Lecture Notes in Physics

The Lecture Notes in Physics

The series Lecture Notes in Physics (LNP), founded in 1969, reports new developments in physics research and teaching – quickly and informally, but with a high quality and the explicit aim to summarize and communicate current knowledge in an accessible way. Books published in this series are conceived as bridging material between advanced graduate textbooks and the forefront of research and to serve three purposes:

- to be a compact and modern up-to-date source of reference on a well-defined topic
- to serve as an accessible introduction to the field to postgraduate students and nonspecialist researchers from related areas
- to be a source of advanced teaching material for specialized seminars, courses and schools

Both monographs and multi-author volumes will be considered for publication. Edited volumes should, however, consist of a very limited number of contributions only. Proceedings will not be considered for LNP.

Volumes published in LNP are disseminated both in print and in electronic formats, the electronic archive being available at springerlink.com. The series content is indexed, abstracted and referenced by many abstracting and information services, bibliographic networks, subscription agencies, library networks, and consortia.

Proposals should be sent to a member of the Editorial Board, or directly to the managing editor at Springer:

Christian Caron
Springer Heidelberg
Physics Editorial Department I
Tiergartenstrasse 17
69121 Heidelberg / Germany
christian.caron@springer.com

H. Weigel

Chiral Soliton Models for Baryons

Springer

Herbert Weigel
Universität Siegen
Fachbereich Physik
Emmy Noether Campus
Siegen 57068
Germany
weigel@physik.uni-siegen.de

H. Weigel, *Chiral Soliton Models for Baryons*, Lect. Notes Phys. 743 (Springer, Berlin Heidelberg 2008), DOI 10.1007/ 978-3-540-75436-7

ISBN: 978-3-540-75435-0 e-ISBN: 978-3-540-75436-7

Lecture Notes in Physics ISSN: 0075-8450

Library of Congress Control Number: 2007938203

Cover design: eStudio Calamar S.L.

Printed on acid-free paper

9 8 7 6 5 4 3 2 1

springer.com

Preface

The purpose of this monograph is to explain and review the chiral soliton picture for baryons and their low-energy properties. Even though this picture by now ages almost half a century, it is currently more than ever under intense investigation. Various revivals have let the model stay modern. Examples that initiated renewed interest are the quark spin contribution to the nucleon spin ("proton spin puzzle") or the quest for pentaquarks and other exotic baryons.

Various motivations for soliton models can be thought of. Mostly they relate to the observed flavor and chiral symmetries of strong interactions and properties of quantum chromodynamics (QCD) when it is generalized to contain infinitely many color degrees of freedom. The author is fully aware that there is anything but an inevitable derivation of the soliton picture from QCD. This probably is a common characteristic of any model attempting to describe baryon properties at low energies. Chiral soliton models certainly do have their limitations. However, they definitely possess a degree of straightforwardness uncommon to other models for hadrons. It is the author's hope that the reader will appreciate the attractive beauty resulting thereof. Quite a number of arguments and conclusions presented in this monograph reflect the author's personal opinion. Yet, the interested reader should be able to gain an objective point of view from the comprehensive list of references that is included.

There are actually many variants of soliton models on the market: starting from the famous Skyrme model of pion fields via vector meson extensions to bosonized formulations of the quark flavor dynamics. They will all be discussed here. Though different variants highlight different issues, it should become clear that they have more features in common than in distinction. In particular, the comprehensive discussion on solitons in models for the quark flavor dynamics (Chaps. 2 and 3) is intended to demonstrate that quark and soliton models have indeed a common base. Even though actual explorations in the soliton picture differ considerably from those in quark models, to a large extent these differences just reflect the use of different field variables.

Some of the topics discussed here have already been reviewed in detail elsewhere. Nevertheless, it might be illuminating to get a different view on similar issues. In addition there are issues that have not been reviewed so far and they motivate this monograph all the more.

Not all the detailed and lengthy calculations will be made explicit. However, the tools provided should enable the interested reader to follow the original research articles or perform the computations independently. Some basic knowledge of quantum field theory, including its path integral formulation, is presupposed. It is also assumed that the reader has some basic knowledge of the representations of the groups $SU(2)$ and $SU(3)$.

These lecture notes distinguish two styles. Chapters 1 through 6 discuss the basics of the soliton model for baryons, i.e., the motivation, the existence of solitons and their interpretation as baryons. These chapters are very detailed and with the help of the appendices the interested reader should be able to redo all the relevant calculations. In particular, beginners in the field will hopefully find this part of the monograph illuminating since one of its major purposes is to cover the gap between standard textbooks and current research. Chapter 1 introduces the subject. The following two chapters review the motivation of soliton models from the quark flavor dynamics. Here we will focus on the Nambu–Jona–Lasino model and explain how the soliton picture emerges from a microscopic quark model that contains all features of chiral symmetry. In Chap. 4 we will particularly examine the Skyrme model and also present the large-N_C arguments that motivate this model. In Chaps. 5 and 6 we will discuss the quantization of the soliton to generate states with good baryon quantum numbers. In particular we will show in Chap. 6 that the baryon number one soliton must be quantized as a fermion. Effectively it is not possible to completely cover the voluminous amount of research that has been assembled in the field. Therefore the remaining chapters serve as survey on static baryon properties (Chap. 7), meson–baryon scattering (Chap. 8), exotic pentaquark baryons (Chap. 9) and systems with baryon number larger than one (Chap. 10). This review part should enable the reader to follow the original research papers that are vastly cited. This Monograph is round off with a short epilogue. A few appendices are included to facilitate comprehension of the calculations in the main body of this monograph.

Many people have contributed to the compilation of this monograph in various ways, e.g., direct collaborations and fruitful discussions over many years. This help is highly appreciated. I am afraid that the following list of names is incomplete: G. Holzwarth, J. Schechter, R. L. Jaffe, H. Reinhardt, H. Walliser, B. Schwesinger, A. Hayashi, N. W. Park, R. Alkofer, Ulf G. Meißner, L. Gamberg, N. N. Scoccola, E. Ruiz Arriola, M. Quandt, O. Schröder. Their insight and expertise has proven indispensable.

The Physics Department at Siegen University is thanked for providing an environment that enabled completion of this monograph.

Siegen, July 2007 Herbert Weigel

Contents

1

Introduction and Motivation

It is of general interest to understand the structure and dynamics of the building blocks of matter. We do well know that matter is composed of atoms. An atom in turn is described as an electron cloud being bound to a nucleus through the electro-magnetic interaction. Furthermore, the nucleus itself contains still more elementary particles, protons and neutrons. They are members of a larger group of particles, the baryons. Together with the mesons (pions, kaons, etc.), the baryons form the even larger group of hadrons that comprise all particles that are subject to the strong interaction. In comparison with the electro-magnetic interaction, our understanding of the strong interaction falls short and many aspects await thorough explanations. Nowadays we utilize relativistic quantum field theories (QFT) to investigate elementary particles and their interactions. For example, the electro-magnetic interaction is understood as the exchange of massless quanta (photons) between charged particles. This theory is called quantum electrodynamics (QED) and formally makes up an abelian gauge group. Unfortunately, the solutions of QFTs are mostly inaccessible outside the perturbation expansion, and often the very knowledge of the relevant quantum theory may be of only limited help to describe observed physical processes.

It is well established that the theory of quantum chromodynamics (QCD) is the fundamental theory for the strong interaction processes of hadrons [1, 2]. In this theory, hadrons are considered as complicated composites of quarks and gluons. The interaction of these fields is described within the framework of a non-abelian gauge theory, the gauge group being color $SU(3)$. The quark fields are assigned to the fundamental representation while the gluons, which are the gauge bosons mediating the interaction, reside in the adjoint representation. In that respect, QCD is a (complicated) generalization of QED. Although we are still lacking a rigorous proof, the confinement hypothesis is commonly accepted. It states that only color singlet objects are observable. These singlet states represent the physical hadrons. The solution to the renormalization group equation tells us that the QCD coupling decreases with increasing momentum transfer (asymptotic freedom). In this energy regime,

H. Weigel: *Introduction and Motivation*, Lect. Notes Phys. **743**, 1–4 (2008)
DOI 10.1007/978-3-540-75436-7_1

QCD can therefore be treated within perturbation theory. The predictions, which result from these analyses of QCD, agree favorably with the experimental data obtained, e.g., in deep inelastic scattering (DIS) processes. However, the behavior of the solution to the renormalization group equation unfortunately prohibits the application of perturbative techniques in the low-energy region. This property of QCD complicates matters significantly and we obviously lack a description of hadrons from first principles, except maybe lattice measurements. In order to describe the low-energy properties of hadrons, it is thus mandatory to revert to models which can be deduced or at least be motivated from QCD.

The motivation of these approaches commonly resides on (i) investigating QCD for special, eventually even unphysical cases for which a deeper insight exists, (ii) exploring the symmetries of QCD, or (iii) both. In the context of building hadron models, the large N_C generalization of QCD and its (approximate) chiral symmetry are of particular importance. The large N_C generalization concerns the number of color degrees of freedom which in reality is $N_\mathrm{C} = 3$, the dimension of the QCD gauge group. Combinatoric considerations allow us to identify the leading contributions to the Green's functions in a $1/N_\mathrm{C}$ expansion which in turn provides an analog classification of hadron properties. The chiral properties of QCD emerge from the observation that in the strong interaction an additional axial symmetry exists besides the expected vector symmetry, due to the smallness of the current quark masses. The interesting feature of the combined, so-called chiral symmetry is that observations from phenomenology dictate this symmetry to be spontaneously broken, i.e., realized in Nambu–Goldstone mode. Implementation of this feature has dramatic consequences on any model for hadron dynamics.

Once a model is given that reflects the symmetries of QCD, it is merely a matter of technical efforts to find the corresponding currents. In turn (static) properties of hadrons can be computed as matrix elements of these currents. Along this path, we will investigate the structure of hadrons in chiral models.

In the course of this monograph, we will extensively explore both the large N_C generalization and the chiral aspects of QCD but will not attempt a detailed exploration of QCD itself. We will find that both motivate the description of baryons as solitons, the so-called Skyrme approach as an outstanding model to analyze baryon properties. This model treats the baryons as collective excitations of meson fields. In particular, the knowledge of the physics of the low-lying mesons provides an exhaustive amount of (almost) parameter-free predictions of properties of baryons. As an additional advantage over many other models, the soliton description represents a means for studying various aspects (spectrum, electromagnetic and axial form factors, meson–baryon scattering, baryon–baryon interaction, etc.) within a unique framework without making any further assumptions about the structure and/or dynamics of particles. Before we analyze the Skyrme approach in detail, it is appropriate to straighten up a few misconceptions about this description. The Skyrme approach has sometimes been criticized as being too crude. This

criticism is based on the issue that the original Skyrme model, which only contains pseudoscalar degrees of freedom, yields qualitatively incorrect predictions on several baryon observables. Many of these problems are linked to the feature that the pseudoscalar fields contain the long-range physics only. Suitable extensions of the model to account for short-range effects as well provide appealing solutions to these problems. Nevertheless, most of the discussion presented here will be limited to the Skyrme model for the pure reason of simplicity. However, such extensions will be explained in more detail when they lead to qualitatively different results.

To begin any thorough discussion of the model, we need to state our understanding of solitons in a field theory. Essentially, this comprises two properties:

- solutions to the (classical) equations of motion,
- localized energy density and finite total energy.

This finite total energy is often referred to as the soliton mass. In order to meet these properties, non-linear features must be operative. Thus, solitons must be non-perturbative structures within the field theory. The incorporation of chiral symmetry and its spontaneous breaking will indeed cause model Lagrangians to be highly non-linear. Furthermore, field configurations that deviate (slightly) from the soliton may be considered. The effects of these deviations can be classified in a $1/N_{\mathrm{C}}$ expansion, thereby making contact with the large N_{C} generalization of QCD. Some of the solitons are additionally characterized by topological properties, in particular a winding number. Though such topological features are crucial and fascinating (The interested reader may, e.g., consult the textbook [3].), this monograph will focus on the relevance of soliton models for hadron phenomenology.

It is worthwhile to reflect on the history of Skyrme soliton models not only because they preceded the development of QCD but also to observe the various ups and downs of these models. Above we have discussed the "modern" justification of the Skyrme model via the $1/N_{\mathrm{C}}$ expansion and spontaneous breaking of chiral symmetry. Naturally, one wonders how they relate to Skyrme's original motivations. We are fortunate in having available a reconstructed talk on just this topic by Skyrme [4]. He mentioned three motivations: (i) the idea of unifying bosons and fermions in a common framework; (ii) the feeling that point particles are inconsistent in the sense that their quantum field theory formulation introduces infinities which are only "swept under the rug" by the renormalization process; and (iii) the desire to eliminate fermions from a fundamental formulation since fermions have no simple classical analog. So, Skyrme did not choose his Lagrangian model to describe spontaneous breakdown of chiral symmetry; rather, the non-linear form was adopted to insure that the pions were "angular" variables which would give multi-valued functions; the crossing of different sheets of these functions might then correspond to singularities which would realize the baryons. The evident "moral" of this historical discussion is just that interesting ideas have an uncanny way of turning out to be useful and true. In the modern framework, the idea

to describe baryons as solitons was revived by Witten in 1979 when he argued that baryons indeed emerge as solitons in the large N_C generalization of QCD [5]. Later, he also showed that the baryon number arises from the topological properties of the soliton [6]. In 1983, first concrete computations on the spectrum and static properties were pioneered by Adkins, Nappi, and Witten in the model with two light flavors [7]. Though that was quite successful, some problems such as the too low prediction for the nucleon axial charge lingered unsolved over the years. A second revival of the Skyrme model was triggered by the EMC observation that the quark spin contribution to the total nucleon spin was unexpectedly small, if not even zero, a feature that was unexpected in quark models but could be nicely understood in the soliton model [8]. This furthermore triggered intensive studies of the three-flavor model [9] and the exploration of the nucleon's strangeness content. In this respect, it is noteworthy that soliton models do not face the so-called missing resonance problem of (non-relativistic) constituent quark models (this notion is misleading as those models predict too many baryon states [10]). Almost naturally, the extension to flavor $SU(3)$ also let into the discussion of exotic baryons because they emerge as (flavor) rotational excitations of the nucleon. For that reason, soliton models predict exotic baryons to be lighter than, e.g., constituent quark models do. Though the early and most stimulating soliton model predictions [11] for properties of exotic baryons were only a little better than just good guesses, they ignited a wealth of research, both on the theory and on the experimental side. At this point of time, we still have to await the ultimate confirmation or rejection of exotic baryons.

References

1. F. J. Ynduráin, *The Theory of Quark and Gluon Interactions*. Springer-Verlag, Berlin, 1993. 1
2. T. Muta, *Foundations of Quantum Chromodynamics*. World Scientific, Singapore, 1987. 1
3. V. G. Makhankov, Y. P. Rybakov, and V. I. Sanyuk, *The Skyrme Model: Fundamentals, Methods, Applications*. Springer series in nuclear and particle physics, 1993. 3
4. T. H. R. Skyrme, *Int. J. Mod. Phys.* **A3** (1988) 2745. Article reconstruced by I. Aitchison. 3
5. E. Witten, *Nucl. Phys.* **B160** (1979) 57. 4
6. E. Witten, *Nucl. Phys.* **B223** (1983) 422, 433. 4
7. G. S. Adkins, C. R. Nappi, and E. Witten, *Nucl. Phys.* **B228** (1983) 552. 4
8. S. J. Brodsky, J. R. Ellis, and M. Karliner, *Phys. Lett.* **B206** (1988) 309. 4
9. H. Weigel, *Int. J. Mod. Phys.* **A11** (1996) 2419. 4
10. D. M. Manley, *J. Phys. Conf. Ser.* **9** (2005) 230. 4
11. D. Diakonov, V. Petrov, and M. V. Polyakov, *Z. Phys.* **A359** (1997) 305. 4

2

Quark Flavor Interaction

The description of the low-energy physics of hadrons requires to model the interaction of the quark constituents. The observation that the (current) quark masses of the up (u) and down (d) quarks (and eventually the strange (s) quark) are significantly smaller than typical strong interaction energy scales serves as a major input. In a first approach it is thus reasonable to ignore the effects of the current quark masses. In that approximation axial transformations leave the QCD Lagrangian invariant and an additional global symmetry, the so-called *chiral symmetry* [1], emerges. This symmetry represents an important tool for model building because the models should be consistent with chiral symmetry. Any such model describes the interaction of light quarks with different flavors: *up*, *down* and eventually *strange*; hence the notion of quark flavor dynamics.

2.1 Chiral Symmetry

In the case of massless Dirac fermions that interact with boson fields via a vector interaction (as in QCD), left- and right-handed components

$$\Psi_{\mathrm{L,R}} = \frac{1}{2}\left(1 \mp \gamma_5\right)\Psi \tag{2.1}$$

of the 4×4 spinors Ψ decouple. As a consequence the QCD Lagrangian with zero current masses decomposes into a sum of two Lagrangians that contain only right-(left-) handed fields, respectively. These two Lagrangians are invariant under global unitary flavor transformations of the corresponding right-(left-) handed fields, so that the QCD Lagrangian possesses an $U_{\mathrm{L}}(N_{\mathrm{f}}) \times U_{\mathrm{R}}(N_{\mathrm{f}})$ symmetry. Here N_{f} is the number of quark flavors whose current quark masses are ignored. Depending on whether we consider the strange current quark mass as large or small we have $N_{\mathrm{f}} = 2$ or $N_{\mathrm{f}} = 3$, respectively. This symmetry group factorizes according to

H. Weigel: *Quark Flavor Interaction*, Lect. Notes Phys. **743**, 5–26 (2008)
DOI 10.1007/978-3-540-75436-7_2

$$U_{\rm L}(N_{\rm f}) \times U_{\rm R}(N_{\rm f}) \cong U_{\rm L+R}(1) \times U_{\rm L-R}(1) \times SU_{\rm L}(N_{\rm f}) \times SU_{\rm R}(N_{\rm f}) \qquad (2.2)$$

and is called the *chiral group*. The invariance under $U_{\rm L+R}(1)$ is responsible for the conservation of baryon number whereas $U_{\rm L-R}(1)$ is subject to a quantum anomaly [2, 3]. This results in $2N_{\rm f} - 1$ conserved flavor currents. The $2N_{\rm f}$ flavor currents are most conveniently presented as linear combination of the left- and right-handed vector currents that are eigenstates of parity: the vector current J^a_μ and the axial vector current A^a_μ,

$$\begin{aligned} J^a_\mu &= \bar{q}_{\rm L}\gamma_\mu \frac{\lambda_a}{2} q_{\rm L} + \bar{q}_{\rm R}\gamma_\mu \frac{\lambda_a}{2} q_{\rm R} = \bar{q}\gamma_\mu \frac{\lambda_a}{2} q \\ A^a_\mu &= -\bar{q}_{\rm L}\gamma_\mu \frac{\lambda_a}{2} q_{\rm L} + \bar{q}_{\rm R}\gamma_\mu \frac{\lambda_a}{2} q_{\rm R} = \bar{q}\gamma_\mu\gamma_5 \frac{\lambda_a}{2} q\,. \end{aligned} \qquad (2.3)$$

Here λ_a $(a = 1, \ldots, N_{\rm f}^2 - 1)$ are the Gell–Mann matrices of $SU(N_{\rm f})$ and $\lambda_0 = \sqrt{2/N_{\rm f}}\,\mathbb{1}$ is proportional to the unit matrix in flavor space. The spinors are additionally column vectors with $N_{\rm f}$ entries of the quark flavors

$$q = \begin{pmatrix} \Psi_1 \\ \Psi_2 \\ \vdots \\ \Psi_{N_{\rm f}} \end{pmatrix} = \begin{pmatrix} \Psi_u \\ \Psi_d \\ \vdots \\ \Psi_{N_{\rm f}} \end{pmatrix}. \qquad (2.4)$$

The properties of these fermion fields under infinitesimal chiral transformations, (2.2), are summarized in Table A.1 of Appendix A. In the limit of vanishing current quark masses the above currents, apart from A^0_μ, are conserved and that property should be reproduced within any model. In case these masses are non-zero but nevertheless identical for all flavors the vector current J^a_μ is still conserved for $a = 0, \ldots, N_{\rm f}$. The non-conservation of A^0_μ can, e.g., be computed in a functional language [4] where it arises from the measure of the fermion fields not being invariant under chiral transformations. This non-conservation can be quantified,

$$\sqrt{\frac{N_{\rm f}}{2}}\,\partial^\mu A^0_\mu = -\frac{g^2}{8\pi^2}\,{\rm tr}\,\left(\widetilde{F}_{\mu\nu}F^{\mu\nu}\right) + \cdots\,. \qquad (2.5)$$

Here the trace goes over all discrete indices of the vector gauge fields to which the fermions, (2.4) couple, e.g., color, charge and/or flavor. Furthermore $F_{\mu\nu}$ is the field strength of the vector field that couples with coupling constant g to the fermions and $\widetilde{F}_{\mu\nu}$ is dual to $F_{\mu\nu}$. The ellipsis refer to contributions that stem from finite current quark masses. A direct consequence of this anomaly is the neutral pion decay into two photons. That effect is discussed in C.4.

2.2 Dynamical Breaking of Chiral Symmetry

In general, symmetries like (2.2) can be realized by the particle content of the theory in two scenarios:

- Wigner–Weyl realization: the vacuum (lowest energy) configuration is invariant under the symmetry and the generators of the symmetry transform degenerate physical states into one another.
- Nambu–Goldstone realization (also called spontaneous symmetry breaking): the vacuum configuration is *not* invariant under the symmetry, rather the lowest energy state is degenerate. Operators that do not transform as singlets under the symmetry develop non-zero vacuum expectation values (VEV). Acting with the symmetry generators on such operators excites massless modes, the so-called Goldstone bosons (instead of transforming into other physical states). States that are related to one another by generators that do not commute with operators that possess non-zero VEVs are *not* degenerate.

Now it is for nature to decide which realization is put into effect. Since states of different chirality carry opposite parity, the question to be answered is whether or not the states of opposite parity are degenerate. For this purpose it is illuminating to consider the spectrum of the low-lying mesons as sketched in Fig. 2.1. Obviously the degeneracy expected in the Wigner–Weyl realization is not seen for the scalar and pseudoscalar mesons. While scalar meson masses are several hundred MeV (these states are quite broad, in addition) the pseudoscalar mesons start at a little above 100 MeV. As a matter of fact, and as we will recognize later, their small masses are solely due to non-zero current quark masses. Stated otherwise, the pseudoscalar mesons would have zero mass in the ideal world of massless current quarks. We conclude that chiral symmetry is realized in the Nambu–Goldstone phase with the pseudoscalar mesons being the (would-be) Goldstone modes. The only exception

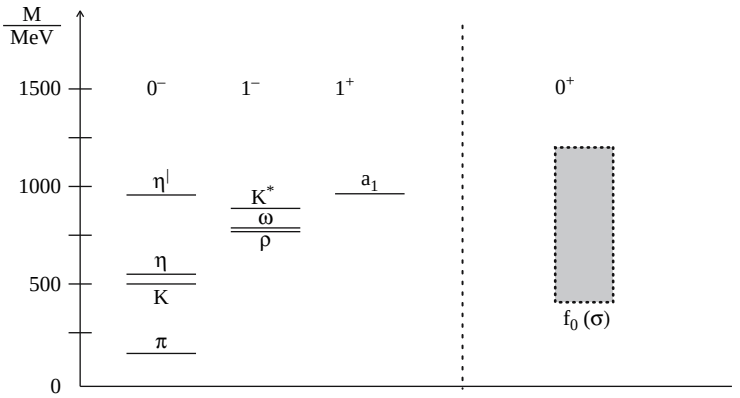

Fig. 2.1. Sketch of the spectrum of the low-lying mesons. *Left panel*: pseudoscalars (0^-), vectors (1^-) and axial vectors (1^+); *right panel*: scalars (0^+). Data taken from the particle data group [5]. This graphic is to illustrate the difference between the 0^- and 0^+ spectra. An updated account on the spectra in the scalar sector is given in the proceedings [6] and references therein

is the η' (or a linear combination of octet and singlet ηs) that remains massive even when the current quark masses are sent to zero. QCD does not have a $U_A(1)$ symmetry because of the anomaly (2.5) and the fact that there are field configurations in QCD (instantons) for which the spatial integral of the right hand side of (2.5) does not vanish even though this four dimensional integral can be transformed into a three dimensional surface integral. Instantons will be discussed in Sect. 2.6; here it suffices to remark that they induce interactions [7] that upon bosonization (to be described in the following section) provide a mass term for pseudoscalar flavor singlet meson [8, 9]. This explains the absence of a (would-be) Goldstone boson for the spontaneously broken $U_A(1)$ symmetry.

Hence the meson spectrum suggests that in the limit of massless quarks only the vector symmetry is realized in the spectrum while the axial symmetry is spontaneously broken. That is, there is an operator that is invariant under vector transformations but not under axial transformations. Noting that vector transformations do alter left- and right-handed spinors equally while axial transformations do not and that

$$\bar{\Psi}\Psi = \bar{\Psi}_{\mathrm{L}}\Psi_{\mathrm{R}} + \bar{\Psi}_{\mathrm{R}}\Psi_{\mathrm{L}}\,, \tag{2.6}$$

it is perspicuous that the simplest such operator is $\bar{q}q$ and that the dynamics of QCD imply a non-zero quark condensate,

$$\langle\bar{q}q\rangle \neq 0\,. \tag{2.7}$$

Model building therefore requires to

(i) Find a simple mechanism that yields such a VEV or
(ii) Start from a formulation that has (2.7) built in.

In the next subsection we will discuss the Nambu–Jona–Lasinio model [10, 11] as a (simple) example to follow path (i). On the other hand, treatments like chiral perturbation theory [12, 13, 14, 15, 16] are designed according to (ii).

2.3 The Nambu–Jona–Lasinio Model

To be specific we will consider the Nambu–Jona–Lasinio (NJL) model described by the Lagrangian (For reviews see, e.g., [17, 18, 19].)

$$\begin{aligned}\mathcal{L}_{\mathrm{NJL}} = \bar{q}(\mathrm{i}\partial\!\!\!/ - \hat{m}_0)q + 2G_1 \sum_{a=0}^{N_{\mathrm{f}}^2-1}\left(\left(\bar{q}\frac{\lambda_a}{2}q\right)^2 + \left(\bar{q}\frac{\lambda_a}{2}\mathrm{i}\gamma_5 q\right)^2\right)\\ -2G_2 \sum_{a=0}^{N_{\mathrm{f}}^2-1}\left(\left(\bar{q}\frac{\lambda_a}{2}\gamma_\mu q\right)^2 + \left(\bar{q}\frac{\lambda_a}{2}\gamma_5\gamma_\mu q\right)^2\right)\,,\end{aligned} \tag{2.8}$$

where $\hat{m}_0 = \mathrm{diag}\,(m_u, m_d, \ldots, m_{N_{\mathrm{f}}})$ is the *current* quark mass matrix and $G_{1,2}$ are two so-far undetermined coupling constants. The discussion and results of Appendix A immediately show that the interaction terms in (2.8) are

invariant under chiral transformations, (2.2). Hence chiral symmetry is only broken by the small current quark masses.

This type of model can, e.g., be motivated from QCD by Fierz-transformation of the *color* current–current interaction that emerges after integrating out the gluon fields [19] and omitting $1/N_{\rm C}$-suppressed diquark-correlations. An easily traceable calculation is that of [20]. Here we only mention that this scenario yields $G_i \propto g^2_{\rm QCD} \times \mathcal{O}(N_C^0)$, where $g_{\rm QCD}$ is the QCD gauge coupling. Later we will argue that a sensible generalization of QCD to arbitrary $N_{\rm C}$ requires $g_{\rm QCD} = \mathcal{O}(1/\sqrt{N_{\rm C}})$, cf. (4.1), and thus $G_i = \mathcal{O}(1/N_{\rm C})$.

We want to express the quark (fermion) theory in (2.8) as an effective meson (boson) theory. Since the interaction is quartic in the quark spinors, this is actually straightforward and merely requires the completion of squares [21]. Consider, e.g.,

$$\frac{1}{8G_1} S_{\rm a}^2 - S_a \bar{q} \frac{\lambda_a}{2} q = \frac{1}{8G_1} \left(S_{\rm a} + 4G_1 \bar{q} \frac{\lambda_a}{2} q \right)^2 - 2G_1 \left(\bar{q} \frac{\lambda_a}{2} q \right)^2 \tag{2.9}$$

and functionally integrate over the auxiliary (meson) field $S_{\rm a}$,

$$\begin{aligned} &\exp\left[\mathrm{i} \int \mathrm{d}^4x \, 2G_1 \left(\bar{q} \frac{\lambda_a}{2} q \right)^2 \right] = \\ &\int [DS_{\rm a}] \exp\left[-\mathrm{i} \int \mathrm{d}^4x \left(\frac{1}{8G_1} S_{\rm a}^2 + S_{\rm a} \bar{q} \frac{\lambda_a}{2} q \right) \right] \end{aligned} \tag{2.10}$$

up to a normalization constant. Of course, analogous relations hold for the remaining interaction terms. Combining all auxiliary fields into a single matrix valued meson field Φ allows us to formally write the generating functional as

$$\begin{aligned} Z_{\rm NJL} &= \int [Dq]\,[D\bar{q}] \, \exp\left(\mathrm{i} \int \mathrm{d}^4x \, \mathcal{L}_{\rm NJL} \right) \\ &= \int [D\Phi] \, \exp\left(-\frac{\mathrm{i}}{2} \int \mathrm{d}^4x \, \mathrm{tr}_F \left[(\Phi - \hat{m}_0) \, Q^{-1} \, (\Phi - \hat{m}_0) \right] \right) \\ &\quad \times \int [Dq]\,[D\bar{q}] \exp\left(\mathrm{i} \int \mathrm{d}^4x \bar{q} \, (\mathrm{i}\partial\!\!\!/ - \Phi \cdot \Lambda) \, q \right) . \end{aligned} \tag{2.11}$$

Here "$\mathrm{tr}_{\rm F}$" denotes the trace in flavor space and the current quark mass matrix has been absorbed into a constant shift of Φ. Furthermore shorthand (matrix) notations are utilized for the flavor–Dirac structure (Λ) and the coupling constants (Q) that occur in the interaction terms of (2.8). Rather than giving them explicitly, we decompose the generic meson field Φ into irreducible Lorentz tensors

$$\Phi \cdot \Lambda = S + \mathrm{i}\gamma_5 P - V\!\!\!/ - A\!\!\!/\gamma_5 \, . \tag{2.12}$$

Here S, P, V and A are scalar, pseudoscalar, vector and axial-vector fields, respectively. They are all hermitian matrices in flavor space. Furthermore the decomposition, (2.12), provides a transparent expression

$$\tfrac{1}{2}\mathrm{tr}(\Phi-\hat{m}_0)Q^{-1}(\Phi-\hat{m}_0) = \tfrac{1}{4G_1}\mathrm{tr}((S-\hat{m}_0)^2+P^2) \\ -\tfrac{1}{4G_2}\mathrm{tr}(V_\mu V^\mu + A_\mu A^\mu)\ , \qquad (2.13)$$

for the argument that appears in the exponential of the mesonic part of the generating functional. When convenient, we will use Φ as a short-hand notation for all fields S, P, V and A and combine scalar and pseudoscalar fields to $M = S + \mathrm{i}P$ and $M^\dagger = S - \mathrm{i}P$.

The generating functional factorizes into mesonic and fermionic parts with a generalized Yukawa interaction between mesons and fermions. In (2.11) the quark field appears bilinearly in the exponent and can now be integrated out. This integration yields the determinant of the operator in between the spinors. Using the identity $\log\mathrm{Det}(A) = \mathrm{Tr}\log(A)$ finally leads to a purely mesonic theory $\mathcal{A}[\Phi]$ that is given by

$$Z_{\mathrm{NJL}} = \int [D\Phi]\exp\left(\mathrm{i}\mathcal{A}[\Phi]\right) \quad \text{with} \\ \mathcal{A}[\Phi] = -\frac{1}{2}\int \mathrm{d}^4x\,(\Phi-\hat{m}_0)Q^{-1}(\Phi-\hat{m}_0) - \mathrm{i}\,\mathrm{Tr}\log(\mathrm{i}\partial\!\!\!/ - \Phi). \qquad (2.14)$$

Here Tr denotes the functional trace that also includes space–time integration on top of summing over discrete indices. The quarks carry color degrees of freedom. Yet the NJL-model interaction is color neutral, so the associated trace merely causes multiplication by N_C, the number of color degrees of freedom, i.e., $\mathrm{Tr} \to N_\mathrm{C}\mathrm{Tr}_\mathrm{DF}$, with the latter trace involving only Dirac and flavor discrete indices (together with space–time integration).

In (2.14) we have essentially met our goal to bosonize the fermion model. Of course, the interaction in (2.8) has been "invented" to exactly facilitate that goal. In (2.14) we sum up all one fermion loop diagrams, i.e., $\mathcal{A}[\Phi]$ is complete at $\mathcal{O}(\hbar)$. The full quantum action of the NJL-model also contains higher order contributions. In the present treatment they do not occur because we have treated the meson fields Φ classically. Higher order terms arise from their quantum properties. For that reason the action, (2.14) is sometimes called the semi-bosonized NJL-model.

Note that the action $\mathcal{A}[\Phi]$ is a non-linear, even non-polynomial function of the meson field Φ; even more, $\mathrm{Tr}\log(\mathrm{i}\partial\!\!\!/ - \Phi)$ is non-local. The quantum theory defined by (2.14) is, however, equivalent to the underlying NJL model defined by the Lagrangian (2.8). On the other hand, the generating functional (2.14) has the advantage that it may be treated semiclassically. In particular, according to (2.10) a stationary point for Φ is to be identified with a VEV of a quark bilinear. This paves the way toward the second goal at which we aim, a microscopic quark model with a non-zero translationally invariant stationary point $S_0 \sim G_1\langle\bar{q}q\rangle$ to parameterize spontaneous chiral symmetry breaking. Unfortunately the action, (2.14) is not yet suited for actual calculations because of ultraviolet divergences in $\mathrm{Tr}\log(\mathrm{i}\partial\!\!\!/ - \Phi)$. A regularization prescription is needed, and as the model (2.8) is not renormalizable

(the coupling constants G_i have dimension $1/(\text{mass})^2$), the model itself is only completely defined when a regularization scheme is provided. For definiteness we will use Schwinger's proper time regularization [22] which introduces an $O(4)$-invariant cut-off Λ after continuation to Euclidean space that is enforced by the Wick rotation.[1] Even though other regularization schemes give similar results [25], its choice is part of the model building. In Euclidean space it is necessary to consider the real and imaginary parts of the non-local piece separately

$$\mathcal{A}_{\mathrm{F}} := -\mathrm{i}\,\mathrm{Tr}\log(\mathrm{i}\partial\!\!\!/ - \Phi\cdot\Lambda) \xrightarrow[\text{rotation}]{\text{Wick}} \mathcal{A}_{\mathrm{R}} + \mathcal{A}_{\mathrm{I}}\,, \tag{2.15}$$

with

$$\mathcal{A}_{\mathrm{R}} = \tfrac{1}{2}\mathrm{Tr}\log(\not{D}_{\mathrm{E}}^{\dagger}\not{D}_{\mathrm{E}}) \qquad \text{and} \qquad \mathcal{A}_{\mathrm{I}} = \tfrac{1}{2}\mathrm{Tr}\log\left((\not{D}_{\mathrm{E}}^{\dagger})^{-1}\not{D}_{\mathrm{E}}\right). \tag{2.16}$$

Here $\not{D}_{\mathrm{E}} = \sum_{\mu=1}^{4} D_{\mathrm{E}\mu}\gamma_\mu$ is the argument of the logarithm in (2.15) analytically continued to Euclidean space ($\mathcal{A}_{\mathrm{F}}$ is real in Minkowski space). The real part $\mathcal{A}_{\mathrm{R}}$ diverges for large momenta p whereas the imaginary part $\mathcal{A}_{\mathrm{I}}$ does not contain ultraviolet divergencies, i.e., it is finite without regularization. Therefore one has the option of keeping $\mathcal{A}_{\mathrm{I}}$ unregularized, or to regularize it in a way consistent with the regularization of $\mathcal{A}_{\mathrm{R}}$. Note that this defines two different models.[2] For the real part of the action the proper time regularization consists in replacing the logarithm by a parameter integral

$$\mathcal{A}_{\mathrm{R}} \to -\frac{1}{2}\int_{1/\Lambda^2}^{\infty}\frac{\mathrm{d}s}{s}\mathrm{Tr}\exp\left(-s\not{D}_{\mathrm{E}}^{\dagger}\not{D}_{\mathrm{E}}\right), \tag{2.17}$$

which for $\Lambda\to\infty$ reproduces the logarithm up to an irrelevant additive constant, cf. (B.18). For finite Λ the contributions from small s in the integral are left out. On the other hand, only the small s values are sensible to the regime where the expectation value of $\not{D}_{\mathrm{E}}^{\dagger}\not{D}_{\mathrm{E}}$ is large. That is, the contributions from large momenta in the functional trace are suppressed. Hence Λ is an ultraviolet cut-off. (The notation Λ for this cut-off should not be confused with the abbreviation for the flavor–Dirac structure in (2.11) and (2.12).)

To discuss chiral symmetry breaking it suffices to consider $\mathcal{A}_{\mathrm{R}}$ as regularized in (2.17) and omit (axial)vector interactions for the time being, i.e., $V_\mu = A_\mu = 0$. Variation with respect to the scalar and pseudoscalar fields yields the Dyson–Schwinger or gap equations. By symmetry, their translationally invariant solutions must be Lorentz scalar and of neutral flavor. However,

[1] Analogous formulations in Minkowski space are reported in [23, 24], see also Sect. 7.7.

[2] The proper reproduction of the anomaly, (2.5) seems to prohibit regularization of $\mathcal{A}_{\mathrm{I}}$, [26]; see, however, [27]. As will be discussed in Chap. 3, the requirement that soliton configurations possess integer baryon number corroborates non-regularization of $\mathcal{A}_{\mathrm{I}}$.

different current quark masses prevent the solution from being proportional to the unit matrix in flavor space. We therefore parameterize $\langle M_{ij}(x)\rangle = \delta_{ij} m_i$ for $i, j = 1, \ldots, N_\mathrm{f}$. From (2.15) it is obvious that m_i acts as a mass for the quark of flavor i. Therefore a non-zero value is called *constituent* quark mass. In the proper time regularization the explicit form of the gap equation is (The calculation may be traced from Appendix B.)

$$m_i = m_{0,i} - 2G_1\langle\bar{q}q\rangle_i \quad \text{where} \quad \langle\bar{q}q\rangle_i = -m_i^3 \frac{N_\mathrm{C}}{4\pi^2}\,\Gamma\left(-1, \frac{m_i^2}{\Lambda^2}\right) . \tag{2.18}$$

The notation already identifies the quark condensate $\bar{q}q$ as it is obtained from the stationary point of the scalar field, (2.10). The interpretation in terms of the quark loop is apparent from (B.15). This leads to the graphical representation

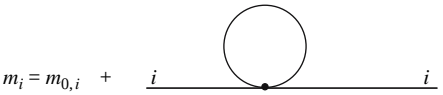

with the mass of the quark in the loop being m_i, the dynamically generated constituent quark mass.

We see from Fig. 2.2 that in the chiral limit ($m_0 = 0$) the quark condensate and therefore also the quark constituent mass is zero when the coupling constant G_1 stays below a critical value whose precise datum depends on the cut-off, Λ. Above this critical value the trivial solution coexists with a

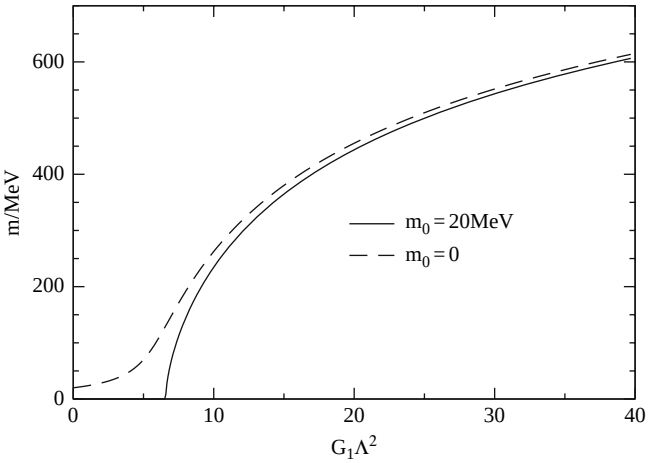

Fig. 2.2. The solution of the gap equation (2.18) for vanishing current mass $m_0 = 20\,\mathrm{MeV}$ (*solid line*) and $m_0 = 0$ (*dashed line*) as function of the coupling constant G_1. In this specific computation $\Lambda = 630\,\mathrm{MeV}$ has been chosen

non-trivial one. The effective potential of a constant scalar field in the chiral limit [20]

$$V_{\text{eff}}(M) = \frac{1}{2G_1}\Sigma^2 + \frac{N_\text{C}}{16\pi^2}\left[\Sigma^4\Gamma\left(0, \frac{\Sigma^2}{\Lambda^2}\right) - \left(\Sigma^2 - \Lambda^2\right)\Lambda^2 \mathrm{e}^{-\Sigma^2/\Lambda^2}\right], \quad (2.19)$$

where $\Sigma = \sqrt{\text{tr}(MM^\dagger)}/N_\text{f}$ shows that the solution with $\Sigma \neq 0$ is energetically favored. Commonly the so-defined Σ is called the chiral radius.

Having established the existence of a non-trivial VEV $\langle\bar{q}q\rangle$, we still have to verify that massless pions emerge, at least for $m_{0,i} = 0$. Fortunately the examination of pion properties also allows us to assign a physical meaning to the above introduced and so far undetermined ultraviolet cut-off Λ. For simplicity we will omit flavor symmetry breaking in this context and call m the solution to the flavor symmetric gap equation, (2.18) with $m_{0,i} \equiv m_0$. The effects of $m_{0,i} \neq m_{0,j\neq i}$ may be traced from the literature [28, 29]. The Goldstone modes are expected to be orthogonal to the mode carrying the VEV. We therefore parameterize

$$M = mU(x) \qquad \text{with} \qquad U(x) = \exp\left[\mathrm{i}\sum_{a=1}^{N_\text{f}^2-1}\phi_a(x)\frac{\lambda_a}{2}\right], \quad (2.20)$$

which also defines the chiral field, $U(x)$. Substituting M and $U = 1 + \mathrm{i}\phi_a(x)\lambda_a/2$ into (2.12) shows that the real fields $\phi_a(x)$ couple to the quarks via γ_5, as pseudoscalars should. In addition, this ensures that the modes ϕ_a are indeed orthogonal to the scalar modes that contain the VEV. The main task is to expand the (regularized) action up to quadratic order in $\phi_a(x)$. The techniques for this calculation are provided in Appendix B. The result is most conveniently presented in (Euclidean) momentum space

$$\mathcal{A}^{(2)} = \frac{1}{2}\int\frac{\mathrm{d}^4q}{(2\pi)^4}\sum_a \widetilde{\phi}_a(q)D^{-1}(q^2)\widetilde{\phi}_a(-q)\,, \quad (2.21)$$

where the superscript indicates the expansion up to second order and $\widetilde{\phi}_a(q)$ is the Fourier transformation of $\phi_a(x)$. The first term in the inverse propagator

$$D^{-1}(q^2) = -\frac{m_0 m}{G_1} - q^2 f(q^2) \qquad \text{with}$$
$$f^2(q^2) = m^2\frac{N_\text{C}}{4\pi^2}\int_0^1 \mathrm{d}x\;\Gamma\left(0, \frac{m^2 + x(1-x)q^2}{\Lambda^2}\right) \quad (2.22)$$

originates from the local part of the action $\mathcal{A}$, (2.14). The mass of $\phi_a(x)$ as extracted from the pole condition, $D^{-1}(-m_\phi^2) = 0$ obviously vanishes in the chiral limit $m_0 = 0$. Identifying the modes $\phi_a(x)$ as pions and comparison with the non-linear σ model (or coupling an external axial current to $\mathcal{A}$, cf. Sect. 2.5 and (B.25)) furthermore shows that the pion decay constant is

$$f_\pi^2 = f^2(-m_\pi^2)\,. \tag{2.23}$$

Imposing the empirical values $f_\pi = 93\,\mathrm{MeV}$ and $m_\pi = 138\,\mathrm{MeV}$ thus yields a further relation between the cut-off Λ and the constituent quark mass m. In practice a value for the constituent quark mass $m \sim 400\,\mathrm{MeV}$ is chosen for the reason discussed later in Sect. 5.6. Equation (2.23) then provides the corresponding value $\Lambda \sim 630\,\mathrm{MeV}$. Subsequently the gap equation, (2.18) yields the coupling constant G_1 and finally the current quark mass m_0 is determined from $D^{-1}(-m_\pi^2) = 0$,

$$m_\pi^2 f_\pi^2 = \frac{m_0 m}{G_1}\,. \tag{2.24}$$

Stated otherwise, the constituent quark mass is considered as the only adjustable model parameter.

We also confirm an important statement of Sect. 2.2: The pion would indeed be a massless Goldstone boson if the current quark mass, m_0, were zero.

Similar computations have been applied to the vector interactions. These investigations determine the coupling constant G_2 from the empirical value of the ρ-meson mass $m_\rho = 770\,\mathrm{MeV}$. In particular the vector interactions contain π–A_1 mixing and the model yields the estimate [30]

$$m_{A_1}^2 = m_\rho^2 + 6m^2 + \mathcal{O}\left(\frac{1}{\Lambda^2}\right) \tag{2.25}$$

according to which the axial-vector mesons are significantly heavier than the vector mesons. Approximate results for the (axial)vector mesons can also be obtained in the gradient expansion that will be subject of the next section. Furthermore exhaustive studies of flavor symmetry breaking effects in the meson sector have been performed. Concerning the three-flavor model it should be noted that there is only one additional parameter, the strange quark current mass.[3] Hence the kaon decay constant, f_K is a prediction. This prediction comes out a bit on the low side: $f_\mathrm{K}/f_\pi \approx 1.11$ vs. 1.21 empirically [5], nevertheless it is in the right ball park. For further details we refer the interested reader to original studies [29, 30, 31] and review articles [17, 18, 19]. In any event, the above discussion is sufficient as a set-up of the model to discuss baryons as solitons in Chap. 3.

We want to conclude this section by discussing the transformation properties of the (pseudo)scalar field M under global chiral transformations. After all, the model for the quark flavor dynamics was built to reflect the chiral properties of QCD. According to the bosonization prescription we explicitly write the flavor indices (color and spin degrees are summed),

[3] We stress that the current quark masses in (2.8) are those of the model. They are model parameters and should not be confused with those in QCD.

$$M_{ij}(x) = \sum_{a=0}^{N_{\rm f}^2-1} M_a(x)\lambda_a^{(ij)} \propto \sum_{a=0}^{N_{\rm f}^2-1} \lambda_a^{(ij)} \left[\bar{q}_m \frac{\lambda_a^{(mn)}}{2} q_n - \bar{q}_m\gamma_5 \frac{\lambda_a^{(mn)}}{2} q_n\right] . \tag{2.26}$$

In general one would expect a bilocal expression on the right hand side. However, here we are only interested in *global* aspects and we may ignore that complication. For the same reason we omit constants of proportionality. From the completeness relation for $SU(N)$ generators ($T_a = \lambda_a/2$)

$$\sum_{a=1}^{N^2-1} (T_a)_{ij} (T_a)_{kl} = \frac{1}{2}\delta_{il}\delta_{jk} - \frac{1}{2N}\delta_{ij}\delta_{kl} \tag{2.27}$$

we find

$$M_{ij}(x) \propto \frac{1}{2}\left[\bar{q}_j q_i - \bar{q}_j\gamma_5 q_i\right] = \bar{q}_{{\rm R}j} q_{{\rm L}i} , \tag{2.28}$$

with explicit reference to chirality. Under global chiral rotations

$$q_{\rm L} \to L\, q_{\rm L} \qquad \text{and} \qquad q_{\rm R} \to R\, q_{\rm R} \tag{2.29}$$

with L and R constant $SU(N_{\rm f})$ matrices, we thus induce

$$M(x) \longrightarrow L M(x) R^\dagger . \tag{2.30}$$

This, of course, is consistent with the requirement that

$$\bar{q}\left({\rm i}\partial\!\!\!/ - M P_{\rm R} - M^\dagger P_{\rm L}\right) q \tag{2.31}$$

is chirally invariant. Seemingly trivial, the coexistence of (2.29) and (2.30) is a very important result: We have just learned how to translate the chiral transformation properties of QCD to the meson fields M. Hence we may identify the internal symmetries of a model for M with those of QCD! Since most of the QCD hadron matrix elements are to be computed from symmetry currents we are allowed to identify the QCD matrix elements with those computed in the model. This is indeed the only venue which permits model calculations of QCD observables. Conversely, model calculations that are based on identifying model degrees of freedom with those of QCD (rather than just identifying currents) are less trustworthy.

2.4 Gradient Expansion

The bosonized action, (2.14), and its regularized version, (2.17), are non-local meson theories. Many of the technical problems in the above-described calculations emerge from this non-locality. It transforms into an infinite series of local derivative terms by a Taylor expansion in the separation. The coefficients of these derivative terms are determined from the non-local action

via the gradient expansion [32, 33, 34]. Assuming that the meson fields Φ vary only slowly in space and thereby mitigating non-local effects, we may approximate this Taylor series by truncating it to a low, say next-to-leading, order. Here we will briefly gather the main results of this approximation for the NJL model, in particular because it serves to construct effective meson theories in which the construction of soliton solutions and their quantization are significantly more perspicuous than in bosonized NJL-type models. In this discussion of the gradient expansion we will mostly follow the treatment of [30]. That calculation counts (axial)vector meson fields at the same order as a single derivative which is suggested by covariant derivatives. For the sum of the local part of the action, (2.14), and the regularized real part of the determinant, (2.17), it yields,

$$\begin{aligned}\mathcal{A}_{\mathrm{R}} = \int \mathrm{d}^4x \Big\{ & -V_{\mathrm{eff}}(M) + \frac{1}{4G_2}\,\mathrm{tr}\,(V_\mu V^\mu + A_\mu A^\mu) \\ & + \frac{1}{2g_{\mathrm{V}}^2}\,\mathrm{tr}\left[3\nabla_\nu M^\dagger \nabla^\nu M - F^V_{\mu\nu}F^{V\mu\nu} - F^A_{\mu\nu}F^{A\mu\nu}\right]\Big\} + \cdots \end{aligned} \tag{2.32}$$

where

$$\nabla^\nu M = \partial^\nu M + \mathrm{i}[V^\nu, M] - \mathrm{i}\gamma_5\{A^\nu, M\} \tag{2.33}$$

denotes the covariant derivative of the scalar–pseudoscalar field M. The vector and axial-vector parts of the field strength tensor are

$$\begin{aligned} F^{\mathrm{V}}_{\mu\nu} &= \partial_\mu V_\nu - \partial_\nu V_\mu + \mathrm{i}[V_\mu, V_\nu] + \mathrm{i}[A_\mu, A_\nu]\,, \\ F^{A}_{\mu\nu} &= \partial_\mu \mathrm{A}_\nu - \partial_\nu A_\mu + \mathrm{i}[A_\mu, V_\nu] + \mathrm{i}[V_\mu, A_\nu]\,, \end{aligned} \tag{2.34}$$

and the effective potential V_{eff} is given in (2.19). The resulting coefficient

$$\frac{1}{g_{\mathrm{V}}^2} = \frac{N_{\mathrm{C}}}{24\pi^2}\Gamma\left(0, \frac{m^2}{\Lambda^2}\right) = \frac{f^2(0)}{6m^2} \tag{2.35}$$

exemplifies the role of the derivative expansion: In momentum space it is a Taylor series about $q^2 = 0$. The substitution of the parameterization, (2.20) into (2.32), suggests $f_\pi = f(0)$ in the absence of (axial)vector mesons. This differs from the exact result, (2.23) by $\mathcal{O}(m_\pi^2/\Lambda^2)$.

Let us now look a bit closer at the vector meson fields. As a consequence of spontaneous chiral symmetry breaking the anti-commutator in (2.33) has a piece that is purely proportional to the axial-vector field. Thus a term of the form $A_\mu \partial^\mu \left(M - M^\dagger\right)$ emerges in the action, (2.32). Essentially this is π–A_1 mixing and requires a redefinition of the axial-vector field to account for the physical particle content. Then the (axial)vector meson masses are identified as

$$m_{\mathrm{V}}^2 = \frac{g_{\mathrm{V}}^2}{4G_2} \quad \text{and} \quad m_{\mathrm{A}}^2 = m_{\mathrm{V}}^2 + 6m^2\,. \tag{2.36}$$

The redefinition of the axial-vector field furthermore induces an additional quadratic derivative term for the pion field from the local part of the action. This requires a renormalization to identify the physical pion field. In total one reads off the pion decay constant

$$f_\pi^2 = \frac{f^2(0)}{1 + 4G_1 f^2(0)} \,. \tag{2.37}$$

In terms of the two flavors with $M = m(1 + \mathrm{i}\boldsymbol{\pi}\cdot\boldsymbol{\tau}/f_\pi + \ldots)$ and $V_\mu = (g_V/2)\boldsymbol{\rho}_\mu \cdot \boldsymbol{\tau}$ the commutator in (2.33) generates the vertex

$$\mathcal{L}_{\rho\pi\pi} = g_\mathrm{V}\, \boldsymbol{\rho}_\mu \cdot (\boldsymbol{\pi} \times \partial^\mu \boldsymbol{\pi}) \tag{2.38}$$

that describes the ρ-meson decay into two pions and identifies g_V as the associated coupling constant, $g_{\rho\pi\pi} = g_\mathrm{V}$. Putting (2.35)–(2.38) together relates observable quantities,

$$\frac{m_\mathrm{V}^2}{m_\mathrm{A}^2} = \frac{g_{\rho\pi\pi}^2 f_\pi^2}{m_\mathrm{A}^2 - m_\mathrm{V}^2} \,. \tag{2.39}$$

As a consequence, the particular choice for G_2 that ensures Weinberg's relation between vector and axial-vector masses $m_\mathrm{A} = \sqrt{2} m_\mathrm{V}$ [35] also gives the KSRF relation $m_\mathrm{V} = \sqrt{2} g_{\rho\pi\pi} f_\pi$ for the ρ-meson decay [36, 37]. The interaction Lagrangian, (2.38) results in the ρ-meson width $\Gamma(\boldsymbol{\rho} \to \boldsymbol{\pi}\boldsymbol{\pi}) = \frac{g_{\rho\pi\pi}^2}{6\pi m_\rho^2} |\boldsymbol{q}_\pi|^3$, where $|\boldsymbol{q}_\pi| \approx 360\,\mathrm{MeV}$ is the pion momentum in the ρ-meson rest frame. The empirical value $\Gamma(\boldsymbol{\rho} \to \boldsymbol{\pi}\boldsymbol{\pi}) \approx 150\,\mathrm{MeV}$ [5] gives $g_{\rho\pi\pi} \approx 6$ vs. 5.85 from KSRF.

The special case that only pseudoscalar fields are considered, i.e., $M = mU$ as in (2.20) has been thoroughly investigated in the context of the gradient expansion. For $U \in SU(N_\mathrm{f})$ the leading term must have at least two derivatives. From (2.32) and (2.35) it is obvious that this term is the non-linear σ-model,

$$\mathcal{L}_{\mathrm{nl}\sigma} = -\frac{f_\pi^2}{4}\,\mathrm{tr}\,(\alpha_\mu \alpha^\mu) = \frac{f_\pi^2}{4}\,\mathrm{tr}\left(\partial_\mu U \partial^\mu U^\dagger\right) \,, \tag{2.40}$$

with $\alpha_\mu = U^\dagger \partial_\mu U$. In the two-flavor case we consider the chiral field $U = \exp(\mathrm{i}\boldsymbol{\tau}\cdot\boldsymbol{\pi}/f_\pi)$ as the non-linear representation for the pion fields and expand,

$$\mathcal{L}_{\mathrm{nl}\sigma} = \frac{1}{2}(\partial_\mu \boldsymbol{\pi})\cdot(\partial^\mu \boldsymbol{\pi}) + \frac{1}{6f_\pi^2}\left[(\boldsymbol{\pi}\cdot\partial_\mu\boldsymbol{\pi})^2 - \boldsymbol{\pi}^2(\partial_\mu\boldsymbol{\pi})\cdot(\partial^\mu\boldsymbol{\pi})\right] + \cdots \,, \tag{2.41}$$

which determines the four pion coupling constant to be proportional to $1/f_\pi^2$. From (2.22) we infer that this effective four pion coupling constant scales as $1/N_\mathrm{C}$. The expansion, (2.41), is the principal starting point of chiral perturbation theory [12, 13, 14, 15, 16]. Higher order derivative terms are also known for the pseudoscalar case. The contribution with four derivatives acting on U is [30, 38]

$$\mathcal{L}^{(4)} = \frac{N_\mathrm{C}}{96\pi^2}\,\Gamma\left(1,\frac{m^2}{\Lambda^2}\right)\,\mathrm{tr}\left\{(\alpha_\mu\alpha^\mu)^2-(\partial_\mu\alpha^\mu)^2\right\} + \frac{N_\mathrm{C}}{192\pi^2}\,\Gamma\left(2,\frac{m^2}{\Lambda^2}\right)\,\mathrm{tr}\left\{\alpha_\mu\alpha_\nu\alpha^\mu\alpha^\nu-2\,(\alpha_\mu\alpha^\mu)^2\right\}\,. \tag{2.42}$$

The coefficients are finite in the limit $\Lambda\to\infty$,

$$\lim_{\Lambda\to\infty}\mathcal{L}^{(4)} = \frac{N_\mathrm{C}}{384\pi^2}\,\mathrm{tr}\left\{[\alpha_\mu,\alpha_\nu]^2-4\,(\partial_\mu\alpha^\mu)^2+2\,(\alpha_\mu\alpha^\mu)^2\right\}\,. \tag{2.43}$$

The commutator term will later play a decisive role in the framework of the Skyrme model.

So far we have only considered the modulus of the fermion determinant in Euclidean space, (2.15). But also the phase is non-zero, even in the absence of vector meson fields. It is related to the anomaly as it arises from the fact that the fermion determinant is not invariant under (local) axial transformations. In leading order of the derivative expansion this phase results in the Wess–Zumino–Witten action [39] when rotated back to Minkowski space. The calculation is somewhat involved and we will only sketch it here.

Starting point is the parameterization

$$M = S+\mathrm{i}P = \xi_\mathrm{L}^\dagger\;\Sigma\;\xi_\mathrm{R}, \tag{2.44}$$

and the observation is that the local chiral transformation

$$\mathrm{i}\widetilde{\not{D}} = \mathcal{T}\,\mathrm{i}\not{D}\mathcal{T}^\dagger,\quad \text{with}\quad \mathcal{T} = \xi_\mathrm{L}+\xi_\mathrm{R}-(\xi_\mathrm{L}-\xi_\mathrm{R})\,\gamma_5 \tag{2.45}$$

removes the pseudoscalar fields from the Dirac operator

$$\mathrm{i}\widetilde{\not{D}} = \mathrm{i}(\not{\partial}+\widetilde{\not{V}}+\widetilde{\not{A}}\,\gamma_5)-\Sigma\,, \tag{2.46}$$

in favor of the induced (axial) vector fields $\widetilde{V}_\mu$ and $\widetilde{A}_\mu$. The idea now is to compute the fermion determinant for $\widetilde{D}$ in the proper time scheme

$$\mathcal{A}_\mathrm{F} = \frac{1}{2}\mathrm{Tr}\int_{1/\Lambda^2}^\infty\frac{\mathrm{d}s}{s}\,\mathrm{e}^{-s\widetilde{D}\widetilde{D}} \tag{2.47}$$

and perform the transformation inverse to (2.45) in order to incorporate the chiral field $U(x)=\xi_\mathrm{L}^\dagger(x)\xi_\mathrm{R}(x)$. Under an infinitesimal local chiral transformation the (axial)vector fields vary as

$$\delta\left(\widetilde{V}_\mu+\mathrm{i}\gamma_5\widetilde{A}_\mu\right) = [\widetilde{D}_\mu,\delta\alpha(x)]+\mathrm{i}[\widetilde{D}_\mu,\delta\beta(x)]\gamma_5\,, \tag{2.48}$$

where $\delta\alpha=\Omega^\dagger\delta\Omega$ and $\delta\beta=\omega^\dagger\delta\omega$ are Cartan matrix fields in flavor space (i.e., Ω and ω are unitary). The regularized fermion determinant transforms as

$$\delta\mathcal{A}_\mathrm{F} = 2\mathrm{i}\,\mathrm{Tr}\left[\mathrm{e}^{-\widetilde{D}\widetilde{D}/\Lambda^2}\omega^\dagger\delta\,\omega\,\gamma_5\right]\,. \tag{2.49}$$

This is actually nothing but Fujikawa's formulation of the chiral anomaly [40]. The regularization has been chosen such that only axial transformations contribute. This guarantees that the vector current is conserved. We consider (2.49) as a differential equation in functional space that must be integrated from $\omega(x) = 1$ to $\omega(x) = U(x)$. This is a complicated calculation that involves various aspects of differential geometry. Details are given in [41], see also [42]. Heat kernel methods [43] may be employed to verify that the right hand side of (2.49) is finite as $\Lambda \to \infty$. In the absence of vector mesons and in leading order of the gradient expansion the calculation yields the Wess–Zumino term

$$\Gamma_{\mathrm{WZ}} = -\frac{\mathrm{i}N_{\mathrm{C}}}{240\pi^2}\int_{M_5} \mathrm{d}^5x\, \epsilon^{\mu\nu\rho\sigma\tau}\mathrm{tr}\,(\alpha_\mu\alpha_\nu\alpha_\rho\alpha_\sigma\alpha_\tau)\ . \tag{2.50}$$

The integral is over a five-dimensional manifold whose boundary is Minkowski space, $\partial M_5 = M_4$. This fifth dimension reflects the auxiliary variable which is introduced to formally integrate the anomaly equation (2.49) in functional space [44]: The additional variable $\tau \in \mathbb{R}$ generalizes $U(x) \to U_\tau(x) = [U(x)]^\tau$. Then also the induced (axial)vector fields $\widetilde{V}_\mu$ and $\widetilde{A}_\mu$ that are contained in $\widetilde{D}$ parametrically depend on τ. The Wess–Zumino term, (2.50) finally arises by integrating the anomaly equation (2.49) from $\tau = 0$ to $\tau = 1$.

Obviously the Wess–Zumino term is non-local. In practice its contribution to an observable in four-dimensional space is computed with the help of Stoke's theorem. Due to the anti-symmetric structure this term vanishes in the two-flavor reduction. However, in the three-flavor version it describes processes like kaon scattering into three pions. Also, when gauged with electromagnetic fields, it properly describes the anomalous π^0 decay into two photons [39], see Appendix C where we repeat that calculation. In the discussion of the soliton picture (Chap. 6) for baryons we will recognize that the Wess–Zumino term has very decisive consequences for the quantization of the soliton: The baryon number one soliton is forced to possess half-integer spin when N_{C} is odd.

2.5 PCAC

In (2.23) we have identified the residuum of the propagator for the pseudoscalar fields ϕ_a as the (square of the) pion decay constant, f_π. We have then normalized the argument of the chiral field in the non-linear σ model accordingly, cf. (2.40). Actually f_π is not a pure strong interaction quantity. Hence that identification appears a bit premature and we will now argue in its favor. The pion decay constant is measured from the pion decay into muon and muon–neutrino. This is an electroweak process and the corresponding (low-energy) interaction is prescribed as a current–current Lagrangian,

$$\mathcal{L}_{\pi\to\mu\nu_\mu} = cA_\mu^{(\mathrm{hadr})}A^{(\mathrm{lept}),\mu} \tag{2.51}$$

where the coupling constant, c, is found from the Weinberg–Salam model for the electroweak interactions. Furthermore $A_\mu^{(\mathrm{hadr})}$ and $A_\mu^{(\mathrm{lept})}$ are the axial current operators for the hadrons (i.e., $\boldsymbol{\pi}$) and leptons (μ, ν_μ), respectively. For simplicity the sum over flavor indices is not made explicit in (2.51). It is now obvious that we have to compute the hadronic matrix element $\langle 0|A_\mu|\boldsymbol{\pi}(p)\rangle$ to investigate the decay of a pion with momentum p. We have dropped the superscript because it is unambiguous that we are concerned with hadronic axial current from now on. Also, eventual vector interactions are not shown in (2.51), because the analog pion matrix element vanishes by parity.

The pion decay constant is simply defined as the pion matrix of the axial current

$$\langle 0|A_\mu^a(x)|\pi^b(q)\rangle = \mathrm{i} f_\pi \delta_{ab}\, q_\mu\, \mathrm{e}^{-\mathrm{i}qx}\,. \tag{2.52}$$

In principle, Lorentz covariance allows f_π to depend on q^2, but the pion is on-shell so $q^2 = m_\pi^2$ is fixed. Of course, it is possible to compute this matrix element in the above-discussed model for the quark flavor dynamics. As sketched at the end of Appendix B this indeed yields (2.23). It is more illuminating to consider this matrix element in the local effective meson theory. In this model the axial current is obtained as the Noether current for the chiral transformation $L = R^\dagger$ in (2.30). The resulting infinitesimal variation of the chiral field is proportional to the anti-commutator $\{U, \boldsymbol{\tau}\}$. To compute the matrix element, (2.52) we only need the part of the axial current that is linear in the pion field. From the non-linear σ model, (2.40) it is straightforwardly found to be

$$\boldsymbol{A}_\mu^{(\mathrm{nl}\sigma)}(x) = \mathrm{i}\frac{f_\pi^2}{2}\mathrm{tr}\left[\frac{\boldsymbol{\tau}}{2}\left(\alpha_\mu + U\alpha_\mu U^\dagger\right)\right] = -f_\pi \partial_\mu \boldsymbol{\pi}(x) + \mathcal{O}\left(\boldsymbol{\pi}^2\right)\,. \tag{2.53}$$

This shows that the previous identification of the pion decay constant is indeed equivalent to its actual definition, (2.52).

We may differentiate (2.52) to find

$$\langle 0|\partial^\mu A_\mu^a(x)|\pi^b(q)\rangle = f_\pi m_\pi^2 \delta_{ab}\, \mathrm{e}^{-\mathrm{i}qx}\,. \tag{2.54}$$

This clearly demonstrates the role of the pion as a would-be Goldstone boson: if the axial current were conserved, the pion would indeed be massless. We reexpress the right hand side of (2.54) as the matrix element $f_\pi m_\pi^2 \langle 0|\hat{\pi}^a(x)|\pi^b(q)\rangle$ where $\hat{\pi}^a(x)$ is the pion field operator. The resulting generalization of (2.54) into an operator identity

$$\partial^\mu \boldsymbol{A}_\mu(x) = f_\pi m_\pi^2 \hat{\boldsymbol{\pi}}(x) \tag{2.55}$$

is called the *partially conserved axial vector current* (PCAC) hypothesis. PCAC relates a current whose matrix elements are measured in the weak interaction to an operator in strong interactions and one is tempted to assume that numerous predictions follow from it. However, in practice more assumptions must often be made to arrive at definite results. Direct relations from

PCAC concern matrix elements at zero momentum transfer and smoothness of the form factors must be taken for granted to extrapolate to the physically relevant regime.

In soliton physics PCAC is sometimes interpreted in the opposite way. While the axial current can be computed as Noether current, the identification of the interpolating pion field operator is not as straightforward because in these models the asymptotic pion field is a superposition of a classical field and fluctuations about it. Then (2.55) is unprejudicedly utilized as a definition of the pion field operator in terms of $\boldsymbol{A}_\mu$. As stated PCAC is a hypothesis, and we will discuss an example in Chap. 9 where that definition (or at least its generalization to the three-flavor case) appears to be inconsistent.

2.6 Relation to Instanton Effects

Often instanton effects are utilized to motivate or even to form the basis for a derivation of the model Lagrangian, (2.8), cf. [45, 46]. This certainly is an overemphasis of such effects. However, instanton effects can be argued to induce dynamical chiral symmetry breaking in a way similar to the quartic quark interaction in (2.8).

To illuminate that point let us briefly recall the nature of instantons and their relevance to QCD. Instantons are localized field configurations that minimize the Euclidean Yang–Mills action

$$S_{\mathrm{E}}[A] = \frac{1}{2g^2} \int \mathrm{d}^4 x_{\mathrm{E}}\, \mathrm{tr}\,(F_{\mu\nu} F_{\mu\nu}) \tag{2.56}$$

where $F_{\mu\nu} = \partial_\mu A_\nu - \partial_\nu A_\mu + \mathrm{i}\,[A_\mu, A_\nu]$ is the field strength tensor. The gauge field, A_μ itself is matrix valued in color space. In the standard realization instantons are embedded in the $SU(2)$ subgroup whose generators are proportional to the Pauli matrices $\boldsymbol{\tau}$,

$$A_\mu^{(\mathrm{inst})} = \frac{x^2}{x^2 + \rho^2} V(x)\, \partial_\mu V^\dagger(x) \quad \text{with} \quad V(x) = \frac{1}{\rho}\,(x_4 + \mathrm{i}\boldsymbol{\tau} \cdot \boldsymbol{x})\ . \tag{2.57}$$

Here x_4 is the Euclidean time, $x^2 = x_4^2 + \boldsymbol{x}^2$ and ρ is a constant scale parameter that measures the extension (size) of the instanton. Rescaling immediately shows that the action, (2.56) does not depend on ρ. Anti-instanton configurations are simply constructed by substituting $V(x) \to V^\dagger(x)$. Vacuum configurations are characterized by $F_{\mu\nu} \equiv 0$ for which it suffices that $A_\mu^{(\mathrm{vac})} = W(x)\partial_\mu W^\dagger(x)$ is pure gauge. Any of these vacuum configurations is characterized by a topological charge n. The instanton configuration, (2.57) mediates between vacua with charges n at $x_4 = -\infty$ and $n+1$ at $x_4 = \infty$. Even more, the semiclassical analysis reveals that the transition amplitude between such two vacua is exactly $\mathrm{e}^{-S_{\mathrm{E}}[A^{(\mathrm{inst})}]} = \mathrm{e}^{-8\pi^2/g^2}$ [1].

In the next step fermions are coupled to the instanton. Consider the eigenvalues, λ_n of the Dirac operator with the instanton background and label their spectral density by $\nu(\lambda_n)$. Then the fermion determinant in the instanton background can formally[4] be written as (in Euclidean space)

$$\log \mathrm{Det}\left(\mathrm{i}\partial\!\!\!/ + A\!\!\!/^{(\mathrm{inst})} + \mathrm{i}m\right) = \frac{1}{2}\int_{-\infty}^{\infty} \mathrm{d}\lambda\, \nu(\lambda) \log\left(\lambda^2 + m^2\right) . \tag{2.58}$$

As in (B.15) the quark condensate $\langle \bar{q}(x)q(x)\rangle$ is obtained from the derivative of the left hand side with respect to the quark mass, m. Utilizing the δ-function representation $\delta(x) = \lim_{\epsilon\to 0^+} \pi\epsilon/(x^2+\epsilon^2)$ yields the famous Casher–Banks relation [47]

$$\langle \bar{q}(x)q(x)\rangle \xrightarrow[m\,\to\,0]{} -\pi\nu(0) \tag{2.59}$$

that relates the quark condensate in the chiral limit to the zero-mode density. The crucial observation is that, as a result of the Atiah–Singer index theorem, an instanton background generates a zero-mode fermion that is right-handed in the limit $m \to 0$. Choosing as above to embed the instanton in the $SU(2)$ color subgroup, the zero-mode spinor reads

$$q_{\mathrm{I}}(x) = \frac{\rho}{\pi\sqrt{2x^2}\,(x^2+\rho^2)^{3/2}}\,\boldsymbol{\gamma}\cdot\boldsymbol{x}\,\Omega\,. \tag{2.60}$$

In the chiral representation of the Dirac matrices Ω is a 4×2 matrix with the upper 2×2 block being zero and the lower one equal to $\mathrm{i}\tau_2$. The right index of Ω denotes color and eventually couples to the instanton, (2.57). An anti-instanton also generates a zero-mode fermion as in (2.60), however, the 2×2 blocks in Ω exchanged. Thus the zero-mode of an anti-instanton is left-handed.

To set up a model (sometimes called the instanton liquid model [48]), assume that the vacuum is filled by an ensemble of (well-separated) instantons and anti-instantons. Such an ensemble produces $\nu(0) \neq 0$ and thus a non-zero quark condensate. It is beyond the scope of this monograph to repeat the actual model calculations,[5] however, the lesson to be learned is that instanton effects in QCD indeed may cause chiral symmetry to be spontaneously broken.

When the fermion propagator S in the single instanton background

$$S(x,y) \;\approx\; S_0(x,y) + \frac{q_{\mathrm{I}}(x)q_{\mathrm{I}}^{\dagger}(y)}{-\mathrm{i}m} \tag{2.61}$$

is approximated by the sum of the free propagator S_0 and the zero-mode component, an action functional that reproduces this fermion propagator can be constructed. This functional contains a non-local interaction of the fermion fields with the spinor of the zero-mode. Essentially $2N_{\mathrm{f}}$ fermions couple to the single instanton. In the instanton liquid model the above approximation

[4] Note that we treat ultraviolet divergent objects as if they were finite.
[5] See, e.g., the review articles [46, 48, 49, 50] and references therein.

scheme is generalized to multi-instanton and anti-instanton configurations in the first step. Subsequently their positions and orientations are integrated over. This induces quark correlations and at the same time defines an effective model for the quark flavor dynamics. For $N_\mathrm{f} = 2$ and in leading order $1/N_\mathrm{C}$ the flavor structure of this effective model relates to the G_1 term in (2.8) [46]. Even though instantons couple only to right-handed fermions and anti-instantons only to left-handed ones, it is not surprising that a chiral invariant quark interaction emerges because instanton and anti-instanton ensembles are independently averaged and in this process neither is favored over the other. Since the (anti)instantons interact with $2N_\mathrm{f}$ fermions, it is more or less obvious that the spin flavor structure of (2.8) results. However, there is one small piece of information that can be gained from the instanton model: Since in that model the interaction is mediated by (the Fourier transformation of) the instanton, the inverse of the average instanton size ($\bar{\rho}$) provides a natural energy cut-off for this four-fermion interaction. Early studies of phenomenological applications of the instanton liquid model yielded $\bar{\rho} \approx \frac{1}{3}\,\mathrm{fm}$ [51, 52] for this a priori free parameter. This result was reproduced within a variational approach to stabilize the (anti)instanton ensemble [53] utilizing the classical instanton anti-instanton interaction. This leads to an energy cut-off in the order of 600 MeV, a value consistent with the NJL model estimate in Sect. 2.3. Rather than from QCD, the instanton liquid estimate of the energy cut-off arises from fits to empirical data. Hence the agreement with NJL model result is not surprising.

Nevertheless there are some conceptual differences between the NJL model action and those instanton-induced interactions. We will briefly consider them for the case $N_\mathrm{f} = 2$. We merely display the result and in doing so it is useful to introduce *non-local* fermion fields [54]

$$\psi(x) = \int \mathrm{d}^4x \int \frac{\mathrm{d}^4k}{(2\pi)^4}\, \mathrm{e}^{\mathrm{i}k(x-y)} r(k)\, q(y)\,, \tag{2.62}$$

where $r(k)$ is extracted from the Fourier transformation of the fermion zero-mode in the instanton background. The non-local transformation, (2.62) suppresses the high-frequency modes and thereby introduces the above-mentioned cut-off. In these non-local fields the instanton-induced (effective) potential seems actually local [46, 50],

$$V_\mathrm{inst.ind.} = -g_\mathrm{I}^2 \left[\left(\bar{\psi}\psi\right)^2 + \left(\bar{\psi}\mathrm{i}\gamma_5 \boldsymbol{\tau}\psi\right)^2 - \left(\bar{\psi}\boldsymbol{\tau}\psi\right)^2 - \left(\bar{\psi}\mathrm{i}\gamma_5\psi\right)^2 \right], \tag{2.63}$$

where the interaction strength, g_I^2, is proportional to the inverse (anti)instanton density in the liquid. While $V_\mathrm{inst.ind.}$ is invariant under $SU_\mathrm{L}(2) \times SU_\mathrm{R}(2)$ chiral transformations, it varies under $U_\mathrm{A}(1)$. In the NJL model interaction, (2.8) this is still a (classical) symmetry and all spin-flavor structures in the G_1 term are attractive (as suggested by the gluon exchange approach [20]), while in (2.63) $\left(\bar{\psi}\boldsymbol{\tau}\psi\right)$ and $\left(\bar{\psi}\mathrm{i}\gamma_5\psi\right)$ are repulsive. Thus the instanton liquid model

would in particular suggest that isovector partners of the scalar isoscalar meson were not bound. This seems at variance with recent empirical studies that suggest the existence of even a nonet of scalar mesons [55].

There is some evidence from lattice measurements for the existence of an (anti)instanton ensemble in the vacuum [56, 57, 58]. An arbitrary gluon configuration on the lattice is dominated by the quantum noise of high-frequency modes. They can be eliminated in a smoothing procedure, so-called *cooling*, which leaves over isolated structures that may indeed be interpreted as an (anti)instanton ensemble. From the cooled configuration average instanton sizes of the order of 0.3 fm are estimated in agreement (and partial support) with the above-mentioned studies. However, it should be mentioned that the cooling procedure is not really converging because after many arbitrary iterations the instantons and anti-instantons will annihilate each other more or less completely. For example, the results displayed in Table 1 of [57] suggest that the number of instantons does not saturate as the number of cooling steps increases. Stated otherwise, the extracted (anti)instanton properties depend on the number of conducted cooling steps. As a way out, it has been proposed to extrapolate this functional behavior to zero cooling steps. This procedure does not seem very conclusive as Table 1 in [58] indicates.

2.7 Final Note on Chiral Quark Models

As a brief summary on this chapter about the quark flavor dynamics it seems fair to say that there many ways to motivate an NJL-type interaction as in (2.8), even from QCD. Most of the considerations contain approximations whose validity is difficult to judge. Probably any bona fide argumentation that respects chiral symmetry and stops one step before completely omitting any interaction will result in such a model. Above we have argued that the current–current approximation and the instanton liquid model do so, the field strength (re)formulation [59] of QCD is yet another example.

The NJL-type models focus on chiral symmetry and a dynamical description of its spontaneous breaking. However, these models lack the important feature of color confinement. This should not be forgotten even though it is not a serious drawback for most applications because they are not affected by unphysical quark anti-quark thresholds. This is particularly the case for static solitons that we will exhaustively discuss in the following chapter.

References

1. T. P. Cheng and L. F. Li, *Gauge Theory of Elementary Particles*, Chapters 5 and 16. Clarendon Press, Oxford, 1988. 5, 21
2. S. L. Adler, *Phys. Rev.* **177** (1969) 2426. 6
3. J. S. Bell and R. Jackiw, *Nuovo Cim.* **A60** (1969) 47. 6

4. K. Fujikawa, *Phys. Rev.* **D21** (1980) 2848. 6
5. S. Eidelman et al. [PDG], *Phys. Lett.* **B592** (2004) 1. 7, 14, 17
6. A. H. Fariborz, ed., *Scalar Mesons: An Interesting Puzzle for QCD. Proceedings, Workshop, Utica, USA, May 16–18, 2003.* American Institute of Physics, New York, 2003. 7
7. G. 't Hooft, *Phys. Rev. Lett.* **37** (1976) 8. 8
8. H. Reinhardt and R. Alkofer, *Phys. Lett.* **B207** (1988) 482. 8
9. R. Alkofer, M. A. Nowak, J. J. M. Verbaarschot, and I. Zahed, *Phys. Lett.* **B233** (1989) 205. 8
10. Y. Nambu and G. Jona-Lasinio, *Phys. Rev.* **122** (1961) 345. 8
11. Y. Nambu and G. Jona-Lasinio, *Phys. Rev.* **124** (1961) 264. 8
12. S. Weinberg, *Physica* **A96** (1979) 327. 8, 17
13. J. Gasser and H. Leutwyler, *Phys. Rep.* **87** (1982) 77. 8, 17
14. J. Gasser and H. Leutwyler, *Ann. Phys.* **158** (1984) 142. 8, 17
15. V. Bernard, N. Kaiser, and U. G. Meißner, *Int. J. Mod. Phys.* **E4** (1995) 193. 8, 17
16. V. Bernard and U. G. Meißner, `hep-ph/0611231`. 8, 17
17. U. Vogl and W. Weise, *Prog. Part. Nucl. Phys.* **27** (1991) 195. 8, 14
18. S. P. Klevansky, *Rev. Mod. Phys.* **64** (1992) 649. 8, 14
19. D. Ebert, H. Reinhardt, and M. K. Volkov, *Prog. Part. Nucl. Phys.* **33** (1994) 1. 8, 9, 14
20. R. Alkofer and H. Reinhardt: *Chiral Quark Dynamics*, Lect. Notes Phys. **M33**, Chap. 2.3. Springer, Heidelberg (1995). 9, 13, 23
21. P. Kopietz: *Bosonization of Interacting Fermions in Arbitrary Dimensions*, Lect. Notes Phys. **M48**. Springer, Heidelberg (1997). 9
22. J. S. Schwinger, *Phys. Rev.* **82** (1951) 664. 11
23. F. Doering, C. Schueren, T. Watabe, K. Goeke, and E. Ruiz Arriola, *Nucl. Phys.* **A603** (1996) 415. 11
24. H. Weigel, E. Ruiz Arriola, and L. P. Gamberg, *Nucl. Phys.* **B560** 1999) 383. 11
25. T. Meissner, E. Ruiz Arriola, and K. Goeke, *Z. Phys.* **A336** (1990) 91. 11
26. A. H. Blin, B. Hiller, and M. Schaden, *Z. Phys.* **A331** (1988) 75. 11
27. R. Alkofer and H. Reinhardt, `hep-ph/921223`. 11
28. R. Alkofer, H. Reinhardt, and H. Weigel, *Phys. Rep.* **265** (1996) 139. 13
29. H. Weigel, R. Alkofer, and H. Reinhardt, *Nucl. Phys.* **A576** (1994) 477. 13, 14
30. D. Ebert and H. Reinhardt, *Nucl. Phys.* **B271** (1986) 188. 14, 16, 17
31. S. Klimt, M. Lutz, U. Vogl, and W. Weise, *Nucl. Phys.* **A516** (1990) 429. 14
32. R. D. Ball, *Phys. Rep.* **182** (1989) 1. 16
33. I. J. R. Aitchison and C. M. Fraser, *Phys. Lett.* **B146** (1984) 63. 16
34. I. J. R. Aitchison and C. M. Fraser, *Phys. Rev.* **D31** (1985) 2605. 16
35. S. Weinberg, *Phys. Rev. Lett.* **18** (1967) 507. 17
36. K. Kawarabayashi and M. Suzuki, *Phys. Rev. Lett.* **16** (1966) 255. 17
37. Riazuddin and Fayyazuddin, *Phys. Rev.* **147** (1966) 1071. 17
38. M. Praszałowicz, *Acta Phys. Polon.* **B22** (1991) 525. 17
39. E. Witten, *Nucl. Phys.* **B223** (1983) 422, 433. 18, 19
40. K. Fujikawa, *Phys. Rev.* **D21** (1980) 2848. 19
41. J. L. Petersen, *Acta Phys. Polon.* **B16** (1985) 271. 19
42. M. Wakamatsu, *Phys. Rev.* **D54** (1996) 6459. 19
43. I. G. Avramidi: *Heat Kernel and Quantum Gravity*, Lect. Notes Phys. **M64**. Springer, Heidelberg (2000). 19
44. J. F. Donoghue, E. Golowich, and B. R. Holstein, *Dynamics of the Standard Model*, Chapter 7. Cambridge Monographs on Particle Physics, 1996. 19

45. D. Diakonov and V. Y. Petrov, *Nucl. Phys.* **B272** (1986) 457. 21
46. D. Diakonov, *Prog. Part. Nucl. Phys.* **51** (2003) 173. 21, 22, 23
47. T. Banks and A. Casher, *Nucl. Phys.* **B169** (1980) 103. 22
48. T. Schäfer and E. V. Shuryak, *Rev. Mod. Phys.* **70** (1998) 323. 22
49. M. A. Nowak, *Acta Phys. Polon.* **B22** (1991) 697. 22
50. D. Diakonov, `hep-ph/9602375`. 22, 23
51. E. V. Shuryak, *Nucl. Phys.* **B203** (1982) 93. 23
52. E. V. Shuryak, *Nucl. Phys.* **B203** (1982) 116. 23
53. D. Diakonov and V. Y. Petrov, *Nucl. Phys.* **B245** (1984) 259. 23
54. G. Ripka, *Quarks Bound to Chiral Fields.* Clarendon Press, Oxford, 1997. 23
55. D. Black, A. H. Fariborz, F. Sannino, and J. Schechter, *Phys. Rev.* **D59** (1999) 074026. 24
56. M. C. Chu, J. M. Grandy, S. Huang, and J. W. Negele, *Phys. Rev. Lett.* **70** (1993) 255. 24
57. M. C. Chu, J. M. Grandy, S. Huang, and J. W. Negele, *Phys. Rev.* **D49** (1994) 6039. 24
58. J. W. Negele, *Nucl. Phys. Proc. Suppl.* **73** (1999) 92. 24
59. M. Schaden, H. Reinhardt, P. A. Amundsen, and M. J. Lavelle, *Nucl. Phys.* **B339** (1990) 595. 24

3

Self-consistent Soliton

This chapter serves to describe how solitons emerge as a self-consistent solution to the (static) field equations in the (regularized) NJL model that was introduced in Chap. 2. Here we will mainly sketch the idea, briefly discuss established soliton solutions and address some unresolved questions. For more details and references on the self-consistent soliton solutions in NJL-type models, we refer the interested reader to the review articles [1, 2].

3.1 Static Energy Functional

As formulated in the introduction, we apprehend solitons as classical solutions of the equations of motion in a non-linear field theory [3]. The energy densities of soliton field configurations are localized in space and their total energy is finite (discussed in Chap. 1). In particular, this implies that soliton configurations are at least equivalent if not identical to the vacuum configuration at spatial infinity. We have already encountered such objects during the discussion of instanton effects in Sect. 2.6. Instanton solutions emerged in Euclidean space where the time and space coordinates are not really distinct so that the instanton may actually be considered as a special type of static field configuration.[1] Being static is actually a major feature of many soliton configurations. This is a mere matter of feasibility: time-dependent solutions with localized energy densities are simply not known for most field theories. For static configurations, it is also quite easy to derive the energy functional because it is proportional to the action of the considered field configuration. In the first step, we will therefore formally construct the energy functional from the unregularized action, (2.11), and then apply the proper time regularization scheme, (2.17), to the ultraviolet divergent vacuum contribution.

[1] The four-dimensional Euclidean space may be embedded in a five-dimensional Minkowski space with an additional time coordinate and the four Euclidean dimensions as spatial coordinates.

H. Weigel: *Self-consistent Soliton*, Lect. Notes Phys. **743**, 27–42 (2008)
DOI 10.1007/978-3-540-75436-7_3

We refer to [2, 4] for a corresponding discussion in the Pauli–Villars scheme, see also Sect. 7.7. Temporal components of vector fields complicate the Wick rotation, (2.15). For the time being, we therefore assume $V_0 = \mathrm{i}V_4 = 0$ as well as $A_0 = \mathrm{i}A_4 = 0$ and relegate the corresponding discussion to Sect. 3.3.

After bosonization, (2.14), we have to compute $\mathrm{Tr}\log(\mathrm{i}\partial\!\!\!/ - \Phi\cdot\Lambda) = \log\mathrm{Det}(\mathrm{i}\partial\!\!\!/ - \Phi\cdot\Lambda)$ in the presence of non-perturbative static meson field configurations $\Phi(x) = \Phi(\boldsymbol{x})$. This determinant is given in terms of the eigenvalues of $\mathrm{i}\partial\!\!\!/ - \Phi\cdot\Lambda$. Since $\det(\mathrm{i}\beta) = 1$, we may equally well consider

$$\beta\,(\mathrm{i}\partial\!\!\!/ - \Phi(\boldsymbol{x})\cdot\Lambda) = \mathrm{i}\partial_t - h(\Phi), \tag{3.1}$$

which introduces the single-particle Hamilton operator $h(\Phi)$ that (parametrically) depends on the shape of the background field, Φ. For static fields, we have $[\mathrm{i}\partial_t, h(\Phi)] = 0$ and the eigenvalues of (3.1) separate into the eigenvalues of $\mathrm{i}\partial_t$ and h. The fermion fields assume anti–periodic boundary conditions on the (arbitrarily large) time interval T. Therefore, the eigenvalues of $\mathrm{i}\partial_t$ are given by the Matsubara frequencies $\Omega_n = (2n+1)\pi/T$ with $n = 0, \pm1, \pm2, \ldots$. In the next step, the single-particle Hamiltian defines the eigenvalue problem[2]

$$h(\Phi)\Psi_\nu = \epsilon_\nu\Psi_\nu\,. \tag{3.2}$$

We achieve discretization of the eigenvalues ϵ_ν by diagonalizing h in an arbitrarily large volume. It also implies that the eigenstates of h are normalized to unity, $\langle\mu|\nu\rangle = \delta_{\mu\nu}$. From these eigenvalues, we compute the unregularized fermion determinant as the product [5]

$$\begin{aligned}\mathrm{Det}\,(\mathrm{i}\partial\!\!\!/ - \Phi(\boldsymbol{r})\cdot\Lambda) &= \prod_{\nu,n}\left(\frac{2n+1}{T}\pi - \epsilon_\nu\right)\\ &= \mathcal{C}(T)\prod_{\nu,n\geq0}\left(1 - \left[\frac{\epsilon_\nu T}{(2n+1)\pi}\right]^2\right).\end{aligned} \tag{3.3}$$

The whole information about the static meson fields is contained in the eigenvalues ϵ_ν. Therefore, the constant

$$\mathcal{C}(T) = \prod_{n\geq0}\left(-\left[\frac{2n+1}{T}\pi\right]^2\right) \tag{3.4}$$

does not depend on the dynamical properties of the system and may hence be absorbed into the normalization of the determinant. Using standard techniques from statistical mechanics and infinite product representations of trigonometrical functions,[3] the functional determinant, (3.3), may be rewritten as [1, 7]

[2] These eigenvalues and eigenfunctions parametrically depend on the background field: $\epsilon_\nu = \epsilon_\nu[\Phi]$ and $\Psi_\nu = \Psi_\nu[\Phi]$.

[3] In particular, $\cos(x) = \prod_{n\geq0}\left(1 - [2x/(2n+1)\pi]^2\right)$ [6].

$$\mathrm{Det}\,(\mathrm{i}\partial\!\!\!/ - \Phi(\boldsymbol{r})\cdot\Lambda) = \widetilde{\mathcal{C}}(T)\exp\left[\mathrm{i}\mathcal{A}_0\right]\sum_{\{\eta_\nu\}}\exp\left[\mathrm{i}\mathcal{A}_V^{\{\eta_\nu\}}\right], \tag{3.5}$$

which provides a natural decomposition into vacuum

$$\mathcal{A}_0 = T\,\frac{N_\mathrm{C}}{2}\sum_\nu |\epsilon_\nu| \tag{3.6}$$

and valence (anti-)quark

$$\mathcal{A}_\mathrm{V}^{\{\eta_\nu\}} = -TN_C\sum_\nu \eta_\nu|\epsilon_\nu| =: -TE_V^{\{\eta_\nu\}} \tag{3.7}$$

contributions. In (3.5), the sum goes over all possible sets of fermion occupation numbers $\eta_\nu = 0, 1$. Since there is no explicit color interaction, the only effect of color is the multiplicative factor N_C which we have made explicit in (3.6) and (3.7). The above assignment of $\mathcal{A}_0$ as the vacuum contribution is based on the definition of the latter as the sole remnant in limit of large Euclidean times when $T\to\infty$. Equation (3.7) should be considered as a definition of the valence energy, $E_\mathrm{V}^{\{\eta_\nu\}}$, for a prescribed set of occupation numbers. These occupation numbers do not have an immanent physical meaning. However, it is obvious that different sets $\{\eta_\nu\}$ in general correspond to different baryon numbers, B, because each occupation of a fermion level adds $1/N_\mathrm{C}$ to B. Stated otherwise, the sum in (3.5) involves configurations with different baryon numbers, and we have to identify contributions that stem from a prescribed value B. To this end, we consider the baryon number current

$$\begin{aligned} j^\mu(x) &= \frac{1}{N_\mathrm{C}}\,\langle\bar{q}(x)\gamma^\mu q(x)\rangle \\ &= \frac{1}{N_\mathrm{C}}\,\frac{\mathrm{i}\delta}{\delta v_\mu(x)}\log\,\mathrm{Det}\,(\mathrm{i}\partial\!\!\!/ - \Phi(\boldsymbol{r})\cdot\Lambda - v_\mu\gamma^\mu)\,\Big|_{v_\mu(x)=0}\,, \end{aligned} \tag{3.8}$$

as a single quark carries baryon number $1/N_\mathrm{C}$. We may regard v_μ as a perturbation in the eigenvalue problem

$$\frac{\delta\epsilon_\nu}{\delta v_\mu(x)}\Big|_{v^\mu(x)=0} = \psi_\nu^\dagger(x)\beta\gamma^\mu\psi_\nu(x) = \left(\psi_\nu^\dagger\psi_\nu(x), \psi_\nu(x)\boldsymbol{\alpha}\,\psi_\nu(x)\right)^\mu\,, \tag{3.9}$$

where $\psi_\nu(x)$ and ϵ_ν are the eigenfunctions and eigenvalues of h. This allows us to apply the functional derivative onto (3.5). Taking furthermore into account that the eigenfunctions are normalized to unity, we immediately find

$$B(\{\eta_\nu\}) = \int \mathrm{d}^3r\, j_0(x) = \sum_\nu\left(\eta_\nu - \frac{1}{2}\right)\mathrm{sign}(\epsilon_\nu) \tag{3.10}$$

for the baryon number associated with a given set of occupation numbers. This relation between baryon number and occupation numbers is obviously not

bijective because a given baryon number may result from various sets $\{\eta_\nu\}$. Once the energy eigenvalues ϵ_ν are known, there is a well-defined set $\{\eta_\nu\}$ with the minimal $E_{\rm V}^{\{\eta_\nu\}}$. This particular set serves to construct the soliton in a sector with fixed baryon number.

So far, the derivation of the energy functional has been formal as the vacuum contribution, (3.6), diverges. Also, the sum in (3.10) is only conditionally convergent. To actually compute $\mathcal{A}_0$, we have to apply the limit $T \to \infty$ and employ the proper time regularization which is an inseparable part of the model definition. Fortunately, the former is straightforward as the Matsubara frequencies become continuous and we may replace

$$\sum_n f\left(\Omega_n\right) \quad \longrightarrow \quad T \int \frac{\mathrm{d}z}{2\pi} f(z)\,. \tag{3.11}$$

The functional trace in (2.17) for static meson fields then becomes

$$\mathcal{A}_R = -TE_0 = -T\frac{N_{\rm C}}{2}\sum_\nu \int_{-\infty}^{\infty}\frac{\mathrm{d}z}{2\pi}\int_{1/\Lambda^2}^{\infty}\frac{\mathrm{d}s}{s}\,\exp\left\{-s\left(z^2+(\epsilon_\nu)^2\right)\right\}\,, \tag{3.12}$$

which at the same time defines the regularized vacuum energy, E_0. The z-integral is Gaußian, and the proper time integral can be written as an incomplete Γ–function with half-integer index to be related to a complementary error function, cf. Appendix B. Then the vacuum energy becomes

$$\begin{aligned} E_0 &= \frac{N_{\rm C}}{4\sqrt{\pi}}\sum_\nu |\epsilon_\nu| \Gamma\left(-\frac{1}{2},\left(\frac{\epsilon_\nu}{\Lambda}\right)^2\right) \\ &= -\frac{N_{\rm C}}{2}\sum_\nu \left\{|\epsilon_\nu|\mathrm{erfc}\left(\left|\frac{\epsilon_\nu}{\Lambda}\right|\right) - \frac{\Lambda}{\sqrt{\pi}}\,\exp\left(-\left(\frac{\epsilon_\nu}{\Lambda}\right)^2\right)\right\}\,. \end{aligned} \tag{3.13}$$

Since the eigenvalues ϵ_ν depend on the shape of the background fields Φ, the total energy (with $\{\eta_\nu\}$ determined as explained above)

$$E_{\rm tot}[\Phi] = N_{\rm C}\sum_\nu \eta_\nu|\epsilon_\nu| + E_0[\Phi] - E_0[\Phi_0] + E_{\rm m}[\Phi] \tag{3.14}$$

is a functional of Φ, i.e., a meson theory. The contribution from the local part on the action is denoted by $E_{\rm m}$ and is straightforwardly obtained by substituting the background field into the integral on the right hand side of (2.14). The vacuum energy of the trivial configuration $\Phi_0 = \mathrm{diag}\left(m_1, m_2, \ldots, m_{N_f}\right)$ is subtracted in (3.14) to set the scale. Eventually, a constant is added such that $E_{\rm m}[\Phi_0] = 0$.

As already indicated, the vacuum contribution to the baryon number in (3.10)

$$B_0 = -\frac{1}{2}\sum_\nu \mathrm{sign}(\epsilon_\nu) \tag{3.15}$$

is only conditionally convergent. The positive and negative energy spectra must be summed symmetrically to obtain a meaningful result.[4] Any kind of (proper time) regularization would multiply each summand in (3.15) with a factor less than unity and thus render an integer baryon number highly unlikely. The analysis in Euclidean space reveals that B_0 originates from the imaginary part of the bosonized action. These are strong arguments in favor of not to regularize the imaginary part of the Euclidean action. The spectrum of $h(\Phi_0)$ is symmetric and thus $B_0[\Phi_0] = 0$. The main result from (3.15) then is that for a background field whose interaction with the quarks induces a spectrum in which an energy eigenvalue has changed its sign from plus to minus, the vacuum carries non-zero baryon number!

To preserve the baryon number when an energy eigenvalue changes sign, the occupation numbers η_ν must be modified along that transition. It is straightforward to verify that the total energy, (3.14), is continuous and smooth when the baryon number is held fixed: Consider the case with baryon number $B = 1$ and denote by ϵ_V the energy eigenvalue of the most strongly bound quark. To ensure $B = 1$, we have to set $\eta_\mathrm{V} = (1 + \mathrm{sign}(\epsilon_\mathrm{V}))/2$ as the occupation number of the most strongly bound quark; all other occupation numbers must be zero. Then we find that

$$E_\mathrm{tot}^{(B=1)}[\Phi] = \frac{N_\mathrm{C}}{2}\,[1 + \mathrm{sign}(\epsilon_\mathrm{V})]\epsilon_\mathrm{V} + E_0[\Phi] - E_0[\Phi_0] + E_\mathrm{m}[\Phi] \tag{3.16}$$

does not develop a cusp when $\epsilon_\mathrm{V} \to 0$.

Obviously the soliton energy is $\mathcal{O}\,(N_\mathrm{C})$ because the fermion action, (2.14), contains the sum over color degrees of freedom.

The goal is to minimize the functional, (3.16). Early attempts employed variational *ansätze* as, e.g., $\Theta(r) = \pi\,(2\mathrm{arctan}(r/R_0) - 1)$ for the chiral angle that appears in the hedgehog *ansatz* for the chiral field, cf. (3.22). Then the functional turns into a function of the variational parameters (here R_0) and a local minimum is searched for [8]. However, such a search is not exhaustive and difficult to use when more fields are considered, as some inspiration is required to invent suitable variational parameters. Fortunately, we can do better and compute the self-consistent solution. That will be the subject of the next section.

3.2 Method

We now describe the construction of the minimal energy configuration with prescribed baryon number. This calculation proceeds in a number of steps. First, profile functions for the fields Φ are *guessed*. These functions serve to compute the eigenvalues, ϵ_μ, and associated eigenfunctions, ψ_μ, of the Dirac–Hamiltonian, $h(\Phi)$, in the second step. As remarked above, h is diagonalized in

[4] This corresponds to taking the *principle value* prescription when integrating over the Matsubara frequencies in the limit $T \to \infty$, cf. (3.11).

a large but finite volume to discretize these states. In particular, the extension of this volume is much larger than any intrinsic scale carried by Φ. Eventually, the volume extension is changed to verify that the results do not depend on it. The implicit equations of motion

$$\begin{aligned} 0 &= \frac{\delta E_{\rm tot}[\Phi]}{\delta\Phi(\boldsymbol{x})} = \sum_\mu \frac{\partial E_{\rm tot}[\Phi]}{\partial\epsilon_\mu}\,\frac{\delta\epsilon_\mu[\Phi]}{\delta\Phi(\boldsymbol{x})} + \frac{\delta E_{\rm m}[\Phi]}{\delta\Phi(\boldsymbol{x})} \\ &= \sum_\mu \left(\eta_\mu {\rm sign}(\epsilon_\mu) + \frac{\partial E_0[\Phi]}{\partial\epsilon_\mu}\right) \psi_\mu^\dagger(\boldsymbol{x}) \left[\frac{\partial h}{\partial\Phi}(\boldsymbol{x})\right] \psi_\mu(\boldsymbol{x}) + \frac{\delta E_{\rm m}[\Phi]}{\delta\Phi(\boldsymbol{x})} \end{aligned} \tag{3.17}$$

relate Φ to quark bilinears $\psi_\mu^\dagger(\boldsymbol{x})\,(\ldots)\,\psi_\mu(\boldsymbol{x})$, that functionally depend on Φ. In the third step, these relations are utilized in a steepest descent approach to construct new profile functions with a lower total energy. The new profile functions are compared to the previous ones, as are the corresponding energies. If convergence is achieved (the changes from one step to the next do not exceed a prescribed limit), the configuration is adopted as the soliton solution. Otherwise, the new profiles are substituted for those that entered h before and the process is restarted. This Hartree iteration method is depicted in Fig. 3.1.

It is very complicated and essentially impossible to obtain the solutions to the equations of motion (3.17) directly. One therefore assumes certain *ansätze* for the background field. In the baryon number one sector these *ansätze* are of the so-called *hedgehog* type [9] which contracts internal (flavor) and spatial indices such that the meson fields are invariant under a combined transformation. The so-constructed spin-flavor operators are then multiplied by radial functions which are ultimately utilized to minimize the total energy. These *ansätze* are similar to the instanton configuration, (2.57), that contains the contraction of color and spatial indices and (four-dimensional) radial functions. As for the instantons, the hedgehog is embedded in the $SU(2)$ subgroup of the symmetry group associated with the internal indices, this time $SU(N_{\rm f})$. The generator of combined spatial and isospin transformations, the so-called *grand spin*

$$\boldsymbol{G} = \boldsymbol{J} + \frac{\boldsymbol{\tau}}{2} = \boldsymbol{L} + \boldsymbol{S} + \frac{\boldsymbol{\tau}}{2}\,, \tag{3.18}$$

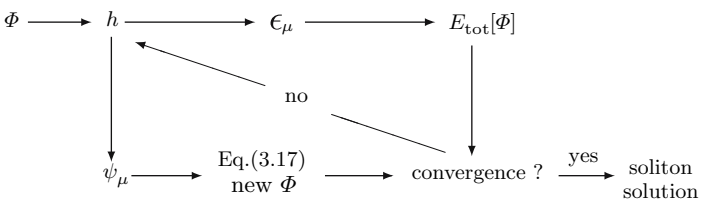

Fig. 3.1. Self-consistent procedure to construct the soliton

commutes with $h(\Phi)$. In (3.18), $\boldsymbol{J}$, $\boldsymbol{L}$ and $\boldsymbol{S}$ are total spin, orbital angular momentum and (internal) spin operators, respectively, while $\boldsymbol{\tau}$ are the isospin Pauli matrices (eventually embedded in $SU(N_\mathrm{f})$). Eigenstates of $\boldsymbol{G}$ are also eigenstates of $h(\Phi)$. The eigenfunctions of $\boldsymbol{G}$ are generalized spherical harmonic functions

$$\left[\mathcal{Y}^M_{GJL}(\hat{\boldsymbol{x}})\right]_{si} = \sum_{m,s_3,i_3,J_3} C^{GM}_{JJ_3,\frac{1}{2}i_3} C^{JJ_3}_{Lm,\frac{1}{2}s_3} Y_{Lm}(\hat{\boldsymbol{x}}) \chi^{(S)}_s(s_3) \chi^{(I)}_i(i_3)\,. \quad (3.19)$$

In the above equation, the $C^{\cdots}_{\cdots}$ are $SU(2)$ Clebsch–Gordan coefficients, the $Y_{Lm}(\hat{\boldsymbol{x}})$ spherical harmonic functions, while the $\chi^{(S)}$ and $\chi^{(I)}$ are each two component spinors in spin and isospin spaces, respectively. A four-component Dirac spinor with $\alpha = 1, \ldots, 4$ in the standard representation (in which γ_0 is diagonal) is constructed by putting two Weyl spinors $[\mathcal{Y}^{\cdots}_{\cdots}(\hat{\boldsymbol{x}})]_{si}$ with $\alpha = s$ and $[\mathcal{Y}^{\cdots}_{\cdots}(\hat{\boldsymbol{x}})]_{s'i}$ and $\alpha = s'+2$ together. Furthermore, the angular dependences of the fields in Φ are chosen to be compatible with the parity of the corresponding Dirac structures in (2.12). Thus, the eigenstates of $h(\Phi)$ are also parity eigenstates with eigenvalues $\Pi = \pm 1$. In full glory, that part of the eigenspinors that carry non-zero isospin reads[5]

$$\Psi^{(G,+)}_\mu = \begin{pmatrix} \mathrm{i} g^{(G,+;1)}_\mu(r) \mathcal{Y}_{GG+\frac{1}{2}G} \\ f^{(G,+;1)}_\mu(r) \mathcal{Y}_{G+1G+\frac{1}{2}G} \end{pmatrix} + \begin{pmatrix} \mathrm{i} g^{(G,+;2)}_\mu(r) \mathcal{Y}_{GG-\frac{1}{2}G} \\ -f^{(G,+;2)}_\mu(r) \mathcal{Y}_{G-1G-\frac{1}{2}G} \end{pmatrix} \quad (3.20)$$

$$\Psi^{(G,-)}_\mu = \begin{pmatrix} \mathrm{i} g^{(G,-;1)}_\mu(r) \mathcal{Y}_{G+1G+\frac{1}{2}G} \\ -f^{(G,-;1)}_\mu(r) \mathcal{Y}_{GG+\frac{1}{2}G} \end{pmatrix} + \begin{pmatrix} \mathrm{i} g^{(G,-;2)}_\mu(r) \mathcal{Y}_{G-1G-\frac{1}{2}G} \\ f^{(G,-;2)}_\mu(r) \mathcal{Y}_{GG-\frac{1}{2}G} \end{pmatrix}, \quad (3.21)$$

where $r = |\boldsymbol{x}|$. The angular dependence and the four Dirac and two isospin indices have not been explicitly written as their appearance is discussed above. The second superscript on the spinors Ψ_μ labels the intrinsic parity Π_intr that enters the parity eigenvalue via $\Pi = (-1)^G \times \Pi_\mathrm{intr}$. The relative phases are chosen such that the equations of motion are compatible with purely real radial functions $g^{(..)}_\mu$ and $f^{(..)}_\mu$. The above-mentioned discretization description transforms into boundary conditions for the radial functions. In accordance with the spherical structure of the box, the finite volume should be a sphere of radius D. As possible boundary condition is to require $g^{(..)}_\mu(D) = 0$, i.e., the upper components of all spinors vanish at the boundary of the finite volume. One of the first studies [11] imposed the boundary condition that the radial function that multiplies the generalized spherical harmonic function with identical grand spin and orbital angular momentum vanished at the boundary. Properties of various boundary conditions are discussed in the literature [12, 13]. The pertinent boundary condition usually depends on the problem under consideration. They all have in common that there is no flux $\langle\psi|\hat{\boldsymbol{x}}\cdot\boldsymbol{\gamma}|\psi\rangle$ through the sphere at $r = D$.

[5] The part with zero isospin (flavor indices $3, \ldots, N_\mathrm{f}$) does not couple with the hedgehog. Hence, those spinors are simply free ones in spherical geometry [10].

Although obvious, it is worth mentioning that the energy eigenvalues obtained by diagonalizing the Dirac–Hamiltonian in a definite channel, G^Π, acquire the degeneracy factor $2G+1$ when summed over as, e.g., in (3.16).

The self-consistency procedure, Fig. 3.1, finally boils down to relating the radial functions $g_\mu^{(..)}$ and $f_\mu^{(..)}$ to the profile functions that parameterize Φ. We will be more explicit on that when discussing specific solutions in Sect. 3.3. Before doing so, we will briefly discuss major features of the spectrum of $h(\Phi)$. To simplify that discussion, we assume that the profile functions in Φ are characterized by a single length scale, a, and we study the spectrum[6] as a function thereof. Of course, we always have $a \ll D$. We also assume that the amplitudes of the profile functions do not exceed certain limits (this is relevant for the scalar–isoscalar component of Φ, see Sect. 3.3.4). We expect the most strongly bound quark to have zero grand spin, $G=0$. Charge and parity conjugation properties of Φ can be arranged such that the corresponding eigenstate has positive parity. Hence, the spectrum of $\Psi_\mu^{(0,+)}$ is of special interest. The scale inherited from the fermion determinant is the VEV (or constituent quark mass) m. Thus, small, moderate and large background configurations correspond to the cases $am \ll 1$, $am \sim 1$ and $am \gg 1$, respectively. For these three cases, the spectrum is outlined in Fig. 3.2. For small extensions, the interaction between the background and the quarks is weak. This causes the lowest lying quark with positive energy to be only loosely bound. For extensions of the order of the Compton wave length of the quarks, the interaction is strong enough to yield a sizable binding energy of that quark. It is expected that this energy gain is sufficient to result in an energetically bound object

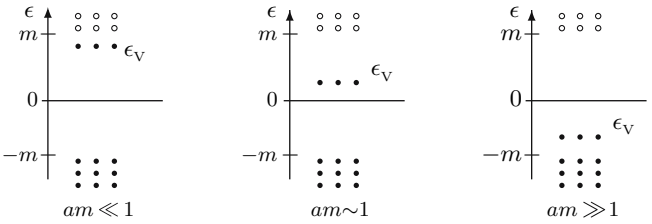

Fig. 3.2. Schematic spectrum in the $G^\Pi = 0^+$ channel for $N_C = 3$. In the Dirac–hole picture, the levels shown with *filled circles* are to be occupied, the *open ones* not. Continuum states with $|\epsilon| \geq m$ are only schematically indicated and ϵ_V is defined before (3.16). Three cases for the extension of the background field are shown small (*left*), moderate (*center*) and large (*right*)

[6] The spectrum is computed by expanding the radial functions in terms of solutions to the free Dirac–Hamiltonian in spherical geometry, $g_\mu^{(G,+;1)} = \sum_n a_n^{(\mu)} j_G(k_n r)$, etc., j_G is a spherical Bessel function and the discretized momenta k_n determined from the boundary condition at $r = D$. The Dirac equation $h\psi_\mu = \epsilon_\mu \psi_\mu$ is thus transformed into an algebraic eigenvalue problem for the vectors $a^{(\mu)}$. Technical details of this calculation are explained in [14].

that carries baryon number. Note that the scenarios with small and moderate extensions still result in a vanishing vacuum baryon number when (3.15) is summed symmetrically over positive and negative energy eigenvalues. To assign unit baryon number to such configurations, the bound state occupation numbers must be taken to be one. This is no longer the case for wide background fields. Then the energy eigenvalue of the most strongly bound quark turns negative and $B_0 = 1$. For very large extensions, this state will eventually join the negative continuum. Whenever $B_0 = 1$, all occupation numbers must be set to zero. Stated otherwise, for $am \gg 1$, the background polarizes the vacuum so strongly that it acquires a baryonic charge.

It is worth to discuss the relation to the suggestive Dirac–hole picture in which the total energy is obtained by summing only over occupied states. According to that picture, the fermion energy of a baryon number one configuration would formally be $E_{\text{fer.}}^{(B=1)} = N_{\text{C}} \sum_{\epsilon_\mu \leq \mu} \epsilon_\mu$ minus the energy assigned to the trivial configuration Φ_0. Again formally, this expression can be argued in favor from (3.6) and (3.7) together with the vanishing trace of the Dirac–Hamiltonian, $\text{tr}(h) = \sum_\mu \epsilon_\mu = 0$. However, once regularization is included, and it is a must here, these trace arguments are no longer valid. In that case, the unique and correct prescription is to sum over all positive and negative energy states as in (3.16). In a quantum field theory approach, that involves regularization (or even renormalization), the Dirac theory must be formulated such that charge conjugation invariance is ensured. This ultimately relates functional traces to sums over *all* states [15].

3.3 Soliton Solutions in NJL-Type Models

In this section, we will finally discuss actual soliton configurations that minimize the regularized energy functional in the baryon number one sector.

3.3.1 Pseudoscalar Fields

Pions are central to chiral symmetry, whence a self-evident approach for the construction of a static configuration that solves the stationary equations (3.17) is to only consider the pseudoscalar Goldstone bosons in the two-flavor reduction. Scalar as well as (axial) vector mesons assume their vacuum values. The hedgehog *ansatz* [9] for static chiral field in (2.20)

$$U(\boldsymbol{x}) = \exp\left(\mathrm{i}\boldsymbol{\tau} \cdot \hat{\boldsymbol{x}}\, \Theta(r)\right) \qquad \text{with} \qquad r = |\boldsymbol{x}| \tag{3.22}$$

defines the chiral angle $\Theta(r)$. It is to be treated self-consistently according to the scheme shown in Fig. 3.1. The corresponding Dirac–Hamiltonian is

$$h = \boldsymbol{\alpha} \cdot \boldsymbol{p} + m\beta\big[\cos\Theta(r) + \mathrm{i}\gamma_5 \boldsymbol{\tau} \cdot \hat{\boldsymbol{x}} \sin\Theta(r)\big]\,. \tag{3.23}$$

For the above *ansatz*, the stationary equation

$$m_\pi^2 f_\pi^2 \sin\Theta(r) = N_\mathrm{C}\, m\, \mathrm{tr}\left\{\left[\sin\Theta(r) - \mathrm{i}\gamma_5 \boldsymbol{\tau}\cdot\hat{\boldsymbol{x}}\cos\Theta(r)\right]\rho\,(\boldsymbol{x},\boldsymbol{x})\right\} \tag{3.24}$$

introduces the regularized density

$$\rho\,(\boldsymbol{x},\boldsymbol{y}) = \theta(\epsilon_\mathrm{V})\Psi_\mathrm{V}(\boldsymbol{x})\bar{\Psi}_\mathrm{V}(\boldsymbol{y}) - \frac{1}{2}\sum_\nu \mathrm{sign}\,(\epsilon_\nu)\,\mathrm{erfc}\left(\frac{|\epsilon_\nu|}{\Lambda}\right)\Psi_\nu(\boldsymbol{x})\bar{\Psi}_\nu(\boldsymbol{y}) \tag{3.25}$$

as a matrix in Dirac and isospin spaces. It defines the steepest descent in the Hartree iteration. As indicated above, $\rho\,(\boldsymbol{x},\boldsymbol{y})$ is continuous as $\epsilon_\mathrm{V} \to 0$. The right- and left-hand sides in (3.24) originate from the regularized fermion determinant. The chiral symmetry breaking piece is

$$E_\mathrm{m} = -\frac{m_0 m}{4G_1}\int \mathrm{d}^3 r\, \mathrm{tr}\left[U + U^\dagger - 2\right] = 4\pi m_\pi^2 f_\pi^2 \int_0^\infty \mathrm{d}r r^2\,\left[1 - \cos(\Theta(r))\right]\,, \tag{3.26}$$

with m_π substituted for m/G_1 according to (2.24). The self-consistency feature is expressed through the fact that the spinors Ψ_ν are eigenstates of the Hamiltonian, (3.23), thus inducing a parametrical dependence of $\rho\,(\boldsymbol{x},\boldsymbol{y})$ on $\Theta(r)$. The subscript "V" denotes the valence level, the most strongly bound quark in the $G^\Pi = 0^+$ channel. Of course, the sum over ν turns into one over the grand spin and parity labels with appropriate degeneracy factors attached as the density matrix is computed using the basis states of (3.20) and (3.21). The sums over the grand spin projection, M in (3.19), and over the discrete indices take care that the right-hand side of (3.24) does not depend on angular variables.

Self-consistent solutions to this system were obtained already some time ago for $N_\mathrm{C} = 3$ [16, 17, 18]. The typical solution has $\Theta(0) - \Theta(\infty) = n\pi$, with n an integer, and one is free to choose $\Theta(\infty) = 0$. Note that these boundary values result from the equation of motion; they are not subject to any topology argument or the requirement of finite energy. For various values of the constituent quark mass, m, the solutions are shown in Fig. 3.3. As explained in Chap. 2, this mass is commonly taken as the only adjustable parameter in the model once pion decay constant, $f_\pi = 93\,\mathrm{MeV}$, and pion mass, $m_\pi = 135\,\mathrm{MeV}$, are fixed. Self-consistent solutions were numerically obtained for $m \geq 325\,\mathrm{MeV}$ [16]. The profile function obviously exhibits only a very mild dependence on m. The soliton energy E_tot, i.e., the energy functional corresponding to the self–consistent chiral angle, similarly varies only scarcely with m as can be seen from Table 3.1. The soliton mass is larger than the three quark thresholds as long as $m \lesssim 420\,\mathrm{MeV}$. Due to the lack of confinement in this model (cf. Chap. 2), the soliton is not stable in this case and may decay into three free quarks.

The total energy, E_tot, or soliton mass, cannot directly be compared to baryon masses (i) because the soliton first has to be projected onto baryon quantum numbers, this will be thoroughly discussed in Chaps. 5 and 6, and

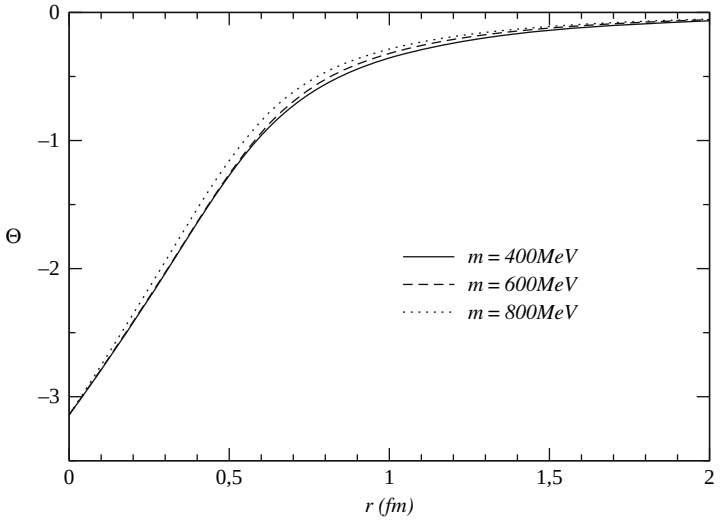

Fig. 3.3. Self-consistent chiral angle Θ as a function of the radial coordinate for different model parameters

(ii) because of the sizeable quantum corrections to the energy due to meson fluctuations[7] to be addressed in Sect. 8.6. In Table 3.1, the various contributions to the soliton mass are also displayed. For small constituent quark masses, the explicit occupation of the valence quark orbit ($\eta_{\rm V} = 1$) provides the dominant contribution to the energy. As m increases the situation is reversed. For $m > 750\,{\rm MeV}$, $E_V = 3\epsilon_{\rm V}$ turns negative. This implies $\eta_{\rm V} = 0$ and the valence quark becomes part of the polarized vacuum which then carries the baryon number. The data confirm that $E_{\rm tot}$ is smooth.

Table 3.1. The soliton energy $E_{\rm tot}$ and its various parts defined (3.16) as functions of the constituent quark mass m. According to (3.16), the entry labeled E_0 contains the vacuum energy with the subtraction of $E_0[\Phi_0]$. All data are in MeV

m	350	400	500	600	700	800
$E_{\rm tot}$	1236	1239	1221	1193	1161	1130
E_V	745	633	460	293	121	−55
E_0	459	571	728	869	1012	1103
E_m	31	34	33	31	28	26

[7] In general, meson loops about the soliton are not renormalizable in these effective models. Hence their quantum effects can only be estimated.

3.3.2 Vector and Axial-Vector Fields

As a first extension, the ρ vector meson field was incorporated [19] according to the Wu–Yang *ansatz*

$$V_\mu = \boldsymbol{\rho}_\mu \cdot \frac{\boldsymbol{\tau}}{2} \quad \text{with} \quad \rho_{0a} = 0 \quad \text{and} \quad \rho_{ia} = \epsilon_{ika}\hat{x}_k G(r)\,. \tag{3.27}$$

This introduces a second radial function, $G(r)$. It can easily be verified that this field configuration commutes with the grand spin generator, (3.18). Except for the pseudoscalar field, for which the hedgehog shape, (3.22), was adopted, all other fields were set to their vacuum expectation values. In that calculation, the lower limit above which solitons exist has been determined to be $m \geq 270\,\text{MeV}$. The incorporation of the ρ-meson does not alter the relation among the model parameters in the pseudoscalar sector. This is no longer the case when also the a_1-meson is included as required by chiral invariance. Mainly $\pi - a_1$ mixing changes the relation between the pion decay constant, f_π, and the cut-off, Λ. The latter is significantly increased for a prescribed value of m, cf. Sect. 2.4. The general *ansatz* for the a_1 meson which is consistent with the grand spin zero assumption and reflects the pseudovector character involves two radial functions, $H(r)$ and $F(r)$,

$$A_\mu = \boldsymbol{a}_{1,\mu} \cdot \frac{\boldsymbol{\tau}}{2} \quad \text{with} \quad a_{1,0a} = 0 \quad \text{and} \quad a_{1,ia} = \delta_{ia}H(r) + \hat{r}_i\hat{r}_a F(r). \tag{3.28}$$

Self-consistent solutions were found for $m \geq 300\,\text{MeV}$ [20, 21]. The full system now involves four functions that are to be treated according to the self–consistent scheme depicted in Fig. 3.3. This numerical program is quite involved, and the resulting radial functions are, e.g., presented in figures 1–3 of [22]. An essential feature of these radial functions is that $H(0) \neq 0$, while the two other profile functions for the (axial) vector meson fields do vanish at the center of the soliton. Thus, in contrast to the vector field, the axial-vector fields do strongly affect the quark modes in the grand spin zero channel. This is in particular the case for the valence quark level whose energy eigenvalue turns negative already for moderate values of the constituent quark mass, m. This is shown in Table 3.2. Hence, the chiral invariant inclusion of vector degrees of freedom in the baryon number one sector of NJL-type models causes the vacuum to be so strongly polarized that it carries the baryon charge. The

Table 3.2. The soliton energy E_{tot} as well as its vacuum and mesonic contributions E_0 and E_m for different values of the constituent quark mass m. The energy of the most strongly bound quark mode is also shown.

m (MeV)	300	350	400
E_{tot} (MeV)	1104	1010	938
E_0 (MeV)	736	615	544
E_m (MeV)	368	395	394
ϵ_{V}/m	-0.04	-0.38	-0.54

same conclusion was drawn from a calculation that eliminated the axial–vector field in a chirally consistent manner by a local chiral transformation on Φ [13].

3.3.3 Remark on the ω Field

The *ansatz* for the isoscalar ω field that is compatible with the grand spin symmetry permits only a radial function in the temporal component, $V_0 = \omega(r)\mathbb{1}$. Hence, this component is subject to variation under the Wick rotation, (2.15). A constant phase factor $\zeta = \mathrm{e}^{\mathrm{i}\varphi}$ that continuously transforms from real and imaginary axes can be attached to verify that the solutions to the Dirac equation with the ω field included are indeed analytic functions [23]. This is a well-known property of ordinary differential equations. The problem emerges with regularization that treats real and imaginary parts of the Euclidean action differently and thus spoils the analytic properties. In addition, the Hamilton operators that enter $\not{D}_E$ and $\not{D}_E^\dagger$, h and $h^\dagger$, respectively, cannot be simultaneously diagonalized. Thus, it appears impossible to construct a meaningful regularized action which, e.g., leads to a regularized energy functional but unregularized vacuum baryon number. This is kind of a pity since in particular the ω meson degree of freedom is affected and from hadron phenomenology we expect this field to play a decisive role. So far, sensible calculations that include the ω field have mainly been carried out in a perturbation expansion [23], i.e., the action is expanded as a power series in ω with non-local contributions.[8]. This power series may then straightforwardly be analytically continued from Euclidean to Minkowski space. The numerical results suggest that it suffices to expand up to quadratic order. It should be noted that *only* the temporal component of the ω field undergoes this expansion, all other (axial) vector meson fields are retained at all orders. In [24], this approach was criticized on the basis that a divergent piece of the action would emerge that couples spatial and temporal components of vector mesons. However, this contribution vanishes identically by the flavor trace because spatial components of the ω field are absent in the generalized hedgehog *ansatz*. In this semi-perturbative treatment of the ω field, its repulsive character is well reproduced [23]. Most importantly, these numerical studies do not alter the above conclusion that for the self-consistent soliton the baryon number is carried by the vacuum, i.e., a fermion level has moved from the positive to the negative spectrum due to the interaction with the background meson fields. This does not come as a surprise. The repulsive character causes the extension of the chiral angle to increase, which in turn decreases the energy of the most strongly bound quark, cf. Fig. 3.2.

This second-order treatment of the ω field can be generalized to all orders [25]. However, for actual computations it becomes tremendously bulky: The analog of the z-integral in (3.12) must be performed numerically because

[8] See [21, 22] for earlier attempts to construct a regularized energy functional in the presence of the ω field.

the generalized Dirac–Hamiltonian parametrically depends on that frequency. In particular, a self-consistent construction of a soliton seems currently infeasible in such a formulation.

3.3.4 Comments on Scalar Fields

In the above considerations, the (pseudo)scalar fields have been constrained to the so-called chiral circle, $MM^\dagger = m^2$, for good reason. It was soon recognized that relaxing this condition causes the soliton to collapse [26], at least as long as (axial) vector fields are omitted. To relax the above condition, the *ansatz*, (3.22), is extended to

$$M = m\,\{[1 + f(r)\cos\Theta(r)] + \mathrm{i} f(r)\boldsymbol{\tau}\cdot\hat{\boldsymbol{x}}\sin\Theta(r)\} \tag{3.29}$$

such that the chiral radius Σ, defined after (2.19), depends on the radial coordinate. Starting from a smooth configuration for the profile function $f(r)$, the iterative procedure of Fig. 3.1 produces a sharp peak at $r = 0$ of arbitrary height. Simultaneously, E_m and E_0 tend to zero. The Dirac spectrum has the interesting feature that the valence level gets transferred from the lower boundary of the positive Dirac spectrum to the upper boundary of negative Dirac spectrum. All other levels in the $G^\pi = 0^+$ channel follow as a consequence of "avoided crossings." Higher partial waves do not get affected. Obviously, the baryon number is then carried by the vacuum, and hence the soliton energy is solely given by the vacuum part E_0 and thus vanishes; but nevertheless the baryon number is one. To some extent, this instability is an artifact of regularizing *only* the real part of the action. For the above-described configuration, the asymmetry of the Dirac spectrum is transferred to ever larger energies. So it is reflected in the baryon number but not in the energy in which the large energy modes are suppressed by regularization.

Early numerical calculations [17, 27] that allowed a radial-dependent scalar field and claimed to have obtained stable solitons already indicated an inflated chiral radius which happens to be at variance with what we know about bag formation in linear sigma models [28]. Those early calculations actually suffered from artifacts in the numerical treatment that were associated with a restricted basis to sum over levels. The self-consistent process essentially requires the expansion of the profile functions in Fourier series, cf. footnote 6, and in a limited basis, arbitrarily sharp peaks cannot be reproduced.

Of course, it should easily be possible to extend the model such that this instability is avoided. First, we recognize that as a consequence of (proper-time) regularization, the effective potential, (2.19), does not generate a large positive definite Σ^4 term that eventually balances negative contributions from derivative terms in the fermion determinant. It does not seem sufficient to change the regularization scheme for $\mathcal{A}_R$ [29], rather a fourth-order term must be put in by hand [30, 31]. This can, e.g., be motivated from models that mock up the trace anomaly of QCD in effective meson theories [32]. Once such a

local term is added, the soliton is again stabile and its properties are similar to the one described in Sect. 3.3.1.

Vector mesons [22] or requiring the regularized baryon number [33] are alternative means to stabilize the chiral radius.

As a brief summary of this chapter, we put on record that NJL-type models for the quark flavor dynamics contain soliton solutions albeit their construction comes with quite some complications which so far are not completely resolved. The most appealing feature is that the chirally consistent incorporation of vector mesons polarizes the vacuum so strongly that it actually carries baryon number. In such a scenario, there are no explicit valence quarks, rather the baryon number must be considered as a property of the meson fields, in particular the chiral field $U(x)$ that triggers the other profile functions.

References

1. R. Alkofer, H. Reinhardt, and H. Weigel, *Phys. Rep.* **265** (1996) 139. 27, 28
2. C. V. Christov et al., *Prog. Part. Nucl. Phys.* **37** (1996) 91. 27, 28
3. R. Rajaraman, *Solitons and Instantons.* North Holland, Amsterdam, 1982. 27
4. H. Weigel, E. Ruiz Arriola, and L. P. Gamberg, *Nucl. Phys.* **B560** (1999) 383. 28
5. R. F. Dashen, B. Hasslacher, and A. Neveu, *Phys. Rev.* **D12** (1975) 2443. 28
6. I. Gradstein and I. Ryshik, *Tables of Series, Products and Integrals I*, chapter 1.431. Harri Deutsch, Thun, 1981. 28
7. H. Reinhardt, *Nucl. Phys.* **A503** (1989) 825. 28
8. D. Diakonov, V. Y. Petrov, and P. V. Pobylitsa, *Nucl. Phys.* **B306** (1988) 809. 31
9. W. Pauli, *Meson Theory of Nuclear Forces.* Interscience Publishes, Inc., New York, 1946. 32, 35
10. C. Itzkson and J.-B. Zuber, *Quantum Field Theory*, chapter 2.3.2. McGraw–Hill, New York, 1980. 33
11. S. Kahana and G. Ripka, *Nucl. Phys.* **A429** (1984) 462. 33
12. H. Weigel, R. Alkofer, and H. Reinhardt, *Nucl. Phys.* **B387** (1992) 638. 33
13. R. Alkofer, H. Reinhardt, J. Schlienz, and H. Weigel, *Z. Phys.* **A354** (1996) 181. 33, 39
14. R. Alkofer and H. Weigel, *Comput. Phys. Commun.* **82** (1994) 30. 34
15. E. Farhi, N. Graham, R. L. Jaffe, and H. Weigel, *Nucl. Phys.* **B585** (2000) 443. 35
16. H. Reinhardt and R. Wünsch, *Phys. Lett.* **B215** (1988) 577. 36
17. T. Meissner, F. Grümmer, and K. Goeke, *Phys. Lett.* **B227** (1989) 296. 36, 40
18. R. Alkofer, *Phys. Lett.* **B236** (1990) 310. 36
19. R. Alkofer and H. Reinhardt, *Phys. Lett.* **B244** (1990) 461. 38
20. R. Alkofer, H. Reinhardt, H. Weigel, and U. Zückert, *Phys. Rev. Lett.* **69** (1992) 1874. 38
21. F. Doering, E. Ruiz Arriola, and K. Goeke, *Z. Phys.* **A344** (1992) 159. 38, 39
22. U. Zückert, R. Alkofer, H. Reinhardt, and H. Weigel, *Nucl. Phys.* **A570** (1994) 445. 38, 39, 41
23. H. Weigel, U. Zückert, R. Alkofer, and H. Reinhardt, *Nucl. Phys.* **A585** (1995) 513. 39
24. I. J. R. Aitchison and G. Ripka, *Nucl. Phys.* **A606** (1996) 292. 39

25. F. Doering, C. Schueren, T. Watabe, K. Goeke, and E. Ruiz Arriola, *Nucl. Phys.* **A603** (1996) 415. 39
26. P. Sieber, T. Meissner, F. Grümmer, and K. Goeke, *Nucl. Phys.* **A547** (1992) 459. 40
27. H. Reinhardt and R. Wünsch, *Phys. Lett.* **B230** (1989) 93. 40
28. P. Jain, R. Johnson, and J. Schechter, *Phys. Rev.* **D35** (1987) 2230. 40
29. J. da Providencia, H. Walliser, and H. Weigel, *Nucl. Phys.* **A671** (2000) 547. 40
30. C. Weiss, R. Alkofer, and H. Weigel, *Mod. Phys. Lett.* **A8** (1993) 79. 40
31. T. Meissner et al., *Phys. Lett.* **B299** (1993) 183. 40
32. J. Schechter, *Phys. Rev.* **D21** (1980) 3393. 40
33. J. Schlienz, H. Weigel, H. Reinhardt, and R. Alkofer, *Phys. Lett.* **B315** (1993) 6. 41

4

The Skyrme Model

In the previous chapters we have considered effective models for the quark flavor dynamics. We have seen that bosonization techniques transform these models into effective meson theories: They can be formulated as functionals of the chiral field U (and other meson fields). We have also seen that self-consistent solitons emerge in such models. However, that results from quite a complicated calculation as integrating out the quarks leads to non-local functionals of the meson fields, though some simplification is achieved by derivative expansions. To complicate matters, we note that so far we have not attacked the problem of quantizing such a soliton to describe states with baryon quantum numbers. Hence the immediate question arises of whether or not it is possible to directly employ a local meson theory and discuss its chiral solitons. In such an approach the baryon number has to be assigned to the meson fields. As we have just learned from the NJL model for quark flavor dynamics this is actually likely. On the other hand it would be particularly intriguing if it were possible to derive or at least motivate that baryons emerge as solitons in effective meson theory directly from QCD. In this chapter we will exactly survey this scenario.

The discussion of chiral meson models and their soliton solutions will be the main subject of this chapter. For the remainder of this monograph we will concentrate on such models and only revert to quark models in case substantially new information is gained as, e.g., in the context of nucleon structure functions that will be discussed in Sect. 7.7.

4.1 Large-N_C Considerations

The application of QCD to low-energy hadron physics is out of the reach of ordinary perturbation theory understood as an expansion in the coupling constant. Nevertheless, 't Hooft already observed some time ago that QCD has a *hidden* expansion parameter that may serve to establish a perturbation theory [1, 2]. The essential procedure is to generalize QCD from an $SU(3)$

H. Weigel: *The Skyrme Model*, Lect. Notes Phys. **743**, 43–64 (2008)
DOI 10.1007/978-3-540-75436-7_4

gauge theory to $SU(N_C)$, where N_C denotes the number of color degrees of freedom. The expansion then is a power series in $1/N_C$. We already became acquainted with that method in the discussion of the NJL-type models for the quark flavor dynamics. Those models do not contain any direct color interaction and N_C solely appeared as combinatorial factor. For example, from (2.22) we observe that the pion decay constant is $\mathcal{O}(N_C)$ while (2.35) and (2.36) together with $G_2 = \mathcal{O}(1/N_C)$ suggest that meson masses approach constant values as $N_C \to \infty$. On the other hand (3.14) tells us that the soliton energy is also $\mathcal{O}(N_C)$. It is not surprising that NJL models without direct color interaction provide an intuitive picture of the $1/N_C$ expansion because in QCD also the large-N_C considerations are essentially combinatorial. In this and the following sections we will present the central issues of these considerations as put forward in [3].

QCD is the non-abelian gauge theory of color interactions. The matter fields (quarks) are members of the fundamental representation and are thus equipped with a single color index.[1] The gauge bosons (gluons) that transmit the interaction dwell in the adjoint representation and have two color indices. One of these indices couples to the quark and the other to the anti-quark. This suggests to consider gluons as composites of quarks and anti-quarks. Of course, this only concerns counting the color degrees of freedom. For large-N_C we may furthermore ignore that the gluon color matrices are traceless; this only supplies a single condition on N_C^2 quantities. Putting these properties together we may find the combinatorial factors of any Feynman diagram by replacing gluon lines with two lines for quarks and anti-quarks. This *double line notation* for the color degrees of freedom is depicted in Fig. 4.1. We may immediately apply this prescription to a typical Feynman diagram that contributes to the gluon self-energy as shown in Fig. 4.2. Obviously the double-line notation reveals the presence of an undetermined color index $(c, \bar{c})$ that must be summed over making up the combinatorial factor N_C. The vertices yield the factor g_{QCD}^2 and thus the full diagram behaves like $g_{QCD}^2 N_C$. To establish a converging $1/N_C$ expansion this diagram must be of order unity. Thus, a well-defined large-N_C generalization of QCD requires

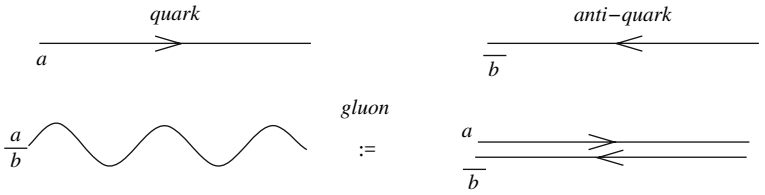

Fig. 4.1. Double-line notation for the gluon color degrees of freedom in Feynman diagrams. Here $a, \bar{b} = 1, \ldots, N_C$ are the color labels

[1] The generalization to arbitrary N_C is not unique [4]. See [5, 6] (and refs. therein) for alternative starting points to study fermions at $N_C \neq 3$.

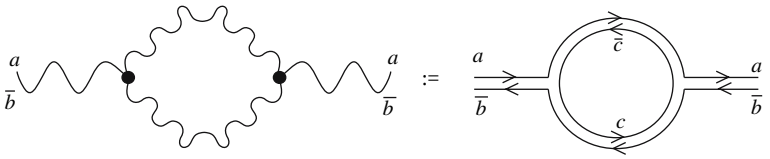

Fig. 4.2. Double-line notation for a typical contribution to the gluon self-energy. The *dots* on the left hand side indicate the gauge coupling constant g_{QCD}

$$g_{\mathrm{QCD}} = \mathcal{O}\left(\frac{1}{\sqrt{N_{\mathrm{C}}}}\right) . \tag{4.1}$$

We are now prepared to compute the combinatorial factors of Feynman diagrams in QCD. In Fig. 4.3 we compare two similar diagrams. The upper diagram has four color loops and the coupling constant enters with power eight. Hence this diagram is $\mathcal{O}(N_{\mathrm{C}}^0)$. The lower diagram has only a single color loop and six factors of the coupling constant, hence it is $\mathcal{O}(1/N_{\mathrm{C}}^2)$. In the upper diagram all gluon lines lie in a single plane. This is not true for the lower one. The generalization of the just-computed combinatorial factors is that all non-planar diagrams are suppressed for large N_{C}. Since there are N_{C}^2 gluons but only N_{C} fermions it is easy to understand that there are fewer possibilities for internal fermion loops than gluon loops and hence the former are suppressed.

The discussion of hadron properties involves matrix elements of color singlet quark bilinears such as $\bar{q}\gamma_\mu q$ or $\bar{q}(\mathrm{i}\partial_\mu - g_{\mathrm{QCD}}A_\mu)q$, where A_μ represents the gluon field. Therefore we need to consider Feynman diagrams with quark lines around the "edges" to which these bilinear operators can couple. These diagrams should have at least a single quark loop at their the edges. A typical representative of this class of diagrams is shown in Fig. 4.4 together with its double-line notation. It is straightforward to verify that this diagram scales as N_{C}. This is actually the leading order for couplings to quark bilinears and is common to diagrams with the following properties [3]:

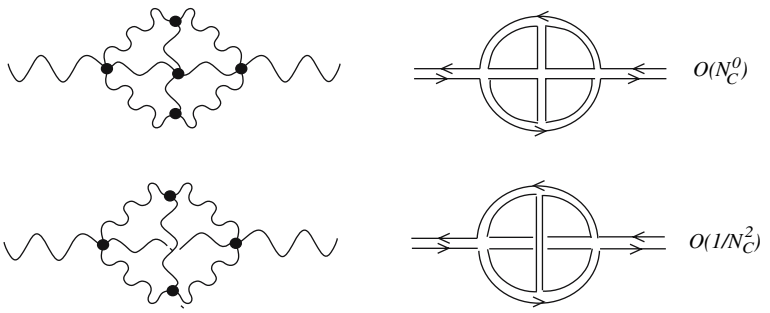

Fig. 4.3. Rephrasing typical QCD Feynman diagrams in the double-line notation. The three gluon vertex gives a factor g_{QCD} while the four gluon vertex has g_{QCD}^2

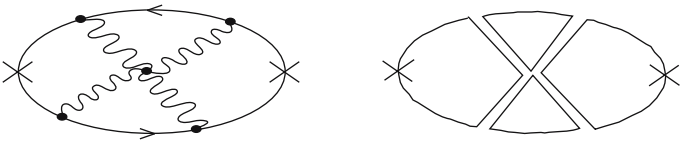

Fig. 4.4. Quark bilinear coupling (indicated by "×") to loops in QCD and its double-line notation

- Internal lines are all made from gluons.
- All lines are in a single plane.
- The edges only have quark lines. (4.2)

In the next step we examine correlation functions of color singlet quark bilinear operators in the large-N_C limit. In particular we can learn about the particle content by considering intermediate states that contribute to such correlation functions. These intermediate states are identified from a diagram that satisfies the criteria (4.2) using Cutkosky's rules [7] according to which we find the intermediate states from the particle content along any cut of the Feynman diagram. Examples for correlation functions of two, three and four quark bilinears are shown in Fig. 4.5. The fact that for large N_C neither non-planar nor diagrams with internal quark loops contribute causes the color indices along any such cut to be combined in a single trace, rather than products of traces. This translates into the statement that in the large-N_C limit all intermediate states are quark bilinear color singlet objects, i.e., single mesons, taking for granted that QCD is a confining theory. The absence of two (or more) meson intermediate states implies that meson loops vanish as $N_\mathrm{C} \to \infty$. The quadratic correlation function of a quark bilinear operator $J(x)$ therefore has the simple spectral decomposition

$$\langle J(x)J(y)\rangle = \int \frac{\mathrm{d}^4k}{(2\pi)^4}\,\mathrm{e}^{\mathrm{i}k(x-y)} \sum_i \frac{a_i(k)a_i^\dagger(k)}{k^2-m_i^2}\,. \tag{4.3}$$

Here the sum goes over all meson states than can couple to $J(x)$. Furthermore $a_n \sim \langle 0|J|i\rangle$ is the amplitude for J to create the meson i (with mass m_i) from the vacuum. We have just learned that the left hand side of (4.3) is linear in N_C. Turning to the right hand side this implies that $a_n \sim \sqrt{N_\mathrm{C}}$ and $\lim_{N_\mathrm{C}\to\infty} m_n = \text{const}$. The latter observation obviously is exactly what we

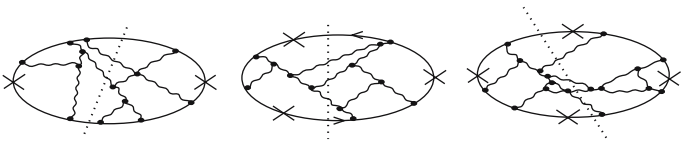

Fig. 4.5. Correlation functions of quark bilinear operators ("×") and their intermediate states (indicated by the *dashed lines*)

found in the NJL model. On the other hand, infinitely many mesons must contribute in the sum, (4.3) in order to reproduce the $\ln(k^2)$ behavior in the asymptotically free regime of QCD. The fact that the amplitude to create a meson from the vacuum scales like $\sqrt{N_C}$ allows us to argue about the leading $1/N_C$ behavior of an n-point meson correlation function. From the diagrams in Fig. 4.5 we know that the correlation function of n quark bilinear operators scales like N_C. In the spectral decomposition this correlation function has contributions of the form

$$\underbrace{\langle 0|J|i_1\rangle \dots \langle 0|J|i_n\rangle}_{n \text{ terms}} \Gamma^{(n)}_{i_1 \dots i_n} = \mathcal{O}\left(N_C^{\frac{n}{2}}\right) \times \Gamma^{(n)}_{i_1 \dots i_n} = \mathcal{O}\left(N_C\right) . \tag{4.4}$$

Hence the coupling constant for the n-meson vertex scales as

$$\Gamma^{(n)}_{i_1 \dots i_n} = \mathcal{O}\left(N_C^{1-\frac{n}{2}}\right) . \tag{4.5}$$

For $n = 4$ this is consistent with what we observed in (2.41), $\Gamma^{(4)} \propto 1/f_\pi^2 = \mathcal{O}\left(1/N_C\right)$.

Accumulating the above results leads to the bold statement or conjecture [3] that in large-N_C QCD becomes equivalent to a meson theory with meson loops and coupling constants getting more and more suppressed as N_C grows. It should be possible to construct this theory from meson phenomenology. The caveat that infinitely many mesons might be involved should not be an obstacle as long as we consider only the low-energy regime in which just a limited number of light mesons should be relevant.

4.2 Baryons in Large-N_C QCD

We now turn to the leading N_C dependences of baryon properties. In particular we would like to understand the role of baryons in the effective meson theory that we just motivated from large-N_C QCD.

Low-lying baryons do not contain (valence) anti-quarks. So we have to build color singlets without the use of anti-quarks. Thus baryons must be composites of (at least) N_C quarks. To make up a color singlet, the baryon wave function should be totally anti-symmetric in the color coordinates and thus symmetric in all other quantum numbers. In a non-relativistic framework we might even assume that the remaining wave function describes a many body "effective boson" with all constituents in the S-wave for the ground state baryon.

In contrast to the discussion of mesons in Sect. 4.1 the examination of typical Feynman diagrams is not helpful in the context of baryons. For baryons not only the combinatoric factors depend on N_C but also the shape of the diagrams itself. In Fig. 4.6 typical Feynman diagrams with one and two gluon exchanges are shown. We expect m single gluon exchange diagrams to contribute

Fig. 4.6. Feynman diagram for a propagating baryon built from $N_{\rm C}$ quarks (indicated by *small dots*) with one and two gluon exchanges. Interaction vertices are shown as *big dots*

$$g_{\rm QCD}^{2m}\frac{1}{m!}\left[N_{\rm C}(N_{\rm C}-1)\right]^{2m}=\mathcal{O}\left(N_{\rm C}^{m}\right)\,. \tag{4.6}$$

Obviously the perturbation expansion does not have a smooth limit as $N_{\rm C}$ tends to infinity. Nevertheless baryon properties do have such a smooth limit. We just have to find the proper way to sum all contributions. This makes use of many body techniques and we will closely follow the arguments of [3] and first consider the many body problem in a non-relativistic framework assuming that the quarks are heavy and then argue that relativistic effects for light quarks do not alter the large-$N_{\rm C}$ results qualitatively.

The non-relativistic many body problem is treated in the Hartree approach assuming that a single quark reacts on an average potential generated by the $N_{\rm C}-1$ remaining quarks. In the non-relativistic case only the two-body forces contribute and the Hamilton operator reads

$$H=N_{\rm C}M+\sum_{i=1}^{N_{\rm C}}\frac{-\boldsymbol{\partial}_i^2}{2M}-\frac{g^2}{N_{\rm C}}\sum_{i<j}^{N_{\rm C}}\frac{1}{|\boldsymbol{r}_i-\boldsymbol{r}_j|}\,, \tag{4.7}$$

where M is the mass of a single quark and $g=\sqrt{N_{\rm C}}g_{\rm QCD}$ is $\mathcal{O}(N_{\rm C}^0)$ in the large-$N_{\rm C}$ limit. Spin-dependent forces have been omitted in compliance with the non-relativistic treatment. As argued above, in the ground state all quarks should be in the S-wave. This motivates the *ansatz* for the (scalar) many body wave function

$$\Psi(\boldsymbol{r}_1,\ldots,\boldsymbol{r}_{N_{\rm C}})=\prod_{i=1}^{N_{\rm C}}\phi(\boldsymbol{r}_i)\,. \tag{4.8}$$

We write $E=N_{\rm C}\epsilon$ and imagine applying the variational principle to

$$\begin{aligned}\langle\Psi|H-E|\Psi\rangle=&-N_{\rm C}\epsilon+N_{\rm C}M+\frac{N_{\rm C}}{2M}\int{\rm d}^3r\,\boldsymbol{\partial}\phi^*(\boldsymbol{r})\cdot\boldsymbol{\partial}\phi(\boldsymbol{r})\\&-\frac{N_{\rm C}(N_{\rm C}-1)}{2}\,\frac{g^2}{N_{\rm C}}\int{\rm d}^3r_1\int{\rm d}^3r_2\frac{|\phi(\boldsymbol{r}_1)|^2|\phi(\boldsymbol{r}_2)|^2}{|\boldsymbol{r}_1-\boldsymbol{r}_2|}\,.\end{aligned} \tag{4.9}$$

Hence $\phi=\mathcal{O}(N_{\rm C}^0)$ and so is ϵ. This implies that baryon masses are $\mathcal{O}(N_{\rm C})$. Note and appreciate that this is exactly the behavior which we observed for the soliton in the NJL model, cf. (3.14). Furthermore the fact that ϕ has

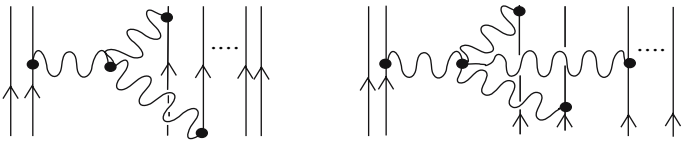

Fig. 4.7. Feynman diagrams that generate three and four-body forces among the constituents of a baryon

a smooth large-N_C limit causes the typical extension of a baryon $\langle r^2 \rangle = \langle \Psi | \sum_i \boldsymbol{r}_i^2 | \Psi \rangle / N_C$ to be $\mathcal{O}(N_C^0)$.

The main observation above is that the average potential seen by a prescribed quark in the baryon is $\mathcal{O}(N_C)$. This is not surprising for the one gluon exchange. When including relativistic effects we also have to consider three- and four-body forces that arise from the non-abelian character of QCD. Typical examples are shown in Fig. 4.7. There are (approximately) N_C^3 and N_C^4 combinations of quarks that interact via three- and four-body forces, respectively. The corresponding coupling constants are $g_{QCD}^4 = g^4/N_C^2$ and $g_{QCD}^6 = g^6/N_C^3$, so that that they contribute at leading order, $\mathcal{O}(N_C)$ but do not induce higher powers of N_C in the variational functional, (4.9). Thus the Hartree character of the wave function remains intact. So, no matter how complicated (and probably infeasible) the relativistic Hartree problem is, baryon masses are $\mathcal{O}(N_C)$ and their radii are $\mathcal{O}(N_C^0)$.

Figure 4.8 shows typical one gluon exchange contributions to baryon–baryon and meson–baryon scattering. In the case of baryon–baryon scattering we may pick the one gluon exchange from N_C^2 constituents. Together with the factor g_{QCD}^2 these diagrams contribute $\mathcal{O}(N_C)$ to the energy of the two-baryon system, i.e., at the same order as the baryon mass. Thus, the Hartree approximation to the corresponding $2N_C$ body wave function

$$\Psi(\boldsymbol{r}_1, \ldots \boldsymbol{r}_{2N_C}) = \sum_P (-1)^P \Big[\prod_{i=1}^{N_C} \phi_1(\boldsymbol{r}_i) \Big] \Big[\prod_{j=1}^{N_C} \phi_2(\boldsymbol{r}_j) \Big] \tag{4.10}$$

with anti-symmetrization between quarks from different baryons insures a smooth large-N_C limit for the single quark components ϕ_i. Hence the baryon–baryon scattering amplitude also has a smooth limit. The situation is different for meson–baryon scattering. Since we can only pick a single quark from

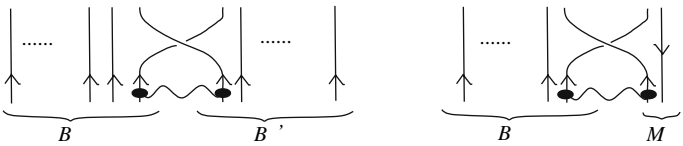

Fig. 4.8. Single gluon exchange contributions to baryon–baryon (*left*) and meson–baryon (*right*) scattering

the meson, the one gluon exchange contribution to the energy functional is $\mathcal{O}(N_C^0)$, i.e., of the same order as the meson mass but suppressed compared to the baryon mass. Since this implies that the (infinitely heavy) baryon is essentially unaffected by the scattering process and only the meson reacts. In a mathematical language this means that the baryon piece (ϕ) in the $N_C + 2$ body Hartree wave function

$$\Psi(\boldsymbol{r}_1, \ldots \boldsymbol{r}_{N_C}; \boldsymbol{x}, \boldsymbol{y}, t) = \sum_P (-1)^P \Big[\prod_{i=1}^{N_C} \phi(\boldsymbol{r}_i, t) \Big] u(\boldsymbol{x}, \boldsymbol{y}, t) \tag{4.11}$$

is the same as in (4.8) up to corrections of $\mathcal{O}(1/N_C)$. In (4.11) we have made explicit the time dependence. The anti-symmetrization is with respect to the color coordinates of the quarks in the baryon and the quark in the meson. Then the wave function is symmetric under the exchange of the quarks' spatial coordinates, $\boldsymbol{r}_i$ and $\boldsymbol{x}$. The meson part of the wave function $u(\boldsymbol{x}, \boldsymbol{y}, t)$ satisfies a *linear* integrodifferential equation [3],

$$\begin{aligned} \mathrm{i}\frac{\partial}{\partial t} u(\boldsymbol{x}, \boldsymbol{y}, t) = {} & \frac{-1}{2M} \left(\boldsymbol{\partial}_x^2 + \boldsymbol{\partial}_y^2 \right) u(\boldsymbol{x}, \boldsymbol{y}, t) - g^2 \frac{u(\boldsymbol{x}, \boldsymbol{y}, t)}{|\boldsymbol{x} - \boldsymbol{y}|} \\ & - g^2 \phi(\boldsymbol{x}) \int \mathrm{d}^3 z \phi^*(\boldsymbol{z}, t)\, u(\boldsymbol{z}, \boldsymbol{y}, t) \left[\frac{1}{|\boldsymbol{z} - \boldsymbol{x}|} + \frac{1}{|\boldsymbol{z} - \boldsymbol{y}|} \right] . \end{aligned} \tag{4.12}$$

The non-symmetric appearance of the coordinates $\boldsymbol{x}$ and $\boldsymbol{y}$ under the integral stems from the fact that the anti-quark coordinate $\boldsymbol{y}$ is not subject to anti-symmetrization in (4.11). The waveequation (4.12) describes the scattering of a meson in a background potential parameterized by $\phi(\boldsymbol{r})$, i.e., generated by the baryon field. Obviously $u(\boldsymbol{x}, \boldsymbol{y}, t)$ is $\mathcal{O}\left(N_C^0\right)$ and so are the meson–baryon scattering data that are extracted thereof.

Finally we have to ask how to put together the large-N_C considerations for mesons and baryons. The two meson scattering processes defines an effective coupling constant, g_{eff} for the (equivalent) meson theory. Equation (4.5) shows that

$$g_{\text{eff}} = \Gamma^{(2)} \propto \frac{1}{N_C} . \tag{4.13}$$

In turn we may rephrase the N_C dependences of baryon properties via g_{eff},

- Baryon masses are proportional to $1/g_{\text{eff}}$.
- Baryon radii are $\mathcal{O}\left(g_{\text{eff}}^0\right)$.
- Meson–baryon scattering amplitudes are also $\mathcal{O}\left(g_{\text{eff}}^0\right)$. (4.14)

In particular the first of these properties is obviously of non-perturbative nature. In Chap. 1 we have already discussed that solitons are non-perturbative objects in field theories. As a matter of fact the behavior (4.14) on the effective meson coupling is characteristic for soliton configurations. In the next section we will verify these properties for the simple example of the kink soliton in the ϕ^4 theory. This congeneric behavior with g_{eff} has led to the conjecture [3] that baryons emerge as the soliton solutions in the effective meson theory that becomes equivalent to QCD in the large-N_C limit.

Note that there is a conceptual difference to the motivation of the soliton picture put forward in Chaps. 2 and 3. In those chapters we intensively studied the fermion determinant and its gradient expansion. In particular the observation that the chiral field carries baryon number via vacuum polarization effects resulted from identifying the gradient expansion of the baryon current, cf. Appendix C. For any gradient expansion to be sensible an energy scale is required to which the potentially small gradients are compared. In the case of the fermion determinant the scale is set by the constituent quark mass, i.e., the scale of dynamical chiral symmetry breaking. On the other hand, the avenue via large $N_{\rm C}$ does not refer to chiral symmetry at all; even the number of flavors is unessential and one would expect these arguments to also hold if QCD had only a single (light) quark. No meson theory (that were to be mainly characterized by the $U_{\rm A}(1)$ anomaly, (2.5)) is known that supports a soliton solution to be identified as a baryon. This has triggered some criticism of the soliton picture [8]. Indeed a sole motivation via large $N_{\rm C}$ is not absolutely compelling. However, the previous chapters have shown that chiral symmetry breaking induces strong enough coupling to the meson fields that solitons with baryon number emerge. In turn their properties are completely consistent with the results of large-$N_{\rm C}$ QCD, (4.14).

4.3 A Simple Soliton

Here we briefly review the so-called kink soliton as a simple example for a classical soliton in $D = 1{+}1$ dimensions. See [9] for a more thorough discussion as well as additional examples. The model Lagrangian contains a fourth order self-interaction

$$\mathcal{L}_{\rm kink} = \frac{1}{2}(\dot{\Phi}^2 - \Phi'^2) - \frac{\lambda}{4}\left(\Phi^2 - \frac{m^2}{\lambda}\right)^2 \tag{4.15}$$

for the scalar field Φ. Obviously we identify $\lambda \sim g_{\rm eff}$ as the effective meson coupling constant, $\Gamma^{(4)}$. To complete the analogy with the large-$N_{\rm C}$ discussion we demand that m remains constant when $g_{\rm eff}$ is changed.

There are two distinct vacuum configurations $\Phi = \pm\frac{m}{\sqrt{\lambda}}$. It is straightforward to verify that classically the Lagrangian, (4.15), has static[2] stationary points

$$\Phi_\pm(x) = \pm\frac{m}{\sqrt{\lambda}}\tanh\left(\frac{m}{\sqrt{2}}\,x\right), \tag{4.16}$$

that mediate between these vacua. This profile function is called the kink soliton and is shown in Fig. 4.9. Obviously this solution exhibits a non-perturbative (even non-analytic) dependence on the coupling constant, λ. Asymptotically, as $x \to \pm\infty$ this profile function approaches either of the

[2] Time-dependent solutions can be constructed via Lorentz boosts.

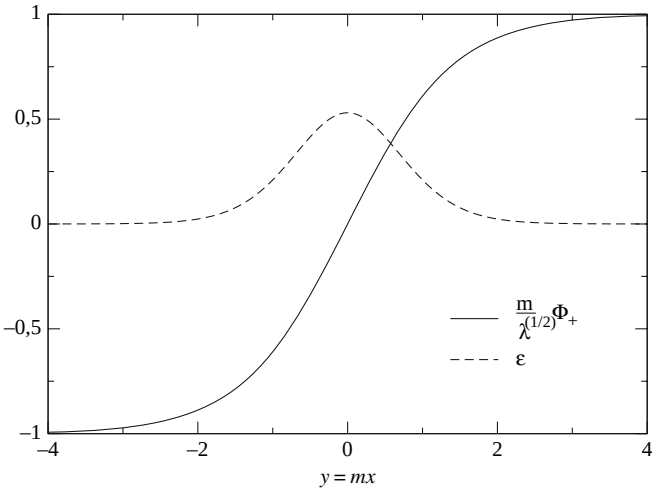

Fig. 4.9. The radial dependence of the kink profile, $\Phi_+(x)$ in units of $m/\sqrt{\lambda}$ and its energy density ϵ, i.e., the normalized integrand of (4.17)

two vacua. This is necessary for the total energy to be finite. This energy functional can be easily obtained from the Lagrangian, (4.15), since for static configurations we always have $E = -\int \mathrm{d}x \mathcal{L}$. Substituting the profile, (4.16), yields

$$E_+ = \int_{-\infty}^{\infty} \mathrm{d}x \left\{ \frac{1}{2}\Phi_+'^2 + \frac{\lambda}{4}\left(\Phi_+^2 - \frac{m^2}{\lambda}\right)^2 \right\} = \frac{2\sqrt{2}}{3}\frac{m^3}{\lambda} = \mathcal{O}\left(1/g_{\mathrm{eff}}\right) , \quad (4.17)$$

where the prime denotes the derivative with respect to the spatial coordinate, x. Equation (4.17) manifestly meets the first of the conditions in (4.14). To measure the extension of the kink we compute the expectation value $\langle x^2 \rangle$ of the kink with respect to the energy density,

$$\begin{aligned} \langle x^2 \rangle &= \frac{1}{E}\int_{-\infty}^{\infty} \mathrm{d}x\, x^2 \left\{ \frac{1}{2}\Phi_+'^2 + \frac{\lambda}{4}\left(\Phi_+^2 - \frac{m^2}{\lambda}\right)^2 \right\} \\ &= \frac{1}{m^2}\left(\frac{\pi^2}{6} - 1\right) = \mathcal{O}\left(g_{\mathrm{eff}}^0\right) , \end{aligned} \quad (4.18)$$

again in correspondence with (4.14). To discuss the analog of meson–baryon scattering we introduce time-dependent fluctuations about the kink, $\Phi(x,t) = \Phi_+(x) + \eta(x,t)$. These fluctuations are the meson wave functions in the kink background and their linearized equations of motion are

$$\begin{aligned} 0 &= \left[\frac{\partial^2}{\partial t^2} - \frac{\partial^2}{\partial x^2} - m^2 + 3\lambda\Phi_+^2(x)\right]\eta(x,t) \\ &= \left[\frac{\partial^2}{\partial t^2} - \frac{\partial^2}{\partial x^2} - m^2 + 3m^2 \tanh\left(\frac{m}{\sqrt{2}}\,x\right)\right]\eta(x,t) . \end{aligned} \quad (4.19)$$

This is the kink model analog to (4.12). In (4.19) any dependence on the effective coupling constant has disappeared. Thus the wave function η and all scattering data extracted thereof are $\mathcal{O}(g_{\rm eff}^0)$. Hence the features of the large-$N_{\rm C}$ picture for baryons is met by this simple soliton.

There is one more interesting feature worth mentioning. The divergence of the current

$$j_\mu = \frac{\sqrt{\lambda}}{m}\,\epsilon_{\mu\nu}\partial^\nu\Phi \tag{4.20}$$

vanishes by pure definition. It is the $D = 1 + 1$ dimensional analog of the Goldstone–Wilczek current [10], see also (C.15). The corresponding (topological) charge

$$Q = \int \mathrm{d}x\, j_0 = \frac{\sqrt{\lambda}}{m}\,\left[\Phi(\infty) - \Phi(-\infty)\right] \tag{4.21}$$

measures the difference between the configurations at the spatial infinities. Since Q is conserved regardless of whether or not the equations of motion are satisfied, fluctuations like $\eta(x,t)$ will not alter its value. Hence profile functions with different charges cannot be smoothly connected by successive infinitesimal changes. For that reason profile functions fall into distinct, so-called topological classes that are characterized by the topological charge Q. In Sect. 4.6 we will observe that the baryon number current as obtained via the gradient expansion to the NJL model, see Appendix C, is the chiral model analog of (4.20).

4.4 Skyrme Model Soliton

Unlasting we will discuss the famous Skyrme model [11] as the prototype soliton picture for baryons. The resulting soliton solution is often referred to as the *Skyrmion*. It is amusing to note that this model for strong interactions emerged before the *invention* of quarks [12]. Essentially we want to apply the results (and conjectures) from the previous sections that baryons emerge as solitons to a physically sensible low-energy meson theory. The basic degrees of freedom should thus be the pions (and kaons for $N_{\rm f} = 3$) and the model Lagrangian should reflect all features of chiral symmetry. Hence the unique starting point is the non-linear σ-model Lagrangian, (2.40),

$$\mathcal{L}_{\rm nl\sigma} = \frac{f_\pi^2}{4}\,\mathrm{tr}\left[\partial_\mu U \partial^\mu U^\dagger\right], \tag{4.22}$$

that we already obtained as the leading order gradient expansion to the NJL model, (2.40). As for the NJL model soliton the *ansatz* of highest symmetry is of hedgehog type,[3] (3.22)

[3] In the Skyrme model context the chiral angle is often denoted $F(r)$ rather than $\Theta(r)$ for the NJL model. Also, as a pure matter of convention, the boundary conditions on $F(r)$ are such that $F(0) - F(\infty) = n\pi$ with positive n.

$$U(\boldsymbol{x}) = U_0(\boldsymbol{x}) \equiv \exp\left(\mathrm{i}\boldsymbol{\tau}\cdot\hat{\boldsymbol{x}}\,F(r)\right) \qquad \text{with} \qquad r = |\boldsymbol{x}|\,. \tag{4.23}$$

For this *ansatz* (4.22) yields the energy functional, $E = -\int \mathrm{d}^3x\mathcal{L}$,

$$E_{\mathrm{nl}\sigma}[F] = 2\pi f_\pi^2 \int_0^\infty \mathrm{d}r\,\left(r^2F'^2 + 2\sin^2 F\right)\,, \tag{4.24}$$

where the prime denotes the derivative with respect to the radial coordinate, r. Simple scaling arguments [13] show that $E_{\mathrm{nl}\sigma}[F(\lambda r)] = E_{\mathrm{nl}\sigma}[F(r)]/\lambda$ so that the chiral angle obtained as the stationary point of $E_{\mathrm{nl}\sigma}$ would ultimately vanish for $r \neq 0$ in any (iterative) variational approach. This conclusion remains unchanged even when explicit chiral symmetry breaking is included via the pion mass term

$$\mathcal{L}_{\mathrm{m}} = \frac{m_\pi^2 f_\pi^2}{4}\,\mathrm{tr}\left[U + U^\dagger - 2\right]\,. \tag{4.25}$$

which adds (3.26) (with $\Theta \to -F$) to the energy functional. A theory that contains stable solutions requires higher derivative terms and Skyrme suggested [11] the four derivative term,

$$\mathcal{L}_{\mathrm{Sk}} = \frac{1}{32e^2}\,\mathrm{tr}\left([\alpha_\mu,\alpha_\nu]\,[\alpha^\mu,\alpha^\nu]\right)\,, \qquad \alpha_\mu = U^\dagger\partial_\mu U\,, \tag{4.26}$$

which is only quadratic in the time derivatives as a result of the use of the commutator. Later this feature will be very advantageous in the quantization procedure. In (4.26) e is a free parameter. From the expansion, $\alpha_\mu = \mathrm{i}\boldsymbol{\tau}\cdot\partial_\mu\boldsymbol{\pi}/f_\pi + \ldots$, we observe that the coefficient of the four pion term is proportional to $1/(e^2f_\pi^4)$. Comparison with (4.5) reveals that $e = \mathcal{O}(1/\sqrt{N_{\mathrm{C}}})$. Putting (4.22), (4.25) and (4.26) together yields the classical energy functional

$$\begin{aligned} E_{\mathrm{cl}}[F] = \frac{2\pi f_\pi}{e}\int_0^\infty \mathrm{d}x\Bigg\{ & x^2F'^2 + 2\sin^2 F + 2\mu_\pi^2x^2\,(1-\cos F) \\ & +\sin^2 F\left(2F'^2 + \frac{\sin^2 F}{x^2}\right)\Bigg\}\,. \end{aligned} \tag{4.27}$$

The dimensionless quantities $x = ef_\pi r$ and $\mu_\pi = m_\pi/(ef_\pi)$ have been introduced and the prime denotes the derivative with respect to x. From what we have learnt about the large-N_{C} behavior of f_π and e we immediately conclude that $E_{\mathrm{cl}} = \mathcal{O}(N_{\mathrm{C}})$, as it should. Upon variation we find the stationary condition,

$$\left(x^2 + 2\sin^2 F\right)F'' + 2xF' - \sin 2F - \sin 2F\left(\frac{\sin^2 F}{x^2} + F'^2\right) = \mu_\pi^2x^2\sin F\,. \tag{4.28}$$

In the following sections we will argue that $F(0) = \pi$ and $F(\infty) = 0$ are suitable boundary conditions to represent unit baryon number configurations.

The corresponding numerical solution to (4.28) has the shape similar to $\Theta(r)$ in Fig. 3.3 with the sign reversed. Nevertheless there is one essential difference between the Skyrmion and the NJL model soliton. As seen from the last term in (4.27) finite static energy requires $F(0) = n\pi$ with n an integer. Stated otherwise, configurations with different values of the chiral angle at $r = 0$ (assuming all these configurations vanish at infinity) are separated by infinite energy barriers in the Skyrme model. Hence all configurations fall into distinct classes that are characterized by the integer $F(0)/\pi$. In Sect. 4.6 we will verify that this integer is indeed the topological charge. The numerical analysis yields $E_{\rm cl} = 72.9 f_\pi/e$ for the solution of (4.28) with $F(0) = \pi$ in the chiral limit $m_\pi = 0$. The parameter dependence cannot be completely factored when $m_\pi \neq 0$, yet the pion mass dependence is only weak.

For completeness we work out the asymptotic behavior of the chiral angle,

$$F(r) \xrightarrow[r\to\infty]{} A\,(1 + m_\pi r)\,\frac{\mathrm{e}^{-m_\pi r}}{r^2}\,. \tag{4.29}$$

This solution is obtained by linearizing the equation of motion (4.28) in F. The constant of proportionality, A, is determined by solving the full differential equation and matching to $F(0) = n\pi$. In the chiral limit, $m_\pi = 0$, the chiral angle decays only with a power law, rather than exponentially.

4.5 Equations of Motion and Wess–Zumino Term

We have already explained that the effective meson action should be augmented by the Wess–Zumino term, (2.50). In Sect. 2.4 we have seen that it arises because the regularized fermion action is not invariant under axial transformations and in Appendix C we argue that it is needed to model the baryon number current after integrating out the fermions. In this section we will repeat Witten's argument for including the Wess–Zumino term [14]. This is particularly interesting because it does not make direct reference to quarks but rather relies on the pseudoscalar nature of the pions and kaons for which the effective meson theory is constructed.

Due to chiral invariance the *local* Lagrangian will be of the form

$$\mathcal{L} = \sum_n c^{(n)}_{\mu_1,\ldots,\mu_{2n}}\ \mathrm{tr}\ [\alpha^{\mu_1,\ldots,\mu_{2n}}]\ . \tag{4.30}$$

The constants $c^{(n)}$ can only be constructed from the tensors $g_{\mu\nu}$ and $\epsilon_{\mu\nu\rho\sigma}$. The $\alpha^{\mu_1,\ldots,\mu_{2n}}$ are either powers of α^μ or derivatives thereof. The contributions that have $c^{(n)}$s completely built from $g_{\mu\nu}$ will ultimately be invariant under parity reflection,

$$\Pi: \quad t \to t \quad \text{and} \quad \boldsymbol{x} \to -\boldsymbol{x}\,. \tag{4.31}$$

The simplest term that involves the Levi–Cevita tensor is

$$\epsilon_{\mu\nu\rho\sigma}\,\mathrm{tr}\,[\alpha^\mu\alpha^\nu\alpha^\rho\alpha^\sigma] = 0\,, \tag{4.32}$$

since this tensor is anti-cyclic in four space–time dimensions. Other (higher order) terms involving $\epsilon_{\mu\nu\rho\sigma}$ can similarly be argued to vanish or to be total derivatives. Hence the effective meson theory seems to be invariant under the transformation, (4.31). However, that is too much of a symmetry. The basic fields of the theory should be pseudoscalars, i.e., under parity they should transform as

$$\Pi: \quad \boldsymbol{\pi}(\boldsymbol{x},t) \to -\boldsymbol{\pi}(-\boldsymbol{x},t) \qquad \Leftrightarrow \qquad U(\boldsymbol{x},t) \to U^\dagger(-\boldsymbol{x},t)\,. \tag{4.33}$$

The theory should be invariant *only* under the combined transformations, (4.31) and (4.33). But we face the difficulty that in $D = 3+1$ dimensions no *local* Lagrangian accomplishes that requirement. The situation is similar to the classical mechanics problem of a particle with charge e moving in the field of a magnetic monopole [15, 16] on a sphere of unit radius.[4] The force on the particle is

$$\boldsymbol{F}_{\mathrm{mag.mon.}} = e\dot{\boldsymbol{x}} \times \boldsymbol{B} = \frac{eg}{r^3}\,\dot{\boldsymbol{x}} \times \boldsymbol{x}\,. \tag{4.34}$$

There is no Lagrange function that via the Euler–Lagrange equations of motion yields this force on the very right hand side. In general, the action

$$e\int \mathrm{d}t^{\cdot} \cdot \boldsymbol{A} = e\int_C \mathrm{d}\boldsymbol{x}\cdot\boldsymbol{A}\,, \tag{4.35}$$

leads upon variation to the Lorentz force in the middle of (4.34). For the special case of the magnetic monopole a singular vector potential, $\boldsymbol{A}$ is required to ensure both, $\boldsymbol{B} = \boldsymbol{\partial}\times\boldsymbol{A}$ and $\boldsymbol{\partial}\cdot\boldsymbol{B} = 0$. In classical mechanics it suffices to consider the equation of motion (4.34) and the actual value of the action is of minor importance. This is no longer the case when quantizing the system. Then we investigate the generating functional

$$Z[T] = \int_{\boldsymbol{x}(T)=\boldsymbol{x}(0)} [\mathrm{d}\boldsymbol{x}]\,\exp\left\{\frac{\mathrm{i}}{\hbar}\left[\ldots + e\oint_C \mathrm{d}\boldsymbol{x}\cdot\boldsymbol{A}\right]\right\}, \tag{4.36}$$

where the ellipsis denote the non-interaction pieces of the action. Obviously only closed trajectories C need to be considered and we may utilize Stoke's theorem to reintroduce the magnetic field,

$$e\oint_{\partial S} \mathrm{d}\boldsymbol{x}\cdot\boldsymbol{A} = e\int_S \mathrm{d}\boldsymbol{S}\cdot\boldsymbol{B}\,. \tag{4.37}$$

The choice of the two-dimensional surface S whose boundary is ∂S, which is the physical trajectory is not unique. There always exists the complementary surface $\bar{S}$ with the same boundary. Since $S\cup\bar{S} \sim \mathbb{S}_2$, which is the surface

[4] The unitary condition $U^\dagger U = \mathbb{1}$ translates into $r = |\boldsymbol{x}| = 1$ for this example.

onto which the particle is constrained, and the orientations of S and $\bar{S}$ are opposite, the fact that the choice should not affect the action implies

$$\frac{e}{\hbar}\oint_{\mathbb{S}_2} \mathrm{d}\boldsymbol{S}\cdot\boldsymbol{B} = 2n\pi\,, \tag{4.38}$$

with n an integer. Substituting the monopole magnetic field yields the celebrated monopole charge quantization rule

$$eg = \frac{n}{2}\,\hbar\,. \tag{4.39}$$

When expressed in terms of the physical field $\boldsymbol{B}$, the action, (4.37), involves integration over an additional coordinate. In analogy we add a five-dimensional integral to the mesonic action [14]

$$\Gamma_{\mathrm{WZ}} = \mathrm{i}\lambda\,\epsilon_{\mu\nu\rho\sigma\tau}\int_{M_5}\mathrm{d}^5x\,\mathrm{tr}\,[\alpha^\mu\alpha^\nu\alpha^\rho\alpha^\sigma\alpha^\tau]\,, \tag{4.40}$$

with the condition that the boundary of the manifold M_5 is the physical four-dimensional Minkowski space, $\partial M_5 = M_4$. At this point λ is still a free parameter. We want to obtain the corresponding equations of motion for the pseudoscalar fields from the variation principle. A possible parameterization of the variation is local chiral transformation of the chiral field

$$U(x) \to U(x)\,\mathrm{e}^{\mathrm{i}\epsilon(x)} \tag{4.41}$$

where $\epsilon(x)$ is a hermitian $N_\mathrm{f}\times N_\mathrm{f}$ matrix field. To linear order we find,

$$\alpha_\mu \to \alpha_\mu + \mathrm{i}\partial_\mu\epsilon + \ldots\,. \tag{4.42}$$

The ellipsis indicate terms that do not contain derivatives of ϵ. Because of the global axial symmetry of the action they ultimately cancel. For the discussion of the parity properties it suffices to consider the non-linear σ model, (4.22), as a representative for the contributions allowed in (4.30). For the variation of $\Gamma = \int \mathrm{d}^4x\mathcal{L}_{\mathrm{nl}\sigma} + \Gamma_{\mathrm{WZ}}$ we find

$$\begin{aligned}\delta\Gamma &= \frac{f_\pi^2}{2}\int_{M_4}\mathrm{d}^4x\,\mathrm{tr}\,[\mathrm{i}\alpha_\mu\partial^\mu\epsilon] + 5\mathrm{i}\lambda\epsilon_{\mu\nu\rho\sigma\tau}\int_{M_5}\mathrm{d}^5x\,\mathrm{tr}\,[(\mathrm{i}\partial^\mu\epsilon)\,\alpha^\nu\alpha^\rho\alpha^\sigma\alpha^\tau]\\ &= \frac{f_\pi^2}{2}\int_{M_4}\mathrm{d}^4x\,\mathrm{tr}\,[\mathrm{i}\alpha_\mu\partial^\mu\epsilon] + 5\mathrm{i}\lambda\epsilon_{\mu\rho\sigma\tau}\int_{M_4}\mathrm{d}^4x\,\mathrm{tr}\,[(\mathrm{i}\partial^\mu\epsilon)\,\alpha^\rho\alpha^\sigma\alpha^\tau]\,,\end{aligned} \tag{4.43}$$

where $\epsilon_{\mu\nu\rho\sigma}\alpha^\mu\alpha^\nu\alpha^\rho\alpha^\sigma = \epsilon_{\mu\nu\rho\sigma}\partial^\mu(\alpha^\nu\alpha^\rho\alpha^\sigma)$ and Stoke's theorem have been used to gain a purely four-dimensional functional. Hence we arrive at the equations of motion

$$\frac{f_\pi^2}{2}\,\partial_\mu\alpha^\mu + 5\mathrm{i}\lambda\epsilon_{\mu\nu\rho\sigma}\alpha^\mu\alpha^\nu\alpha^\rho\alpha^\sigma = 0\,. \tag{4.44}$$

The first term is odd in α_μ, as are all other contributions from (4.30), but the last term is even. Thus the transformation (4.33) that translates to

$$\alpha_\mu \to -U\alpha_\mu U^\dagger \quad \text{and} \quad \partial_\mu \alpha^\mu \to -U\partial_\mu \alpha^\mu U^\dagger\,, \tag{4.45}$$

causes a relative sign in (4.44). This is exactly compensated by the sign change due to (4.32). We have reached the desired result: The Wess–Zumino action is required in the effective meson theory to enforce the pseudoscalar nature of the Goldstone bosons.

4.6 Topological Structures

We have not yet determined the coefficient λ. The topological structure of the Wess–Zumino action can be used to further specify λ. But first we note that $\lambda \in \mathbb{R}$ follows from the equation of motion (4.44) and $\alpha_\mu^\dagger = -\alpha_\mu$.

There is a complementary manifold $\bar{M}_5$ that has the same boundary, M_4 as M_5 itself. As in the monopole example above, the choice on which of the two manifolds the Wess–Zumino action is computed must not alter the physics and therefore we demand,

$$\mathrm{i}\lambda\epsilon_{\mu\nu\rho\sigma\tau}\int_{M_5\cup\bar{M}_5} \mathrm{d}^5x\,\mathrm{tr}\,[\alpha^\mu\alpha^\nu\alpha^\rho\alpha^\sigma\alpha^\tau] = 2\pi n\,, \tag{4.46}$$

where n again is an integer. We evaluate the generating functional with initial and final time steps identified and thus $M_5 \cup \bar{M}_5$ is compact and isomorphic to $\mathbb{S}_5$. Consequently the left hand side of (4.46) is proportional to $Q = \int_{\mathbb{S}_5} \mathrm{d}^5x\, j_0$ where[5]

$$j_\mu(x) = \frac{\mathrm{i}}{480\pi^3}\,\epsilon_{\mu\nu\kappa\rho\sigma\tau}\mathrm{tr}\,[\alpha^\nu\alpha^\kappa\alpha^\rho\alpha^\sigma\alpha^\tau] \tag{4.47}$$

is the winding number current for the mapping $\mathbb{S}_5 \mapsto SU(3)$, cf. (4.20) that has the same structure in a lower dimensional context. Again "it" j_μ has zero divergence regardless of whether or not the equations of motion are satisfied. Therefore Q is conserved and actually is an integer for topological reasons.[6] Thus the condition, (4.46) translates into

$$\lambda = \frac{n}{240\pi^2}\,. \tag{4.48}$$

The physics requirement that upon gauging Γ_{WZ} with respect to the electromagnetic interaction reproduces the QCD result for the decay $\pi^0 \to \gamma\gamma$ finally gives the condition that this integer equals the number of color degrees of freedom, i.e., $n = \pm N_{\mathrm{C}}$; see Sect. C.4 in Appendix C. A particular choice of the phase yields (2.50), which is repeated here for completeness,

[5] In general, the winding number of the mapping $\mathbb{S}_{2n+1} \mapsto SU(n+1)$ is $Q = \left(\frac{\mathrm{i}}{2\pi}\right)^{n-1}\frac{n!}{(2n+1)!}\,\epsilon_{\mu_1\cdots\mu_{2n+1}}\int \mathrm{d}^{2n+1}x\,\mathrm{tr}\left[(U^\dagger\partial^{\mu_1}U)\cdots(U^\dagger\partial^{\mu_{2n+1}}U)\right]$ for $U \in SU(n+1)$ [17].

[6] The homotopy structure is $\Pi_5(SU(3)) \sim \Pi_5(\mathbb{S}_5) = \mathbb{Z}$.

$$\Gamma_{\rm WZ} = -\frac{{\rm i}N_C}{240\pi^2}\int_{M_5} {\rm d}^5x\,\epsilon^{\mu\nu\rho\sigma\tau}{\rm tr}\left[\alpha_\mu\alpha_\nu\alpha_\rho\alpha_\sigma\alpha_\tau\right]\,. \tag{4.49}$$

In Appendix C we discuss that the variation of the Wess–Zumino term due to gauge transformations of α_μ is local in ordinary space. So are the associated symmetry currents. In particular, gauging the $U_{\rm V}(1)$ symmetry defines the baryon number current, (C.26)

$$B_\mu = \frac{1}{24\pi^2}\,\epsilon_{\mu\nu\rho\sigma}\,{\rm tr}\left[\alpha^\nu\alpha^\rho\alpha^\sigma\right]\,, \tag{4.50}$$

which also has the form of a winding number current as in (4.20) and (4.47). It is the topological current for the mapping $\mathbb{S}_3 \mapsto SU(2)$. The soliton configurations assume the same values for all points at spatial infinity, e.g., $\lim_{r\to\infty} = \mathbb{1}$. That is, to characterize the mapping all these points are identified and the space $\mathbb{R}^3$ is compactified to $\mathbb{S}_3$. To describe mappings into $SU(N)$ we may consider pertinent $SU(2)$ subgroups thereof. Therefore $\mathbb{S}_3 \mapsto SU(2)$ is indeed the appropriate mapping for solitons in the chiral model. Most importantly it implies that the baryon number is not only conserved but indeed integer.

Substituting the hedgehog configuration, (4.23) yields

$$B_\mu = -F'\frac{\sin^2 F}{2\pi^2}\,g_{\mu 0}. \tag{4.51}$$

Hence configurations with boundary conditions $F(\infty) = 0$ and $F(0) = n\pi$ have baryon number n. In particular, the configuration with $F(0) = \pi$ has unit baryon number.

There is a lower bound for the energy of a configuration with a prescribed baryon number. Consider

$${\rm tr}\left(\frac{f_\pi}{2}\alpha_i \pm \frac{1}{4e}\epsilon_{ijk}\alpha_j\alpha_k\right)^2 = {\rm tr}\left(\frac{f_\pi^2}{4}\alpha_i\alpha_i + \frac{1}{32e^2}\left[\alpha_i,\alpha_j\right]^2 \pm 6\frac{\pi^2}{e}f_\pi B_0\right)\,. \tag{4.52}$$

By construction the left hand side is non-negative. Hence integrating the right hand side yields the inequality

$$E_{\rm cl} \geq 6\frac{\pi^2}{e}f_\pi|B_0|\,, \tag{4.53}$$

for $m_\pi = 0$. This relation is often called the Bogomol'ny [18] bound because of its similarity to the energy bound for the 't Hooft–Polyakov monopole [19, 20], see also [9]. However, this bound was already known to Skyrme [11]. The unit baryon number hedgehog solution, (4.23), exceeds that bound by about 20%.

The Skyrme term, (4.26), is just one possibility to stabilize the soliton. Sometimes the six-order term

$$\mathcal{L}_6 = -\frac{\epsilon_6^2}{2}B_\mu\,B^\mu \tag{4.54}$$

is used instead or in addition to the Skyrme term, see e.g., [21, 22, 23]. This stabilizing term only has two time derivatives, as does the Skyrme term.

4.7 Vector Interactions

Certainly the Skyrmion is just the simplest possible soliton within hadron models. Actually it fails to properly describe a number of phenomena. Most of them can be accounted for by extending the effective model to also contain vector meson degrees of freedom. Here we will briefly sketch the idea of introducing them. For more details we refer to the reviews [24, 25, 26] on the incorporation of vector mesons into chiral Lagrangians and chiral soliton models. These vector meson models also provide some phenomenological motivation for the stabilizing terms (4.26) and (4.54).

Here we will present a phenomenologically motivated approach to incorporate vector degrees of freedom in a chiral invariant manner. We particularly sketch the so-called *massive gauge approach* of [27, 28, 29]. The *hidden symmetry approach* [26] applies different techniques to incorporate the ρ-meson in a chirally invariant way but ends up with the identical Lagrangian.

The major problem arises when one wishes to eliminate the axial vector field a_1 while keeping the ρ-meson *without* breaking the chiral symmetry. This elimination is desirable as the large a_1 mass suggests that it is not important for the description of low-energy hadron properties and keeping a_1 inflates the model and reduces its predictability. However, the corresponding field variable cannot simply be set to zero, after all the a_1 and ρ-mesons are chiral partners. We therefore start from the non-linear σ model, (4.22), together with left- and right-handed vector fields that transform like gauge fields under *local* chiral transformations that are defined by $U(x) \to L(x)U(x)R^\dagger(x)$:

$$\begin{aligned} A^\mu_{\mathrm{L}}(x) &\to L(x)\left(A^\mu_{\mathrm{L}}(x) + \frac{\mathrm{i}}{g}\,\partial^\mu\right) L^\dagger(x) \\ A^\mu_{\mathrm{R}}(x) &\to R(x)\left(A^\mu_{\mathrm{R}}(x) + \frac{\mathrm{i}}{g}\,\partial^\mu\right) R^\dagger(x)\,, \end{aligned} \tag{4.55}$$

which introduces the gauge coupling, g, as a new parameter. Its physical interpretation will be discussed shortly. Under parity these chiral fields transform into one another, $A^{\mathrm{L}}_\mu \leftrightarrow A^{\mathrm{R}\mu}$. The vector and axial-vector meson fields as introduced in Sect. 2.4 are sum and differences of A_L and A_R. It is then straightforward to gauge $\mathcal{L}_{\mathrm{nl}\sigma}$ to become invariant under local chiral symmetries. In the next step either of the fields A_{L} and A_{R} is to be eliminated in a chirally consistent way. This can, e.g., be accomplished by imposing the condition,

$$A^\mu_{\mathrm{L}} = U\left(A^\mu_{\mathrm{R}} + \frac{\mathrm{i}}{g}\,\partial^\mu\right) U^\dagger. \tag{4.56}$$

A convenient realization thereof introduces the ρ-meson field,

$$A^\mu_{\mathrm{L}} = \xi\left(\rho^\mu + \frac{\mathrm{i}}{g}\,\partial^\mu\right)\xi^\dagger \quad \text{and} \quad A^\mu_{\mathrm{R}} = \xi^\dagger\left(\rho^\mu + \frac{\mathrm{i}}{g}\,\partial^\mu\right)\xi \tag{4.57}$$

where $\xi = U^{1/2}$ is the root of the chiral field. Since under parity $\xi \leftrightarrow \xi^\dagger$, it is easy to verify that ρ^μ contains vector meson degrees of freedom only. Under the chiral transformation this vector field also behaves like a gauge field [30]

$$\rho_\mu \to K\left(\rho_\mu + \frac{\mathrm{i}}{g}\partial_\mu\right)K^\dagger \quad \text{and} \quad \xi \to L\xi K^\dagger = K\xi R^\dagger. \tag{4.58}$$

The last equation defines the matrix K. For vector transformations it is trivially solved by $L = R = K$ while for axial transformations, $L = R^\dagger$, the matrix K depends on the meson field configuration ξ.

As the realization (4.57) is merely a gauge transformation for the fields $A^\mu_{\mathrm{L,R}}$, the kinetic part for the vector mesons is uniquely given by

$$-\frac{1}{2}\mathrm{tr}\left[F_{\mu\nu}(\rho)F^{\mu\nu}(\rho)\right]. \tag{4.59}$$

Here $F_{\mu\nu}(\rho)$ denotes the field tensor associated with the vector mesons ρ and ω, which are incorporated via $\rho_\mu = (\omega_\mu \mathbb{1} + \boldsymbol{\rho}_\mu \cdot \boldsymbol{\tau})/2$ in the two-flavor reduction. The ρ-meson field acquires a mass by adding terms quadratic in $A^\mu_{\mathrm{L,R}}$ which are invariant under global chiral transformations only

$$\frac{m_0^2}{2}\mathrm{tr}\left[A_{\mathrm{L}\mu}A^\mu_{\mathrm{L}} + A_{\mathrm{R}\mu}A^\mu_{\mathrm{R}}\right] - \frac{B}{2}\mathrm{tr}\left[A_{\mathrm{L}\mu}UA^\mu_{\mathrm{R}}U^\dagger\right]. \tag{4.60}$$

The identical coefficients of the first two terms are demanded by parity invariance. Since (4.57) is a local chiral transformation that maps the chiral field U to the identity matrix, the gauged non-linear σ-model Lagrangian vanishes identically in this realization. Nevertheless $\mathcal{L}_{\mathrm{nl}\sigma}$ arises in the model when substituting the realization, (4.57), into the mass-type terms, (4.60). Identifying the parameters $4m_0^2 - 2B = m_{\mathrm{V}}^2$ and $4m_0^2 + 2B = g^2 f_\pi^2$ (m_{V} denotes the average ρ–ω meson mass) and adding a pseudoscalar mass term yields the normal parity part of the Lagrangian for pseudoscalar and vector mesons,

$$\begin{aligned}\mathcal{L}_{\mathrm{S}} = {} & f_\pi^2\mathrm{tr}\left[p_\mu p^\mu\right] + \frac{m_\pi^2 f_\pi^2}{2}\mathrm{tr}\left[U + U^\dagger - 2\right] \\ & -\frac{1}{2}\mathrm{tr}\left[F_{\mu\nu}(\rho)\,F^{\mu\nu}(\rho)\right] + m_{\mathrm{V}}^2\mathrm{tr}\left[R_\mu R^\mu\right].\end{aligned} \tag{4.61}$$

The fields

$$p_\mu = \frac{\mathrm{i}}{2}\left(\xi\partial_\mu\xi^\dagger - \xi^\dagger\partial_\mu\xi\right) \quad \text{and} \quad v_\mu = \frac{\mathrm{i}}{2}\left(\xi\partial_\mu\xi^\dagger + \xi^\dagger\partial_\mu\xi\right) \tag{4.62}$$

are proportional to the induced fields in (2.46) for the special choice $\xi_{\mathrm{L}}^\dagger = \xi_{\mathrm{R}} = \xi$. Since $p_\mu = \frac{\mathrm{i}}{2}\xi^\dagger\alpha_\mu\xi$, the first term is indeed $\mathcal{L}_{\mathrm{nl}\sigma}$. Furthermore the construction (4.58) ensures that $R_\mu = \rho_\mu - v_\mu/g$ transforms simply under chiral transformations: $R_\mu \to KR_\mu K^\dagger$. The last term in (4.61) not only contains the ρ-meson mass term but also the $\rho\pi\pi$ vertex

$$m_{\rm V}^2 {\rm tr}\left[R_\mu R^\mu\right] = \frac{m_{\rm V}^2}{2}\left\{\boldsymbol{\rho}_\mu\cdot\boldsymbol{\rho}^\mu + \frac{1}{gf_\pi^2}\,\boldsymbol{\rho}_\mu\cdot(\boldsymbol{\pi}\times\partial^\mu\boldsymbol{\pi}) + \ldots\right\}. \tag{4.63}$$

Utilizing the experimental data for the pion decay constant $f_\pi = 93\,\mathrm{MeV}$ and the width $\Gamma(\rho\to 2\pi)\approx 151\,\mathrm{MeV}$ [31] finally fixes the gauge coupling constant $g\approx 5.6$.

It is interesting to consider a large mass expansion for the ρ-meson. The leading order term $R_\mu = 0$ gives $\rho_\mu = \frac{v_\mu}{g}$. Subsequent substitution,[7]

$$-\frac{1}{2}{\rm tr}\left[F_{\mu\nu}\left(\frac{v}{g}\right)F^{\mu\nu}\left(\frac{v}{g}\right)\right] = \frac{1}{32g^2}\,{\rm tr}\left\{[\alpha_\mu,\alpha_\nu]\,[\alpha^\mu,\alpha^\nu]\right\} \tag{4.64}$$

suggests to identify the Skyrme constant (4.26) as $e = g$ and thus extract it from meson phenomenology.

In order to complete the vector meson model Lagrangian the anomalous terms that contain the Levi–Cevita tensor, $\epsilon_{\mu\nu\alpha\beta}$ have to be added. For their presentation it is most useful to introduce the notation of differential forms: $A^{\rm R} = A^{\rm R}_\mu {\rm d}x^\mu$, ${\rm d} = \partial_\mu {\rm d}x^\mu$, etc. (cf. Appendix C). Since the left and right "gauge fields" are related via the chiral constraint, (4.56), the number of linear independent terms, which transform properly under the chiral transformation as well as parity and charge conjugation, is quite limited [27, 28, 29]:

$$A^{\rm L}\alpha^3\,,\ {\rm d}A^{\rm L}\alpha A^{\rm L} - A^{\rm L}\alpha\,{\rm d}A^{\rm L} + A^{\rm L}\alpha A^{\rm L}\alpha\,,\ 2\left(A^{\rm L}\right)^3\alpha + \frac{\rm i}{g}A^{\rm L}\alpha A^{\rm L}\alpha\,. \tag{4.65}$$

Rewriting these combinations in terms of the field variables of (4.61) yields the abnormal parity part of the action

$$\begin{aligned}\Gamma_{\rm an} = {}& \frac{2N_{\rm C}}{15\pi^2}\int {\rm Tr}(p^5) \\ & + \int {\rm Tr}\left[\frac{4{\rm i}}{3}(\gamma_1+\frac{3}{2}\gamma_2)Rp^3 - \frac{g}{2}\gamma_2 F(\rho)(pR-Rp) - 2{\rm i}g^2(\gamma_2+2\gamma_3)R^3p\right].\end{aligned} \tag{4.66}$$

The first term is nothing but the Wess–Zumino term. The additional parameters γ_1,γ_2 and γ_3 correspond to the invariant terms listed in (4.65). These parameters should ultimately be fixed from meson properties. In [29] two of the three unknown constants, $\gamma_{1,2,3}$ were determined from purely strong interaction processes like $\omega\to 3\pi$. Defining $\tilde{h} = -2\sqrt{2}\gamma_1/3$, $\tilde{g}_{VV\phi} = g\gamma_2$ and $\kappa = \gamma_3/\gamma_2$ the central values $\tilde{h} = \pm 0.4$ and $\tilde{g}_{VV\phi} = \pm 1.9$ were found. Within experimental uncertainties (stemming from the errors in the $\omega-\phi$ mixing angle) these may vary in the range $\tilde{h} = -0.15,\ldots,0.7$ and $\tilde{g}_{VV\phi} = 1.3,\ldots,2.2$ subject to the condition $|\tilde{g}_{VV\phi} - \tilde{h}|\approx 1.5$. The third parameter, κ could not be fixed in the meson sector. As we will see later, a value around $\kappa\approx 1$ is favored from predictions on baryon properties in the soliton picture.

[7] Direct computation gives $F_{\mu\nu}\left(\frac{v}{g}\right) = \frac{-{\rm i}}{4g}\xi^\dagger\,[\alpha_\mu,\alpha_\nu]\,\xi$ [24]. The conventions of [24] for the ρ-field and the coupling g differ from the present ones such that the product $g\rho_\mu$ is the same.

As mentioned before, the action, (4.66) contains the ω–3π coupling. It is of the form $\mathcal{L}_{\omega 3\pi} = g_\omega \omega_\mu B^\mu$ with $g_\omega = 2\pi^2(2\gamma_1 + 3\gamma_2)$. Eliminating the ω-meson in a large mass expansion similar to (4.64) produces the sixth order term, (4.54), with $\epsilon_6^2 = \dfrac{g_\omega^2}{m_{\rm V}^2}$.

The full vector meson action, $\int \mathrm{d}^4x \mathcal{L}_{\rm S} + \Gamma_{\rm an}$, contains static soliton solutions. The appropriate *ansätze* with zero grand spin are

$$\xi(\boldsymbol{x}) = \exp\left(\frac{\mathrm{i}}{2}\hat{\boldsymbol{x}}\cdot\boldsymbol{\tau}F(r)\right)\ ,\ \omega_0(\boldsymbol{x}) = \frac{\omega(r)}{g}\ ,\ \rho_{i,a}(\boldsymbol{x}) = \frac{G(r)}{gr}\,\epsilon_{ija}\hat{x}_j\ , \quad (4.67)$$

while all other field components vanish. Again, the isovector component of the vector fields assumes the Wu–Yang structure. Typical profile functions that minimize the energy functional (primes denote derivatives with respect to the radial coordinate r)

$$\begin{aligned} E[F,\omega,G] = 4\pi \int \mathrm{d}r \Big\{ & \frac{f_\pi^2}{2}\left(F'^2 r^2 + 2\sin^2 F\right) + m_\pi^2 f_\pi^2 (1-\cos F) r^2 \\ & -\frac{r^2}{2g^2}(\omega'^2 + m_{\rm V}^2\omega^2) + \frac{1}{g^2}\left[G'^2 + \frac{G^2}{2r^2}(G+2)^2\right] \\ & +\frac{m_{\rm V}^2}{g^2}\left(1+G-\cos F\right)^2 + \frac{\gamma_1}{g}F'\omega\sin^2 F \\ & -\frac{\gamma_2}{g}G'\omega\sin^2 F + \frac{\gamma_3}{g}F'\omega\, G(G+2) \\ & +\frac{1}{g}\left(\gamma_2+\gamma_3\right)F'\omega\left[1-2(G+1)\cos F + \cos^2 F\right]\Big\} \end{aligned} \quad (4.68)$$

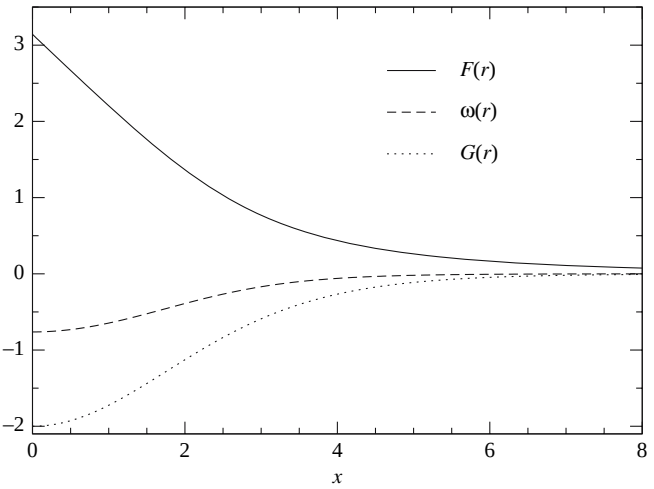

Fig. 4.10. Profile functions of the soliton configuration, (4.67) as functions of the dimensionless quantity $x = \sqrt{2} g f_\pi r$

are shown in Fig. 4.10. Again the boundary condition $F(0) = \pi$ and $F(\infty) = 0$ is chosen to comply with unit baryon number because the baryon number current is that of the purely pseudoscalar model, (4.50). Having established these boundary conditions for the chiral angle, the boundary values for the other fields, e.g., $G(0) = -2$, follow from the finite energy condition.

So far we have succeeded in constructing the soliton solutions in various models (NJL, Skyrme, vector mesons) and showing that these configurations carry unit baryon number. However, no other quantum number has been identified so far. That project will be the subject of the following chapters.

References

1. G. 't Hooft, *Nucl. Phys.* **B72** (1974) 461. 43
2. G. 't Hooft, *Nucl. Phys.* **B75** (1974) 461. 43
3. E. Witten, *Nucl. Phys.* **B160** (1979) 57. 44, 45, 47, 48, 50
4. E. Corrigan and P. Ramond, *Phys. Lett.* **B87** (1979) 73. 44
5. A. Cherman and T. D. Cohen, *JHEP* **0612** (2006) 035. 44
6. F. Sannino and J. Schechter, *Phys. Rev.* **D76** (2007) 014014. 44
7. C. Itzkson and J.-B. Zuber, *Quantum Field Theory*, Chap. 6.3.4. McGraw–Hill, New York, 1980. 46
8. R. L. Jaffe, *Phys. Rep.* **409** (2005) 1. 51
9. R. Rajaraman, *Solitons and Instantons*, Chapters 2 and 3. North Holland, Amsterdam, 1982. 51, 59
10. J. Goldstone and F. Wilczek, *Phys. Rev. Lett.* **47** (1981) 986. 53
11. T. H. R. Skyrme, *Proc. R. Soc. Lond.* **A260** (1961) 127. 53, 54, 59
12. M. Gell-Mann, *Phys. Lett.* **8** (1964) 214. 53
13. G. H. Derrick, *J. Math. Phys.* **5** (1964) 1252. 54
14. E. Witten, *Nucl. Phys.* **B223** (1983) 422, 433. 55, 57
15. P. A. M. Dirac, *Proc. R. Soc. Lond.* **A133** (1931) 60. 56
16. P. A. M. Dirac, *Phys. Rev.* **74** (1948) 817. 56
17. R. Bott and R. Seeley, *Commun. Math. Phys.* **62** (1978) 235. 58
18. E. B. Bogomolny, *Sov. J. Nucl. Phys.* **24** (1976) 449. 59
19. G. 't Hooft, *Nucl. Phys.* **B79** (1974) 276. 59
20. A. M. Polyakov, *JETP Lett.* **20** (1974) 194. 59
21. A. Jackson, A. D. Jackson, A. S. Goldhaber, G. E. Brown, and L. C. Castillejo, *Phys. Lett.* **B154** (1985) 101. 59
22. B. Schwesinger and H. Weigel, *Nucl. Phys.* **A465** (1987) 733. 59
23. B. Schwesinger and H. Weigel, *Nucl. Phys.* **A540** (1992) 461. 59
24. B. Schwesinger, H. Weigel, G. Holzwarth, and A. Hayashi, *Phys. Rep.* **173** (1989) 173. 60, 62
25. U. G. Meißner, *Phys. Rep.* **161** (1988) 213. 60
26. M. Bando, T. Kugo, and K. Yamawaki, *Phys. Rep.* **164** (1988) 217. 60
27. O. Kaymakcalan, S. Rajeev, and J. Schechter, *Phys. Rev.* **D30** (1984) 594. 60, 62
28. O. Kaymakcalan and J. Schechter, *Phys. Rev.* **D31** (1985) 1109. 60, 62
29. P. Jain, R. Johnson, U. G. Meißner, N. W. Park, and J. Schechter, *Phys. Rev.* **D37** (1988) 3252. 60, 62
30. C. G. J. Callan Jr., S. R. Coleman, J. Wess, and B. Zumino, *Phys. Rev.* **177** (1969) 2247. 61
31. S. Eidelman et al. [PDG], *Phys. Lett.* **B592** (2004) 1. 62

5

Soliton Quantization in Flavor SU(2)

In this chapter, we will illustrate the interpretation of the soliton solutions in effective meson theories as baryons. So far, we have not accomplished the important task of assigning good spin and flavor quantum numbers to the soliton. For this purpose, we will have to quantize rotational degrees of freedom both in coordinate and in flavor spaces. The hedgehog configuration, (4.23), is invariant under a combined coordinate and flavor rotation but not with respect to either of them separately. This means that the soliton "spontaneously" breaks rotational and flavor invariance: The ground state (in the unit baryon number sector) does not maintain the symmetries of the theory. On the other hand, any configuration that is related to the hedgehog by constant rotations in coordinate or flavor spaces is equally well a solution to the static equations of motion.

Ordinary quantization in field theory introduces (small amplitude) fluctuations and quantizes these degrees of freedom canonically. However, for a system with spontaneous symmetry breaking, there is an obstacle to that treatment. Due to the rotational symmetry, there is no restoring force for rotational excitations about the soliton. They become large amplitude fluctuations and must be treated differently. A common approach is to canonically quantize the collective coordinates that parameterize those large amplitude fluctuations. We will first establish that approach with the help of a simple quantum mechanical example. Before actually applying it to build nucleon and Δ states, we will discuss the quantization of the rigid top and introduce the concept of Euler angles as collective coordinates of the symmetry group $SU(N)$.

5.1 Collective Coordinates

Consider a mechanical system that is defined by a radially symmetric potential, $V(r)$, which supports a minimum at $r_0 \neq 0$. There are infinitely many

H. Weigel: *Soliton Quantization in Flavor SU(2)*, Lect. Notes Phys. **743**, 65–83 (2008)
DOI 10.1007/978-3-540-75436-7_5

configurations that minimize the system; all are related to one another by constant rotations.

The quantum mechanics for a particle of mass m is described by the Schrödinger-type equation in a partial wave decomposition

$$\mathrm{i}\frac{\partial}{\partial t}\psi_\ell(t,r) = \left[-\frac{1}{2m}\frac{\partial^2}{\partial r^2} + \frac{\ell(\ell+1)}{2mr^2} + V(r)\right]\psi_\ell(t,r)\,, \tag{5.1}$$

where ℓ is the orbital angular momentum quantum number. We assume that the potential V_0 is characterized by a coupling constant and that the angular barrier is of subleading order in the respective expansion. In the case of the chiral soliton that suppression factor is $1/N_\mathrm{C}$. In such a scenario, it is legitimate to first consider the potential separately and solve the eigenvalue equation for the S-wave channel, $\ell = 0$. The solutions are radial excitations just as, e.g., the harmonic oscillator levels in one dimension with wave functions $\psi_{n,\ell=0}(r)$. The corresponding rotational excitation energies are then obtained in first-order perturbation theory:

$$E^{(\mathrm{rot})}_{n,\ell} = \frac{\ell(\ell+1)}{2m\langle r_n^2\rangle}\,. \tag{5.2}$$

Here $\langle r_n^2\rangle = \langle n,0|r^2|n,0\rangle$ are the matrix elements with respect to the beforehand constructed states $\langle r|n\ell\rangle = \psi_{n,\ell}(r)$. In particular, we have for the ground state $\langle r_0^2\rangle = r_0^2$, which is the position of the minimum of the potential $V(r)$.

We will now explain how to obtain the spectrum, (5.2), in a semiclassical treatment with the help of collective coordinates. Classically, we want to solve for the trajectory $\boldsymbol{r}(t)$. The potential has a minimum at a non-zero value of the radius vector. To specify a solution we have to pick a direction, say $\boldsymbol{r}_0 = r_0\hat{\boldsymbol{e}}_z$. Of course, that is nothing but spontaneous symmetry breaking and provides a static solution to the classical problem. For quantization, however, we need to construct time-dependent trajectories. By construction, the (constant) transformation

$$\boldsymbol{r}_0 \longrightarrow D\,\boldsymbol{r}_0, \tag{5.3}$$

where $D = (D_{ij})$ is an orthogonal rotation matrix, does not alter the potential. It transforms the (spontaneously) chosen solution along the symmetries of the theory. It is thus suggestive that

$$\boldsymbol{r}(t) = r_0 D(t)\,\hat{\boldsymbol{e}}_z \tag{5.4}$$

is a reasonable approximation to the exact time-dependent solution. We substitute the *ansatz* equation (5.4) into the Lagrange function

$$L = \frac{m}{2}\,\dot{\boldsymbol{r}}^2 - V(r) = \frac{mr_0^2}{2}\left(\Omega_1^2 + \Omega_2^2\right) - V(r_0), \tag{5.5}$$

where the time derivative of the rotation matrixes enter via the angular velocities:

$$\Omega_i = \frac{1}{2}\epsilon_{ijk} D_{jl} \dot{D}_{kl} \,. \tag{5.6}$$

We consider (5.5) as a starting point and attempt to quantize the time-dependent degrees of freedom contained in D. These degrees of freedom are the collective coordinates and are suitably chosen as the three Euler angles:

$$D_{ij}(\Phi,\Theta,\Psi) = \begin{pmatrix} \cos\Phi & \sin\Phi & 0 \\ -\sin\Phi & \cos\Phi & 0 \\ 0 & 0 & 1 \end{pmatrix} \begin{pmatrix} 1 & 0 & 0 \\ 0 & \cos\Theta & \sin\Theta \\ 0 & -\sin\Theta & \cos\Theta \end{pmatrix} \begin{pmatrix} \cos\Psi & \sin\Psi & 0 \\ -\sin\Psi & \cos\Psi & 0 \\ 0 & 0 & 1 \end{pmatrix}_{ij} . \tag{5.7}$$

The resulting Lagrangian reads

$$L = \frac{m r_0^2}{2} \left(\dot{\Theta}^2 + \sin^2\Theta \, \dot{\Phi}^2 \right) - V(r_0) \,. \tag{5.8}$$

The kinetic part is of the general form $\dot{\xi}_i g_{ij}(\xi) \dot{\xi}_j$ where ξ_i are the dynamical variables while $g_{ij}(\xi)$ is a coordinate-dependent metric tensor. Such a term is quantized by substituting it in the Hamiltonian according to [1]:

$$\frac{1}{2} \dot{\xi}_i g_{ij}(\xi) \dot{\xi}_j \longrightarrow -\frac{1}{2\sqrt{g}} \frac{\partial}{\partial \xi_i} \left(g^{-1} \right)_{ij} \sqrt{g} \, \frac{\partial}{\partial \xi_j}, \tag{5.9}$$

where $g = \det(g_{ij})$. This yields

$$H = -\frac{1}{2 m r_0^2} \left(\frac{1}{\sin\Theta} \frac{\partial}{\partial\Theta} \sin\Theta \, \frac{\partial}{\partial\Theta} + \frac{\partial^2}{\partial\Phi^2} \right) + V(r_0) \,. \tag{5.10}$$

Obviously, the first part is nothing but the angular part of the three-dimensional Laplace operator written in Euler rather than polar and azimuthal angles. It can readily be diagonalized resulting in the energy eigenvalues

$$E_\ell = \frac{\ell(\ell+1)}{2 m r_0^2} + V(r_0) \,. \tag{5.11}$$

This is nothing but (5.2) for $n = 0$. We have thus established that collective coordinate quantization is a well-suited means to obtain the energy eigenvalues for rotational excitations on top of a degenerate ground state configuration. This treatment is absolutely legitimate and accurate when the rotational energy is of lower order in an eventual coupling constant than the potential energy.

5.2 Quantization of the $SU(N)$ Rigid Top

We will now apply the collective coordinate quantization to the Skyrmion. As in the mechanics analog above, the Skyrmion is a (ground state) configuration

that does not respect the basic symmetries of the theory, the rotations in coordinate and flavor spaces. And again, we will introduce collective coordinates that transform the chosen configuration along the symmetries of the model. Due to the hedgehog structure rotations in flavor and coordinate spaces are related and collective coordinates must only be introduced for one of the two symmetries. Stated otherwise, there is a combined flavor–coordinate transformation that leaves the hedgehog unchanged, and collective coordinates for that transformation do not appear in the Lagrangian. In the above example that corresponds to the angle Ψ. It parameterized rotations around the z-axis, which left the chosen ground state unchanged.

Let us first consider the $SU(2)$ case and then make a few general statements on $SU(N)$. The original rigid rotator quantization of the two-flavor soliton was performed by Adkins, Nappi and Witten [2]. For reviews, see [3, 4]. The *ansatz* analog to (5.4) is to introduce time-dependent $SU(2)$ matrices:

$$A(t) = \exp\left(\mathrm{i}\Phi(t)\frac{\tau_3}{2}\right)\exp\left(\mathrm{i}\Theta(t)\frac{\tau_2}{2}\right)\exp\left(\mathrm{i}\Psi(t)\frac{\tau_3}{2}\right) . \tag{5.12}$$

They parameterize the orientation of the hedgehog and approximate a time-dependent configuration via

$$U(\boldsymbol{x},t) = A(t)U_0(\boldsymbol{x})A^\dagger(t), \tag{5.13}$$

where $U_0(\boldsymbol{x})$ is the hedgehog configuration of (4.23). Originally, the authors of [2] used the parameterization $A(t) = a_4(t)+\mathrm{i}\boldsymbol{a}(t)\cdot\boldsymbol{\tau}$. However, this complicates matters because of the constraint $\sum_{i=1}^4 a_i^2(t) = 1$ and evades a straightforward generalization to $SU(3)$.

The Lagrange function of the rigid top arises from substituting the *ansatz*, (5.13), into the Skyrme model Lagrangian, $\mathcal{L}_{\mathrm{nl}\sigma}+\mathcal{L}_{\mathrm{Sk}}$, (4.22) and (4.26). Note that this Lagrangian is only quadratic in the time derivatives which simplifies matters and yields

$$L = \frac{1}{2}\alpha^2[F]\,\boldsymbol{\Omega}\cdot\boldsymbol{\Omega} - E_{\mathrm{cl}}[F], \tag{5.14}$$

where[1]

$$\alpha^2[F] = \frac{8\pi}{3}\int_0^\infty \mathrm{d}r r^2 \sin^2 F\left[f_\pi^2 + \frac{1}{e^2}\left(F'^2 + \frac{\sin^2 F}{r^2}\right)\right] \tag{5.15}$$

is a moment of inertia and

$$\boldsymbol{\Omega} = -\mathrm{itr}\left(A^\dagger(t)\dot{A}(t)\boldsymbol{\tau}\right) \tag{5.16}$$

is again an angular velocity. Numerically, one finds for the solution to (4.28) with $m_\pi = 0$ that $\alpha^2 = 51.2/(e^3 f_\pi)$. The scaling behavior of f_π and e shows that $\alpha^2 = \mathcal{O}(N_{\mathrm{C}})$. It is worth mentioning that α^2 quickly decreases as m_π is

[1] We adopt the notation of [5] although that is a paper on the $SU(3)$ Skyrmion.

switched on because the additional r^2 in the integrand pronounces the long-range behavior of the soliton. We explicitly write the Lagrange function in terms of the Euler angles, (5.12),

$$L = \frac{1}{2}\alpha^2[F]\left(\dot{\Phi}^2 + \dot{\Theta}^2 + \dot{\Psi}^2 + 2\cos\Theta\dot{\Phi}\dot{\Psi}\right) - E_{\rm cl}[F] \tag{5.17}$$

and apply the quantization rule (5.9) to obtain the Hamilton operator

$$\begin{aligned} H = E_{\rm cl}[F] - \frac{1}{2\alpha^2[F]}\Bigg[&\frac{1}{\sin\Theta}\frac{\partial}{\partial\Theta}\sin\Theta\frac{\partial}{\partial\Theta} \\ &+\frac{1}{\sin^2\Theta}\left(\frac{\partial^2}{\partial\Phi^2} - 2\cos\Theta\frac{\partial^2}{\partial\Phi\partial\Psi} + \frac{\partial^2}{\partial\Psi^2}\right)\Bigg]\,. \end{aligned} \tag{5.18}$$

The differential operator in H is nothing but the spin operator for the Wigner D-functions [6]:

$$HD^j_{mm'}(\Phi,\Theta,\Psi) = \left[E_{\rm cl}[F] + \frac{j(j+1)}{2\alpha^2[F]}\right]D^j_{mm'}(\Phi,\Theta,\Psi)\,. \tag{5.19}$$

So we have found the rotational spectrum of the Skyrmion. The rotational energy is proportional to $1/\alpha^2$. Hence, the eventual order parameter is $1/N_{\rm C}$ and indeed the rotational contribution to the energy is subleading which a posteriori justifies the collective coordinate method. We stress that the spectrum of any other two-flavor hedgehog soliton (e.g., NJL model, or vector mesons) is of identical structure in the two-flavor version, merely the numerical values for $E_{\rm cl}$ and α^2 vary; though their computation may become quite complicated as will be exemplified later.

We still have to provide a physical interpretation to the quantum numbers j, m and m'. To this end, consider

$$\begin{aligned} \boldsymbol{J} = \frac{\partial L}{\partial\boldsymbol{\Omega}} &= \alpha^2[F]\boldsymbol{\Omega} \\ &= \frac{1}{\sin\Theta}\begin{pmatrix}\cos\Psi\\ \sin\Psi\\ 0\end{pmatrix}p_\Phi + \begin{pmatrix}-\sin\Psi\\ \cos\Psi\\ 0\end{pmatrix}p_\Theta + \begin{pmatrix}-\cos\Psi\cot\Theta\\ -\sin\Psi\cot\Theta\\ 1\end{pmatrix}p_\Psi, \end{aligned} \tag{5.20}$$

where the time derivatives in $\boldsymbol{\Omega}$ have been replaced in favor of the conjugate momenta $p_\Phi = \frac{\partial L}{\partial\dot{\Phi}}$, etc. Assuming canonical commutation relations among the Euler angles and their conjugate momenta ($[\Psi, p_\Psi] = i$, etc.) yields

$$[J_a, J_b] = \mathrm{i}\epsilon_{abc}J_c. \tag{5.21}$$

i.e., these are $SU(2)$ operators and (minus) m' is the eigenvalue of J_3 [6]. The differential operator in (5.18) is nothing but $\boldsymbol{J}^2$ with eigenvalues $j(j+1)$. The rotated operators

$$I_a = -D_{ab}(A)J_b \quad \text{where} \quad D_{ab}(A) = \frac{1}{2}\mathrm{tr}\left[\tau_a A\tau_b A^\dagger\right] = D^{(1)}_{ab}(\Phi,\Theta,\Psi) \tag{5.22}$$

similarly satisfy $[I_a, I_b] = \mathrm{i}\epsilon_{abc} I_c$ while $[I_a, J_b] = 0$. In the next section, we will show that $\boldsymbol{I}$ and $\boldsymbol{J}$ indeed must be identified with the physical isospin and spin operators, respectively. Before doing so, we will find the generalization of (5.21) to $SU(N)$.

We parameterize the $N \times N$ unitary matrix A (with unit determinant) by collective coordinates ξ_a where $a = 1, \ldots, N^2 - 1$. Then we introduce angular velocities as

$$\Omega_a = h_{ba}(\xi_a)\dot{\xi}_b \quad \text{with} \quad h_{ba} = -2\mathrm{i}\,\mathrm{tr}\left[T_a A^\dagger \frac{\partial A}{\partial \xi_b}\right] . \tag{5.23}$$

The T_a are the generators in the defining representation, e.g., $T_a = \tau_a/2$ and $T_a = \lambda_a/2$ in $SU(2)$ and $SU(3)$, respectively. The h_{ba} are the Maurer–Cartan forms. Next we consider the general Lagrangian for the collective coordinates

$$L = \frac{1}{2}\Omega_a \Theta_{ab} \Omega_b - E_0 . \tag{5.24}$$

Here Θ_{ab} is a symmetric inertia tensor and E_0 a quantity that does not contain the generalized velocities $\dot{\xi}_b$. Neither Θ_{ab} nor E_0 depend on ξ_a. The conjugate momenta are

$$\pi_c = \frac{\partial L}{\partial \dot{\xi}_c} = h_{ca}\Theta_{ab} h_{b'b}\dot{\xi}_{b'} . \tag{5.25}$$

We furthermore define "spin" operators as

$$J_a = \frac{\partial L}{\partial \Omega_a} = \Theta_{ab} h_{b'b}\dot{\xi}_{b'} = \left(h^{-1}\right)_{aa'} \pi_{a'} . \tag{5.26}$$

We compute the commutator of the spin operators from the canonical commutators $[\pi_a, \xi_b] = -\mathrm{i}\delta_{ab}$;

$$\begin{aligned} [J_a, J_b] &= \left[\left(h^{-1}\right)_{aa'} \pi_{a'}, \left(h^{-1}\right)_{bb'} \pi_{b'}\right] \\ &= \mathrm{i}\left(h^{-1}\right)_{aa'} \left(h^{-1}\right)_{bb'} \left[\frac{\partial h_{b'c}}{\partial \xi_{a'}} - \frac{\partial h_{a'c}}{\partial \xi_{b'}}\right] J_c . \end{aligned} \tag{5.27}$$

Explicit commutation based on the definition, (5.23), reveals

$$\frac{\partial h_{ab}}{\partial \xi_c} = \frac{1}{2} h_{cc'} h_{aa'} f_{bc'a'} + \mathrm{i} H^{(b)}_{ac} , \tag{5.28}$$

where f_{abc} are the anti-symmetric structure constants of $SU(N)$ and the $H^{(b)}_{ac}$ are complicated functions of the coordinates ξ_a that are invariant under the exchange $a \leftrightarrow c$ and hence drop out when substituted into (5.27). Putting things together yields the expected generalization of (5.21):

$$[J_a, J_b] = \mathrm{i} f_{abc} J_c , \tag{5.29}$$

which is nothing but the $SU(N)$ algebra. That is, the "spin" operators are actually $SU(N)$ generators. Finally, we note that $\pi_a \dot{\xi}_a = J_a \Omega_a$ so that Hamiltonian is

$$H = J_a \Omega_a - L = \frac{1}{2} J_a \left(\Theta^{-1}\right)_{ab} J_b + E_0 \,. \tag{5.30}$$

For further interpretation, we compute the commutator

$$[J_a, A] = \frac{1}{\mathrm{i}} \left(h^{-1}\right)_{aa'} \frac{\partial A}{\partial \xi_{a'}} = A T_a \,. \tag{5.31}$$

That is, the spin operators are the *right* generators of $SU(N)$. They act like multiplying with generators from the *right* in the defining representation. Finally, we define *left* generators

$$L_a = -D_{ab} J_b \quad \text{with} \quad D_{ab} = 2\mathrm{tr}\left[T_a A T_b A^\dagger\right] . \tag{5.32}$$

L_a can be shown to satisfy $[L_a, A] = T_a A$ using the completeness relation, (2.27). Obviously, the left generators act as left multiplication with T_a. They also obey an $SU(N)$ algebra, $[L_a, L_b] = \mathrm{i} f_{abc} L_c$. In the context of the three-flavor model (Chap. 6), we will redefine $R_a = -J_a$ to compensate for the minus sign in (5.32). The R_a are sometimes referred to as the generators of the intrinsic $SU(N)$ group. The matrices D_{ab} describe the adjoint representation and satisfy $D \cdot D^\dagger = \mathbb{1}$, which follows again from the completeness relation and the fact that $A T_a A^\dagger$ is traceless.

It is amusing to note that the toy model in Sect. 5.1 can also be solved using the above-introduced $SU(N)$ techniques. We just have to supplement the Hamiltonian, (5.18), by the constraint $J_3 \equiv 0$. Since $[H, J_3] = 0$, this constraint can be immediately imposed onto the states, yielding the selection rule $m' = 0$. Then the eigenfunctions are spherical harmonics as $D^j_{m0}(\Phi, \Theta, \Psi) = \frac{4\pi}{\sqrt{j(j+1)}} Y_{jm}(\Theta, \Phi)$ and the eigenvalues are proportional to $j(j+1)$. Of course, the possibility to apply the $SU(2)$ rigid rotator techniques to that toy model merely reflects the isomorphism between $SU(2)$ and $SO(3)$.

5.3 Nucleon and Δ States

As indicated in the previous section, we identify indices m and m' in (5.19) with the isospin and spin projection quantum numbers of baryons. To this end, we have to construct the Noether currents and charges that arise from the infinitesimal transformations

$$U \to U - \boldsymbol{\epsilon} \cdot \left[U, \frac{\boldsymbol{\tau}}{2}\right] + \ldots \quad \text{and} \quad U \to U - \boldsymbol{\epsilon}' \cdot [\mathrm{i}\boldsymbol{x} \times \boldsymbol{\partial}, U] + \ldots \tag{5.33}$$

for isospin and coordinate rotations, respectively. Though we consider such Noether currents in the next section, there actually is a more elegant way to establish the desired identity. We can formally write the isospin charge as

$$\boldsymbol{I} = -\int \mathrm{d}^3 x \, \mathrm{tr} \left\{ \frac{\partial \mathcal{L}(\mathcal{U})}{\partial \dot{U}} \left[U, \frac{\boldsymbol{\tau}}{2}\right] + \mathrm{h.c.} \right\} , \tag{5.34}$$

where h.c. stands for Hermitian conjugate and $\mathcal{L}$ is the Lagrangian density under consideration, which is not necessarily constrained to be the Skyrme model. The rigid rotator parameterization, (5.13), implies

$$\dot{U} = A\left[\frac{\mathrm{i}}{2}\boldsymbol{\tau}\cdot\Omega, U_0\right]A^\dagger = \left[\frac{\mathrm{i}}{2}\boldsymbol{\tau}\cdot\boldsymbol{\Omega}', U\right], \tag{5.35}$$

where the definition of the angular velocity (5.16) has been inserted and $A\boldsymbol{\tau}\cdot\boldsymbol{\Omega}A^\dagger = \boldsymbol{\tau}\cdot\boldsymbol{\Omega}'$ implies that $\Omega_a = \Omega'_b D_{ba}$, cf. (5.22). Note that the only time dependence of the field configuration stems from the collective coordinates. We utilize the chain rule to write

$$\begin{aligned}\boldsymbol{I} &= -\int \mathrm{d}^3x\,\mathrm{tr}\left\{\frac{\partial\mathcal{L}(\mathcal{U})}{\partial\dot{U}}\frac{\partial\dot{U}}{\partial\boldsymbol{\Omega}'} + \mathrm{h.c.}\right\}\\ &= -\frac{\partial L[U]}{\partial\boldsymbol{\Omega}'} = -D\cdot\frac{\partial L[U]}{\partial\boldsymbol{\Omega}} = -\alpha^2 D\cdot\boldsymbol{\Omega}\end{aligned} \tag{5.36}$$

from (5.14). The hedgehog structure, (4.23), implies

$$[\mathrm{i}\boldsymbol{x}\times\boldsymbol{\partial}, U] = -\left[U, A\frac{\boldsymbol{\tau}}{2}A^\dagger\right] = -D^\dagger\cdot\left[U, \frac{\boldsymbol{\tau}}{2}\right], \tag{5.37}$$

and therefore

$$\boldsymbol{J} = -D^\dagger\cdot\boldsymbol{I} = \frac{\partial L[U]}{\partial\boldsymbol{\Omega}} = \alpha^2\boldsymbol{\Omega}\,. \tag{5.38}$$

The comparison with (5.20) and (5.22) shows that the "spin" operator that appears when quantizing the rigid top is indeed the physical spin, the quantity conserved because of rotational invariance. In addition, $\boldsymbol{I}$ is the isospin of the soliton. As already indicated above, the indices of the Wigner$D$- functions are associated with the left and right generators, the latter being minus the spin (in $SU(2)$). Therefore, the properly normalized baryon wave functions are (up to phase factors)

$$\langle A|J=I, I_3, J_3\rangle = \langle\Phi,\Theta,\Psi|J=I, I_3, J_3\rangle = \left[\frac{2J+1}{8\pi^2}\right]^{1/2} D^{J=I}_{I_3,-J_3}(\Phi,\Theta,\Psi) \tag{5.39}$$

in the space of the collective coordinates. To fully establish that the rigidly rotating Skyrmion describes baryons, we still have to show that only half-integer values are allowed for the spin quantum number J. This proof has to wait until we generalize the rigid rotator quantization to flavor $SU(3)$ and incorporate the important Wess–Zumino term, (4.40), that vanishes in $SU(2)$.

In the current treatment, the rotational excitations of the nucleon appear as stable states even though nature tells us that they are merely (quickly decaying) resonances. At the moment, it suffices to note that in the large-N_C limit these excitations become degenerate and thus may indeed be considered stable states in that limit. We will discuss decay mechanisms in more detail later.

We would like to round up this section by discussing the computation of the relevant matrix elements between baryon states. Once the hedgehog configuration is substituted the field operators turn into functions of the collective coordinates, A, and their time derivatives, $\dot{A}$. These can be immediately expressed in terms of the adjoint representation $D_{ij}(A) = D^{(1)}_{m,m'}(\Phi, \Theta, \Psi)$ and the angular velocities $\mathbf{\Omega}$. The matrix elements of $\mathbf{\Omega}$ are straightforwardly related to those of the spin operator via (5.38) and are thus standard. The matrix elements of D_{ij} are obtained by integrating over the Euler angles,

$$\frac{8\pi^2}{\sqrt{(2I'+1)(2I+1)}} \langle J' = I', I'_3, J'_3 | D^{(1)}_{m,m'} | J = I, I_3, J_3 \rangle = \tag{5.40}$$
$$\int \mathrm{d}A \left[D^{J'=I'}_{I'_3,-J'_3}(A) \right]^* D^{(1)}_{m,m'}(A) D^{J=I}_{I_3,-J_3}(A) = \frac{8\pi^2}{2I'+1} C^{I'I'_3}_{II_3,1m} C^{J'-J'_3}_{J-J_3,1m'} ,$$

where the integration measure is $\int \mathrm{d}A = \int_0^{2\pi} \mathrm{d}\Phi \int_0^{\pi} \mathrm{d}\Theta \sin\Theta \int_0^{2\pi} \mathrm{d}\Psi$ and the C's are $SU(2)$ Clebsch–Gordan coefficients [6].

In some cases, these matrix elements simplify by the Wigner–Eckart theorem. The left index of the collective coordinate matrix A behaves like an isospinor and, due to the hedgehog structure of the soliton, the right index like an ordinary spinor. This transfers to the transformation properties of the adjoint representation:

$$D_{ij} \sim I_i J_j \,. \tag{5.41}$$

When the D-function is sandwiched between states of equal spin (and isospin), we have

$$\langle J = I, I'_3, J'_3 | D_{ij} | J = I, I_3, J_3 \rangle = c(J) \langle J = I, I'_3, J'_3 | \hat{I}_i \hat{J}_j | J = I, I_3, J_3 \rangle \,, \tag{5.42}$$

where $c(j)$ is the reduced matrix element. Furthermore, $\hat{I}$ and $\hat{J}$ are $SU(2)$ generators that act on the I_3 and J_3 labels, respectively. From (5.38), we then compute the reduced matrix element via

$$\langle I_i \rangle = \langle -D_{ij} J_j \rangle = -c(J) J(J+1) \langle I_i \rangle \,. \tag{5.43}$$

Hence, the diagonal piece in (5.40) simplifies to

$$\langle J = I, I'_3, J'_3 | D_{ij} | J = I, I_3, J_3 \rangle = -\frac{\langle J = I, I'_3, J'_3 | \hat{I}_i \hat{J}_j | J = I, I_3, J_3 \rangle}{J(J+1)} \tag{5.44}$$

for states within a given spin (isospin) representation. In particular, we have $\langle N | D_{ai} | N \rangle = -\frac{1}{3} \langle \sigma_i \tau^a \rangle$ for the nucleon, where $\boldsymbol{\sigma}$ and $\boldsymbol{\tau}$, respectively, denote (twice) the spin and isospin operators in the $J = I = \frac{1}{2}$ representation.

5.4 Nucleon Static Properties

The predictions for baryon static properties will be exhaustively discussed in Chap. 7. Here we will mainly illuminate the use of the above-developed description of baryons.

The first prediction for baryons to be drawn from the spectrum, (5.19), is the mass difference between the Δ-resonance and the nucleon[2]:

$$M_\Delta - M_N = \frac{1}{2\alpha^2}\left(\frac{15}{4} - \frac{3}{4}\right) = \frac{3}{2\alpha^2}\,. \tag{5.45}$$

Comparison with the empirical mass difference (293 MeV) indicates that $\alpha \approx 5.11\,\mathrm{GeV}^{-1}$. This fixes the Skyrme term parameter to $e = 4.77$ when we choose the physical value $f_\pi = 93\,\mathrm{MeV}$ in the chiral limit ($m_\pi = 0$) as can be seen from the data presented after (5.16). For any non-zero pion mass, the simple scaling argument does not apply for the equation of motion (4.28) and the moment of inertia, (5.15). Then these integrations must be repeated individually. For the physical pion mass, $m_\pi = 138\,\mathrm{MeV}$, the identification of the Δ-nucleon mass difference yields $e = 4.25$.

The Skyrme parameter obtained from this fit to the Δ–nucleon mass differences then fully settles the model from which static properties of baryons are evaluated. In order to do so, one first constructs the Noether currents associated with the symmetry transformation (2.30). A convenient method is to extend these global symmetries to local ones by introducing external gauge fields (e.g., the gauge fields of the electroweak interactions) into the Skyrme model action. The Noether currents are subsequently read off as the expressions which couple linearly to these gauge fields. This procedure is especially appropriate for the Wess–Zumino term (4.40) because this non-local term can only be made gauge invariant by a trial and error type procedure [7, 8, 9], see Appendix C.2 for more details. The covariant form of the $SU(2) \times U(1)$ vector (V_μ^a) and axial-vector (A_μ^a) currents ($a = 0, \ldots, 3$) is again most conveniently written in terms of the forms $\alpha_\mu = U^\dagger \partial_\mu U$ and $\beta_\mu = U \partial_\mu U^\dagger$ [10] for $N_\mathrm{C} = 3$:

$$\begin{aligned} V_\mu^a(A_\mu^a) = {} & \mp\frac{\mathrm{i}}{2} f_\pi^2 \,\mathrm{tr}\left\{Q^a\left(\alpha_\mu \pm \beta_\mu\right)\right\} \\ & \mp\frac{\mathrm{i}}{8e^2}\mathrm{tr}\left\{Q^a\left([\alpha_\nu,[\alpha_\mu,\alpha^\nu]] \pm [\beta_\nu,[\beta_\mu,\beta^\nu]]\right)\right\} \\ & \pm\frac{1}{16\pi^2}\epsilon^{\mu\nu\rho\sigma}\mathrm{tr}\left\{Q^a\left(\alpha_\nu\alpha_\rho\alpha_\sigma \mp \beta_\nu\beta_\rho\beta_\sigma\right)\right\}\,, \end{aligned} \tag{5.46}$$

where $Q^a = (\frac{1}{2}\mathbb{1}, \frac{\tau^1}{2}, \ldots, \frac{\tau^3}{2})$ denote the hermitian $SU(2) \times U(1)$ generators. The combination, again for $N_\mathrm{C} = 3$,

$$Q^{\mathrm{e.m.}} = \mathrm{diag}\left(\frac{2}{3}, -\frac{1}{3}\right) = \frac{\tau_3}{2} + \frac{1}{6}\mathbb{1} = Q^3 + \frac{1}{2}Q^{\mathrm{baryon}} \tag{5.47}$$

is of special interest because it enters the computation of the electromagnetic properties.

[2] Originally, Adkins Nappi and Witten [2] attempted to also match the absolute masses. We will see in Sect. 8.6 that E_cl is subject to sizable quantum corrections which prevent us from directly identifying the eigenvalues of (5.19) with the physical masses.

We substitute the collectively rotating hedgehog configuration, (5.13), into the covariant form (5.46) and find the relevant vector current components to be

$$\begin{aligned} \tfrac{1}{3}V_0^0 &= \tfrac{1}{2}b(r)\,, & \tfrac{1}{3}V_i^0 &= \tfrac{1}{2}b(r)\epsilon_{ijk}\Omega_j x_k\,, \\ V_0^a &= -\tfrac{2}{3}v(r)D_{ai}\Omega_i\,, & V_i^a &= \tfrac{v(r)}{r^2}\epsilon_{ijk}x_j D_{ak}\,, \end{aligned} \tag{5.48}$$

with the radial functions, cf. (4.51),

$$b(r) = -F'\frac{\sin^2 F}{2\pi^2} \quad \text{and} \quad v(r) = \sin^2 F\left[f_\pi^2 + \frac{1}{e^2}\left(F'^2 + \frac{\sin^2 F}{r^2}\right)\right]. \tag{5.49}$$

Primes denote derivatives with respect to the radial coordinate r. Obviously, the integrals $\int \mathrm{d}^3 r b(r) = 1$ and $\int \mathrm{d}^3 r v(r) = \frac{3}{2}\alpha^2$ ensure proper normalization of the baryon charges, since according to the quantization rules of the previous section, we have $\int \mathrm{d}^3 r \left(\frac{1}{3}V_0^0 + V_0^3\right) = \frac{1}{2} + I_3$ in agreement with (5.47). Similarly, we find the spatial components of the (non-singlet) axial currents to be

$$A_i^a = \left[a_1(r)\delta_{ik} + a_2(r)\hat{x}_i\hat{x_k}\right] D_{ak}\,, \tag{5.50}$$

with

$$\begin{aligned} a_1(r) &= \frac{\sin 2F}{2r}\left[f_\pi^2 + \frac{1}{e^2}\left(F'^2 + \frac{\sin^2 F}{r^2}\right)\right], \\ a_2(r) &= -a_1(r) + F'\left[f_\pi^2 + \frac{2}{e^2}\frac{\sin^2 F}{r^2}\right]. \end{aligned} \tag{5.51}$$

Before proceeding in calculating baryon properties, it is actually interesting to note that $\partial_i A_i^a$ is proportional to the right-hand side of the equation of motion (4.28) for the chiral angle in the Skyrme model. Hence PCAC, (2.55), is equivalent to the stationary condition for the soliton profile. This equivalence is true in any soliton model, at least at the classical level. Thus the PCAC relation is satisfied in all soliton models classically. Yet, in soliton models, PCAC is not necessarily a statement on the pion field operator.

In the first place, we want to compute the nucleon magnetic moments as the matrix elements

$$\mu_N = \langle N J_3 = \tfrac{1}{2}| \int \mathrm{d}^3 x \left(\boldsymbol{x} \times \boldsymbol{V}^{\mathrm{e.m.}}\right)_3 |N J_3 = \tfrac{1}{2}\rangle\,, \tag{5.52}$$

where the linear combination, (5.47), is indicated. Upon substitution of the collectively rotating hedgehog and evaluation of the matrix elements according to the rules derived in Sect. 5.3, the magnetic moments are

$$\frac{\mu_N}{\mu_{\mathrm{n.m.}}} = \frac{2\pi}{3}M_N \int_0^\infty \mathrm{d}r r^2 \left[\pm\frac{2}{3}v(r) + \frac{r^2}{2\alpha^2}b(r)\right], \tag{5.53}$$

when measured in nucleon magnetons $\mu_{\mathrm{n.m.}} = \frac{e\hbar}{2M_N}$ with $M_N = 939\,\mathrm{MeV}$ being the physical nucleon mass. The two signs in (5.53) refer to proton and

neutron, respectively. Numerical results are shown in Table 5.1. As discussed above, the Skyrme constant is chosen to reproduce the Δ-nucleon mass difference. While it is nowadays common to keep the pion decay constant at its experimental value, $f_\pi = 93\,\mathrm{MeV}$, we also include the results of the earlier computation [12] that fitted $f_\pi = 54\,\mathrm{MeV}$ to reproduce the nucleon mass according to (5.19).

While the ratio of proton and neutron magnetic moments is reasonably well reproduced, the absolute values are significantly underestimated. We will observe in Chap. 7 when we discuss baryon properties in more detail that the inclusion of vector meson fields favorably improves these predictions.

Similar to (5.52), we find the charge radii as the matrix element

$$\begin{aligned}\langle r_N^2 \rangle &= \left\langle N J_3 = \tfrac{1}{2} \left| \int d^3x\, \boldsymbol{x}^2\, V_0^{\mathrm{e.m.}} \right| N J_3 = \tfrac{1}{2} \right\rangle \\ &= 4\pi \int_0^\infty \mathrm{d}r r^4 \left[\pm \frac{1}{3\alpha^2} v(r) + \frac{1}{2} b(r) \right] . \end{aligned} \tag{5.54}$$

Numerical results are shown in Table 5.1 for two sets of model parameters mentioned above. In contrast to the magnetic moments, we observe a pronounced dependence of the results on f_π. To discuss that dependence in more detail, it is appropriate to consider isoscalar ($I = 0$) and isovector ($I = 1$) radii

$$r_{I=0}^2 = r_p^2 + r_n^2 \qquad \text{and} \qquad r_{I=1}^2 = r_p^2 - r_n^2 \tag{5.55}$$

separately because they are not affected by potential cancellations between the two terms in (5.54). Leaving the pion mass dependence aside for the moment, dimensional considerations tell us that the radii, (5.55), should scale like $1/f_\pi^2$. Thus, we would expect an increase by a factor four when going from parameter set A to B in Table 5.1. This is mitigated by the additional change of the Skyrme parameter, e, and the increase of the dimensionless ratio μ_π when f_π is lowered but the pion mass is held fixed, cf. (4.29). This effect causes the soliton to become narrower. In total, the parameter change yields a factor two for the squared charge radii. It is very interesting to note that $r_n^2 < 0$, in agreement with data. This is a result of the delicate cancellation in (5.54). Being so, the predicted absolute value is actually quite model dependent. Nevertheless, all known soliton model calculations predict negative values for r_n^2.

The just discussed numerical results only refer to the case with the pion mass term included. The unphysical case $m_\pi = 0$ is somewhat troublesome because not all of the radial integrals that appear in the calculation of nucleon static properties converge well when the chiral angle decays with a power law as $r \to \infty$, cf. (4.29). The reason is that we actually have to consider momentum-dependent form factors of the currents as, e.g., in Sect. 7.1. They may possess cusps when the momentum approaches time-like multiples of m_π.

Table 5.1. Predictions for nucleon static properties in the Skyrme model compared to experimental data [11]. Two parameter sets are considered: (A: $f_\pi = 93\,\mathrm{MeV}$ $e = 4.25$) and (B:$f_\pi = 54\,\mathrm{MeV}$ $e = 4.84$ [12])

	A	B	expt.
μ_p	1.78	1.97	2.79
μ_n	−1.42	−1.24	−1.91
$\frac{\mu_p}{\mu_n}$	−1.26	−1.59	−1.46
r_p^2	0.48	0.77	0.74
r_n^2	−0.23	−0.31	−0.12
$r_{I=0}^2$	0.25	0.46	0.62
$r_{I=1}^2$	0.71	1.08	0.86
g_A	0.90	0.65	1.26

These cusps become visible at zero momentum when $m_\pi = 0$. Yet, the form factors are always well behaved, rather moments of the currents are ill-defined.

Let us next explore the axial charge, i.e., the proton matrix element $\langle 2A_3^3 \rangle$ which is obtained from (5.51):

$$g_\mathrm{A} = -\frac{8\pi}{3} \int dr r^2 \left[a_1(r) + \frac{1}{3} a_2(r) \right] . \tag{5.56}$$

Experimentally, the quantity is extracted from the neutron-beta decay together with isospin invariance, as the relevant transition Hamiltonian couples the electroweak axial current to the nucleon axial current.

We compare the Skyrme model prediction to the experimental data for g_A in Table 5.1 as well. Again, the model prediction is sensible to the parameters. Turning again to dimensionless variables, the dependence of g_A on f_π only enters via μ_π in the equation of motion (4.28); a larger f_π corresponds to a smaller μ_π and in turn to a wider chiral angle, cf. (4.29). Since g_A is sensitive to the large distance behavior of the chiral angle, the increase of g_A with f_π shown in Table 5.1 is well understood. Nevertheless, the empirical value for g_A is significantly underestimated.

Let us round up this section by a short discussion on subtleties of the axial charge in the chiral limit, with vanishing pion mass. In that case, the axial current is conserved and the Lorentz covariant decomposition for its nucleon matrix element requires the Dirac structure $\gamma_5 \left(\gamma_\mu - 2M_N q_\mu / q^2 \right)$, where q_μ is the difference of the momenta of the nucleon states. Then the non-relativistic reduction of the matrix element that defines g_A becomes

$$\langle N(\boldsymbol{p}) | 2A_3^3 | N(\boldsymbol{p}') \rangle = g_\mathrm{A} \left(\delta_{3a} - \frac{q_3 q_a}{\boldsymbol{q}^2} \right) (4 J_a I_3) \qquad \text{for} \quad \boldsymbol{q} = \boldsymbol{p} - \boldsymbol{p}' \to 0 \,. \tag{5.57}$$

The limit $\boldsymbol{q} \to 0$ is ambiguous[3] and commonly [2] it is taken in a symmetric way: $\langle N(\boldsymbol{p})|2A_3^3|N(\boldsymbol{p}')\rangle = \frac{2}{3}g_{\rm A}$. The numerical analysis verifies that the prefactor (2/3) is required to render the integral, (5.56), smooth when $m_\pi \to 0$. We make use of the conservation of the axial current in the chiral limit when evaluating the matrix element:

$$\int \mathrm{d}^3 r\, \partial_i \left(x_3 A_i^3\right) = \int \mathrm{d}^3 r A_3^3 \,. \tag{5.58}$$

Naïvely, one expects the left-hand side to vanish because it may be turned into a surface integral at spatial infinity. However, (4.29) shows that the chiral angle decays only with a power law in the chiral limit so that this surface integral actually is non-zero. Collecting pieces, we alternatively find

$$g_{\rm A} = \frac{8\pi}{3} f_\pi^2 A \tag{5.59}$$

for the axial charge when $m_\pi = 0$. Here we have employed the definition of A in (4.29), expanded the radial functions a_i in (5.50) to leading order in $1/r$ and evaluated the spin–isospin matrix elements from (5.44). In Section (10.3), we will argue that the long-range behavior of the pion field defines the coupling constant $g_{\pi NN}$ seen in the one-pion-exchange contribution to the nucleon–nucleon potential via

$$\pi^a \longrightarrow -\frac{g_{\pi NN}}{8\pi M_N} \langle \sigma_i \tau^a \rangle \, \frac{x_i}{r^3} \qquad \text{as} \quad r \longrightarrow \infty \,, \tag{5.60}$$

where (twice) the nucleon spin and isospin matrix elements are indicated. For the rigidly rotating hedgehog, we extract the asymptotic form of the pion field from

$$U \sim \mathbb{1} + \mathrm{i} \frac{\boldsymbol{\pi} \cdot \boldsymbol{\tau}}{f_\pi} \sim = \mathbb{1} + \mathrm{i} F(r) \hat{x}_i D_{ai} \tau^a \,. \tag{5.61}$$

The nucleon matrix elements, (5.44), and again the large r behavior of the chiral angle, (4.29), identify $\frac{g_{\pi NN}}{8\pi M_N} = \frac{1}{3} f_\pi A$. Eliminating A then yields

$$g_{\rm A} = \frac{f_\pi g_{\pi NN}}{M_N} \,. \tag{5.62}$$

This is the celebrated Goldberger–Treimann relation (GTR) between the nucleon axial charge that is measured in weak interactions and the pion–nucleon coupling constant that is a strong interaction property. Commonly, the GTR is obtained from sandwiching the PCAC relation (2.55) as an operator equation between nucleon states. While the left-hand side of that matrix element gives the axial charge of the nucleon, the LSZ reduction formalism can be

[3] For $m_\pi \neq 0$, the denominator is $\boldsymbol{q}^2 + m_\pi^2$ and the limit can be taken straightforwardly.

utilized to relate the right-hand side to the pion–nucleon form factor whose zero momentum limit defines the coupling constant $g_{\pi NN}$.[4]

In the Skyrme model, the situation changes considerably away from the chiral limit. Then the axial current is not conserved and asymptotically the chiral angle decays exponentially. Thus, (5.58) turns into

$$0 = \int \mathrm{d}^3 r\, \partial_i \left(x_3 A_i^3\right) = \int \mathrm{d}^3 r A_3^3 + \int \mathrm{d}^3 r\, x_3 f_\pi^2 m_\pi^2 \sin F \hat{x}_k D_{3k}\,. \qquad (5.63)$$

It is tempting to use the PCAC relation (2.55), identify the pion field as $\pi^a = f_\pi \sin F \hat{x}_k D_{ak}$ and compute $g_{\pi NN}$ as the nucleon matrix element thereof. By pure construction, that procedure renders the Goldberger–Treimann relation, (5.62). However, some care needs to be taken with this definition of the pion–nucleon coupling constant because it remains unclear how it is related to the one-pion-exchange contribution in the nucleon–nucleon potential or even pion–nucleon scattering; after all this pion field is confined in space and thus cannot correspond to an asymptotic state. Generalizations of this definition of $g_{\pi NN}$ to coupling constants for baryon resonances (e.g., $g_{\pi N\Delta} \sim \frac{2M_N}{f_\pi}\langle N|A_3^3|\Delta\rangle$) to compute its decay width seem even more questionable. In fact, in Sect. 9.3, we will discuss a case where this approach fails.

5.5 Quantization in Vector Meson Models

A short note on the analogous computation in vector meson models is in order because there is a major technical difference. With time-dependent rotations, the field equations for components that vanish on the classical soliton level are augmented by source terms proportional to the angular velocities. This induces additional radial functions for these components. Essentially, the time components of the ρ and the spatial components of the ω meson fields are affected:

$$\rho_{0,a} = \frac{1}{2g} A(t) \left[\xi_1(r)\Omega_a + \xi_2(r)(\hat{\boldsymbol{x}} \cdot \boldsymbol{\Omega})\hat{x}_a\right] A^\dagger(t)\,,\ \omega_i = \frac{\phi(r)}{2g}\epsilon_{ijk}\Omega_j \hat{x}_k\,. \quad (5.64)$$

These additional profile functions are determined from a variational principle to the moment of inertia, α^2 [13, 14, 15]. In the case of the model generalized to $U(2)$, a two-flavor psedouscalar–isoscalar field of the from $\eta_T(\boldsymbol{r}) = \frac{1}{f_\pi}\eta(r)\hat{\boldsymbol{r}} \cdot \boldsymbol{\Omega}$ is also induced. (Section 7.4 contains a comprehensive discussion of η fields in chiral models.) To be precise, the moment of inertia in the vector meson model described in Sect. 4.7 reads

[4] Strictly speaking the GTR is valid only at zero momentum transfer and smoothness is assumed to extrapolate to the physical point.

$$
\begin{aligned}
\alpha^2 = \frac{8\pi}{3}\int \mathrm{d}r \Bigg\{ & f_\pi^2 r^2 \sin^2 F - \frac{4}{g^2}(\phi'^2 + 2\frac{\phi^2}{r^2} + m_\rho^2\phi^2) \\
& + \frac{m_\rho^2}{2g^2} r^2 \left[(\xi_1+\xi_2)^2 + 2(\xi_1 - 1 + \cos F)^2\right] \\
& + \frac{1}{2g^2}\left[(3\xi_1'^2 + 2\xi_1'\xi_2' + \xi_2'^2)r^2 + 2(G^2+2G+2)\xi_2^2\right. \\
& \left. + 4G^2(\xi_1^2 + \xi_1\xi_2 - 2\xi_1 - \xi_2 + 1)\right] + \frac{4\gamma_1}{g}\phi F' \sin^2 F \\
& + \frac{4\gamma_3}{g}\phi F'\left[(G-\xi_1)(1-\cos F) + (1-\cos F)^2 - G\xi_1\right] \\
& + \frac{2\gamma_2}{g}\Big\{\phi' \sin F(G - \xi_1 + 2 - 2\cos F) + \phi \sin F(\xi_1' - G') \\
& + \phi F'\left[2 + 2\sin^2 F + (\xi_1 - G - 2)\cos F - 2(\xi_1+\xi_2)\right]\Big\} \\
& - \frac{1}{2}\left[\eta'^2 r^2 + 2\eta^2 + m_\eta^2 r^2 \eta^2\right] + \frac{\gamma_2 g}{2f_\pi}\left[\eta(\phi\omega' - \omega\phi') - \eta'\phi\omega\right] \\
& - \frac{\gamma_1}{3gf_\pi}\left[\eta'(\xi_1+\xi_2)\sin^2 F + 2\eta F'(G+\xi_1)\sin F\right] \\
& - \frac{3\gamma_3}{gf_\pi}\eta'(G + 1 - \cos F)^2(\xi_1+\xi_2) \\
& - \frac{\gamma_2}{gf_\pi}\left\{\eta'\left[(G+\xi_1)G + (\xi_1+\xi_2)[(1-\cos F)^2 - 2G\cos F]\right]\right. \\
& \left. + \eta(G\xi_1' - G'\xi_1)\right\}\Bigg\}. \qquad (5.65)
\end{aligned}
$$

In future, we will refrain from displaying such lengthy formulas and rather refer to the literature. In any event, it should be obvious that the inclusion of vector mesons significantly complicates matters. Of course, these additional fields must also be taken into account when computing the analog of the radial functions in (5.48), etc., in vector meson models [13, 14, 15]. Otherwise, the charges, etc., are not properly normalized.

There is, however, a significant effect of the vector meson fields. Without their presence, there is no term that is only linear in the isoscalar pseudoscalar field η, as evident from (5.65). That is, without vector mesons this component does not get excited. This is one of the features that make qualitative differences to the Skyrme model. Although the effect of the induced η field is negligibly small for most quantities, there are special ones that vanish without the η and in such cases it plays an important role, cf. Sects. 7.4 and 7.6.

Once the moment of inertia, α^2, is computed, the spectrum is again determined from (5.19). In order to obtain $\alpha^2 \approx 5\,\mathrm{GeV}^{-1}$ as deduced from the Δ-nucleon mass difference, a value of $\kappa = \gamma_3/\gamma_2 \approx 1$ is needed for the so far undetermined parameter (discussed after (4.66)). The corresponding piece in the Lagrangian is repulsive, and thus too small a value (in particular a negative one) yields too small a soliton extension and in turn too big a Δ-nucleon mass difference [14].

5.6 Quantization in Chiral Quark Models

Let us also briefly discuss the method of collective coordinate quantization in chiral quark models. Actually, the quantization prescription is the same as in the mesonic models, i.e., the spectrum is given by (5.19). However, the computation of the moment of inertia, α^2, is again significantly more complicated than in the Skyrme model, (5.15). Also, in chiral quark models, the connection to the famous cranking procedure [16] is more obvious and so justifies the notion of *cranking the hedgehog* for the collective coordinate approach.

Starting point is the observation that the rotation of the hedgehog, (5.13), can be phrased as a vector transformation of the quark fields. Then the Dirac operator becomes

$$\mathrm{i}\beta\not{D} = A(t)\left\{\mathrm{i}\partial_t - h - \frac{1}{2}\boldsymbol{\tau}\cdot\boldsymbol{\Omega}\right\}A^\dagger(t)\,. \tag{5.66}$$

Here h is the single-particle Dirac–Hamiltonian of (3.23) if only pseudoscalar fields are considered. The computation proceeds by expanding the bosonized action, (2.14), in powers of $\boldsymbol{\Omega}$ to quadratic order. The coefficient of that term is then identified as the moment of inertia. As in the case of the classical energy, the action separates into valence quark and vacuum pieces. The former is analyzed by treating the extended Dirac equation for the valence quark state in stationary perturbation theory. The corresponding contribution to the moment of inertia tensor is

$$\Theta^{(\mathrm{V})}_{ab} = \frac{N_\mathrm{C}}{2}\sum_{\mu\neq\mathrm{V}}\frac{\langle\mathrm{V}|\tau_a|\mu\rangle\langle\mu|\tau_b|\mathrm{V}\rangle}{\epsilon_\mu - \epsilon_\mathrm{V}}\,, \tag{5.67}$$

where μ refers to the eigenstates of h and V denotes the (strongly bound) valence level. This expression illustrates the cranking-type structure of the collective rotations [16]. Similarly, we find the first-order rotational correction to the valence quark wave function

$$\Psi^{(\mathrm{rot})}_\mathrm{V}(\boldsymbol{r}\,,t) = \mathrm{e}^{-\mathrm{i}\epsilon_\mathrm{V}t}A(t)\left\{\Psi_\mathrm{V}(\boldsymbol{r}\,) + \frac{1}{2}\sum_{\mu\neq\mathrm{V}}\Psi_\mu(\boldsymbol{r}\,)\frac{\langle\mu|\boldsymbol{\tau}\cdot\boldsymbol{\Omega}|\mathrm{V}\rangle}{\epsilon_\mathrm{V}-\epsilon_\mu}\right\}, \tag{5.68}$$

with $\Psi_\mu(\boldsymbol{r}\,)$ being the eigenfunctions of h in (3.23).

The expansion of the vacuum part complicates the computation of the inertia parameter. Since regularization is mandatory and we employ the proper time prescription, the detour over Euclidean space is unavoidable. In Euclidean space $h_{rot} = \frac{1}{2}\boldsymbol{\tau}\cdot\boldsymbol{\Omega}$ is an anti-hermitian quantity since it is linear in the time derivative. The real part of the regularized action is[5]

[5] We do not discuss the imaginary part here. It does not contribute in the two-flavor case. This is different when collective coordinates are introduced for flavor $SU(3)$ [17].

$$\mathcal{A}_R = -\frac{1}{2}\int_{1/\Lambda^2}^{\infty}\frac{\mathrm{d}s}{s}\mathrm{Tr}\,\exp\left\{-s\left[-\partial_\tau^2 + h^2 + [h, h_{\mathrm{rot}}] - h_{\mathrm{rot}}^2\right]\right\}. \tag{5.69}$$

This expression is analyzed using the general formula, (B.23), for an expansion up to quadratic order for operator-valued objects. Since the perturbation is taken to be static, the temporal part of the functional trace is straightforwardly converted into Gaußian-type integrals as in (3.12). The remainder of the trace is evaluated using the eigenstates, $|\mu\rangle$, of the Dirac Hamiltonian in the background of the chiral soliton, (3.2). Having obtained the expanded Euclidean action, the coefficients of $\Omega_a\Omega_b$ are extracted after continuing back to Minkowski space. This yields the vacuum contribution to the moment of inertia tensor

$$\Theta_{ab}^{(0)} = \frac{N_{\mathrm{C}}}{2}\sum_{\mu\nu} f_\Lambda(\epsilon_\mu, \epsilon_\nu)\langle\mu|\tau^a|\nu\rangle\langle\nu|\tau^b|\mu\rangle\,. \tag{5.70}$$

The cut-off function

$$f_\Lambda(\epsilon_\mu, \epsilon_\nu) = \frac{\Lambda}{\sqrt{\pi}}\frac{\mathrm{e}^{-(\epsilon_\mu/\Lambda)^2} - \mathrm{e}^{-(\epsilon_\nu/\Lambda)^2}}{\epsilon_\nu^2 - \epsilon_\mu^2} + \frac{\mathrm{sign}(\epsilon_\mu)\mathrm{erfc}\left(\left|\frac{\epsilon_\mu}{\Lambda}\right|\right) - \mathrm{sign}(\epsilon_\nu)\mathrm{erfc}\left(\left|\frac{\epsilon_\nu}{\Lambda}\right|\right)}{2(\epsilon_\mu - \epsilon_\nu)} \tag{5.71}$$

vanishes in the case $\epsilon_\mu = \epsilon_\nu$ [18]. When regularization is removed

$$\lim_{\Lambda\to\infty} f_\Lambda(\epsilon_\mu, \epsilon_\nu) = \frac{\mathrm{sign}(\epsilon_\mu) - \mathrm{sign}(\epsilon_\nu)}{2\,(\epsilon_\mu - \epsilon_\nu)}, \tag{5.72}$$

the typical cranking structure of particle–hole excitations becomes obvious. Because of flavor $SU(2)$ symmetry, the moment of inertia tensor is proportional to the unit matrix. Therefore, the moment of inertia that enters the Δ-nucleon mass difference, (5.45), becomes

$$\alpha^2 = \frac{1}{2}\left[1 + \mathrm{sign}(\epsilon_{\mathrm{V}})\right]\Theta_{33}^{(\mathrm{V})} + \Theta_{33}^{(0)}\,. \tag{5.73}$$

The first coefficient measures whether or not the baryon number is carried by the polarized vacuum, cf. Sect. 3.1. As for the classical energy, (3.16), the right-hand side of (5.73) is smooth as ϵ_{V} changes sign. Again, the value $\alpha^2 \approx 5\,\mathrm{GeV}^{-1}$ is often used to fix the remaining model parameter (after fitting meson observables). In Sect. 3.3, we have discussed that this may be phrased in terms of the constituent quark mass m. For the model of only pseudoscalar fields (Sect. 3.3.1), one finds $m \approx 400\,\mathrm{MeV}$.

This has just been a sketch of the computation of the moment of inertia in chiral quark soliton models. For a more detailed discussion, we recommend to consult the original references [18, 19] as well as the reviews on the (NJL) chiral quark soliton model [20, 21].

References

1. T. D. Lee, *Particle Physics and Introduction to Field Theory*, Chap. 7. Harwood Acad. Publ., Chur, 1982. 67
2. G. S. Adkins, C. R. Nappi, and E. Witten, *Nucl. Phys.* **B228** (1983) 552. 68, 74, 78
3. G. Holzwarth and B. Schwesinger, *Rep. Prog. Phys.* **49** (1986) 825. 68
4. I. Zahed and G. E. Brown, *Phys. Rep.* **142** (1986) 1. 68
5. H. Yabu and K. Ando, *Nucl. Phys.* **B301** (1988) 601. 68
6. D. A. Varshalovich, A. N. Moskalev, and V. K. Khersonskii, *Quantum Theory of Angular Momentum*, Chap. 4. World Scientific, Singapore, 1988. 69, 73
7. E. Witten, *Nucl. Phys.* **B223** (1983) 422, 433. 74
8. O. Kaymakcalan, S. Rajeev, and J. Schechter, *Phys. Rev.* **D30** (1984) 594. 74
9. O. Kaymakcalan and J. Schechter, *Phys. Rev.* **D31** (1985) 1109. 74
10. N. W. Park, J. Schechter, and H. Weigel, *Phys. Rev.* **D43** (1991) 869. 74
11. S. Eidelman et al. [PDG], *Phys. Lett.* **B592** (2004) 1. 77
12. G. S. Adkins and C. R. Nappi, *Nucl. Phys.* **B233** (1984) 109. 76, 77
13. U. G. Meißner, N. Kaiser, and W. Weise, *Nucl. Phys.* **A466** (1987) 685. 79, 80
14. U. G. Meißner, N. Kaiser, H. Weigel, and J. Schechter, *Phys. Rev.* **D39** (1989) 1956. 79, 80
15. N. W. Park and H. Weigel, *Nucl. Phys.* **A541** (1992) 453. 79, 80
16. D. R. Inglis, *Phys. Rev.* **96** (1954) 1059. 81
17. H. Weigel, R. Alkofer, and H. Reinhardt, *Nucl. Phys.* **B387** (1992) 638. 81
18. H. Reinhardt, *Nucl. Phys.* **A503** (1989) 825. 82
19. K. Goeke et al., *Phys. Lett.* **B256** (1991) 321. 82
20. R. Alkofer, H. Reinhardt, and H. Weigel, *Phys. Rep.* **265** (1996) 139. 82
21. C. V. Christov et al., *Prog. Part. Nucl. Phys.* **37** (1996) 91. 82

6

Soliton Quantization in Flavor SU(3)

The extension to three flavors is essential to establish the fermionic character of the Skyrmion. As explained in Chap. 5, the N_C dependences are almost trivial in two-flavor soliton models. They merely effect the scaling of constants in the effective meson Lagrangian while the quantization rules for spin and isospin are not affected. The eigenstates of the collective coordinate Hamiltonian, (5.18), are members of $SU(2)$ representations that are completely determined by the prescribed values of spin and isospin, (5.39). This will turn out to be very different when we extend the model such that it is based on a three-flavor effective meson Lagrangian. We will see that the allowed $SU(3)$ representations depend on the value of N_C. As is to be expected this results from the Wess–Zumino term, the representative for the QCD axial anomaly in the effective meson theory. Another major difference to the two-flavor version is the fact that $SU(3)$ is not an exact symmetry in nature.[1] This feature must also be incorporated when generating baryon states from the soliton.

6.1 Baryon States in the Non-relativistic Quark Model

We will first briefly review the non-relativistic quark model for three flavors to establish the role of $SU(3)$ representations. In the non-relativistic quark model, baryons are built out of three quarks that are bound by a potential. The details of that potential are not important here. It suffices to know that for the low-lying baryons the three quarks are in the same spatial wave function $\phi(x)$ and that the product wave function is completely symmetric in spin and flavor. This is due to the fact that the overall anti-symmetry solely results from the permutation properties of the color wave function. For the spin–flavor component of the product of three quarks, we consider the Clebsch–Gordan

[1] Though also isospin is not exact, we may ignore isospin breaking effects at the scale of strong interactions.

H. Weigel: *Soliton Quantization in Flavor SU(3)*, Lect. Notes Phys. **743**, 85–112 (2008)
DOI 10.1007/978-3-540-75436-7_6

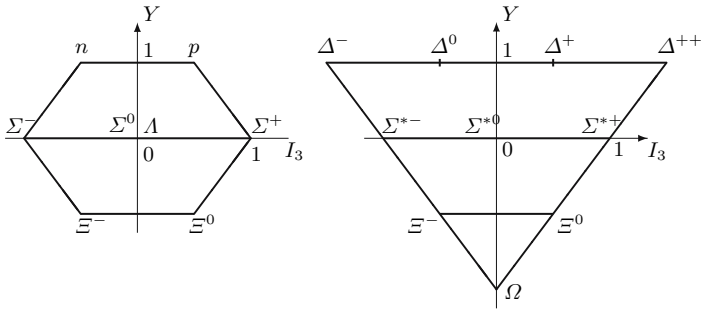

Fig. 6.1. The low-lying baryons in the octet (*left*) and decuplet (*right*) representations of flavor $SU(3)$. These baryons are characterized by their isospin projection (I_3) and hypercharge (Y) quantum numbers. The $Y = I_3 = 0$ state in the octet is twofold degenerate

expansion (in the language of Young tableaux)

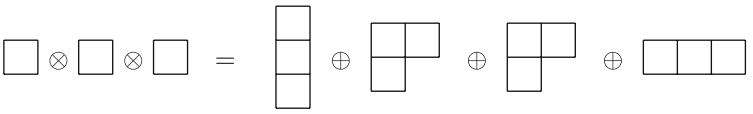

(6.1)

which is valid for both spin $SU(2)$ and flavor $SU(3)$. In the case of $SU(2)$, the totally anti-symmetric combination  is not available. Therefore, the possible product wave functions that are totally symmetric in the spin and flavor quantum numbers are

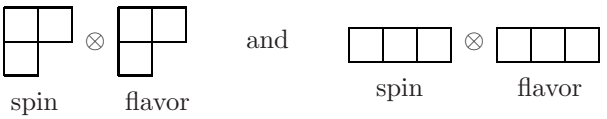

(6.2)

The states in the first product carry spin $s = \frac{1}{2}$ because  in $SU(2)$, i.e., these states belong to the fundamental doublet. The states in the second product form an $SU(2)$ quartet with $s = \frac{3}{2}$. The flavor representations are octet and decuplet on the left- and right-hand sides, respectively. The flavor content of these multiplets is shown in Fig. 6.1 where the states are ordered according to their hypercharge and isospin projection quantum numbers, i.e., the eigenvalues of the Cartan operators of $SU(3)$.

6.2 Quantization of the Soliton in the Flavor Symmetric Case

In this section, we will discuss the quantization of the Skyrmion in the simplified case of zero flavor symmetry breaking. This comprises the rigid rotator

approach to the chiral soliton in flavor $SU(3)$. Compared to the quantization in the two-flavor reduction, there are already two major differences. The first one is the emergence of the Wess–Zumino term, cf. Sect. 4.5. It no longer vanishes because in $SU(3)$ sufficiently many linear independent generators are present. We will in particular see that it enforces to quantize the soliton a spin $\frac{1}{2}$ object, at least for odd N_C. The second difference is actually obvious. We still want to quantize the modes about the hedgehog configuration, (4.23). However, there are several $SU(2)$ sub-manifolds in $SU(3)$ that could be chosen to embed the hedgehog. Eventually, we want to quantize about an extremal point of the action when flavor symmetry breaking is included. Any embedding outside the isospin sub-group will change the classical energy by a positive amount proportional to the mass difference between the strange and non-strange quark masses. In the effective Lagrangian, that mass difference is represented by the one between the kaon and the pion, cf. (2.24).

The initial configuration in the three-flavor model is

$$U_H(\boldsymbol{x}\,) = \left(\begin{array}{cc|c} \multicolumn{2}{c|}{\exp\left[\mathrm{i}\hat{\boldsymbol{x}}\cdot\boldsymbol{\tau}\,F(r)\right]} & \begin{array}{c}0\\0\end{array} \\ \hline 0 & 0 & 1 \end{array}\right), \tag{6.3}$$

where, for the Skyrme model case, $F(r)$ is again the solution to the equation of motion (4.28). We introduce collective coordinates for the zero modes in the $SU(3)$ symmetric model

$$U(\boldsymbol{x}\,,t) = A(t)U_H(\boldsymbol{x})A^\dagger(t) \tag{6.4}$$

to parameterize time-dependent configurations as in (5.13). Here the soliton rotates without deformation (i.e., rigidly) in flavor space. Therefore treatments based on (6.4) are commonly summarized as the *rigid rotator approach* (RRA). When we substitute this ansatz into the sum $\int \mathrm{d}^4x\,[\mathcal{L}_{\mathrm{nl}\sigma} + \mathcal{L}_{\mathrm{Sk}}] + \Gamma_{\mathrm{WZ}}$, we obtain the Lagrange function for the collective coordinates

$$L(A,\Omega_a) = -E_\mathrm{cl} + \frac{1}{2}\alpha^2\sum_{i=1}^{3}\Omega_i^2 + \frac{1}{2}\beta^2\sum_{\alpha=4}^{7}\Omega_\alpha^2 - \frac{N_\mathrm{C}B}{2\sqrt{3}}\Omega_8\,, \tag{6.5}$$

where

$$\frac{\mathrm{i}}{2}\sum_{a=1}^{8}\Omega_a\lambda_a = A^\dagger(t)\,\frac{\mathrm{d}A(t)}{\mathrm{d}t} \tag{6.6}$$

defines the $SU(3)$ angular velocities, cf. (5.16). The classical energy, E_cl and the moment of inertia associated with the first three rotations, α^2, are the same as in $SU(2)$, cf. (4.27) and (5.15), respectively. Again, the α^2 term arises because the Skyrmion breaks rotational invariance and the hedgehog structure allows to express spatial rotations as flavor transformations. Similarly, the third term is caused by the Skyrmion breaking the $SU(3)$ symmetry. The corresponding moment of inertia is again a functional of the chiral angle:

$$\beta^2 = \pi \int \mathrm{d}r\, r^2 \sin^2\frac{F}{2}\left[4f_\pi^2 + \frac{1}{e^2}\left(F'^2 + \frac{2}{r^2}\sin^2 F\right)\right] . \tag{6.7}$$

Induced kaon fields, required by partial conservation of the axial current [1], are not explicitly shown. Typical model results for this inertia parameter are about $4\,\mathrm{GeV}^{-1}$. The last term in (6.5) is less easily understood. Note that λ_8 commutes with the soliton configuration (6.3). Hence one does not expect Ω_8 to appear at all in the collective coordinate Lagrangian. And indeed, there is no Ω_8^2 contribution from either the non-linear σ or the Skyrme Lagrangians. However, this commutator argument applies only to local pieces of the action. The Wess–Zumino term is non-local and yields the last term in (6.5). Since the Wess–Zumino term has at most one time derivative, it is obvious that its contribution to the collective coordinate Lagrangian is linear in the angular velocities. This piece in the Lagrangian can easily be worked out from (C.27) in Appendix C with $V \equiv A(t)$. We stress that exactly the same term arises in chiral quark soliton models (Chap. 3) from $\mathcal{A}_I$ (2.16) [2, 3]. This is not surprising, after all Γ_{WZ} is included to mock up $\mathcal{A}_I$.

The discussion and results of Sect. 5.2 are valid for any dimension of the special unitary group. To quantize the system, (6.5), we may hence simply identify the (intrinsic) $SU(3)$ generators

$$R_a = -\frac{\partial L}{\partial \Omega_a} = \begin{cases} -\alpha^2\Omega_a = -J_a, & a = 1,2,3 \\ -\beta^2\Omega_a, & a = 4,..,7 \\ \frac{N_{\mathrm{C}}B}{2\sqrt{3}}, & a = 8 \end{cases} \tag{6.8}$$

and impose the commutation relations[2]

$$[R_a, R_b] = -\mathrm{i} f_{abc} R_c\,, \tag{6.9}$$

where f_{abc} are the $SU(3)$ structure constants. The fact that the first three generators are identified with the spin operator is a mere consequence of the hedgehog structure that identifies spin and isospin rotations. We easily find the Hamiltonian of (6.5) from the Legendre transformation eq. (5.30)

$$\begin{aligned} H &= E_{\mathrm{cl}} + \frac{1}{2\alpha^2}\boldsymbol{J}^{\,2} + \frac{1}{2\beta^2}\sum_{\alpha=4}^{7} R_\alpha^2 \\ &= E_{\mathrm{cl}} + \frac{1}{2}\left(\frac{1}{\alpha^2} - \frac{1}{\beta^2}\right)\boldsymbol{J}^{\,2} + \frac{1}{2\beta^2}C_2[SU(3)] - \frac{N_{\mathrm{C}}^2 B^2}{24\beta^2}\,, \end{aligned} \tag{6.10}$$

where $C_2[SU(2)] = \sum_{a=1}^{8} R_a^2$ is the quadratic Casimir operator of $SU(3)$. The main task is now to find the eigenstates of (6.10) subject to the constraint $R_8 = \frac{N_{\mathrm{C}}B}{2\sqrt{3}}$. In (5.20), the Euler angle representation of the $SU(2)$ generators is given. Of course, an analog for R_a in terms of the eight $SU(3)$ Euler exists

[2] Note the different phase convention.

as well. The detailed expressions are listed in Appendix D. Techniques based on expressing H in terms of the Euler angles will become more important when incorporating flavor symmetry breaking.

In the absence of flavor symmetry breaking, the diagonalization problem is simple because members of definite $SU(3)$ representations are also eigenstates of the $SU(3)$ Casimir operators. It is important to recall that we have to consider *two* sets of multiplets, one for the right generators R_a and one for the left generators L_a that are related via (5.32). Since $\sum_{a=1}^{8} R_a^2 = \sum_{a=1}^{8} L_a^2$, these two multiplets have *identical* sets of p and q values that characterize $SU(3)$ multiplets. Thus, in similarity to the quark model wave function which can be viewed as a product of $SU(2)$-spin and $SU(3)$-flavor multiplets, the soliton quantization produces states that are represented by a product of two identical $SU(3)$ representations. The states in $SU(3)$ representations are labeled by $SU(2)$ and $U(1)$ quantum numbers. In the case of flavor, this is isospin and flavor, cf. Fig. 6.1. In the case of the $SU(3)$ representation for the right generators, the $SU(2)$ quantum number describes spin since $R_i = -J_i$ for $i = 1, 2, 3$. The corresponding $U(1)$ label is the *right hypercharge* that is fixed by the constraint to be $Y_{\mathrm{R}} = \frac{2}{\sqrt{3}} R_8 = \frac{N_{\mathrm{C}} B}{3}$. The constraint actually commutes with the Hamiltonian for the collective coordinates. It may thus be considered as a condition for the allowed multiplets. The energy eigenvalue of states within a given multiplet is then straightforwardly found to be[3]

$$E = E_{\mathrm{cl}} + \frac{1}{2}\left(\frac{1}{\alpha^2} - \frac{1}{\beta^2}\right) j(j+1) + \frac{1}{6\beta^2}\left(p^2 + q^2 + pq + 3p + 3q\right) - \frac{N_{\mathrm{C}}^2 B^2}{24\beta^2}\,, \tag{6.11}$$

where j is the spin eigenvalue of the considered state. At the moment, we are not really interested in the resulting spectrum for which the so far omitted flavor symmetry breaking is an important ingredient.

We will now work out the allowed multiplets in detail. To enlighten the following discussion a bit, the state content of a typical (higher dimensional) $SU(3)$ multiplet is displayed in Fig. 6.2. In terms of the two integers p and q, the hypercharge of the states at the top of an $SU(3)$ multiplet is $Y^{(\mathrm{top})} = \frac{p+2q}{3}$. The hypercharge of any other state in that multiplet differs by an integer $t \leq p + q$. Hence, the constraint implies

$$p + 2q = N_{\mathrm{C}} B + 3t \tag{6.12}$$

for the allowed multiplets. Actually, the integer t plays the role of Biedenharn's triality [6].

The states with a fixed hypercharge form a multiplet concerning the $SU(2)$ subgroup. Let us denote the largest $SU(2)$ eigenvalue within such a multiplet by $m_{\max}$. For the states at the top of the $SU(3)$ multiplet, we have $m_{\max}^{(\mathrm{top})} = \frac{p}{2}$. Thus, this maximal quantum number for the other states in the multiplet is (determined from the states farthest to the right in Fig. 6.2)

[3] For details on $SU(3)$ representation theory, we refer to the textbooks [4, 5].

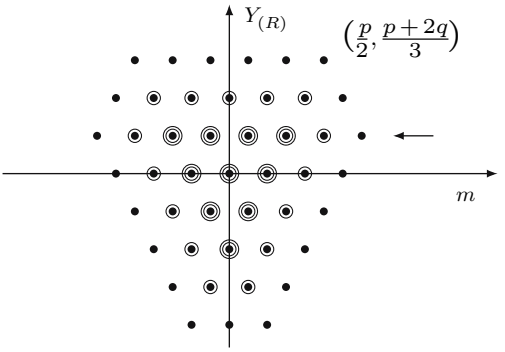

Fig. 6.2. A typical higher dimensional $SU(3)$ multiplet with $p = 5$ and $q = 2$. The dimension of this multiplet is $D = \frac{1}{2}(p+1)(q+1)(p+q+2) = 81$. Multiply occupied states are indicated by circles. The arrow indicates the $SU(2)$ submultiplet that satisfies the constraint $Y_{\mathrm{R}} = 1$ and carries $t = 2$, cf. (6.12). Also the state that possesses the largest m and Y quantum numbers is made explicit at the *top right*

$$m_{\max} = \begin{cases} \frac{p}{2} + \frac{t}{2} & t \leq q \\ \frac{p}{2} - \frac{t}{2} + q & t \geq q\,. \end{cases} \tag{6.13}$$

Eliminating the label p via the constraint, (6.12) yields

$$m_{\max} = \frac{N_{\mathrm{C}} B}{2} + \begin{cases} 2t - q & t \leq q \\ t & t \geq q\,. \end{cases} \tag{6.14}$$

This implies that $m_{\max}$ is half-integer valued whenever the product $N_{\mathrm{C}} B$ is odd, regardless of the considered multiplet and the value of t. This is an important result as $m_{\max}$ being half-integer causes the eigenvalues for J_3 to be half-integer as well. Hence, for the particularly interesting case of $B = 1$, the quantized Skyrmion describes fermions for N_{C} odd and bosons for N_{C} even, just as in the quark model. Recalling that the constraint emerged from the Wess–Zumino term, we see that reproducing the anomaly structure of QCD induces the proper statistics upon the Skyrmion.

It is furthermore important to note that $m_{\max}$ is just the largest allowed $SU(2)$ quantum number. States in the interior of an $SU(3)$ multiplet may be degenerate and are distinguished by the *highest weight* that they carry with respect to the $SU(2)$ subgroup. For example, in the 81-dimensional representation shown in Fig. 6.2, the allowed states are up to threefold occupied and spin eigenvalues of $J = \frac{7}{2}$, $\frac{5}{2}$ and $\frac{3}{2}$ emerge. The latter may eventually mix with Δ-type baryons when flavor symmetry is abandoned.

The starting picture to quantize the Skyrmion is obviously quite different from the quark model, where the wave functions are products of $SU_{\mathrm{S}}(2)$ and $SU_{\mathrm{F}}(3)$ representations for spin and flavor, respectively. The Skyrmion quantization is that of a product of two identical $SU(3)$ representations, one

of which contains the spin degrees of freedom. At the end, the constraint from the Wess–Zumino terms takes care that in this representation only those states are allowed that have the same spin properties as the baryon states in the $SU(6)$ constituent quark model when decomposed with respect to the $SU_{\rm S}(2) \times SU_{\rm F}(3)$ content [7]. Nevertheless, matrix elements turn out equivalent in the two models as $N_{\rm C} \to \infty$ [8].

We may actually understand the important result that the constraint leads to half-integer spin without going into the details of group theory. There is a simple analogy in particle phenomenology which, after all, has already solved $SU(3)$ representation theory for us for the physical case of $B = 1$ and $N_{\rm C} = 3$. Similar to the Gell–Mann-Nishijima relation for the electric charge, we may define a right charge operator

$$Q_{\rm R} = R_3 + \frac{1}{2} Y_{\rm R} = -J_3 + \frac{1}{2} Y_{\rm R} \,. \tag{6.15}$$

Its eigenvalues are completely determined by the $SU(3)$ algebra. Fortunately, we do not have to calculate them because the quark model tells us that possible eigenvalues are $Q_{\rm R} = 0, \pm\frac{1}{3}, \pm\frac{2}{3}, \pm 1, \pm\frac{4}{3}, \ldots$; no half–integer charge is allowed. For $Y_{\rm R} = 1$, this eigenvalue relation, (6.15), can only be consistently accommodated with J_3 being half-integer. This argument can be generalized to arbitrary (odd) $N_{\rm C}$. The electric charges of hadrons that are built from such quarks are $Q = ne/N_{\rm C}$, where n is an integer and e the elementary charge (cf. footnote 1 in Appendix C). The analogy with the quark model also teaches us to write $Q_{\rm R} = n_{\rm R}/N_{\rm C} = -J_3 + (B_{\rm R} + S_{\rm R})/2 = m/N_{\rm C}$, where $B_{\rm R}$ and $S_{\rm R}$ are right baryon and strangeness numbers, respectively. While $S_{\rm R}$ is integer, we eliminate $B_{\rm R}$ in favor of the constraint in the form $N_{\rm C} B = 3Y_{\rm R} = N_{\rm C} B_{\rm R} + 3S_{\rm R}$ so that the condition

$$n_{\rm R} = N_{\rm C} \left(\frac{B}{2} - J_3 \right) + \frac{S_{\rm R}}{2} \, (N_{\rm C} - 3) \tag{6.16}$$

demands half-integer J_3 when B is odd because $n_{\rm R} - S_{\rm R}(N_{\rm C} - 3)/2$ is integer for odd $N_{\rm C}$ regardless of what integer value $S_{\rm R}$ assumes.

In Sect. 5.2, we have already seen that the left generators are the isospin charges in the two-flavor model, cf. (5.36). This generalizes to the flavor charges in $SU(3)$ which we label by the eight-dimensional vector $\boldsymbol{Q}$:

$$\boldsymbol{Q} = -D^\dagger \cdot \frac{\partial L}{\partial \boldsymbol{\Omega}} = -D^\dagger \boldsymbol{R} = \boldsymbol{L} \,. \tag{6.17}$$

As was to be expected, this identity shows that the multiplets associated with the left $SU(3)$ are flavor multiplets alike in the quark model. The interesting feature is that the allowed multiplets are selected by the Wess–Zumino term.

We will say more about the resulting spectrum at arbitrary $N_{\rm C}$ in Sect. 9.4. Let us next discuss that in more detail for the physically interesting case of $N_{\rm C} = 3$ and $B = 1$. For $t = 0$, the constraint, (6.12), becomes $p + 2q = 3$,

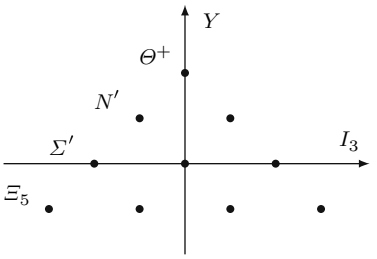

Fig. 6.3. The flavor content of the anti-decuplet

which can be accommodated by $(p,q) = (1,1)$ and $(p,q) = (3,0)$. The former is the octet (**8**) and the latter is the decuplet (**10**) whose flavor (left) states are depicted in Fig. 6.1. Concerning the right quantum numbers, (6.13) immediately shows that the octet may only contain $J = \frac{1}{2}$ states. These are to be identified with nucleon and the ordinary hyperons. In general, $m_{\max} = \frac{3}{2}$ would allow for $J = \frac{3}{2}$ and $J = \frac{1}{2}$ states in the decuplet. Since the decuplet is a triangle representation, there is no degeneracy and the $Y_{\mathrm{R}} = 1$ submultiplet only has $J = \frac{3}{2}$ states. These are to be identified with the Δ-type resonances, including the excited hyperons Σ^*, Ξ^* and Ω. As long as we do not consider any flavor symmetry breaking, the states within a given multiplet are predicted to possess identical masses, as can be easily deduced from (6.11).

The lowest dimensional multiplet with $t = 1$ is the anti-decuplet. It will be of particular relevance when discussing exotic states in Chap. 9. It is the complex conjugate of the decuplet and has $(p,q) = (0,3)$. Hence, we expect the states in that multiplet to lie roughly $\frac{3}{2\beta^2} \approx 500\,\mathrm{MeV}$ above the nucleon [6, 9, 10]. The corresponding Young–Tableaux is $\begin{array}{|c|c|c|}\hline \\ \hline \end{array}$ and the flavor content is shown in Fig. 6.3. The states on the top (Θ^+) and the bottom (Ξ_5) have strangeness $S = +1$ and $S = -2$ and isospin $I = 0$ and $I = \frac{3}{2}$, respectively. These states cannot be built from three quarks; rather these quantum numbers require configurations with four quarks and an anti-quark. This motivates the notion of pentaquarks. The anti-decuplet also contains a nucleon-type state (N') as well as Σ-type states. These are sometimes referred to as crypto-exotic pentaquarks. Once flavor symmetry breaking is switched on, these states mix with the nucleon and Σ from the octet. The $SU(2)$ submultiplet of the anti-decuplet with $Y = 1$ is a doublet. Turning to the right multiplet $Y_{\mathrm{R}} = 1$, thus implies that the anti-decuplet states have $J = \frac{1}{2}$. Of course, all flavor rotational excitations have the same parity as the nucleon, which by convention is $+1$.

6.3 Flavor Symmetry Breaking

So far, we have considered the unrealistic flavor symmetric case. Though that has been extremely fruitful to understand the quantization of the chiral soliton in flavor $SU(3)$, we may not expect to reproduce empirical data reliably. After all, nucleons and hyperons are not degenerate.

To construct the model Lagrangian, we have to understand the chiral transformation properties of a general flavor symmetry breaking term $\mathcal{L}_{\rm sb}$ in the effective meson Lagrangian. Upon bosonization of the quark flavor interaction such terms arise from the mass term of QCD, which has the same chiral properties as the mass term in the NJL model (2.8). We may characterize its bosonization by

$$\sum_{i,j=1}^{N_f} (\hat{m}_0)_{ij} \left(\bar{q}_{{\rm R}j} q_{{\rm L}i} + \bar{q}_{{\rm L}j} q_{{\rm R}i}\right) \longrightarrow \sum_{i,j=1}^{N_f} (\hat{m}_0)_{ij} \left(M + M^\dagger\right)_{ij} , \tag{6.18}$$

where $\hat{m}_0$ is the (diagonal) current quark mass matrix and M is the meson field that arises after bosonization (2.28). The bosonization of the interaction terms will alter the chiral symmetric pieces, and also higher order derivative contributions will eventually emerge in the effective meson Lagrangian. Though that complicates matters, the above prescription teaches us two important features about the structure of the flavor symmetry breaking terms in the chiral Lagrangian:

- Flavor symmetry breaking terms will involve powers of the current quark mass matrix. Under the assumption of isospin symmetry ($m_{0,u} = m_{0,d}$), the current quark mass matrix can be parameterized as

$$\hat{m}_0 = \frac{1}{3}\left[2m_{0,u}\left(\mathbb{1} + \frac{\sqrt{3}}{2}\lambda_8\right) + m_{0,s}\left(\mathbb{1} - \sqrt{3}\lambda_8\right)\right] \tag{6.19}$$

  in the three-flavor case. Since $m_{0,u} \ll m_{0,s}$, the second term dominates.
- To linear order in $\hat{m}_0$, we may generally write

$$\mathcal{L}_{\rm sb} = \sum_i c_i {\rm tr}\left\{F_i\left(M, \partial_\mu M\right) + {\rm h.c.}\right\} + \sum_i \tilde{c}_i {\rm tr}\left\{\lambda_8 \tilde{F}_i\left(M, \partial_\mu M\right) + {\rm h.c.}\right\} , \tag{6.20}$$

  where h.c. stands for Hermitian conjugate. The c_i and $\tilde{c}_i$ arise from bosonization but may in practice be determined form experimental data. They vanish in the flavor symmetric limit. The important issue is that the functions F_i and $\tilde{F}_i$ unambiguously transform under global chiral transformations, (2.30),

$$F_i\left(LMR^\dagger, \partial_\mu(LMR^\dagger)\right) = LF_i\left(M, \partial_\mu M\right)R^\dagger \tag{6.21}$$

  and similarly for $\tilde{F}_i$. One way of arguing is that under the assumption $\hat{m}_0 \to R\hat{m}_0 L^\dagger$, all terms transform like singlets.

In the Skyrme model, matters simplify a bit since we only have pseudoscalar fields $M \propto f_\pi U$. Also, we wish to consider a minimal set of flavor symmetry breaking terms. We merely want $\mathcal{L}_{\rm sb}$ to describe the differences between the kaon and pion masses as well as the associated decay constants. To

this end, it is sufficient to only consider contributions linear in flavor symmetry breaking:

$$\mathcal{L}_{\rm sb} = \frac{f_\pi^2 m_\pi^2 + 2 f_K^2 m_K^2}{12} {\rm tr}\left[U + U^\dagger - 2\right] + \sqrt{3}\frac{f_\pi^2 m_\pi^2 - f_K^2 m_K^2}{6} {\rm tr}\left[\lambda_8 \left(U + U^\dagger\right)\right] + \frac{f_K^2 - f_\pi^2}{12} {\rm tr}\left[\left(1 - \sqrt{3}\lambda_8\right)\left(U\partial_\mu U^\dagger \partial^\mu U + U^\dagger \partial_\mu U \partial^\mu U^\dagger\right)\right] . \tag{6.22}$$

In total, we therefore consider the effective meson action

$$\Gamma = \int {\rm d}^4 x \left\{\mathcal{L}_{{\rm nl}\sigma} + \mathcal{L}_{\rm Sk} + \mathcal{L}_{\rm sb}\right\} + \Gamma_{\rm WZ}, \tag{6.23}$$

with the various pieces listed in (4.23), (4.26), (6.22) and (4.40) as a realistic starting point for a soliton description of baryons in flavor $SU(3)$. We expand the chiral field in terms of pseudoscalar modes, normalize them properly and extract the axial current to easily verify that f_π and f_K are the respective decay constants [11].

At this point only $\mathcal{L}_{\rm sb}$ is new. Substituting the rigidly rotating chiral soliton, (6.4) adds

$$L_{\rm sb} = -\frac{1}{2}\gamma[F]\left(1 - D_{88}(A)\right) \tag{6.24}$$

to the Lagrange function for the collective coordinates, (6.5). Since flavor symmetry is explicitly broken, the collective coordinates appear explicitly. In (6.24), this appearance is parameterized by the adjoint representation, cf. (5.32) with $T_a = \lambda_a/2$. The constant of proportionality is a functional of the chiral angle and contains the information about different masses and decay constants of the pseudoscalar mesons:

$$\gamma[F] = \frac{4}{3}\int {\rm d}^3 r \left\{ \left(m_K^2 f_K^2 - m_\pi^2 f_\pi^2\right)\left(1 - \cos F\right) + \frac{1}{2}\left(f_K^2 - f_\pi^2\right)\cos F \left(F'^2 + 2\frac{\sin^2 F}{r^2}\right)\right\}. \tag{6.25}$$

Note that we have omitted contributions from $\mathcal{L}_{\rm sb}$ that are quadratic in the angular velocities. Those would emerge from the term proportional to the $(f_K^2 - f_\pi^2)$. As we will see later, the direct influence of that term is minor. Neither did we make explicit contribution from $\mathcal{L}_{\rm sb}$ to the functionals $E_{\rm cl}$, α^2 and β^2. Actual computations take this into account. It is straightforward to include $L_{\rm sb}$ in the Legendre transformation to get the Hamiltonian for the collective coordinates with symmetry breaking effects included,

$$H(A, R_a) = E_{\rm cl} + \frac{1}{2}\left[\frac{1}{\alpha^2} - \frac{1}{\beta^2}\right]\boldsymbol{J}^2 + \frac{1}{2\beta^2}C_2(SU(3)) - \frac{3}{8\beta^2} + \frac{1}{2}\gamma\left(1 - D_{88}(A)\right) . \tag{6.26}$$

We still have to recognize the constraint on $Y_{\rm R}$. Fortunately, it commutes with $H(A, R_a)$ even in the presence of symmetry breaking. So we may apply it

solely onto the states. Since $[R_a, D_{88}] \neq 0$ as well as $\left[\sum_{a=1}^{8} R_a^2, D_{88}\right] \neq 0$, it is obvious that definite $SU(3)$ representations will no longer serve to diagonalize this Hamiltonian. In a first attempt, one might want to treat the Hamiltonian, (6.26), in perturbation theory. Noting that the symmetry breaking part can be written in terms of an $SU(3)$ D-function, $D_{88} = D^{\mathbf{8}}_{000,000}$, the required matrix elements are given in terms of $SU(3)$ Clebsch–Gordan coefficients [12]:

$$\begin{aligned}(-1)^{J+J'-J_3-J_3'}&\langle \mu'; Y', I', I_3'; Y_{\mathrm{R}}', J', J_3'|D_{88}(A)|\mu; Y, I, I_3; Y_{\mathrm{R}}, J, J_3\rangle \\ &= \sqrt{\frac{\dim\mu}{\dim\mu'}} \sum_{\gamma} \begin{pmatrix} \mathbf{8} & \mu & \mu'_\gamma \\ 000\ Y I I_3 & Y', I', I_3' \end{pmatrix} \begin{pmatrix} \mathbf{8} & \mu & \mu'_\gamma \\ 000\ Y_{\mathrm{R}} J - J_3 & Y_{\mathrm{R}}', J', -J_3' \end{pmatrix} . \quad (6.27)\end{aligned}$$

The sum (over γ) occurs because the Clebsch–Gordan expansion of the product $\mathbf{8} \otimes \mu$ may contain the $SU(3)$ representation μ' more than once, e.g.,

$$\mathbf{8} \otimes \mathbf{8} = \mathbf{1} \oplus \mathbf{8}_1 \oplus \mathbf{8}_2 \oplus \mathbf{10} \oplus \overline{\mathbf{10}} \oplus \mathbf{27}\,. \quad (6.28)$$

Turning to the interesting value $Y_{\mathrm{R}} = 1$, the first-order modification of the energy eigenvalues for the octet baryons due to the flavor symmetry breaking is readily evaluated to be [13]

$$\begin{aligned} 2\beta^2 \Delta M_N &= -\frac{1}{5}\,\omega^2\,; \qquad 2\beta^2 \Delta M_\Lambda = -\frac{1}{15}\,\omega^2\,; \\ 2\beta^2 \Delta M_\Sigma &= \frac{1}{15}\,\omega^2\,; \qquad 2\beta^2 \Delta M_\Xi = \frac{2}{15}\,\omega^2\,, \end{aligned} \quad (6.29)$$

where the effective symmetry breaking parameter $\omega^2 = \frac{3}{2}\gamma\beta^2$ (ratio of symmetry breaking potential to flavor rotation energy) has been introduced [14]. In a similar fashion the change of the baryon wave functions may be obtained. This results in deviations from pure octet (or decuplet) states. Of course, the admixture may only contain contributions from states that have identical identical spin–flavor quantum numbers and are members of representations that satisfy the constraint, (6.12). For example, to $\mathcal{O}\left(\omega^2\right)$, the octet nucleon state is perturbed by nucleon-type states in the anti-decuplet, cf. Fig. 6.3, and the **27**-plet [15]:

$$|N\rangle = |N, \mathbf{8}\rangle + 0.0497\omega^2 |N, \overline{\mathbf{10}}\rangle + 0.0327\omega^2 |N, \mathbf{27}\rangle + \cdots \quad (6.30)$$

We will later see that calculations up to only first order are generally not sufficient for convergence. The obvious way to preceed is the inclusion of higher order terms. Numerically, it turns our that for physically relevant values of ω^2, convergence appears at third order. Here it is worth to mention that in the perturbation series for the octet baryons up to third order in ω, only the two representations $\overline{\mathbf{10}}$ and $\mathbf{27}$ occur [15]. Similarly, one can adopt all states in representations that are allowed by the constraint, (6.12), as basis states, compute the matrix elements of the symmetry breaker according to (6.27) and numerically diagonalize the (truncated) matrix of the Hamiltonian

operator, (6.26), to obtain the exact energy eigenvalues and states [10, 16]. Equivalently, we achieve exact diagonalization by abandoning the concept of $SU(3)$ representations but introducing eight $SU(3)$ Euler angles to parameterize the collective rotations $A(t)$ and quantize these angles canonically. This procedure is known as the Yabu–Ando approach [14], and we will explain it in more detail in the next section.

6.4 Diagonalization with Flavor Symmetry Breaking

A suitable Euler angle parameterization of the collective rotations A is given in (D.1) and (D.2). The crucial feature that makes possible the exact diagonalization of the Hamiltonian, (6.26), is that the potential depends only on a *single* of the eight Euler angles:

$$1 - D_{88} = \frac{3}{2}\sin^2\nu\,. \tag{6.31}$$

This particular angle parameterizes the soliton's collective flavor rotation into strangeness direction; it is the strangeness changing Euler angle. With this simplification, the Schrödinger-type equation

$$\left[C_2 + \omega^2 \sin^2\nu\right]\Psi = \epsilon_{\rm SB}\Psi\,, \tag{6.32}$$

which in the general Euler angle description is a coupled partial differential equation in eight variables, boils down to a set of coupled ordinary differential equations for only a single variable, the strangeness changing angle ν. These equations are numerically integrated in each spin–isospin channel separately. Technical details of that treatment may be traced from Appendix D. The so-computed eigenvalue, $\epsilon_{\rm SB}$, then enters the mass formula for the baryons:

$$M_{\rm B} = E_{\rm cl} + \frac{1}{2}\left(\frac{1}{\alpha^2} - \frac{1}{\beta^2}\right) J(J+1) - \frac{N_{\rm C}^2 B^2}{24\beta^2} + \frac{1}{2\beta^2}\epsilon_{\rm SB}\,. \tag{6.33}$$

This represents the *exact* eigenvalue of the collective coordinate Hamiltonian (6.26). Since this diagonalization procedure does not make explicit contact with $SU(3)$ representations, the constraint on $Y_{\rm R}$ can easily be implemented by simply substituting the appropriate numerical value in (D.9). Although this approach was originally formulated for $N_{\rm C} = 3$ [14], the generalization to arbitrary (odd) $N_{\rm C}$ is straightforward [17].

For physical applications, we surely consider the case $Y_{\rm R} = 1$. In Table 6.1, we compare the predicted mass differences (with respect to the nucleon) from (6.33) with the experimental data. Note that the employed Skyrme model only has a single free parameter, which we take to be $e = 4.0$, i.e., only slightly different from the two-flavor model. The decay constants and the

Table 6.1. Comparison of predicted mass differences to the experimental data for the low-lying $J = \frac{1}{2}$ and $J = \frac{1}{3}$ baryons in the Skyrme and vector meson (VM) models

baryon	Skyrme	VM	expt.
$\Lambda - N$	163	159	177
$\Sigma - N$	264	270	254
$\Xi - N$	388	398	379
$\Delta - N$	268	311	293
$\Sigma^* - N$	406	448	446
$\Xi^* - N$	545	592	591
$\Omega - N$	680	718	733

meson masses are fixed to their empirical values. As of such, the 10% or better agreement should be characterized as good.

A similar computation has been performed in the vector meson model that has been presented in Sect. 4.7 [1, 18]. In comparison with the Skyrme model, the three-flavor treatment of this vector meson model is conceptually more complicated because of two reasons:

(i) additional symmetry breaking terms

$$\alpha_1[U] \sum_{i=1}^{3} D_{8i} R_i \,, \quad \beta_1[U] \sum_{\alpha=4}^{7} D_{8\alpha} R_\alpha \,, \quad \text{etc.}, \tag{6.34}$$

occur that must be expressed in Euler angles as (6.31) and included in the eigenvalue problem, (6.32),

(ii) strange vector meson field components that vanish classically get induced by the collective rotations into strangeness direction in addition to those already induced by the $SU(2)$ rotations, (5.64).

We refrain from exploring these complications in detail, but merely quote the numerical results in Table 6.1. Obviously, the model describes the spectrum well. Again this computation supports the choice $\kappa \approx 1$ for the parameter that could not be fixed from meson properties, cf. the discussion after (4.66).

For the spin $\frac{1}{2}$ baryons, the exact diagonalization is important as significant deviations from the first-order approximation, (6.29), occur. This becomes most obvious from the ratios of mass differences shown in Table 6.2. This comparison not only shows that the first-order treatment is insufficient

Table 6.2. Ratios of mass differences between baryons with spin $\frac{1}{2}$. The entry "exact" gives the predictions from the exact diagonalization of (6.32), while the last column refers to the approximation of (6.29). The empirical data are shown in column "expt."

baryon mass diff.	exact	expt.	1. ord.
$(M_\Lambda - M_N) : (M_\Sigma - M_\Lambda) : (M_\Xi - M_\Sigma)$	1:0.61:0.76	1:0.43:0.69	1:1:0.5

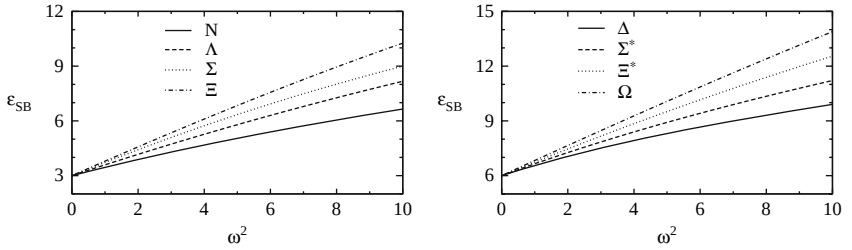

Fig. 6.4. Solutions to the Schrödinger-type equation (6.32) as functions of the strength of the symmetry breaking, ω^2. The left and right panels contain the spin $\frac{1}{2}$ and $\frac{3}{2}$ states, respectively

for convergence but also that it predicts the Σ hyperon far too low. There are other approaches which cure this shortcoming by introducing a symmetry breaker that is linear in the hypercharge. Though such a term is indeed permitted by the symmetries, it requires a contribution to $\mathcal{L}_{\rm sb}$, (6.22), that is linear in the time derivatives. This cannot be constructed from $\alpha_\mu = U^\dagger \partial_\mu U$ in a Lorentz covariant fashion. Vector or chiral quark interactions as in [2, 3, 18] must be added. In any event, the symmetry breaker proportional to $1 - D_{88}$ dominates in all these models so that higher order contributions in symmetry breaking are sizable and important.

The first-order treatment yields an equal spacing in the spectrum of the spin $\frac{3}{2}$ baryons [13]. Higher order contributions cause only minor modifications thereof. These results are summarized in Fig. 6.4 which shows the dependences of the eigenvalues $\epsilon_{\rm SB}$ on the symmetry breaking strength for all low-lying spin $\frac{1}{2}$ and spin $\frac{3}{2}$ baryons.

6.5 Beyond the Classical Hedgehog Solution

So far, we have treated the three-flavor soliton by rigidly rotating the two-flavor hedgehog in $SU_{\rm F}(3)$. It is pretty obvious that this can only be an approximation. Consider, e.g., the asymptotic behavior of the chiral field U. Regardless of the flavor orientation $A \in SU(3)$, it is solely determined by the pion mass as in (4.29). However, the symmetry breaking terms imply that the kaonic components of U should asymptotically approach the vacuum value with a Yukawa tail that is governed by the kaon mass. To improve the rigid rotator approximation, we assume that the soliton rotates so slowly[4] that its shape adjusts itself to the forces exerted by symmetry breaking and the time derivatives of the collective coordinates may be omitted in a first step. Since spin and isospin coordinates can be absorbed by global symmetry transformations, this corresponds to the field parameterization

[4] This motivates the nomenclature *slow rotator approach* (SRA).

$$U(\boldsymbol{x},\nu) = \mathrm{e}^{-\mathrm{i}\nu\lambda_4} U_H(\boldsymbol{x})\, \mathrm{e}^{\mathrm{i}\nu\lambda_4}\,, \tag{6.35}$$

with constant strangeness changing angle ν, cf. (D.1). Substituting this field configuration into the Lagrangian yields an energy functional that parametrically depends on ν [19]:

$$\begin{aligned} E(\nu)[F] = \int \mathrm{d}^3 r \Bigg[& \frac{f_\pi^2}{2}\left(F'^2 + 2\frac{\sin^2 F}{r^2}\right) + \frac{\sin^2 F}{e^2 r^2}\left(F'^2 + \frac{\sin^2 F}{2r^2}\right) \\ & + m_\pi^2 f_\pi^2 (1-\cos F) \\ & + \sin^2\nu \Big[\frac{1}{2}\left(f_K^2 - f_\pi^2\right)\left(F'^2 + \frac{2\sin^2 F}{r^2}\right)\cos F \\ & + \left(m_K^2 f_K^2 - m_\pi^2 f_\pi^2\right)(1-\cos F) \Big] \Bigg]\,. \end{aligned} \tag{6.36}$$

The minimum of the energy functional (6.36) is obtained by varying this functional with respect to $F(r)$ at fixed $\nu \in [0, \pi/2]$. Hence, the chiral angle is a function not only of the radial distance but also of the strangeness changing Euler angle ν: $F = F(r,\nu)$. It is then obvious that the symmetry breaking forces yield $F(r,\pi/2) \to \exp(-m_K r)$ for $r \to \infty$, i.e., in the slow rotator approach, the kaon field has the proper asymptotic behavior (Yukawa tail). This chiral angle also causes the (minimal) classical energy to implicitly depend on ν on top of the $\sin^2\nu$ term in (6.36).

In the second step, the quantization of the slow rotator proceeds along the line of the rigid rotator by subsequently taking all Euler angles to be time dependent. Essentially, this yields the moments of inertia to be ν dependent. Accounting for ordering ambiguities by hermitionizing, the Hamilton operator reads

$$\begin{aligned} H = E(\nu) & + \left(\frac{1}{2\alpha^2(\nu)} - \frac{1}{2\beta^2(\nu)}\right)\mathbf{J}^2 \\ & + \frac{1}{2}\left\{\frac{1}{2\beta^2(\nu)}, C_2\left[SU(3)\right]\right\} - \frac{3}{8\beta^2(\nu)}\,. \end{aligned} \tag{6.37}$$

An additional contribution proportional to $\left(\frac{\mathrm{d}\nu}{\mathrm{d}t}\right)^2$ has been shown to be negligibly small [19] and is further on omitted. Since the quadratic Casimir operator may essentially be considered as a second-order differential operator of the strangeness changing angle ν, the eigenvalue problem $H\Psi = \epsilon\Psi$ is solved with

Table 6.3. Slow rotator results [19] for the baryon mass differences with respect to the nucleon compared to experimental data

baryon	Λ	Σ	Ξ	Δ	Σ^*	Ξ^*	Ω
model	177	285	381	298	477	619	731
expt.	177	254	379	293	446	591	733

the techniques introduced in Sect. 6.4. Table 6.3 contains the comparison of the resulting mass differences with the experimental data. In that calculation, the only free parameter was adjusted to $e = 3.46$ leading to a best fit for the overall picture of the mass differences. The resulting mass differences are similar to those obtained in the rigid rotator approach. As we will observe in Chap. 7 (cf. Table 7.2), the main feature of the chiral angle being sensitive to symmetry breaking is more strongly reflected in deviations of predicted static baryon properties from $SU(3)$ relations, most notably the magnetic moments.

Finally, we note that an additional technique exists to reflect symmetry breaking in the soliton extension. In [20, 21], a collective coordinate, $\mu(t)$ for the size of the soliton was introduced and included in the quantization of the rigid rotator. (This coordinate is often called *breathing mode*.) The symmetry breaking terms in the Lagrangian build a common potential for this new collective coordinate and the strangeness changing angle ν. Hence, the forces exerted on the size of the soliton vary even within a flavor multiplet and the quantization of μ also depends on the quantum numbers of the considered baryon: The expectation value of the size of the chiral angle decreases with (the modulos of) strangeness. In essence, this approach corresponds to a strangeness-dependent chiral angle similar to the slow rotator approach discussed above. It is thus not surprising that the results for baryon properties are similar in the two approaches. However, the quantization of μ also allows us to study radially excited baryons. Here we will not further elaborate on this approach but eventually reconsider it and present numerical results in the framework of non-harmonic excitations in Sect. 8.5 and when discussing exotic baryons in Chap. 9.

6.6 Bound State Approach

In the previous sections, we have discussed several treatments of the three-flavor soliton model. They were based on the assumption that the time-dependent solution to the Euler–Lagrange equations is reasonably approximated by elevating the coordinates which parameterize the flavor orientation to time-dependent quantities. Of course, such treatments are motivated by considering the flavor symmetry to be approximately realized, allowing for large amplitude fluctuations into the direction of the "would-be" symmetry. Subsequently, the symmetry breaking effects are treated within the space of these collective coordinates. The exact diagonalization of the resulting collective Hamiltonian is possible according to the Yabu–Ando approach [14] and yields the baryon masses and wave functions. Adopting, however, the contrary point of view that only small amplitude fluctuations are permitted for the broken symmetry, implying that the corresponding restoring forces are significant, leads to the treatment that has become known as the *bound state approach* (BSA). The reason for this notion is that hyperons are constructed out of the soliton and a kaon mode, which is bound in the background field of the soliton. This treatment has been initiated by Callan and Klebanov [22, 23]

and later been employed in many aspects, as will be partially sketched in this section. Actually, this approach is comparable to the old compound hypothesis, where hyperons are considered as molecules consisting of a nucleon and a kaon [24].

To introduce the strangeness degrees of freedom as small amplitude fluctuations, we consider the parameterization

$$U(\boldsymbol{x},t) = \xi_\pi \mathrm{e}^{\mathrm{i}Z} \xi_\pi \quad \text{with} \quad Z = \frac{\sqrt{2}}{f_K} \left(\begin{array}{c|c} 0 & K(\boldsymbol{x},t) \\ \hline K^\dagger(\boldsymbol{x},t) & 0 \end{array} \right) , \tag{6.38}$$

where ξ_π is a unitary matrix that differs only in the $SU(2)$ subgroup from the unit matrix such that $\xi_\pi^2 = U_H$ in (6.3). Furthermore, $K(\boldsymbol{x},t)$ is the isospinor that parameterizes the small amplitude kaon field. Expanding up to quadratic order in K yields the Lagrangian

$$\begin{aligned} \mathcal{L}_K = {} & (D_\mu K)^\dagger D^\mu K - m_K^2 K^\dagger K - \frac{f_\pi^2 m_\pi^2}{4 f_K^2} K^\dagger \left(\xi_\pi + \xi_\pi^\dagger - 2 \right) K \\ & - \frac{1}{2} K^\dagger K \mathrm{tr} \left(p_\mu p^\mu + \frac{1}{16 e^2 f_K^2} \left[\xi_\pi^\dagger \partial_\mu \xi_\pi, \xi_\pi^\dagger \partial_\nu \xi_\pi \right]^2 \right) \\ & + \frac{1}{2 e^2 f_K^2} \Big\{ (D_\mu K)^\dagger D_\nu K \mathrm{tr} \left(p^\mu p^\nu \right) - (D_\mu K)^\dagger D^\mu K \left(p_\nu p^\nu \right) \\ & - 3 (D_\mu K)^\dagger \left[p^\mu, p^\nu \right] D_\nu K \Big\} - \frac{\mathrm{i} N_\mathrm{C}}{4 f_K^2} B_\mu \left[K^\dagger D^\mu K - (D_\mu K)^\dagger K \right] . \end{aligned} \tag{6.39}$$

The covariant derivative is $D_\mu = \partial_\mu - \mathrm{i} v_\mu$ with p_μ and v_μ are those of (4.62) with ξ substituted[5] by ξ_π. The last term stems from the Wess–Zumino term (4.49). The derivation of its special from in (6.39) is outlined in Appendix C.

The factor $\frac{1}{f_K}$ in the parameterization, (6.38), causes all coefficients in the Lagrangian, (6.39), to be $\mathcal{O}\left(N_\mathrm{C}^0\right)$. Hence, the isospinor field $K(\boldsymbol{x},t)$ has a smooth limit as $N_\mathrm{C} \to \infty$. We will see in Chap. 8 that this feature is common to all harmonic fluctuations about the soliton. Furthermore, any higher order term in the expansion with respect to $K(\boldsymbol{x},t)$ will also contain additional powers of $\frac{1}{f_K}$ and thus vanish in the limit $N_\mathrm{C} \to \infty$. This implies the important feature that the bound state approach is exact in the large N_C limit [25].

While the general case for the field $K(\boldsymbol{x},t)$ is of physical relevance for scattering data (cf. Sect. 8), the P-wave channel is of particular interest for examining the spectrum and static properties of the low-lying baryons. This channel contains a bound state, evolving from the zero-mode that, in the flavor symmetric case, is associated with the rotation into the strange flavor direction. That is, this bound state is the "would-be" Goldstone boson of the

[5] We adopt that convention (for ξ and ξ_π) *only* in the context of the bound state approach to the Skyrme model, i.e., here and in Appendix C.3.

flavor rotations into strangeness direction. The suitable *ansatz* for this P-wave mode reads

$$K_{\rm P}(\boldsymbol{x},t) = \int \frac{{\rm d}\omega}{2\pi}\, {\rm e}^{-{\rm i}\omega t} k_{\rm P}(r,\omega)\hat{\boldsymbol{x}}\cdot\boldsymbol{\tau}\begin{pmatrix} a_1(\omega) \\ a_2(\omega)\end{pmatrix} . \tag{6.40}$$

The spectral functions $a_i(\omega)$ become creation and annihilation operators in the process of canonical quantization.

The Schrödinger-type equation for $k_{\rm P}(r,\omega)$ obtained from the Lagrangian, (6.39), can be cast in the form

$$\left\{-\frac{1}{r^2}\frac{\rm d}{{\rm d}r}\left(r^2 h(r)\frac{\rm d}{{\rm d}r}\right)+m_K^2+V_{\rm P}(r)-f(r)\omega^2+2\lambda(r)\omega\right\}k_{\rm P}(r,\omega)=0\,. \tag{6.41}$$

The explicit expressions of the radial functions h, $V_{\rm P}$, f and λ may be traced from the literature[6] [22, 23, 26]. The term linear in the frequency ω originates from the Wess–Zumino action and removes the degeneracy between solutions of positive and negative ω. From the orthogonality condition associated with the above differential equation, the normalization

$$2\int {\rm d}r r^2 k_{\rm P}(r,\omega)\left(f(r)\omega-\lambda(r)\right)k_{\rm P}(r,\omega)={\rm sgn}(\omega) \tag{6.42}$$

emerges. The so-normalized solutions to the bound state equation (6.41) are drawn in Fig. 6.5. In particular, it is illustrated how the bound state wave function evolves from the zero mode, which is proportional to $\sin(F/2)$, when the parameters are tuned from those describing the flavor symmetric case to physical ones. The bound state energy computed with the physical parameters ($m_K = 495\,{\rm MeV}$, $f_K = 1.22 f_\pi$) is $\omega_0 = 252\,{\rm MeV}$ for the Skyrme parameter $e = 4.25$. Note that the asymptotic form of the bound state wave function is $\exp(-\sqrt{m_K^2-\omega_0^2}\,r)$ rather than $\exp(-m_K r)$ as one would expect for a (static) kaon field.

The sign of the bound state energy also determines its strangeness because the integrand of the normalization condition, (6.42), arises from a derivative of the Lagrangian with respect to the kaon frequency, i.e., the phase of the kaon field. The corresponding Noether charge is strangeness. In correspondence to the quark model definition of strangeness, we have adopted sign conventions such that a positive frequency yields negative strangeness. To identify spin and flavor quantum numbers, we again resort to collective coordinate quantization. Since the kaon fields are already parameterized by the small amplitude fluctuations, we only require $A_2(t) \in SU(2)$ embedded in a 3×3 matrix:

$$U(\boldsymbol{x},t) = \left(\begin{array}{cc|c} & & 0 \\ & A_2(t) & 0 \\ \hline 0 & 0 & 1 \end{array}\right)\xi_\pi {\rm e}^{{\rm i}Z}\xi_\pi \left(\begin{array}{cc|c} & & 0 \\ & A_2^\dagger(t) & 0 \\ \hline 0 & 0 & 1 \end{array}\right) . \tag{6.43}$$

[6] If we only considered the non-linear model, (2.40), we would have $f \equiv 1$.

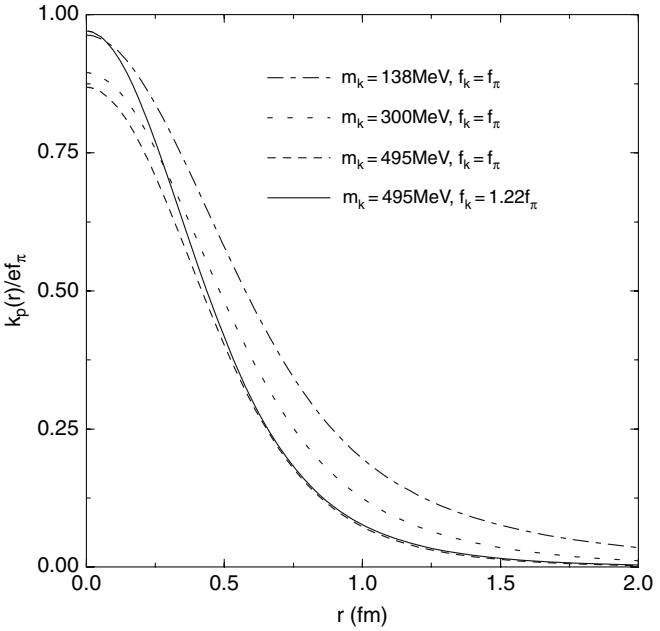

Fig. 6.5. The radial dependence of the bound state wave function in the Skyrme model. The normalization is according to (6.42). The parameters in the non-strange sector are $f_\pi = 93\,\mathrm{MeV}$, $e = 4.25$ and $m_\pi = 138\,\mathrm{MeV}$

This inclusion of the collective coordinates adds a term to the Lagrangian,

$$\Delta L = \frac{1}{2}\chi\,[F, k_\mathrm{P}]\,\boldsymbol{\Omega}\cdot\left(\sum_{i,j=1}^{2} a_i^\dagger \boldsymbol{\tau}_{ij} a_j\right) . \tag{6.44}$$

The angular velocity $\boldsymbol{\Omega}$ is obtained from $A_2(t)$ as in (5.16), while the operators a_i are defined in (6.40). The dimensionless constant of proportionality, χ, is a radial integral that involves the chiral angle, $F(r)$, and the normalized bound state wave function, $k_\mathrm{P}(r, \omega_0)$ [26]. We find $\chi = 0.332$ for $e = 4.25$. The quantization is made simple by the observation that the last factor in (6.44) is twice the total grand spin: the vector sum of the total spin and isospin in the intrinsic frame: $G_i = J_i + D_{ji} I_j$. The D-matrix for this transformation to the intrinsic frame is given in (5.22) and the isospin is conjugate to $\boldsymbol{\Omega}'$ as in (5.36). At the end, it should be obvious that the above term gives rise to a spin–isospin coupling proportional to $\boldsymbol{J}\cdot\boldsymbol{I}$ that can be reexpressed in terms of total spin ($J(J+1)$) and isospin ($I(I+1)$). Finally, the quantization of this system, which is discussed at length in the literature, cf. [23], yields the mass formula

$$M_\mathrm{B} = E_\mathrm{cl} + |S|\omega_0 + \frac{1}{2\alpha^2}\left[\chi J(J+1) + (1-\chi) I(I+1)\right] , \tag{6.45}$$

Table 6.4. Mass differences of the low-lying baryons with respect to the nucleon in the bound state approach to the Skyrme model. The Skyrme model parameter is taken $e = 4.25$ to properly reproduce $M_\Delta - M_N$. All data are in MeV

baryon	Λ	Σ	Ξ	Δ	Σ^*	Ξ^*	Ω
model, (6.45)	205	334	505	293	431	602	805
expt.	177	254	379	293	446	591	733

for the low-lying P-wave baryons with strangeness $S = 0, -1, -2, -3$. Obviously, χ parameterizes the hyperfine splitting. For consistency with the expansion, (6.39), contributions of order χ^2 and $\boldsymbol{G}^2 \sim (a_i)^4$ are omitted in the derivation of (6.45). The resulting mass differences are shown in Table 6.4. The approach overestimates the mass differences significantly, in particular for $S \leq -2$. This indicates that non-linear effects that are omitted in the bound state approach (but included in the rigid rotator treatment) are indeed important.

We have already seen that there is no degeneracy between the solutions to the Schrödinger-type equation (6.41) for $\pm\omega$. This implies that the spectrum in the $S = +1$ channel differs from the above studied case with $S = -1$. Actually, the $S = +1$ channel does not contain a bound state unless m_K is tuned to unphysically large values [27] or the strength of the Wess–Zumino term is artificially reduced [28]. Even more, above threshold this channel does not even posses a clear resonance, as can be seen from Fig. 9.5. Originally, that was interpreted as the absence of pentaquarks ($S = +1$ states must at least be built from four quarks and an anti-quark) in the Skyrme model [29]. In Chap. 9, we will discuss that issue in more detail and observe that this conclusion is premature.

We round up the discussion of the P-wave kaon fluctuations by noting that the bound state energy can reliably be estimated by sandwiching the equation of motion (6.41) between the properly normalized (would be) zero mode wave function (for the time being we assume $f_\pi = f_K$)

$$z(r) = \sqrt{4\pi}\frac{f_\pi}{\sqrt{\beta^2}}\sin\frac{F(r)}{2} \qquad \text{with} \qquad \int \mathrm{d}r r^2 z(r) f(r) z(r) \,=\, 1 \tag{6.46}$$

and solving for ω. We first define (not to be confused with the exact eigenvalue computed above)

$$\omega_0 = \int r^2 \mathrm{d}r z^2(r) 2\lambda(r) = \frac{N_\mathrm{C}}{4\beta^2}, \tag{6.47}$$

which is $\mathcal{O}(N_\mathrm{C}^0)$. Then the equation for ω reads

$$\omega^2 = \frac{3\gamma}{8\beta^2} + \omega_0\,\omega\,, \tag{6.48}$$

with the functional γ given in (6.25). This quadratic equation for ω has the negative valued solution $-\omega_\Lambda$ with

$$\omega_\Lambda = \frac{1}{2}\left[\sqrt{\omega_0^2 + \frac{3\gamma}{2\beta^2}} - \omega_0\right] . \tag{6.49}$$

The second solution for ω estimates the energy of the potential $S = +1$ pentaquark Θ^+, cf. Fig. 6.3,

$$\omega_\Theta = \frac{1}{2}\left[\sqrt{\omega_0^2 + \frac{3\gamma}{2\beta^2}} + \omega_0\right] . \tag{6.50}$$

Models typically yield $\omega_\Theta > m_K$ and $3\gamma/2\beta^2 > \omega_0^2$. This is in accordance with the above observation that there is no $S = +1$ bound state and suggests that a perturbation treatment in flavor symmetry breaking is bound to fail.

Utilizing the zero mode wave function to estimate the hyperfine parameters yields

$$\chi_- = 1 - \frac{4\alpha^2\omega_\Lambda}{8\beta^2\omega_\Lambda + N_\mathrm{C}} \qquad \text{and} \qquad \chi_+ = 1 - \frac{4\alpha^2\omega_\Theta}{8\beta^2\omega_\Theta - N_\mathrm{C}} , \tag{6.51}$$

where the subscript labels strangeness. The above estimates (6.49–6.51) may also be interpreted as the BSA results when the Hilbert space for the fluctuations is restricted to the collective modes of the soliton. We will return to that estimate in Sect. 9.4.

Finally, we remark that also the S-wave channel,

$$K_\mathrm{S}(\boldsymbol{x}, t) = \int \frac{\mathrm{d}\omega}{2\pi}\, \mathrm{e}^{-\mathrm{i}\omega t} k_\mathrm{S}(r, \omega) \begin{pmatrix} a_1(\omega) \\ a_2(\omega) \end{pmatrix} , \tag{6.52}$$

contains a bound state solution with negative strangeness. This state has been employed to describe the $\Lambda(1405)$ resonance [26].

6.7 Baryons with a Heavy Valence Quark

The description of baryons with heavy quarks is a voluminous subject on its own. Here we will merely allude to it because the techniques involved are very similar to those of the bound state approach discussed in the previous section. The interested reader may want to consult the numerous references listed in [30] for more thorough explorations of this subject.

Starting point for the treatment of heavy quarks is the important observation that QCD allows for an expansion in the inverse current quark mass. This expansion defines the heavy quark effective theory (HQET) [31]. A crucial result is that the spin-dependent forces are suppressed in the limit that this mass tends to infinity. As a consequence, pseudoscalar and vector mesons built from the same quarks become degenerate in that limit. This feature is indeed reflected in the data [32]:

$$m_{\mathrm{D}^{\pm *}} - m_{\mathrm{D}^\pm} \approx 138\,\mathrm{MeV} \qquad \text{and} \qquad m_{\mathrm{B}^{\pm *}} - m_{\mathrm{B}^\pm} \approx 46\,\mathrm{MeV} . \tag{6.53}$$

To construct an effective theory for these mesons, the pseudoscalar (P) and vector mesons (Q_ν) are first reparameterized such that the frequency of the fluctuating modes account for the large masses

$$\widetilde{P} = \mathrm{e}^{\mathrm{i}MV\cdot x}P \qquad \text{and} \qquad \widetilde{Q_\nu} = \mathrm{e}^{\mathrm{i}M^*V\cdot x}Q_\nu\,. \tag{6.54}$$

Here M and M^* are the (almost degenerate) pseudoscalar and vector meson masses, respectively. The four-velocity V^μ characterizes the reference frame of the heavy quark. The exponential functions take care that the leading order terms cancel in the effective meson Lagrangian when a large mass expansion is performed. Secondly, these fields are combined in a single heavy meson multiplet:

$$\mathcal{H} = \frac{1}{2}\left(1+\gamma_\mu V^\mu\right)\left(\mathrm{i}\gamma_5\widetilde{P}+\gamma^\nu\widetilde{Q}_\nu\right) \quad \text{and} \quad \bar{\mathcal{H}} = \gamma_0\mathcal{H}^\dagger\gamma_0\,. \tag{6.55}$$

The heavy meson fields P and Q_ν are isospinors for the case of two light flavors and so is $\mathcal{H}$. The corresponding components refer to the bound states of the heavy quark and the light (anti)quarks *up* and *down*, respectively. We are mostly interested in the interaction between heavy and light mesons. Of course, that should be governed by chiral symmetry for the light degrees of freedom of $\mathcal{H}$. A model Lagrangian with as few as possible derivatives acting on the light pseudoscalar meson fields reads

$$\frac{1}{M}\mathcal{L}_H \to \mathrm{i}V^\mu\mathrm{Tr}\left\{\mathcal{H}\left(\partial_\mu-\mathrm{i}v_\mu\right)\bar{\mathcal{H}}\right\} - \mathrm{d}\,\mathrm{Tr}\left\{\mathcal{H}\gamma_\mu\gamma_5 p^\mu\bar{\mathcal{H}}\right\}+\cdots\,, \tag{6.56}$$

where the ellipsis indicate subleading pieces in $1/M$. The currents v_μ and p_μ are defined in (4.62). The single new parameter can be determined from the semi-leptonic $D\to K$ transition: $d\approx 0.53$ [33, 34]. In [30, 35], the coupling to the light vector mesons ρ and ω was also studied. For clarity of presentation, their interaction with $\mathcal{H}$ is not made explicit in (6.56).

Having set up the model for the interaction between the heavy and light mesons, we attempt to construct a bound state solution for $\mathcal{H}$ in the same fashion as we did for the kaon field in Sect. 6.6. The soliton–bound state combination will describe a baryon with a heavy quark. In the first step, we substitute the hedgehog configuration for v_μ and p_μ. As for the kaon bound state, we require an *ansatz* for the $\mathcal{H}$. In the rest frame $V_\mu=(1,\mathbf{0})_\mu$, we have

$$\mathcal{H}^a = \begin{pmatrix} 0 & 0 \\ H^a & 0 \end{pmatrix} \tag{6.57}$$

in the standard representation for the Dirac matrices. Here $a=1,2$ ($\sim$*up*, *down*) is the isospin index and $H^a=(H^a_{\mathrm{lh}})$ is (for a prescribed value of a) a 2×2 matrix whose indices represent the spin projections of the light (l) and heavy (h) quarks inside the heavy meson. Again we expect the bound state to reside in the P-wave channel. In Fourier space for the frequency, the corresponding wave function reads

$$H^a_{\rm lh} = {\rm e}^{-{\rm i}\omega_{\rm B} t}\, \frac{u(r)}{\sqrt{2M}}\, (\boldsymbol{x}\cdot\boldsymbol{\tau})_{ad}\, \epsilon_{dl}\chi_{\rm h}\,. \tag{6.58}$$

The two-dimensional ϵ–tensor emerges from the contraction of the light isospin and spin components according to the hedgehog symmetry [36]. We now only require the solution to the Schrödinger equation for the radial function $u(r)$ to compute the binding energy $\omega_{\rm B}$. This is also simple because we already observe from Fig. 6.5 that the bound state wave function gets more and more concentrated at the center of the soliton as the meson mass increases. Hence, in the ultimate heavy quark limit, the bound state wave function is fully determined by the properties of the soliton at $r = 0$. To this end, the binding energy is found to be

$$\omega_{\rm B} = \frac{3}{2}{\rm d}F'(0) - \frac{3\sqrt{2}c}{gm_V}G''(0) + \frac{\alpha}{2}\omega(0)\,, \tag{6.59}$$

where primes denote derivatives with respect to the radial coordinate. In (6.59), we have again made explicit the contributions from the light vector meson profiles computed in Sect. 4.7. The coupling constant c can be estimated from the semi-leptonic decay $D \to K^*$ [34][7] to be $c \approx 1.60$. Unfortunately, there is no direct experimental evidence for the value of α. (It would be unity if a possible definition of light vector meson dominance for the electromagnetic form factors of the heavy mesons were to be adopted.) So α is commonly considered as a parameter. Typical numerical results for ω_B are of the order $700 - 900\,{\rm MeV}$ [35] and the difference $M - \omega_{\rm B}$ is the heavy quark limit of the mass difference between the nucleon and a heavy baryon, up to $1/N_{\rm C}$ corrections. In the bottom sector, the corresponding prediction $4260 - 4460\,{\rm MeV}$ underestimates the empirical value $M(\Lambda_{\rm B}) - M(N) = 4680 \pm 2\,{\rm MeV}$ somewhat. That is, the predicted binding energy is too large. Of course, we would ultimately like to investigate the finite heavy meson mass case and eventually compare its predictions to the above result. This will be sketched in the reminder of this section.

To consider finite heavy meson masses, we have to resort to the field variables P and Q_ν in (6.55) and develop a relativistic Lagrangian that yields (6.56) as M and M^* tend to infinity. With the transformation, (6.54), it is a matter of straightforward algebra to verify that the Lagrangian

$$\begin{aligned}\mathcal{L}_H = {} & (D^\mu P)^\dagger\, D_\mu P - \frac{1}{2}\,(Q^{\mu\nu})^\dagger\, Q_{\mu\nu} - M^2 P P^\dagger + M^{*2} Q^\dagger_\mu Q^\mu \\ & + 2{\rm i}Md\left[P^\dagger p_\mu Q^\mu - Q^\dagger_\mu p^\mu P\right] - \frac{d}{2}\,\epsilon^{\alpha\beta\mu\nu}\left[Q^\dagger_{\nu\alpha} p_\mu Q_\beta + Q^\dagger_\beta p_\mu Q_{\nu\alpha}\right]\,,\end{aligned} \tag{6.60}$$

with $Q_{\mu\nu} = D_\mu Q_\nu - D_\nu Q_\mu$ indeed turns into (6.56). In the absence of light vector mesons, the covariant derivative is as in (6.56), $D_\mu = \partial_\mu - {\rm i}v_\mu$. In fact,

[7] The sign of c (as well as d) is fixed by the assumption that there exists a continuous transition from the chiral Lagrangian to the HQET model [34].

the condition to reproduce (6.56) in the infinite mass limit enforces the coefficients of the two last terms in (6.60) in the specific way they are presented. Lorentz and chiral invariance alone do not relate these two terms.

When light vector mesons are included, the covariant derivative contains the undetermined parameter α, $D_\mu = \partial_\mu - \mathrm{i}\alpha g \rho_\mu - \mathrm{i}\,(1-\alpha)\,v_\mu$. Also, two more terms enter the Lagrangian,

$$\Delta\mathcal{L}_H = -\frac{2\sqrt{2}\mathrm{i}cM}{m_V}\left\{2Q_\mu^\dagger F^{\mu\nu}\,(\rho)\,Q_\nu \right. \\ \left. -\frac{\mathrm{i}}{M}\epsilon^{\alpha\beta\mu\nu}\left[(D_\beta P)^\dagger\,F_{\mu\nu}\,(\rho)\,Q_\alpha + Q_\alpha^\dagger F_{\mu\nu}\,(\rho)\,D_\beta P\right]\right\}, \quad (6.61)$$

that are related to each other via the heavy quark symmetry as are the two last terms in (6.60). We refer to Sect. 4.7 for further definitions regarding the light vector meson fields.

Again, the most strongly bound states are expected in the P-wave channel. The corresponding *ansätze* read

$$P = \frac{1}{\sqrt{4\pi}}\Phi(r)\hat{\boldsymbol{x}}\cdot\hat{\boldsymbol{\tau}}\chi\mathrm{e}^{\mathrm{i}\epsilon t}, \qquad Q_0 = \frac{1}{\sqrt{4\pi}}\Psi_0(r)\chi\mathrm{e}^{\mathrm{i}\epsilon t}\,, \quad (6.62)$$

$$Q_i = \frac{1}{\sqrt{4\pi}}\left[\mathrm{i}\Psi_1(r)\hat{x}_i + \frac{1}{2}\Psi_2(r)\epsilon_{ijk}\hat{x}_j\tau_k\right]\chi\mathrm{e}^{\mathrm{i}\epsilon t}\,, \quad (6.63)$$

where $\chi\begin{pmatrix}a_1\\a_2\end{pmatrix}$ is a space-independent spinor, as in (6.40). Phases are introduced such that all four profile functions are real. The (eigen) frequency and binding energy are related via $\epsilon = M - \omega_\mathrm{B}$. In the heavy quark limit, the multiplet $\mathcal{H}$ is characterized by a single radial function (6.58). This implies that for $M = M^* \to \infty$ the radial functions in (6.63) must satisfy the linear relations

$$\Psi_1 = -\Phi, \quad \Psi_2 = -2\Phi \quad (6.64)$$

together with $\Psi_0 = 0$. In general, however, a set of second-order differential equations similar to (6.41) is obtained for these radial functions [35] from which the binding energies are computed. Numerical results for a typical value of the Skyrme model parameter are displayed in Table 6.5. They clearly demonstrate that the heavy limit does not apply to the charm sector and only hardly to the bottom sector when it comes to predict the masses of the lowest lying baryons in the respective sectors. Even though the relations (6.64) are reasonably well satisfied, it seems inappropriate to assume that these profile functions are localized at the center of the soliton. For a sensible model prediction, furthermore, the projection onto states with good spin and isospin quantum numbers as in (6.45) is necessary. This has been done not only for the above-discussed P-wave bound state but also for the S-wave channel for the heavy mesons [30]. Results based on both the Skyrme model and the vector meson solitons are presented in

Table 6.5. Binding energies from the relativistic model, (6.60), for the Skyrme model parameter $e = 6.4$. All data are in GeV and the entry "∞" is obtained from (6.59). The picture on the right shows typical bound state profile functions. They correspond to the B-meson case in the table

M	M^*	$\omega_{\rm B}$
∞	∞	1.016
50.0	50.0	0.869
40.0	40.0	0.853
30.0	30.0	0.831
20.0	20.0	0.796
10.0	10.0	0.721
5.279	5.325	0.595
1.865	2.007	0.314

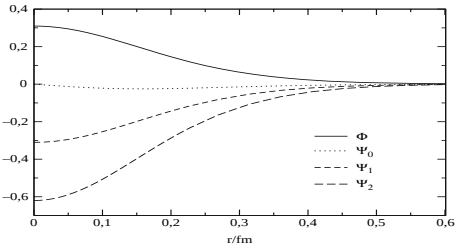

Table 6.6. In either case, the model parameters in the light sector are chosen to reproduce the Δ-nucleon mass difference. Despite the fact that the parameter α is undetermined, the predicted $\Lambda_c - N$ mass difference (row N in the table) undoubtedly shows the necessity to include light vector meson degrees of freedom. The model predictions for non–ground state b-quark baryons, $M(\Sigma_{\rm B}) - M(\Lambda_{\rm B}) \approx 190\,{\rm MeV}$ and $M(\Sigma^*_{\rm B}) - M(\Lambda_{\rm B}) \approx 205\,{\rm MeV}$ [30], favorably agree with the data (192 ± 2) MeV and (212 ± 2) MeV that very recently became available [39]. This prediction for the hyperfine splitting dominantly arises higher derivative terms in (6.60) and (6.61) that do not manifestly break heavy flavor symmetry [40]. Their main effect is to push the heavy meson fields away from the center of the soliton. In this respect, the present method differs from earlier approaches that assigned the hyperfine splitting to an additional piece in the Lagrangian that breaks the symmetry explicitly [41]. Hence, the above quoted data represent

Table 6.6. Heavy baryon mass differences with respect to Λ_c. Primes indicate negative parity, i.e., S-wave bound states. Baryons with spin $\frac{3}{2}$ carry a star. The physical meson masses 1865 MeV and 5279 MeV are used when computing the mass differences to the nucleon and the Λ_b. The empirical data are taken from the PDG [32], see also [37, 38]. All energies are in MeV. Question marks denote baryon states not observed so far

α	-0.1	0.0	0.1	0.2	0.3	Expt.	Skyrme
Σ_c	171	172	174	175	177	168	185
Σ_c^*	215	214	213	212	211	233	201
Λ_c'	250	249	245	242	238	308	208
Σ_c'	415	413	408	402	397	?	335
$\Sigma_c'^*$	468	467	464	461	458	?	437
N	-1237	-1257	-1278	-1299	-1321	-1345	-1553
Λ_b	3160	3164	3167	3170	3173	3335 ± 9	3215

an important verification of the method based on (6.60) and (6.61): it requires no further extension to reasonably describe baryons with a heavy valence quark.

6.8 Brief Summary on Soliton Quantization

In this and the preceding chapters we have extensively described the quantization of chiral solitons. The main motivation has been the generation of baryons states from solitons in effective meson theories. As explained in the case of a simple quantum mechanical example, we have accomplished that goal by introducing and canonically quantizing collective coordinates that characterize the symmetries which are broken by the classical solution to the field equations. In the case of the soliton, the collective coordinates parameterize the flavor and coordinate space rotations, the latter are absorbed into the former by means of the hedgehog structure of the soliton.

Having established that procedure as a legitimate approximation and applying it to the case of three light flavors (up, down, strange), i.e., the $SU(3)$ group structure, unambiguously and straightforwardly yielded the correct quantum numbers for the low-lying baryons. The Wess–Zumino term that transfers the quark anomaly from QCD to the effective meson theory is essential to obtain that result.[8] It must be stressed that no assumption has been made about the quark content and structure of the baryons: neither did the idea enter that baryons are built from three (valence) quarks nor was any prejudice made about a symmetric spin–flavor and anti-symmetric color wave function. The analogy with the $SU_{\rm S}(2) \times SU_{\rm F}(3)$ decomposition of the baryon wave function is an immediate result of the soliton quantization. To the knowledge of the author, the chiral soliton picture is unique in actually predicting the quantum numbers of the low-lying baryons.

Originally, we gained these conclusions in the somewhat unrealistic case of light flavor symmetry, which naïvely occurs as the only allowed regime for the $SU(3)$ collective coordinates. However, as the studies in [17] unambiguously show, the introduction of collective coordinates need not be limited to exact symmetries, see also Sect. 8.5. So, by exactly diagonalizing the system including flavor symmetry breaking, we observed little changes in the structure (and definitely not in the quantum numbers) of the wave functions, just an expected mixing between different irreducible representations of the broken symmetry. However, we have also seen that in the particular limit of large $N_{\rm C}$, in which the bound state approach reproduces the exact solution of the soliton model, the $SU_{\rm F}(3)$ structure may be well hidden. This is merely because that limit omits the important non-linearities of the flavor rotations. And indeed, generalizing the treatment of Sect. 6.4 to arbitrarily large $N_{\rm C}$ on the one side

[8] In chiral quark models (Chap. 2), it directly emerges from the imaginary part of the Euclidian action, (2.16) [42].

and on the other side constraining the bound state approach such that the bound state wave function dwells in the subspace of rotational excitations yields identical spectra [17]. We will thoroughly explore that feature later in Sect. 9.4.

References

1. H. Weigel, *Int. J. Mod. Phys.* **A11** (1996) 2419. 88, 97
2. H. Weigel, R. Alkofer, and H. Reinhardt, *Nucl. Phys.* **B387** (1992) 638. 88, 98
3. A. Blotz et al., *Nucl. Phys.* **A555** (1993) 765. 88, 98
4. H. Georgi, *Lie Algebras in Particle Physics. From Isospin to Unified Theories*, vol. 54. Westview Press, Boulder, CO, 1982. 89
5. F. Stancu, *Group Theory in Subnuclear Physics*, Vol. 19. Oxford Science Publications, Oxford, 1996. 89
6. L. C. Biedenharn and Y. Dothan, Print-84-1039 (DUKE). 89, 92
7. A. V. Manohar, "Large N QCD," in *Probing the Standard Model of Particle Interactions*, F. David and R. Gupta, eds. North Holland, Amsterdam, 1998. 91
8. A. V. Manohar, *Nucl. Phys.* **B248** (1984) 19. 91
9. M. Praszałowicz, "$SU(n)$ Skyrme Model," in *Skyrmions and Anomalies*, M. Jezabek and M. Prasałowicz, eds. American Institute of Physics, New York, 1987. 92
10. H. Walliser, *Nucl. Phys.* **A548** (1992) 649. 92, 96
11. P. Jain, R. Johnson, N. W. Park, J. Schechter, and H. Weigel, *Phys. Rev.* **D40** (1989) 855. 94
12. J. J. de Swart, *Rev. Mod. Phys.* **35** (1963) 916. 95
13. E. Guadagnini, *Nucl. Phys.* **B236** (1984) 35. 95, 98
14. H. Yabu and K. Ando, *Nucl. Phys.* **B301** (1988) 601. 95, 96, 100
15. N. W. Park, J. Schechter, and H. Weigel, *Phys. Lett.* **B224** (1989) 171. 95
16. H. Walliser and V. B. Kopeliovich, *J. Exp. Theor. Phys.* **97** (2003) 433. 96
17. H. Walliser and H. Weigel, *Eur. Phys. J.* **A26** (2005) 361. 96, 110, 111
18. N. W. Park and H. Weigel, *Nucl. Phys.* **A541** (1992) 453. 97, 98
19. B. Schwesinger and H. Weigel, *Nucl. Phys.* **A540** (1992) 461. 99
20. J. Schechter and H. Weigel, *Phys. Rev.* **D44** (1991) 2916. 100
21. J. Schechter and H. Weigel, *Phys. Lett.* **B261** (1991) 235. 100
22. C. G. J. Callan Jr., and I. R. Klebanov, *Nucl. Phys.* **B262** (1985) 365. 100, 102
23. C. G. J. Callan Jr., K. Hornbostel, and I. R. Klebanov, *Phys. Lett.* **B202** (1988) 269. 100, 102, 103
24. H. Goldhaber, *Phys. Lett.* **101** (1956) 433. 101
25. I. R. Klebanov. Lectures given at NATO ASI on Hadron and Hadronic Matter, Cargese, France, Aug 8–18, 1989. 101
26. C. L. Schat, N. N. Scoccola, and C. Gobbi, *Nucl. Phys.* **A585** (1995) 627. 102, 103, 105
27. H. Weigel, *Eur. Phys. J.* **A2** (1998) 391. 104
28. N. Itzhaki, I. R. Klebanov, P. Ouyang, and L. Rastelli, *Nucl. Phys.* **B684** (2004) 264. 104
29. M. Karliner and M. P. Mattis, *Phys. Rev.* **D34** (1986) 1991. 104
30. M. Harada, A. Qamar, F. Sannino, J. Schechter, and H. Weigel, *Nucl. Phys.* **A625** (1997) 789. 105, 106, 108, 109

31. A. V. Manohar and M. B. Wise, *Camb. Monogr. Part. Phys. Nucl. Phys. Cosmol.* **10** (2000) 1; D. Blaschke, M. A. Invanov, and T. Mannel: *Heavy Quark Physics*, Lect. Notes Phys. **647**. Springer, Heidelberg (2004). 105
32. S. Eidelman et al. [PDG], *Phys. Lett.* **B592** (2004) 1. 105, 109
33. K. S. Gupta, M. Arshad Momen, J. Schechter, and A. Subbaraman, *Phys. Rev.* **D47** (1993) 4835. 106
34. P. Jain, A. Momen, and J. Schechter, *Int. J. Mod. Phys.* **A10** (1995) 2467. 106, 107
35. J. Schechter, A. Subbaraman, S. Vaidya, and H. Weigel, *Nucl. Phys.* **A590** (1995) 655. 106, 107, 108
36. J. Schechter and A. Subbaraman, *Phys. Rev.* **D51** (1995) 2311. 107
37. CLEO Collaboration, G. Brandenburg et al., *Phys. Rev. Lett.* **78** (1997) 2304. 109
38. CDF Collaboration, D. Acosta et al., *Phys. Rev. Lett.* **96** (2006) 202001. 109
39. CDF Collaboration, T. Aaltonen, `arXiv:0706.3868 [hep-ex]`. 109
40. M. Harada, A. Qamar, F. Sannino, J. Schechter, and H. Weigel, *Phys. Lett.* **B390** (1997) 329. 109
41. E. E. Jenkins and A. V. Manohar, *Phys. Lett.* **B294** (1992) 273. 109
42. H. Weigel, H. Reinhardt, and R. Alkofer, *Phys. Lett.* **B313** (1993) 377. 110

7

Baryon Properties

Empirically most of the baryon properties are obtained by testing baryons with electro–weak probes. In the QCD language these probes couple to the baryon constituents as electroweak gauge currents. Therefore, baryon properties may in general be computed as matrix elements of these currents. Since the chiral Lagrangians emulate the QCD symmetries, the corresponding currents must be identified as the QCD symmetry currents. This paves the way to soliton model studies of baryon properties as the matrix elements of the associated symmetry currents. This is a two-step program. First, we find the currents in the model and substitute the soliton configuration. Second, we employ the techniques of the previous chapters to generate baryon states from which the matrix elements are computed.

We have already discussed some soliton model predictions for properties of the nucleon in Sect. 5.4. He we will refine those considerations and especially generalize them to flavor $SU(3)$ utilizing the quantization techniques discussed in the previous chapter. Essentially, we will concentrate on the Skyrmion in the rigid rotator quantization of Sect. 6.4. We will also comment on effects of the other quantization procedures, in particular those that incorporate symmetry breaking effects on the soliton extension (Sect. 6.5). In addition, we will address effects that cannot be correctly described in the model with pseudoscalar fields only but require the inclusion of short-range effects via either chiral quarks or vector meson fields.

We start by writing the covariant form of the vector (V_μ^a) and axial-vector (A_μ^a) currents in the Skyrme model. These are the symmetry currents associated with the transformations $U \to U + [U, Q^a]$ and $U \to U + \{U, Q^a\}$, respectively. The Q^a are the matrices that generate the infinitesimal transformation in flavor space, e.g., the Gell–Mann matrices of $SU(3)$. We have already presented the contributions from the flavor symmetry part of the action in (5.46) which we now supplement by the contribution from the flavor symmetry breaking term, (6.22)

H. Weigel: *Baryon Properties*, Lect. Notes Phys. **743**, 113–145 (2008)
DOI 10.1007/978-3-540-75436-7_7

$$
\begin{aligned}
V_\mu^a(A_\mu^a) = & \mp\frac{\mathrm{i}}{2}f_\pi^2\ \mathrm{tr}\left\{Q^a\left(\alpha_\mu \pm \beta_\mu\right)\right\} \\
& \mp\frac{\mathrm{i}}{8e^2}\mathrm{tr}\left\{Q^a\left([\alpha_\nu,[\alpha_\mu,\alpha^\nu]] \pm [\beta_\nu,[\beta_\mu,\beta^\nu]]\right)\right\} \\
& \pm\frac{1}{16\pi^2}\epsilon^{\mu\nu\rho\sigma}\mathrm{tr}\left\{Q^a\left(\alpha_\nu\alpha_\rho\alpha_\sigma \mp \beta_\nu\beta_\rho\beta_\sigma\right)\right\} \\
& \mp\mathrm{i}\beta'\mathrm{tr}\left\{Q^a\left(\{U\mathcal{M}+\mathcal{M}U^\dagger,\alpha_\mu\} \pm \{\mathcal{M}U+U^\dagger\mathcal{M},\beta_\mu\}\right)\right\}\,,
\end{aligned}
\tag{7.1}
$$

where we again set $N_\mathrm{C} = 3$ and also included terms that arise from the first term in (6.19). We recall our previous conventions $\alpha_\mu = U^\dagger\partial_\mu U$ and $\beta_\mu = U\partial_\mu U^\dagger$. The matrix $\mathcal{M} = \mathrm{diag}(1,1,x)$ is proportional to the current quark mass matrix with $x = \frac{m_K^2}{m_\pi^2} - 1$ and the parameter β' is determined from difference of the decay constants [1, 2]

$$
\left(\frac{f_K}{f_\pi}\right)^2 = 1 + \frac{4}{f_\pi^2}\beta'(1-x)\,. \tag{7.2}
$$

7.1 Electromagnetic Properties

In a first step, we are interested in the electromagnetic properties of the spin-$\frac{1}{2}$ baryons. For this purpose, we consider the electromagnetic vector current $V_\mu^{\mathrm{e.m.}}$ that is obtained from (7.1) employing the linear combination (see footnote 1 of Appendix C for the generalization to $N_\mathrm{C} \neq 3$)

$$
Q^{\mathrm{e.m.}} = \mathrm{diag}\left(\frac{2}{3},-\frac{1}{3},-\frac{1}{3}\right) = Q^3 + \frac{1}{\sqrt{3}}Q^8\,. \tag{7.3}
$$

Its matrix elements define Dirac and Pauli form factors via

$$
\langle B(\boldsymbol{p}')|V_\mu^{\mathrm{e.m.}}|B(\boldsymbol{p})\rangle = \overline{u}(\boldsymbol{p}')\left[\gamma_\mu F_1^B(q^2) + \frac{\sigma_{\mu\nu}q^\nu}{2M_B}F_2^B(q^2)\right]u(\boldsymbol{p})\,, \tag{7.4}
$$

where p_μ and p'_μ are the on-shell momenta of the initial and final baryons and $q_\mu = p_\mu - p'_\mu$ is the momentum transfer. The above definition is the standard Lorentz covariant parameterization of the matrix elements of the conserved electromagnetic current, in which $u(\boldsymbol{p})$ is the Dirac spinor for the baryon B. Note that M_B is just a parameter in this decomposition and refers to the empirical mass rather than the model result. It is convenient to introduce "electric" and "magnetic" (so-called Sachs) form factors :

$$
G_\mathrm{E}^B(q^2) = F_1^B(q^2) - \frac{q^2}{4M_B^2}F_2^B(q^2)\,, \qquad G_\mathrm{M}^B(q^2) = F_1^B(q^2) + F_2^B(q^2)\,. \tag{7.5}
$$

In the next step, we have to substitute the (collectively) rotating hedgehog, (6.4), into the covariant expression above. This is a straightforward but

eventually quite a tedious task. The resulting expression is a sum in which each term is a product of a radial function and a function that depends on the collective coordinates $A(t)$ (and their time derivative measured by the angular velocities $\Omega_{\rm a}$ (6.6)). For the spatial part of the vector current, we find[1]

$$V_i^a = V_1(r)\epsilon_{ijk}x_j D_{ak} + \frac{\sqrt{3}}{2}B(r)\epsilon_{ijk}\Omega_j x_k D_{a8} + V_2(r)\epsilon_{ijk}x_j d_{d\alpha\beta}D_{a\alpha}\Omega_\beta + V_3(r)\epsilon_{ijk}x_j D_{88}D_{ak} + V_4(r)\epsilon_{ijk}x_j d_{d\alpha\beta}D_{8\alpha}D_{a\beta} + \cdots . \tag{7.6}$$

The first two terms may straightforwardly be identified from the second column in (5.48) when noting that $D_{\rm a8} \to \delta_{\rm a8}$ and $V_i^8 \to V_i^0$ in the two-flavor reduction. The third term arises from the Wess–Zumino term and does not have a two-flavor counterpart. The remaining contributions that are only partially listed stem from flavor symmetry breaking terms in the chiral Lagrangian. Essentially, this Skyrme model structure of the current is recovered in all soliton models. However, the radial functions that are obtained from the soliton profiles and eventually induced components differ substantially. For example, in vector meson models, the V_2 term also acquires contributions from the $\epsilon_{\mu\nu\rho\sigma}$ terms in (4.66). We refer to the literature for the explicit expressions in various models, cf. [3, 4].

Employing the tools of Appendix E, we find the momentum-dependent magnetic form factor to be[2]

$$G_{\rm M}^B(q^2) = -8\pi M_B \int_0^\infty r^2 {\rm d}r \frac{r}{|\boldsymbol{q}|} j_1(r|\boldsymbol{q}|)\Bigg\{ V_1(r)\langle D_{e3}\rangle_B - \frac{1}{2\alpha^2}B(r)\langle D_{e8}R_8\rangle_B - \frac{1}{\beta^2}V_2(r)\langle d_{3\alpha\beta}D_{e\alpha}R_\beta\rangle_B + V_3(r)\langle D_{88}D_{e3}\rangle_B + V_4(r)\langle d_{3\alpha\beta}D_{e\alpha}D_{8\beta}\rangle_B \Bigg\} . \tag{7.7}$$

The subscript "e" refers to the electromagnetic combination of (7.3), while "B" indicates the respective baryon matrix elements. They are to be computed from the collective coordinate wave functions that diagonalize the Hamiltonian, with $SU(3)$ symmetry breaking included (6.26). The relevant techniques are sketched in Appendix D. Note that the above identification of the form factors is obtained in the Breit frame with $p_0 = p_0'$ and $\boldsymbol{p} = -\boldsymbol{p}' = \frac{\boldsymbol{q}}{2}$ for the momenta of the incoming and outgoing photons. This is suitable for the (large-$N_{\rm C}$) soliton picture, as the target is assumed to be infinitely heavy implying zero energy transfer. Recoil corrections stemming from $M_N < \infty$ will be discussed below.

[1] We impose the notation that doubled indices are summed with the ranges $i, j, k, \ldots = 1, 2, 3$ and $\alpha, \beta, \gamma, \ldots = 4, \ldots, 7$.

[2] According to the quantization rule, (6.8), angular velocities are replaced by the $SU(3)$ generators.

Table 7.1. The Skyrme (Sk) [5] and vector meson (VM) [3] model predictions for the magnetic moments of the spin-$\frac{1}{2}$ baryons compared to experimental data. Also shown are the ratios with resect to the proton magnetic moment

baryon	p	n	Λ	Σ^+	Σ^-	Ξ^0	Ξ^-	$\Sigma^0 \to \Lambda$
μ (Sk)	2.03	−1.58	−0.71	1.99	−0.79	−1.55	−0.64	−1.39
μ (VM)	2.36	−1.87	−0.60	2.41	−1.10	−1.96	−0.84	−1.74
$\mu_{\rm exp.}$	2.79	−1.91	−0.61	2.42	−1.16	−1.25	−0.69	−1.61
μ/μ_p (Sk)	1	−0.78	−0.35	0.98	−0.39	−0.76	−0.32	−0.68
μ/μ_p (VM)	1	−0.79	−0.25	1.02	−0.47	−0.83	−0.36	−0.74
$(\mu/\mu_p)_{\rm exp.}$	1	−0.68	−0.22	0.87	−0.42	−0.45	−0.25	−0.58

In Table 7.1, we summarize the results for the magnetic moments of the low-lying spin-$\frac{1}{2}$ baryons. As in the two-flavor model, cf. Sect. 5.4, the isovector part of the magnetic moments is underestimated while the isoscalar part is reasonably well reproduced. This is the case for both, the Skyrme model of pseudoscalar fields only and its vector meson extension.

We recall from Sect. 4.7 that the vector meson model contains a parameter (κ) that could not be determined from meson properties and argued that it should be close to unity. The results shown in Table 7.1 have been obtained with $\kappa = 1.2$. A significantly smaller (or even negative) value yields unacceptable magnetic moments. On the other hand, even larger values spoil the agreement for the baryon spectrum.

Despite the fact that the flavor symmetry breaking is large for the baryon wave functions, the predicted magnetic moments do not strongly deviate from the $SU(3)$ relations [6]:

$$\mu_{\Sigma^+} = \mu_p \ , \quad \mu_{\Sigma^0} = \frac{1}{2}(\mu_{\Sigma^+} + \mu_{\Sigma^-}) \ , \quad \mu_{\Sigma^-} = \mu_{\Xi^-} \ ,$$
$$2\mu_\Lambda = -(\mu_{\Sigma^+} + \mu_{\Sigma^-}) = -2\mu_{\Sigma^0} = \mu_n = \mu_{\Xi^0} = \frac{2}{\sqrt{3}}\,\mu_{\Sigma^0\Lambda} \ . \qquad (7.8)$$

Hence, a more elaborate treatment of the flavor symmetry breaking is necessary to accommodate the experimentally observed details of breaking the U-spin symmetry which, e.g., is reflected in the approximate equalities $\mu_{\Sigma^+} \approx \mu_p$ and $\mu_{\Xi^0} \approx \mu_n$. In Sect. 6.5, we have already been acquainted with the slow rotator approach that incorporates the symmetry breaking effects onto the static soliton. In that quantization, the radial functions $V_1, \ldots, V_4$ in (7.7) additionally depend on the strangeness changing angle ν, as do the classical mass and the moments of inertia, cf. (6.36). Then the collective coordinate parts of the matrix elements are of the form $\langle V_1(r,\nu) D_{e3}\rangle_B$, etc., that can be numerically computed with the techniques provided in Sect. 6.5 and Appendix D. The numerical results of this slow rotator approach (SRA) calculation [7] and those previously obtained in the rigid rotator approach (RRA) are confronted to the experimental data in Table 7.2. Obviously, the forces exerted by symmetry breaking upon the soliton are adequate to explain

Table 7.2. Skyrme model predictions for the ratios of hyperon magnetic moments in the rigid rotator (RRA) and slow rotator (SRA) approaches compared to experimental data

baryon	n	Λ	Σ^+	Σ^-	Ξ^0	Ξ^-	$\Sigma^0 \to \Lambda$
μ/μ_p (RRA)	-0.78	-0.35	0.98	-0.39	-0.76	-0.32	-0.68
μ/μ_p (SRA)	-0.83	-0.25	0.85	-0.40	-0.54	-0.20	-0.62
$(\mu/\mu_p)_{\rm exp.}$	-0.68	-0.22	0.87	-0.42	-0.45	-0.25	-0.58

the observed violation from the U-spin symmetry for the hyperon magnetic moments. The same conclusion can be drawn from an approach that introduces a dynamical scale variable for the size of the soliton [8, 9]. This so-called breathing mode quantization will be briefly discussed in Sects. 8.5 and 9.2. For other applications of the SRA to electromagnetic properties of hyperons, we refer to the literature [7, 10, 11].

We return to the RRA and similarly to (7.7); we find the electric form factor by Fourier transforming the time component of the electromagnetic current

$$G_{\rm E}^B(q^2) = 4\pi \int_0^\infty r^2 {\rm d}r j_0(r|\boldsymbol{q}|) \left\{ \frac{\sqrt{3}}{2} B(r) \langle D_{e8} \rangle_B + \frac{1}{\alpha^2} V_7(r) \langle D_{ei} R_i \rangle_B + \frac{1}{\beta^2} V_8(r) \langle D_{e\alpha} R_\alpha \rangle_B \right\} . \tag{7.9}$$

The identities

$$4\pi \int_0^\infty r^2 {\rm d}r \, V_7(r) = \alpha^2 \qquad \text{and} \qquad 4\pi \int_0^\infty r^2 {\rm d}r \, V_7(r) = \beta^2 \tag{7.10}$$

ensure proper normalization of the electric charges because then $G_{\rm E}^B(0) = \sum_{a=1}^8 \langle D_{ea} R_a \rangle_B = \langle L_e \rangle_B$ due to the constraint on R_8 (6.8). In Fig. 7.1, we compare the Skyrme model predictions for the momentum-dependent electric

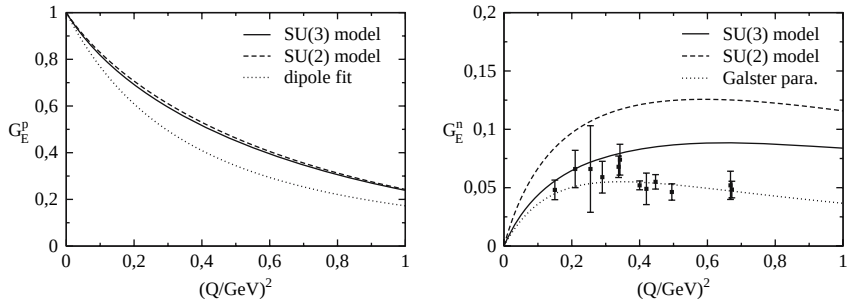

Fig. 7.1. Skyrme model (with $e = 4.0$) prediction for the momentum-dependent electric form factors of the proton (*left*) and neutron (*right*). The proton prediction is compared to the dipole fit and the neutron to the Galster parameterization, cf. (7.11). Data are from [12, 13, 14, 15, 16, 17, 18, 19, 20]

form factors of the nucleon to empirical data. The latter are often presented in the form of established parameterizations. With Q measured in GeV, the standard dipole and Galster [21] parameterizations of the empirical form factors are

$$G_{\rm D}^{\rm p}(Q^2) = \frac{1}{\left(1+Q^2/0.71\right)^2} \qquad \text{and} \qquad G_{\rm G}^{\rm n}(Q^2) = \frac{0.54Q^2}{1+1.54Q^2}\, G_{\rm D}^{\rm p}(Q^2) \tag{7.11}$$

for proton and neutron, respectively.

While the inclusion of strange degrees of freedom does little to the proton form factor, the neutron form factor is strongly affected and acquires a significant reduction. This can be deduced from the neutron collective coordinate matrix elements that enter (7.9). In case of exact flavor symmetry, they are

$$\frac{\sqrt{3}}{2}\langle D_{e8}\rangle_{\rm n} = \frac{1}{10} \quad \langle D_{ei}R_i\rangle_{\rm n} = -\frac{3}{10} \quad \langle D_{e\alpha}R_\alpha\rangle_{\rm n} = \frac{1}{5}, \tag{7.12}$$

while the $SU(2)$ analogs are $\frac{1}{2}, -\frac{1}{2}$ and 0. When symmetry breaking is included according to Sect. 6.4, the numerical values for these matrix elements are somewhere in between those of (7.12) and the $SU(2)$ ones. Hence, the magnitude of the neutron electric form factor is noticeably reduced by $SU(3)$ effects. This is also noticed in the neutron electric radius, the slope of $G_{\rm E}^{\rm n}$. For $e = 4.0$ is reduced (in magnitude) from $-0.24\,\mathrm{fm}^2$ to $-0.16\,\mathrm{fm}^2$ when generalizing from two to three flavors. Strangeness degrees of freedom bring $\langle r_{\rm E}^{\rm n2}\rangle$ closer to the empirical value of $(-0.116 \pm 0.002)\mathrm{fm}^2$ [22]. In case of the proton, this cancellation effect is less dramatic, after all then these three matrix elements always have to add to one. To be precise, they are $\frac{1}{2}, \frac{1}{2}$ and 0 for $SU(2)$ and $\frac{1}{5}$,$\frac{2}{5}$ and $\frac{2}{5}$ in exact $SU(3)$. In the pseudoscalar model, the corresponding radius is always predicted a bit on the low side, $\langle r_{\rm E}^{\rm p2}\rangle \approx 0.55\,\mathrm{fm}^2$ compared to $\langle r_{\rm E}^{\rm p2}\rangle_{\rm exp} = (0.76 \pm 0.01)\mathrm{fm}^2$. This changes significantly when including vector meson fields. Typical predictions within these models are around $1\,\mathrm{fm}^2$, both in $SU(2)$ [23] and in $SU(3)$ [3]. This can be easily understood without going into the complicated details of the vector meson model calculation. In the pseudoscalar model, the time component of the isoscalar part, V_0^0 (V_0^8 in $SU(3)$) of the electromagnetic current, is essentially given by the baryon density, $b(r)$, as is easily observed from (5.48). In simplified vector meson models, the current field identity of the vector meson dominance picture [24] holds. In the current context, it states that the isoscalar component of the vector current is proportional to the ω–field. On the other hand, the baryon current essentially acts as the source for the ω–field. In vector meson models, V_0^0 therefore is subject to an equation of the form

$$\left(\boldsymbol{\partial}^2 - m_\omega^2\right) V_0^0 \sim -m_\omega^2 b(r)\,. \tag{7.13}$$

Multiplying by $\boldsymbol{x}^2$ and integrating over space yields [25]

$$\int \mathrm{d}^3x\, \boldsymbol{x}^2 V_0^0 = \langle r^2\rangle_{I=0} = \langle r^2\rangle_B + \frac{6}{m_\rho^2}\,, \tag{7.14}$$

where $\langle r^2 \rangle_B$ is the radius of the baryon density that equals the isoscalar radius in the pseudoscalar model. This clearly shows that vector meson effects cause a sizable increase ($6/m_\rho^2 \approx 0.4\,\mathrm{fm}^2$) of the electromagnetic radii of baryons in soliton models.

7.2 Relativistic Corrections

Using the techniques of Appendix E, we may extend the nucleon form factor calculation to larger momenta by the transformation

$$G_\mathrm{E}(Q^2) \longrightarrow \gamma^{-2n_\mathrm{E}} Q_\mathrm{E}\left(\frac{Q^2}{\gamma^2}\right) \qquad \text{and} \qquad G_\mathrm{M}(Q^2) \longrightarrow \gamma^{-2n_\mathrm{M}} Q_\mathrm{M}\left(\frac{Q^2}{\gamma^2}\right), \tag{7.15}$$

where $\gamma^2 = 1 + \frac{Q^2}{4M_N^2}$ is the Lorentz boost factor. The result, (E.18), which is based on the Lorentz boost, suggests to put $n_\mathrm{E} = 0$ and $n_\mathrm{M} = 1$. Before discussing numerical results based on the transformation, (7.15), it is instructive to reflect on its nature. Most evidently, the momentum interval $[0, 4M_N^2]$ of the rest frame is mapped onto the space-like momenta in the Breit frame. While small momenta are almost unaffected, the form factors at infinity in the Breit frame are obtained from those in the rest frame at $Q^2 = 4M_N^2$. Even though the latter may be small, there is no general reason for them to vanish. In particular, this implies that the form factors do not match the empirical dipole form (7.11) unless $n_\mathrm{E} = n_\mathrm{M} \geq 2$. In contrast to the result from (E.18), the values $n_\mathrm{E} = n_\mathrm{M} \geq 2$ are also frequently adopted [26] because they are strongly motivated by regarding the baryon as a cluster of particles whose leading Fock component is a three-particle state [27, 28]. In any case, the large Q^2 behavior is not a profound model result but merely originates from the boost prescription and thus mainly reflects the kinematical situation.

Numerical results are shown in Fig. 7.2. For those calculations, quite a small Skyrme constant $e = 3.5$ was used. The magnetic form factors are nor-

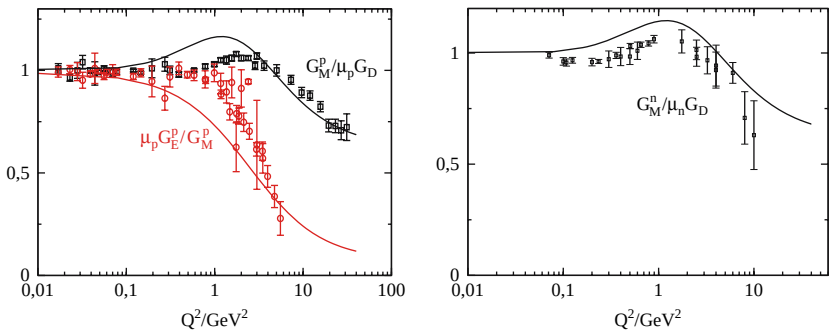

Fig. 7.2. Proton (*left*) and neutron (*right*) form factors computed in the $SU(3)$ Skyrme model as a function of momentum transfer after applying the boost (E.18). Data are from [28, 29, 30, 31, 32, 33] (proton) and [34, 35, 36, 37, 38, 39, 40] (neutron)

malized to the respective magnetic moments, which this calculation predicts to be $\mu_{\rm p} = 2.71$ and $\mu_{\rm n} = -2.30$. This figure clearly demonstrates that soliton models are able to reproduce the gross features of the empirical form factors. The reader may consult [26] for a more thorough investigation in a vector meson soliton model that strongly supports this statement. The Lorentz boost, (E.18), is crucial to gain that agreement. As explained in [26], the strong decrease of the ratio $\mu_{\rm p} G_{\rm E}^{\rm p}(Q^2)/G_{\rm M}^{\rm p}(Q^2)$ then emerges naturally in chiral soliton models as it basically stems from the isospin being generated from a rigid rotation in flavor space.

7.3 Axial Charges and Hyperon Decays

We now turn to the discussion of matrix elements of the axial-vector current, A_μ^a in (7.1). These matrix elements are very interesting as they enter the hadronic part of the low-energy effective current–current interaction for the standard model. Hence, they are directly connected to semi-leptonic decays of baryons, most prominently the neutron β-decay. Historically, their analysis gave profound reason that flavor symmetry would be well reflected among the hyperons.

Here we will concentrate on the octet components, $a = 1, \ldots, 8$, and postpone a thorough study of the singlet component, A_μ^0, to the next section. We substitute the rotating hedgehog, (6.4), and find the spatial components to be

$$\begin{aligned} A_i^a = {} & \left[A_1(r)\delta_{ik} + A_2(r)\hat{x}_i\hat{x}_k\right] D_{ak} + \left[A_3(r)\delta_{ik} + A_4(r)\hat{x}_i\hat{x}_k\right] d_{k\alpha\beta} D_{a\alpha}\Omega_\beta \\ & + \left[A_5(r)\delta_{ik} + A_6(r)\hat{x}_i\hat{x}_k\right] D_{a8}\Omega_k + \left[A_7(r)\delta_{ik} + A_8(r)\hat{x}_i\hat{x}_k\right] D_{ak}(D_{88} - 1) \\ & + \left[A_9(r)\delta_{ik} + A_{10}(r)\hat{x}_i\hat{x}_k\right] d_{k\alpha\beta} D_{a\alpha} D_{8\beta}\,. \end{aligned} \tag{7.16}$$

Again, the radial functions $A_1(r), \ldots, A_{10}(r)$ contain the profile fields and are thus model dependent. We refer to the literature [3, 25, 41] for explicit expressions. It is interesting to note that in the two-flavor model only the A_1 and A_2 terms are present, cf. (5.50). Though the A_3 and A_4 terms have major contributions from the vector meson profiles, they also have contributions from the Wess–Zumino term [42] and are thus also present in the model with only pseudoscalar mesons. On the other hand, the A_5 and A_6 terms vanish in the latter model. The remaining terms stem from the symmetry breaking part of the effective meson Lagrangian.

We define form factors as the covariant matrix elements

$$\langle B'(\boldsymbol{p}')|A_\mu^a|B(\boldsymbol{p})\rangle = \overline{u}'(\boldsymbol{p}')\left[\gamma_\mu\gamma_5 G_{\rm A}^{BB'}(q^2) + \gamma_5 q_\mu \widetilde{G}_{\rm A}^{BB'}(q^2)\right] u(\boldsymbol{p}). \tag{7.17}$$

Here $G_{\rm A}$ and $\widetilde{G}_{\rm A}$ are the main and induced axial form factors, respectively. The involved baryons B and B' select the pertinent octet components, e.g., the semi-leptonic $\Lambda \to N$ transition demands to choose $a = 4 + {\rm i}5$. Again we

compute these form factors by Fourier transformation of the soliton model current, (7.16), in the Breit frame. We are mostly interested in the low-energy properties of baryons and will not discuss the induced form factor $\widetilde{G}$. The main axial form factor describes the neutron β-decay which, upon isospin invariance, is obtained as the proton matrix element of $2A_3^3$,

$$G_{\rm A}(q^2) = \frac{8\pi M_N}{E} \int {\rm d}r r^2 \left\{ \left[j_0(|\boldsymbol{q}|r) A_1(r) + \frac{j_1(|\boldsymbol{q}|r)}{|\boldsymbol{q}|r} A_2(r) \right] \langle D_{33} \rangle_{\rm p} \ldots \right\} , \tag{7.18}$$

where $E = \sqrt{M_N^2 + \boldsymbol{p}^2} = \sqrt{M_N^2 + (\boldsymbol{q}/4)^2}$. The ellipsis represents the matrix element associated with the $A_3 \ldots A_{10}$ components in (7.16). They are not displayed because they are completely analogous in structure to the A_1 and A_2 contributions. Even though $|\langle D_{33} \rangle_{\rm p}|$ decreases from 1/3 in flavor $SU(2)$ to 7/30 in the symmetric case of $SU(3)$, the axial charge of the nucleon, $g_{\rm A} = G_{\rm A}(0)$, does not significantly change when adding strange degrees of freedom. There are two main reasons: (i) when symmetry breaking is properly included, this matrix element tends toward its two-flavor limit[3] and (ii) the additional terms, in particular $\rm A_3$ and $\rm A_4$, make up major parts of the difference. To be specific, the $SU(3)$ vector meson model of [3] predicts $g_{\rm A} = 0.93$. Even though that model calculation is characterized by quite an extended soliton (achieved by $\kappa \approx 1$), and the axial charge is sensible to the soliton size, it underestimates the empirical value ($\sim$1.26) by more than a quarter. The too-small prediction has always been a problem in chiral soliton models. The situation seems a bit different for solitons in the NJL model that we discussed in Chap. 3. As, e.g., is seen from (3.5), these approaches require the evaluation of fermion functional determinants, which implies to arrange products of operators according to their time ordering. In [43, 44], it has been argued that this ordering prescription yields subleading (in $1/N_{\rm C}$) contributions to $g_{\rm A}$ that match the difference to the empirical data. However, there is an inconsistency in that approach as there is no analog to this contribution in the equation of motion of the chiral field which would be needed to comply with PCAC [45], even in the two-flavor reduction. We will therefore, and also because it is technically involved, not discuss that analysis in further detail.

In the context of the three-flavor soliton, the most interesting aspect of the axial current matrix elements is their analysis in the framework of flavor symmetry breaking because the various amplitudes favorably agree with predictions solely based on flavor $SU(3)$ symmetry. Commonly, the $g_{\rm A}/g_{\rm V}$ ratios are considered in this context. We have already defined $g_{\rm A}$ as the zero momentum transfer limit of $G_{\rm A}^{BB'}$ in (7.17). The vector current matrix elements are computed from the appropriate flavor component V_μ^a similar to (7.4), just that we have to consider different baryons in the initial and final states.

[3] As a matter of fact and consistency, handling such matrix elements according to the rules of Sect. 6.4 shows that they approach their $SU(2)$ values for arbitrarily large flavor symmetry breaking, when strange degrees of freedom are frozen.

Table 7.3. The matrix elements of the axial-vector current between different baryon states, $g_{\rm A}$, in the flavor symmetric limit. Displayed are both the strangeness conserving (upper part) and the strangeness changing (lower part) processes. The first column gives the relevant flavor component of the axial current

	$n \to p$	$\Sigma^- \to \Lambda$	$\Sigma^- \to \Sigma^0$	$\Xi^- \to \Xi^0$
A^{π^-}	$F + D$	$2D/\sqrt{6}$	$\sqrt{2}F$	$D - F$
	$\Lambda \to p$	$\Sigma^- \to n$	$\Xi^- \to \Lambda$	$\Xi^- \to \Sigma^0$
A^{K^-}	$(3F + D)/\sqrt{6}$	$D - F$	$(3F - D)/\sqrt{6}$	$(F + D)/\sqrt{2}$

This generalizes the form factor $G_{\rm E}^B(Q^2)$ to $G_{\rm V}^{BB'}(Q^2)$. We obtain $g_{\rm V}$ from its $Q^2 \to 0$ limit.[4] In the $SU(3)$ symmetric case, the $g_{\rm V}$ measure the $SU(3)$ charges and thus are directly expressed by Clebsch–Gordan coefficients. The axial current itself carries octet quantum numbers, and there two ways to couple it to the octet baryons via the Clebsch–Gordan series, cf. (6.28). By $SU(3)$ symmetry there are thus two independent coupling constants between the axial current and the bilinear baryon operators. They are commonly called F and D constants, and their coupling to the baryon operators is shown in Table 7.3. If $SU(3)$ were a good symmetry, the $g_{\rm A}/g_{\rm V}$ ratios for six measured semi-leptonic baryon decays must therefore be describable by only two parameters. And indeed, that is possible as can easily be observed from Table 7.4. It is interesting to note that the dominating collective coordinate operators in (7.16) (D_{ak} and $d_{k\alpha\beta}D_\alpha R_\beta$) yield $F/D = 5/9$ when computed in the $SU(3)$ limit. This agrees with the empirical fit, cf. Table 7.4. From this point of view, the reasoning of Sect. 6.4 that flavor symmetry might be strongly violated seems questionable. Yet, we will soon see that such a conclusion is premature [50]. Two essential modifications arise for $g_{\rm A}/g_{\rm V}$ from the inclusion of symmetry breaking effects. First, the matrix elements of the vector current at zero momentum transfer,

$$\int {\rm d}^3 r V_0^{(a)} = \sum_{b=1}^{8} D_{ab} R_b = L_a \,, \tag{7.19}$$

Table 7.4. The measured values of $g_{\rm A}/g_{\rm V}$ fitted by $SU(3)$ relations with $F + D = 1.26$ and $F/D = 0.58$. Data are from [22, 46, 47, 48]; see also [49]

	$n \to p$	$\Lambda \to p$	$\Sigma \to n$	$\Xi \to \Lambda$	$\Xi^0 \to \Sigma^+$	$\Sigma \to \Lambda$
emp.	1.26	0.72 ± 0.02	0.34 ± 0.02	0.25 ± 0.05	1.29 ± 0.16	0.61 ± 0.02
$F\&D$	1.26	0.73 ± 0.01	0.34 ± 0.03	0.19 ± 0.02	$1.26 = g_{\rm A}(n \to p)$	0.65 ± 0.01

[4] For simplicity, we omit the superscripts B and B' on $g_{\rm V}$ and $g_{\rm A}$. The designated baryon states should be obvious from the context.

are no longer given by simple Clebsch–Gordan coefficients even though they are still computed as matrix elements of $SU(3)$ generators. The reason is that the baryon states are no longer pure states that dwell in definite $SU(3)$ representations. As a consequence of the Ademollo–Gatto theorem [51], the deviation from the Clebsch–Gordan coefficients is at least quadratic in the symmetry breaking parameter, i.e., $\mathcal{O}(\omega^4)$ in the notation of Sect. 6.4. Nevertheless, this must not be small [52]. Second, the notion of F and D parameters is strictly limited to the flavor symmetric case and there is no use for them to parameterize the axial current matrix elements in the presence of flavor symmetry breaking. In the soliton description, the effect of the derivative-type symmetry breaking terms is mainly indirect. They provide the splitting between the various decay constants and thus increase γ [53] since it is proportional to $f_K^2 m_K^2 - f_\pi^2 m_\pi^2 \approx 1.5 f_\pi^2 (m_K^2 - m_\pi^2)$. Otherwise, the derivative-type symmetry breaking terms are negligible. Hence symmetry breaking terms can be omitted in the current operators and the non-singlet axial charge operator is parameterized as ($a = 1, \ldots, 8$, $i = 1, 2, 3$)

$$\int \mathrm{d}^3 r A_i^{(a)} = c_1 D_{ai} - c_2 D_{a8} R_i + c_3 \sum_{\alpha,\beta=4}^{7} d_{i\alpha\beta} D_{a\alpha} R_\beta \,. \tag{7.20}$$

The coefficients c_i are model-dependent functionals of the soliton profiles. For the moment, we will treat them as free parameters. For $\omega^2 \to \infty$ (infinitely heavy *strange* degrees of freedom), the strangeness contribution to the nucleon axial charge should vanish. Noting that $\langle N|D_{83}|N\rangle \to 0$ and $\langle N|\sum_{\alpha,\beta=4}^{7} d_{3\alpha\beta} D_{8\alpha} R_\beta|N\rangle \to 0$ while $\langle N|D_{88}|N\rangle \to 1$ for $\omega^2 \to \infty$, we therefore demand

$$\int \mathrm{d}^3 r A_i^{(0)} = -2\sqrt{3} c_2 R_i \quad \text{with} \quad i = 1, 2, 3 \,, \tag{7.21}$$

for the axial singlet current because it consistently causes the strangeness projection, $A_i^{(s)} = (A_i^{(0)} - 2\sqrt{3} A_i^{(8)})/3$, to vanish when $\omega^2 \to \infty$. Actually, all model calculations in the literature [3, 54] satisfy this relation between singlet and octet currents. The singlet current matrix element, $\triangle\Sigma_B = \sqrt{3} c_2$, is the quark spin contribution to the spin of the considered baryon, B. We will study that quantity thoroughly in the following section. Here it suffices to note that the empirical value for the nucleon matrix element $\triangle\Sigma_N \approx 0.20 \pm 0.10$ [55] is insensitive to the strength of flavor symmetry breaking [56]. This suggests to adjust c_2 accordingly.

The values for g_A and g_V (only g_A for $\Sigma^+ \to \Lambda e^+ \nu_e$) are obtained from the matrix elements of the operators in (7.20) and (7.19), respectively, sandwiched between the eigenstates of the full Hamiltonian (6.26). We still have to specify c_1 and c_3. As in [50], we determine these two parameters such that the empirical nucleon axial charge and the $g_\mathrm{A}/g_\mathrm{V}$ ratio for $\Lambda \to p e^- \bar{\nu}_e$ are reproduced at a prescribed strength of flavor symmetry breaking, say $\omega_\mathrm{fix}^2 = 6.0$. Then we are not only left with predictions for the other decay parameters

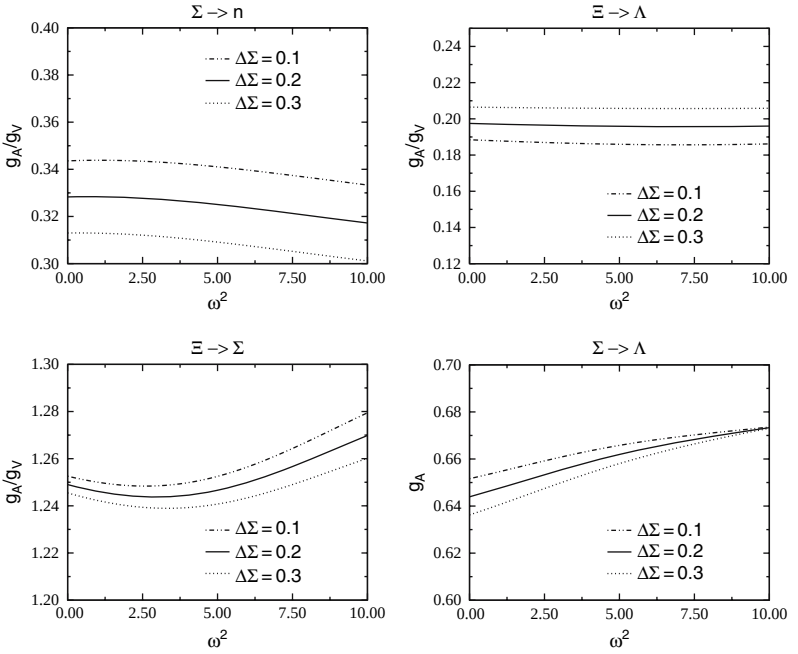

Fig. 7.3. The predicted decay parameters for the hyperon β-decays using $\omega^2_{\rm fix} = 6.0$. The errors originating from those in $\Delta\Sigma_N$ are indicated

but we can in particular study the variation with symmetry breaking. This is shown in Fig. 7.3. The dependence on flavor symmetry breaking is very moderate,[5] and the results can be viewed as reasonably agreeing with the empirical data, cf. Table 7.4. The observed independence of ω^2 shows that these predictions are not sensitive to the choice of $\omega^2_{\rm fix}$. The two transitions, $n \to p$ and $\Lambda \to p$, which are not shown in Fig. 7.3, exhibit a similar negligible dependence on ω^2. We therefore have a two-parameter (c_1 and c_3, c_2 is fixed from $\Delta\Sigma_N$) fit of the hyperon β-decays. Comparing the results in Fig. 7.3 with the data in Table 7.4, we see that the present calculation using strongly distorted wave functions agrees equally well with the empirical data as the flavor symmetric $F\&D$ fit. Stated otherwise, the possibility to fit the decay parameters of hyperon decays in a flavor covariant manner is no proof for the validity of flavor symmetry. In this context, it is worthwhile to remark that lattice results are available for the $g_{\rm A}/g_{\rm V}$ ratio of the $\Sigma \to n$ transition [57]. They are consistent with empirical data and, as in the above soliton model study, they exhibit only minor changes when flavor symmetry breaking effects are incorporated.

[5] However, the individual matrix elements that enter the ratios $g_{\rm A}/g_{\rm V}$ as factors of the parameters c_i vary strongly with ω^2 [50].

To complete the discussion of the octet axial currents, a general comment on PCAC (2.55) in conjuction with the axial current, (7.16), is in order. Even if the symmetry breaking contributions, $A_5, \ldots, A_{10}$, were absent, PCAC is not satisfied in the sense that $\partial^\mu A^a_\mu = 0$ in the chiral limit. As already mentioned in Sect. 5.4, the equations of motion for the profile functions are equivalent to this divergence equation. However, the equations of motion are solved classically only, i.e., in leading order of the $1/N_\mathrm{C}$ expansion. But in flavor $SU(3)$, the axial current contains pieces in A_3 and A_4 that are down by one order, at least when nucleon matrix elements are taken.[6] It is then obvious that away from the chiral limit the right-hand side of $\partial^\mu A^a_\mu$ cannot be identified as the (interpolating) pseudoscalar field as suggested at the end of Sect. 5.4. This questions computations of coupling constants for hadronic decays of baryon resonances as matrix elements of the axial current (7.16). We will discuss that matter exhaustively in Sect. 9.3. Here just remark that the resulting discrepancy for $g_{\pi NN}$ from the Goldberger–Treimann relation was already observed by Kanazawa [42]. As a solution to that problem, induced kaon fields were introduced [53, 58] similar to what we have already discussed for the vector meson model in Sect. 5.5. However, this is not the final word because double counting problems emerge for the kaon fields. A comprehensive investigation requires a thorough treatment of the rotation–vibration coupling for the kaon fields, cf. Sect. 9.5.

7.4 Proton Spin Puzzle

The proton spin puzzle concerns the nucleon matrix element of the axial singlet current, i.e., the coefficient c_2 in (7.21). In the (non-relativistic) quark model, this matrix element equals twice the contribution of the quark spin to the total nucleon spin.[7] It is not completely devious to assume that this gives a guidance for the structure of the nucleon. Thus, a value of order unity is expected for this matrix element. Yet this matrix element has been experimentally determined to be considerably smaller. This suggests that the nucleon structure is more complicated than assumed in the quark model picture. At least for a short while that represented a puzzle.

There is an immediate problem that we face in the soliton model of only pseudoscalar mesons. Straightforward evaluation from (7.1) shows that the axial singlet current vanishes in the Skyrme model Lagrangian with $U \in SU(3)$. This changes when kinetic symmetry breaking terms as in (6.22) are included [59]:

[6] One must be careful in this $1/N_\mathrm{C}$ counting because the matrix elements of D_{ai} and $d_{i\alpha\beta}D_{a\alpha}R_\beta$ have different N_C dependences when evaluated between different baryon states. This is particularly the case for members of the anti-decuplet, Fig. 6.3, are concerned.

[7] For a review, see [55].

$$A_\mu^{(0)} = \sqrt{3}\mathrm{i}\left(f_K^2 - f_\pi^2\right)\partial_\mu \,\mathrm{tr}\left[\lambda_8\left(U - U^\dagger\right)\right] + \cdots . \tag{7.22}$$

This is a total derivative and hence its nucleon matrix element at zero momentum transfer vanishes.[8] This is a general issue in soliton models that are based only on pseudoscalar degrees of freedom. The extension from $U \in SU(3)$ to $U \in U(3)$ merely adds a contribution proportional to $\partial_\mu\left[\ln \det(U)\right]$ to $A_\mu^{(0)}$. There have been attempts to generate a non-zero axial singlet charge in such models from higher derivative terms by choosing a favorable order for the collective coordinate operators [61] or including terms in the effective Lagrangian that are products of flavor traces [62] (rather than single traces) which are suppressed in the large N_C expansion. The quantization scheme in the former approach is not consistent with G-parity constraints [56], and the additional terms invented in the latter are actually generated from vector meson interactions involving the Levi–Cevita tensor, $\epsilon_{\mu\nu\rho\sigma}$, as suggested in (4.66). It is more appealing to directly employ vector meson models because their interaction strength can be deduced from meson phenomenology, cf. Sect. 4.7, at least partially. Already some time ago it has been noticed that even in a $U(2)$ approach, the $\epsilon_{\mu\nu\rho\sigma}$ terms in (4.66) provide the source terms for a singlet component of the pseudoscalar mesons upon collective coordinate quantization of the (iso)spin degrees of freedom [23, 63]. Exactly, these source terms recur when separating the derivative of the flavor singlet component, η', from the current

$$A_\mu^{(0)} = \sqrt{6} f_\pi \partial_\mu \eta' + \overline{A}_\mu^{(0)} , \tag{7.23}$$

since the anomaly equation, $\partial^\mu A_\mu^{(0)} = \sqrt{6} f_\pi m_{\eta'}^2 \eta'$, is the stationary condition for η'. A non-trivial η' thus implies a non-zero $\overline{A}_\mu^{(0)}$ which in turn might yield a non-zero axial singlet current matrix element at $q^2 = 0$. Because of the pseudoscalar nature, the η and/or η' fields must be of the form $\eta(r)\hat{\boldsymbol{x}} \cdot \boldsymbol{\Omega}$, where $\boldsymbol{\Omega}$ is the angular velocity for the (iso)spin rotations, (5.16). Due to the embedding of the static soliton in the isospin subgroup, (6.3), initially only the non-strange component of η' can get excited as long as neither $SU(3)$ nor $U(1)$ symmetry breaking is included. We therefore parameterize the singlet and octet η fields with two profile functions [1, 64]

$$\eta_0 \mathbb{1}_3 + \eta_8 \lambda_8 = \left(\begin{array}{cc|c} \multicolumn{2}{c|}{\eta_\mathrm{T}(r)\hat{\boldsymbol{x}} \cdot \boldsymbol{\Omega}\, \mathbb{1}_2} & \begin{array}{c} 0 \\ 0 \end{array} \\ \hline 0 \quad & 0 & \eta_\mathrm{S}(r)\hat{\boldsymbol{x}} \cdot \boldsymbol{\Omega} \end{array}\right) . \tag{7.24}$$

These profile functions are obtained by a variational approach to the non-strange moment of inertia, α^2, together with the induced vector meson components, (5.64). As a matter of fact, even the inclusion of $SU(3)$ breaking terms does not induce the strange component, η_S. For this to happen $U(1)$,

[8] This is at odds with the claims of [60] who merely estimated $\langle A_i^0 \rangle$ from PCAC rather than from a thorough calculation.

breaking terms that involve powers and derivatives of the trace $2\eta_{\rm T}+\eta_{\rm S}$ are required.

From the above consideration, it is obvious that a careful discussion of the axial singlet current also requires a detailed investigation of the physics of the η-mesons. This in particular concerns the mixing of the η and η' mesons. Let us begin this discussion by just listing two typical $U(1)$ symmetry breaking terms

$$\left[\ln\left(\det(U)/\det(U^\dagger)\right)\right]^2 \quad , \quad \left[{\rm tr}(U\partial_\mu U^\dagger)\right]^2 \tag{7.25}$$

and refer to [1] for more details, especially for a thorough discussion on implementing the $U_{\rm A}(1)$ anomaly via an effective pseudoscalar ghost gluon field. Nevertheless, a few general remarks on the mixing scenario as it emerges from terms like those in (7.25) are worthwhile, also because the η mesons turn out to be crucial for the proper description of the neutron–proton mass difference under the inclusion of (small) isospin breaking as we will discuss in Sect. 7.6. Early and standard textbook descriptions picture the mixing scenario by an orthogonal transformation that is parameterized by a single mixing angle, θ, cf. [65]. However, this is empirically insufficient [66], and a more general transformation from the singlet (η_1) and octet (η_8) to the physical isoscalar pseudoscalar mesons η and η' must be effective. According to the singular value decomposition theorem, we can write this transformation as

$$\begin{pmatrix}\eta_0\\ \eta_8\end{pmatrix} = S\begin{pmatrix}\eta\\ \eta'\end{pmatrix} \quad \text{with} \quad S = R(\theta_{\rm id})R(\theta_1)\hat{K}^{-1/2}R(\theta_2), \tag{7.26}$$

where $R(\theta)$ are rotation matrices and $\hat{K}$ is diagonal. The angle $\theta_{\rm id}$ merely describes the ideal mixing that transfers the non-strange component ($\eta_{\rm T}\sim(u\bar{u}+d\bar{d})/\sqrt{2}$) and purely strange component ($\eta_{\rm S}\sim s\bar{s}$) into the group theoretical basis η_0 and η_8. In [1], the entries of the parameterization in (7.26) were determined by first writing down a general effective Lagrangian for the η fields, including $SU(3)$ and $U(1)$ symmetry breaking, and expanding to quadratic order in the η fields:

$$\mathcal{L}_\eta^{(2)} = -\frac{1}{2}\partial_\mu\begin{pmatrix}\eta_{\rm T}\\ \eta_{\rm S}\end{pmatrix}^{\rm t} K\partial^\mu\begin{pmatrix}\eta_{\rm T}\\ \eta_{\rm S}\end{pmatrix} + \frac{1}{2}\begin{pmatrix}\eta_{\rm T}\\ \eta_{\rm S}\end{pmatrix}^{\rm t} M\begin{pmatrix}\eta_{\rm T}\\ \eta_{\rm S}\end{pmatrix}, \tag{7.27}$$

where K and M are real symmetric 2×2 matrices that contain three unknown coupling constants. It is worth noting that the non-diagonal matrix elements of K and M solely emerge from OZI violating contributions in the effective meson Lagrangian. The θ_1 rotations diagonalize K to $\hat{K}$ and θ_2 diagonalizes M in the basis constructed from the original one by renormalization with $\hat{K}^{-1/2}$. The four parameters $\theta_{1,2}$ and $\hat{K}_{1,2}$ are not independent but related by their functional dependence on the three coupling constants. Nevertheless, it was possible to reproduce the empirical data of four quantities: two masses of the η's and two widths for their decays into two photons. The latter is determined by the $U(3)$ generalization of the computation that in Appendix C.4 is described for $\pi^0\to\gamma\gamma$. Substituting the so-determined coupling constants yields

$$\theta_1 = 7.4^\circ\,, \quad \theta_2 = 34.7^\circ\,, \quad \hat{K}_1^{1/2} = 1.07\,, \quad \hat{K}_2^{1/2} = 1.36\,. \tag{7.28}$$

Among other issues, a big ado, both in theory [67] and in experiment [68], was later made of the fact that θ_1 is quite small[9] allowing the simplified approximation $S \sim R(\theta_{\rm id})\hat{K}^{-1/2}R(\tilde{\theta})$, but that might be purely accidental.

After this interlude on the physics of η mesons, we return to the discussion of the axial singlet current. Following [1], we define axial form factors of the nucleon for the flavor $l = u, d, s$ via

$$\frac{\sqrt{p_0 p_0'}}{M_N}\ \langle P(\boldsymbol{p}')|\overline{q}_l\gamma_\mu\gamma_5 q_l|P(\boldsymbol{p})\rangle = \overline{u}(\boldsymbol{p}')\left[\gamma_\mu\gamma_5 H_l(q^2) + \frac{\mathrm{i}q_\mu}{2M_N}\gamma_5\tilde{H}_l(q^2)\right]u(\boldsymbol{p}) \tag{7.29}$$

with $q_\mu = p_\mu - p'_\mu$. In this notation, we identify the difference $g_{\rm A} = H_1(0) - H_2(0)$ as the axial charge for neutron β-decay. The relevant quantity for the axial singlet current is

$$H(q^2) = \sum_{l=1}^{3} H_l(q^2). \tag{7.30}$$

Obviously, the first term in (7.23) only contributes to the induced form factor $\tilde{H}(q^2) = \sum_{l=1}^{3}\tilde{H}_l(q^2)$. In the notation of Sect. 4.7, we find the non-derivative piece $\overline{A}_\mu^{(0)}$ to be

$$\overline{A}_\mu^{(0)} = \sqrt{2}\epsilon_{\mu\nu\rho\sigma}\mathrm{tr}\left\{2\mathrm{i}\big(\frac{\gamma_1}{3} + \frac{\gamma_2}{2}\big)p^\nu p^\rho R^\sigma - \sqrt{2}g\gamma_2 F^{\nu\rho}(\rho)R^\sigma - 2\mathrm{i}g^2(\gamma_2 + 2\gamma_3)R^\nu R^\rho R^\sigma\right\}. \tag{7.31}$$

As for other axial charges, $H(q^2)$ is obtained from the spatial components. We substitute the classical as well as the induced profile functions in the covariant expression and find

$$\overline{A}_i^{(0)} = \frac{2}{\sqrt{3}}\left[A_5(r)\Omega_i + A_6(r)\hat{x}_i\hat{\boldsymbol{x}}\cdot\boldsymbol{\Omega}\right]. \tag{7.32}$$

The radial functions, A_5 and A_6, have already been quoted in (7.16). Even though the η meson profiles do not appear explicitly therein, they affect the induced vector meson profiles (5.64) via the corresponding equations of motion. According to the quantization prescription for the collective coordinates, (5.20), we have to replace the angular velocity by the spin operator when computing matrix elements $\boldsymbol{\Omega} \to \boldsymbol{J}/\alpha^2$, with α^2 the moment of inertia for spatial rotations, cf. (5.65). Taking the proton polarization to be $S_z = +\frac{1}{2}$ then yields

$$H(0) = \Sigma_N = \sqrt{3}c_2 = \frac{4\pi}{\sqrt{3}\alpha^2}\int_0^\infty r^2\mathrm{d}r\,[3A_5(r) + A_6(r)] \tag{7.33}$$

[9] It simply reflects that OZI violation associated with derivatives of the η fields, alike the second term in (7.25), is small.

for the Fourier transformation of $3A_i^{(0)}$. This result holds in both the two- and the three-flavor versions of the model and does not depend on the strength of flavor symmetry breaking. It is the same for all spin-$\frac{1}{2}$ baryons. (Generally, the quantization prescription $\boldsymbol{\Omega} \to \boldsymbol{J}/\alpha^2$ is contaminated by symmetry breaking; so small variations are nevertheless possible.) Numerically the vector meson models predict

$$\Sigma_N = 0.30 \pm 0.05, \tag{7.34}$$

where the error has been estimated from the range of allowed parameters in the effective vector meson Lagrangian. This agrees favorably with the empirical data quoted in the previous section. In particular, it is significantly less than one, the prediction of the non-relativistic quark model in which the axial singlet matrix element equals twice the contribution to the proton spin that is carried by the quarks spin. Certainly, this must be considered as one of the major successes of soliton models. The above calculation shows that in chiral soliton models significant efforts need to be taken to actually get a small but non-zero result. Given the small experimental datum for Σ_N, this demonstrates that chiral symmetry is crucial for the nucleon structure.

7.5 Strangeness in the Nucleon

In a flavor symmetric world, the excitation of virtual strange and non-strange quark anti-quark pairs is equally probable. In such a scenario, we actually expect sizable effects of strange degrees of freedom in the nucleon. On the other hand and as a consequence of the Appelquist–Carazzone theorem [69], virtual strangeness excitations do not appear when the corresponding field degrees of freedom are infinitely heavy. The latter scenario is realized in the two-flavor reduction of chiral Lagrangians. Hence, we conclude that the effect of strangeness in the nucleon depends on the effective size of flavor symmetry breaking. We have already seen in Chap. 6 that the collective coordinate quantization scheme allows us to treat flavor symmetry breaking as a variable parameter in the form of $\omega^2 = \frac{3}{2}\gamma\beta^2$, the product of explicit symmetry breaking, cf. (6.25), and the moment of inertia for collective rotations of the soliton into strangeness direction, cf. (6.7). In Sect. 7.3, we have made ample use thereof to demonstrate that the phenomenological parameters of semi-leptonic hyperon decays are essentially independent of the strength of symmetry breaking and that those empirical data cannot be used to argue in favor of a flavor symmetric world. In the context of that discussion, we did, however, not discuss in detail the sensitivity of the nucleon matrix element of the strange axial current, $\Delta s = \langle N|A_i^{(s)}|N\rangle$ on ω^2. That relation is displayed in Fig. 7.4 in the same fashion as the other axial current matrix elements in Sect. 7.3. Obviously, Δs shows a significantly stronger dependence on ω^2 than the matrix elements for the hyperon decays. The matrix element decreases clearly as symmetry breaking grows. Of course, that is not unexpected as Δs

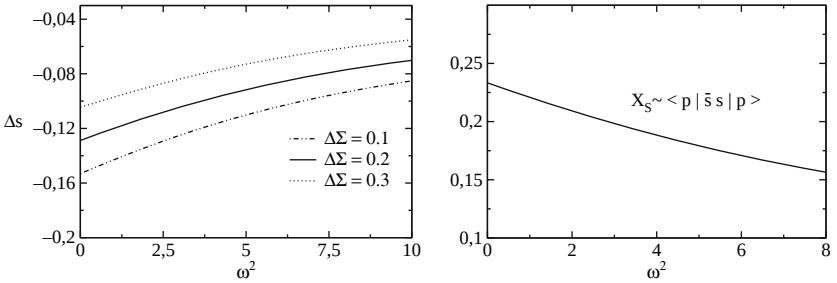

Fig. 7.4. Dependence of nucleon matrix elements on the effective symmetry breaking ω^2. *Left panel*: axial current; *right panel*: scalar $\bar{s}s$ as defined in (7.35). Note that the ordinate does not start at zero

must vanish for infinite ω^2. This result questions estimates of Δs that apply $SU(3)$ flavor symmetry relations to compute the nucleon matrix element of $A_i^{(8)}$ [60] and subsequently extract Δs from the measured value of $\Delta\Sigma$. Such procedures most likely overestimate Δs.

In Fig. 7.4, we also show the ω^2 dependence of the (normalized) scalar matrix element

$$X_{\mathrm{S}} = \frac{\langle p|\bar{s}s|p\rangle - \langle 0|\bar{s}s|0\rangle}{\langle p|\bar{u}u + \bar{d}d + \bar{s}s|p\rangle - \langle 0|\bar{u}u + \bar{d}d + \bar{s}s|0\rangle} =: \frac{y}{2+y}. \tag{7.35}$$

Here the state $|0\rangle$ refers to the soliton being absent and $y = \frac{2\langle p|\bar{s}s|p\rangle}{\langle p|\bar{u}u+\bar{d}d|p\rangle}$ is a definition often used within chiral perturbation theory; e.g., [70] estimated $y = 0.21\pm0.20$ which translates into $X_{\mathrm{S}} = 0.10\pm0.08$. This quantity has a wide spectrum of interesting applications reaching from its contribution to the nucleon σ-term in pion–nucleon scattering [71] to its influence on the neutralino-nucleon cross-section [72] which, as indicated in supersymmetric approaches, may be important for eventually detecting dark matter directly. Models for the quark flavor dynamics, as, e.g., the one of Nambu–Jona–Lasinio, indicate that in soliton models the matrix elements of quark bilinears $\bar{q}\lambda_a q$ should be proportional to the matrix elements of $\mathrm{tr}\left[\lambda_a\left(U + U^\dagger - 2\right)\right]$, cf. (2.28). Then we straightforwardly get

$$X_{\mathrm{S}} = \frac{1}{3}\langle p|1 - D_{88}|p\rangle \approx \frac{7}{30} - \frac{43}{2250}\gamma\beta^2 + \cdots, \tag{7.36}$$

with the deviation from the flavor symmetric value ($X_{\mathrm{S}} \approx 0.233$ [73]) indicated. As for Δs, this scalar strangeness content decreases as symmetry breaking increases. Such a significant reduction from the flavor symmetric prediction is also needed to establish agreement with the above-quoted estimate from chiral perturbation theory. However, the actual amount of deviation from the symmetric limit is smaller than for the axial vector counterpart, Δs.

The three-flavor Skyrme model also provides a convenient way to study the nucleon matrix elements of the vector current $\bar{s}\gamma_\mu s$. They are theoretically

interesting because they would vanish in a pure valence quark model of the nucleon and so test finer details of nucleon structure. Experimentally, they can be extracted from measurements of the parity violating asymmetry in the elastic scattering of polarized electrons from the proton [74, 75, 76, 77]. The strange vector form factors are defined as

$$\langle P(\boldsymbol{p}')|\overline{q}_{\rm s}\gamma_\mu q_{\rm s}|P(\boldsymbol{p})\rangle = \overline{u}(\boldsymbol{p}')\left[\gamma_\mu F_{\rm s}(q^2) + \frac{\sigma_{\mu\nu}q^\nu}{2M_p}\tilde{F}_{\rm s}(q^2)\right]u(\boldsymbol{p}) \qquad (7.37)$$

and have been estimated in various models. They range from vector–meson–pole fits [78] of dispersion relations [29] through vector meson dominance approaches [5] and kaon–loop calculations with [79] and without [80] vector meson dominance contributions via constituent quark models [81] to soliton model calculations [3, 5, 82, 83, 84]. The numerical results for the strange magnetic moment $\mu_{\rm S} = \tilde{F}_{\rm s}(0) \approx -0.31 \pm 0.09 \ \ldots \ 0.25$ are quite diverse. The predictions for the strange charge radius $r_{\rm S}^2 = -6{\rm d}F_{\rm s}(q^2)/{\rm d}q^2|_{q=0}$ are almost equally scattered $r_{\rm S}^2 \approx -0.20 \ \ldots \ 0.14\,{\rm fm}^2$.

In order to evaluate these form factors in the three-flavor Skyrme model, one requires the matrix elements of the "strange" combination

$$Q^{\rm s} = \frac{1}{3}\mathbb{1} - \frac{1}{\sqrt{3}}\lambda_8 = Q^0 - \frac{2}{\sqrt{3}}Q^8 \qquad (7.38)$$

rather than the electromagnetic one (7.3) between proton states. Using the same value $e = 4.0$ as used consistently for the three-flavor pseudoscalar model yields the predictions

$$\mu_{\rm S} = -0.13{\rm n.m.} \quad \text{and} \quad r_{\rm S}^2 = -0.10\,{\rm fm}^2 \ . \qquad (7.39)$$

Here n.m. stands for nuclear magnetons. These results are obtained under full recognition of flavor symmetry breaking in the collective coordinate wave functions, cf. Sect. 6.4. If a pure octet wave function were employed to compute the matrix elements of the collective operators, the strange magnetic moment would have been $\mu_{\rm S} = -0.33$. The proper inclusion of symmetry breaking into the nucleon wave function is again seen to reduce the effect of the strange degrees of freedom in the nucleon. The vector meson model of [3] predicts an even smaller (in magnitude) strange magnetic moment, $\mu_{\rm S} \approx -0.05$n.m. So it seems likely that this strange nucleon property may actually be compatible with zero, a result supported by the latest (accurate) experiments [77].

7.6 Neutron–Proton Mass Difference

The neutron–proton mass difference is another famous problem whose solution in the nucleon-as-soliton picture requires the addition of vector mesons to the effective Lagrangian. We will find that major contributions to this difference

are integrals over the η-meson profiles, (7.24) that require vector meson fields to be non-zero, cf. (7.23) and (7.31).

After correcting for the electromagnetic interaction (photon loop) the remaining "strong" part of the neutron–proton mass difference should be $(M_\mathrm{n} - M_\mathrm{p})_\mathrm{strong} \approx (2.0 \pm 0.3)\mathrm{MeV}$ [85]. At the quark level, this arises from the down quark-up quark mass difference, $m_{0,\mathrm{d}} - m_{0,\mathrm{u}}$. So we have to generalize (6.19) to account for (small) isospin breaking:

$$\begin{aligned}\hat{m}_0 &= \frac{m_{0,\mathrm{u}} + m_{0,\mathrm{d}}}{3}\left(\mathbb{1} + \frac{\sqrt{3}}{2}\lambda_8\right) + \frac{m_{0,\mathrm{d}} - m_{0,\mathrm{u}}}{2}\lambda_3 + \frac{m_{0,\mathrm{s}}}{3}\left(\mathbb{1} - \sqrt{3}\lambda_8\right) \\ &\propto \frac{2 + x^{(\mathrm{s})}}{3}\mathbb{1} + x^{(i)}\lambda_3 + \frac{1 - x^{(\mathrm{s})}}{\sqrt{3}}\lambda_8\,. \end{aligned} \tag{7.40}$$

In (6.22), we have estimated the strangeness symmetry breaking coefficient from kaon and pion properties, $x^{(\mathrm{s})} = \left(f_K^2 m_K^2 - f_\pi^2 m_\pi^2\right)/f_\pi^2 m_\pi^2$. Similarly, we gain the isospin parameter from investigating appropriate mass differences. For example, the pseudoscalar sector predicts $x^{(i)} = m_K\left(m_{K^+} - m_{K^0}\right)/m_\pi^2 + \cdots$, where contributions from derivative symmetry breakers in the effective Lagrangian are not made explicit. Alternatively, one could use the $\rho^0 - \omega$ mass difference in the vector meson model. These approaches agree in predicting $x^{(i)} = -0.4 \cdots - 0.2$ [1].

To understand the problem, it is helpful to consider the contribution of the dominating mass-type symmetry breaker to the neutron–proton mass difference. Since the d–u quark mass difference clearly exists with only two flavors, it is interesting to first consider the problem at this level. The relevant term is proportional to

$$\mathrm{tr}\left[\tau_3\left(U + U^\dagger\right)\right]. \tag{7.41}$$

From (7.24), we see that $U = \exp(\mathrm{i}\eta_\mathrm{T}(\boldsymbol{x}))\left[\cos(F) + \mathrm{i}\hat{\boldsymbol{x}}\cdot\boldsymbol{\tau}\sin(F)\right]$ in the two-flavor reduction. Hence, the expression (7.41) is proportional to $\sin(\eta_\mathrm{T})$. In other words, the contribution vanishes unless the field η_T gets excited due to the collective rotation (or any kind of symmetry breaking). The discussion around (7.23) shows that this will not happen if only pseudoscalars are present in the effective Lagrangian; the vector meson contribution $\overline{A}_\mu^{(0)}$ must also be present. This is analogous to just discussed proton spin puzzle. The contribution of the mass-type symmetry breaking term turns out to be

$$(M_\mathrm{n} - M_\mathrm{p})_\mathrm{strong} = -\frac{8x^{(i)} f_\pi^2 m_\pi^2}{3\alpha^2}\int \mathrm{d}^3 r \sin F(r)\eta_\mathrm{T}(r) + \cdots\,, \tag{7.42}$$

where only the contribution linear in the angular velocity ($\boldsymbol{\Omega}$) is kept. Its nucleon matrix element has been evaluated according to the rules of Sect. 5.3, as the appearance of the moment of inertia, α^2, suggests. Using the full two-flavor vector meson result for $\overline{A}_\mu^{(0)}$ which was already employed to compute the axial singlet matrix element yields [1, 86]

$$\Delta = (M_{\rm n} - M_{\rm p})_{\rm strong} \approx 1.4\,{\rm MeV}\,. \tag{7.43}$$

Not surprisingly, this numerical result turns out to be about as robust against (permitted) changes of the parameters as is $H(0)$. In any event, the induced η profile function enters crucially and thus the above result is sensitive to the $\eta - \eta'$ mixing scenario described above. Nevertheless, the prediction, (7.43), is still somewhat too small when compared to the empirical value. It turns out that the missing ~ 0.5MeV can be attributed to three flavor effects that we will discuss next. They are already present at the classical level. Straightforward substitution of the collectively rotating hedgehog configuration, (6.4), yields

$$\text{Eq. (7.41)} = \frac{4}{\sqrt{3}} D_{38}\,(\cos F - 1)\,. \tag{7.44}$$

For finite symmetry breaking $\omega^2 < \infty$, the nucleon matrix element of D_{38} is non-zero and hence there is a contribution to the neutron proton matrix element

$$\Delta_{SU(3)} = \Gamma_3\,(\langle n|D_{38}|n\rangle - \langle p|D_{38}|p\rangle) \tag{7.45}$$

with

$$\Gamma_3 = \frac{4\pi x^{(i)} m_\pi^2 f_\pi^2}{\sqrt{3}} \int_0^\infty {\rm d}r r^2\ \{(1-\cos F)\ldots\}\,, \tag{7.46}$$

where contributions from the derivative-type symmetry breaker and vector mesons are not listed explicitly.[10] Typical values for the functional Γ_3 turn out to be around $-15\,{\rm MeV}$ [1]. The collective coordinate matrix element in (7.45) gives $\langle N|D_{38}|N\rangle = \frac{I_3}{5\sqrt{3}}$ when $SU(3)$ symmetric nucleon wave functions are substituted, where $I_3 = \pm\frac{1}{2}$ is the nucleon isospin projection. This corresponds to $\Gamma_3 \approx 1.7\,{\rm MeV}$. Together with the two-flavor result, (7.43), this would overestimate the empirical value considerably. However, we have already seen that collective coordinate matrix elements may considerably deviate from their flavor symmetric values. This is particularly the case for D_{38}, as shown in Fig. 7.5. For the realistic symmetry breaking $\omega^2 \approx 6$, this matrix element is reduced to a about a third of the above mentioned symmetric value. Hence, the $SU(3)$ contribution to the neutron–proton mass difference is only of the order of $0.5\,{\rm MeV}$. Together with the dominating two-flavor contribution this adds to about $2\,{\rm MeV}$, exactly what is expected for the strong interaction part of $M_{\rm n} - M_{\rm p}$.

As an interim conclusion, we realize that the axial singlet current matrix element as well as the neutron–proton mass difference pinpoints shortcomings of the original Skyrme model with only pseudoscalar degrees of freedom. However, they are not general problems of chiral soliton models as they can be nicely solved by appropriate extensions of the effective meson action. Here we

[10] In addition, the full three-flavor result embodies other collective coordinate operators than the one shown in (7.45), as, e.g., $\sum_{i=1}^3 D_{3i} D_{8i}$. The detailed discussion is given in [1].

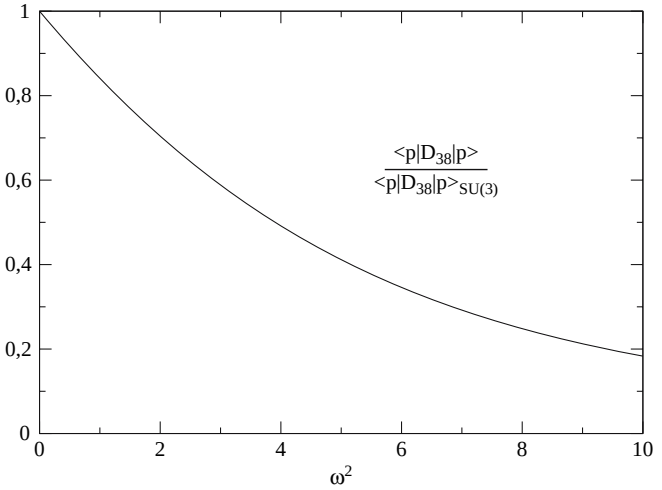

Fig. 7.5. Dependence of proton matrix element $\langle p|D_{38}|p\rangle$ on the effective symmetry breaking ω^2. The displayed matrix element is normalized to the result at $\omega^2 = 0$

have extensively discussed the vector meson scenario. References [56, 86, 87] show that extensions by chiral quarks as in the NJL model, cf. Chap. 3, do a similar job.

7.7 Nucleon Structure Functions

So far we have considered baryon properties that can be computed in any chiral soliton model with more or less success and agreement between predictions and empirical data. We will now consider a particular set of properties for which this does not seem to be true. Structure functions parameterize hadron properties in deep inelastic scattering (DIS). In (perturbative) QCD, these functions are matrix elements of bilinear quark operators that are also bilocal. Thus, it seems plausible that models based on a meson action cannot account for such matrix elements because then the field degrees of freedom represent local bilinear quark operators. Many of the computations [88, 89][11] essentially identify the quark operators of chiral quark models (as those discussed in Chap. 3) with those in the DIS matrix elements. The latter actually refer to the field degrees of freedom in perturbative QCD, and thus this identification seems a bit ad hoc. We will therefore concentrate on approaches that only require the QCD chiral symmetries to be identified in the considered chiral quark model. After all, DIS refers to photon nucleon reactions in

[11] See [90, 91, 92] for more recent discussions and exhaustive lists of further references.

a certain kinematical regime. Thus, DIS properties must be computable from appropriate matrix elements of the electromagnetic current, which is one of the symmetry currents in chiral models. As a matter of fact, this weaker identification was used in the first computations of nucleon structure functions in [93, 94, 95]. The approach builds up from virtual Compton scattering at large momentum transfer. Hence, it requires to consider the two-photon coupling to the nucleon in chiral quark models in the respective kinematical regime [96]. We will first discuss pion structure functions in the chiral quark model of Sect. 2.3 to set up the approach and proceed with investigating some of the nucleon structure functions. A comprehensive discussion on chiral quark model computations for nucleon structure functions is beyond the scope of this monograph and we rather refer to the research articles quoted above and in footnote 11.

We are actually interested in the absorptive (i.e., imaginary) part of the forward virtual Compton amplitude. In order to properly identify this imaginary part, it is most appropriate to explore the chiral quark model, that we considered earlier in Euclidean space, in Minkowski space. This is actually straightforward and leads to the regularized action functional [96, 97]

$$-\mathrm{i}\,\mathrm{Tr}_\Lambda \log\left[\mathrm{i}\partial\!\!\!/ - (S + \mathrm{i}\gamma_5 P)\right] = -\mathrm{i}\frac{N_\mathrm{C}}{2}\sum_{n=0}^{2} c_n \,\mathrm{Tr}\log\left[-\mathbf{D}\mathbf{D}_5 + \Lambda_n^2 - \mathrm{i}\epsilon\right] \\ -\mathrm{i}\frac{N_\mathrm{C}}{2}\mathrm{Tr}\log\left[-\mathbf{D}\left(\mathbf{D}_5\right)^{-1} - \mathrm{i}\epsilon\right] , \qquad (7.47)$$

with

$$\mathrm{i}\mathbf{D} = \mathrm{i}\partial\!\!\!/ - (S + \mathrm{i}\gamma_5 P) \quad \text{and} \quad \mathrm{i}\mathbf{D}_5 = -\mathrm{i}\partial\!\!\!/ - (S - \mathrm{i}\gamma_5 P) \; . \qquad (7.48)$$

These definitions replace (2.16) and (2.17) in the case that only scalar (S) and pseudoscalar (P) quark bilinear fields are considered. We have switched to the Pauli–Villars (PV) regularization scheme for the anomaly free part of the action. The anomalous part is (conditionally) finite and does not get regularized. The choice $c_0 = 1,\ \Lambda_0 = 0,\ \sum_{n=0}^{2} c_n = 0$ renders the functional finite and formally reproduces the action listed in (2.15) when the cut-offs $\Lambda_{1,2}$ approach infinity. We may also employ the chiral circle condition, (2.20), for $M = S + \mathrm{i}P$. Then (7.47) exhibits only a logarithmic divergence and a single subtraction is sufficient. The reason for modifying the regularization prescription will soon become more obvious.

As in the proper time scheme, the PV-regularization parameters are determined to reproduce meson properties. In the PV scheme, the gap equation (2.18) reads

$$\frac{1}{2G}\left(m - m_0\right) = 4\mathrm{i}N_\mathrm{C} m \sum_{n=0}^{2} c_n \int \frac{\mathrm{d}^4 k}{(2\pi)^4}\left[k^2 - m^2 - \Lambda_n^2 + \mathrm{i}\epsilon\right]^{-1} . \qquad (7.49)$$

Defining the polarization function

$$\Pi(q^2,x)=\sum_{n=0}^{2} c_n \frac{\mathrm{d}^4k}{(2\pi)^4\mathrm{i}} \left[k^2+x(1-x)m_\pi^2-m^2-\Lambda_n^2+\mathrm{i}\epsilon\right]^{-2}, \qquad (7.50)$$

the (on-shell) pion decay constant becomes

$$f_\pi = 4N_\mathrm{C} m g \int_0^1 \mathrm{d}x\, \Pi(m_\pi^2,x)\,. \qquad (7.51)$$

The pole and unit residue of the pion propagator implicitly relate the pion mass and meson–quark coupling constant to the model parameters:

$$\begin{aligned} m_0 &= 4\,N_\mathrm{C}\,m\,G\,m_\pi^2 \int_0^1 \mathrm{d}x\,\Pi(m_\pi^2,x)\,,\\ \frac{1}{g^2} &= 4N_\mathrm{C}\frac{\mathrm{d}}{\mathrm{d}m_\pi^2}\int_0^1 \mathrm{d}x\,\left[m_\pi^2\Pi(m_\pi^2,x)\right]\,. \end{aligned} \qquad (7.52)$$

These equations replace (2.22), (2.23) and (2.24) from the proper-time regularization scheme.

DIS off hadrons is parameterized by the hadronic tensor $W^{\mu\nu}(p,q)$. Here q is the momentum transmitted from the photon to the hadron with momentum p. The tensor $W^{\mu\nu}(p,q)$ is obtained from the hadron matrix element of the current commutator by the Fourier transformation[12]

$$W_{\mu\nu}(p,q)=\frac{1}{4\pi}\int \mathrm{d}^4x\,\mathrm{e}^{\mathrm{i}q\cdot\xi}\,\langle p,s|[J_\mu(\xi),J_\nu^\dagger(0)]|p,s\rangle\,. \qquad (7.53)$$

Subsequently, $W_{\mu\nu}(p,q)$ is parameterized in terms of form factors that multiply the allowed Lorentz structures. These form factors are extracted by pertinent projection of the hadronic tensor. Finally, the structure functions are the leading terms of the twist expansion[13] for the form factors. These contributions are obtained from computing $W^{\mu\nu}(p,q)$ in the Bjorken limit: $Q^2=-q^2\to\infty$ with the Bjorken variable $x=Q^2/p\cdot q$ fixed. That is, subleading contributions in $1/Q^2$ are omitted.

An essential feature of bosonized quark models is that the derivative term in (7.48) is formally identical to that of a non-interacting (or asymptotically free) quark model. In the framework of DIS studies, chiral quark models are therefore favored over models that are directly formulated in meson field variables.[14] More explicitly, the vector current operator is given as $J^\mu=\bar{q}\mathcal{Q}\gamma^\mu q$,

[12] Eventually, the spin of the hadron is called s. For simplicity, we do not make explicit the flavor labels on J_μ.

[13] Roughly spoken, twist refers to the expansion of the structure functions in inverse powers of the momentum Q^2[98].

[14] See, however, [99] for an early attempt to compute structure functions in the Skyrme model.

with $\mathcal{Q}$ a flavor matrix in chiral quark models. Expectation values of currents are conveniently computed by introducing pertinent sources v_μ in (7.48)

$$\mathrm{i}\mathbf{D} \longrightarrow \mathrm{i}\mathbf{D} + \mathcal{Q}\not{v} \qquad \text{and} \qquad \mathrm{i}\mathbf{D}_5 \longrightarrow \mathrm{i}\mathbf{D}_5 - \mathcal{Q}\not{v} \tag{7.54}$$

and differentiating the so-gauged action (7.48) with respect to v_μ. In bosonized quark models, it is convenient to identify $W^{\mu\nu}(p,q)$ from the absorptive part

$$W^{\mu\nu}(p,q) = \frac{1}{2\pi}\mathsf{Im}\left[T^{\mu\nu}(p,q)\right] \tag{7.55}$$

of the forward virtual Compton amplitude

$$T^{\mu\nu}(p,q) = \int \mathrm{d}^4\xi\, \mathrm{e}^{\mathrm{i}q\cdot\xi}\, \langle p,s|T\left(J^\mu(\xi)J^\nu(0)\right)|p,s\rangle \tag{7.56}$$

because the time-ordered product is straightforwardly obtained from

$$T\left(J^\mu(\xi)J^\nu(0)\right) = \frac{\delta^2}{\delta v_\mu(\xi)\,\delta v_\nu(0)}\,\mathrm{Tr}_\Lambda \log\left[\mathrm{i}\partial\!\!\!/ - (S + \mathrm{i}\gamma_5 P) + \mathcal{Q}\not{v}\right]\Big|_{v_\mu=0}, \tag{7.57}$$

as defined from (7.48) with the substitution (7.54).

We compute the pion–photon scattering amplitude by expanding (7.48) to second order in both $\boldsymbol{\pi}$ and v_μ. From this term, we read off the single structure function, $F(x)$, that characterizes pion-DIS. Due to the separation into $\mathbf{D}$ and $\mathbf{D}_5$, this calculation differs considerably from the simple evaluation of the "handbag" diagram. For example, isospin violating and dimension-five operators appear for the action (7.48). Fortunately, all isospin violating pieces cancel yielding

$$F(x) = \frac{5}{9}(4N_\mathrm{C}g^2)\frac{\mathrm{d}}{\mathrm{d}m_\pi^2}\left[m_\pi^2\Pi(m_\pi^2,x)\right], \quad 0 \le x \le 1\,. \tag{7.58}$$

It appears to be a fortuitousness that the same result is obtained by a formal treatment of the divergent handbag diagram and ad hoc regularization[100]. The cancellation of the isospin violating pieces is a feature of the Bjorken limit: insertions of the pion field on the propagator that carries the infinitely large photon momentum can be safely omitted. Furthermore, this propagator can be taken to be the one for non-interacting massless fermions. This implies that also the Pauli–Villars cut-offs can be omitted for this propagator. That, in turn, leads to the desired scaling behavior of the structure function in this model and is a particular feature of the Pauli–Villars regularization. A priori it is not obvious for an arbitrary regularization scheme that terms of the form Q^2/Λ_n^2 drop out in the Bjorken limit.

From (7.52) and (7.58), it is obvious that $F(x) = 5/9$ for $0 \le x \le 1$ in the chiral limit ($m_\pi = 0$). We note that this is the structure function at the (low) energy scale of the model. To compare with empirical data that are at a higher

energy scale, the DGLAP[15] program of perturbative QCD has to be applied onto $F(x)$ to incorporate the leading $\ln Q^2$ corrections. Such studies [103, 104] show good agreement with the experimental data for $F(x)$.

DIS off nucleons is described by four structure functions: $F_1(x)$ and $F_2(x)$ are insensitive to the nucleon spin, while the polarized structure functions, $g_1(x)$ and $g_2(x)$, multiply Lorentz structures that contain the nucleon spin. An important consequence of the formal identity between the current operators in the model and in QCD is that the Callan–Gross relation $F_2(x) = 2xF_1(x)$ that originally identified the charged partons as spin-$\frac{1}{2}$ particles is reproduced in this soliton model.

We will now outline the model calculation of structure functions. As argued in the context of the pion structure function, the quark propagator with the (infinitely) large photon momentum should be taken to be the one for free and massless fermions. Thus, it is sufficient to differentiate (Here $\mathbf{D}$ and $\mathbf{D}_5$ are those of (7.48), i.e., with $v_\mu = 0$.)

$$\frac{N_\mathrm{C}}{4\mathrm{i}} \sum_{n=0}^{2} c_n \mathrm{Tr}\left\{\left(-\mathbf{D}\mathbf{D}_5 + \Lambda_n^2\right)^{-1}\left[\mathcal{Q}^2 \not{p}\,(\not{\partial})^{-1}\not{p}\mathbf{D}_5 - \mathbf{D}(\not{p}\,(\not{\partial})^{-1}\not{p})_5\mathcal{Q}^2\right]\right\}$$
$$+\ \frac{N_\mathrm{C}}{4\mathrm{i}}\mathrm{Tr}\left\{(-\mathbf{D}\mathbf{D}_5)^{-1}\left[\mathcal{Q}^2\not{p}\,(\not{\partial})^{-1}\not{p}\mathbf{D}_5 + \mathbf{D}(\not{p}\,(\not{\partial})^{-1}\not{p})_5\mathcal{Q}^2\right]\right\}, \qquad (7.59)$$

with respect to the photon field v_μ. The $(\ldots)_5$ description

$$\gamma_\mu\gamma_\rho\gamma_\nu = S_{\mu\rho\nu\sigma}\gamma^\sigma - \mathrm{i}\epsilon_{\mu\rho\nu\sigma}\gamma^\sigma\gamma^5, \quad (\gamma_\mu\gamma_\rho\gamma_\nu)_5 = S_{\mu\rho\nu\sigma}\gamma^\sigma + \mathrm{i}\epsilon_{\mu\rho\nu\sigma}\gamma^\sigma\gamma^5, \qquad (7.60)$$

accounts for the unconventional appearance of axial sources in $\mathbf{D}_5$, cf. [96]. Substituting (5.13) for the meson fields[16] in $\mathbf{D}$ and $\mathbf{D}_5$, computing the functional trace up to subleading order in $1/N_\mathrm{C}$ in the basis $\{\Psi_\alpha(\boldsymbol{x})\}$ that diagonalizes the Dirac–Hamiltonian (3.23) yields the model results for the structure functions. The detailed formulas are listed in [96], so is the verification of the sum rules that relate static nucleon properties to integrals of the structure functions over the Bjorken variable x. As an example, we display the isovector contribution to $g_1(x)$ which in leading order $1/N_\mathrm{C}$ reads

$$g_1(x) = \frac{M_N N_\mathrm{C}}{36\mathrm{i}}\left\langle N\middle|I_3\middle|N\right\rangle \int\frac{\mathrm{d}\omega}{2\pi}\sum_\alpha\int\mathrm{d}^3\xi\int\frac{\mathrm{d}\lambda}{2\pi}\,\mathrm{e}^{\mathrm{i}M_N x\lambda}$$
$$\times\left(\sum_{n=0}^{2}\frac{c_n\,(\omega+\epsilon_\alpha)}{\omega^2-\epsilon_\alpha^2-\Lambda_n^2+\mathrm{i}\epsilon}\right)_\mathrm{P}\left[\Psi_\alpha^\dagger(\boldsymbol{\xi}\,)\tau_3\,(1-\alpha_3)\,\gamma_5\Psi_\alpha(\boldsymbol{\xi}+\lambda\hat{e}_3)\mathrm{e}^{-\mathrm{i}\omega\lambda}\right.$$

[15] These are non-local, linear differential equations for the structure functions that sum the logarithmic corrections in Q^2 which arise from absorption and emission of gluons and quarks. The coefficient functionals, the so-called splitting functions, can be computed in perturbative QCD and we refer to standard textbooks [98, 101, 102] for more details.

[16] In the context of nucleon structure functions, we only consider two flavor degrees of freedom. The three-flavor case is e.g., discussed in [105].

$$+\ \Psi_\alpha^\dagger(\boldsymbol{\xi})\tau_3\,(1-\alpha_3)\,\gamma_5\Psi_\alpha(\boldsymbol{\xi}-\lambda\hat{e}_3)\mathrm{e}^{\mathrm{i}\omega\lambda}\Big]\,. \tag{7.61}$$

Here the subscript (P) indicates the pole term that is to be computed according to Cutkosky's rules. This essentially takes care of the frequency (ω) integration. The two quark bilinears in the squared brackets emerge from the two orders in which the functional derivatives in (7.57) act. In the diagrammatic language, these two terms reflect forward and backward propagating quarks.

To verify sum rules, observe that an x-integration yields $\delta(\lambda)$ and thus renders the quark bilinears local.

There is one peculiarity that is thoroughly worked out in [96] and worth to be briefly noted here. The structure function that enters the Gottfried sum rule for the unpolarized structure function is related to the γ_5-odd piece of the action and hence does not undergo regularization. This is surprising because in the parton model this structure function differs from the one associated with the Adler sum rule (observed in neutrino proton DIS) only by the sign of the anti-quark distribution. In the present model, however, this structure function gets regularized, in agreement with the quantization rule for the collective coordinates for the isospin orientation that involves the regularized moment of inertia, α^2. This is the technical reason for this unexpected difference: for the isovector contribution associated with the backward propagating quark, the exchanges of a photon and a charged left-handed gauge boson in neutrino scattering come with opposite signs. In turn that selects different pieces from (7.59). Yet, it is sensitive to commence the model calculation of structure functions from a fully regularized action for the interaction with gauge bosons. Merely identifying QCD quark bilinears within the model does not reveal this peculiarity.

Unfortunately, numerical results for the full structure functions in the double Pauli–Villars regularization scheme, i.e., including the properly regularized vacuum piece are not yet available. Once the self-consistent soliton is substituted, the axial charges are saturated to 95% or even more by their valence quark contributions (the strongly bound level in the soliton background, cf. Fig. 3.2). This provides sufficient justification to consider its contribution to the polarized structure functions as a reliable approximation since, e.g., the sum rule for the leading polarized structure function is nothing but the axial current matrix element, $\int_0^1 \mathrm{d}x g_1(x) = c g_\mathrm{A}$, with c being a numerical constant determined by the quark charges. Technically, this approximation corresponds to replacing the quarks levels in (7.61) by the cranked valence level of (5.68), omitting the regularization parameters as well as the sum over α. As already stressed, this level is defined within the chiral soliton model, (5.68), and its contributions to the structure functions should not at all be confused with valence quark distributions in parton models. In general, these model calculations yield structure functions that parameterize the hadronic tensor, but not (anti)-quark distributions. The latter would require the identification of model degrees of freedom with those in QCD. However, here only

the symmetries (namely the chiral symmetry) and thus the current operators in the hadronic tensor are identified.

As in the case for the pion, the model calculation yields the nucleon structure function at a low-energy scale and $\ln Q^2$ corrections must be accounted for. Another obstacle arises because the soliton is a localized object. Thus, the computed structure functions are frame-dependent and one frame has to be picked. The appropriate choice is the infinite momentum frame (IMF) not only because it makes contact with the parton model but also because in this frame the support of the structure functions is limited to the physical regime $0 \leq x \leq 1$. Choosing the IMF amounts to the transformation [106, 107]

$$f_{\mathrm{IMF}}(x) = \frac{1}{1-x}\, f_{\mathrm{RF}}(-\ln(1-x))\,, \tag{7.62}$$

where $f_{\mathrm{RF}}(x)$ denotes the structure function as computed in the nucleon rest frame. So, even after the soliton model structure function has been worked out, a two-stage program must be conducted: first the transformation to the IMF according to (7.62) and subsequently the DGLAP evolution program[17] to incorporate the resumed $\ln Q^2$ corrections. In the current context, it is appropriate to restrain oneself to the leading order (in α_{s}) in the evolution program because higher orders require the identification of quark and anti-quark distributions in the parton model sense. This does not seem possible without further assumptions.[18] The low-energy scale, $Q_0^2 = 0.4\,\mathrm{GeV}^2$, at which the model is assumed to approximate QCD has been estimated in [93, 94, 95] from a best fit to the experimental data of the unpolarized structure function, $F_2(x)$. The same boundary value is taken to evolve the model prediction for polarized structure function, $g_1(x)$, in the IMF to the scale $Q^2 \sim 4 \ldots 10\,\mathrm{GeV}^2$ at which the experimental data are available. For the structure function $g_2(x)$, the situation is a bit more complicated. First the twist-2 piece must be separated according to [109]

$$g_2^{WW}(x) = -g_1(x) + \int_x^1 \frac{\mathrm{d}y}{y}\, g_1(y) \tag{7.63}$$

and evolved analogously to $g_1(x)$ (which also is twist-2). The remainder, $g_2(x) - g_2^{WW}(x)$, is twist-3 and is evolved according to the large N_C scheme of [110]. Finally, the two pieces are again put together at the endpoint of the evolution, Q^2. In Fig. 7.6, the model predictions for the linearly independent polarized structure functions of the proton are confronted with the experimental data from [111]. Obviously, the model reproduces the gross features of the data. Figure 7.7 compares the model predictions for g_2 of both the proton and the neutron (in form of the deuteron) not only to the recently accumulated data but also to other model predictions. Surprisingly, the twist-2

[17] In addition to footnote 15, we refer to [108] for the splitting functions that concern the polarized nucleon structure functions.

[18] We assume, however, that the gluon distribution is zero at the model scale.

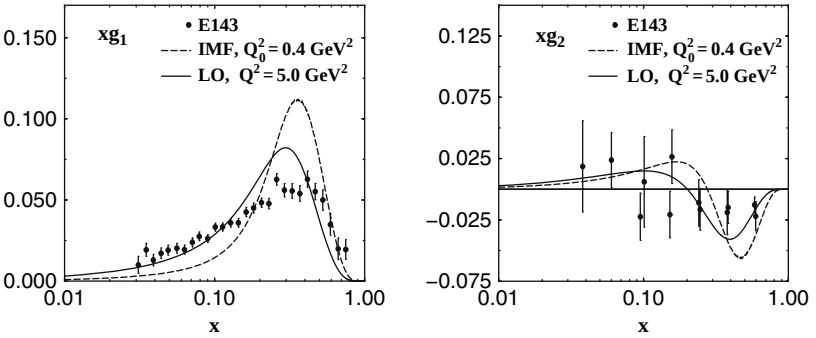

Fig. 7.6. Model predictions for the polarized proton structure functions xg_1 (*left panel*) and xg_2 (*right panel*). The curves labeled "RF" denote the results as obtained from the valence quark contribution to (7.59). These undergo a projection to the infinite momentum frame "IMF" (7.62) and a leading order "LO" DGLAP evolution, cf. footnote 17. Data are from SLAC–E143 [111].

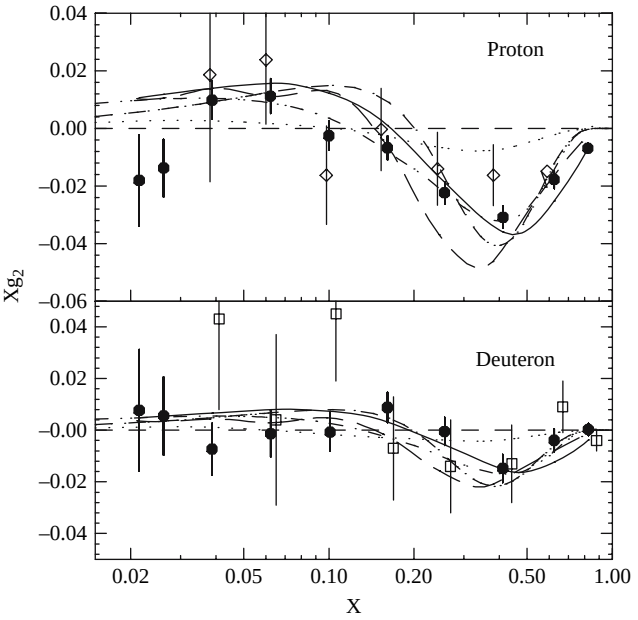

Fig. 7.7. Model predictions for the polarized proton structure functions xg_2 for proton and neutron (deuteron) and comparison with data from E143 [111] (*open diamond*) and E155 [112] (*open square*) and their combination (*solid circle*). The *full line* is the twist-2 truncation, (7.63), with data for $g_1(x)$. *Dashed-dotted* [113] and *dotted* [114] lines are bag model calculations; the *short dashed lines* represent the present chiral soliton model [95] and *long dashed line* that of [115] (this is a slightly modified figure from [112])

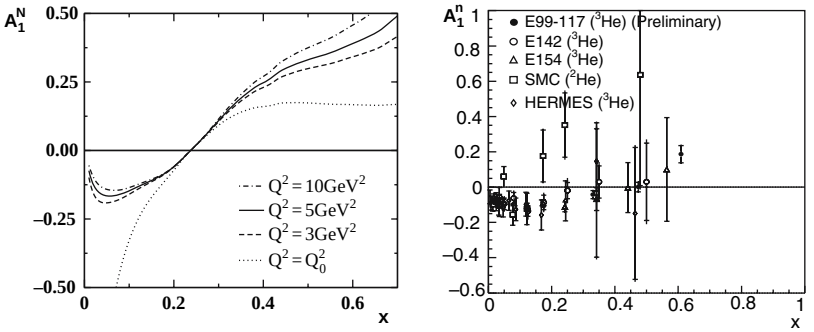

Fig. 7.8. Model prediction for A_1^N at different Q^2. The right panel shows various experimental data [116]. Most recent (and precise) JLab data are labeled E99–117

truncation, i.e., (7.63) with the data for $g_1(x)$ at the right-hand side, gives the most accurate description of the data. However, also the chiral soliton model predictions reproduce the data well. Bag model predictions have a less pronounced structure.

Recently, precise data [116] have become available for the neutron asymmetry

$$A_1 = \frac{g_1(x,Q^2) - \frac{4M^2x^2}{Q^2} g_2(x,Q^2)}{F_1(x,Q^2)} \,. \tag{7.64}$$

It is therefore challenging to study this quantity in the present model. As subleading twist contributions are omitted, this amounts to computing the ratio $g_1(x,Q^2)/F_1(x,Q^2)$ for the neutron. The resulting ratio is shown in Fig.7.8 together with data. It is interesting to note that while the ratio at the model scale, Q_0, becomes large and negative at small x, the DGLAP evolution causes it to bend around so that it actually tends to zero as $x \to 0$. This behavior is also observed from the data, as is the change in sign at moderate x. The position ($x \approx 0.25$) at which this change occurs seems somewhat lower than the preliminary JLab-data [116] suggest and also appears to be insensitive to the endpoint of evolution. Once evolution has set in at a moderate point Q^2, the evolution to even higher Q^2 has insignificant effect.

Though the studies discussed in this section represent an interesting application of the chiral quark soliton model, the ultimate goal is the investigation of nucleon structure functions in any chiral soliton model without reference to any underlying quark flavor dynamics. In particular, it is challenging to reproduce the Callan–Gross relation from the Wess–Zumino term which, according to Chap. 6, dictates the fermion nature of the soliton.

References

1. J. Schechter, A. Subbaraman, and H. Weigel, *Phys. Rev.* **D48** (1993) 339. 114, 126, 127, 12
2. M. Harada and J. Schechter, *Phys. Rev.* **D54** (1996) 3394. 114
3. N. W. Park and H. Weigel, *Nucl. Phys.* **A541** (1992) 453. 115, 116, 118, 120, 121, 123, 131
4. H.-C. Kim, A. Blotz, M. V. Polyakov, and K. Goeke, *Phys. Rev.* **D53** (1996) 4013. 115
5. N. W. Park, J. Schechter, and H. Weigel, *Phys. Rev.* **D43** (1991) 869. 116, 131
6. G. S. Adkins and C. R. Nappi, *Nucl. Phys.* **B249** (1985) 507. 116
7. B. Schwesinger and H. Weigel, *Nucl. Phys.* **A540** (1992) 461. 116, 117
8. J. Schechter and H. Weigel, *Phys. Rev.* **D44** (1991) 2916. 117
9. J. Schechter and H. Weigel, *Phys. Lett.* **B261** (1991) 235. 117
10. T. Haberichter, H. Reinhardt, N. N. Scoccola, and H. Weigel, *Nucl. Phys.* **A615** (1997) 291. 117
11. N. N. Scoccola, H. Weigel, and B. Schwesinger, *Phys. Lett.* **B389** (1996) 433. 117
12. T. Eden et al., *Phys. Rev.* **C50** (1994) 1749. 117
13. C. Herberg et al., *Eur. Phys. J.* **A5** (1999) 131. 117
14. M. Ostrick et al., *Phys. Rev. Lett.* **83** (1999) 276. 117
15. D. Rohe et al., *Phys. Rev. Lett.* **83** (1999) 4257. 117
16. I. Passchier et al., *Phys. Rev. Lett.* **82** (1999) 4988. 117
17. J. Golak, G. Ziemer, H. Kamada, H. Witala, and W. Gloeckle, *Phys. Rev.* **C63** (2001) 034006. 117
18. E93026 Collaboration, H. Zhu et al., *Phys. Rev. Lett.* **87** (2001) 081801. 117
19. J. Bermuth et al., *Phys. Lett.* **B564** (2003) 199. 117
20. E93-038 Collaboration, R. Madey et al., *Phys. Rev. Lett.* **91** (2003) 122002. 117
21. S. Galster et al., *Nucl. Phys.* **B32** (1971) 221. 118
22. S. Eidelman et al. [PDG], *Phys. Lett.* **B592** (2004) 1. 118, 122
23. U. G. Meißner, N. Kaiser, H. Weigel, and J. Schechter, *Phys. Rev.* **D39** (1989) 1956. 118, 126
24. J. J. Sakurai, *Currents and Mesons*. University of Chicago Press, Chicago, IL, 1969. 118
25. U. G. Meißner, N. Kaiser, and W. Weise, *Nucl. Phys.* **A466** (1987) 685. 118, 120
26. G. Holzwarth, `hep-ph/0511194`. Talk at Workshop on Nucleon Form Factors (N05), Frascati. 119, 120
27. A. N. Mitra and I. Kumari, *Phys. Rev.* **D15** (1977) 261. 119
28. J. J. Kelly, *Phys. Rev.* **C66** (2002) 065203. 119
29. G. Hohler et al., *Nucl. Phys.* **B114** (1976) 505. 119, 131
30. A. F. Sill et al., *Phys. Rev.* **D48** (1993) 29. 119
31. R. C. Walker et al., *Phys. Rev.* **D49** (1994) 5671. 119
32. Jefferson Lab Hall A Collaboration, O. Gayou et al., *Phys. Rev. Lett.* **88** (2002) 092301. 119
33. V. Punjabi et al., *Phys. Rev.* **C71** (2005) 055202. 119
34. S. Rock et al., *Phys. Rev. Lett.* **49** (1982) 1139. 119
35. A. Lung et al., *Phys. Rev. Lett.* **70** (1993) 718. 119
36. H. Anklin et al., *Phys. Lett.* **B336** (1994) 313. 119
37. H. Anklin et al., *Phys. Lett.* **B428** (1998) 248. 119
38. G. Kubon et al., *Phys. Lett.* **B524** (2002) 26. 119
39. W. Xu et al., *Phys. Rev. Lett.* **85** (2000) 2900. 119
40. Jefferson Lab E95-001 Collaboration, W. Xu et al., *Phys. Rev.* **C67** (2003) 012201. 119

41. C. V. Christov et al., *Prog. Part. Nucl. Phys.* **37** (1996) 91. 120
42. A. Kanazawa, *Prog. Theor. Phys.* **77** (1987) 1240. 120, 125
43. M. Wakamatsu and T. Watabe, *Phys. Lett.* **B312** (1993) 184. 121
44. A. Blotz, M. Praszałowicz, and K. Goeke, *Phys. Lett.* **B317** (1993) 195. 121
45. R. Alkofer and H. Weigel, *Phys. Lett.* **B319** (1993) 1. 121
46. Bristol-Geneva-Heidelberg-Orsay-Rutherford-Strasbourg Collaboration, M. Bourquin et al., *Z. Phys.* **C12** (1982) 307. 122
47. Bristol-Geneva-Heidelberg-Orsay-Rutherford-Strasbourg Collaboration, M. Bourquin et al., *Z. Phys.* **C21** (1983) 1. 122
48. R. Flores-Mendieta, E. Jenkins, and A. V. Manohar, *Phys. Rev.* **D58** (1998) 094028. 122
49. N. Cabibbo, E. C. Swallow, and R. Winston, *Phys. Rev. Lett.* **92** (2004) 251803. 122
50. H. Weigel, *Nucl. Phys.* **A690** (2001) 595. 122, 123, 124
51. M. Ademollo and R. Gatto, *Phys. Rev. Lett.* **13** (1964) 264. 123
52. N. W. Park, J. Schechter, and H. Weigel, *Phys. Rev.* **D41** (1990) 2836. 123
53. H. Weigel, J. Schechter, N. W. Park, and U. G. Meißner, *Phys. Rev.* **D42** (1990) 3177. 123, 125
54. A. Blotz et al., *Nucl. Phys.* **A555** (1993) 765. 123
55. J. R. Ellis and M. Karliner, `hep-ph/0606181`. 123, 125
56. R. Johnson, N. W. Park, J. Schechter, V. Soni, and H. Weigel, *Phys. Rev.* **D42** (1990) 2998. 123, 126, 134
57. D. Guadagnoli, V. Lubicz, M. Papinutto, and S. Simula, *Nucl. phys.* **B761** (2007) 63. 124
58. J. A. McGovern and M. C. Birse, *Phys. Lett.* **B200** (1988) 401. 125
59. N. W. Park, J. Schechter, and H. Weigel, *Phys. Lett.* **B228** (1989) 420. 125
60. S. J. Brodsky, J. R. Ellis, and M. Karliner, *Phys. Lett.* **B206** (1988) 309. 126, 130
61. Z. Ryzak, *Phys. Lett.* **B217** (1989) 325. 126
62. T. D. Cohen and M. K. Banerjee, *Phys. Lett.* **B230** (1989) 129. 126
63. P. Jain, R. Johnson, U. G. Meißner, N. W. Park, and J. Schechter, *Phys. Rev.* **D37** (1988) 3252. 126
64. H. Weigel, "The proton spin structure in Skyrme type models," in *Particle and Nuclei Pan XIII*, A. Pascolini, ed. World Scientific, Singapore, 1993. `hep-ph/9310293`. 126
65. J. Gasser and H. Leutwyler, *Nucl. Phys.* **B250** (1985) 465. 127
66. A. V. Kiselev and V. A. Petrov, *Z. Phys.* **C58** (1993) 595. 127
67. T. Feldmann, P. Kroll, and B. Stech, *Phys. Rev.* **D58** (1998) 114006. 128
68. KLOE Collaboration, F. Ambrosino, `hep-ex/0612029`. 128
69. T. Appelquist and J. Carazzone, *Phys. Rev.* **D11** (1975) 2856. 129
70. B. Borasoy and U. G. Meißner, *Ann. Phys.* **254** (1997) 192. 130
71. J. Gasser, *Ann. Phys.* **136** (1981) 62. 130
72. A. Bottino, F. Donato, N. Fornengo, and S. Scopel, *Astropart. Phys.* **13** (2000) 215. 130
73. J. F. Donoghue and C. R. Nappi, *Phys. Lett.* **B168** (1986) 105. 130
74. SAMPLE Collaboration, B. Mueller et al., *Phys. Rev. Lett.* **78** (1997) 3824. 131
75. HAPPEX Collaboration, K. A. Aniol et al., *Phys. Lett.* **B509** (2001) 211. 131
76. A4 Collaboration, F. E. Maas, *Eur. Phys. J.* **A17** (2003) 339. 131
77. G0 Collaboration, D. S. Armstrong et al., *Phys. Rev. Lett.* **95** (2005) 092001. See also references in here. 131

78. R. L. Jaffe, *Phys. Lett.* **B229** (1989) 275. 131
79. M. J. Musolf and T. W. Donnelly, *Z. Phys.* **C57** (1993) 559. 131
80. H. Forkel, M. Nielsen, X.-m. Jin, and T. D. Cohen, *Phys. Rev.* **C50** (1994) 3108. 131
81. A. Faessler, T. Gutsche, V. E. Lyubovitskij, and K. Pumsa-ard, *Phys. Rev.* **D73** (2006) 114021. 131
82. H. Weigel, A. Abada, R. Alkofer, and H. Reinhardt, *Phys. Lett.* **B353** (1995) 20. 131
83. A. Silva, H.-C. Kim, and K. Goeke, *Phys. Rev.* **D65** (2002) 014016. 131
84. A. Silva, H.-C. Kim, D. Urbano, and K. Goeke, *Phys. Rev.* **D74** (2006) 054011. 131
85. J. Gasser and H. Leutwyler, *Ann. Phys.* **158** (1984) 142. 132
86. P. Jain, R. Johnson, N. W. Park, J. Schechter, and H. Weigel, *Phys. Rev.* **D40** (1989) 855. 132, 134
87. M. Praszałowicz, A. Blotz, and K. Goeke, *Phys. Rev.* **D47** (1993) 1127. 134
88. D. Diakonov, V. Petrov, P. Pobylitsa, M. V. Polyakov, and C. Weiss, *Nucl. Phys.* **B480** (1996) 341. 134
89. D. Diakonov, V. Y. Petrov, P. V. Pobylitsa, M. V. Polyakov, and C. Weiss, *Phys. Rev.* **D56** (1997) 4069. 134
90. M. Wakamatsu, *Phys. Rev.* **D67** (2003) 034005. 134
91. M. Wakamatsu, *Phys. Rev.* **D67** (2003) 034006. 134
92. H. Weigel, *Pramana* **61** (2003) 921. 134
93. H. Weigel, L. P. Gamberg, and H. Reinhardt, *Mod. Phys. Lett.* **A11** (1996) 3021. 135, 140
94. H. Weigel, L. P. Gamberg, and H. Reinhardt, *Phys. Lett.* **B399** (1997) 287. 135, 140
95. H. Weigel, L. P. Gamberg, and H. Reinhardt, *Phys. Rev.* **D55** (1997) 6910. 135, 140, 141
96. H. Weigel, E. Ruiz Arriola, and L. P. Gamberg, *Nucl. Phys.* **B560** (1999) 383. 135, 138, 139
97. F. Doering, C. Schueren, T. Watabe, K. Goeke, and E. Ruiz Arriola, *Nucl. Phys.* **A603** (1996) 415. 135
98. T. Muta, *Foundations of Quantum Chromodynamics*. World Scientific, Singapore, 1987. 136, 138
99. M. Chemtob, *Nucl. Phys.* **A473** (1987) 613. 136
100. T. Frederico and G. A. Miller, *Phys. Rev.* **D50** (1994) 210. 137
101. F. J. Ynduráin, *The Theory of Quark and Gluon Interactions*. Springer-Verlag, Berlin, 1993. 138
102. M. E. Peskin and D. V. Schroeder, *An Introduction to Quantum Field Theory*, Chap. 19.3. Perseus Books, Reading, MA, 1995. 138
103. R. M. Davidson and E. Ruiz Arriola, *Acta Phys. Polon.* **B33** (2002) 1791. 138
104. E. Ruiz Arriola and W. Broniowski, *Phys. Rev.* **D66** (2002) 094016. 138
105. O. Schroeder, H. Reinhardt, and H. Weigel, *Phys. Lett.* **B439** (1998) 398. 138
106. R. L. Jaffe, *Ann. Phys.* **132** (1981) 32. 140
107. L. P. Gamberg, H. Reinhardt, and H. Weigel, *Int. J. Mod. Phys.* **A13** (1998) 5519. 140
108. G. Altarelli, P. Nason, and G. Ridolfi, *Phys. Lett.* **B320** (1994) 152. 140
109. S. Wandzura and F. Wilczek, *Phys. Lett.* **B72** (1977) 195. 140
110. A. Ali, V. M. Braun, and G. Hiller, *Phys. Lett.* **B266** (1991) 117. 140
111. E143 Collaboration, K. Abe et al., *Phys. Rev.* **D58** (1998) 112003. 140, 141
112. E155 Collaboration, P. L. Anthony et al., *Phys. Lett.* **B553** (2003) 18. 141
113. M. Stratmann, *Z. Phys.* **C60** (1993) 763. 141
114. X. Song, *Phys. Rev.* **D54** (1996) 1955. 141
115. M. Wakamatsu, *Phys. Lett.* **B487** (2000) 118. 141
116. Z. E. Meziani, *Nucl. Phys.* **A721** (2003) 118. 142

8

Meson–Baryon Scattering in Chiral Soliton Models

In this chapter we will discuss approaches to describe meson–baryon scattering in soliton models. Here we will concentrate on the two-flavor description and leave an important $SU(3)$ application to Sect. 9.5. Although this subject is very interesting and challenging because it deals with properties of baryon resonances, we will concise ourselves and only sketch the main ideas. We will quickly observe that most of the computations are very involved: We require not only the quantization of the classical soliton field configuration but also the small amplitude fluctuations about it. The reader may get an impression of that formidable task from the appendices of [1].

The first important observation is that soliton models contain both the meson and baryon degrees of freedom in terms of meson fields. While mesons are the fundamental fields, baryons emerge as soliton configurations and we may investigate meson–baryon interactions by considering small amplitude fluctuations about the soliton. Only in a limited number of soliton models such calculations have been performed exhaustively, i.e., for arbitrary angular momentum of the fluctuations. In vector meson models the computation is inflated by the number of field components involved [1, 2]. In chiral quark models it gets out of hand because the fluctuations couple quark modes of different grand spins, that are displayed in (3.20) and (3.21); the larger the angular momentum of the fluctuations, the more grand spins are affected. For that reason only fluctuations with low angular momenta have been studied in chiral quark models [3]. As we will see in the course of this chapter this is insufficient to make concrete statements about physical meson–baryon scattering.

In terms of the chiral field the most suggestive parameterization for the fluctuations about the soliton is [4, 5][1]

[1] For calculational purposes it is sometimes more appropriate to introduce the fluctuations of pseudoscalar mesons as chiral rotations of the soliton $U(\boldsymbol{x},t) = A\exp\left[\mathrm{i}\eta(\boldsymbol{x},t)/2\right]\exp\left[\mathrm{i}\boldsymbol{\tau}\cdot\hat{\boldsymbol{x}}F(r)\right]\exp\left[\mathrm{i}\eta(\boldsymbol{x},t)/2\right]A^\dagger$. Different parameterizations yield the same scattering matrix as the single particle spectrum is unchanged in the asymptotic regime [6].

H. Weigel: *Meson–Baryon Scattering in Chiral Soliton Models*, Lect. Notes Phys. **743**, 147–180 (2008)
DOI 10.1007/978-3-540-75436-7_8

$$U(\boldsymbol{x},t) = A\exp\left[\mathrm{i}\boldsymbol{\tau}\cdot\hat{\boldsymbol{x}}F(r) + \mathrm{i}\eta(\boldsymbol{x},t)\right]\, A^\dagger\,, \tag{8.1}$$

where A represents the collective coordinates that describes the flavor orientation of the meson–baryon system. Obviously, $\eta(\boldsymbol{x},t)$ is matrix valued in flavor space. The generalization to fluctuations about vector meson type soliton configurations is straightforward but tedious [1]. Since $\eta(\boldsymbol{x},t)$ collectively co-rotates with the soliton in flavor space it defines fluctuations in the intrinsic (or body-fixed) frame. The laboratory fluctuations are $A(t)\eta(\boldsymbol{x},t)A^\dagger(t)$.

A severe problem arises because modes for the flavor orientation of the soliton are contained in both the small amplitude fluctuations η and the collective coordinates A. In general, constraints must be implemented that avoid double counting and that allow us to quantize the system.

8.1 Adiabatic Approximation

The adiabatic approximation is defined by taking the collective coordinates in (8.1) to be time independent, i.e., $\dot{A} = 0$. In that case they are not dynamical degrees of freedom and the double counting problem does not arise. This is also reflected by the fact that time-independent collective coordinates do not couple to the fluctuations, at least in a flavor symmetric model.

It is quite tedious but nevertheless straightforward to expand the action function of the given chiral model to quadratic order in the fluctuations. Since the soliton is a stationary configuration, the term of linear order vanishes and we may generally write [1, 5]

$$L = E_{\mathrm{cl}} + \frac{1}{2}\int \mathrm{d}^3r\,\left[\dot{\eta}_i(\boldsymbol{x},t)M_{ij}(\boldsymbol{x})\dot{\eta}_j(\boldsymbol{x},t) - \eta_i(\boldsymbol{x},t)V_{ij}(\boldsymbol{x})\eta_j(\boldsymbol{x},t)\right]\,. \tag{8.2}$$

Here M_{ij} and V_{ij} are metric and potential matrices, respectively. Their spatial dependences arise from the background soliton, as, e.g., $M_{ij}(\boldsymbol{x}) = M_{ij}(U_0(\boldsymbol{x}))$ in the Skyrme model. Note that $V_{ij}(\boldsymbol{x})$ contains differential operators that act on $\eta_j(\boldsymbol{x},t)$, the components of the matrix $\eta(\boldsymbol{x},t)$ when expanded in the N_{f}^2-1 Pauli or Gell–Mann matrices. The Euler–Lagrange equations

$$M_{ij}(\boldsymbol{x})\ddot{\eta}_j(\boldsymbol{x},t) + V_{ij}(\boldsymbol{x})\eta_j(\boldsymbol{x},t) = 0 \tag{8.3}$$

reduce to Klein–Gordon equations asymptotically, i.e., $|\boldsymbol{x}|\to\infty$: $M_{ij}(\boldsymbol{x})\to M_{ij}^{(0)} = \delta_{ij}$ and $V_{ij}(\boldsymbol{x})\to V_{ij}^{(0)} = m_i^2\delta_{ij}$, where m_i are meson masses. Upon Fourier decomposition, $\eta_i(\boldsymbol{x},t)\to\eta_i(\boldsymbol{x},\omega)\exp(\mathrm{i}\omega t)$, no imaginary frequency solutions ($\mathsf{Im}(\omega)\neq 0$) have been found in all soliton models considered. This is important because it establishes that the hedgehog configuration minimizes the action functional, at least locally in functional space.

A general remark on the adiabatic approximation is in order. To identify the fluctuations about the soliton as single particle states, the wave function must be scaled by a factor f_π, as in the discussion of (2.41). Hence the expansion in η actually is an expansion in $1/N_{\mathrm{C}}$. If the collective rotations were

considered dynamical degrees they could, at least formally, be compensated by higher orders in the fluctuations. Thus the adiabatic approximation is exact at next to leading order in the $1/N_C$ expansion, which is N_C^0.

We will now concentrate on pion baryon scattering in the two-flavor model. We notice again that the soliton itself is invariant under combined spin and flavor rotations. This invariance is manifested for the fluctuations as follows: There exists a generalized angular momentum, the grand spin

$$\boldsymbol{G} = \boldsymbol{J} + \boldsymbol{I} \tag{8.4}$$

that is the vector sum of the fluctuations of total spin ($\boldsymbol{J}$) and isospin ($\boldsymbol{I}$). In general, the former is the vector sum of angular momentum and spin, $\boldsymbol{J} = \boldsymbol{L} + \boldsymbol{S}$. When decomposing the fluctuations with respect to grand spin

$$\eta_j(\boldsymbol{x}, \omega) = \sum_{GJM} \eta_{GJ}(r, \omega) \left[\boldsymbol{Y}_{GJM}(\hat{\boldsymbol{x}})\right]_j \,, \tag{8.5}$$

the differential equations for the fluctuations decouple in the grand spin quantum number G and do not contain its projection quantum number (M) explicitly. The vector spherical harmonic function $\boldsymbol{Y}_{GJM}(\hat{\boldsymbol{x}})$ in (8.5) arises from coupling total angular momentum $\boldsymbol{J}$ and isospin ($I = 1$)

$$\boldsymbol{Y}_{GJM}(\hat{\boldsymbol{x}}) = \sum_{m\nu} C^{GM}_{Jm,1\nu} Y_{Jm}(\hat{\boldsymbol{x}}) \boldsymbol{e}_{t_3} \tag{8.6}$$

to $\boldsymbol{G}$. Of course, as long as we only consider pseudoscalar fields the total angular momentum equals the orbital angular momentum L of the fluctuations and the coupling induces the selection rules $G = L \pm 1, L$. Since parity is also conserved, the fluctuations further decouple into magnetic modes with $G = L$ and electric modes with $G = L \pm 1$. Finally standard potential scattering methods [7, 8] may be employed to compute the corresponding elements of the scattering matrix, $\widetilde{S}_{G,L,L'}$, which is the so-called *intrinsic* S-matrix because it refers to scattering in the body-fixed frame. For the magnetic modes this is just the phase shift $\widetilde{S}_{G,G,G} = \mathrm{e}^{2\mathrm{i}\delta_{G,G,G}}$ but a 2×2 matrix for the electric modes. (Computational techniques are explained in Appendix F.) To obtain the S-matrix in the laboratory frame from $\widetilde{S}$ we have to project onto physical channels. So far we have considered the scattering of spinless mesons about the soliton. A more general consideration also includes vector mesons, as in the soliton model of Sect. 4.7. In such cases we first couple the fluctuations' orbital angular momentum and their isospin to an intermediate grand spin $\boldsymbol{K} = \boldsymbol{L} + \boldsymbol{I}_\phi$, where $\boldsymbol{I}_\phi$ is the isospin of the meson. In general the total spin $\boldsymbol{J} = \boldsymbol{L} + \boldsymbol{s}_\phi$ also includes the meson spin $\boldsymbol{s}_\phi$. Thus $\boldsymbol{K}$ is not the grand spin but an additional, non-conserved quantum number in the body-fix frame. In total, the intrinsic S-matrix is labeled as $\widetilde{S}_{GKK',LL'}(\phi \to \psi)$ for scattering of a meson ϕ to another meson ψ about the soliton. On top we have the (geometrical) transformation to the laboratory system via [4, 9]

$$S(\phi B \to \psi B') = \delta_{\boldsymbol{II'}}\delta_{\boldsymbol{JJ'}} \sum_{GKK'} \zeta\zeta' \widetilde{S}_{GKK',LL'}\,(\phi \to \psi) \tag{8.7}$$

with the recoupling coefficient written as a 9–j symbol

$$\zeta = [(2G+1)(2K+1)(2s+1)(2S_{\mathrm{t}}+1)]^{\frac{1}{2}} \begin{Bmatrix} L & I_\phi & K \\ S_{\mathrm{t}} & s & s_\phi \\ J & I & G \end{Bmatrix}. \tag{8.8}$$

The coefficient ζ' is obtained from ζ by substituting all non-conserved quantum numbers with primed ones and ϕ by ψ. The total spin (including orbital angular momentum) and isospin of the meson–baryon system are J and I, respectively and S_{t} denotes the spin quantum number that is associated with the sum of the meson and baryon spins (without orbital angular momentum). In the $SU(2)$ soliton models baryons have identical isospin and spin s; furthermore s_ϕ and I_ϕ are the spin and isospin quantum numbers of the meson ϕ. The derivation of this recoupling scheme is reviewed in Appendix F.

When only pions are involved, i.e., for $s_\phi = 0$ and $I_\phi = 1$, the recoupling coefficient collapses to a 6–j symbol,

$$\zeta_\pi = (-1)^{L+s+J}\,[(2G+1)(2s+1)]^{\frac{1}{2}} \begin{Bmatrix} I & 1 & s \\ L & J & G \end{Bmatrix}. \tag{8.9}$$

There are more physical S-matrix elements than there are for the intrinsic S-matrix. So $\widetilde{S}$ may be eliminated in favor of linear relations among the physical S-matrix elements. For the elastic pion–nucleon scattering this leads to a linear dependence of the $I = \frac{3}{2}$ and $I = \frac{1}{2}$ scattering amplitudes [4],

$$\begin{aligned} 2\,(2L+1)\,S_{L32L+1} &= 3LS_{L12L+1} + (L+2)\,S_{L12L+1} \\ 2\,(2L+1)\,S_{L32L-1} &= (L-1)\,S_{L12L-1} + 3\,(L+2)\,S_{L12L-1}\,, \end{aligned} \tag{8.10}$$

with the notation S_{L2I2J} for the physical S-matrix elements. (As usually the letters S, P, D and F are introduced for $L = 0, 1, 2$ and 4, respectively.) These relations are valid in the adiabatic approximation regardless of the specific soliton model. Hence they are actually large N_{C} results [10, 11], and confronting these relations with experimental data serves as a check of the adiabatic approximation. This is shown in Fig. 8.1. We find perfect agreement in the $L = 3$ channel[2] but observe that these relations do not work well for the pion angular momentum $L = 0, 1$ and 2. We may actually identify the reason for this discrepancy. The adiabatic approximation does not account for the Δ resonance which, according to (5.45), emerges at order $1/N_{\mathrm{C}}$ while this approximation is valid only to $\mathcal{O}\left(N_{\mathrm{C}}^0\right)$. The P-wave comparison indeed reveals that this resonance is missing. Within the collective coordinate scheme resonances arise from quantizing the rotational zero mode of the soliton and

[2] The momentum shift of the resonance position corresponds to a mass difference of order $1/N_{\mathrm{C}}$.

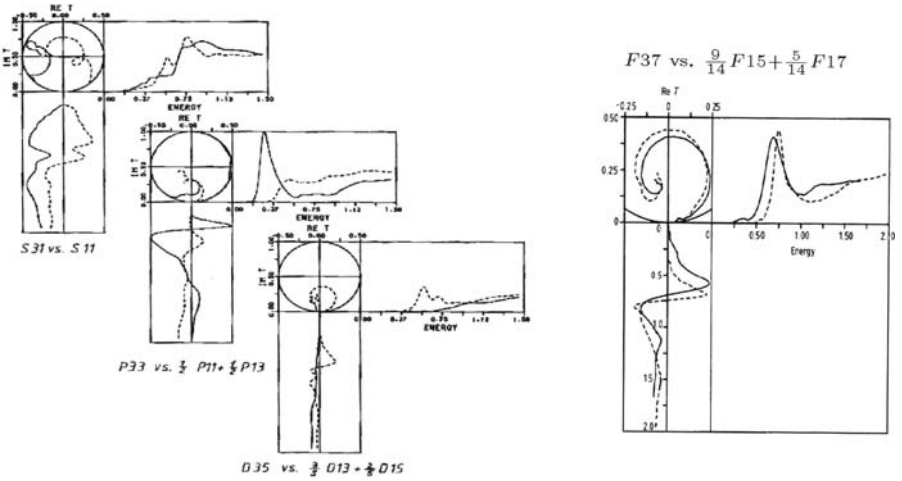

Fig. 8.1. Model independent (large N_C) relations among the scattering amplitudes (T-matrix Argand diagrams) from the recoupling scheme, (8.10). The *full* and *dashed lines* refer to the $I = \frac{1}{2}$ and $I = \frac{3}{2}$ parts of those relations, respectively. The left panel concerns the channels that intrinsically contain zero modes while the right panel shows the F-wave channel. Taken from [12]

hence we cannot expect the adiabatic approximation to yield perfect results in those channels that contain zero-mode fluctuations. These are the grand spin $G = 1$ channels that carry forward to the physical S, P and D-wave channels via the large-N_C coupling scheme, (8.7). On the other hand, the intrinsic $G = 1$ channel does not show up in the physical F-wave channel. It is hence no longer surprising that in this channel the large-N_C relations from (8.10) are nicely satisfied and we thus expect soliton models to reliably predict these scattering amplitudes. This is shown in Fig. 8.2. Obviously the key features of the empirical data are reproduced: The $F15$ and $F37$ partial waves exhibit pronounced structures (resonances) while the $F35$ and $F17$ channels are essentially flat.

We complete this section by discussing an important difference between the Skyrme and vector meson soliton models. It is indicated in Fig. 8.2 and exhaustively explained in [14] that the Skyrme model phase shifts rise linearly with momentum k which is not acceptable. It is actually a consequence of the contact interactions contained in the Skyrme term, (4.26). Its presence causes the metric function M to be different from the coefficient of the second derivative operator in V, cf. (8.2). At large momenta $k = \sqrt{\omega^2 - m_\pi^2}$ the differential equation for the fluctuations η is then roughly approximated by

$$\left[\partial_r^2 + k^2\,(1 + m(r))\right]\eta(r,\omega) = 0\,, \tag{8.11}$$

in any grand spin channel. A non-zero result for $m(r)$ arises solely from the Skyrme term or other higher order derivative terms in the chiral Lagrangian.

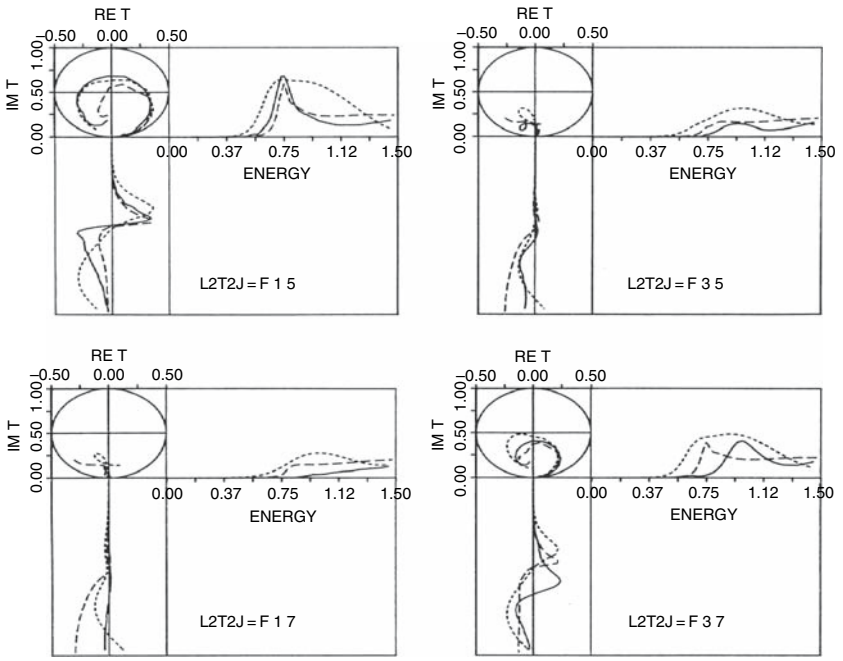

Fig. 8.2. Soliton model prediction for the F-channel πN scattering amplitudes shown as Argand diagrams for the T-matrix. The *full lines* represent the empirical data [13], the *short dashed lines* give the Skyrme model results and the *long dashed lines* those obtained in a vector meson model (a slight variant of the model discussed in Sect. 4.7. Different versions of vector meson models yield comparable results for πN scattering [2]). Taken from [12]

The above equation is solved by

$$\eta(r,\omega) = \mathrm{e}^{\mathrm{i}k\xi(r)} \quad \text{with} \quad \xi(r) = \int_{r_0}^{r} \mathrm{d}r' \sqrt{1+m(r')} + \mathcal{O}\left(\frac{1}{k}\right) \tag{8.12}$$

and induces the phase shift that rises linearly with momentum,

$$\delta(k) = k \int_{r_0}^{\infty} \mathrm{d}r [\sqrt{1+m(r)} - 1]\,. \tag{8.13}$$

This small calculation reveals the bad large momentum behavior and actually raises the question of whether or not the resonant behavior in the Skyrme model F-wave corresponds to a real resonance. In the context of (4.64) we discussed that the Skyrme term may be understood as a local (contact) approximation for the more complicated $\pi - \rho$ effective Lagrangian. And indeed, the full vector meson Lagrangians with the higher order derivative terms replaced by propagating vector (or scalar) mesons do not lead to ever-rising phase shifts. This may also be inferred from Fig. 8.2 and is thoroughly discussed in [15]. We conclude that the resonant behavior found in the Skyrme model

indeed describes actual resonances rather than being a technical artifact. The effect at work here is similar to the incorporation of massive vector mesons in the electroweak interaction: the substitution of a contact interaction by a propagating mode.

We refer to the literature for studies of the three flavor scattering problem. The flavor symmetric case was considered already early [16, 17, 18]. Important flavor symmetry breaking effects have been studied in [19].

We will now turn to the discussion of the more problematic low partial waves of elastic pion nucleon scattering with zero-mode contamination. In these cases we must go beyond the adiabatic approximation.

8.2 S-Wave Scattering

We first consider the case when the relative orbital angular momentum between the pion and the nucleon vanishes. In the adiabatic approximation only a single intrinsic S-matrix element, $\widetilde{S}_{1,00}$, contributes to the S-wave S-matrix of elastic πN scattering (for which we may omit the intermediate grand spin $\boldsymbol{K}$). This intrinsic channel has unit grand spin and contains the translational zero mode. With only a single intrinsic S-matrix element available, the adiabatic approximation predicts identical scattering amplitudes for the two available isospin channels $I = \frac{1}{2}$ and $I = \frac{3}{2}$. This can also be inferred from the top of the two equations (8.10). As is immediately observed from Fig. 8.1, this strongly contradicts the experimental situation.

Before discussing non-adiabatic effects, it is illuminating to review the standard current algebra results for the S-wave scattering amplitude and make contact with Tomozawa–Weinberg relation [20, 21]. In general the isospin covariant scattering amplitude is parameterized by two functions b_0 and b_1 that only depend on the pion momentum k. They enter the R-matrix[3] via

$$-R(k) = b_0(k) + 2b_1(k)\boldsymbol{I}_\pi \cdot \boldsymbol{I}_\mathrm{N}\,. \tag{8.14}$$

Here $\boldsymbol{I}_\pi$ and $\boldsymbol{I}_\mathrm{N}$ are the pion and nucleon isospin operators, respectively. The matrix elements are related to the phase shifts δ_I via,

$$-\langle I|R(k)|I\rangle = \frac{\tan\delta_I(k)}{k}\,, \tag{8.15}$$

where $I = \frac{1}{2}, \frac{3}{2}$ is the total (conserved) isospin of the πN system. A phase shift analysis yields [13]

$$\lim_{k\to 0} b_0(k) = \frac{a_1 + 2a_3}{3} \approx -\frac{0.010}{m_\pi} \quad \text{and} \quad \lim_{k\to 0} b_1(k) = \frac{a_3 - a_1}{3} \approx -\frac{0.091}{m_\pi}\,, \tag{8.16}$$

[3] We choose to call that standard scattering theory quantity *reaction* matrix, sometimes the synonym K-matrix is used. The phase convention is dictated by the Lippmann–Schwinger equation (9.42).

where $a_1 \approx 0.173/m_\pi$ and $a_3 \approx -0.101/m_\pi$ are the scattering lengths associated with the total isospin $I = \frac{1}{2}$ and $I = \frac{3}{2}$ channels, respectively. The current algebra analysis [20, 21]

$$a_1 = -2a_3 = \frac{m_\pi}{4\pi f_\pi^2} \approx \frac{0.175}{m_\pi} \tag{8.17}$$

favorably explains the smallness of b_0. Since the $I = \frac{1}{2}$ and $I = \frac{3}{2}$ scattering amplitudes are identical in the adiabatic approximation, the S-wave scattering amplitude computed in the previous section yields the leading large-N_C contribution to b_0. We denote that piece by $b_0^{(0)}$. Unfortunately it suffers from sizable model dependences. In the original Skyrme model the zero momentum limit is found to be about $0.077/m_\pi$ for $e = 4.0$ while in the six-order stabilization scenario, (4.54), it turns out negligibly small, $-0.005/m_\pi$ [22]. So the adiabatic approximation not only incorrectly predicts $b_1 = 0$ as discussed above but also gives an unsatisfactory result for b_0. This calls for the incorporation of non-adiabatic effects. They arise from the time dependence of the collective coordinates in (8.1), that we have omitted so far. Then the angular velocity $\boldsymbol{\Omega}$, (5.16) enters and couples to a bilinear of the pionic fluctuations.[4] Since $\boldsymbol{\Omega}$ transforms like an isovector, the pion fluctuations must also combine to an isovector when constructing the relevant interaction Lagrangian. Since we also have to accommodate two time derivatives, the required term must be of the form $\boldsymbol{\Omega} \cdot (\boldsymbol{\eta} \times \dot{\boldsymbol{\eta}})$ multiplied by a radial function that contains the classical soliton. Conceptually such a term is not much different from the hyperfine splitting, (6.44), that emerged from the time dependence of the isospin rotations for the kaonic bound state; yet here we deal with scattering states and with the triplet rather than the doublet representation of $SU(2)$. The vector product is again associated with the grand spin operator $\boldsymbol{G}$ (similar to the last factor in (6.44)). It is thus intuitively clear that non-adiabatic effects induce interaction Hamiltonians with $\boldsymbol{J} \cdot \boldsymbol{G}$. As already argued, S-wave scattering emerges from the unit grand spin channel. Squaring the relation given after (6.45) between grand spin, $\boldsymbol{G}$, total spin, $\boldsymbol{J} = \boldsymbol{J}_\mathrm{N} + \boldsymbol{L}$ and total isospin $\boldsymbol{I} = \boldsymbol{I}_\mathrm{N} + \boldsymbol{I}_\pi$ implies $\boldsymbol{J} \cdot \boldsymbol{G} = -\boldsymbol{I}_\mathrm{N} \cdot \boldsymbol{I}_\pi$. Hence the non-adiabatic effects yield $b_1 \neq 0$. The full Skyrme model calculation has been performed in [23] and in [24] for a vector meson model. The results may be comprised in form of the non-adiabatic contribution to the R-matrix

$$\begin{aligned} -R^{(1)}(k) \;&=\; -\frac{\omega}{4\pi\alpha^2}\boldsymbol{I}_\mathrm{N} \cdot \boldsymbol{I}_\pi \, A(k,k) - \frac{\omega}{2\pi\alpha^2} \int \frac{\mathrm{d}^3k'}{(2\pi)^3} \, A(k,k')A(k',k) \\ &=: b_1(k)\boldsymbol{I}_\mathrm{N} \cdot \boldsymbol{I}_\pi + b_0^{(1)}(k)\,. \end{aligned} \tag{8.18}$$

Explicit expressions for the matrix elements $A(k,k')$ are provided in [23, 24]. They arise from sandwiching functions of the soliton profile between S-wave

[4] It also couples linearly to the zero-mode fluctuations, but that is only relevant to P-wave scattering, cf. next section.

scattering states computed in the adiabatic approximation. Hence $R^{(1)}(k)$ is the distorted wave Born approximation (DWBA) for non-adiabatic effects. The non-adiabaticity of $R^{(1)}(k)$ is also reflected by the appearance of the moment of inertia, α^2, showing that $R^{(1)}(k)$ is of subleading order in the $1/N_{\rm C}$ expansion. The Skyrme model results [23] for the R-matrix coefficients at threshold ($k \to 0$) are shown in Table 8.1. We recall from Sect. 5.4 that $e = 4.25$ is favored because it properly predicts the Δ-nucleon mass difference. The second term in (8.18) contains the non-adiabatic correction $b_0^{(1)}$ to the isoscalar part of the R-matrix and is quartic in the fluctuations. It originates from squaring $\boldsymbol{\eta} \times \dot{\boldsymbol{\eta}}$ when Legendre transforming to obtain the interaction Hamiltonian. Though there are other terms at that order which have not been included (as in the bound state approach) we see from Table 8.1 that it favorably contributes to $b_0 = b_0^{(0)} + b_0^{(1)}$. Also, its inclusion somewhat mitigates the model dependence of b_0. Obviously, the non-adiabatic corrections not only significantly improve the isoscalar part of the R-matrix that came out badly in the adiabatic approximation but also nicely reproduce the isospin splitting among the two S-wave scattering amplitudes. In [23] the momentum dependence was studied for momenta up to 300 MeV. The results match the empirical data well but not perfectly. Such an agreement has finally been accomplished in a vector meson model [24].

The non-adiabatic corrections to the S-wave scattering problem could be implemented in tedious but nevertheless straightforward computations. These corrections stem from coupling the vibrational modes ($\boldsymbol{\eta}$) to dynamical collective rotations of the soliton. In general, flavor rotations are also contained in the fluctuations as zero modes. However, they do not dwell in the S-wave channel[5] because the fluctuations associated with the flavor rotations have the same orbital angular momentum as the soliton, i.e., $L = 1$. So there is no double counting problem in the S-wave channel, yet it unavoidably shows up in P-wave scattering that we will discuss next.

Table 8.1. The R-matrix coefficients b_0 and b_1 at zero momentum as function of the Skyrme model parameter e. These results are adopted from [23] and are measured in units of inverse pion mass. For the background contribution the separation between the adiabatic piece ($b_0^{(0)}$) and its non-adiabatic correction ($b_0^{(1)}$) is also given, cf. (8.18)

e	$b_0^{(0)}$	$b_0^{(1)}$	b_0	b_1
3.75	0.095	−0.080	0.015	−0.113
4.00	0.077	−0.076	0.001	−0.109
4.25	0.061	−0.072	−0.011	−0.106
4.50	0.052	−0.070	−0.018	−0.104
4.75	0.044	−0.068	−0.024	−0.101

[5] The translational zero mode has a S-wave component. But we do not treat it dynamically in the scattering problem.

8.3 P-Wave Scattering and the Yukawa Problem

The particular role of the Δ resonance in P-wave pion nucleon scattering has been a long-standing problem for the soliton picture. Figure 8.1 reveals that the Δ is not accounted for in adiabatic approximation. This is not surprising as the Δ is stable for $N_{\rm C} \to \infty$. Many attempts to incorporate this resonance as an intermediate state have been put forward. Common to most of those attempts is the computation of an effective pion–nucleon–Δ vertex that is subsequently substituted in Feynman diagram calculations like those in Fig. 8.3. Naïvely, soliton models do not generate a single meson vertex, as the contribution linear in the fluctuations about the soliton seemingly vanishes by definition. The absence of the vertex is known as the *Yukawa problem* in soliton models. The motivation to nevertheless construct such a vertex from dynamical collective coordinates are far reaching: from Hamiltonian mechanics [25] to functional integral methods [26]. There are many papers on this subject, e.g., [27, 28, 29, 30, 31, 32, 33, 34, 35, 36].[6] Here we will discuss only a particular approach [33, 34], the problems thereof and suggest a potential solution to the Yukawa problem along the approach of [1]. The latter acquires further support from the studies that will be described in Sect. 9.5: It survives an $1/N_{\rm C}$ consistency test for kaon nucleon scattering.

Previously we have argued that the Δ comes about as a rotational excitation of the soliton and is to be treated as a collective resonance. We therefore have to treat the collective rotations dynamically and explore their coupling to the small amplitude fluctuations, η. This immediately leads to the double counting problem that the collective rotations are also contained as zero-mode fluctuation in the intrinsic $G = 1$ channel that dominates the physical $L = 1$ partial wave.

To investigate the role of the zero mode and the potential linear terms we will somewhat modify the parameterization, (8.1), of the fluctuations (cf. footnote 1) [38]

$$\begin{aligned} U(\boldsymbol{x},t) &= \exp\left[\mathrm{i}\boldsymbol{\tau}\cdot\boldsymbol{\xi}(\boldsymbol{x},t)/2\right]\, A(t)\exp\left[\mathrm{i}\boldsymbol{\tau}\cdot\hat{\boldsymbol{x}}F(r)\right] A^{\dagger}(t)\exp\left[\mathrm{i}\boldsymbol{\tau}\cdot\boldsymbol{\xi}(\boldsymbol{x},t)/2\right] \\ &= \exp\left[\mathrm{i}\boldsymbol{\tau}\cdot\boldsymbol{\xi}(\boldsymbol{x},t)/2\right]\, U_{\rm R}(\boldsymbol{x},t)\exp\left[\mathrm{i}\boldsymbol{\tau}\cdot\boldsymbol{\xi}(\boldsymbol{x},t)/2\right]\,, \end{aligned} \tag{8.19}$$

with $U_{\rm R}$ and $\xi_i = D_{ij}\eta_j$ being the collectively rotating hedgehog and the fluctuations in the laboratory frame, respectively. Linear terms (in $\boldsymbol{\xi}$) only

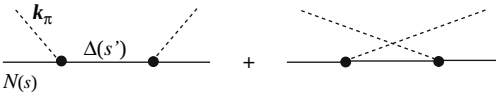

Fig. 8.3. Feynman diagrams for πN scattering with an intermediate Δ resonance. The *dot* denotes the form factor defined in (8.23)

[6] Those studies are summarized in Chap. IV of [37].

emerge because $U_{\rm R}$ is not a solution to the full equations of motion. If it were, linear terms, that eventually mimic the Yukawa coupling to a resonance (and allow us to identify an effective pion–nucleon–Δ vertex), would definitely be absent. The expansion of U to linear order in the fluctuations

$$\delta U(\boldsymbol{x},t) = \mathrm{i}\boldsymbol{\xi}(\boldsymbol{x},t)\cdot\left\{\frac{\boldsymbol{\tau}}{2}\,,\,U_{\rm R}(\boldsymbol{x},t)\right\} \tag{8.20}$$

involves the generator for axial transformations of $U_{\rm R}$. Therefore the linear term in the Lagrangian will be of the form

$$\delta\mathcal{L} = \boldsymbol{A}^{\mu}\cdot\partial_{\mu}\boldsymbol{\xi}(\boldsymbol{x},t) + \ldots \tag{8.21}$$

where $\boldsymbol{A}^{\mu}$ is the axial current for $U_{\rm R}$ and the ellipses represent terms $\mathcal{O}\left(m_{\pi}^2\right)$ that originate from the explicit breaking of chiral symmetry. The equation of motion for the chiral angle does not account for time-dependent rotations, rather it yields $\partial_i \boldsymbol{A}^i = \mathcal{O}\left(m_{\pi}^2\right)$. Thus the linear term reduces to

$$\delta\mathcal{L} = \boldsymbol{A}^0\cdot\dot{\boldsymbol{\xi}}(\boldsymbol{x},t)\,. \tag{8.22}$$

This interaction term is linear in the angular velocities $\Omega_{\rm a}$ defined in (5.16) because $\boldsymbol{A}_0$ contains a time derivative. This linear term has been exhaustively employed in perturbative treatments to incorporate the effects of an intermediate Δ resonance by taking matrix elements [33, 34]

$$\langle s|\delta\mathcal{L}|\boldsymbol{k},\boldsymbol{I}_{\pi};s'\rangle = \frac{3f_{\pi ss'}(k^2)}{2\mathrm{i}\alpha^2\omega}\langle s|\boldsymbol{I}_{\pi}\cdot\boldsymbol{I}_B\boldsymbol{k}\cdot\boldsymbol{J}_B|s'\rangle\,, \tag{8.23}$$

that defines the hadronic form factor $f_{\pi ss'}(k^2)$ for emission (or absorption) of a pion with momentum $\boldsymbol{k}$ from a baryon. The factor $\boldsymbol{k}$ emerges because of the P-wave coupling. This form factor essentially involves the Fourier transformation of $\boldsymbol{A}_0$ and parameterizes the vertices in Fig. 8.3. The baryonic matrix element is computed from the collective coordinate operators contained in $\boldsymbol{A}_0$ with the quantization rules (5.38) and (5.40). The structure $A_i^0 \propto D_{ia}\epsilon_{abc}\Omega_b\,\hat{x}_c\,(\sin 2F + \ldots)$ implies that diagonal matrix elements alike $\langle N|\boldsymbol{A}^0|N\rangle$ vanish when the operator product is hermitionized. Thus the spins s and s' of the baryons in the in and out states differ by one unit, In particular $f_{\pi NN} = 0$ and the intermediate state for πN scattering must be the Δ resonance. Though this approach fairly well describes the phase shift of the $P33$ channel in πN scattering we will now discuss that a serious problem remains [39]. As noted above, $f_{\pi ss'}(k^2)$ is a Fourier transform and as such reflects the plane wave Born approximation (PWBA) treatment of $\delta\mathcal{L}$. In the previous section we have argued that actually the DWBA should be employed. In that approach the solutions to (8.3) rather than plane waves (via spherical Bessel functions in the Fourier transform) are to be substituted into $\delta\mathcal{L}$. To reveal the resulting problem we choose an alternative derivation of the linear interaction, (8.22). We require the contribution to the Lagrangian that is linear in both the time derivative of the fluctuations and the angular velocity. In the Skyrme model they originate from the time derivative of the chiral field,

$$\dot{U} = \frac{i}{2} A(t) D_{ij}(A) \left(\dot{\xi}_i + \Omega_{\rm a} \xi^{\rm a}_{0,i} \right) \{\tau_j, U_0\} \, A^\dagger(t) \,, \tag{8.24}$$

where the adjoint representation of the collective rotations in defined in (5.22), see also (5.32). Furthermore

$$\xi^{\rm a}_{0,i} = D_{il} \eta^{\rm a}_{0,l} = D_{il} \epsilon_{ikl} \hat{x}_l \tan F \tag{8.25}$$

are the three zero modes (labeled by a) for the rotation of the classical soliton in the laboratory frame. Equation (8.24) suggests that the linear term may be obtained from the second order Lagrangian (8.2) by replacing $\dot{\eta}_i \to \dot{\xi}_i + \Omega_{\rm a} \xi^{\rm a}_{0,i}$. Then we have

$$\mathcal{L}^{(1)} = \Omega_{\rm a} \dot{\xi}_i \xi^{\rm a}_{0,j} M_{ij} = \Omega_{\rm a} \dot{\boldsymbol{\xi}} \cdot \boldsymbol{\xi}^{\rm a}_0 \, M \,, \tag{8.26}$$

with the metric function taken from the adiabatic approximation. In the second equation we used $M \propto \mathbb{1}$, which is valid in the relevant subspace of transverse magnetic modes. The DWBA corresponds to replacing $\boldsymbol{\xi} \to D \cdot \boldsymbol{\eta}$ with η_j being the solutions to (8.3),

$$\mathcal{L}^{(1)} \Big|_{\rm DWBA} = \Omega_{\rm a} \dot{\boldsymbol{\eta}} \cdot \boldsymbol{\eta}^{\rm a}_0 \, M \,. \tag{8.27}$$

Now the spatial integral projects out the zero-mode piece from the fluctuation $\boldsymbol{\eta}$ due to the orthogonality condition associated with (8.3). However, the zero mode has $\dot{\boldsymbol{\eta}} = 0$ and thus this linear interaction vanishes in DWBA.

For a sensible investigation we need to consider the contribution in the Lagrangian which is linear in the fluctuations and has both time derivatives acting on the collective rotations, i.e., the term $\mathcal{O}\left(\boldsymbol{\Omega}^2 \times \boldsymbol{\eta}\right)$. For the intrinsic fluctuations, (8.1), this linear interaction term is of the form

$$\mathcal{L}^{(1)} = H_{\rm L}(r) \left[\boldsymbol{\Omega}^2 - (\boldsymbol{\Omega} \cdot \hat{\boldsymbol{x}})^2 \right] \hat{\boldsymbol{x}} \cdot \boldsymbol{\eta} - H_{\rm T}(r) \boldsymbol{\Omega} \cdot \hat{\boldsymbol{x}} \left[\boldsymbol{\Omega} - (\boldsymbol{\Omega} \cdot \hat{\boldsymbol{x}}) \, \hat{\boldsymbol{x}} \right] \cdot \boldsymbol{\eta} \,. \tag{8.28}$$

The radial functions $H_{\rm L}(r)$ and $H_{\rm T}(r)$ are determined from the classical soliton profiles. In Chap. 10 of [1] they are listed for the Skyrme and a vector meson model.

The interaction (8.28) can, e.g., be treated with the techniques of reaction theory [40]. It is similar to the Lee model [41, 42, 43] and the result can be phrased in terms of a width function $\Gamma(k)$ and an energy shift δE. The width function reads

$$\Gamma(k) = 2\pi \frac{\omega}{k} \left| \langle \Delta | H^{(1)} | N; \pi(\boldsymbol{k}) \rangle \right|^2 \,, \tag{8.29}$$

where $H^{(1)}$ is the Hamiltonian obtained from the interaction Lagrangian[7] (8.28) via a standard Legendre transformation that substitutes the angular velocities

[7] The present normalization of the pion field differs by a factor k from that in Chap. 10 of [1]. The radial functions of the grand spin decomposition, (8.5) turn into spherical Bessel functions when the background is switched off, cf. Appendix F.

by spin operators as in (5.38). The ket state in the above matrix element has good total spin (J), isospin (I) and pion angular momentum (L). It is obtained from states representing (pion) fluctuations with good grand spin (G)

$$|kL, JM; II_3\rangle = (-1)^{L+J+\frac{1}{2}} \sum_{GG_3I_3'} \sqrt{4G+2} \begin{Bmatrix} I & 1 & \frac{1}{2} \\ L & J & G \end{Bmatrix} \times C^{JM}_{GG_3,II_3'} |kL, GG_3\rangle D^I_{I_3',-I_3}(A)\,, \tag{8.30}$$

which is a combination of (F.7) and (F.8) for the nucleon with spin $s = \frac{1}{2}$. The state $|k, GG_3, L\rangle$ represents a fluctuating meson in the intrinsic frame. It connects to a pion state with momentum $\boldsymbol{k}$ and isospin projection t in the laboratory system by[8]

$$|kL, GG_3\rangle = \sum_{mt} \int \mathrm{d}\Omega_k\, C^{GG_3}_{Lm,1G_3-m}\, Y^*_{Lm}(\hat{\boldsymbol{k}})\, D^{(1)}_{G_3-m,t}(A)\, |\boldsymbol{k}, t\rangle\,. \tag{8.31}$$

The Clebsch–Gordan coefficient arises from the coupling according to (8.4) (with $s_\phi = 0$) and the Wigner D-function from the transformation $\boldsymbol{\xi} = D \cdot \boldsymbol{\eta}$. The bra state in the matrix element, (8.29) is represented by the Wigner D-function with Δ quantum numbers: $D^{\frac{3}{2}}_{J_3,-I_3}(A)$. Note that in general ordering ambiguities emerge when computing the collective coordinate part of the matrix element. Commonly they are fixed by demanding that the non-resonant piece $\langle N|H^{(1)}|N;\pi(k)\rangle$ vanishes [44]. In the final matrix element, $|kL, GG_3\rangle$ projects out the radial function in the expansion (8.5). Having obtained the width function we may straightforwardly compute the energy shift

$$\delta E(k) = \mathcal{P} \int \frac{\mathrm{d}q}{2\pi} \frac{q}{\omega_q} \frac{\Gamma(q)}{\omega - \omega_q} \quad \text{with} \quad \omega_q = \sqrt{q^2 - m_\pi^2} \tag{8.32}$$

Here $\mathcal{P}$ refers to the Cauchy principal value of the momentum integral, which is finite. In the end $\Gamma(k)$ and $\delta E(k)$ combine to the phase shift

$$\mathrm{e}^{2\mathrm{i}\delta} = 1 - \frac{\mathrm{i}\Gamma}{\omega - (M_\Delta - M_\mathrm{N}) - \delta E + \frac{\mathrm{i}}{2}\Gamma}\,, \tag{8.33}$$

which can be computed numerically once the profile functions and pion scattering wave functions are known. Unfortunately, numerical results are only available in the plane wave approximation, i.e., when the relevant radial part of the pion wave function is replaced by the spherical Bessel function $j_1(kr)$, appropriate for the P-wave channel. These results are shown in Fig. 8.4. Obviously the key features of the phase shift are reproduced. However, the resulting width seems too small and the predicted phase shift is too large at

[8] This and similar transformation relations are most straightforwardly verified from the requirement that they must also be valid in the absence of the soliton, i.e., for plane waves.

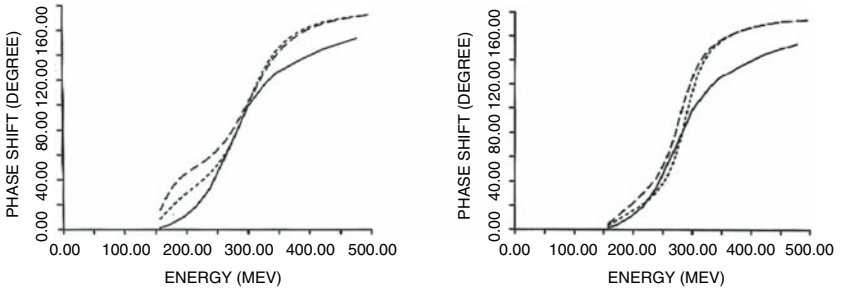

Fig. 8.4. The phase shift, δ for the $P33$ channel of πN scattering as function of the pion energy (ω) obtained from (8.33) (*long-dashed lines*); the *short-dashed lines* omit the energy shift δE and the *full lines* are data [13]. *Left panel*: Skyrme model, *right panel*: vector meson model. Taken from [12]

the high-energy part. Of course, it would be interesting to see whether these shortcomings get corrected within the DWBA, as it has been the case for the S-wave channel.

We repeat that the linear term in the form of (8.28) emerges only because the collectively rotating hedgehog is not a solution to the full equations of motion. Another puzzle arises because the linear terms in (8.22) and (8.28) are of different order in the $1/N_{\mathrm{C}}$ counting because a time derivative of the fluctuation is $\mathcal{O}\left(N_{\mathrm{C}}^{0}\right)$ while a time derivative of the collective coordinates is $\mathcal{O}\left(N_{\mathrm{C}}^{-1}\right)$. Again this discrepancy is a consequence of the incomplete treatment of the field equations. They are solved at the two leading orders in $1/N_{\mathrm{C}}$ (classically and subsequently for the fluctuations) and therefore inconsistencies arise at the next order.

Here we have concentrated on the Δ P-wave channel. However, also the nucleon P-wave channel contains a prominent excitation, the Roper resonance at about 1440 MeV. At this point we just mention that in adiabatic approximation no significant structure is obtained, in neither the Skyrme nor the vector meson models [1]. We will further discuss this issue in Sect. 8.5.

In summary, despite the huge amount of work that has already been done, the description of the P-wave pion nucleon scattering in soliton models still leaves space for improvement.

8.4 Photoproduction

In the previous sections we have seen that fluctuations about the soliton can be identified as meson states that scatter off the nucleon. Even more, in adiabatic approximation the recoupling scheme allows us to construct proper meson scattering states. These states may be interpreted as asymptotic states for the meson nucleon system and it is thus suggestive to study other processes that lead to similar final states; the most prominent one is their photoproduction:

$\gamma N \to \pi N$. Other mesons than the pion can be considered but currently we will not do so. Here we will mainly review the central ideas for such studies in the soliton model pioneered by Eckart and Schwesinger [45] in the Skyrme model and upgraded to a vector meson model in [1].

To describe photoproduction processes we will have to find the interaction Lagrangian that is linear in both the photon and the pion fields. As a matter of fact, we have already performed parts of that calculation when studying baryon electromagnetic properties in Sect. 7.1. At that time we computed the electromagnetic current $V_\mu^{\text{e.m.}}$ which couples linearly to the photon field A_μ. However, we only considered the contribution from the collectively rotating hedgehog to $V_\mu^{\text{e.m.}}$. To include meson scattering states, we have to expand (7.1) (and their analogs in other soliton models) to linear order in the fluctuations η when substituting the parameterization (8.1). One might wonder whether additional terms would arise from the response of the soliton on the photon field. At least in adiabatic approximation this is not the case because the soliton is a stationary point of the action so that this response would be quadratic in the photon field. Hence, we obtain the leading contribution to pion photoproduction by simultaneously expanding the model Lagrangian in the electric charge e and $1/N_{\text{C}}$. The latter is metered by inverse powers of the pion decay constant, f_π.

In radiation gauge, $A_0 = 0$, which is most appropriate because it minimizes the number time derivatives action on the chiral field, the relevant interaction Lagrangian is of the form

$$\mathcal{L}_{\boldsymbol{\pi}\gamma} = \frac{e}{f_\pi} D_{3i} R_{ijm}(\boldsymbol{x}) \eta_j(\boldsymbol{x}, t) A_m(\boldsymbol{x}, t)\,, \tag{8.34}$$

where the expansion parameters are made explicit. The static functions, $R_{ijm}(\boldsymbol{x})$, are determined from the background soliton. Because of parity invariance only three structures emerge

$$R_{ijm}(\boldsymbol{x}) = R_1(r)\epsilon_{ijm} + R_2(r)\epsilon_{ilm}\hat{x}_l\hat{x}_j + R_3(r)\epsilon_{ijn}\hat{x}_n\hat{x}_m\,. \tag{8.35}$$

Explicit expressions for the radial functions R_i in terms of soliton profiles may be traced from [1, 45]. The rotation matrix D_{3i} appears in (8.34) because the pion fluctuations η_j as well as the soliton profiles dwell in the intrinsic frame while the photon field resides in the laboratory system. The isospin index "3" follows from the reduction of the charge operator, (7.3), to flavor $SU(2)$. Together with the ϵ-tensor in (8.35) it insures that in the laboratory system only charged pions ($\xi^\pm = (\xi_1 \pm \mathrm{i}\xi_2)/\sqrt{2}$) couple.

Equation (8.31) relates the pion states whose creation and annihilation operators are contained in $\boldsymbol{\eta}$ to the physical pion states with good momentum $\boldsymbol{k}$ and isospin projection t. So we know how to evaluate the pion matrix element of the interaction, (8.34). For the photon field we adopt the standard multi-pole decomposition that defines electric and magnetic modes,

$$\boldsymbol{A}(\boldsymbol{x},t) = \sum_{\ell\mu}^{\lambda=\text{el.,mag.}} \int_0^\infty q\,\mathrm{d}q \left[(\mathrm{i})^\ell \alpha^\lambda_{\ell\mu}(q) \widetilde{\boldsymbol{A}}^\lambda_{\ell\mu}(q,\boldsymbol{x}) + \text{h.c.} \right] . \tag{8.36}$$

The multi-pole fields are expressed in terms of vector spherical harmonics and Bessel functions [46],

$$\begin{aligned} \widetilde{\boldsymbol{A}}^{\text{el.}}_{\ell\mu}(q,\boldsymbol{x}) &= \sqrt{\frac{q}{\pi}} \left(\frac{1}{\mathrm{i}q} \boldsymbol{\partial} \right) \times \left[j_\ell(qr) \boldsymbol{Y}_{\ell\ell\mu}(\hat{\boldsymbol{x}}) \right] , \\ \widetilde{\boldsymbol{A}}^{\text{mag.}}_{\ell\mu}(q,\boldsymbol{x}) &= \sqrt{\frac{q}{\pi}} j_\ell(qr) \boldsymbol{Y}_{\ell\ell\mu}(\hat{\boldsymbol{x}}) . \end{aligned} \tag{8.37}$$

In this decomposition $\left[\alpha^\lambda_{\ell\mu}(q)\right]^\dagger$ creates a photon with orbital angular momentum quantum numbers (ℓ,μ) and momentum $\boldsymbol{q} = q\hat{\boldsymbol{e}}_z$. The electric and magnetic modes have parity $(-1)^{\ell+1}$ and $(-1)^\ell$, respectively. We are now fully equipped to compute the transition amplitude

$$S_{\text{fi}} = \langle \boldsymbol{k}t; s'; J_3', I_3' | \int \mathrm{d}^4x\, \mathcal{L}_{\boldsymbol{\pi}\gamma} | \boldsymbol{q}\mu; s; J_3, I_3 \rangle \tag{8.38}$$

from the interaction Lagrangian, (8.34). The labels s and s' refer to the identical spin and isospin quantum numbers of the baryon in the initial and final states, respectively. The corresponding projection quantum numbers are also made explicit. For the nucleon with $s = s' = \frac{1}{2}$ it is convenient to introduce reduced electric and magnetic multi-pole moments, $M^{(\text{e})}$ and $M^{(\text{m})}$ via [45]

$$\begin{aligned} S_{\text{fi}} = \mathrm{i}\delta(q-\omega) \frac{\sqrt{\alpha}}{q\sqrt{2\pi\omega}} \sum_{JL\ell} \sqrt{(2L+1)(2\ell+1)} (\mathrm{i})^{\ell-L+1} D^{(J)}_{J_3+\mu,J_3'}(\phi,\theta,-\phi) \\ \times C^{JJ_3'}_{L0,\frac{1}{2}J_3'} C^{JJ_3+\mu}_{\ell\mu,\frac{1}{2}J_3} \left(\mathrm{i} M^{(\text{e})}_{\ell LJ} + \mu M^{(\text{m})}_{\ell LJ} \right) , \end{aligned} \tag{8.39}$$

where $\alpha = \frac{e^2}{4\pi} = 1/137$ is the electromagnetic fine structure constant while ϕ and θ are the azimuthal and polar angles of the pion momentum $\boldsymbol{k}$. This part of the transition amplitude arises from writing the spherical harmonic function in (8.31) as a matrix element of the rotation operator, $\langle L0|\hat{D}(\hat{\boldsymbol{k}})|Lm\rangle$ and projecting $\hat{D}$ onto grand spin states, (8.30) on the left and nucleon photon states (coupled to good total spin) on the right. This also explains the specific indices of the resulting Clebsch–Gordan coefficients. In (8.39) the δ function that identifies photon and pion energies arises because in the adiabatic approximation the nucleon is infinitely heavy and does not take away any energy.

As suggested by (8.34) the reduced multi-pole moments in (8.39) are computed as radial integrals that essentially involve three factors: (i) a function of the classical soliton, (ii) a Bessel function for the incident photon and (iii) the radial part of the pion scattering wave function computed in adiabatic approximation. The resulting bulky expressions are listed in [45] and [1] for the Skyrme and a vector meson model, respectively. The $M^{(\text{m})}_{\ell LJ}$ transfer the

orbital angular momentum directly from the photon to the pion, $L = \ell$ while the electric ones, $M^{(\mathrm{e})}_{\ell LJ}$, change it by one unit, $L = \ell \pm 1$. The momentum arguments of the wave functions under items (ii) and (iii) are related by the δ function in (8.39), so that these moments not only depend on the displayed quantum numbers but are additionally functions of a single momentum that is not made explicit. Finally these moments are related to the *helicity elements* in Walker's [47] definition via [45]

$$\begin{aligned} M^{(\mathrm{e})}_{\ell LJ} &= \sqrt{\frac{q}{8\pi\alpha}} \left[\delta_{\ell L+1}\delta_{JL+\frac{1}{2}} \sqrt{\frac{L+2}{L+1}} \left(A_{L+} + \frac{L}{2} B_{L-} \right) \right. \\ &\qquad \left. -\delta_{\ell L-1}\delta_{JL-\frac{1}{2}} \sqrt{\frac{L-2}{L}} \left(A_{L-} - \frac{L+1}{2} B_{L-} \right) \right] \\ M^{(\mathrm{m})}_{\ell LJ} &= -\sqrt{\frac{q}{8\pi\alpha L(L+1)}} \delta_{\ell L} \left(1 - \delta_{\ell 0}\right) \left[\delta_{JL+\frac{1}{2}} L \left(A_{L+} - \frac{L+2}{2} B_{L+} \right) \right. \\ &\qquad \left. +\delta_{JL-\frac{1}{2}} (L+1) \left(A_{L-} + \frac{L-1}{2} B_{L-} \right) \right] , \end{aligned} \tag{8.40}$$

in terms of which the data are commonly discussed. The A and B type amplitudes correspond to helicities $\frac{1}{2}$ and $\frac{3}{2}$, respectively. The subscript indicates the pion orbital angular momentum and its relation to the total angular momentum, $L\pm : J = L \pm \frac{1}{2}$. Isospin labels are not shown. A huge amount of numerical results exists for the helicity amplitudes computed in various soliton models [1, 45]. A sample from a vector meson soliton model is presented in Figs. 8.5 and 8.6. Figure 8.5 shows helicity amplitudes that correspond to S- and P-channels of pion nucleon scattering. It is not astonishing that the model calculations for A_{0+} do not reproduce the prominent structure of the empirical data. They are directly linked to the $S11(1540)$ resonance that is not contained in the adiabatic approximation presently adopted for the pion field. In Sect. 8.2 we have described how to address that problem. Most likely, the application of that approach to photoproduction will be successful as well. More surprisingly, the data in the P-wave channel (i.e., A_{1-}) are reasonably well reproduced. That is, effects of the Roper resonance ($P11(1440)$) are captured in the model calculation of pion photoproduction. Recall that the model failed to describe that effect in πN scattering, at least in adiabatic approximation. In that case the contribution of intrinsic $L = 1$ zero mode strongly dominates over the $L = 0$ piece that reflects the scaling (or breathing) excitation of the soliton. While the latter indeed is resonant [5, 49, 50] the phase shift in the zero-mode channel is essentially flat, leaching out the breathing mode structure. In photoproduction an additional suppression factor emerges for the intrinsic $L = 1$ contribution so that the breathing excitation dominates.

In Fig. 8.6 helicity amplitudes in those higher partial waves are shown that correspond to D- and F-wave channels of πN scattering. Though these computations do not reproduce all details of the data, they describe the gross features reasonably well. This again supports the conclusion that the adiabatic

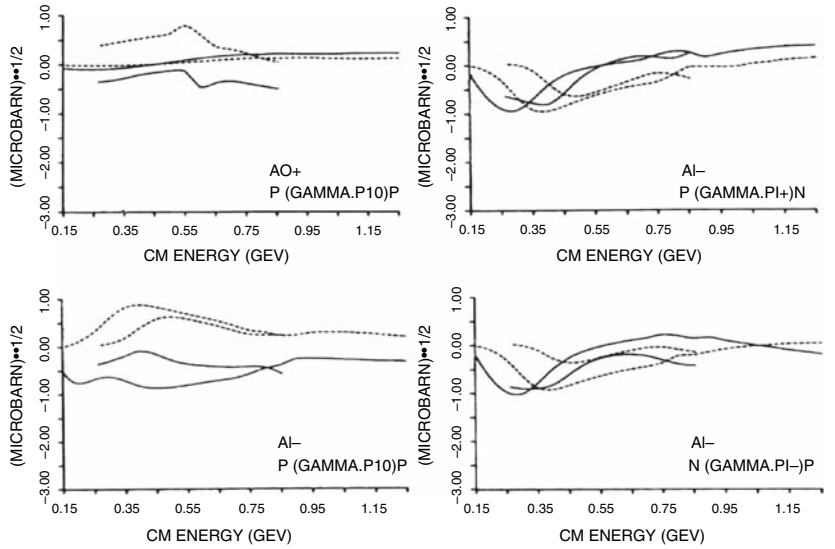

Fig. 8.5. The helicity amplitudes A_{0+} and A_{1-} in units of $\sqrt{\mu b}$ from a vector meson soliton model compared to empirical data [48]. *Full lines* show the real, *dashed lines* the imaginary parts. The *short lines* that range from $W - M_N = 0.26 \ldots 0.86$GeV represent the data. This graph is adopted from [12]

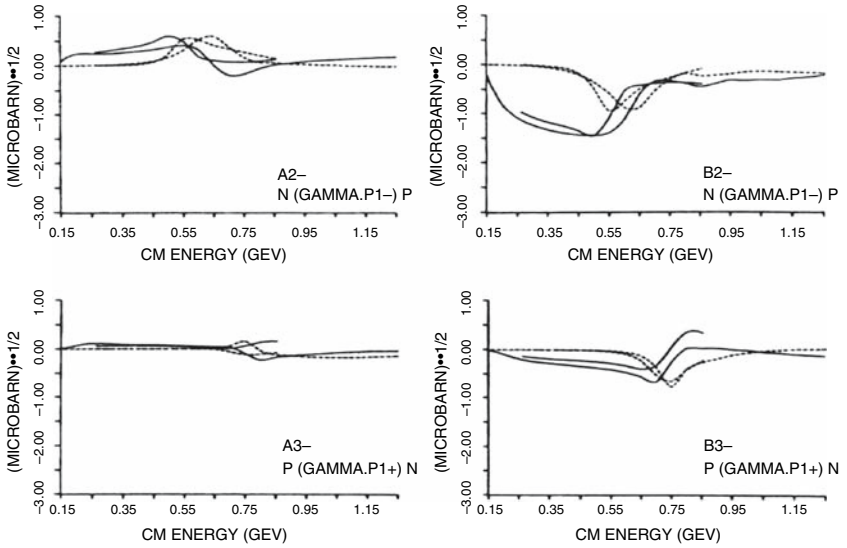

Fig. 8.6. Same as Fig. 8.5 for the amplitudes $A_{2,3-}$ and $B_{2,3-}$

Table 8.2. Nucleon–photon couplings in units of $10^{-3}\mathrm{GeV}^{-\frac{1}{2}}$ for various resonances of the πN system. The respective upper entries are the empirical data [51] while the lower ones result from a vector meson soliton calculation [1]. Some resonances couple only very weakly to photons, e.g., $D13(1700)$, and are omitted here

$L2I2J$	mass (MeV)	$A^{(p)}_{\frac{3}{2}}$	$A^{(p)}_{\frac{1}{2}}$	$A^{(n)}_{\frac{3}{2}}$	$A^{(n)}_{\frac{1}{2}}$
$P11$	1440		-65 ± 4		40 ± 10
	1340		-134		134
$D13$	1520	166 ± 05	-24 ± 09	-139 ± 11	-59 ± 13
	1590	171	-117	-126	-36
$S11$	1535		90 ± 30		-46 ± 27
	1590		57		64
$S11$	1650		53 ± 16		-15 ± 21
	1340		51		32
$D15$	1675	15 ± 9	19 ± 8	-58 ± 13	-43 ± 12
	1600	0	-22	-110	-55
$F15$	1680	133 ± 12	-15 ± 6	-33 ± 9	29 ± 10
	1690	110	0	0	171
$P13$	1720	-19 ± 15	18 ± 20	-29 ± 61	1 ± 15
	1540	27	-9	-27	9

approximation works well for the higher partial waves that are not afflicted with contaminations from zero-mode channels.

Let us now compare to the empirical resonance couplings. The PDG [51] usually quotes them in the form

$$\mathrm{Im}A^{\beta}_{L\pm} = \mp f A^{\beta}_{\frac{1}{2}} \qquad \text{and} \qquad \mathrm{Im}B^{\beta}_{L\pm} = \pm f\sqrt{16}(2J-1)(2J+3)A^{\beta}_{\frac{3}{2}}\,, \quad (8.41)$$

where the superscripts label isospin (proton, neutron or Δ). In principle the kinematical factor f must be formulated in terms of the position and width of the hadronic resonance implying a Breit–Wigner fit to the πN scattering data, reflecting background subtraction. This is not really appropriate here because photoproduction and resonance formation is computed in a single step. For that reason an average value for f has been used in [1] to perform a meaningful comparison with data. The model results for A^{β}_{h} are extracted in a two-step procedure from the momentum-dependent helicity amplitudes: First, in a prescribed LIJ channel the position of the maximum of the imaginary part of the amplitude is determined. This value is identified as the mass of the resonance. Second, the value at this mass is substituted into (8.41) to evaluate the resonance coupling. We recognize from Table 8.2 that many of the resonance couplings are reasonably reproduced by the model calculation, at least for the phases. Certainly the S-wave channel ($A^{(n)}$) is an exception, and we blame it again on the adiabatic approximation. Remarkably, the model calculation predicts the Roper resonance ($P11(1440)$) to strongly couple to the photon, though its resonance energy comes out a bit on the low side.

Table 8.3. The Δ-photon resonance couplings. In the $P33(1232)$ case the model prediction arises from (8.42) and (8.43). All other results are obtained as in table 8.2

$L2I2J$	mass (MeV)	$A^{(\Delta)}_{\frac{3}{2}}$	$A^{(\Delta)}_{\frac{1}{2}}$
$P33$	1232	-250 ± 8	-135 ± 6
	1240	-255	-140
$S31$	1620		27 ± 11
	1600		13
$D33$	1700	85 ± 15	85 ± 22
	1600	36	99
$F35$	1905	-45 ± 11	26 ± 11
	1690	0	44
$F37$	1950	-97 ± 10	-76 ± 12
	1690	-102	-76

So far we have not discussed model predictions for the A_{1+} and B_{1+} amplitudes. As can, e.g., be observed from Fig. 2 in [45], soliton models predict essentially flat amplitudes. Yet, the empirical data exhibit pronounced structures that correspond to the photo-excitation of the Δ-resonance. Hence, we certainly do not expect these amplitudes to be reproduced in adiabatic approximation. We must resort to the collective coordinate approach to consider the photo-induced Δ nucleon transition. Essentially the methods of Sects. 5.3 and 5.4 are to be applied and the results can be phrased in terms of the above-discussed resonance couplings. The linear combinations

$$M_1 = \frac{-1}{2\sqrt{3}} \left(3A^{\Delta}_{\frac{3}{2}} + \sqrt{3} A^{\Delta}_{\frac{2}{2}} \right) \quad \text{and} \quad E_2 = \frac{1}{2\sqrt{3}} \left(A^{\Delta}_{\frac{3}{2}} - \sqrt{3} A^{\Delta}_{\frac{2}{2}} \right) \tag{8.42}$$

describe the coupling of the Δ nucleon system to magnetic and electric photons with orbital angular momentum $\ell = 1$ and $\ell = 2$, respectively. These couplings are related to the magnetic dipole and electric quadrupole transition matrix elements [52, 53, 54]

$$\begin{aligned} M_1 &= \tfrac{1}{3} \langle \Delta | \int \mathrm{d}^3 r j_2(qr) \left(\frac{3z^2}{r^2} - 1 \right) V_0^{\text{e.m.}}(\boldsymbol{x}) | N \rangle \,, \\ E_2 &= \tfrac{1}{2} \langle \Delta | \int \mathrm{d}^3 r j_1(qr) j_1(qr) \epsilon_{3ij} \hat{x}_i V_j^{\text{e.m.}}(\boldsymbol{x}) | N \rangle \,, \end{aligned} \tag{8.43}$$

where $V_\mu^{\text{e.m.}}(\boldsymbol{x})$ refers to the electromagnetic current in the soliton model, e.g., (5.48). This current also contains collective coordinate operators in the space of which the matrix elements are computed. The couplings between the photon and $I = \frac{3}{2}$ resonances are shown in Table 8.3. The agreement with data is about as good (or meager) as for the $I = \frac{1}{2}$ channels. In total, it is comfortable to see how far one can go with soliton models for baryons. Being able to compute energy-dependent helicity amplitudes (and phase shifts) starting from a simple Lagrangian distinguishes soliton models positively from many other baryon models.

8.5 Non-harmonic Excitations

In Sects. 8.2 and 8.3 we have already seen that in some cases it is necessary to respect the coupling of the collective flavor rotations to other excitations of the soliton. Unfortunately we have also seen that this becomes quite cumbersome in the context of small amplitude fluctuations about the soliton. In this section we discuss an alternative treatment that introduces collective coordinates for presumably important modes. Of course, the introduction of additional collective coordinates is a matter of educated guesses. We will especially consider the use of collective coordinates for the scaling (or breathing or monopole) excitation of the soliton. As mentioned above, the small amplitude approach indeed shows that the monopole channel is resonant [5, 49, 50]. In the adiabatic approximation to πN scattering this resonance is washed out by the (geometrical) coupling to the zero-mode channel of the flavor rotation. In order to treat that coupling dynamically and to allow for large amplitudes in the resonant channel, the idea is then to introduce collective coordinates for both the breathing and the rotational modes and investigate their interaction. As a particular result we will find that this procedure describes the Roper resonance as expected from the photoproduction results, i.e., the resonance energy is slightly under-estimated.

We will initially motivate the introduction of the collective breathing mode in the much simpler case of the kink soliton model,[9] cf. Sect. 4.3. We introduce the corresponding collective coordinate $\mu = \mu(t)$ via the parameterization for the field

$$\Phi(x,t) = \Phi_+\left(\frac{x}{\mu(t)}\right) = \frac{m}{\sqrt{\lambda}}\tanh\left(\frac{mx}{\sqrt{2}\mu(t)}\right). \tag{8.44}$$

Upon substitution into the Lagrangian, (4.15), and spatial integration we find the Lagrange function

$$L(\mu,\dot{\mu}) = \frac{E_+}{2\omega_+^2}\frac{\dot{\mu}^2}{\mu} - \frac{E_+}{\omega_+}\left(\mu + \frac{1}{\mu}\right) \tag{8.45}$$

for the collective coordinate μ. The mass, E_+ is given in (4.17) while $\omega_+ = m\sqrt{6/(\pi^2-6)}$. The quantization prescription, (5.9), yields the Schrödinger equation

$$\left\{-\frac{\omega_+^2}{2E_+}\sqrt{\mu}\frac{\partial}{\partial\mu}\sqrt{\mu}\frac{\partial}{\partial\mu} + \frac{E_+}{\omega_+}\left(\mu+\frac{1}{\mu}\right)\right\}\Psi(\mu) = E\Psi(\mu)\,. \tag{8.46}$$

Introducing the variable $\rho^2 = \mu$ and the wave function $\phi(\rho) = \Psi(\rho^2)/\sqrt{\rho}$ directly maps this Schrödinger equation onto that of an axially symmetric harmonic oscillator with (non-integer) angular momentum $\ell = \frac{2}{\omega_+}\sqrt{E_+^2 + \frac{\omega_+^2}{16}}$. The energy eigenvalues are readily obtained as

[9] The author is grateful to H. Walliser for pointing out this analog.

$$E_n = \frac{\omega_+}{2}\,(2n+1+\ell) = \sqrt{E_+^2 + \frac{\omega_+^2}{16}} + \omega_+ \left(n+\frac{1}{2}\right). \tag{8.47}$$

In particular we find the energy of the first excitation to be $\Delta E = E_1 - E_0 = \omega_+ \approx 1.245m$. Similar to (8.3) small amplitude fluctuations can be considered for the kink, cf. (4.19). Besides the scattering states a zero-mode bound state (for the translation) and a discrete bound state at $\omega_1 = \sqrt{\frac{3}{2}}m \approx 1.225m$ emerge [55]. The approximate agreement, $\Delta E \approx \omega_1$, shows that the breathing mode approach to the kink predicts the lowest excitation energy with an accuracy of better than 2%. This also establishes that collective coordinate quantization is very useful for modes which parameterize transformations that are not exact invariances but have low excitation energies.[10]

So we have very good reason to apply the breathing mode technique to the chiral soliton and particularly study the interaction between this and the rotational modes. Similar to the kink example, the collective breathing mode is introduced via the *ansatz* for the chiral field

$$U(\boldsymbol{x},t) = A(t)\exp\left[\mathrm{i}\hat{\boldsymbol{x}}\cdot\boldsymbol{\tau}F\left(\frac{r}{\mu(t)}\right)\right]A^\dagger(t)\,, \tag{8.48}$$

where again $A(t)$ contains the collective coordinates for the rotations and $F(r)$ is the classical soliton profile. Substituting this parameterization into the two-flavor Skyrme model Lagrangian yields a Lagrange function for the collective coordinates,

$$\begin{aligned} L(x,\dot{x},A,\dot{A}) = \frac{4}{9}\left(a_1 + a_2 x^{-\frac{4}{3}}\right)\dot{x}^2 - \left(b_1 x^{\frac{2}{3}} + b_2 x^{-\frac{2}{3}} + b_3 x^2\right) \\ + \frac{1}{2}\left(\alpha_1 x^2 + \alpha_2 x^{\frac{2}{3}}\right)\boldsymbol{\Omega}^2\,, \end{aligned} \tag{8.49}$$

with the redefinition $x(t) = \mu^{\frac{3}{2}}(t)$. The time derivative of the rotational degrees of freedom is contained in the angular velocities, (5.16). The coefficients $a_1, a_2, \ldots, \alpha_2$ are functionals of the chiral angle and can easily be computed numerically. Explicit expressions and numerical values are, e.g., listed in [56]. The b_i and α_i add up to the classical mass E_{cl} and moment of inertia α^2, respectively. Since $F(r)$ is a stationary point of the action, the potential part of L is minimized for $x = 1$. This implies $b_1 - b_2 + 3b_3 = 0$ and serves as a good test for the accuracy of the numerical soliton to the classical equation of motion. The Schrödinger equation is straightforwardly obtained from the prescription (5.9)

[10] The absolute energy scale is not reliably reproduced; after all E_0 is not zero. This deficiency is related to fact that the quantum corrections associated with the breathing mode are not included. Therefore it is most appropriate to only consider mass differences.

Table 8.4. Mass splittings (measured in MeV) with respect to the nucleon for radially and rotationally excited baryons in the Skyrme model (SM) with $e = 6.0$ and a scalar extended Skyrme model (sSM) compared to the empirical data (expt.) in the $P11$ and $P33$ channel. For the Roper resonance [$N(1440)$] both the Breit–Wigner (BW) mass and the pole position (PP) estimates are listed [51]

$n, 2j$	SM	sSM	expt.
$1, 1$	342	380	501 BW 426 PP
$2, 1$	664	756	771
$0, 3$	268	276	293
$1, 3$	598	660	661
$2, 3$	914	1040	981

$$\left\{ -\frac{1}{2\sqrt{m\alpha^3}} \frac{\partial}{\partial x} \sqrt{\frac{\alpha^3}{m}} \frac{\partial}{\partial x} + b + \frac{1}{2\alpha} \boldsymbol{J}^2 \right\} \Psi(x, A) = E\, \Psi(x, A)\,, \tag{8.50}$$

with the abbreviations $m = m(x) = \frac{8}{9}(a_1 + a_2 x^{-\frac{4}{3}})$, $b = b(x) = b_1 x^{\frac{2}{3}} + b_2 x^{-\frac{2}{3}} + b_3 x^2$ and $\alpha = \alpha(x) = \alpha_1 x^2 + \alpha_2 x^{\frac{2}{3}}$. The spin operator emerges via (5.20) since the momenta conjugate to A commute with the breathing variable. The eigenfunctions are easily obtained from the separation $\Psi(x, A) = f_j(x) D^{(j)}_{mm'}(A)$, where the Wigner D-functions represent the rotational part of the baryon wave function, cf. Sect. 5.2. This approach is still constrained to baryons with identical spin and isospin because the hedgehog structure is not altered. We end up with an ordinary differential equation for the breathing mode wave functions $f_j(x)$ whose j dependences arise from $\boldsymbol{J}^2 \to j(j+1)$. Hence the discrete eigenenergies are E_{nj}, where n labels the analog of the radial quantum number of an ordinary spherically symmetric quantum mechanical system. In this notation the nucleon is $(n, 2j) = (0, 1)$ while the Δ is $(0, 3)$. The Roper is interpreted as first radial excitation of the nucleon and hence corresponds to $(1, 1)$. In Table 8.4 the predicted mass differences (with respect to the nucleon) are compared to the empirical data. We observe that a significant alteration for the Skyrme parameter is needed to accommodate the Δ nucleon mass difference. This strongly indicates that the breathing mode, though not an exact zero mode, is indeed soft as small modifications cause sizable variations. As announced, the eigenenergy associated with the Roper resonance comes out somewhat on the low side. Nevertheless, this state is definitely contained in the soliton model, just well hidden in πN scattering and the dynamic interplay with the rotational modes seems important. The other radial excitations of the nucleon and Δ are reasonably reproduced in this approach as well. Similar (maybe even better) results are obtained when quantizing the breathing mode in a model that also contains a scalar field.[11] This scalar

[11] It is highly desirable to employ a vector meson model. Ingenuously scaling the time components leads to a non-integer baryon charges. The reason is that the

Table 8.5. The mass differences with respect to the nucleon in the three-flavor breathing mode approach in a scalar extended Skyrme model. All numbers are in MeV. Experimental data are taken from [51], if available. Unless otherwise noted, they denote four- and three-star resonances. The experimental states furnished with "?" in the Ξ row are potential isospin $\frac{1}{2}$ candidates whose spin–parity quantum numbers are not yet determined

	sSM	expt.	sSM	expt.	sSM	expt.
N	Input		445	501 BW 426 PP	869	771
Λ	173	177	688	661	1129	871
Σ	284	254	722	721	1096	831 (∗) 941 (∗∗)
Ξ	380	379	971	751 1011 (?)	1324	—
Δ	276	293	680	661	1010	981
Σ^*	460	446	878	901	1148	1141
Ξ^*	617	591	1068	—	1269	—
Ω	745	733	1386	—	1719	—

model (Its Lagrangian is actually displayed in (10.35).) is discussed in detail in [57]. Essentially only the numerical values of the parameters $a_1, \ldots, \alpha_2$ alter when adopting this scalar Skyrme model (sSM).

A conceptually very interesting question arises. Above we have seen that soliton models predicted a radial excitation about 400 MeV above the nucleon. Simultaneously, in flavor $SU(3)$ a state with nucleon quantum numbers dwells in the $\overline{\mathbf{10}}$ representation, cf. Fig. 6.3. Apart from symmetry breaking effects its mass difference to the nucleon is given in terms of the moment of inertia for rotations into strangeness direction $\frac{3}{2\beta^2} \approx 400\,\mathrm{MeV}$, i.e., it is in the same ballpark. The immediate puzzle is whether or not soliton models predict two nearby states. To decide on that question, the breathing mode approach must be generalized to three flavors and take $A \in SU(3)$ in (8.48). In sect. 9.2 we will thoroughly discuss technical issues of this generalization. Here we restrict ourselves to the presentation of the numerical results in Table 8.5. The model gives a fair account of the low-lying baryons with spin $\frac{1}{2}$ and $\frac{3}{2}$ as well as the corresponding excited states. Especially, only a single state is predicted with excitation energy around 400 MeV in the nucleon channel. Its wave function is a complicated mixture of radial and rotational excitations. The same is the case for the following nucleon type state which might be associated with the observed $N(1720)$. So the suspected inconsistency is avoided. Being of such a complicated nature questions approaches that identify the $N(1720)$ as a pure $SU(3)$ anti-decuplet (crypto-exotic) state [58]. The results in Table 8.5

corresponding field equations are actually constraints that must always be satisfied. Stated otherwise, the breathing mode approach to vector meson models requires to solve the stationary condition for any value of the scaling variable.

suggest that the model overestimates the resonance energy of $N(1720)$ by about 100 MeV. Yet, more recent data analysis indicate the resonance mass to be about 1.8 GeV [59]. Finally the model suggests not to assert $P11$ quantum numbers to the $\Xi(1690)$ resonance, rather $\Xi(1950)$ should carry these labels [60]. This is also concluded from a recent study within the bound state approach to the $SU(3)$ Skyrme model [61]. So far the exact quantum numbers of these two resonances are not determined experimentally [51].

Let us round up this section by mentioning that Hajduk and Schwesinger considered additional non-harmonic excitations [62]. On top of the breathing mode they allowed for deformations of the soliton to describe quadrupole resonances in the two-flavor model. Furthermore the breathing mode approach was employed to analyze color transparency in the Skyrme model [63].

8.6 Estimate of Quantum Corrections in Soliton Models

In the final section of this chapter we will consider the vacuum polarization energy that emerges by summing the zero-point energies of the meson fluctuations in the soliton background. Often this energy is also referred to as the Casimir energy. We have already argued after (8.3) that all properties computed from meson fluctuations are $\mathcal{O}\left(N_C^0\right)$. So this vacuum polarization energy is the next to leading order contribution to the soliton energy. This is very interesting because it teaches us important aspects about the absolute energy scale in soliton models. After all, up to now we have merely considered mass differences when investigating baryon spectra. Various attempts have been made to estimate their quantum corrections [3, 64, 65, 66]. Here we will in particular discuss the progress made in [66]. Before we go into details we note that chiral theories $D = 3+1$ are not renormalizable as far as the meson fluctuations are concerned. Thus, a rigorous calculation, with renormalization conditions for only a finite set of Green's functions, is not possible.

To motivate the use of the techniques from the beginning of this chapter, we first give an heuristic argument for the important role of phase shifts when computing vacuum polarization energies. We imagine placing the system in a box by imposing the boundary condition $\psi_k(x) = 0$ at $x = L$ for L much larger than the typical soliton extension.[12] The boundary condition $\sin(kL + \delta(k)) = 0$ yields a discrete spectrum of allowed values of k, which we enumerate as

$$k_n L + \delta(k_n) = n\pi\,. \tag{8.51}$$

We subtract the n and $n+1$ entries from each other. Since L is large, $k_{n+1} - k_n$ must be small and we approximate the difference of phase shifts by its derivative,

[12] In [67] the relation between phase shifts and vacuum polarization energy is derived without reference to artificial boundaries.

$$\frac{1}{\pi}\left(L+\frac{\mathrm{d}\delta(k)}{\mathrm{d}k}\right)=\frac{1}{k_{n+1}-k_n}=\rho(k). \tag{8.52}$$

The right hand side is the inverse of the spacing between adjacent levels, i.e., the density of states $\rho(k)$. The continuum limit is obtained by sending $L\to\infty$. To find the change in the density of meson states induced by the soliton we compare $\rho(k)$ in the presence of the potential (e.g., $M_{ij}(\boldsymbol{x})$ and $V_{ij}(\boldsymbol{x})$ in (8.2)) to the free density of states $\rho^{(0)}(k)=\frac{L}{\pi}$ from $M_{ij}^{(0)}$ and $V_{ij}^{(0)}$,

$$\Delta\rho(k)=\rho(k)-\rho^{(0)}(k)=\frac{1}{\pi}\frac{\mathrm{d}\delta(k)}{\mathrm{d}k}\,. \tag{8.53}$$

We find the vacuum polarization energy by summing the change of zero- point energies weighted with the so-computed variation of the density,

$$\Delta E=\frac{1}{2}\left\{\sum_j\omega_j+\int_0^\infty\mathrm{d}k\;\Delta\rho(k)\right\}=\frac{1}{2}\sum_j\omega_j+\int_0^\infty\frac{\mathrm{d}k}{2\pi}\frac{\mathrm{d}\delta(k)}{\mathrm{d}k}\sqrt{k^2+m^2}\,, \tag{8.54}$$

where ω_j labels the (absolute value of the) discrete bound states and m is the mass of the fluctuating meson field.

This expression for the vacuum polarization energy can almost straightforwardly be adopted in chiral soliton models, at least in the adiabatic approximation. The only complication arises from the emergence of various channels in the scattering problem. If we dealt only with channels that would not mix under scattering, we could directly employ (8.54) by merely summing over those channels. Otherwise we have to diagonalize the S-matrix and extract the phases of these eigenvalues.[13] As already noted, the total grand spin, (8.4) is conserved and thus the S-matrix is block diagonal. We then need to diagonalize each such block. Due to the invariance of the trace under diagonalization, the sum over the so-computed phases with grand spin G is

$$\delta_G^{\mathrm{tot}}(k)=\frac{1}{2\mathrm{i}}\mathrm{tr}\ln\widetilde{S}_G\,. \tag{8.55}$$

As discussed in Appendix F we find δ_G^{tot} directly from the equation of motion for the fluctuations about the soliton, (8.3). To this end the (unrenormalized) vacuum polarization energy of the soliton formally reads

$$\Delta E[U]=\tfrac{1}{2}\sum_{jG}(2G+1)\omega_{jG}+\sum_G(2G+1)\int_0^\infty\frac{\mathrm{d}k}{2\pi}\frac{\mathrm{d}\delta_G^{\mathrm{tot}}(k)}{\mathrm{d}k}\sqrt{k^2+m^2}\,, \tag{8.56}$$

where ω_{jG} is the jth bound state in the channel of grand spin G.

As explained at the end of Sect. 8.1 the Skyrme model phase shifts rise linearly with momentum for any given grand spin G. Summing with degeneracy $2G+1$ effectively adds two further dimensions so that

[13] Unitarity of the S-matrix implies that these eigenvalues have unit absolute value.

$$\delta^{\rm tot}(k) \longrightarrow \sum_G (2G+1)\,\delta_G^{\rm tot}(k) \to a_0 k^3 + a_1 k + \frac{a_2}{k} \tag{8.57}$$

as $k \to \infty$. The constants a_i can at least be extracted numerically from the asymptotic behavior of $\delta^{\rm tot}(k)$. In some cases they are known as functionals of the chiral field [65, 68]. Substituting the expansion (8.57) into (8.56) immediately reveals the quartic ultraviolet divergence of the vacuum polarization energy in the Skyrme model. Actually, all terms displayed in (8.57) yield divergent contributions to the vacuum polarization energy.

Ultraviolet divergences are compensated by counterterms in the renormalization program. The non-renormalizability of chiral Lagrangians induces infinitely many counterterms. They are classified according to the chiral expansion, a simultaneous expansion in the number of derivatives acting on the chiral field and the violation of exact chiral symmetry, as measured by the pion mass. In this scheme (called chiral perturbation theory), the non-linear σ term, (2.40), and the pion mass term, (4.25), are of second order, while the Skyrme term, (4.26), is of fourth order. In this way we label any piece in the chiral Lagrangian by $\mathcal{L}_i^{(N)}$, where $i = 1, \ldots, i_N$ counts the independent terms of a prescribed chiral order N. The general chiral Lagrangian is the sum

$$\mathcal{L} = \sum_{i,N} \left[c_{i,N}^{(0)} + c_{i,N}^{(1)}(D,\mu) \right] \mathcal{L}_i^{(N)} \,. \tag{8.58}$$

The superscript $r = 0, 1$ on the coefficients $c_{i,N}^{(r)}$ (so-called low-energy constants) labels the order in $\hbar$. If we were interested in two-loop or even higher quantum corrections we would additionally require $r = 2, \ldots$ pieces. The computation of a specific observable proceeds as follows: First, there are the classical (or tree level) contributions that solely involve $c_{i,N}^{(0)}$. Second there are $\mathcal{O}(\hbar)$ (or one loop) quantum corrections computed from the interactions described by $c_{i,N}^{(0)} \mathcal{L}_i^{(N)}$. These involve ultraviolet divergent loop integrals that are regularized in a specific scenario so that a finite value is attached to these integrals as long as the regularization parameter is not taken at its singular limit. In dimensional regularization this is the deviation, $\epsilon > 0$, from the physical space time dimension $D = 4 - 2\epsilon$. In the third step counterterms, $c_{i,N}^{(1)}(D,\mu) \mathcal{L}_i^{(N)}$, are added to the Lagrangian. Their contribution to the chosen observable is computed at tree level only because the induced quantum corrections would be $\mathcal{O}\left(\hbar^2\right)$. The coefficients $c_{i,N}^{(1)}(D,\mu)$ diverge in the singular limit such that they cancel the $r = 0$ one-loop singularities. Since the finite part of an infinite quantity is ambiguous, a scale μ emerges that parameterizes this ambiguity. This must be fixed by some renormalization prescription that commonly demands specific values for Green's functions at prescribed external momenta. In chiral perturbation theory this is transferred to matching empirical scattering data. For actual computations only a finite number of pieces $\mathcal{L}_i^{(N)}$ can be considered and one starts from a specific set of low-energy constants $\left\{ c_{i,N}^{(0)} \middle| N \leq N_{\rm max} \right\}$. If the considered model were renormalizable,

quantum corrections would only require counterterms of the same kind that are parameterized by the set $\left\{c^{(1)}_{i,N} \middle| N \leq N_{\max}\right\}$. Since chiral Lagrangians are not renormalizable the interactions of chiral order N induce counterterms of higher order. Hence sensible calculations of quantum corrections are impossible unless some criterion is established to control and eventually omit such higher order pieces in the Lagrangian. In chiral perturbation theory the higher order terms come together with higher powers of the external momenta (q) of the considered process. Hence small q (e.g., in the threshold region) allows one to ignore higher chiral orders. The typical expansion parameter is $q/4\pi f_\pi$. Unfortunately for soliton configurations that decay from π to zero within a fm is of the order one and the chiral truncation scheme cannot be blindly adopted. We will nevertheless do so and use the argument of [66] to justify the truncation a posteriori. As already explained, the computation of a specific observable, say Γ, results in a sum of the classical, quantum and counterterm contributions, $\Gamma^{(0)}$, $\Gamma^{(1)}$ and $\Gamma^{(1)}_{\text{ct.}}$, respectively. The singular pieces of the latter two cancel and the regulator may be taken at the physical value. They also have finite pieces that are characterized by a scale. The scale dependence cancels by the renormalization conditions. We can compute $\Gamma^{(1)}$ (in some regularization scheme) but we do not know $\Gamma^{(1)}_{\text{ct.}}$ to all chiral orders. However, we can read off its singular pieces from $\Gamma^{(1)}$. We will find a finite answer by taking $\Gamma^{(1)}_{\text{ct.}}$ identical to these singular parts. This finite result will be scale dependent because we were unable to eliminate the scale dependence of $\Gamma^{(1)}$. If we are lucky, the final (numerical) value depends only mildly on the scale and we may argue that the omission of the (unknown) counterterms is an acceptable approximation. Exactly this is the strategy and result of [66].

After these general remarks on renormalization in chiral theories we compute the vacuum polarization energy in the two-flavor Skyrme model. We subtract the asymptotic behavior (8.57) from the formal expression (8.56)

$$\begin{aligned}\Delta E[U] = {} & \tfrac{1}{2}\sum_{jG}(2G+1)\omega_{jG} \\ & + \int_0^\infty \frac{\mathrm{d}k}{2\pi}\sqrt{k^2+m^2}\left\{\frac{\mathrm{d}}{\mathrm{d}k}\left[\delta^{\text{tot}}(k) - a_0k^3 - a_1k\right] + \frac{a_2}{k^2+m^2}\right\} \\ & + E_{\text{sub}}\,, \end{aligned} \tag{8.59}$$

where the subtractions, E_{sub} refer to the pieces that have been subtracted under the integral and must be added back in. Furthermore the a_2 term has been slightly altered to avoid infrared divergences; that finite modification will be included in E_{sub}. We integrate by parts (this implies the use of an intermediate regulator) and find[14]

$$\Delta E[U] = \tfrac{1}{2}\sum_{jG}(2G+1)(\omega_{jG} - m) + \frac{a_2}{2\pi}$$

[14] Chapter 5.4 of [55] contains an heuristic argument that yields the analog expression without integration by parts.

$$-\int_0^\infty \frac{\mathrm{d}k}{2\pi}\left\{\frac{k}{\sqrt{k^2+m^2}}\left[\delta^{\mathrm{tot}}(k)-a_0k^3-a_1k\right]-\frac{a_2}{\sqrt{k^2+m^2}}\right\}$$
$$+E_{\mathrm{sub}}\,. \tag{8.60}$$

The second piece in the surface contribution, $\propto a_2 - m\delta^{\mathrm{tot}}(0)$, is identified from the asymptotic behavior, (8.57). It has entered the sum over bound states via Levinson's theorem according to which $\delta^{\mathrm{tot}}(0)/\pi$ counts the number of bound states. (In view of the asymptotic behavior, (8.13), this merely is a convention.) Next, we treat the subtractions in dimensional regularization that generalizes integrals like those above according to [69]

$$\int_0^\infty \mathrm{d}^D k \frac{\left(\boldsymbol{k}^2\right)^\alpha}{\left(\boldsymbol{k}^2+m^2\right)^\beta} = \left(\frac{\sqrt{\pi}}{2}\right)^D \left(m^2\right)^{\frac{D}{2}+\alpha-\beta} \frac{\Gamma\left(\alpha+\frac{D}{2}\right)\Gamma\left(\beta-\alpha-\frac{D}{2}\right)}{\Gamma\left(\frac{D}{2}\right)\Gamma\left(\beta\right)}\,. \tag{8.61}$$

We identify the subtractions from (8.60) and write

$$\begin{aligned}
2\pi E_{\mathrm{sub}} &= -\int_0^\infty \frac{\mathrm{d}k}{\sqrt{k^2+m^2}}\left[a_0k^4+a_1k^2+a_2\right] \\
&\longrightarrow -\mu^{4-D}\int_0^\infty \mathrm{d}^{D-3}k\,\frac{a_0k^4+a_1k^2+a_2}{\sqrt{k^2+m^2}} \\
&= \frac{\lambda(D)}{2}\left[\frac{3m^4a_0}{4}-m^2a_1+2a_2\right]+\frac{m^4a_0}{16}\left[3\ln\left(\frac{m^2}{\mu^2}\right)+\frac{1}{2}\right] \\
&\quad -\frac{m^2a_1}{4}\ln\left(\frac{m^2}{\mu^2}\right)+\frac{a_2}{2}\left[\ln\left(\frac{m^2}{\mu^2}\right)-1\right]+\mathcal{O}\left(D-4\right)\,,
\end{aligned} \tag{8.62}$$

where the scale μ has been introduced to preserve the dimensionality of the integral. The divergences are parameterized by

$$\lambda(D)=\frac{1}{D-4}+\frac{1}{2}\left[\gamma-1-\ln\left(4\pi\right)\right] \quad \text{with} \quad \gamma=0.5772157\ldots\,. \tag{8.63}$$

This is singular at the physical dimension $D = 4$. Any finite change $\Delta\lambda$ is compensated by a multiplicative renormalization $\mu \to \mathrm{e}^{-\Delta\lambda}\mu$. The divergent λ piece is absorbed in the (partially unknown) higher order counterterms. Collecting pieces we find the scale-dependent vacuum polarization energy

$$\begin{aligned}
\Delta E(\mu) = -3m &- \int_0^\infty \frac{\mathrm{d}k}{2\pi}\frac{k\delta^{\mathrm{tot}}(k)-a_0k^4-a_1k^2-a_2}{\sqrt{k^2+m^2}} \\
&+\frac{m^4a_0}{32\pi}\left[3\ln\left(\frac{m^2}{\mu^2}\right)+\frac{1}{2}\right]-\frac{m^2a_1}{8\pi}\ln\left(\frac{m^2}{\mu^2}\right)+\frac{a_2}{4\pi}\left[\ln\left(\frac{m^2}{\mu^2}\right)+1\right]\,.
\end{aligned} \tag{8.64}$$

Here we made use of the fact that the only bound states are the translational and rotational zero modes in the $G = 1$ channel. Equation (8.64) is the result derived in [66]. Unfortunately there are some ambiguities. We have already mentioned the intermediate use of a regulator when integrating a divergent integral by parts. Also recall that we subtracted

$$\int_0^\infty \frac{\mathrm{d}k}{2\pi}\sqrt{k^2+m^2}\left[3a_0k^2+a_1+\frac{a_2}{k^2+m^2}\right]$$

in (8.59), but only added back the dimensionally regularized form of

$$\int_0^\infty \frac{\mathrm{d}k}{2\pi}\frac{a_0k^4+a_1k^2+a_2}{\sqrt{k^2+m^2}}$$

in (8.62). In general the difference between these two expressions diverges. Fortunately in dimensional regularization the corresponding poles cancel at $D=4$, yet a finite scale-independent ambiguity remains.

To make the cancellation of divergences more explicit we read off finite coefficients, $\gamma_{i,N}$ via

$$3m^4a_0-4m^2a_1+8a_2=\frac{1}{\pi}\sum_{i,N}\gamma_{i,N}\int \mathrm{d}^3r\mathcal{L}_i^{(N)}\,. \tag{8.65}$$

In principle, the $\gamma_{i,N}$ are identified from the chiral perturbation expansion at one loop. Naturally, only those for the low chiral orders are known [68]. The divergent contributions are compensated by counterterms

$$\begin{aligned} E_{\mathrm{sub}}+E_{\mathrm{c.t.}} &= -\int \mathrm{d}^3x\, c_{i,N}^{(1,R)}(\mu)\,\mathcal{L}_i^{(N)} \\ c_{i,N}^{(1,R)}(\mu) &= \lim_{D\to 4}\left[c_{i,N}^{(1)}(D,\mu)-\frac{\gamma_{i,N}}{16\pi^2}\lambda(D)\right]\,, \end{aligned} \tag{8.66}$$

with the soliton configuration substituted in $\mathcal{L}_i^{(N)}$. The second equation defines renormalized counterterm coefficients and the invariance discussed after (8.63) suggests $c_{i,N}^{(1,R)}(\mu)=c_{i,N}^{(1,R)}(m_\rho)-\frac{\gamma_{i,N}}{16\pi^2}\ln(\mu/m_\rho)$ where, in the scenario of chiral perturbation theory, the ρ-meson mass is chosen as absolute scale.

The classical energy is computed with $c_{i,N}^{(1)}(D,\mu)\to c_{i,N}^{(1,R)}(\mu)$ in (8.58); so the scale dependence propagates to $E_{\mathrm{cl}}=E_{\mathrm{cl}}(\mu)$, such that the total energy

$$E_{\mathrm{tot}}=E_{\mathrm{cl}}(\mu)+\Delta E(\mu)\,, \tag{8.67}$$

is scale independent.

As discussed, in general a residual scale dependence emerges in the actual calculation. The numerical results from [66] show only a mild scale dependence. This mitigates the non-renormalizability problem in chiral soliton models. Two entries have proven important to reach that result:

1. The full scale dependence is kept for the counterterms that are of the same form as the tree level terms.
2. The field configuration must be taken at the stationary point, i.e., the soliton. Then the scale dependence from the soliton emerges at $\mathcal{O}(1/N_{\mathrm{C}})$.

Especially issue (2) shows that this procedure does not have much in common with conventional renormalization which must be applicable to *all* field

Table 8.6. Quantum corrections computed in the Skyrme model for the renormalized Skyrme constant $e^{(0)} + e^{(1,R)}(m_\rho) = 4.25$. Results taken from [66]. The electric isoscalar radius shown here differs from that in table 5.1 by the vector meson exchange contribution, cf. (7.14)

	classical	one loop	total	expt.
$E_{\rm tot}$ (MeV)	1629	−683	946	939
$g_{\rm A}$	0.91	−0.25	0.66	1.26
$\mu_{I=1}$	1.62	0.62	2.24	2.35
$r^2_{E,I=0}$ (fm^2)	0.62	−0.11	0.51	0.62
$r^2_{M,I=1}$ (fm^2)	0.77	−0.13	0.64	0.73
σ (MeV)	54	−22	32	60-80

configurations. Nevertheless it is a worthwhile study to obtain valuable information about the structure of quantum corrections to baryon properties, in particular because the too large prediction for the absolute baryon masses at the classical level is unsettling. The quantum corrections to nucleon observables whose tree level computation does not involve time derivatives of the collective coordinates (angular velocities, (5.16)) require only a moderate extension, though it is numerically exhaustive. The Lagrangian is augmented by a small perturbation

$$\delta\mathcal{L} = \epsilon^a j_a(U)\,, \tag{8.68}$$

where $j_a(U)$ is the current density for the observable. With this modification the renormalized total energy, (8.67), turns into a function of the ϵ^a and observables are computed from the nucleon matrix element

$$\langle N \Big| \frac{\partial E_{\rm tot}(\{\epsilon^a\})}{\partial \epsilon^a}\Big|_{\epsilon^a=0} \Big| N\rangle\,. \tag{8.69}$$

We will now discuss numerical results that stem from the above-introduced program. We concentrate on the Skyrme model with $e^{(0)} + e^{(1,R)}(m_\rho) = 4.25$ because it exhibits the mildest scale dependence of all results presented in [66]: $E_{\rm tot}$ is essentially flat in the regime $\mu = 500 \ldots 1100\,\text{MeV}$.

The most important observation is the fact that the classical energy indeed has sizable quantum corrections that cause a reduction of about 40% and bring the total energy close to the actual nucleon mass. A major share of this correction is due to the zero mode as $3m_\pi \approx 400\,\text{MeV}$. Thus the large tree level mass mainly results from the violation of translational and rotational invariances. Also in the case of the isovector magnetic moment $\mu_{I=0} = (\mu_p - \mu_n)/2$ the quantum corrections contribute very favorably to the Skyrme model prediction. The corrections from quantum fluctuations to the isoscalar magnetic moment are not considered here because they are $\mathcal{O}(1/N_{\rm C})$. Those electromagnetic radii that have classical contributions are only mildly affected by the quantum corrections. They turn out negative for all variants of the model considered in [66]. Unfortunately, the nucleon axial charge, $g_{\rm A}$, continues to

cause concern. Its quantum contributions point into the wrong direction and amplify the disagreement with the empirical value.

The last row of Table 8.6 shows results for the nucleon σ term, that we have not discussed so far. In Sect. 9.1 we will elaborate on σ in more detail. It measures the explicit chiral symmetry breaking via the pion mass term in the chiral Lagrangian. Its extraction from empirical data of pion nucleon scattering is somewhat involved [70, 71]. Obviously, it suffers significant quantum corrections in soliton models. This is not surprising since it must be considered on the same level as the classical mass.

In [72, 73] quantum corrections were estimated for the three-flavor model. The main qualitative result is the fact that the vacuum polarization energy from kaon loops approximately compensates the rotational energy from the collective rotations into strangeness direction (the $1/\beta^2$ piece in (6.10)). The main contribution for this compensation originates from the kaon zero-mode analog of the first term on the right hand side of (8.64). This teaches an important lesson: The zero-mode contribution carries the major share of the vacuum polarization energy. This contribution can therefore be used for a rough estimate of the quantum correction to the nucleon mass. This was done in [3] for the soliton of the Nambu–Jona–Lasinio model (cf. Chap. 3). This estimate also teaches us that quantum corrections has severe consequences when comparing energies of configurations with different baryon numbers. Quantum corrections reduce the energy by an amount that is approximately proportional to the number of zero modes. This number is dictated by the symmetries of the Lagrangian rather than the baryon number. The subtractions for the $B > 1$ objects are significantly smaller than B times the subtractions for the single Skyrmion. Eventually this reduces the soliton model predictions for binding energies of compound baryons considerably. We will return to that issue in the context of the H-dibaryon in Sect. 10.6.

References

1. B. Schwesinger, H. Weigel, G. Holzwarth, and A. Hayashi, *Phys. Rep.* **173** (1989) 173. 147, 148, 156, 158, 160, 161, 162, 163, 165
2. H. Weigel, *Phys. Lett.* **B215** (1988) 24. 147, 152
3. H. Weigel, R. Alkofer, and H. Reinhardt, *Nucl. Phys.* **A582** (1995) 484. 147, 171, 178
4. A. Hayashi, G. Eckart, G. Holzwarth, and H. Walliser, *Phys. Lett.* **B147** (1984) 5. 147, 149, 150
5. H. Walliser and G. Eckart, *Nucl. Phys.* **A429** (1984) 514. 147, 148, 163, 167
6. R. Haag, *Phys. Rev.* **112** (1958) 669. 147
7. R. G. Newton, *Scattering Theory of Waves and Particles.* Springer, New York, 1982. 149
8. K. Chadan and P. C. Sabatier, *Inverse Problems in Quantum Scattering Theory.* Springer, New York, 1977. 149
9. M. P. Mattis, *Phys. Rev. Lett.* **56** (1986) 1103. 149
10. M. P. Mattis and R. R. Silbar, *Phys. Rev.* **D51** (1995) 3267. 150

11. T. D. Cohen and R. F. Lebed, *Phys. Rev. Lett.* **91** (2003) 012001. 150
12. H. Weigel, *Baryon Resonances in an Effective Meson Theory.* PhD thesis, Siegen University, 1988. Unpublished. See also [1, 4]. 151, 152, 160, 164
13. G. Hohler, F. Kaiser, R. Koch, and E. Pietarinen, "Handbook of pion nucleon scattering." Physics Data, No. 12-1 (1979). 152, 153, 160
14. G. Eckart, A. Hayashi, and G. Holzwarth, *Nucl. Phys.* **A448** (1986) 732. 151
15. B. Schwesinger and H. Weigel, *Nucl. Phys.* **A465** (1987) 733. 152
16. M. Karliner and M. P. Mattis, *Phys. Rev.* **D34** (1986) 1991. 153
17. M. P. Mattis and M. Karliner, *Phys. Rev.* **D31** (1985) 2833. 153
18. M. Karliner and M. P. Mattis, *Phys. Rev. Lett.* **56** (1986) 428. 153
19. B. Schwesinger, *Nucl. Phys.* **A537** (1992) 253. 153
20. Y. Tomozawa, *Nuovo Cim.* **46A** (1966) 707. 153, 154
21. S. Weinberg, *Phys. Rev. Lett.* **17** (1966) 616. 153, 154
22. G. Holzwarth, H. Walliser, and H. Pari, *Z. Phys.* **A339** (1991) 195. 154
23. H. Walliser, *Nucl. Phys.* **A524** (1991) 706. 154, 155
24. D. Masak, H. Walliser, and G. Holzwarth, *Nucl. Phys.* **A536** (1992) 583. 154, 155
25. N. Dorey, J. Hughes, and M. P. Mattis, *Phys. Rev.* **D50** (1994) 5816. 156
26. D. Diakonov, V. Y. Petrov, and P. V. Pobylitsa, *Phys. Lett.* **B205** (1988) 372. 156
27. M. Uehara, *Prog. Theor. Phys.* **75** (1986) 212. 156
28. G. Holzwarth, A. Hayashi, and B. Schwesinger, *Phys. Lett.* **B191** (1987) 27. 156
29. M. Uehara, *Prog. Theor. Phys.* **78** (1987) 984. 156
30. S. Saito, *Prog. Theor. Phys.* **78** (1987) 746. 156
31. H. Verschelde, *Phys. Lett.* **B209** (1988) 34. 156
32. A. Hayashi, S. Saito, and M. Uehara, *Phys. Lett.* **B246** (1990) 15. 156
33. G. Holzwarth, *Phys. Lett.* **B241** (1990) 165. 156, 157
34. G. Holzwarth, G. Pari, and B. K. Jennings, *Nucl. Phys.* **A515** (1990) 665. 156, 157
35. A. Hayashi, S. Saito, and M. Uehara, *Phys. Rev.* **D43** (1991) 1520. 156
36. A. Hayashi, S. Saito, and M. Uehara, *Prog. Theor. Phys. Suppl.* **109** (1992) 45. 156
37. G. Holzwarth, ed., *Baryons as Skyrme Solitons. Proceedings, International Workshop, Siegen, Germany, September 28–30, 1992.* World Scientific, Singapore, 1993, 445 p. 156, 179
38. H. J. Schnitzer, *Phys. Lett.* **B139** (1984) 217. 156
39. G. Holzwarth. p. 279 in [37]. 157
40. H. Feshbach, *Theoretical Nuclear Physics*, Chap. 2. Wiley Interscience Publication, New York, 1991. 158
41. T. D. Lee, *Phys. Rev.* **95** (1954) 1329. 158
42. E. M. Henley and W. Thirring, *Elementary Qunatum Field Theory*, chap. 13. McGraw-Hill, New York, 1962. 158
43. C. R. Hagen, *Phys. Rev.* **A61** (2000) 032715. 158
44. S. Saito, *Nucl. Phys.* **A463** (1987) 169c. 159
45. G. Eckart and B. Schwesinger, *Nucl. Phys.* **A458** (1986) 620. 161, 162, 163, 166
46. J. D. Jackson, *Classical Electro Dynamics*, Chap. 10. Wiley Interscience Publication, New York, 3rd Ed., 1998. 162
47. R. L. Walker, *Phys. Rev.* **182** (1969) 1729. 163
48. P. Noelle, *Prog. Theor. Phys.* **60** (1978) 778. 164
49. J. D. Breit and C. R. Nappi, *Phys. Rev. Lett.* **53** (1984) 889. 163, 167
50. U. B. Kaulfuss and U. G. Meißner, *Phys. Lett.* **B154** (1985) 193. 163, 167
51. S. Eidelman et al. [PDG], *Phys. Lett.* **B592** (2004) 1. 165, 169, 170, 171

52. T. Haberichter, H. Reinhardt, N. N. Scoccola, and H. Weigel, *Nucl. Phys.* **A615** (1997) 291. 166
53. A. Wirzba and W. Weise, *Phys. Lett.* **B188** (1987) 6. 166
54. H. Walliser and G. Holzwarth, *Z. Phys.* **A357** (1997) 317. 166
55. R. Rajaraman, *Solitons and Instantons.* North Holland, Amsterdam, 1982. 168, 174
56. J. Schechter and H. Weigel, *Phys. Rev.* **D44** (1991) 2916. 168
57. J. Schechter and H. Weigel, *Phys. Lett.* **B261** (1991) 235. 170
58. D. Diakonov, V. Petrov, and M. V. Polyakov, *Z. Phys.* **A359** (1997) 305. 170
59. G. Y. Chen, S. S. Kamalov, S. N. Yang, D. Drechsel, and L. Tiator, *Phys. Rev.* **C76** (2007) 035206. 171
60. H. Weigel, *Eur. Phys. J.* **A21** (2004) 133. 171
61. Y. Oh, *Phys. Rev.* **D75** (2007) 074002.. 171
62. C. Hajduk and B. Schwesinger, *Phys. Lett.* **B145** (1984) 171. 171
63. P. Jain, J. Schechter, and H. Weigel, *Phys. Rev.* **D45** (1992) 1470. 171
64. B. Moussallam, *Ann. Phys.* **225** (1993) 264. 171
65. B. Moussallam and D. Kalafatis, *Phys. Lett.* **B272** (1991) 196. 171, 173
66. F. Meier and H. Walliser, *Phys. Rept.* **289** (1997) 383. 171, 174, 175, 176, 177
67. N. Graham et al., *Nucl. Phys.* **B645** (2002) 49. 171
68. J. Gasser and H. Leutwyler, *Ann. Phys.* **158** (1984) 142. 173, 176
69. J. Collins, *Renormalization*, chapter 4. Cambridge Monographs on Mathematical Physics, 1984. 175
70. J. Gasser, H. Leutwyler, and M. E. Sainio, *Phys. Lett.* **B253** (1991) 252. 178
71. M. M. Pavan, I. I. Strakovsky, R. L. Workman, and R. A. Arndt, *PiN Newslett.* **16** (2002) 110. 178
72. H. Walliser, *Phys. Lett.* **B432** (1998) 15. 178
73. N. N. Scoccola and H. Walliser, *Phys. Rev.* **D58** (1998) 094037. 178

9

Exotic Baryons

This topic became very popular after the LEPS collaboration announced the observation of a very narrow strangeness $S = +1$ baryon [1]. Typically, a width of at most some 10 MeV is quoted, an order of magnitude less than ordinary hadronic widths! Due to its quantum numbers, such a state cannot be built from three quarks. It must contain (at least) four quarks and an antiquark. Here soliton models played a very decisive role because that search was initiated by a paper from Diakonov et al. [2]. Even though the calculations from Diakonov et al. are just a little better than a guess (as we will see in the course of this chapter), the apparent agreement with the observations from LEPS initiated many more experimental analysis and theoretical studies.[1]

By now a second round of experiments with significant higher statistics has been completed. Most of them do not confirm earlier claims of pentaquark findings, at least with regard to a very narrow light pentaquark.[2]

The soliton model calculations of [2, 5] may have been most influential on the pentaquark front. They have triggered the interest in the field of both exotic baryons and soliton models en bloc. Larger parts of this chapter deal with working out the assumptions that underly those results. A major assumption is the use of the $SU(3)$ rigid rotator approach. Though we have good arguments in favor of this approach, cf. Chap. 6, we must not forget that it is an approximation to quantizing the full system. Within that approach as many parameters of collective coordinate operators, e.g., moments of inertia, as possible were related to empirical data rather than evaluating them in a particular chiral model. For that reason, the resulting predictions are often claimed to be model independent. In a sense, that scenario can be viewed as using the optimal soliton model. If indeed these predictions were absolutely model independent, their failure to match data would immediately imply the failure of all chiral soliton models. Such a conclusion is definitely

[1] The numerous papers that have appeared since then may be downloaded from `http://www.rcnp.osaka-u.ac.jp/~hyodo/research/Thetapub.html`.

[2] At the time of writing, [3, 4] fairly account for the experimental situation.

H. Weigel: *Exotic Baryons*, Lect. Notes Phys. **743**, 181–206 (2008)
DOI 10.1007/978-3-540-75436-7_9

premature when profound assumptions enter. Thus, there is a general interest to elaborate how rigorous these results really are. For this purpose, we will closely follow and review the arguments of [2, 5] in Sects. 9.1 and 9.3 without failing to critically intervene when appropriate.

9.1 Exotic Flavor Structure and Spectrum

In Chap. 8, we have seen that anti-decuplet baryons naturally emerge in the rigid rotator treatment of soliton models. That representation is depicted in Fig. 6.3. Most interesting are the states at the top and bottom of that diagram. At the top we have the Θ^+ with hypercharge $Y = +2$, i.e., strangeness $S = 1$. In the quark model picture, this necessarily requires an anti-strange quark constituent, the flavor structure is $uudd\overline{s}$. The states at the bottom have isospin $I = 3/2$ and strangeness $S = -2$. The member at the far right of this isospin multiplet possesses the minimal quark model content $uu\overline{d}ss$. Obviously, the anti-decuplet baryons do not correspond to ordinary quark model states with three constituents. In that sense, they are exotic and require (at least) five constituents, therefore the notation *pentaquarks*.

In soliton models, the anti-decuplet baryons (and those from other higher dimensional representations) appear as collective soliton excitations whose energy gap to the nucleon

$$M_{\overline{\mathbf{10}}} - M_{\mathbf{8}} = \frac{3}{2\beta^2} + \text{flavor sym. breaking cont.} \tag{9.1}$$

may be as low as 400 MeV [6, 7, 8, 9], depending on the model prediction for the moment of inertia β^2 cf. (6.7). This is different from the quark model, in which at least some 600 MeV is required to construct these states from the mere addition of two constituents.[3] There is another very noticeable difference to quark models where four quarks and an anti-quark in the orbital ground states build a negative parity baryon. In the soliton model, the pentaquarks from the anti-decuplet can be understood as flavor excitations of the nucleon, whence they should carry positive parity.

Equation (9.1) unfortunately also hints a dilemma of the soliton approach. A dependable prediction for the pentaquark spectrum relies on the solid knowledge of the inertia parameter β^2. However, model predictions for β^2 vary strongly [11, 12]. It is thus desirable to find some model-independent result for β^2. In [2], it was therefore suggested to identify the $P11(1720)$ nucleon resonance as the nucleon-type state in the anti-decuplet to fix the scale for β^2. As we have already observed in Sect. 8.5 and will further discuss in Sect. 9.2, this assumption is anything but rock solid because it does not consider mixing with states that are outside the rigid rotator approach, which unavoidably occurs for $P11(1720)$. By ignoring this mixing, this identification falls back

[3] See [10] for an exhaustive discussion of pentaquarks in quark models.

on the level of a model assumption. Still, just choosing a value for β^2 is not sufficient to predict the pentaquark mass without reference to a specific rigid rotator model, as flavor symmetry breaking is not yet accounted for. In the next step, it was then assumed that symmetry breaking is only moderate so that the expansion can be truncated after the linear order. Symmetry breaking contributions that involve angular velocities were also kept only to linear order. With these approximations, the general $SU(2)$ invariant form of the symmetry breaking part of the Hamiltonian reads, cf. (6.24) and (6.34),

$$\begin{aligned} H_{\rm sb} &= \frac{1}{2}\gamma\,(1 - D_{88}) + \alpha_1 \sum_{i=1}^{3} D_{8i} R_i + \beta_1 \sum_{\alpha=4}^{7} D_{8\alpha} R_\alpha \\ &= \frac{1}{2}\gamma + \widetilde{\alpha} D_{88} + \widetilde{\beta} Y + \frac{\widetilde{\gamma}}{\sqrt{3}} \sum_{i=1}^{3} D_{8i} J_i \,, \end{aligned} \tag{9.2}$$

where the hypercharge $Y = \frac{2}{\sqrt{3}} \sum_{a=1}^{8} D_{8a} R_a$ is introduced and the quantization rules (6.8) are used to make contact with the notation of [2]: $\widetilde{\alpha}+\widetilde{\beta} = -\gamma/2$, etc. We recall from Chap. 6 that the $\widetilde{\beta}$ and $\widetilde{\gamma}$ terms are not contained in the Skyrme model and that the $\widetilde{\alpha}$ term is the dominating symmetry breaking term in all known soliton models. Continuing to restrict oneself to linear order in flavor symmetry breaking to compute the mass splittings[4] among the spin $\frac{1}{2}$ and $\frac{3}{2}$ baryons shows that they are fully determined by the two linear combinations $2\widetilde{\alpha} + 3\widetilde{\gamma}$ and $2\widetilde{\alpha} + 16\widetilde{\beta} - 5\widetilde{\gamma}$. Hence, it is impossible to determine these three parameters from the spectrum without reference to a specific soliton model. In [2], it was suggested to determine the remaining symmetry breaking parameter from the pion–nucleon σ-term. We have already encountered that quantity in Sect. 8.6 and we will now discuss its computation in chiral soliton models in more detail. Conventionally, the σ-term is defined as the nucleon matrix element of the equal time double commutator of the axial generators, Q_i^5, with the Hamiltonian [14]

$$\sigma = \frac{1}{3} \sum_{i=1}^{3} \langle N | \left[Q_i^5, \left[Q_i^5, H \right] \right] | N \rangle \,. \tag{9.3}$$

Here we only consider zero momentum transfer for this factor. Equation (9.3) is the quadratic term in the expansion of the small parameter $\boldsymbol{\epsilon}$ that enters the axial transformation of the chiral field, cf. (2.30) $U \to \mathrm{e}^{\mathrm{i}\boldsymbol{\epsilon}\cdot\boldsymbol{\tau}} U \mathrm{e}^{\mathrm{i}\boldsymbol{\epsilon}\cdot\boldsymbol{\tau}}$. Here we already encounter a problem for the model-independent approach: this axial transformation cannot be transferred to the collective coordinates, $A(t)$, that only parameterize vector degrees of freedom.

Obviously mass terms violate chiral symmetry. The second-order variation of the pion mass term, (4.25), yields

[4] According to Sect. 6.4, this may be too crude a restriction. An exact diagonalization of $H_{\rm sb}$ was performed in [13] for pentaquark studies.

$$\frac{1}{3}\sum_{i=1}^{3}\left[Q_i^5,\left[Q_i^5,H\right]\right] = m_\pi^2 f_\pi^2 \mathrm{tr}\left(U+U^\dagger-2\right)\,. \tag{9.4}$$

This indeed suggests that the σ-terms contain information about the symmetry breaking parameter γ (6.25). The rigid rotator analysis yields [15]

$$\sigma = \frac{2+\langle N|D_{88}|N\rangle}{2(\xi-1)}\,\gamma\,, \tag{9.5}$$

where $\xi = 2(f_K m_K/f_\pi m_\pi)^2 - 1 = 2m_\mathrm{s}/(m_\mathrm{u}+m_\mathrm{d})$. The latter identification as a ratio of current quark masses is suggested by the Gell-Mann–Oakes–Renner relation [16] and can be motivated from the pole condition to (2.22) in the approximation that the constituent quark masses are flavor invariant. Using the techniques of Sect. 6.4 shows that the nucleon matrix element of D_{88} is a monotonous function of flavor symmetry breaking that varies between $\frac{3}{10}$ and 1 for the extreme cases of $m_K = m_\pi$ and $m_K \to \infty$. Furthermore, $\xi \gg 1$ so that the crude approximation

$$\sigma = \frac{3}{2\xi}\gamma \quad \Leftrightarrow \quad \widetilde{\alpha}+\widetilde{\beta} = -\frac{\xi}{3}\,\sigma \tag{9.6}$$

seems helpful to obtain the third empirical information for the parameters in (9.2). We stress, however, that this information is model dependent and that the analog of the $\widetilde{\gamma}$ term (that naturally arises) is not taken into account. In principle, it must contribute to σ because any vector symmetry breaker by definition also violates the axial symmetry.[5] Furthermore, we have observed in Table 8.6 that σ is subject to sizable quantum corrections, after all it behaves like absolute energies rather than mass differences. Putting things together, (9.5), is only a rough guide to the parameters in H_sb. With the so-adopted parameters, the estimated masses of anti-decuplet pentaquarks are shown in Table 9.1. The authors of [5] used various model results for some of the parameters in H_sb to estimate the masses of Θ and $\Xi_{\frac{3}{2}}$. Additional errors stem from the experimental uncertainty of the σ term. (In [2] only the then actual central value $\sigma = 45\,\mathrm{MeV}$ was considered.) Subsequently, they used the empirical data for these baryons [1, 17] to predict the masses of the anti-decuplet N and Σ, the so-called crypto-exotic pentaquarks. In view of these errors, it is amazing to see how fortuitously the early results [2] coincided with the first data [1] of pentaquark masses. Taking all the facts together,

[5] To leading order in flavor symmetry breaking, the correct relation is

$$(\xi-1)\,\sigma = -\left\langle N\middle|2\widetilde{\alpha}+3\widetilde{\beta}+\widetilde{\alpha}D_{88}-\frac{\widetilde{\gamma}}{\sqrt{3}}\sum_{i=1}^{3}D_{8i}J_i\middle|N\right\rangle.$$

The last collective coordinate matrix element is small and may indeed be neglected while the approximate treatment of D_{88} causes errors on σ of up to 10 MeV for the parameters of [5].

Table 9.1. Pentaquark spectrum in rigid rotator based approaches. DPP [2] is discussed in the text. EKP [5] used various model results for parameters in $H_{\rm sb}$ to estimate the Θ and $\Xi_{\frac{3}{2}}$ masses. Subsequently, they used data for these baryons [1, 17] to predict the masses of the anti-decuplet N and Σ. The WK calculation [13] diagonalized the collective coordinate Hamiltonian exactly and fitted parameters from the ordinary spin-$\frac{1}{2}$ baryons as well as Θ. All data are in MeV

	DPP	EKP	WK	expt. ?
Θ	1530	1545 ± 110	1540	~ 1540 [1]
N	input	1646	1650	
Σ	1890	1745	1750	
$\Xi_{\frac{3}{2}}$	2070	1878 ± 92	1780	~ 1862 [17]

that calculation was not much more than a good guess. This becomes even more obvious when observing that its prediction for the $\Xi_{3/2}$ fails to reproduce empirical datum by a couple of hundred MeV. (So far only a single such empirical result has been reported [17], which has never been reproduced.)

Approaches that pursue the opposite path, i.e., fitting parameters in $H_{\rm sb}$ from data for pentaquark masses and estimating the σ term via (9.6) [18], must be regarded with even more skepticism.

9.2 Spectrum and Mixing Mechanisms

The above discussion assumes that nucleon and Σ-type states in the anti-decuplet are observable baryons, at least in the absence of flavor symmetry breaking. With symmetry breaking switched on, $SU(3)$ quantum numbers are no longer conserved and mixing with, e.g., (ordinary) octet baryons occurs. Then there is also no reason for these states not to mix with radial excitations of (ordinary) octet baryons as well. This is even more likely because the mass gap between such radial excitations and anti-decuplet states is presumably small, cf. (9.1). A reliable study of pentaquark physics may not eschew that mixing. In view of the approaches discussed above, there are specific reasons to study this mixing in soliton models: (i) the identification of the anti-decuplet nucleon as $N(1710)$ yielded quite a heavy $\Xi_{3/2}$. Regardless of whether or not the datum of [17] withstands future experimental analysis, it seems unlikely that the mass splitting between the top and bottom states in the anti-decuplet is 100 MeV larger than in the decuplet; (ii) the parameters of [5] suggest an additional nucleon state at 1650 MeV for which there is only little experimental indication.[6] A first thorough soliton model study of the mixing phenomena between exotic states and radial excitations of ordinary baryons was performed in [20, 21]. The immediate consequences for the Θ^+ pentaquark were investigated in [22].

[6] Reference [19] reports a narrow structure around 1.65 GeV in η-photoproduction off the neutron.

The interplay between flavor rotational and radial excitations is studied by treating the soliton extension as a dynamical quantity, cf. Sect. 8.5. When we generalize (8.50) to flavor $SU(3)$, the Hamiltonian is essentially augmented by two terms,

$$H_{3\mathrm{fl}} = \frac{1}{2\beta(x)} \sum_{\alpha=4}^{7} R_\alpha^2 \quad \text{and} \quad H_{\mathrm{sb}} = s(x)\,[1 - D_{88}(A)]\ . \tag{9.7}$$

They originate from the collective rotations into strangeness direction and the flavor symmetry breaking, respectively. As in (8.49), the dependence on the scaling variable x is computed from the classical soliton. Since H_{sb} contains both the collective scaling and rotation variables explicitly, a simple separation *ansatz* as in the two-flavor problem is no longer possible. Rather a two-step program is pursued. First, a basis is constructed by diagonalizing the Hamiltonian without the D_{88} piece. At this stage, flavor representation mixing does not yet occur and the eigenstates are products $|\mu, n_\mu\rangle = |\mu\rangle|n_\mu\rangle$, where μ denotes the $SU(3)$ representation and n_μ is the corresponding radial (or breathing) quantum number. We denote the eigenvalues of this truncated Hamiltonian $\mathcal{E}_{\mu,n_\mu}$ and compute matrix elements of the full Hamiltonian:

$$H_{\mu,n_\mu;\mu',n'_{\mu'}} = \mathcal{E}_{\mu,n_\mu}\delta_{\mu,\mu'}\delta_{n_\mu,n'_{\mu'}} - \langle\mu|D_{88}(A)|\mu'\rangle\langle n_\mu|s(x)|n'_{\mu'}\rangle\ . \tag{9.8}$$

The linear combinations

$$|B, m\rangle = \sum_{\mu,n_\mu} C^{(B,m)}_{\mu,n_\mu}|\mu, n_\mu\rangle \tag{9.9}$$

diagonalize this Hamiltonian with energy eigenvalues $E_{B,m}$. Here B refers to the baryon quantum numbers while m counts its excitations. We have already presented model results for the baryons with non-exotic quantum numbers in Table 8.5. The corresponding results for the pentaquarks (Θ^+ and $\Xi_{3/2}$) are added in Fig. 9.1. Ignoring for the time being excited states that would be absent if the **27**-plet baryons were infinitely heavy (indicated by dashed lines) and counting the isospin degeneracy, there are 18 states predicted in the energy regime up to about 2 GeV. Thus, it is plausible that the $J^\pi = \frac{1}{2}^+$ baryons in the energy regime between 1.3 and 1.8 GeV may be viewed as members of the direct sum $\mathbf{8} \oplus \overline{\mathbf{10}}$ of $SU_{\mathrm{F}}(3)$ representations, modulo representation mixing induced by flavor symmetry breaking. These octet states would be (radial) excitations of the ordinary spin-$\frac{1}{2}$ baryons. In such an $\mathbf{8} \oplus \overline{\mathbf{10}}$ scenario, the Λ and Ξ resonances are pure octet while Θ^+ and $\Xi_{3/2}$ are pure anti-decuplet. Mixing can only occur for nucleon and Σ-type states. There are two approaches to arrange the excited baryons within such a direct sum. In [23], a diquark picture has been adopted that leads to an ideal mixing between baryons of identical quantum numbers of the **8** and $\overline{\mathbf{10}}$ representations such that the eigenstates have minimal or maximal strangeness content. Then, the octet nucleon and the anti-decuplet nucleon (N' in Fig. 6.3) mix to build eigenstates

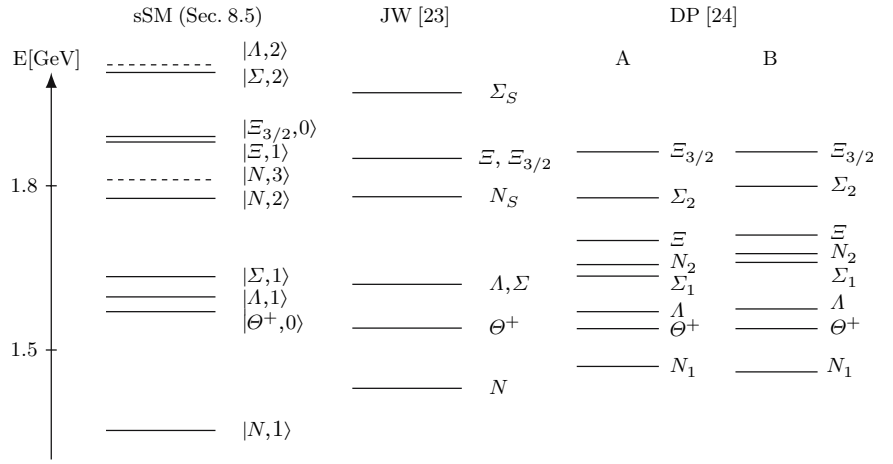

Fig. 9.1. Predicted spectra of baryons with $J = \frac{1}{2}$ in various models for pentaquarks. For the non-exotic states, the model results are taken from Table 8.5 with the physical nucleon. JW denotes a calculation within the diquark model with parameters $M_0 = 1.44\,\mathrm{GeV}$, $m_\mathrm{s} = 0.11\,\mathrm{GeV}$ and $\alpha = 0.06\,\mathrm{GeV}$ in the mass formula of [23]. In columns A and B, the results for the two scenarios of [24] are shown. We have adopted the notation used in the respective papers

with the quark structure $uud(\bar{u}u)$ and $uud(\bar{s}s)$, modulo their isospin partners. The baryon mass formula developed in [23] essentially counts the number of strange quarks and anti-quarks of the considered resonance. In [24], the $\mathbf{8} \oplus \overline{\mathbf{10}}$ decomposition was taken as starting point. For these octet and anti-decuplet states, the pattern of flavor symmetry breaking was adopted from the first-order calculation in soliton models. Additionally, it was assumed that $\Xi(1690)$—whose spin–parity quantum numbers are yet to be determined [25]—was the octet partner of $\Lambda(1600)$ to estimate the octet mass parameters and fix the anti-decuplet mass parameters from $\Theta^+(1535)$ and $\Xi_{3/2}(1862)$. With that input, the authors [24] computed the mixing angle between the $\mathbf{8}$ and $\overline{\mathbf{10}}$ representations and predicted so far unobserved nucleon and Σ resonances in the $1650 - 1810\,\mathrm{MeV}$ region. In Fig. 9.1, we compare the mass spectra of these two $\mathbf{8} \oplus \overline{\mathbf{10}}$ scenarios with the present model calculation. Surprisingly, the spectra obtained in the current model calculation and that of the ideal mixing diquark scenario are very similar. The most apparent similarity is the (almost) degeneracy of the $\Xi_{3/2}$ and the first-excited Ξ. The model of [23] also has degenerate Λ and Σ states. In the present approach, such a degeneracy is also indicated but not very pronounced. Furthermore, both treatments yield the second-excited Σ way above the $\Xi_{3/2}$ as well as a large gap between the first-exited Σ and the second-exited nucleon. The most obvious difference in the analysis of [24] is the large gap between Ξ and $\Xi_{3/2}$, with the second-excited Σ sitting in between. For that conclusion, it was crucial to assume that the $\Xi(1690)$ forms an $SU(3)$ multiplet with the $\Lambda(1600)$ that has $J^\pi = \frac{1}{2}^+$.

If this assumption was true, we would expect such a Ξ state in quark model calculations. However, in that model, the first-excited Ξ with $J^\pi = \frac{1}{2}^+$ shows up significantly higher, at about 1850 MeV [26], i.e., similar to the present prediction for $|\Xi, 1\rangle$, cf. Table 8.5. As already argued in Sect. 8.5, it seems more plausible to assign $J^\pi = \frac{1}{2}^+$ to $\Xi(1950)$.

In the nucleon channel, the model calculations yield the $m = 3$ state to be only about 40 MeV higher than the $m = 2$ state, i.e., still within the regime where the model is assumed to be applicable. This is interesting because data analysis [27, 28] suggests that there might exist more than only one nucleon resonance in the concerned energy region.

Although the spectrum in the present model turns out to be similar to the diquark scenario, the mixing pattern is considerably more complicated than an ideal direct sum $\mathbf{8} \oplus \overline{\mathbf{10}}$. In Table 9.2, we give the mixing in the form of the probabilities

$$P_\mu = \sum_{n_\mu} \left[C^{(B,m)}_{\mu,n_\mu} \right]^2 \tag{9.10}$$

that sum the squared amplitudes within a given $SU(3)$ multiplet. In the $\mathbf{8} \oplus \overline{\mathbf{10}}$ scenarios of [23, 24], both the $|\Lambda, 1\rangle$ and the $|\Xi, 1\rangle$ would be pure octet states. In the present model calculation, we find, however, that there is significant admixture of the partners from the **27**-plet, at the order of 40% in P_μ. Furthermore, the states $|N, 1\rangle$ and $|N, 2\rangle$ as well as $|\Sigma, 1\rangle$ and $|\Sigma, 2\rangle$ are not simple linear combinations of the corresponding octet and anti-decuplet states but contain sizable contributions from their partners in the **27**-plet. In [23], the mixing pattern for the **8** and $\overline{\mathbf{10}}$ states is ideal for the strangeness content, i.e., N and Σ have minimal strangeness content while it is maximal for N_S and Σ_S.

Table 9.2. Mixing pattern as measured by the probabilities P_μ, (9.10), for the low-lying $J^\pi = \frac{1}{2}^+$ baryons and the states shown in Fig. 6.3

B, m	$\mu = \mathbf{8}$	$\mu = \overline{\mathbf{10}}$	$\mu = \mathbf{27}$	$\mu = \overline{\mathbf{35}}$	$\mu = \mathbf{64}$
$\|N, 0\rangle$	0.87	0.06	0.05	0.01	0.00
$\|N, 1\rangle$	0.59	0.15	0.16	0.05	0.03
$\|N, 2\rangle$	0.12	0.68	0.10	0.05	0.04
$\|N, 3\rangle$	0.57	0.17	0.08	0.12	0.03
$\|\Lambda, 0\rangle$	0.93	–	0.06	–	0.00
$\|\Lambda, 1\rangle$	0.58	–	0.34	–	0.07
$\|\Lambda, 2\rangle$	0.58	–	0.23	–	0.17
$\|\Sigma, 0\rangle$	0.88	0.08	0.04	0.01	0.00
$\|\Sigma, 1\rangle$	0.37	0.33	0.15	0.10	0.03
$\|\Sigma, 2\rangle$	0.11	0.69	0.13	0.04	0.04
$\|\Xi, 0\rangle$	0.96	–	0.04	–	0.00
$\|\Xi, 1\rangle$	0.49	–	0.42	–	0.07
$\|\Theta^+, 0\rangle$	–	0.85	–	0.14	–
$\|\Xi_{3/2}, 0\rangle$	–	0.76	0.12	0.10	0.01

There is an important effect of mixing between radially excited octet and anti-decuplet nucleon states. We can compute transition magnetic moments of anti-decuplet to octet states by evaluating pertinent collective coordinate matrix elements as we did in (7.7). In the flavor symmetric limit, the proton transition moment vanishes while it is comparable to ordinary magnetic moments in the neutron channel [29], cf. last entry in Table 9.3. Once the breathing mode is elevated to a dynamical degree of freedom (and symmetry breaking is included), the computations become more involved. The coefficient functions V_i parametrically depend on the scaling variable and we have to sandwich them between the states $|n_\mu\rangle$. Subsequently, we project these matrix elements onto physical baryon states via the configuration mixing, (9.9). The numerical results for the scalar extended soliton model (Sect. 8.5) are listed in Table 9.3. For completeness, the predictions from that model for the magnetic moments of the ordinary spin-$\frac{1}{2}$ baryons are also included for which the now dynamical breathing mode produces the proper description of the empirically observed deviation from the U-spin symmetry, cf. discussion after (7.8). This is not surprising since, similarly to the slow rotator approach introduced in Sect. 6.5, the current treatment allows the soliton configuration to respond to flavor symmetry breaking. Here this feature is incorporated by $H_{\rm sb}$, (9.7), that generates differences in the radial parts of the spin-$\frac{1}{2}$ baryons. Apart from the problem of too small absolute magnetic moments (that seems common to most soliton models), we find agreement with the empirical data that is superior to the rigid rotator approach, cf. Table 7.1. So we should take seriously the predictions for the transition magnetic moments of the crypto-exotic nucleon-type baryons in the breathing mode treatment. They are shown in Table 9.3. Most importantly, we observe that the rigid rotator

Table 9.3. Magnetic moments in the breathing mode quantization scheme. Results are given in nucleon magnetons (n.m.) and normalized to the proton magnetic moment, $\mu_{\rm p}$. The upper and lower parts list the magnetic moments of the spin-$\frac{1}{2}$ ground state baryons and the magnetic moments of excited nucleons in the proton and neutron channels, respectively. Table adopted from [21, 30]

	p	n	Λ	Σ^+	Σ^-	Ξ^0	Ξ^-	$\Sigma^0 \to \Lambda$
μ (n.m.)	2.21	−1.84	−0.52	1.82	−0.94	−1.06	−0.41	−1.37
$\mu/\mu_{\rm p}$	1	−0.83	−0.24	0.82	−0.42	−0.48	−0.19	−0.62
$(\mu/\mu_{\rm p})_{\rm exp.}$	1	−0.68	−0.22	0.87	−0.42	−0.45	−0.25	−0.58

	proton		neutron	
m	μ (n.m.)	$\mu/\mu_{\rm p}$	μ (n.m.)	$\mu/\mu_{\rm p}$
1 (Roper)	−0.90	−0.41	0.89	0.40
2 ($N1710$)	−0.28	−0.13	−0.17	−0.08
3	−0.24	−0.11	−0.19	−0.09
$\|\mathbf{8},1\rangle \to \|\mathbf{8},0\rangle$	−0.53	−0.24	0.40	0.18
$\|\overline{\mathbf{10}},0\rangle \to \|\mathbf{8},0\rangle$	0.00	0.00	−0.62	−0.28

prediction, according to which the transition magnetic moment of the crypto-exotic proton is strongly suppressed compared to that of the neutron [29], is almost reversed. This must be attributed to sizable admixtures of radial octet excitations in the $N(1710)$ state.

Though this description of excited nucleons may be somewhat crude as it incorporates only a few modes collectively, we definitely learn that admixtures of radially excited states, against which there is no general argument, play a significant role. In particular, they drastically modify the predicted magnetic part of the transition to the ground state nucleon.

9.3 The Myth of the Narrow Pentaquark

Much of the ado around pentaquarks has been ignited by the prediction of a very narrow pentaquark in [2]. Here we will illustrate that (ill)famed calculation because we must address the question of whether it is a rigorous prediction of chiral soliton models. Only if it were, the non-observation of a narrow pentaquark (which be seems almost certain by now [3, 4]) would frame a severe problem for soliton models. The small width prediction seemed welcome to motivate exhaustive searches for pentaquarks. Only such narrow states could have escaped earlier searches and/or could be identified without laborious phase shift analysis of (new) data. In the course of this and the following sections, we will observe that the statement that chiral soliton models predict a *narrow* pentaquark baryon in the $S = +1$ channel essentially is a myth. This myth has been aggressively sold by some and, unfortunately, bought as truth by too many.

Of course, the non-observation of a narrow pentaquark does not completely forbid its existence. In that context, we recall indications for pentaquarks seen earlier in kaon–nucleon scattering [31, 32, 33]. At that time, the quantum numbers $P_{01}(1830)$, $P_{13}(1810)$, $D_{03}(1790)$ and $D_{15}(2070)$ were assigned to the structures seen in the $S = +1$ channel. In chiral soliton models, the latter can only be interpreted as a quadrupole excitation of a rotational ground state in the P_{01} channel. The structure observed in that channel is actually higher in energy than both the P_{13} and the D_{03} structures. It is thus suggestive that this P_{01} structure is not the rotational ground state whose mass should thus be significantly lower than 1790 MeV. This would be a further hint for a Θ^+ pentaquark with $M_\Theta \lesssim 1700\,\mathrm{MeV}$.

We have already learned in Sect. 8.3 that it is difficult to compute widths for hadronic decays of resonances in soliton models. The essential reason is that mesons and baryons are described by the same field variable, the chiral field U. This distinguishes them drastically from models with explicit baryon (B) and meson (Φ) fields that commonly have trilinear Yukawa interactions (the fields are multi-valued in flavor space):

$$\mathcal{L}_{\mathrm{int}} = \frac{g_{\phi BB'}}{M_B + M'_B}\, \bar{\Psi}_B \gamma_5 \gamma_\mu \left(\partial^\mu \Phi\right) \Psi_{B'} \,. \tag{9.11}$$

The derivative interaction reflects chiral symmetry and γ_5 the pseudoscalar nature of the lightest mesons. With this interaction, the computation of decay widths for the hadronic decay of the excited baryon (B') is standard:

$$\Gamma(B' \to B\Phi) = \frac{\overline{|\mathcal{M}|^2}}{8\pi M_B M_{B'}} \, |\boldsymbol{p}_\Phi| \,, \tag{9.12}$$

where $\mathcal{M}$ is the spin–flavor matrix element resulting from (9.11). The overbar denotes summing and averaging over spins. Since $\mathcal{M}$ is linear in both, the coupling $g_{\phi BB'}$ and the momentum of the final meson, $\boldsymbol{p}_\Phi$ (due to the pseudoscalar nature of Φ), we have $\Gamma \propto g^2_{\phi BB'} |\boldsymbol{p}_\Phi|^3$.

In soliton models, the situation is significantly different. Since the soliton is a stationary point of the action, there is no straightforward identification of an interaction which is linear in the asymptotic meson field and that provides the coupling constant $g_{\phi BB'}$. As discussed in Sect. 8.3, this subtlety in known as the Yukawa problem. Hence profound assumptions are necessary to make use of (9.12). The profound assumption often made in soliton models is to generalize the Goldberger–Treimann relation (GTR), (5.62), to the $SU(3)$ relatives of pions and nucleons:

$$\frac{1}{2} \, (M_B + M_{B'}) \, g_{\rm A}^{BB'} = f_\phi g_{\phi BB'} \,. \tag{9.13}$$

Certainly, one should doubt that this $SU(3)$ generalization is as fundamental as (5.62). After all, the latter only adheres to asymptotically stable states. The profound assumption then computes $g_{\rm A}^{BB'}$ as axial current transition matrix elements uses (9.13) to identify $g_{\phi BB'}$ and substitutes it into (9.12) to compute the decay width. In the rigid rotator approach, the axial current operator has the model independent from, cf. (7.16),

$$A_i^a = \sum_{k=1,2,3} A_{ik}^{(0)}(\boldsymbol{x}) D_{ak} + \sum_{\substack{k=1,2,3 \\ \alpha,\beta=4,\ldots,7}} A_{ik}^{(1)}(\boldsymbol{x}) \, d_{k\alpha\beta} D_{a\alpha} R_\beta + \sum_{k=1,2,3} A_{ik}^{(2)}(\boldsymbol{x}) \, D_{a8} R_k \tag{9.14}$$

up to omitted flavor symmetry breaking. The structure of the coefficient functions is $A_{ik}^{(m)}(\boldsymbol{x}) = A_1^{(m)}(r)\delta_{ik} + A_2^{(m)}(r)\hat{x}_i\hat{x}_k$. The $A_{1,2}^{(m)}(r)$ are radial functions through the profile function $F(r)$. It is legitimate to use isospin invariance and compute $g_{\rm A}$ as the nucleon matrix element $\langle 2A_3^3 \rangle$. Then (9.13) implies [2, 5]

$$g_{\pi NN} = \frac{7}{10} \left[G_0 + \frac{1}{2} G_1 + \frac{1}{14} G_2 \right]$$

with

$$G_m = -\frac{8\pi M_N}{3 f_\pi} \int_0^\infty {\rm d}r r^2 \left[A_1^{(m)}(r) + \frac{1}{3} A_2^{(m)}(r) \right] . \tag{9.15}$$

The relative coefficients stem from the nucleon matrix elements of the collective coordinate operators in (9.14). They are readily obtained from $SU(3)$

Clebsch–Gordan coefficients, e.g., $\langle p\uparrow|D_{33}|p\uparrow\rangle = -7/30$ (again omitting flavor symmetry breaking for simplicity). Generalizing the above result for $g_{\pi NN}$ to flavor $SU(3)$ yields coupling constants

$$G_{10} = G_0 + \frac{1}{2}G_1 \qquad \text{and} \qquad G_{\overline{10}} = G_0 - G_1 - \frac{1}{2}G_2 \tag{9.16}$$

that, respectively, measure the coupling of baryons from the decuplet (Δ) and the anti-decuplet (Θ^+) to those in the octet (nucleon, hyperons) via (9.13). These coupling constants enter the matrix element $\mathcal{M}$ and yield widths for hadronic baryon decays via (9.12): $\Gamma(\Delta \to N\pi) \propto G_{10}^2|\boldsymbol{p}_\pi|^3$ and $\Gamma(\Theta^+ \to NK) \propto G_{\overline{10}}^2|\boldsymbol{p}_K|^3$. The omitted constants of proportionality are merely kinematical factors. Model calculations [11, 34, 35] indicate that G_0 and G_1 are comparable. That is, significant cancellations cause $G_{\overline{10}}$ to be rather small. This has been the main argument for claiming a Θ^+ width of the order of only a few MeV, or even less. For example, [36] quotes a value as small as 2.3 MeV. The cancellations between G_0 and G_1 persist when the number (N_C) of color degrees of freedom is sent to infinity [37]. This completes the way of thinking about pentaquark decay widths put forward in [2, 5] and frequently adopted later on.[7] Yet a careful analysis shows that correcting the original computation of [2] for an intrinsic arithmetical error [22, 38][8] increases the estimate for $\Gamma(\Theta \to KN)$ to about 30 or 40 MeV, which is not so small anymore and thus less exciting.

Further subtleties doubt this GTR-based approach already afore we test it against incontrovertible results from the phase shift analysis:

- The classical field equations affect only the first part $\partial_i A_{ik}^{(0)} = \mathcal{O}\left(m_\pi^2\right)$. The last term ($A^{(2)}$) vanishes or is at least small because it essentially is the axial singlet matrix element. On the other hand, $\partial_i A_{ik}^{(1)}$ is not part of any equation of motion. Hence, the axial current computed solely from the classical profile functions violates PCAC (Induced kaon fields were considered as an early attempt to solve the problem, cf. Appendix C in [11]). As a consequence, the use of GTR in $SU(3)$ soliton models is questionable because a major entry is not met.
- The above derivation only involves the classical soliton and there is no reference to asymptotic meson states in the decay products. In two-flavor soliton models the GTR arises from the long-range behavior of the soliton profile [41] and has been identified from the one-pion exchange contribution to the nucleon–nucleon interaction; see also (5.60) and Sect. 10.3.

  However, this process does not require asymptotic pion states. Also, that argument strongly relies on pions being massless. For $m_\pi > 0$, g_A cannot be read off from the long range behavior and thus not related to $g_{\pi NN}$.

[7] Many additional references on this approach can be traced from `http://www.rcnp.osaka-u.ac.jp/~hyodo/research/Thetapub.html`.

[8] The interested reader may want to survey [39, 40] for a striking example for reinterpretation of reproducible errors.

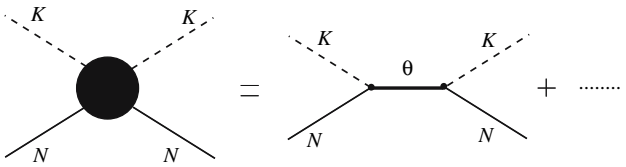

Fig. 9.2. Θ^+ resonance exchange buried in kaon–nucleon scattering

It is thus not surprising that $SU(3)$ Skyrme model calculations severely fail to reproduce GTR when $g_{\pi NN}$ is extracted from the long-range behavior of the soliton [34]. Evidently, it is not possible to directly map soliton models onto the Yukawa model. Hence, any soliton model motivated computation of pentaquark (and probably any other excited baryon) widths that is based on the identification of an effective Yukawa coupling constant must be doubted.

In the next section, we will describe the soliton model approach to kaon–nucleon scattering in the spin–isospin channel with pentaquark quantum numbers. As in experiment, that process should reflect all information about pentaquark widths. A decisive feature of that approach is its consistency with the large-N_C limit, in which the model prediction for the scattering data is unambiguously known from the adiabatic approximation, cf. Sect. 8.1. Since that treatment is quite technical, we will state a main conclusion already here: only a *single* collective coordinate operator contributes to the Θ^+ width function, at least in the flavor symmetric limit. This definitely proves incorrect the cancellation scenario for $G_{\overline{10}}$ and the resultant small width prediction. Earlier we asked whether or not the small width prediction would be a rigorous chiral soliton model prediction. Given the precedent discussion, we obviously must deny this question.

Though unlikely, there is still a scenario for a narrow pentaquark. It could couple weakly to a bound state, e.g., in the vector meson channel. This mechanism is quite general and this possibility can also be inferred from soliton model studies as, e.g., Fig. 7.5a in [42], though that concerns a different process.

9.4 Rigid Rotator at Arbitrary N_C

We now want to work toward a better understanding of the decay $\Theta \to KN$ within chiral soliton models. This is actually a subprocess of kaon–nucleon scattering in the $S = +1$ channel as depicted in Fig. 9.2. In Sect. 8.1, we have learned that we can compute the scattering data reliably to $\mathcal{O}\left(N_C^0\right)$ within a soliton model. Here we will discuss the spectrum of the rigid rotator at arbitrary N_C to establish that the mass gap between the Θ^+ and the nucleon is $\mathcal{O}\left(N_C^0\right)$ and thus non-zero in the large-N_C limit. Hence, the Θ^+ is unstable for $N_C \to \infty$ and we should be able to extract its width from scattering computations, at least for $N_C \to \infty$. That will be subject of the next section.

In Sect. 6.6, we found that the BSA is exact for $N_C \to \infty$. In this limit, the RRA should therefore reproduce the BSA results when the fluctuations are constrained to the collective modes of the soliton, (6.49), (6.50) and (6.51). We will first explore the RRA findings that emerge from the use of (D.9) with $Y_R = N_C/3$ analytically in the flavor symmetric case and then present numerical results for the general case.

In (6.12), (6.13) and (6.14), we have derived the general conditions for the eigenstates within the RRA when symmetry breaking is ignored. Equation (6.11) describes the corresponding spectrum. Now we fix $B = 1$ and arrange these states conveniently according to increasing triality, t, that has been defined in (6.12). For $t = 0$ they are

$$(p,q) = \left(2J, \frac{N_C - 2J}{2}\right), \tag{9.17}$$

where $J = \frac{1}{2}, \frac{3}{2}, \ldots, \frac{N_C}{2}$ ($= m_{\max}$ in the notation of Sect. 6.2) are the allowed spin eigenvalues, i.e., $\sum_{i=1}^{3} \langle R_i^2 \rangle = J(J+1)$. From (6.11), we compute the corresponding energies

$$E_0 = E_{cl} + \frac{J(J+1)}{2\alpha^2} + \frac{N_C}{4\beta^2}\,. \tag{9.18}$$

This coincides with the $SU(2)$ mass formula, (5.19), up to an additive constant for nucleon and Δ-type states. For $t = 1$ we find

$$\begin{aligned} (p,q) &= \left(2J \mp 1, \frac{N_C + 3}{2} - \frac{2J \mp 1}{2}\right), \\ E_\mp &= E_{cl} + \frac{J(J+1)}{2\alpha^2} + \frac{2N_C + 4 \mp (2J+1)}{4\beta^2}\,, \end{aligned} \tag{9.19}$$

with $J = \frac{1}{2}, \frac{3}{2}, \ldots, \frac{N_C}{2} + 1$.

The lowest lying multiplets with spins $J = \frac{1}{2}$ and $J = \frac{3}{2}$ are

$$\begin{aligned} J = \frac{1}{2} : (p,q) &= \left(1, \frac{N_C - 1}{2}\right), \left(0, \frac{N_C + 3}{2}\right), \ldots = \text{“}\mathbf{8}\text{”}, \text{“}\overline{\mathbf{10}}\text{”}, \ldots \\ J = \frac{3}{2} : (p,q) &= \left(3, \frac{N_C - 3}{2}\right), \left(2, \frac{N_C + 1}{2}\right), \ldots = \text{“}\mathbf{10}\text{”}, \text{“}\mathbf{27}\text{”}, \ldots . \end{aligned} \tag{9.20}$$

In each case, the first representation stems from (9.17) while the second ones are associated with (9.19). The numbers in quotation marks label the dimensionalities of the representations for $N_C = 3$. The above assignments are unique in soliton models and so are the flavor quantum numbers attributed to the lowest lying baryon states within the multiplets. This is inferred from the fact that these assignments minimize the energy functional. For example, for large N_C the symmetry breaking term contributes

$$\frac{\gamma}{2}\langle 1 - D_{88} \rangle \to \frac{\gamma}{2}\left(1 - \frac{3}{N_C} Y\right) = -\frac{3\gamma}{2N_C} S \qquad (S \le t) \tag{9.21}$$

to the energy functional if symmetry breaking was treated in first-order perturbation. For finite N_C, this generalizes to the fact that symmetry breaking causes the masses of baryons within a multiplet to decrease with increasing strangeness. For $t = 0$, we therefore obtain the lightest $J = \frac{1}{2}$ baryon, the "nucleon" with zero strangeness and isospin $I = \frac{1}{2}$ and the lightest $J = \frac{3}{2}$ baryon, the "Δ" with zero strangeness and isospin $I = \frac{3}{2}$. For $t = 1$, the lowest lying "pentaquarks" with $J = \frac{1}{2}$ and $J = \frac{3}{2}$ carry strangeness $S = +1$ and isospins $I = 0$ and $I = 1$, respectively. For finite symmetry breaking, mixing with higher dimensional multiplets occurs. Although such non-linear effects may not be omitted, the spin–flavor assignments are unaffected.

The lowest lying pentaquarks with $S = +1$ dwell in $t = 1$ representations. For these pentaquarks, the two mass formulas (9.19) refer to the spin–isospin relations $I = J \mp \frac{1}{2}$. It is straightforward to derive the corresponding energies

$$E_{\mp} = M + \frac{J(J+1)}{2\alpha^2} + \frac{N_C}{2\beta^2} + \frac{1}{2\beta^2}\left[I(I+1) - J(J+1) + \frac{9}{4}\right] . \qquad (9.22)$$

The terms $\mathcal{O}(1/N_C)$ exactly match[9] those in (6.45) when equating those contributions to the hyperfine energies that are of quartic order in the fluctuations to $\frac{9}{8\beta^2}$. Even more, we may compute the mass difference between the nucleon (in "$\mathbf{8}$") and pentaquarks with $I = 0$ and $J = \frac{1}{2}$ (in "$\overline{\mathbf{10}}$")

$$E_{\overline{\mathbf{10}}} - E_{\mathbf{8}} = \frac{N_C + 3}{4\beta^2} , \qquad (9.23)$$

which coincides with ω_Θ (6.50 with $\gamma = 0$) when $N_C \to \infty$, as it should. Thus, we conclude that the BSA and RRA are consistent when flavor symmetry breaking is omitted. Note that the above mass difference acquires a factor 2 for $N_C = 3$.

For the physical case of non-zero flavor symmetry breaking, a perturbative treatment seems tempting because it reproduces the Gell-Mann–Okubo mass relations [43, 44] in the RRA for $N_C = 3$ [45]. We already argued in the context of (6.49) and (6.50) that the perturbation series in γ does not converge for the BSA. Many pentaquark studies in the RRA treated flavor symmetry breaking perturbatively to first or (at best) to second order [2, 5].[10] This seems at odds with the BSA. Also, the Gell-Mann–Okubo relations are not reproduced in the BSA [11]. Hence, we have to solve the eigenvalue problem

$$\left\{M + \frac{J(J+1)}{2\alpha^2} + \frac{R_\alpha^2}{2\beta^2} + \frac{1}{2}\gamma\,(1 - D_{88})\right\}\Psi = E\Psi \qquad (9.24)$$

together with $R_8\Psi = \frac{N_C}{2\sqrt{3}}\Psi$ (numerically) exactly. For $N_C = 3$, we have discussed that scenario in Sect. 6.4. It can be straightforwardly generalized by

[9] Without symmetry breaking, we have $\omega_\Theta = N_C/4\beta^2$ and thus $1 - \chi_+ = \alpha^2/\beta^2$ in (6.51).

[10] In the RRA to pentaquarks, symmetry breaking was treated exactly in [8, 13, 22, 46].

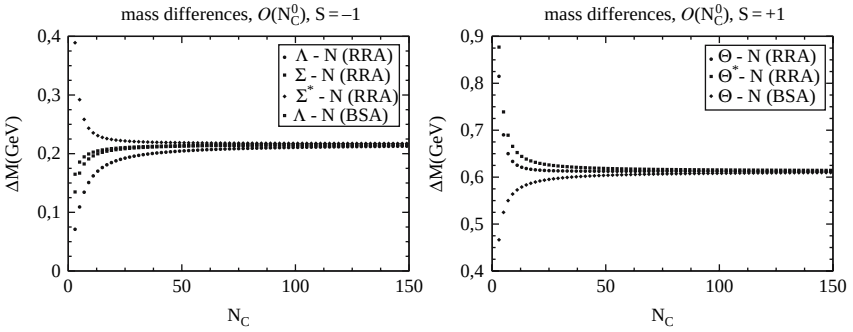

Fig. 9.3. Mass differences at $\mathcal{O}(N_{\rm C}^0)$ computed in the Skyrme model as functions of $N_{\rm C}$. In the RRA, they are the corresponding differences of the eigenvalues in (9.24), while in the BSA they are extracted from (6.45). *Left panel* $\Delta S = -1$; *right panel* $\Delta S = +1$. Model parameters are chosen to reproduce the Δ–N mass difference at $N_{\rm C} = 3$

putting $Y_{\rm R} = 2R_8/\sqrt{3} = N_{\rm C}/3$ in (D.9), together with the linear $N_{\rm C}$ dependencies of the functionals α^2, β^2 and γ via $\alpha^2 \to \alpha^2(N_{\rm C} = 3)N_{\rm C}/3$, etc. The only condition on $N_{\rm C}$ is that it must be taken odd. For typical model parameters, we display the resulting mass differences in Figs. 9.3 and 9.4. In Fig. 9.3, we concentrate on mass differences that scale like $\mathcal{O}(N_{\rm C}^0)$, i.e., between baryons whose strangeness quantum numbers differ by one unit. As $N_{\rm C} \to \infty$, the BSA for fluctuations in the rotational subspace predicts ω_Λ and ω_Θ for those mass differences regardless of spin and isospin. Obviously this is matched by the RRA. In Fig. 9.4, we display the mass differences that scale like $\mathcal{O}(1/N_{\rm C})$, i.e., we compute the hyperfine splitting in both approaches. In doing so, we always consider baryons with identical strangeness since then the ordering ambiguities and omissions from $\mathcal{O}(\eta_\alpha^4)$ terms in the BSA cancel. Again, perfect

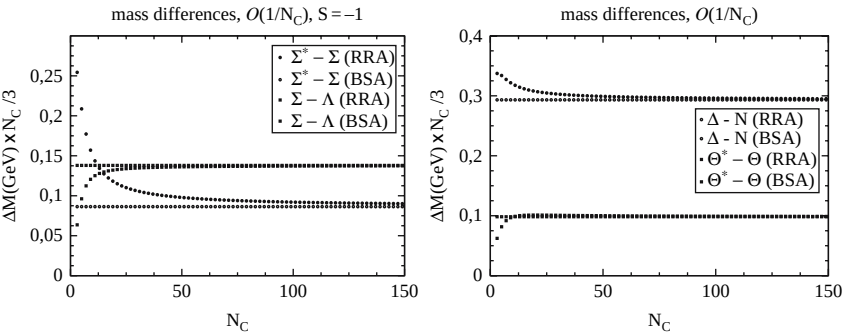

Fig. 9.4. Mass differences at $\mathcal{O}(1/N_{\rm C})$ computed in the Skyrme model as functions of $N_{\rm C}$. *Left panel*: baryons with strangeness $S = 0, 1$; *right panel* $S = -1$. See also caption of Fig. 9.3

agreement between the two approaches is observed for $N_C \to \infty$. However, at $N_C = 3$, sizable $1/N_C$ corrections occur that cannot be accounted for by the BSA.

In Sect. 9.6, we will employ the eigenfunctions of (9.24) to compute matrix elements of collective coordinate operators for arbitrary odd N_C and non-zero symmetry breaking.

9.5 Solution to the Yukawa Problem

The discussion in Sect. 9.3 showed that chiral soliton models improbably describe pentaquark widths of the order of only a few MeV. Yet the intensive discussion of exotic baryons has paved a way toward solving the long-standing Yukawa problem that we first encountered in Sect. 8.3. As a matter of fact, it concerns the description of all hadronic decays of excited baryons in soliton models. So, at last, the arguable prediction of very narrow pentaquarks nevertheless turned into a fortune for soliton models. We will explain that solution in this section. We will give explicit formulas for the specific case of flavor symmetry. For the general case, which is more laborious and thoroughly discussed in [47], we will confine ourselves to the presentation of numerical results. The main result will be the momentum-dependent width function for the pentaquark decay that supercedes the approach of [2] that was discussed in Sect. 9.3 .

The bold statement of having solved the Yukawa problem is based on the fact that we have available a litmus test in the pentaquark channel. This test can be inferred from (9.23). In contrast to the intensively discussed Δ resonance (Sect. 8.3), the Θ^+ maintains a non-zero mass gap to the nucleon when N_C is sent to infinity. Hence, its width must not vanish for $N_C \to \infty$: $\Gamma(\Theta \to KN) = \mathcal{O}\left(N_C^0\right)$. Simultaneously, we know that the adiabatic approximation (Sect. 8.1) is exact at this order. So we merely have to extract the properties from the phase shifts from the solutions to (6.41) via the recoupling scheme from Appendix F. This is simple in the Θ^+ channel because only the intrinsic P-wave channel for kaon–nucleon scattering is affected. The corresponding Skyrme model result for the phase shift is shown as the full line in Fig. 9.5. We immediately observe that no clear resonance structure is visible; the phase shift hardly reaches $\pi/2$. The absence of such a resonance has previously lead to the criticism that no bound pentaquark existed in the large N_C limit and that it were a pure artifact of the RRA [48, 49, 50, 51]. Though this conclusion is premature, it indicates that the extraction of Θ^+ properties from the phase shift is a formidable task. Essentially, we have to disentangle the contribution from the collective modes to this phase shift. To do so, we need to incorporate the dynamical coupling between the small amplitude fluctuations and the collective modes. This induces couplings that are of subleading order in the $1/N_C$ expansion. Actually, (9.23) shows that they must be important as the resonance energy changes by a factor two in

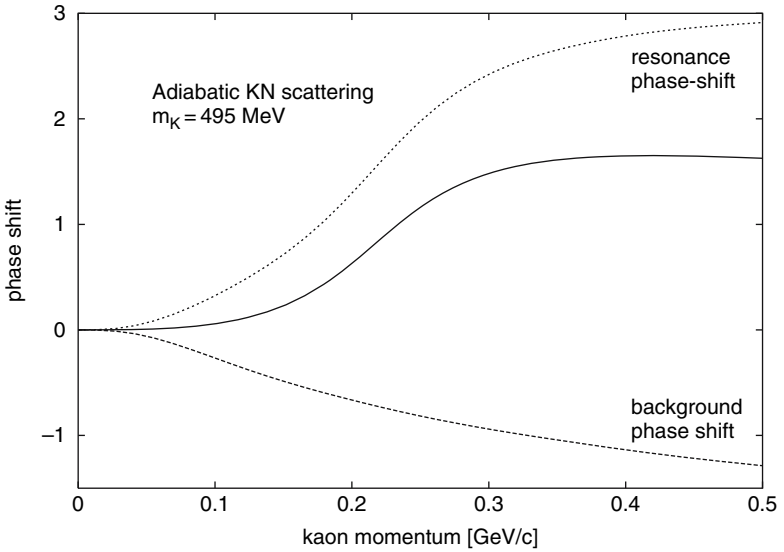

Fig. 9.5. Skyrme model prediction for the phase shift in the $S = +1$ channel (*full line*). The *long–dashed line* (background) gives the phase shift when the fluctuations are constrained to be orthogonal to the rigid rotation, cf. (9.35), and the *short-dashed line* is the difference between the full and long–dashed line, *the resonance phase shift*

between $N_{\rm C} = 3 \ldots \infty$. At the end, we have to apply the litmus test: in the limit $N_{\rm C} \to \infty$, our treatment *must* reproduce the phase shift represented by the full line in Fig. 9.5.

We consider (8.1)

$$U(\boldsymbol{x},t) = A(t)\sqrt{U_0(\boldsymbol{x})}\exp\left[\frac{\mathrm{i}}{f_\pi}\lambda_\alpha\widetilde{\eta}_\alpha(\boldsymbol{x},t)\right]\sqrt{U_0(\boldsymbol{x})}A^\dagger(t)\,, \tag{9.25}$$

for dynamical, i.e., time-dependent collective rotations, $A(t) \in SU(3)$. The fluctuations $\widetilde{\eta}_\alpha$ dwell in the intrinsic system as they rotate along with the soliton. These modes differ from the η_α in Sect. 6.6 through the coupling to $A(t)$. An immediate problem arises for the *ansatz* (9.25): dynamical flavor rotational modes are contained in both $A(t)$ and $\widetilde{\eta}_\alpha$. These double counting effects are reflected by the linear relation ($x = \{t, \boldsymbol{x}\}$)

$$R_\alpha := -\frac{\partial L}{\partial\Omega_\alpha} = \sqrt{\beta^2}\int \mathrm{d}^3r\, z^\alpha_\beta(\boldsymbol{x})\left[\frac{\delta L}{\delta\dot{\widetilde{\eta}}_\alpha(x)} - \frac{2}{\sqrt{3}}\lambda(r)f_{8\beta\gamma}\widetilde{\eta}_\gamma(x)\right] \tag{9.26}$$

between the conjugate momenta. The radial function $\lambda(r) = \frac{N_{\rm C}}{4f_\pi^2}B_0(r)$ is proportional to the baryon density (4.51), and stems from the Wess–Zumino term. Furthermore,

$$z^\alpha_\beta(\boldsymbol{x}) = \frac{2f_\pi}{\sqrt{\beta^2}} \sin\frac{F(r)}{2}\, \hat{x}_i f_{i\beta\alpha} = \frac{z(r)}{\sqrt{\pi}}\, \hat{x}_i f_{i\beta\alpha} \tag{9.27}$$

is the properly normalized collective mode wave function written in the flavor basis, cf. (6.46). The first term in square brackets in (9.26) results from the chain rule applied to the time derivative of $U(\boldsymbol{x}\,,t)$ and will emerge for any local chiral Lagrangian. The second term is unexpected and reflects the nonlocal structure of the Wess–Zumino term.

To eliminate double counting effects, we demand that the momenta conjugate to the collective coordinates do not contain any fluctuation parts: $R_\alpha = -\beta^2\Omega_\alpha$. The linear relation, (9.26), then translates into the *primary constraints*

$$\Psi_\alpha = \int \mathrm{d}^3r\, z^\alpha_\beta(\boldsymbol{x}) \left[\widetilde{\Pi}_\beta(x) - \frac{2}{\sqrt{3}}\lambda(r) f_{8\beta\gamma}\widetilde{\eta}_\gamma(x)\right] = 0\,. \tag{9.28}$$

The momenta $\widetilde{\Pi}_\beta$ differ from those that are conjugate to $\widetilde{\eta}_\alpha$ exactly by the collective part,

$$\Pi_\beta = \frac{\partial L}{\partial\dot{\widetilde{\eta}}_\alpha} = \widetilde{\Pi}_\beta - \sqrt{\beta^2}\Omega_\beta z^\alpha_\beta(\boldsymbol{x}) f(r)\,, \tag{9.29}$$

where $f(r)$ is the metric function from (6.41). The induced *secondary constraints* require the fluctuations to be orthogonal to the collective mode

$$\chi_\alpha = \int \mathrm{d}^3r\, z^\alpha_\beta(\boldsymbol{x})\, f(r)\widetilde{\eta}_\beta(x) = 0\,. \tag{9.30}$$

These constraints are linear functionals of the fluctuations and their conjugate momenta. They satisfy the Poisson brackets $\{\Psi_\alpha, \chi_\beta\} = \delta_{ab}$ so that $\widetilde{\Pi}_\alpha$ and $\widetilde{\eta}_\beta$ are conjugate to each other in the constrained subspace [52]. We then construct the Hamiltonian by Legendre transforming, adding the constraints with Lagrange multipliers α_α and β_α

$$H = -L + \Omega_\alpha \frac{\partial L}{\partial\Omega_\alpha} + \int \mathrm{d}^3r\, \frac{\delta L}{\delta\dot{\widetilde{\eta}}_\alpha(x)}\, \dot{\widetilde{\eta}}_\alpha(x) + \alpha_\alpha\Psi_\alpha + \beta_\alpha\chi_\alpha \tag{9.31}$$

and expressing it as functions of the constrained fluctuations

$$\begin{aligned} H = {} & \frac{R^2_\alpha}{2\beta^2} + \frac{1}{2}\int \frac{\mathrm{d}^3r}{f(r)} \left[\widetilde{\Pi}_\alpha(x) + \frac{2}{\sqrt{3}}\lambda(r) f_{8\alpha\beta}\, \widetilde{\eta}_\beta(x)\right]^2 \\ & + \frac{R_\alpha}{\sqrt{\beta^2}} \int \mathrm{d}^3r\, z^\alpha_\beta(\boldsymbol{x}) \left[\widetilde{\Pi}_\alpha(x) + \frac{2}{\sqrt{3}}\lambda(r) f_{8\alpha\beta}\, \widetilde{\eta}_\beta(x)\right] \\ & + \frac{1}{2}\int \mathrm{d}^3r\, \widetilde{\eta}_\alpha(x)\, h^2_{\alpha\beta}(\boldsymbol{x})\, \widetilde{\eta}_\beta(x) + \alpha_\alpha\Psi_\alpha + \beta_\alpha\chi_\alpha\,. \end{aligned} \tag{9.32}$$

From this Hamiltonian, we derive the canonical equations of motion and determine the Lagrange multipliers from the requirement that the constraints are fulfilled for all times, i.e., $\dot{\Psi}_\alpha = 0$ and $\dot{\chi}_\alpha = 0$:

$$\alpha_\alpha = -\frac{R_\alpha}{\sqrt{\beta^2}} - \frac{4}{\sqrt{3}} \int \mathrm{d}^3 r\, \lambda(r) z_\beta^\alpha(\boldsymbol{x}) f_{8\beta\gamma} \widetilde{\eta}_\gamma(x) \quad \text{and} \quad \beta_\alpha = -\frac{2}{\sqrt{3}}\, \omega_0\, f_{8\alpha\beta}\alpha_\beta\,, \tag{9.33}$$

with ω_0 given in (6.47). Terms that are linear in both, the collective and fluctuating modes, emerge not only explicitly but also implicitly through the Lagrange multipliers (9.33). We collect all these terms in the interaction Hamiltonian,

$$\begin{aligned} H_{\mathrm{int}} &= \frac{2R_\alpha}{\sqrt{3\beta^2}} f_{8\beta\gamma} \int \mathrm{d}^3 r\, z_\beta^\alpha(\boldsymbol{x}) \left[2\lambda(r) - \omega_0 f(r)\right] \widetilde{\eta}_\gamma(x) \\ &= \frac{2}{\sqrt{4\pi\beta^2}}\, d_{i\alpha\beta}\, R_\beta \int \mathrm{d}^3 r\, z(r) \left[2\lambda(r) - \omega_0 f(r)\right] \hat{x}_i \widetilde{\eta}_\alpha(x,t)\,, \end{aligned} \tag{9.34}$$

where we substituted (6.46) and (9.27) and utilized identities for products of $SU(3)$ structure constants. This completes the derivation of the coupling between the collective and fluctuating modes in the Skyrme model when flavor symmetry breaking is omitted. The analogous derivation in the general case is given in Appendix A of [47].

The second part of (9.34) reveals that only the P-wave channel of the strange fluctuations is concerned. In the discussion of the equation of motion, we therefore return to the single radial function $\widetilde{\eta}(r)$ defined in analogy to (6.40). This radial function is subject to an inhomogeneous linear differential equation. We first discuss the solution $\overline{\eta}$ to the homogeneous part of that differential equation (still assuming flavor symmetry):

$$\begin{aligned} &h^2\overline{\eta}(r) + \omega \left[2\lambda(r) - \omega f(r)\right] \overline{\eta}(r) \\ &\qquad = -\left[2\lambda(r) - (\omega + \omega_0)\, f(r)\right]\, z(r) \int_0^\infty r'^2 \mathrm{d}r' z(r') 2\lambda(r') \overline{\eta}(r')\,. \end{aligned} \tag{9.35}$$

This equation differs from (6.41) only by the non-local term on the right-hand side. It enforces the constraint, (9.30), as can easily be verified by multiplying with $z(r)$ and integrating over space (recall that $h^2 z(r) = 0$ and $\int \mathrm{d}r r^2 z^2 \lambda = \omega_0/2$). The phase shift extracted from $\overline{\eta}$ is shown as the *background* phase shift in Fig. 9.5. Obviously, it is repulsive such that the difference between the total phase shift and this background phase shift shows a resonant behavior. This behavior incipiently indicates that the pentaquark channel indeed resonates in the large-N_{C} limit.

For large N_{C}, $\widetilde{\eta}$ must carry the same phase shift as η . Hence, the effects of H_{int} on $\overline{\eta}$ must be to reincorporate the resonance, at least for $N_{\mathrm{C}} \to \infty$. We will now demonstrate exactly that. Essentially, we have to integrate out the collective modes in the sector relevant to kaon–nucleon scattering. For zero total isospin and total spin $\frac{1}{2}$, only Λ and Θ^+ couple as intermediate states. Standard second-order perturbation theory yields

$$\frac{\left|\langle \Theta | H_{\mathrm{int}} | (KN)_{I=0} \rangle\right|^2}{\omega_\Theta - \omega} + \frac{\left|\langle \Lambda | H_{\mathrm{int}} | (KN)_{I=0} \rangle\right|^2}{\omega_\Lambda + \omega}\,, \tag{9.36}$$

where $\omega_{\Theta,\Lambda}$ are the corresponding, N_C-dependent, excitation energies extracted from the RRA Hamiltonian, (9.24) (in the flavor symmetric case they are $\omega_\Theta = \omega_0$ and $\omega_\Lambda = 0$). The signs in the propagators reflect the opposite strangeness between Λ and Θ^+. The kaon states in (9.36) refer to those in the laboratory frame while $\widetilde{\eta}$ rotates along with the soliton in the intrinsic frame. The corresponding transformation, (F.3), brings an additional D-function into the game. At the end, the matrix element becomes

$$\begin{aligned}\langle\Theta|H_{\rm int}|(KN)_{I=0}\rangle &= X_\Theta\sqrt{\frac{N_C}{4\pi\beta^2}}\,\frac{k}{\sqrt{\omega}}\int_0^\infty {\rm d}r r^2 z(r)\left[2\lambda(r)-\omega_0 f(r)\right]\widetilde{\eta}(r)\\ &= X_\Theta\sqrt{\frac{N_C}{4\pi\beta^2}}\,\frac{k}{\sqrt{\omega}}\int_0^\infty {\rm d}r r^2 z(r) 2\lambda(r)\widetilde{\eta}(r)\,,\end{aligned} \tag{9.37}$$

where the second relation recognizes the constraint (9.30). The collective coordinate matrix element

$$X_\Theta := \sqrt{\frac{32}{N_C}}\langle\Theta^+|d_{3\alpha\beta}D_{+\alpha}R_\beta|n\rangle \tag{9.38}$$

is normalized such that $\lim_{N_C\to\infty} X_\Theta = 1$ in the flavor symmetric case. Since the analogously defined X_Λ vanishes under the same conditions, we will ignore the Λ channel for the time being. Quantum mechanically we consider a state that lies in the continuum. This is the structure of the Lee model [53, 54, 55] and we readily find the width arising from coupling the state to the continuum via $H_{\rm int}$,

$$\Gamma(k) = 2\pi\frac{\omega}{k}\left|\langle\Theta|H_{\rm int}|(KN)_{I=0}\rangle\right|^2 = 2k\omega_0 X_\Theta^2\left|\int_0^\infty r^2{\rm d}r\, z(r)2\lambda(r)\overline{\eta}(r)\right|^2 . \tag{9.39}$$

Note the appearance of $\overline{\eta}$ rather than $\widetilde{\eta}$ as in (9.37) because $H_{\rm int}$ is a perturbation to the homogeneous problem that is solved by $\overline{\eta}$.

Exactly the same width can be attributed to an additional separable potential that is induced by the exchanged particles. In reaction theory, we get the width function from the (real) reaction matrix R via

$$-k\int_0^\infty {\rm d}r r^2\int_0^\infty {\rm d}r' r'^2 R(\omega;r,r') = \tan\left(\delta_{\rm R}(k)\right) = \frac{\Gamma(\omega)/2}{\omega_\Theta-\omega+\delta E(\omega)}\,, \tag{9.40}$$

with the pole shift ($\omega_q = \sqrt{q^2+m_K^2}$)

$$\delta E(\omega) = \frac{1}{2\pi\omega}\,\mathcal{P}\int_0^\infty q{\rm d}q\left[\frac{\Gamma(\omega_q)}{\omega-\omega_q}+\frac{\Gamma(-\omega_q)}{\omega+\omega_q}\right]. \tag{9.41}$$

Even though $\omega_\Theta = \omega_0$ for the considered simplification, we distinguish them in the energy denominators for later use. Formally, R obeys the Lippmann–Schwinger equation (the "$\cdot$" includes spatial integration)

$$R = V + V \cdot \overline{G}_0 \cdot R\,, \tag{9.42}$$

where $\overline{G}_0$ the Green's function for the constrained system,

$$\overline{G}_0(\omega; r, r') = \frac{1}{\pi\omega}\,\mathcal{P}\int_0^\infty q^2 \mathrm{d}q\,\left[\frac{\overline{\eta}_{\omega_q}(r)\overline{\eta}_{\omega_q}(r')}{\omega-\omega_q} + \frac{\overline{\eta}_{-\omega_q}(r)\overline{\eta}_{-\omega_q}(r')}{\omega+\omega_q}\right]. \tag{9.43}$$

Here $\mathcal{P}$ denotes the principle value prescription. It is then straightforward to verify that

$$V(\omega; r, r') = -\frac{\omega_0}{\omega_\Theta - \omega} X_\Theta^2\, z(r)\,[2\lambda(r) - \omega_0 f(r)]\,[2\lambda(r') - \omega_0 f(r')]\, z(r') \tag{9.44}$$

indeed reproduces the Lee model width function (9.39). Obviously, the potential is nothing but the first term in (9.36). Numerical analysis indeed verifies [47, 56] that the phase shift, (9.40) and (9.41), exactly matches the *resonance* phase shift in Fig. 9.5, which was originally obtained as the difference between the phase shifts of the BSA and the background phase shift from the constrained fluctuations.

We add this non-local potential and the Λ analog to the Schrödinger equation for $\overline{\eta}$ and thus obtain the Schrödinger equation for $\widetilde{\eta}$:

$$\begin{aligned} h^2\widetilde{\eta}(r) + \omega\,[2\lambda(r) - \omega f(r)]\,\widetilde{\eta}(r) &= -z(r)\left[\int_0^\infty r'^2 \mathrm{d}r' z(r') 2\lambda(r')\widetilde{\eta}(r')\right] \\ &\times \left[2\lambda(r) - (\omega+\omega_0)\,f(r) - \omega_0\left(\frac{X_\Theta^2}{\omega_\Theta - \omega} + \frac{X_\Lambda^2}{\omega}\right)(2\lambda(r) - \omega_0 f(r))\right]. \end{aligned} \tag{9.45}$$

The essential observation is that this equation has a simple solution as $N_\mathrm{C} \to \infty$ ($X_\Theta = 1$ and $X_\Lambda = 0$):

$$\widetilde{\eta}(r) = \eta(r) - a z(r) \qquad \text{with} \qquad a = \int_0^\infty \mathrm{d}r r^2\, z(r) f(r) \eta(r)\,. \tag{9.46}$$

Here $\eta(r)$ is the solution to the unconstrained equation (6.41) in the BSA. The radial function, $z(r)$, is localized in space. Thus, the phase shifts of η and $\widetilde{\eta}$, which are extracted from the respective asymptotic behaviors, are identical. This explicitly verifies the earlier explained litmus test beyond the above-mentioned numerical analysis.

We have established that (9.39) is the unambiguous width function of the Θ^+ pentaquark in the Skyrme model when symmetry breaking is set aside. It dramatically differs from the one we discussed in Sect. 9.3 and what was historically adopted. Most importantly, only a *single* collective coordinate matrix element emerges. Hence, there cannot be any cancellation between several of them, and we must conclude that such an explanation for a small pentaquark width is invalid [57]. Yet even more than a year after this cancellation argument has been proven incorrect [47], it is still adopted [58, 59, 60].

9.6 Skyrme Model Results for the Pentaquark Width

Though the discussion in the previous section was carried out along the Skyrme model Lagrangian, the qualitative results generalize as they only effect the treatment of strangeness degrees of freedom. On the other hand, the quantitative results may suffer considerable model dependences.

In Fig. 9.6, we show the resonance phase shift computed from (9.40) for various values of N_C. First we observe that the resonance position quickly moves toward larger energies as N_C decreases. This is mainly due to the strong N_C dependence of pole position $\omega_\Theta \to E_{\overline{\mathbf{10}}} - E_{\mathbf{8}}$: in the flavor symmetric case, it is twice as large for $N_C = 3$ as it is when $N_C \to \infty$, cf. (9.23). The pole shift δE is actually quite small (some 10 MeV) so that $E_{\overline{\mathbf{10}}} - E_{\mathbf{8}}$ is indeed a reliable estimate of the resonance energy. Second, the resonance becomes shaper as N_C decreases. Mainly this is caused by the reduction of X_Θ.

We now turn to more quantitative results for which we also include flavor symmetry breaking effects. Two principle differences arise for the width calculations. First, the interaction Hamiltonian acquires an additional term

$$H_{\rm int}^{\rm sb} = \left(m_K^2 - m_\pi^2\right) d_{i\alpha\beta} D_{8\beta} \int {\rm d}^3 r\, z(r) \gamma(r) \widetilde{\eta}_\alpha(\boldsymbol{x}, t) \hat{x}_i \,. \tag{9.47}$$

This turns the width function to

$$\Gamma(\omega) = 2k\omega_0 \left| \int_0^\infty r^2 {\rm d}r\, z(r) \left[2X_\Theta \lambda(r) + \frac{Y_\Theta}{\omega_0} \left(m_K^2 - m_\pi^2\right) \right] \overline{\eta}_\omega(r) \right|^2 , \tag{9.48}$$

where X_Θ and $Y_\Theta = \sqrt{8N_C/3} \langle \Theta^+ | d_{3\alpha\beta} D_{+\alpha} D_{8\beta} | n \rangle$. Contributions of the form $\int {\rm d}r r^2 z(r) f(r) \overline{\eta}(r)$ vanish due to the constraint in (9.30).

Second, X_Λ does not vanish as $N_C \to \infty$ and the R-matrix formalism is always two dimensional. Nevertheless, the large N_C solution is always of the form (9.46) and the BSA phase shift is recovered. For this to happen, the matrix elements must satisfy

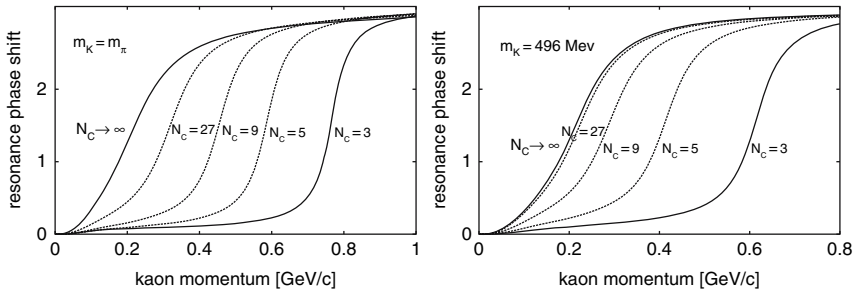

Fig. 9.6. The resonance phase shift, (9.40), as a function of N_C for $m_K = m_\pi$ (*left panel*) and $m_K = 495\,{\rm MeV}$ (*right panel*)

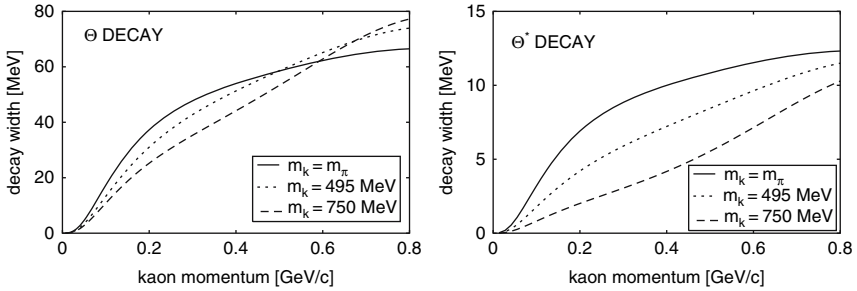

Fig. 9.7. Model prediction for the width $\Gamma(\omega)$ of Θ^+ (*left*) and Θ^{*+} (*right*) for $N_C = 3$ as function of the momentum $k = \sqrt{\omega^2 - m_K^2}$ for three values of the kaon mass measuring flavor symmetry breaking. Note the different scales of two figures

$$X_\Theta = \frac{\omega_\Theta}{\omega_0} Y_\Theta \,, \qquad X_\Lambda = -\frac{\omega_\Lambda}{\omega_0} Y_\Lambda \,, \qquad Y_\Theta = Y_\Lambda = \sqrt{\frac{\omega_0}{\omega_\Theta + \omega_\Lambda}} \,, \tag{9.49}$$

as $N_C \to \infty$. And indeed, the techniques of Sect. 9.4 reproduce these relations! Besides sandwiching the collective coordinate matrix operators between the eigenfunctions of (9.24), this also requires to substitute

$$\omega_\Lambda \longrightarrow E_\Lambda - E_N \qquad \text{and} \qquad \omega_\Theta \longrightarrow E_\Theta - E_N \,, \tag{9.50}$$

on the right hand sides of (9.49), with $E_{N,\Theta,\Lambda}$ being the eigenvalues of (9.24) in the respective channels. In this case, we have actually introduced collective coordinates for a non-zero mode. As in Sect. 8.5, this proves such techniques appropriate beyond the parameterization of exact symmetries.

Having collected all these entries, the resonance phase shift is computed according to (9.40), cf. Fig. 9.6. Again the resonance narrows as N_C approaches its physical value.

The width functions for Θ and its isovector partner Θ^* are shown in Fig. 9.7 for $N_C = 3$. The Θ^* case merely requires the appropriate modification of the matrix elements in (9.48). Most importantly, the k^3 behavior of the width function, as suggested by the treatment discussed in Sect. 9.3, is reproduced only right above threshold, afterward it levels off. Second, and somewhat surprising, the width of the non-ground state pentaquark is smaller than that of the lowest lying pentaquark. The particular model suggests $\Gamma_\Theta \approx 40\,\text{MeV}$ and $\Gamma_{\Theta^*} \approx 20\,\text{MeV}$.

References

1. LEPS Collaboration, T. Nakano et al., *Phys. Rev. Lett.* **91** (2003) 012002. 181, 184, 185
2. D. Diakonov, V. Petrov, and M. V. Polyakov, *Z. Phys.* **A359** (1997) 305. 181, 182, 183, 184,
3. K. Hicks, `hep-ph/0703004`. 181, 190
4. M. Danilov and R. Mizuk, `arXiv:0704.3531 [hep-ex]`. 181, 190

5. J. R. Ellis, M. Karliner, and M. Praszałowicz, *JHEP* **05** (2004) 002. 181, 182, 184, 185, 191,
6. L. C. Biedenharn and Y. Dothan, Print-84-1039 (DUKE). 182
7. M. Praszałowicz, "$SU(n)$ Skyrme Model," in *Skyrmions and Anomalies*, M. Jezabek and M. Prasałowicz, eds. American Institute of Physics, New York, 1987. 182
8. H. Walliser, *Nucl. Phys.* **A548** (1992) 649. 182, 195
9. M. Chemtob, *Nucl. Phys.* **B256** (1985) 600. 182
10. B. K. Jennings and K. Maltman, *Phys. Rev.* **D69** (2004) 094020. 182
11. H. Weigel, *Int. J. Mod. Phys.* **A11** (1996) 2419. 182, 192, 195
12. G. Pari, B. Schwesinger, and H. Walliser, *Phys. Lett.* **B255** (1991) 1. 182
13. H. Walliser and V. B. Kopeliovich, *J. Exp. Theor. Phys.* **97** (2003) 433. 183, 185, 195
14. H. Pagels, *Phys. Rep.* **16** (1975) 219. 183
15. N. W. Park and H. Weigel, *Nucl. Phys.* **A541** (1992) 453. 184
16. M. Gell-Mann, R. J. Oakes, and B. Renner, *Phys. Rev.* **175** (1968) 2195. 184
17. NA49 Collaboration, C. Alt et al., *Phys. Rev. Lett.* **92** (2004) 042003. 184, 185
18. P. Schweitzer, *Eur. Phys. J.* **A22** (2004) 89. 185
19. GRAAL Collaboration, V. Kuznetsov, `hep-ex/0606065`. 185
20. J. Schechter and H. Weigel, *Phys. Rev.* **D44** (1991) 2916. 185
21. J. Schechter and H. Weigel, *Phys. Lett.* **B261** (1991) 235. 185, 189
22. H. Weigel, *Eur. Phys. J.* **A2** (1998) 391. 185, 192, 195
23. R. L. Jaffe and F. Wilczek, *Phys. Rev. Lett.* **91** (2003) 232003. 186, 187, 188
24. D. Diakonov and V. Petrov, *Phys. Rev.* **D69** (2004) 094011. 187, 188
25. S. Eidelman et al. [PDG], *Phys. Lett.* **B592** (2004) 1. 187
26. L. Y. Glozman, W. Plessas, K. Varga, and R. F. Wagenbrunn, *Phys. Rev.* **D58** (1998) 094030. 188
27. M. Batinic, I. Slaus, A. Svarc, and B. M. K. Nefkens, *Phys. Rev.* **C51** (1995) 2310. Err.: *Phys. Rev.* **C57** (1998) 1004. 188
28. D. G. Ireland, S. Janssen, and J. Ryckebusch, `nucl-th/0312103`. 188
29. M. V. Polyakov and A. Rathke, *Eur. Phys. J.* **A18** (2003) 691. 189, 190
30. H. Weigel, "Pentaquarks in a breathing mode approach to chiral solitons," in *Pentaquarks 2004*. `hep-ph/0410066`. 189
31. B. C. Wilson et al., *Nucl. Phys.* **B42** (1972) 445. 190
32. Particle Data Group Collaboration, M. Aguilar-Benitez et al., *Phys. Lett.* **B170** (1986) 1. 190
33. J. S. Hyslop, R. A. Arndt, L. D. Roper, and R. L. Workman, *Phys. Rev.* **D46** (1992) 961. 190
34. A. Kanazawa, *Prog. Theor. Phys.* **77** (1987) 1240. 192, 193
35. A. Blotz, M. Praszalowicz, and K. Goeke, *Phys. Rev.* **D53** (1996) 485. 192
36. C. Lorce, *Phys. Rev.* **D74** (2006) 054019. 192
37. M. Praszalowicz, *Phys. Lett.* **B583** (2004) 96. 192
38. R. L. Jaffe, *Eur. Phys. J.* **C35** (2004) 221. See also refs. [39, 40] 192
39. D. Diakonov, V. Petrov, and M. Polyakov, `hep-ph/0404212`. 192
40. R. L. Jaffe, `hep-ph/0405268`. 192
41. G. S. Adkins, C. R. Nappi, and E. Witten, *Nucl. Phys.* **B228** (1983) 552. 192
42. B. Schwesinger, H. Weigel, G. Holzwarth, and A. Hayashi, *Phys. Rep.* **173** (1989) 173. 193
43. S. Okubo, *Prog. Theor. Phys.* **27** (1962) 949. 195
44. M. Gell-Mann and Y. Neemam, *The Eightfold Way: a Review with a Collection of Reprints*. Benjamin, New York, 1964. 195

45. E. Guadagnini, *Nucl. Phys.* **B236** (1984) 35. 195
46. H. Walliser, p. 247 in G. Holzwarth, ed., *Baryons as Skyrme Solitons. Proceedings, International Workshop, Siegen, Germany, September 28–30, 1992*. World Scientific, Singapore, 1993, 445 pp. 195
47. H. Walliser and H. Weigel, *Eur. Phys. J.* **A26** (2005) 361. 197, 200, 202
48. N. Itzhaki, I. R. Klebanov, P. Ouyang, and L. Rastelli, *Nucl. Phys.* **B684** (2004) 264. 197
49. T. D. Cohen, *Phys. Lett.* **B581** (2004) 175. 197
50. T. D. Cohen, *Phys. Rev.* **D70** (2004) 014011. 197
51. A. Cherman, T. D. Cohen, T. R. Dulaney, and E. M. Lynch, *Phys. Rev.* **D72** (2005) 094015. 197
52. P. A. M. Dirac, *Can. J. Math.* **2** (1950) 129. 199
53. T. D. Lee, *Phys. Rev.* **95** (1954) 1329. 201
54. E. M. Henley and W. Thirring, *Elementary Quantum Field Theory*, Chap. 13. McGraw-Hill, New York, 1962. 201
55. C. R. Hagen, *Phys. Rev.* **A61** (2000) 032715. 201
56. H. Weigel, *Eur. Phys. J.* **A31** (2007) 495. 202
57. H. Weigel, *Phys. Rev.* **D75** (2007) 114018. 202
58. G.-S. Yang, H.-C. Kim, and K. Goeke, *Phys. Rev.* **D75** (2007) 094004. 202
59. K. Piesciuk and M. Praszałowicz, `arXiv:0704.0196 [hep-ph]`. 202
60. H. C. Kim, G. S. Yang, and K. Goeke, `arXiv:0704.1777 [hep-ph]`. 202

10

Multi-baryon Systems in the Skyrme Model

Here we will communicate some basic ideas for studying hadrons with higher baryon numbers in soliton models. The main reason for not being able to make concrete predictions in this regard is the fact that quantum corrections affect configurations with different winding (or baryon) numbers differently and significantly alter the binding energies. We have seen in Sect 8.6 that these corrections are difficult (if at all) to handle, mainly because the effective meson models are non-renormalizable, at least in the sense that only a finite number of counterterms is required. In Sect. 10.6 we will discuss an illuminating example for how significant these corrections are in multi-baryon systems.

Nevertheless there are interesting issues about $B \geq 2$ configurations in soliton models that are worth discussing. Likewise, it is interesting to apply the concept of baryons being topological singularities in chiral models to heavy ion collision issues.

10.1 Static Configurations with $B \geq 2$

The identification of the baryon number with the winding number of a meson configuration is central to the soliton picture, cf. (4.50). So far we have only considered configurations with unit winding number. Of course, the soliton description of baryons is not limited to that sector. As already indicated after (4.51) the very first guess for a baryon number two object in the Skyrme model is to require boundary conditions $F(\infty) = 0$ and $F(0) = 2\pi$. In the Skyrme model the classical mass (4.27) of the corresponding solutions to the equation of motion (4.28) turns out to be about three times as large as that of the $B = 1$ hedgehog. Hence this $B = 2$ configuration is classically unstable. It achieves the twofold mapping by doubling the speed in the chiral angle. Alternatively one might attempt to double the speed of the azimuthal angle φ via the *ansatz* [1]

H. Weigel: *Multi-baryon Systems in the Skyrme Model*, Lect. Notes Phys. **743**, 207–230 (2008)
DOI 10.1007/978-3-540-75436-7_10

$$U(\boldsymbol{x}) = \exp\left[\mathrm{i}\boldsymbol{\tau}\cdot\boldsymbol{\Pi}_2(\boldsymbol{x})F_2(r)\right] \qquad \text{where} \qquad \boldsymbol{\Pi}_n(\boldsymbol{x}) = \begin{pmatrix}\sin(\theta)\cos(n\varphi)\\ \sin(\theta)\sin(n\varphi)\\ \cos(\theta)\end{pmatrix}, \tag{10.1}$$

with θ being the polar angle in coordinate space. Direct computation verifies that this parameterization has winding number two (or more generally n) since the baryon density is formally that of (4.51) with an extra factor n. The classical mass is only slightly generalized when compared to (4.27)

$$E_{\mathrm{cl}}[F_n] = \frac{2\pi f_\pi}{e}\int_0^\infty \mathrm{d}x\Bigg\{n^2x^2F_n'^2 + (n^2+1)\sin^2F_n + 2\mu_\pi^2x^2\,(1-\cos F_n) \\ +\sin^2F_n\left[(n^2+1)F_n'^2 + \frac{n^2\sin^2F_n}{x^2}\right]\Bigg\}, \tag{10.2}$$

where again $x = ef_\pi r$. Numerical minimization in the corresponding winding number sectors yields $E_{\mathrm{cl}}[F_2] = 2.14\ E_{\mathrm{cl}}[F_1]$ [1]. Despite the sizable decrease compared to the hedgehog with $F(0) = 2\pi$, this is still an unbound baryon number two configuration. (The vector meson and chiral quark model analogs have been considered in [2, 3], respectively.) In a next step one might take into account that the *ansatz* has only axial rather than spherical symmetry. This should be reflected by a deformation of the chiral angle,

$$F_n(\boldsymbol{x}) = F_n\left(\sqrt{x^2+y^2+\lambda z^2}\right). \tag{10.3}$$

Here λ is a parameter that is varied to further reduce the classical energy. While this is not sufficient to bind the corresponding $B = 2$ Skyrmion, it accomplishes that goal when stabilization is accounted for by the sixth order Lagrangian in (4.54) [4]. The configuration of (10.3) depends only on a single variable. To properly reflect the axial symmetry, the radial and axial coordinates should be treated differently. This affects both the chiral and the polar angles [5],

$$U_n(\boldsymbol{x}) = \exp\left[\mathrm{i}\boldsymbol{\tau}\cdot\boldsymbol{\Pi}_n(\boldsymbol{x})F_n(\rho,z)\right] \quad \text{where} \quad \boldsymbol{\Pi}_n(\boldsymbol{x}) = \begin{pmatrix}\sin\alpha_n(\rho,z)\cos(n\varphi)\\ \sin\alpha_n(\rho,z)\sin(n\varphi)\\ \cos\alpha_n(\rho,z)\end{pmatrix}. \tag{10.4}$$

Here cylindrical coordinates prove to be appropriate $\rho = \sqrt{x^2+y^2}$. This *ansatz* allows for more general deformations of the parameterization (10.1) than does (10.3). These deformations should be continuous thereby implying that $F_n(\rho,z)$ is invariant while $\alpha_n(\rho,z) \to \pi - \alpha_n(\rho,z)$ under spatial reflection. We introduce differential forms $(f,f) = (\partial_\rho f)^2 + (\partial_z f)^2$ and $[f,g] = \partial_\rho f\partial_z g - \partial_\rho g\partial_z f$ for a compact presentation of the classical energy functional

$$E_{\rm cl}[U_n] = 2\pi \int {\rm d}z\rho{\rm d}\rho \left\{ \frac{f_\pi^2}{2} \left[(F,F) + \left((\alpha,\alpha) + \frac{n^2}{\rho^2} \sin^2\alpha \right) \sin^2 F \right] \right. \qquad (10.5)$$
$$\left. + \frac{\sin^2 F}{2e^2} \left[[F,\alpha]^2 + \frac{n^2}{\rho^2} ((F,F) + (\alpha,\alpha)\sin^2 F) \right] + m_\pi^2 f_\pi^2 \, (1 - \cos F) \right\}$$

in the Skyrme model. The variational problem is more complicated than previously because coupled partial differential equations must be solved for $F = F_n(\rho, z)$ and $\alpha = \alpha_n(\rho, z)$. The numerical accuracy is usually checked from the baryon number to be sufficiently close to the integer n [6]. For typical Skyrme model parameters the $n = 2$ configuration is indeed classically bound by some 10 MeV [5]. The contour lines of equal mass density (integrand in (10.5)) are (approximately) circles centered at $z = 0$ and $\rho = \rho_0 > 0$ rather than the origin of the ρ–z plane. In three dimensions these configurations are tori; for which reasons they are often called *donuts*.

In [5] the tori configurations were found to be bound not only in the case of $B = 2$ but also for $B = 3, 4, 5$. As an aside, for $B = 1$ the hedgehog solution was confirmed from this extended *ansatz*. In the baryon number 2 case, the donut structure of the lowest energy solution was also argued for in [7] by comparison with scattering of Bogomolny–Prasad–Sommerfeld [8, 9] monopoles. Finally the donut shape of the $B = 2$ minimal energy configuration was confirmed with lattice calculations without reference to a variational *ansatz* at approximately the same time [10, 11, 12].

Let us consider the $B = 2$ donut in more detail. We want to utilize collective coordinates for its quantization and generate states with physical quantum numbers. In particular it is challenging to identify light nuclei. The symmetries that are (spontaneously) broken by the soliton configuration are rotations in both coordinate and flavor space. In contrast to the hedgehog configuration, (4.23), rotations in either space cannot be formulated mutually and collective coordinates must be introduced separately,

$$U(\boldsymbol{x}, t) = A(t) U_2(\boldsymbol{\xi}(t)) A^\dagger(t) \qquad \text{with} \qquad \xi_i(t) = [D(t)]_{ij} \, x_j \, . \qquad (10.6)$$

That is, $A(t) \in SU(2)$ (or $SU(3)$) parameterizes the unitary flavor transformations and $D(t) \in SO(3)$ contains the collective coordinates for rotations in coordinate space. In analogy to (5.16) and (5.6) we define intrinsic (or body-fixed) angular velocities ω_a and Ω_n for A and D, respectively. A rotation about the angle γ around the z-axis transforms the azimuthal angle $\varphi \to \varphi + \gamma$. On the other hand, a rotation around the third isospin axis induces $\pi_1 \to \pi_1 \cos\gamma + \pi_2 \sin\gamma$ and $\pi_2 \to -\pi_1 \sin\gamma + \pi_2 \cos\gamma$ in the space of the pion fields π_i. For the *ansatz* (10.4) this implies that $n\varphi \to n\varphi - \gamma$ is a symmetry. When quantizing the donut, the equivalence of these two transformation induces the constraint $J_3^{\rm b.f.} + n I_3^{\rm b.f.} = 0$ for the projection quantum numbers of spin and isospin in the intrinsic frames. In terms of the respective sets of Euler angles the eigenfunctions are (setting $n = 2$)

$$\langle A, D|II_3, JJ_3, \ell\rangle = \frac{(2I+1)(2J+1)}{8\pi^2}\, D^I_{I_3,\ell}(A) D^J_{J_3,-2\ell}(D)\,. \tag{10.7}$$

The physical spin (isospin) emerges from the associated rotation of the intrinsic frame, $J_i = D_{ij} J_j^{\text{b.f.}}$ ($I_i = \frac{1}{2}\text{tr}(\tau_i A \tau_j A^\dagger) I_j^{\text{b.f.}}$). The resulting spectrum is

$$E - E_{\text{cl}} = \frac{I(I+1)}{2\Theta_I} + \frac{J(J+1)}{2\Theta_J} + \frac{\ell^2}{2}\left(\frac{1}{\Theta_3} - \frac{1}{\Theta_I} - \frac{4}{\Theta_J}\right), \tag{10.8}$$

where the moments of inertia Θ_I, Θ_J and Θ_3 are functionals of the profiles F_2 and α_2. Immediately we question the physics interpretation of the intrinsic quantum number ℓ. The above-discussed symmetry properties of α_n under $z \to -z$ cause the first and second component of $\mathbf{\Pi}_2$ not to change sign under spatial reflection while the third component does. From (4.33) we recall that the pseudoscalar nature gives rise to an additional overall sign for $\mathbf{\Pi}_2$. Hence the parity operation on $\mathbf{\Pi}_2$ is equivalent to a rotation in isospace $A \to A\exp(\text{i}\pi\tau_3/2)$. This symmetry operation induces the phase $\text{e}^{\text{i}\pi\ell}$ for the wave function in (10.7). Hence ℓ must be an integer and, due to the constraint between $J_3^{\text{b.f.}}$ and $I_3^{\text{b.f.}}$, spin and isospin must be integers too. This, of course, is expected for a $B = 2$ configuration. The low-lying positive parity states have $\ell = 0$ and thus the last term in (10.8) does not contribute. The potentially lowest energy state with $I = 0$ and $J = 0$ can be built neither from six quarks nor from two nucleons [1]. Rather this state should be interpreted as a two boson composite. Its occurrence here results from the $SU(2)$ quantization which allows to assign integer spin to the $B = 1$ hedgehog. This state does not emerge in the $SU(3)$ quantization scheme [13].[1] Model calculations show that $\Theta_J < \Theta_I$ and thus the deuteron-like system ($I = 0$, $J = 1$) has lower energy than the singlet scattering state ($I = 1$, $J = 0$); a remarkable qualitative agreement with the existence of the deuteron and non-existence of a dineutron-type state. Any negative parity state must have $J \geq 2$ so that the rotational energy unbinds them.

In [15] the energy functional was minimized for $B \leq 6$ with lattice techniques and the surfaces of equal mass density have been classified as tetrahedrical and cubic for $B = 3$ and $B = 4$, respectively. Each of these configurations can be constructed by joining several (deformed) torus-like structures. In analogy to the above discussion, the $B = 3$ tetrahedra was quantized in [16] and identified with ^{3}He and ^{3}H nuclei. We refrain from presenting numerical results for the binding energies because of significant parameter dependences as well as the unresolved issue of quantum corrections. However, with the above-constructed $B = 2$ and $B = 3$ [16] wave functions it is possible to compute matrix elements of symmetry currents just alike described in Chap. 7 for the $B = 1$ system. In Table 10.1 we compare predictions for magnetic moments with empirical data for light nuclei. Given the addressed

[1] Demanding the existence of a closed path to a configuration with two well-separated $B = 1$ configurations of half-integer spin also excludes this state [14].

Table 10.1. Magnetic moments for $B = 2$ and $B = 3$ states in the Skyrme model with parameters from [17]. Table adopted from [6]

mag. mom.	p	n	^{2}D	^{3}He	^{3}H
$f_\pi = 54\,\mathrm{MeV}$, $e = 4.84$	1.97	−1.24	0.74	−1.92	2.72
expt.	2.79	−1.91	0.86	−2.13	2.98

reservations, the agreement is astonishingly good. For axial properties the situation is similar to that of the nucleon: the predicted axial ^{3}He–^{3}H transition matrix element is only about half as large as the experimental value (0.58 vs. 1.21) [16].

10.2 Product Ansatz

Even though we have investigated the construction of exact solutions with $B > 1$ in the preceding section for the exploration of the multi-baryon system, a different approach is more illuminating for the physics interpretation. For this we particularly want to exploit the additive character of the baryon number and attempt to identify the quantum numbers of the individual baryons that participate. Above we only considered the quantum numbers of the composite configuration.

We compute the baryon number from the spatial integral over the time component of the topological current, (4.50). In the notation of differential forms (in three space dimensions) as in Appendix C the baryon number is

$$B[U] = \int \mathrm{d}^3 r B_0 = \frac{1}{24\pi^2} \int \mathrm{tr}\,[\alpha\alpha\alpha] = -\frac{1}{24\pi^2} \int \mathrm{tr}\,[\beta\beta\beta]\ , \tag{10.9}$$

where again $\alpha = U^\dagger \mathrm{d}U$ and $\beta = U\mathrm{d}U^\dagger = -U\alpha U^\dagger$. Here we want to examine the baryon number for field configurations that are parameterized as a product of two unitary matrices,

$$U(\boldsymbol{x}, t) = U_1(\boldsymbol{x}, t) U_2(\boldsymbol{x}, t)\,. \tag{10.10}$$

This implies $\alpha = U_2^\dagger \alpha_1 U_2 + \alpha_2 = U_2^\dagger\,(\alpha_1 - \beta_2)\,U_2$ where the subscripts are attached according to (10.10). Hence the associated baryon number is

$$\begin{aligned} B[U_1 U_2] &= \frac{1}{24\pi^2} \int \mathrm{tr}\left[\alpha_1^3 - \beta_2^3 - 3\beta_2\alpha_1^2 + 3\beta_2^2\alpha_1\right] \\ &= \frac{1}{24\pi^2} \int \mathrm{tr}\left[\alpha_1^3 + \alpha_2^3 + 3\beta_2(\mathrm{d}\alpha_1) - 3(\mathrm{d}\beta_2)\alpha_1\right]\ . \end{aligned} \tag{10.11}$$

Since the last two terms combine to a total derivative they may be dropped. Thus the baryon number is additive for the product configuration, (10.10),

$$B[U_1U_2] = B[U_1] + B[U_2]\,. \tag{10.12}$$

Accordingly, in the soliton picture the superposition of two distinct baryons is described by the product of the chiral fields for the individual soliton configurations. This paves the way to consider a two-nucleon system

$$U_i(\boldsymbol{x},t) = A_i(t)U_0(\boldsymbol{x}_i)A_i^\dagger(t) \qquad \text{for} \quad i=1,2 \tag{10.13}$$

where $U_0(\boldsymbol{x})$ is the static configuration of (4.23) representing a single baryon. The spatial separation of these hedgehogs is parameterized by $\boldsymbol{x}_i = \boldsymbol{x} \pm \boldsymbol{R}/2$ and $A_i(t) \in SU(N_\mathrm{f})$ contains the respective spin-flavor collective coordinates. Though this is not a solution to the variational problem, it presumably does so for configurations that have the baryon density peaked at well-separated regions in space because then distortions of the hedgehog get suppressed.

10.3 Nucleon–Nucleon Potential

We now want to employ the just-constructed $B=2$ configuration to exploit the potential interaction between the two solitons centered at $\pm\boldsymbol{R}/2$. It is obtained by subtracting the single Skyrmion energies from that of the product, (10.10) [18]

$$V(\boldsymbol{R},A_1,A_2) = E[U_1U_2] - E[U_1] - E[U_2]\,. \tag{10.14}$$

Let us first discuss the adiabatic behavior at large distances, $|\boldsymbol{R}| \to \infty$, the region in which the product *ansatz* is assumed to resemble the $B=2$ solution reasonably well. Then the interaction approaches

$$V(\boldsymbol{R},A_1,A_2) \longrightarrow 4\pi A^2 f_\pi^2 D_{ai}(A_1)D_{aj}(A_2)\frac{\partial}{\partial R_i}\frac{\partial}{\partial R_j}\frac{\mathrm{e}^{-m_\pi|\boldsymbol{R}|}}{|\boldsymbol{R}|}\,, \tag{10.15}$$

where the amplitude A is read off from (4.29). To sketch the derivation of (10.15) we note that $U_1 \approx \mathbb{1}$ in the spatial regime where $\alpha_2^\mu \neq 0$ when $|\boldsymbol{R}|$ is large; and vice versa. For large $|\boldsymbol{R}|$ only the leading derivative terms are essential. Parameterizing $U_0(\boldsymbol{x}_i) = \exp(\mathrm{i}\boldsymbol{\tau}\cdot\boldsymbol{\pi}_i/f_\pi)$ enables us to express the leading contribution as

$$V(\boldsymbol{R},A_1,A_2) \longrightarrow -D_{ai}(A_1)D_{aj}(A_2)\int \mathrm{d}^3x \left[(\boldsymbol{\partial}^2+m_\pi^2)\pi_1^{(i)}\right]\pi_2^{(j)} \tag{10.16}$$

after an integration by parts. The major contribution to the integral stems from regions where it is save to adopt the asymptotic behavior (4.29) that we write as $\boldsymbol{\pi}_\mathrm{a} = Af_\pi\boldsymbol{\partial}[\mathrm{e}^{-m_\pi r_\mathrm{a}}/r_\mathrm{a}]$. This furthermore implies $(\boldsymbol{\partial}^2+m_\pi^2)\boldsymbol{\pi}_1 \approx -4\pi Af_\pi\boldsymbol{\partial}[\delta^3(\boldsymbol{x_1})]$. We shift the integration variable $\boldsymbol{x}$ by $\boldsymbol{R}/2$, write the gradients as those for the external parameter $\boldsymbol{R}$ and move them out of the integral to finally obtain the result of (10.15).

Sandwiching $V(\boldsymbol{R}, A_1, A_2)$ between states that contain two uncorrelated nucleons and evaluating the individual collective coordinate matrix elements according to (5.44) yields

$$\langle 1,2|V(\boldsymbol{R},A_1,A_2)|1,2\rangle \longrightarrow 4\pi\left(\frac{Af_\pi}{3}\right)^2 \langle 1|\boldsymbol{\tau}\,(\boldsymbol{\sigma}\cdot\boldsymbol{\partial}_{\boldsymbol{R}})\,|1\rangle \cdot \langle 2|\boldsymbol{\tau}\,(\boldsymbol{\sigma}\cdot\boldsymbol{\partial}_{\boldsymbol{R}})\,|2\rangle \frac{\mathrm{e}^{-m_\pi|\boldsymbol{R}|}}{|\boldsymbol{R}|} \tag{10.17}$$

where in the standard notation $\boldsymbol{\tau}$ and $\boldsymbol{\sigma}$ represent (twice) the nucleon isospin and spin operators, respectively. The scalar product affects the ispspion operators. Equation (10.17) assumes the established form of the one-pion exchange contribution to the nucleon–nucleon potential in the boson exchange model [19, 20, 21] once the identification

$$A = \frac{3}{8\pi}\frac{g_{\pi NN}}{f_\pi M_{\mathrm{N}}} \tag{10.18}$$

is made. This is not surprising since the utilized large $\boldsymbol{R}$ approximations correspond to the description of the pion field at $\boldsymbol{R}$ in the presence of a pointlike nucleon source at the center.

Hence we find that to leading order of the large separation expansion the Skyrmion–Skyrmion interaction can indeed be mapped onto the boson exchange model and the coupling constant for the one-pion exchange can be extracted from the Skyrmion. Even though this does not imply the mapping of the Skyrme model onto a Yukawa model in general, substituting A in favor of the axial charge via (5.59) indeed reproduces the Goldberger–Treimann relation, (5.62), in the chiral limit.

Studies beyond the large separation expansion can only be performed numerically and we will sketch the results which are mostly taken from [22, 23, 24, 25].

In the adiabatic approximation we ignore the time derivatives of the collective coordinates $A_i(t)$. Then only the relative orientation $C = A_1^\dagger A_2$ of the two hedgehogs is relevant. Writing $C = c_4 + \mathrm{i}\boldsymbol{\tau}\cdot\boldsymbol{c}$ and ignoring the unitary constraint $C^\dagger C = \sum_{i=1}^4 c_i^2 = 1$ for a moment, the $SU(2)$ Skyrme model interaction potential is a sum of terms that are quadratic and quartic in c_i. Even though α_μ is already quadratic in c_i and the Lagrangian contains terms up to fourth order in α_μ, the interaction only picks up terms of the structure $\alpha_1\alpha_2\alpha_1\alpha_2$, i.e., an equal number of contributions from either hedgehog, and is thus at most quartic in c_i. From rotational and isospin invariance, the general form of the quadratic term is

$$v_2(\boldsymbol{R}, C) = \alpha_1(R)\,\boldsymbol{c}^2 + \alpha_2(R)\,c_4^2 + \alpha_3(R)\left(\boldsymbol{c}\cdot\hat{\boldsymbol{R}}\right)^2, \tag{10.19}$$

with $R = |\boldsymbol{R}|$. The radial functions $\alpha_i(R)$ are extracted from pertinent choices of coordinates. For example, $C = \mathrm{i}\tau_1$ and $\boldsymbol{R} = R\hat{e}_z$ provides $\alpha_1(R)$. For the quartic pieces a similar but somewhat more complicated decomposition exists

that defines six radial functions $\beta_1(R), \ldots, \beta_6(R)$ [22]. Once the nine radial functions are (numerically) computed, the constraint $C^\dagger C = 1$ is reinforced and two-nucleon matrix elements are computed by noting that [26]

$$D^j_{mm'}(A_1^\dagger A_2) = \sum_{m''=-j}^{j} D^j_{mm''}(A_1^\dagger)\, D^j_{m''m'}(A_2)\,. \tag{10.20}$$

Finally linear combinations of the α_i and β_i are mapped onto the radial functions that are contained in the general decomposition of the nucleon–nucleon potential [19]. This potential is parameterized by six linearly independent operators in the product space of two nucleons,

$$\begin{aligned} V(\boldsymbol{R}) = {} & V_C^+(R) + \boldsymbol{\tau}_1\cdot\boldsymbol{\tau}_2 V_C^-(R) + \boldsymbol{\sigma}_1\cdot\boldsymbol{\sigma}_2\left[V_{SS}^+(R) + \boldsymbol{\tau}_1\cdot\boldsymbol{\tau}_2 V_{SS}^-(R)\right] \\ & + \left[3(\boldsymbol{\sigma}_1\cdot\hat{\boldsymbol{R}})(\boldsymbol{\sigma}_2\cdot\hat{\boldsymbol{R}}) - \boldsymbol{\sigma}_1\cdot\boldsymbol{\sigma}_2\right]\left[V_T^+(R) + \boldsymbol{\tau}_1\cdot\boldsymbol{\tau}_2 V_T^-(R)\right]\,. \end{aligned} \tag{10.21}$$

Here $\boldsymbol{\tau}_i$ and $\boldsymbol{\sigma}_i$ are (twice) the isospin and spin operators for the two nucleons $i = 1, 2$. An exemplary mapping is [22],

$$V_T^-(R) = \frac{\alpha_3(R) + \beta_3(R)}{54} + \frac{\beta_5(R)}{432} + \frac{\beta_6(R)}{72}\,. \tag{10.22}$$

In the adiabatic approximation the three radial functions V_C^-, V_{SS}^+ and V_T^+ vanish identically. Results for the remaining three radial functions are depicted in Fig. 10.1. From the large R regime we immediately observe that the one-pion exchange contributions to V_{SS}^- and V_T^- and thus the Golberger–Treimann relation are reproduced as discussed above, though the method is different this time. In the intermediate range, $1\,\mathrm{fm} \leq R \leq 2\,\mathrm{fm}$ the predicted components V_{SS}^- and V_T^- deviate from the one-pion exchange contribution by approximately the ρ-meson contribution within phenomenological potential models. The ρ-meson is not explicitly incorporated in the model (only in the static approximation via the Skyrme term, cf. (4.64)). Hence the deficiency is expected and cannot be viewed as a shortcoming of the model. On the other hand, the central potential V_C^+ does not reflect the intermediate range attraction. This raises some concern because this attraction is the major cause for nucleons to bind to nuclei. However, this attraction originates from interactions with scalar mesons in the meson exchange models for the potential [19, 20, 21]. These field degrees of freedom are not contained in the Skyrme model. In [27] vector and scalar meson fields were explicitly considered in the context of the nucleon–nucleon potential. That exhaustive study shows that indeed the scalar mesons give rise to attractive forces in the intermediate range.

Attempts to compute the nucleon–nucleon interaction beyond the product *ansatz* have also been made. Essentially the field equations must be numerically solved in the winding number two sector. Simultaneously two distinct baryons must be identified that are separated by a prescribed distance to extract the potential, (10.14). The main complication in these computations is

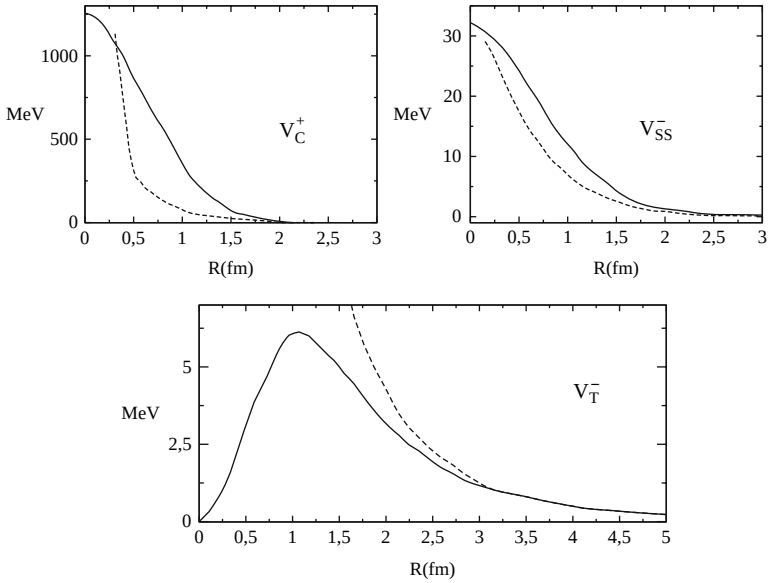

Fig. 10.1. The nucleon–nucleon potential from the Skyrme model. The *dashed lines* are comparisons to specific parts of the Paris nucleon–nucleon potential [19]: ω-exchange for V_C^+ and one-pion exchange for both V_{SS}^- and V_T^-. Figure adopted from [22]

the non-obvious projection onto physical two-nucleon states and the identification of the separation. To compute the nucleon matrix elements the relative isospin orientation C must be identified. To this end use is made of the invariance under exchange of position and orientation of the two distinct baryons [28, 29]. Let $\boldsymbol{n}$ be a unit vector perpendicular to the connecting line between the location of the two baryons, e.g., the points with $U = -1$. The exchange of position is a rotation by π around $\boldsymbol{n}$. The single baryons are hedgehogs (at least for large separation) so we must undo that rotation in isospace. The remaining difference to the unrotated configuration defines the relative isospin orientation, C. Stated otherwise, the configuration with two distinct baryons has the symmetry

$$U(\boldsymbol{x}, t) = C\,(\boldsymbol{n}\cdot\boldsymbol{\tau})\,U(2\boldsymbol{n}(\boldsymbol{n}\cdot\boldsymbol{x}) - \boldsymbol{x}, t)\,(\boldsymbol{n}\cdot\boldsymbol{\tau})\,C^\dagger\,, \tag{10.23}$$

provided C commutes with $\boldsymbol{n}\cdot\boldsymbol{\tau}$. This is indeed a symmetry of the product *ansatz* and, since these rotations are global, it is also a symmetry of the action. That is, in a relaxation scenario that is based on the field equations a prescribed relative orientation C is always maintained. Similar to the analysis of the product *ansatz* only a few choices for C are required to identify the coefficient functions in the general decomposition of the nucleon–nucleon potential, (10.21). So the initial configuration of the relaxation scenario is taken

to be the product of two well-separated hedgehogs with prescribed (and conserved) relative isospin orientation. Finally the separation must be fixed. This can, e.g., be accomplished with the help of Lagrange multipliers [11]. This augments the action by

$$L \longrightarrow L - \frac{\lambda}{2}\,(R - R_0)^2 \tag{10.24}$$

with

$$R_0 = 2\int_{z\geq 0} \mathrm{d}^3 r B_0(\boldsymbol{r}) z \tag{10.25}$$

when the initial configuration was separated along the z-axis. As expected, these computations reproduce the radial functions of the product *ansatz* for large separations, $R \gtrsim 2\,\mathrm{fm}$. At smaller distances, this *ansatz* only reproduces the repulsion for the orientations $C = 1$ and $C = \mathrm{i}\tau_3$. In contrast, the exact solution exhibits sizable attraction for $C = \mathrm{i}\tau_2$. This not only provides the intermediate range attraction for the central potential, $V_C(R)$, but also significantly improves the agreement with the empirical meson exchange picture for the nucleon–nucleon interaction, cf. Fig. 3 in [29].

As in the framework of the product *ansatz*, the radial functions V_C^-, V_{SS}^+ and V_T^+ vanish in the above-described exact calculation. They are induced once mixing through intermediate states is incorporated. Essentially one aims at the diagonalization of the two-baryon Schrödinger equation with the potential $V(\boldsymbol{R}, A_1, A_2)$. Perturbatively the solution looks alike [30][2]

$$\begin{aligned} V_{NN}(\boldsymbol{R}) &= \langle NN|V(\boldsymbol{R}, A_1, A_2)|NN\rangle \\ &\quad + \sum_s \frac{\langle NN|V(\boldsymbol{R}, A_1, A_2)|s\rangle\langle s|V(\boldsymbol{R}, A_1, A_2)|NN\rangle}{E_{NN}(\boldsymbol{R}) - E_s(\boldsymbol{R})}\,, \end{aligned} \tag{10.26}$$

where the intermediate states are $s = |N\Delta\rangle, |\Delta N\rangle, |\Delta\Delta\rangle$ with total isospin T, total spin J, orbital angular momentum L and spin projection S along $\hat{\boldsymbol{R}}$. According to the Pauli principle the condition $L + S + T = \text{odd}$ is enforced. For $R \approx 1\,\mathrm{fm}$ the mixing amplitudes are about 10%. These corrections yield additional attraction, in particular for the NN channel with $J = L = S = 0$ and thus further improve the agreement with empirical descriptions. The additional attraction in the S-wave $T = 0$ channel is less pronounced [29].

These formidable efforts (especially numerically) show that the Skyrme soliton model is capable to describe the physics of the two-nucleon system reasonably well. In [31] these studies have been generalized to flavor $SU(3)$ with flavor symmetry breaking included.

[2] For a given separation $\boldsymbol{R}$ the problem has actually been solved exactly; this resembles a Born Oppenheimer treatment.

10.4 Towards Dense Matter

Here we will discuss the application of the soliton picture for baryons to aspects of nuclear matter. As a first attempt it is plausible to study a Skyrmion crystal on a lattice by imposing twisted boundary conditions [32] to minimize the frustration energies from Skyrmions on neighboring cells. At low density (small number of Skyrmion cells on the lattice) the Skyrmions are well separated while they grow with increasing density and *melt* into a high density phase. The latter is characterized by approximately homogeneous energy and baryon densities [33], so that the single Skyrmions lose their identities. There is a couple of drawbacks besides being of intransparent numerical nature. For example, the boundary conditions motivated in the low-density regime are airily adopted for all densities. Also, the order of the phase transition was found to be sensitive to the prescribed boundary conditions. While the twisted boundary conditions suggest a first order transition, rectangular boundary conditions indicate a second order transition [34].

Here we will therefore take a different path to investigate large densities which is also interesting from the mathematics point of view. We consider a single Skyrmion on compact manifolds, to be precise, on three spheres of radius L: $\mathbb{S}_3(L)$ [35, 36]. The density of this matter increases as L decreases. In contrast to numerical studies of Skyrmion crystals on a lattice this treatment provides information that is deduced analytically.

We embed $\mathbb{S}_3(L)$ in $\mathbb{R}^4$ by introducing a second polar angle $0 \leq \mu \leq \pi$, such that $x \in \mathbb{R}^4$ is parameterized as [37, 38, 39, 40]

$$\begin{aligned} ef_\pi x &= L\,(\cos\mu, \sin\mu\cos\theta, \sin\mu\sin\theta\cos\phi, \sin\mu\sin\theta\sin\phi) \\ &= L\,(\cos\mu, \sin\mu\;\hat{\boldsymbol{r}})\;, \end{aligned} \tag{10.27}$$

where θ and ϕ can be thought of as ordinary polar and azimuthal angles. Skyrme model parameters are used to turn L into a dimensionless quantity. The (static) hedgehog *ansatz* for the chiral field reads

$$U(x) = \mathbb{1}\cos f(\mu) + \mathrm{i}\boldsymbol{\tau}\cdot\hat{\boldsymbol{r}}\sin f(\mu)\,. \tag{10.28}$$

To fill the cell with one baryon the *radial* profile function $f(\mu)$ must obey the boundary conditions $f(0) = 0$ and $f(\pi) = \pi$. The Skyrme model energy functional (without pion mass term) for this manifold is straightforwardly computed,

$$E[f] = \frac{f_\pi}{2e}\int \mathrm{d}m\left\{L\left[f'^2\sin^2\mu + 2\sin^2 f\right] + \frac{1}{L}\left[2f'^2\sin^2 f + \frac{\sin^4 f}{\sin^2\mu}\right]\right\}, \tag{10.29}$$

where primes denote derivatives with respect to the argument and the integration measure is $\mathrm{d}m = \sin\theta\,\mathrm{d}\theta\,\mathrm{d}\phi\,\mathrm{d}\mu$. Variation yields the equation of motion,

$$\left[\sin^2\mu + \frac{2}{L^2}\sin^2 f\right] f'' = -\sin 2\mu - \frac{1}{L^2}\sin 2f\, f'^2 + \sin 2f \left[1 + \frac{1}{L^2}\frac{\sin^2 f}{\sin^2\mu}\right] . \tag{10.30}$$

Obviously the so-called *identity map* $f_{\rm I}(\mu) = \mu$ always solves this equation and also respects the boundary condition. The corresponding energy is evaluated to be

$$E[f_{\rm I}] = 3\frac{\pi^2}{e} f_\pi \left(L + \frac{1}{L}\right) . \tag{10.31}$$

It saturates the Bogomol'ny bound, (4.53), at its minimum, $L = 1$. Hence for this radius the identity map is the true solution. For large L the hypersphere turns into $\mathbb{R}^3$ in which case the hedgehog is the known solution. Hence there is an intermediate value L_0 for which the identity map ceases to be a local minimum. This value L_0 can be determined from the variational problem that introduces (static) fluctuations ψ about $f_{\rm I}$. The resulting change in energy can be formally written as,

$$\Delta E[f_{\rm I}] = \frac{f_\pi}{2e} \int {\rm d}m\, \psi \cdot V \cdot \psi \, . \tag{10.32}$$

The lowest eigenvalue λ_0 of the differential operator V is known [36, 38],

$$\lambda_0 = -L + \frac{2}{L} \, . \tag{10.33}$$

Therefore $f_{\rm I}$ is stable for $L < \sqrt{2}$ but unstable for $L > \sqrt{2}$. In the latter regime the solution must be constructed by numerically integrating the differential equation (10.30). This solution is localized like $1/L$ as the radius grows and the corresponding energy saturates at the $73 f_\pi/e$, i.e., the classical energy of a single Skyrmion for $m_\pi = 0$ [41], cf. Sect. 4.4. Hence the structure of the solution changes at $L = \sqrt{2}$ and we observe a phase transition. This corresponds to a critical density of about $0.25\,{\rm fm}^{-3}$ if $e f_\pi \approx 0.5\,{\rm GeV}$ is assumed (note that $V(\mathbb{S}_3(1)) = 2\pi^2$), which is only little larger than nuclear matter density, $\approx 0.17\,{\rm fm}^{-3}$.

We need to establish an order parameter that distinguishes between these phases. A possible choice would be to use the different structures ($f_{\rm I}$ vs. localized Skyrmions) and consider deviations from the mean energy and/or baryon densities because these deviations vanish only for the identity map. However, this is a particular property for the baryon number one solution; for configurations on $\mathbb{S}_3$ with larger baryon number these deviations do not completely vanish in the high-density phase [37]. It is more appropriate to write $U = \sigma \mathbb{1} + {\rm i}\boldsymbol{\tau}\cdot\boldsymbol{\pi}$ and consider the chiral average

$$\Phi := \langle\sigma\rangle^2 + \langle\boldsymbol{\pi}\rangle^2 \, , \tag{10.34}$$

obtained by integrating the respective fields over $\mathbb{S}_3$. Since the hedgehog configuration, (10.28), has $\boldsymbol{\pi}(\hat{\boldsymbol{r}}) = -\boldsymbol{\pi}(-\hat{\boldsymbol{r}})$ this average only affects the isoscalar

field σ. Obviously $\langle\sigma\rangle$ vanishes for the identity map. For localized configuration, $U = \mathbb{1}$ everywhere in space except around the center of the soliton. Hence $\langle\sigma\rangle$ approaches unity as $L \to \infty$. Numerical studies [38] show that Φ is a continuous but not smooth function of L, evidencing that the phase transition is second order. In the high-density phase we have $\Phi = 0$, i.e., chiral symmetry is restored. This suggests to relate the observed phase transition to the chiral phase transition, even though that is supposed to occur at significantly higher densities. There are many ways to extend these studies, e.g., incorporate higher derivative terms in the chiral Lagrangian, adding vector mesons or construct solitons on $\mathbb{S}_3$ with baryon number larger than one. These extension seem to increase the critical density somewhat but still it appears to be too small [40]. All these extensions signal a second order phase transition.[3] However, there is one exception. Consider the Skyrme model augmented by a scalar (glueball) field to account for the QCD scale anomaly [42]

$$\mathcal{L} = \chi^2 \mathcal{L}_{\mathrm{nl}\sigma} + \mathcal{L}_{\mathrm{Sk}} + \frac{\chi_0^2}{2} (\partial_\mu \chi)^2 - B \left[1 + \chi^4 \left(\ln \chi^4 - 1\right)\right] , \tag{10.35}$$

with $\mathcal{L}_{\mathrm{nl}\sigma}$ and $\mathcal{L}_{\mathrm{Sk}}$ defined in (4.22) and (4.26). Furthermore χ is the scalar glueball field normalized to its vacuum expectation value χ_0. The parameter B determines the regime in which χ deviates from unity and forms a bag [43] (a region in space with $\chi \approx 0$ for the $\mathbb{R}_3$ model). On $\mathbb{S}_3(L)$ the equation of motion for this scalar field reads

$$\chi_0^2 \left(\chi'' + 2\frac{\cos\mu}{\sin\mu}\chi'\right) - \chi f_\pi^2 \left[f'^2 + 2\frac{\sin^2 f}{\sin^2\mu}\right] - 4BL^2\chi^3 \ln\chi^4 = 0 . \tag{10.36}$$

This equation must be integrated in conjunction with (10.30) modified by the appearance of χ in $\mathcal{L}_{\mathrm{nl}\sigma}$. In the localized Skyrmion phase the scalar field obeys the boundary condition $\chi(\pi) = 1$ since that point corresponds to spatial infinity for $\mathbb{R}^3$. For the identity map the expression square brackets is a nonzero constant even at $\mu = \pi$ so that $\chi(\pi) < 1$. Hence χ jumps at the phase transition which therefore is first order in this model.

The Skyrmion on $\mathbb{S}_3(L)$ not only is an interesting mathematical play ground but also gives comprehensive insight in the way chiral symmetry can be restored at high density. For various model Lagrangians this analytical approach yields critical densities approximately equal to those from lattice measurements [33, 34, 44]. Admittedly this critical density comes out in the order of nuclear matter density, too low to be of physical significance. Eventually subleading $1/N_{\mathrm{C}}$ corrections may help to cure this shortcoming.

[3] The pion mass term causes explicit chiral symmetry breaking and thus smoothes the cusp at the phase transition.

10.5 An Application to Heavy Ion Collisions

The chiral phase transition obviously challenges models in which the chiral symmetry is spontaneously broken. Here we report on soliton model motivated lattice measurements that explore the chiral phase transition and thus yield information that are relevant for heavy ion collisions (HIC) [45, 46, 47, 48]. We will focus on the studies of [48] as an example for how the idea that baryons emerge as topological objects in chirally symmetric Lagrangians (and thus the soliton picture) is basic to these investigations. A scalar field must be introduced to parameterize deviations from the chiral circle,

$$U(x) \longrightarrow \phi_4(x) + \mathrm{i}\boldsymbol{\tau} \cdot \boldsymbol{\phi}(x) \tag{10.37}$$

without constraints for the isovector field $\boldsymbol{\Phi} = (\phi_1, \ldots, \phi_4)$. Initially the configuration is chosen randomly. While it evolves in time it rapidly expands in one (longitudinal) direction. This expansion is described by boosting to the local co-moving frame, the Bjorken rod [49], characterized by the proper time τ and the rapidity η,

$$t = \tau \cosh \eta \qquad \text{and} \qquad z = \tau \sinh \eta \,. \tag{10.38}$$

The transverse coordinate (x in $D = 2 + 1$ dimensions) is unchanged. In the $D = 3+1$ dimensional case the transverse components form a two dimensional subspace. In this co-moving frame the kinetic energy from the non-linear σ term, (2.40) acquires a factor of the proper time,

$$T = \frac{\tau}{2} \int \mathrm{d}x \, \mathrm{d}\eta \, (\partial_\tau \boldsymbol{\Phi}) \cdot (\partial_\tau \boldsymbol{\Phi}) \;, \tag{10.39}$$

in units of f_π^2. The time evolution is governed by the equation of motion

$$\frac{1}{\tau} \partial_\tau \boldsymbol{\Phi} + \partial_\tau^2 \boldsymbol{\Phi} = \hat{O} \boldsymbol{\Phi} \,, \tag{10.40}$$

where $\hat{O}$ is a complicated linear operator that inter alia contains gradients and Laplacians in x and η directions. The explicit expression for $\hat{O}$ is, of course, model dependent. During the time evolution various observables are monitored. In particular the modulus of the baryon density $|\rho|$ and the related numbers of baryonic structures (or defects) $n(t) = \int \mathrm{d}V |\rho|$. This is not a conserved quantity; neither need it be an integer.

To reduce the numerical complexity, most of the lattice measurements are performed in $D = 2 + 1$ dimensions. Topologically non-trivial structures are constructed from the compactified map $\mathbb{R}^2 \to \mathbb{S}_2$. This implies to consider the chiral field in O(3), i.e., $\phi_4 \equiv 0$ but there is no constraint on $\boldsymbol{\phi}$. The numerical study is defined through a rectangular lattice for $x, \eta = (ia, jb)$: $\boldsymbol{\Phi}(\tau, x, \eta) \to \boldsymbol{\Phi}_{ij}(\tau)$ with Fourier transformation (in $D = 3 + 1$ dimensions i, k and a have two components)

$$\mathbf{\Phi}_{ij}(\tau) = \frac{1}{2N} \sum_{k,l=-N/2+1}^{N/2} \widetilde{\mathbf{\Phi}}_{kl}(\tau) \exp\left[\frac{2\pi}{N}\,(ik+jl)\right] + \text{h.c.}\,. \tag{10.41}$$

Chiral ensembles are constructed by taking the amplitudes $\widetilde{\mathbf{\Phi}}_{kl}$ at the initial time from a Gaußian deviate

$$G_{kl} = \frac{1}{\sqrt{2\pi\sigma_{kl}}} \exp\left(-\frac{|\widetilde{\mathbf{\Phi}}_{kl}|^2}{2\sigma_{kl}^2}\right) \tag{10.42}$$

where

$$\sigma_{kl}^2 = \frac{\sigma_0^2}{Z} \exp\left(-\frac{\sqrt{p^2+q^2+m^2}}{\mathcal{T}}\right) \quad \text{and} \quad \sum_{k,l=-N/2+1}^{N/2} \sigma_{kl}^2 = N\sigma_0^2\,, \tag{10.43}$$

with coordinates $(p,q) = 2\pi(k,l)/(aN)$. The average occupation numbers follow a Boltzmann distribution

$$n_{kl}^{\alpha} = \langle\langle|\widetilde{\Phi}_{kl}^{\alpha}|^2\rangle\rangle = \sigma_{kl}^2\,, \tag{10.44}$$

for each component α. The above average is over the distribution (10.43). This deviate obviously defines the (effective) temperature $\mathcal{T}$. The range of temperatures that can be realized in such lattice measurements is estimated from the relation between temperatures and correlation lengths. The latter are defined through normalized correlation functions[4] (at a given time, τ)

$$C_i^{\perp} = \frac{1}{D\sigma_0^2 N^2}\left[\left\langle\left\langle \sum_{mn} \mathbf{\Phi}_{mn}\cdot\mathbf{\Phi}_{m+i,n}\right\rangle\right\rangle - \frac{1}{N^2}\left\langle\left\langle\sum_{mn}\mathbf{\Phi}_{mn}\right\rangle\right\rangle^2\right]. \tag{10.45}$$

The parallel correlation function affects the second index; $C_i^{\parallel}$: $\mathbf{\Phi}_{m+i,n} \to \mathbf{\Phi}_{m,n+i}$. The angular averaged correlation may be defined via $\bar{C}(r)$: $\mathbf{\Phi}_{m+i,n} \to \mathbf{\Phi}_{m+i,n+j}$, while summing over all points (i,j) that are separated by r from the lattice site (m,n). The correlation length R_α, is the distance at which C_i^{α} drops to $1/e$:

$$C_{i_0}^{\alpha} = \frac{1}{e} \Longrightarrow R_\alpha = i_0 \times \begin{cases} a & \text{for} \quad \alpha = \perp \\ b & \text{for} \quad \alpha = \parallel \end{cases}. \tag{10.46}$$

The distribution, (10.42) and (10.43), is rotationally symmetric and thus $R = R_\perp = R_\parallel$. In that case the continuum limit of the correlation function can be computed as Fourier transform of the average occupation numbers $\sigma_{kl}^2 \to \sigma^2(p,q)$, yielding $R \approx 1/\mathcal{T}$ in the special case with $m = 0$ [48]. For $m \neq 0$ the decrease of R with $\mathcal{T}$ is modified to $R \propto \mathcal{T}^{-\kappa}$ and the lattice measurements suggest κ slightly smaller than one. The lattice is defined by lattice

[4] According to (10.44) each isovector component contributes $\sigma_0^2 N^2$. The normalization $1/D$ arises as we consider O(D) models in the respective dimensions.

unit size a and the number of sites N with total length $\ell = Na$ for each dimension. The correlation should cover at least a single lattice unit but should also fit well on the whole lattice. So the range of accessible temperatures is estimated as $\frac{1}{l} \lesssim \mathcal{T} \lesssim \frac{1}{a}$.

Once an initial high-density configuration is prepared, its time evolution is determined by the evolution equation (10.40). The evolution is driven towards chiral symmetry via a Mexican hat potential of the form

$$V(\mathbf{\Phi}, \mathcal{T}) = \frac{\lambda}{4} \left[\mathbf{\Phi}^2 - f^2(\mathcal{T})\right]^2 - H\phi_4 \tag{10.47}$$

when

$$f^2(\mathcal{T}) := f_0^2(\mathcal{T}) - \frac{H}{\lambda f_0(\mathcal{T})} \tag{10.48}$$

is negative. (The reduction to the O(3) model in $D = 2+1$ is obvious.) Generically $f_0^2(\mathcal{T})$ decreases monotonously from unity to zero when $\mathcal{T}$ increases from zero to infinity. This implies that $f^2(\mathcal{T})$ changes sign at, say $\mathcal{T} = \mathcal{T}_C$. Thus at high temperature the configuration that minimizes the potential vanishes up to impurities from the explicit symmetry breaking that is measured by H. The specific form of $f_0^2(\mathcal{T})$ is not crucial. A reasonable approximation is to assume that it varies such that at $\tau = \tau_0$ the sign of $f^2(\mathcal{T})$ changes from negative to positive, so that the minimizing field configuration changes from $\mathbf{\Phi} \sim \mathcal{O}(H)$ to $\mathbf{\Phi}_0 = (0, 0, 0, f_0)$. This scenario is called the *sudden quench* approximation.

After the sudden quench the structures interact with each other and in particular nearby baryon and anti-baryon structures tend to annihilate. Thus, with a short delay τ_1, the average number of structures decays with a power law $n(\tau) \propto (\tau/\tau_0)^{-\gamma}$. This is the so-called *roll-down* period which proceeds until the system *freezes out* at $\tau_{\rm f}$ when $n(t)$ saturates at $n_{\rm f}$. The power is parameterized as $\gamma = \alpha d$ where $d = D-1$ is the number of spatial dimensions. The constant of proportionality is measured on the lattice as $\alpha \approx 0.20 \ldots 0.25$, in agreement with statistical arguments [48].

The rapidity gradients decrease like $1/\tau$ and it is thus legitimate to discard them after the sudden quench. Contributions from higher derivative terms in $\hat{O}$ are similarly suppressed. With these omissions the evolution equation

$$\frac{1}{\tau}\partial_\tau \mathbf{\Phi} + \partial_\tau^2 \mathbf{\Phi} - \partial_x^2 \mathbf{\Phi} - m^2 \mathbf{\Phi} = 0 \tag{10.49}$$

describes the propagation of waves in transverse direction. This equation is solved by simple Bessel functions

$$A(\tau, x) \sim \mathrm{e}^{\mathrm{i}px} \times \begin{cases} J_0\left(\tau\sqrt{p^2 - m^2}\right) & \text{for } p^2 > m^2 \\ \\ I_0\left(\tau\sqrt{p^2 - m^2}\right) & \text{for } p^2 < m^2 \ . \end{cases} \tag{10.50}$$

The mass parameter $m^2 = \lambda f^2$, that characterizes the fluctuations about $\mathbf{\Phi} \sim \mathcal{O}(H)$, is negative before the sudden quench. After the sudden quench, m^2 is positive and a few modes with small p actually get amplified. Because of this amplification the potential (and Skyrme) term becomes important for the evolution and the roll-down commences and continues until the true vacuum $\mathbf{\Phi}_0$ is reached. In the co-moving frame the averaged integrated potential $U = \int \mathrm{d}^d x\, V(\mathbf{\Phi}, \mathcal{T})$ ((10.47) with $\mathbf{\Phi}^2 \to \langle\langle \mathbf{\Phi}^2 \rangle\rangle$) increases linearly with τ until $\langle\langle \mathbf{\Phi}^2 \rangle\rangle$ starts to rise at τ_1, the onset of the roll-down. The modified behavior of $\langle\langle \mathbf{\Phi}^2 \rangle\rangle$ is a consequence of amplified low momentum ($p^2 < m^2$) transverse modes. Thus τ_1 can roughly be estimated from (10.50). For example, at $\tau_1 \approx 2.5/m$ the $p = 0$ mode is enhanced by about a factor e from its value at τ_0 if $\tau_0 m \leq 1$. During the roll-down period these modes receive further amplification. For $\tau \geq \tau_1$ we may approximate $I_0(\tau m) \propto \mathrm{e}^{\tau m}$ and thus the end of the roll-down at $\tau = \tau_\mathrm{f}$ is obtained from the respective amplitudes, $m\tau_\mathrm{f} \approx m\tau_1 + \ln\left(\frac{A(\tau_\mathrm{f})}{A(\tau_1)}\right)$. An amplification factor of about 10 then suggests $\tau_\mathrm{f} \approx 4/m$. These estimates for τ_1 and τ_f are reproduced by the lattice measurement within the O(3) model for $D = 2 + 1$ [48].

For large arguments, the Bessel functions decay like $1/\sqrt{\tau}$ so that factors τ as in the kinetic energy T, (10.39), are eventually compensated. Once the dynamics is dominated by the transverse gradients the linear rise of T levels off into a constant.

The average number of structures $\langle\langle n \rangle\rangle$ is closely connected to the coherence length R. On a $d = D - 1$ dimensional cubic lattice the field orientations $\mathbf{\Phi}$ are statistically independent on sublattices of size R. Since in total there are $(Na/R)^d$ such sublattices, one estimates

$$\langle\langle n \rangle\rangle = \nu_d (Na/R)^d \,, \tag{10.51}$$

where ν_d is the average number of defects for a lattice cell. Essentially ν_d is the winding density and has been determined for various manifolds [50, 51],[5] e.g., $\nu_2 = \frac{1}{4}$ and $\nu_3 = \frac{5}{16}$ for the O(3) and O(4) models, respectively. The relation (10.51) can be tested on the lattice by following the number of defects and the correlation length as functions of the initial temperature $\mathcal{T}$. Indeed the $\langle\langle n \rangle\rangle \propto (Na/R)^2$ behavior is reproduced for $d = 2$, however, the constant of proportionality is somewhat smaller ($\approx 1/5$) than the topology argument suggests. During roll-down the average number of defects decreases power-like from the initial value n_0 at the time of the sudden quench. At freeze-out time it smoothly approaches a constant value, n_f that measures the number of surviving baryons plus anti-baryons. Somewhat surprisingly the reduction n_f/n_0 is numerically found to be only about 50%. At all times the proportionality $\langle\langle n \rangle\rangle \propto (N/\bar{R})^2$ for the mean correlation length defined from $\bar{C}$ is approximately maintained.

[5] The scenario behind this picture of defect formation is similar to structure formation in cosmology [52].

For meson production the interesting quantity is the average number of pions (and sigmas) that are produced during roll-down and may be counted after freeze-out. This number can be extracted from the spectral analysis of the energy T. There are two contributions to T, (i) an average background $\bar{T}$ that is stored in the baryons and anti-baryons, (ii) oscillations about $\bar{T}$ that arise from the meson fluctuations. The complex Fourier amplitudes

$$\mathcal{C}(\omega) = \int_{\tau_a}^{\tau_b} \langle\langle T(\tau) - \bar{T}(\tau)\rangle\rangle \, \mathrm{e}^{\mathrm{i}\omega\tau} \, \mathrm{d}\tau \tag{10.52}$$

cover a large time interval after the freeze-out: $\tau_\mathrm{f} \ll \tau_a \ll \tau_b$. Then $\epsilon(\omega) = |\mathcal{C}(\omega)|$ and $n(\omega) = \epsilon(\omega)/\omega$ are the spectral energy and particle number densities, respectively. The latter has the mode sum representation[6]

$$n(\omega) = \sum_{ij} n_{ij}^{(\pi)} \, \delta\left(\omega - 2\omega_{ij}^{(\pi)}\right) + \sum_{ij} n_{ij}^{(\sigma)} \, \delta\left(\omega - 2\omega_{ij}^{(\sigma)}\right) \tag{10.53}$$

where $\omega_{ij}^{(\pi,\sigma)} = \sqrt{m_{\pi,\sigma}^2 + \left(\frac{2\pi}{aN} i\right)^2 + \left(\frac{2\pi}{bN} j\right)^2}$ are the frequencies available on the lattice. The respective masses are the curvatures for the small amplitude fluctuations about $\mathbf{\Phi}_0$: $m_\pi^2 = H/f_0$ and $m_\sigma^2 - m_\pi^2 = 2\lambda f_0^2 = 2m^2$. Numerically, the δ-function type peaks of $n(\omega)$ are reproduced and the corresponding amplitudes level off exponentially with ω such that the σ fluctuations may be ignored for the subsequent discussion of particle multiplicities.

For large proper times only those parts contribute to the energy that carry the overall factor τ, alike T in (10.39). In contrast to T all other remaining terms do not contain derivatives with respect to τ. Hence scaling arguments show that the solutions to the equation of motion (10.40) store exactly half of their energy in T. Numerically it is found that the saturation value of T can be roughly estimated from the potential at $\tau_1 \approx 5/2m \approx 5/\sqrt{2}m_\sigma$. Then the energy stored in the fluctuations can be approximated as

$$2T \approx f_\pi^2 \tau_1 \frac{\lambda}{4} \mathcal{V} = f_\pi^2 \frac{5m_\sigma}{8\sqrt{2}} \, abN^2 \,, \tag{10.54}$$

where $\mathcal{V}$ refers to the lattice volume in rapidity and transverse directions; contributions $\mathcal{O}(H)$ have been omitted. We divide by the lowest possible pion energy, to obtain the number of emitted pions

$$n_\pi = f_\pi^2 \frac{5}{8\sqrt{2}} \frac{m_\sigma}{m_\pi} \, abN^2 \,. \tag{10.55}$$

The total baryon number B is conserved. Hence $n(\tau_\mathrm{f})$ equals half the number of surviving (anti)baryons for configurations with $B = 0$. From the time dependence of $n(\tau)$ and the statistical argument, (10.51), the ratio of produced anti-baryons ($\bar{B}$) to pions in $D = 2 + 1$ is then estimated as

[6] The factors 2 in the δ-function arguments arise because T is quadratic in the meson fields, cf. (10.39).

$$\frac{n_{\bar{B}}}{n_\pi} \approx 0.15\,\frac{a}{b}\,\frac{m_\pi}{m_\sigma f_\pi^2}\,\frac{(\tau_0 m_\sigma)^{2\alpha}}{R_0^2}\,, \tag{10.56}$$

where R_0 is the correlation length at τ_0 and the numerical factor arises from taking $\nu_2 = 0.25$. The result, (10.56), is not free of lattice parameters. However, the ratio a/b of spatial and rapidity lattice constants equals that of the (initial) transverse and longitudinal coherence lengths and should thus be of the order τ_0. Rough estimates based on assuming $\tau_0 m_\sigma \approx 1$ yield multiplicity ratios of 5–10%.

For $D = 3+1$ the data for the multiplicities (6.5–8.5% [53]) can be utilized to substantiate the above assumptions for R_0 and τ_0. The data are reproduced for $0.2\,\mathrm{fm} \leq \tau_0 \leq 0.5\,\mathrm{fm}$, $0.7\,\mathrm{fm} \leq R_0 \leq 1.2\,\mathrm{fm}$ in connection with $R_0 \approx (3\tau_0)^{3\alpha+1}$ which essentially washes out the τ_0 dependence of the multiplicity ratio [48]. Together with the arguments about the initial coherence length discussed after (10.46) this suggests a chiral phase transition temperature of $\mathcal{T} \approx 200\,\mathrm{MeV}$.

This single example already shows that numerous interesting features of heavy ion collisions can be explored in a framework that is based on the concept that baryons emerge as topological defects of chiral fields.

10.6 The H-dibaryon

The H-dibaryon is a potential $B = 2$ state with strangeness $S = -2$. It was first studied in the framework of the MIT-bag model [54] and later also in the Skyrme model [55, 56]. We will particularly study this example to substantiate that quantum corrections to the static soliton energy [57] are crucial when determining the binding energy of configurations with baryon number larger than one.

The H-dibaryon configuration refers to a specific $SO(3)$ embedding in $SU(3)$. The corresponding $SO(3)$ generators are

$$\Lambda_1 = \lambda_7 \quad \Lambda_2 = -\lambda_5 \quad \Lambda_3 = \lambda_2\,, \tag{10.57}$$

so that $(\boldsymbol{\Lambda}\cdot\hat{\boldsymbol{v}})_{ij} = \mathrm{i}\epsilon_{ikj}v_k$ for an arbitrary vector $\boldsymbol{v}$. The *ansatz* for the H-dibaryon configuration reads [55, 58]

$$V_{\mathrm{H}} = \mathbb{1}\,\mathrm{e}^{\mathrm{i}\psi} + \mathrm{i}\boldsymbol{\Lambda}\cdot\hat{\boldsymbol{x}}\,\mathrm{e}^{-\mathrm{i}\psi/2}\sin\chi + (\boldsymbol{\Lambda}\cdot\hat{\boldsymbol{x}})^2\,[\mathrm{e}^{-\mathrm{i}\psi/2}\cos\chi - \mathrm{e}^{\mathrm{i}\psi}]\,, \tag{10.58}$$

where ψ and χ are functions of the radial coordinate $r = |\boldsymbol{x}|$. The baryon number for this configuration is solely given by the boundary values of χ,

$$B[V_{\mathrm{H}}] = \frac{2}{\pi}\,[\chi(0) - \chi(\infty)]\,. \tag{10.59}$$

Insertion of (10.58) into the Skyrme model Lagrangian, (4.22) and (4.26), yields the energy functional

$$E_{\rm cl}[V_{\rm H}] = 2\pi\frac{f_\pi}{e}\int_0^\infty {\rm d}x\,\Big\{\tfrac{3}{4}x^2\psi'^2 + x^2\chi'^2 + 4\left[1-\cos\chi\cos\left(\tfrac{3}{2}\psi\right)\right] + \tfrac{1}{4}\left(1-\cos\chi\cos\left(\tfrac{3}{2}\psi\right)\right)\left(9\psi'^2+4\chi'^2\right) + 3\sin\chi\sin\left(\tfrac{3}{2}\psi\right)\phi'\chi' + \tfrac{1}{x^2}\left[3\sin^2\chi\sin^2\left(\tfrac{3}{2}\psi\right) + \left(1-\cos\chi\cos\left(\tfrac{3}{2}\psi\right)\right)^2\right]\Big\}, \quad (10.60)$$

where, again, primes denote derivatives with respect to the dimensionless variable $x = ef_\pi r$. The minimal value for this energy functional is found to be $140 f_\pi/e$ which is about 4% less than twice the energy of the $B = 1$ hedgehog, cf. discussion after (4.28). This suggests that $V_{\rm H}$ is significantly bound. Further numerical analysis [57] shows that $E_{\rm cl}[V_{\rm H}]$ is slightly larger than the actual $B = 2$ (torus type) solution discussed in Sect. 10.1. When chiral symmetry breaking (i.e., m_π) is included, the $SO(3)$ configuration is even lighter than the torus.

To make more definite statements on whether or not $V_{\rm H}$ represents a stable particle we have to (i) project it on physical states by means of collective coordinate quantization, (ii) incorporate flavor symmetry breaking and (iii) estimate quantum corrections to the energy. Actually items (i) and (ii) are even simpler than in the case of the hedgehog. Any transformation $\Lambda = \exp({\rm i}\boldsymbol{a}\cdot\boldsymbol{\Lambda})$ on $V_{\rm H}$ generated by the subgroup, (10.57), can be reexpressed as a coordinate rotation,

$$\Lambda V_{\rm H}(\boldsymbol{x})\Lambda^\dagger = V_{\rm H}(D\boldsymbol{x})\,, \quad (10.61)$$

where D is a rotation matrix that depends on the constant transformation parameters $\boldsymbol{a}$. Hence any spatial integrals over those parts of the Lagrange density that do not contain time derivatives are invariant under Λ. Furthermore under (10.61) the contribution from the Wess–Zumino term, (C.27), gives

$$(A^\dagger\dot{A})\Lambda\int {\rm d}^3x\,\epsilon_{ijk}\left(\alpha_i^{({\rm H})}\alpha_j^{({\rm H})}\alpha_k^{({\rm H})} + V_H\alpha_i^{({\rm H})}\alpha_j^{({\rm H})}\alpha_k^{({\rm H})}V_{\rm H}^\dagger\right)\Lambda = (A^\dagger\dot{A})\int {\rm d}^3x\,\epsilon_{ijk}\left(\alpha_i^{({\rm H})}\alpha_j^{({\rm H})}\alpha_k^{({\rm H})} + V_{\rm H}\alpha_i^{({\rm H})}\alpha_j^{({\rm H})}\alpha_k^{({\rm H})}V_{\rm H}^\dagger\right), \quad (10.62)$$

where $\alpha_i^{({\rm H})} = V_{\rm H}^\dagger\partial_i V_{\rm H}$. Since Λ is irreducible in $SU(3)$, the integral must be proportional to the unit matrix in flavor space and the flavor trace of (10.62) vanishes. Consequently, there is no such constraint as for the right hypercharge in the hedgehog quantization, (6.8).[7] The same argument can be applied to the flavor symmetry breaking terms in (6.22) (again, omitting time derivatives) to observe that the λ_8 terms do not contribute. Hence flavor symmetry breaking merely adds a constant to the energy functional that is independent of the collective coordinates, A. In analogy to the computation in Sect. 6.3 the collective coordinate Hamiltonian is finally found to be

$$H = E_{\rm cl}[V_{\rm H}] + \frac{1}{\alpha^2[V_{\rm H}]}\boldsymbol{J}^2 + \frac{1}{\beta^2[V_{\rm H}]}C_2(SU(3)) + \frac{1}{2}\gamma[V_{\rm H}]\,. \quad (10.63)$$

[7] There is a symmetry similar to (10.61) for the hedgehog. However, in that case the transformation reduces with respect to isospin and hypercharge.

The constants of proportionality are numerically computed for the configuration that minimizes the classical energy,

$$\alpha^2[V_{\rm H}] \approx \frac{121}{f_\pi e^3}\,, \quad \beta^2[V_{\rm H}] \approx \frac{183}{f_\pi e^3}\,, \quad \gamma[V_{\rm H}] \approx \frac{13.4}{f_\pi e^3}\left(m_{\rm K}^2 - m_\pi^2\right)\,. \qquad (10.64)$$

Since there is no constraint, the lowest energy state is the $SU(3)$ singlet, with mass $M_{\rm H} = E_{\rm cl}[V_{\rm H}] + \frac{1}{2}\gamma[V_{\rm H}]$. Since this state has zero hypercharge and baryon number two, it must carry strangeness $S = -2$. Therefore this state should decay into two Λ baryons, if at all unstable. The corresponding mass difference is $M_{\rm H} - 2M_\Lambda \sim 1\,{\rm GeV}$, when the physical value for f_π is substituted. Of course, this is huge and mainly due to the large absolute value of M_Λ. We have previously argued that this absolute value cannot be trusted because it contains big quantum corrections. We have studied such corrections for the hedgehog in Sect. 8.6 and it is obviously necessary to at least estimate them for $V_{\rm H}$, this is issue (iii).

In Sect. 8.6 we saw that the major contribution to the quantum correction to the soliton energy (i.e., the Casimir or vacuum polarization energy ΔE) originates from the zero modes. The numerical results available for $\Delta E[V_{\rm H}]$ utilize that issue as only the zero-mode contribution is considered within a specific formulation of the Casimir energy. In [59] this approximation has been studied for the kink (cf. Sect. 4.3) and sine-Gordon soliton models for which these quantum corrections are exactly known [60, 61]. It turned out that in these models the zero-mode approximation underestimated the full result by about 10–15%. Comparing the results of [59] for the Skyrme to the more elaborate computations of [62], cf. Sect. 8.6, exhibits an underestimation of about 20%. So the zero-mode approximation should be viewed as a trustworthy bound for ΔE. This should be sufficient to address the question of whether or not the soliton picture predicts a strongly bound dibaryon with strangeness $S = -2$. For consistency this approximation is then applied to estimate ΔE in both the $B = 1$ and $B = 2$ sectors. The zero-mode treatment of [59] works reasonably well because this specific formulation favorably imposes the so-called *no–tadpole* renormalization scheme, that is standard for the evaluation of ΔE [63]. We will explain that briefly. We write the equation of motion for the fluctuations, (8.3), as

$$H_{\rm S}^2\eta(\boldsymbol{x},\omega) = \left(H_0^2 + V\right)\eta(\boldsymbol{x},\omega) = \omega^2\eta(\boldsymbol{x},\omega)\,, \qquad (10.65)$$

where $H_{\rm S}^2$ is the Klein–Gordon Hamiltonian for fluctuations in the background of the soliton and H_0^2 is that for a free Klein–Gordon field. Hence V is the potential induced by the soliton. The no-tadpole condition corresponds to omitting the $\mathcal{O}(V)$ contribution in the mode sum for the Casimir energy, (8.54). Formally we write this operation as [64]

Table 10.2. Masses of the $J = \frac{1}{2}$ baryons and the $SO(3)$ H-dibaryon in the Skyrme model with $e = 4.0$ as listed in [57]. All data are in MeV

	$B = 1$	$2 \times (B = 1)$	$B = 2$
$E_{\rm cl}$	1756.5	3513.0	3375.4
ΔE	−1234.8	−2496.6	−1642.1
$E_{\rm coll.}$	400.2	800.4	0.0
$E_{\rm tot}$	921.9	1843.8	1733.3

$$\Delta E \sim \frac{1}{2}\mathrm{tr}\left[H_{\rm S} - H_0 - \frac{1}{2}H_0^{-1}V\right] = -\frac{1}{4}\mathrm{tr}\left[H_0^{-1}\left(H_0 - H_{\rm S}\right)^2\right]$$
$$\sim \; -\frac{1}{4}\sum\!\!\!\!\!\!\int_{n,n'} \langle n|H_0^{-1}\left(H_0 - H_{\rm S}\right)^2|n'\rangle\langle n'|n\rangle \tag{10.66}$$

where $|n\rangle$ and $|n'\rangle$ label the eigenstates of H_0 and $H_{\rm S}$, respectively. The zero-mode approximation amounts to restricting the n' sum (integral) accordingly,

$$\Delta E \sim -\frac{1}{4}\sum_{n'}\int_0^\infty k^2 \mathrm{d}k\sqrt{k^2+m_\pi^2}\,|\langle \boldsymbol{k}|z_{n'}\rangle|^2 \; . \tag{10.67}$$

We have used that $H_{\rm S}z_{n'} = 0$ and that there are no discrete states in the free Klein–Gordon spectrum. The zero-mode wave functions, $z_{n'}(\boldsymbol{x})$ are determined by operating with the symmetry generators $\hat{X}_{n'}$ on the soliton configurations,

$$z_{n'}^{(B=1)}(\boldsymbol{x}) \propto \left[\hat{X}_{n'}, U_0(\boldsymbol{x})\right] \quad \text{and} \quad z_{n'}^{(B=2)}(\boldsymbol{x}) \propto \left[\hat{X}_{n'}, V_{\rm H}(\boldsymbol{x})\right] \; . \tag{10.68}$$

In practical computations [57, 59, 65, 66] the square root of the metric, 8.3, according to which the eigenstates of $H_{\rm S}$ are normalized, is included to render the matrix element in (10.67) independent of the parameterization for the fluctuations, cf. footnote 1 in Chap. 8. These wave functions are localized in space and their Fourier transforms $\langle \boldsymbol{k}|z_{n'}\rangle$ level off with increasing $k = |\boldsymbol{k}|$. Therefore the integral, (10.67) is finite and actually negative definite.

The calculations that compare the Casimir energies for the $B = 1$ hedgehog and the $B = 2$ dibaryon have been performed by Scholtz et al. [57]. Their results are listed in Table 10.2. The Casimir energy of the single hedgehog is only little smaller (in magnitude) than the Casimir energy of the $SO(3)$ dibaryon. We may easily understand this: The number of zero modes is determined by the symmetries of the model but not by the configuration itself. Thus it is not surprising that the Casimir energy is roughly independent of the baryon number. As a result the dibaryon becomes unstable. Yet, this is not the end of the story. As discussed, the lowest $B = 2$ state is a spin-flavor singlet hence it does not acquire any rotational energy. However, the $B = 1$ states receive rotational energies upon collective coordinate quantization. In

particular for three flavors (computed from (6.11) since the current discussion omits flavor symmetry breaking) they substantially increase the baryon mass. This ends up in a loosely bound H-dibaryon as seen in Table 10.2. This does not seem a very robust statement in view of the many approximations made. However, it occurs certain that the quantum corrections are important and invalidate the prediction of a strongly bound dibaryon with strangeness $S = -2$. This also questions that the classically stable objects constructed in Sect. 10.1 realize as observable baryons.

References

1. H. Weigel, B. Schwesinger, and G. Holzwarth, *Phys. Lett.* **B168** (1986) 321. 207, 208, 210
2. H. Imai, A. Kobayashi, H. Otsu, and S. Sawada, *Prog. Theor. Phys.* **82** (1989) 141. 208
3. S. Komori, N. Sawado, and N. Shiiki, *Ann. Phys.* **311** (2004) 1. 208
4. H. Weigel, *Investigations in the $B = 0$ and $B = 2$ Sectors of the Skyrme Model (in German).* Diploma thesis, Siegen University, 1986. Unpublished. 208
5. V. B. Kopeliovich and B. E. Stern, *JETP Lett.* **45** (1987) 203. 208, 209
6. V. B. Kopeliovich, "Bound skyrmions: the properties and physics consequences of their existence." p. 363 in G. Holzwarth, ed., *Baryons as Skyrme Solitons, Proceedings, International Workshop, Seigen, Germany, September 28–30, 1992.* World Scientific, Singapore, 1993, 445pp. 209, 211
7. N. S. Manton, *Phys. Lett.* **B192** (1987) 177. 209
8. E. B. Bogomolny, *Sov. J. Nucl. Phys.* **24** (1976) 449. 209
9. M. K. Prasad and C. M. Sommerfield, *Phys. Rev. Lett.* **35** (1975) 760. 209
10. J. J. M. Verbaarschot, *Phys. Lett.* **B195** (1987) 235. 209
11. J. J. M. Verbaarschot, T. S. Walhout, J. Wambach, and H. W. Wyld, *Nucl. Phys.* **A468** (1987) 520. 209, 216
12. A. J. Schramm, Y. Dothan, and L. C. Biedenharn, *Phys. Lett.* **B205** (1988) 151. 209
13. V. B. Kopeliovich, B. Schwesinger, and B. E. Stern, *Nucl. Phys.* **A549** (1992) 485. 210
14. E. Braaten and L. Carson, *Phys. Rev.* **D38** (1988) 3525. 210
15. E. Braaten, S. Townsend, and L. Carson, *Phys. Lett.* **B235** (1990) 147. 210
16. L. Carson, *Nucl. Phys.* **A535** (1991) 479. 210, 211
17. G. S. Adkins and C. R. Nappi, *Nucl. Phys.* **B233** (1984) 109. 211
18. T. H. R. Skyrme, *Nucl. Phys.* **31** (1962) 556. 212
19. M. Lacombe, et al., *Phys. Rev.* **C21** (1980) 861. 213, 214, 215
20. R. Machleidt, K. Holinde, and C. Elster, *Phys. Rep.* **149** (1987) 1. 213, 214
21. R. Machleidt, *Adv. Nucl. Phys.* **19** (1989) 189. 213, 214
22. R. Vinh Mau, M. Lacombe, B. Loiseau, W. N. Cottingham, and P. Lisboa, *Phys. Lett.* **B150** (1985) 259. 213, 214, 215
23. A. Jackson, A. D. Jackson, and V. Pasquier, *Nucl. Phys.* **A432** (1985) 567. 213
24. H. Yabu and K. Ando, *Prog. Theor. Phys.* **74** (1985) 750. 213
25. R. Vinh Mau, *Prog. Part. Nucl. Phys.* **20** (1988) 221. 213
26. D. A. Varshalovich, A. N. Moskalev, and V. K. Khersonskii, *Quantum Theory of Angular Momentum*, Chap. 4. World Scientific, Singapore, 1988. 214

27. D. Kalafatis and R. Vinh Mau, *Phys. Rev.* **D46** (1992) 3903. 214
28. T. S. Walhout and J. Wambach, *Phys. Rev. Lett.* **67** (1991) 314. 215
29. T. S. Walhout, p. 339 in G. Holzwarth, ed., *Baryons as Skyrme Solitons, Proceedings, International Workshop, Seigen, Germany, September 28–30, 1992*. World Scientific, Singapore, 1993, 445pp. 215, 216
30. N. R. Walet and R. D. Amado, *Phys. Rev. Lett.* **68** (1992) 3849. 216
31. B. Schwesinger, F. G. Scholtz, and H. B. Geyer, *Phys. Rev.* **D51** (1995) 1228. 216
32. I. R. Klebanov, *Nucl. Phys.* **B262** (1985) 133. 217
33. E. Wuest, G. E. Brown, and A. D. Jackson, *Nucl. Phys.* **A468** (1987) 450. 217, 219
34. A. D. Jackson and J. J. M. Verbaarschot, *Nucl. Phys.* **A484** (1988) 419. 217, 219
35. N. S. Manton and P. J. Ruback, *Phys. Lett.* **B181** (1986) 137. 217
36. N. S. Manton, *Commun. Math. Phys.* **111** (1987) 469. 217, 218
37. A. D. Jackson, A. Wirzba, and N. S. Manton, *Nucl. Phys.* **A495** (1989) 499. 217, 218
38. A. D. Jackson, *Prog. Part. Nucl. Phys.* **20** (1988) 65. 217, 218, 219
39. H. Reinhardt and B. V. Dang, *Phys. Rev.* **D38** (1988) 2881. 217
40. A. Wirzba, "Nuclear matter aspects of skyrmions." p. 411 in G. Holzwarth, ed., *Baryons as Skyrme Solitons, Proceedings, International Workshop, Seigen, Germany, September 28–30, 1992*. World Scientific, Singapore, 1993, 445pp. 217, 219
41. G. S. Adkins, C. R. Nappi, and E. Witten, *Nucl. Phys.* **B228** (1983) 552. 218
42. R. Gomm, P. Jain, R. Johnson, and J. Schechter, *Phys. Rev.* **D33** (1986) 801. 219
43. H. Gomm, P. Jain, R. Johnson, and J. Schechter, *Phys. Rev.* **D33** (1986) 3476. 219
44. L. Castillejo, P. S. J. Jones, A. D. Jackson, J. J. M. Verbaarschot, and A. Jackson, *Nucl. Phys.* **A501** (1989) 801. 219
45. G. Holzwarth, *Nucl. Phys.* **A672** (2000) 167. 220
46. G. Holzwarth, `hep-ph/0107034`. 220
47. G. Holzwarth and J. Klomfass, *Phys. Rev.* **D66** (2002) 045032. 220
48. G. Holzwarth, *Phys. Rev.* **D70** (2004) 036001. 220, 221, 222, 223, 225
49. J. D. Bjorken, *Phys. Rev.* **D27** (1983) 140. 220
50. J. R. Ellis and H. Kowalski, *Phys. Lett.* **B214** (1988) 161. 223
51. N. H. Christ, R. Friedberg, and T. D. Lee, *Nucl. Phys.* **B202** (1982) 89. 223
52. T. W. B. Kibble, *J. Phys.* **A9** (1976) 1387. 223
53. PHENIX Collaboration, K. Adcox et al., *Phys. Rev. Lett.* **88** (2002) 242301. 225
54. R. L. Jaffe, *Phys. Rev. Lett.* **38** (1977) 195. 225
55. A. P. Balachandran, F. Lizzi, V. G. J. Rodgers, and A. Stern, *Nucl. Phys.* **B256** (1985) 525. 225
56. G. L. Thomas, N. N. Scoccola, and A. Wirzba, *Nucl. Phys.* **A575** (1994) 623. 225
57. F. G. Scholtz, B. Schwesinger, and H. B. Geyer, *Nucl. Phys.* **A561** (1993) 542. 225, 226, 228
58. A. P. Balachandran, A. Barducci, F. Lizzi, V. G. J. Rodgers, and A. Stern, *Phys. Rev. Lett.* **52** (1984) 887. 225
59. G. Holzwarth, *Phys. Lett.* **B291** (1992) 218. 227, 228
60. R. F. Dashen, B. Hasslacher, and A. Neveu, *Phys. Rev.* **D10** (1974) 4130. 227
61. R. F. Dashen, B. Hasslacher, and A. Neveu, *Phys. Rev.* **D11** (1975) 3424. 227
62. F. Meier and H. Walliser, *Phys. Rep.* **289** (1997) 383. 227
63. N. Graham, R. L. Jaffe, and H. Weigel, *Int. J. Mod. Phys.* **A17** (2002) 846. 227
64. K. E. Cahill, A. Comtet, and R. J. Glauber, *Phys. Lett.* **B64** (1976) 283. 227
65. H. Weigel, R. Alkofer, and H. Reinhardt, *Nucl. Phys.* **A582** (1995) 484. 228
66. G. Holzwarth, *Nucl. Phys.* **A572** (1994) 69. 228

Epilogue

In this monograph, we have reviewed the concept of chiral soliton models for baryons. In these models, the baryons emerge as (topological) defects of the chiral field. The elementary starting point is a chiral Lagrangian that fully contains the dynamics of the chiral field and/or other fields that parameterize meson degrees of freedom. Once it is set, in the sense that all pieces in the chiral Lagrangian are established, no further assumptions about the interaction are required. In particular, no additional information must be supplemented from outside, and any question on low-energy baryon properties or resonances has, in principle, a definite answer within the model. Even though reaching testable predictions may still involve complicated and lengthy computations and eventually simplifying approximations in a number of cases, this feature of straightforwardness nicely distinguishes the soliton picture from many other baryon models. A particularly fascinating feature is the fact that the soliton must indeed be quantized as a fermion. This result strictly emerged from reproducing the symmetries of QCD in the effective model.

We have encountered many applications of the soliton description. Starting from the baryon spectrum they reach from static baryon properties via nucleon resonances and deep inelastic scattering to even heavy ion collisions. Though we have only discussed some specific exemplary studies, which we will not itemize here, the reader may have recognized and appreciated the vast range of successful activities.

As physicists, we have the common interest of confronting theory with experiment. We do not expect the soliton picture to produce highly accurate results that survive comparison with data on the few percent level, or even better. After all in reality, $1/N_{\rm C}$, which is the rough expansion parameter within the soliton picture, is not small. Yet we certainly gain reliable qualitative insight into the physics of baryons. A particular example is the smallness of the singlet axial current matrix element which is nicely explained in the soliton picture of the nucleon. Simultaneously, we stress that this picture in principle represents a parameter-free approach once the chiral Lagrangian is set to correctly describe meson properties.

H. Weigel: *Epilogue*, Lect. Notes Phys. **743**, 231–232 (2008)
DOI 10.1007/978-3-540-75436-7_11

In this monograph, we have discussed numerous successful applications of the soliton picture for baryons. Nevertheless, challenging problems remain that should be subjected to future investigations. Here is a short list containing those that are of general interest:

- We have seen that the nucleon–nucleon potential allows us to extract the pion–nucleon coupling $g_{\pi NN}$ for the boson exchange model stemming from Yukawa interactions. On the other hand, the soliton predictions for meson baryon scattering cannot be associated with simple Yukawa interactions. So, why can we map one sector of the model on the Yukawa theory but not the other?
- Certainly, we want to improve our understanding of quantum corrections to baryon properties, in particular the spectrum. After all, they contribute already at the next to leading order in the $1/N_{\mathrm{C}}$ expansion. This is also desirable to obtain reliable information about multi-baryon systems and eventually nuclei. In particular, it concerns their binding energies.
- We have discussed the computation of nucleon structure functions in the NJL chiral quark model. In that model, the Callan–Gross relation resulted naturally. This relation reflects the fermionic nature of the nucleon. After the gradient expansion, this information is contained in the Wess–Zumino term. Hence, it should also be possible to extract this relation from there.

Additionally, it is very likely that in future the soliton picture will find further specific applications so that the soliton picture prospectively promises to further enrich our understanding of the structure of baryons and their dynamics in the low and intermediate energy regimes.

In conclusion, the author hopes that the presented material not only comprehensively explains the soliton picture for baryons and leads to further insight but also initiates further progress on the subject.

Appendix A

Chiral Properties of Quark Bilinears

In this appendix we briefly summarize the behavior of quark bilinears under infinitesimal flavor and chiral transformations. These results can be employed to verify the invariance of the Lagrangian, (2.8), under these transformations.

Under flavor rotations the quark spinors as defined in (2.4) transform as

$$q \to q' = \mathrm{e}^{(\mathrm{i}/2)\epsilon_a \lambda_a}\, q\,, \quad \bar{q} \to \bar{q}' = \bar{q}\, \mathrm{e}^{-(\mathrm{i}/2)\epsilon_a \lambda_a}\,, \tag{A.1}$$

where $\bar{q} = q^\dagger \gamma_0$ and ϵ_a with $a = 0, \ldots, N_\mathrm{f}$ being the (infinitesimal) parameters that characterize the transformation. The Gell–Mann matrices λ_a are defined in Chap. 2. The sum $a = 1, \ldots, N_\mathrm{f}$ is implied in the notation of (A.1). Chiral rotations involve γ_5 in addition,

$$q \to q' = \mathrm{e}^{(\mathrm{i}/2)\eta_a \lambda_a \gamma_5}\, q\,, \quad \bar{q} \to \bar{q}' = \bar{q}\, \mathrm{e}^{(\mathrm{i}/2)\eta_a \lambda_a \gamma_5}\,, \tag{A.2}$$

with some different (infinitesimal) parameters η_a. The difference in the signs of the exponentials multiplying $\bar{q}$ in (A.1) and (A.2) arise from the anti-commutator $\gamma_0\gamma_5 + \gamma_5\gamma_0 = 0$. Note that under this transformation the chirality of a spinor is conserved, i.e., the properties $(1 \pm \gamma_5)\, q = 0$ are not affected. Transformations that act on purely left- and right-handed spinors as defined in (2.1) are characterized by $\epsilon_a = \eta_a$ and $\epsilon_a = -\eta_a$, respectively.

To summarize the transformation properties of quark bilinears under infinitesimal flavor and chiral rotations we first define the symmetric (d_{abc}) and anti-symmetric (f_{abc}) structure constants of the generators introduced in Chap. 2:

$$\lambda_a \lambda_b = \frac{2}{N_\mathrm{f}} \delta_{ab} + d_{abc} \lambda_c + \mathrm{i} f_{abc} \lambda_c\,. \tag{A.3}$$

This also includes the unit matrix in form of $\lambda_0 = \sqrt{2/N_\mathrm{f}}\, \mathbb{1}$. Though this is a notational convenience it brings into the game the complication that those

H. Weigel: *Chiral Properties of Quark Bilinears*, Lect. Notes Phys. **743**, 233–235 (2008)
DOI 10.1007/978-3-540-75436-7_12

components of d_{abc} with one or more of the subscripts being zero are not totally symmetric; using $i, j = 1, \ldots, N_{\rm f}^2 - 1$ we rather have

$$d_{000} = d_{00i} = d_{0i0} = 0 \quad d_{0ij} = d_{i0j} = \sqrt{\frac{2}{N_{\rm f}}}\,\delta_{ij} \quad \text{but} \quad d_{ij0} = 0\,. \tag{A.4}$$

In case none of the indices is zero, the d_{abc} are the well-known totally symmetric structure constants of $SU(N_{\rm f})$. The transformation properties are finally listed in Table A.1. Actually some of the flavor singlet ($a = 0$) bilinears are invariant since $f_{0bc} = 0$. With these transformation properties at hand it is straightforward to confirm that the combinations in (2.8) are indeed invariant under flavor and chiral rotations. As an example we consider the chiral transformation for the term multiplying G_1:

$$\begin{aligned}\Delta \sum_{a=0}^{N_{\rm f}^2-1} \left((\bar{q}\lambda_a q)^2 - (\bar{q}\lambda_a\gamma_5 q)^2\right) &= \frac{4{\rm i}}{N_{\rm f}} \sum_{i=1}^{N_{\rm f}^2-1} \eta_i \left[\bar{q}\lambda_i q\,\bar{q}\gamma_5 q - \bar{q}\lambda_i\gamma_5 q\,\bar{q}q\right] \\ &\quad + 2\,{\rm i} \sum_{\substack{a,b=0\\ i=1}}^{N_{\rm f}^2-1} d_{aib}\eta_i \left[\bar{q}\lambda_a q\,\bar{q}\lambda_b\gamma_5 q - \bar{q}\lambda_a\gamma_5 q\,\bar{q}\lambda_b q\right]. \end{aligned} \tag{A.5}$$

Naïvely the symmetry of d_{abc} suggests the last term to vanish. As already mentioned in (A.4), the symmetry does not hold in case one or more indices are zero and we have to discuss the case $a = 0$ separately,

$$\begin{aligned}\Delta \sum_{a=0}^{N_{\rm f}^2-1} \left((\bar{q}\lambda_a q)^2 - (\bar{q}\lambda_a\gamma_5 q)^2\right) &= \frac{4{\rm i}}{N_{\rm f}} \sum_{i=1}^{N_{\rm f}^2-1} \eta_i \left[\bar{q}\lambda_i q\,\bar{q}\gamma_5 q - \bar{q}\lambda_i\gamma_5 q\,\bar{q}q\right] \\ &\quad + 2\,{\rm i}\sqrt{\frac{2}{N_{\rm f}}} \sum_{\substack{b=0\\ i=1}}^{N_{\rm f}^2-1} d_{0ib}\eta_i \left[\bar{q}q\,\bar{q}\lambda_b\gamma_5 q - \bar{q}\gamma_5 q\,\bar{q}\lambda_b q\right]. \end{aligned} \tag{A.6}$$

Table A.1. Infinitesimal variations of selected quark bilinears under flavor and chiral rotations. According to the summation convention in (A.1) and (A.2) we have $\epsilon_0 = \eta_0 = 0$. In [1] a list may be found that does not utilize this condensed form including the $a = 0$ components

quark bilinear	flavor rot. (A.1)	chiral rot. (A.2)
$\Delta\bar{q}\lambda_a q$	$-f_{abc}\epsilon_b\bar{q}\lambda_c q$	${\rm i}\,\bar{q}\gamma_5\left(\frac{2}{N_{\rm f}}\eta_a + d_{abc}\eta_b\lambda_c\right) q$
$\Delta\bar{q}\gamma_5\lambda_a q$	$-f_{abc}\epsilon_b\bar{q}\gamma_5\lambda_c q$	${\rm i}\,\bar{q}\left(\frac{2}{N_{\rm f}}\eta_b + d_{abc}\eta_b\lambda_c\right) q$
$\Delta\bar{q}\gamma_\mu\lambda_a q$	$-f_{abc}\epsilon_b\bar{q}\gamma_\mu\lambda_c q$	$-f_{abc}\eta_b\bar{q}\gamma_\mu\gamma_5\lambda_c q$
$\Delta\bar{q}\gamma_\mu\gamma_5\lambda_a q$	$-f_{abc}\epsilon_b\bar{q}\gamma_\mu\gamma_5\lambda_c q$	$-f_{abc}\eta_b\bar{q}\gamma_\mu\lambda_c q$

Inserting (A.4) for d_{0ib} finally shows that the right hand side vanishes. That is, the considered combination of quark bilinears is indeed invariant under chiral rotations.

Reference

1. G. Ripka, *Quarks Bound to Chiral Fields.* Clarendon Press, Oxford, 1997. 234

Appendix B

Functional Techniques

In field theory, we often encounter quadratic actions (cf. Chaps. 2 and 3)

$$S[\phi] = \int \mathrm{d}^4x\, \phi(x)\hat{O}\phi(x) \tag{B.1}$$

for some linear operator $\hat{O}$ in path integrals alike (2.11),

$$Z = \int [D\phi]\, \mathrm{e}^{-\mathrm{i}S[\phi]}\,. \tag{B.2}$$

Formally, we expand ϕ in terms of eigenfunctions of $\hat{O}$,

$$\phi(x) = \sum_n a_n \phi_n(x) \qquad \text{with} \qquad \hat{O}\phi_n(x) = \lambda_n \phi_n(x)\,. \tag{B.3}$$

Orthogonality of the ϕ_n and Gaußian integration for a_n yield

$$\begin{aligned} Z &\propto \left[\prod_{n=1}^{\infty}\int_{-\infty}^{\infty}\mathrm{d}a_n\right] \exp\left[-\mathrm{i}\int \mathrm{d}^4x \sum_{k=1}^{\infty}\sum_{k'=1}^{\infty} a_k\phi_l(x)a_{k'}\lambda_{k'}\phi_{k'}(x)\right] \propto \prod_{n=1}^{\infty}\frac{1}{\sqrt{\lambda_n}} \\ &= N\left[\mathrm{Det}(\hat{O})\right]^{-\frac{1}{2}}\,. \end{aligned} \tag{B.4}$$

The normalization constant N is irrelevant to the logarithm

$$\ln\left(\frac{Z}{N}\right) = \ln\left[\mathrm{Det}(\hat{O})\right]^{-\frac{1}{2}} = -\frac{1}{2}\,\mathrm{Tr}\ln\left[\hat{O}\right]\,. \tag{B.5}$$

Commonly $\hat{O} = \hat{O}_0 + \hat{O}_{\mathrm{int}}$ where the second term contains the dynamics. Then the formal expansion

$$\begin{aligned} \ln\left[\hat{O}\right] &= \ln\left[\hat{O}_0\right] + \ln\left[1 + \hat{O}_0^{-1}\hat{O}_{\mathrm{int}}\right] \\ &= \ln\left[\hat{O}_0\right] + \hat{O}_0^{-1}\hat{O}_{\mathrm{int}} - \frac{1}{2}\hat{O}_0^{-1}\hat{O}_{\mathrm{int}}\hat{O}_0^{-1}\hat{O}_{\mathrm{int}} + \cdots \end{aligned} \tag{B.6}$$

defines the Feynman series. So far ϕ has been a real boson field. For complex boson fields, the integration space is twice as large, hence the factor $\frac{1}{2}$ on the right hand side of (B.5) is dropped in that case.

H. Weigel: *Functional Techniques*, Lect. Notes Phys. **743**, 237–241 (2008)
DOI 10.1007/978-3-540-75436-7_13

In case of fermions, the a_n are anti-commuting Grassman variables,

$$a_n a_m = -a_m a_n \,, \tag{B.7}$$

which implies $a_n^2 = 0$. The basic integration rules

$$\int \mathrm{d}a_n = 0 \qquad \text{and} \qquad \int \mathrm{d}a_n a_m = \delta_{nm} \tag{B.8}$$

follow from translational invariance of the measure. The eventual normalization on the right hand is set to unity. To evaluate the path integral

$$Z[M] = \left[\prod_{n=1}^{\infty} \int \mathrm{d}\bar{a}_n\right] \left[\prod_{m=1}^{\infty} \int \mathrm{d}a_m\right] \exp\left[\bar{a} \cdot M \cdot a\right] \tag{B.9}$$

for the c-number valued matrix M, we expand the exponential function. The rules in (B.7) and (B.8) enforce that any matrix element M_{nm} appears exactly once. In addition the result must be totally anti-symmetric. Therefore,

$$Z[M] \propto \mathrm{Det}(M) = \exp\left\{\mathrm{Tr}\,\left[\ln(M)\right]\right\}, \tag{B.10}$$

which can easily be verified for a low-dimensional matrix M. In field theory, the above result turns into expressions alike (2.14).

The basic identification for the computation of the above-encountered functional traces is

$$\mathrm{Tr}\{\ldots\} \longrightarrow \mathrm{tr} \int \mathrm{d}^{\bar{4}}x \, \langle x|\{\ldots\}|x\rangle \,. \tag{B.11}$$

Here "tr" involves discrete indices only and $|x\rangle$ is an eigenstate of the position operator, i.e., $\hat{x}|x\rangle = x|x\rangle$. In this space, the unit operator reads

$$\mathbb{1} = \int \mathrm{d}^4x \, |x\rangle\langle x| = \int \frac{\mathrm{d}^4k}{(2\pi)^4} |k\rangle\langle k| \,, \tag{B.12}$$

with $|k\rangle$ being momentum state conjugate to $|x\rangle$: $\langle k|x\rangle = \mathrm{e}^{\mathrm{i}k\cdot x}$. Matrix elements of local functions are diagonal:

$$\langle x|\phi(\hat{x})|y\rangle = \phi(x)\delta^4(x-y) \,. \tag{B.13}$$

In this functional language, the Fourier transform of a field has the compact notation

$$\widetilde{\phi}(q-k) = \int \mathrm{d}^4x \, \mathrm{e}^{\mathrm{i}(q-k)}\phi(x) = \langle q|\phi(\hat{x})|k\rangle, \tag{B.14}$$

with $|k\rangle$ and $|q\rangle$ eigenstates of the momentum operator. Then the gap equation that has been introduced in Chap. 2 is computed via

$$\frac{\delta}{\delta M_{ij}(y)}\mathrm{Tr}\log\left(\mathrm{i}\partial\!\!\!/ - M\right) = N_\mathrm{C}\mathrm{tr}_\mathrm{D}\langle y|\left(\mathrm{i}\partial\!\!\!/ - M\right)^{-1}_{ij}|y\rangle$$
$$= 4N_\mathrm{C}\int\frac{\mathrm{d}^4k}{(2\pi)^4}\left(k^2 - MM^\dagger\right)^{-1}_{ij}\,. \qquad \text{(B.15)}$$

Note that right hand side of the first equation defines the quark condensate, $\langle\bar{q}(x)q(x)\rangle$. The trace in that equation only concerns the Dirac indices of the γ-matrices. For the regularized action, (2.17), one finds under the assumption that the solution to the gap equation is diagonal in flavor space

$$4N_\mathrm{C}\delta_{ij}\int\frac{\mathrm{d}^4k}{(2\pi)^4}\int_{1/\Lambda^2}^\infty \mathrm{d}s\,\mathrm{e}^{-s\left(k^2+m_i^2\right)} = \frac{N_\mathrm{C}\delta_{ij}}{\pi^2}\int_{1/\Lambda^2}^\infty\frac{\mathrm{d}s}{s^2}\,\mathrm{e}^{-sm_i^2}\,, \quad \text{(B.16)}$$

since after Wick rotation the momentum integral is merely Gaußian. The result, (2.18), can be readily obtained from the definition of the incomplete Γ-function

$$\Gamma(u,x) = \int_x^\infty \mathrm{d}\tau\tau^{u-1}\mathrm{e}^{-\tau}\,, \qquad \text{(B.17)}$$

especially

$$\Gamma(0,x) = -\log x + \gamma + \mathcal{O}(x) \quad \text{for} \quad x\to 0^+ \qquad (\gamma = 0.57721\cdots) \quad \text{(B.18)}$$

motivates the regularization prescription (2.17). Other Γ-functions are obtained from the recursion relation

$$\Gamma(a+1,x) = a\Gamma(a,x) + x^a\mathrm{e}^{-x}\,. \qquad \text{(B.19)}$$

In Chap. 3, Γ-functions with half-integer index occur. The above recursion relates them to the complementary error function

$$\Gamma(\tfrac{1}{2},x^2) = \sqrt{\pi}\,\mathrm{erfc}(|x|)\,. \qquad \text{(B.20)}$$

Next we expand the regularized real part of the Euclidean action up to quadratic order in the pseudoscalar meson fields ϕ_a, cf. (2.20), starting from

$$\not{D}^\dagger_\mathrm{E}\not{D}_\mathrm{E} = A_0 + A_1 + A_2 + \cdots\,. \qquad \text{(B.21)}$$

The subscripts indicate the order at which ϕ_a appears. Explicitly we have

$$A_0 = \partial^2 + m^2\,, \quad A_1 = m\gamma_5\left[\partial\!\!\!/\sum_a\phi_a\lambda_a\right] \quad \text{and} \quad A_2 = 0\,, \qquad \text{(B.22)}$$

where m is the constituent quark mass, recall that flavor symmetry is assumed. Obviously, only derivatives of ϕ occur. This is a consequence of the chiral invariance of $\mathrm{Det}\not{D}^\dagger_\mathrm{E}\not{D}_\mathrm{E}$. The formal series

$$\begin{aligned}\mathcal{A}_{\rm F} &= -\frac{1}{2}\int_{1/\Lambda^2}^{\infty}\frac{{\rm d}s}{s}\,{\rm Tr}\,\exp\left(-s\not{D}_{\rm E}^{\dagger}\not{D}_{\rm E}\right)\\ &= -\frac{1}{2}\int_{1/\Lambda^2}^{\infty}\frac{{\rm d}s}{s}\,{\rm Tr}\,{\rm e}^{-sA_0}+\frac{1}{2}\int_{1/\Lambda^2}^{\infty}{\rm d}s\int_0^1{\rm d}\zeta\,{\rm Tr}\,{\rm e}^{-s\zeta A_0}A_2{\rm e}^{-s(1-\zeta)A_0}\\ &\quad -\frac{1}{2}\int_{1/\Lambda^2}^{\infty}{\rm d}s s\int_0^1{\rm d}\zeta\int_0^{1-\zeta}{\rm d}\eta\,{\rm Tr}\,{\rm e}^{-s\eta A_0}A_1{\rm e}^{-s(1-\zeta-\eta)A_0}A_1{\rm e}^{-s\zeta A_0}\\ &\quad +\mathcal{O}(\phi_a^3)\end{aligned}\tag{B.23}$$

allows us to systematically expand $\mathcal{A}_{\rm F}$. It is convenient to evaluate the functional trace in (Euclidian) momentum space since $\langle k|A_0|q\rangle = (-k^2+m^2)\,\delta(k-q)$. The matrix elements of the operators in $A_{1,2}$ that are local in coordinate space may be expressed in terms of the corresponding Fourier transformation (B.14). Due to the cyclic property of the trace, only the linear combination $\alpha=\zeta+\eta\in[0,1]$ occurs in the exponential functions and we may straightforwardly integrate over $\beta=\zeta-\eta\in[-\alpha,\alpha]$. The α-integral is simplified by the symmetry $\alpha\leftrightarrow 1-\alpha$,

$$\begin{aligned}\mathcal{A}_{\rm F}^{(2)} &= -\frac{m^2N_{\rm C}}{4}\int_{1/\Lambda^2}^{\infty}{\rm d}s s\int_0^1{\rm d}\alpha\int\frac{{\rm d}^4q}{(2\pi)^4}\int\frac{{\rm d}^4k}{(2\pi)^4}\,{\rm tr}_{\rm DF}\\ &\quad\times{\rm e}^{-s\alpha(k^2+m^2)}\gamma_5\not{q}\widetilde{\phi}_a(q)\lambda_a{\rm e}^{-s(1-\alpha)((k-q)^2+m^2)}\gamma_5(-\not{q})\widetilde{\phi}_b(-q)\lambda_b\,.\end{aligned}\tag{B.24}$$

After the shift $k\to k-(1-\alpha)q$ that integral is computed as in (B.16) and the s-integral is expressed as an incomplete Γ-function. Final evaluation of the Dirac and flavor traces yields (2.21) and (2.22).

Let us round off this appendix by an outline for the computation of the pion matrix element of the axial current $\langle 0|\bar{q}(x)\gamma_\mu\gamma_5\frac{\tau^a}{2}q(x)|\pi^b(q)\rangle = if_\pi(q^2)q_\mu\delta_{ab}\,{\rm e}^{-{\rm i}qx}$. Here $a,b=1,2,3$ refers to the isovector components of ϕ. This matrix element defines the pion decay constant, f_π, cf. Sect. 2.5. First we note that we formally get the expectation value of the axial current for prescribed meson fields (ϕ_a, etc.) from a functional derivative of the extended action

$$\langle\bar{q}(x)\gamma_\mu\gamma_5\frac{\tau^a}{2}q(x)\rangle=\frac{\delta}{\delta a^{a,\mu}(x)}\,{\rm Tr}_\Lambda\log\left[{\rm i}\not{D}+\boldsymbol{a}_\nu(\hat{x})\cdot\frac{\boldsymbol{\tau}}{2}\gamma_\nu\gamma_5\right]\Big|_{\boldsymbol{a}_\mu=0},\tag{B.25}$$

where the need for regularization is indicated. This equation just tells us to expand the full action to linear order in the external source $\boldsymbol{a}_\mu(x)$ which can easily be accomplished by adding $\boldsymbol{a}_\mu(x)\gamma^\mu\gamma_5\frac{\boldsymbol{\tau}}{2}$ to the operator A_1 in (B.22). For the one-pion matrix element, it suffices to expand up to linear order in the pseudoscalar fields. Then the relevant part of the action will be similar to (B.24), with one of the $q_\nu\widetilde{\phi}_a\lambda_a$ replaced by $\widetilde{\boldsymbol{a}}_\nu(q)\cdot\frac{\boldsymbol{\tau}}{2}$. The remainder of the calculation proceeds as for (B.24). In the final matrix element with the pion state, the q-integral disappears. Finally $\frac{\delta}{\delta a^{a,\mu}(x)}\widetilde{a}_{b,\nu}(q)=g_{\mu\nu}\delta_{ab}\,{\rm e}^{{\rm i}qx}$ renders the functional form of the above definition. Note that the pion and ϕ fields are differently normalized, $\boldsymbol{\pi}=f_\pi\boldsymbol{\phi}$, since the propagator of a field operator

associated with a one-particle state has unit residue. This similarity between the expansion of the action up to quadratic order in ϕ^a and the computation of the axial current matrix element clearly shows that (2.23) equals the pion decay constant (squared).

Appendix C

Baryon Current and Wess–Zumino Term

Here we will review the calculations showing that the topological current arises from the gradient expansion of the expectation value of a baryon source and as a symmetry current from the Wess–Zumino term. Furthermore we gauge the Wess–Zumino by photon fields and discuss the relevance for the decay of π^0.

C.1 Gradient Expansion of the Fermion Determinant with a Baryon Source

It is well known that the topological current arises as the leading term in the gradient expansion of the corresponding one-quark-loop expectation value [1]. Nevertheless we repeat the essential points of that calculation because this relation is essential for many of the arguments in the main text. In doing so, we apply the functional techniques of Appendix A to the approach of [2]. Essentially we only consider the coupling of the quarks to the chiral field U as in (2.20),

$$M(x) = mU(x) = g\,[\sigma(x) + \mathrm{i}\boldsymbol{\tau}\cdot\boldsymbol{\pi}(x)] \quad \text{with} \quad \sigma^2(x) + \boldsymbol{\pi}^2(x) = f_\pi^2\,. \quad \text{(C.1)}$$

We explicitly use neither the limitation to two flavors nor the unitary condition for σ and $\boldsymbol{\pi}$. However, we omit flavor symmetry breaking effects. We have defined the coupling constant $g = m/f_\pi$ because it is customary to parameterize the vacuum expectation value $\langle\sigma\rangle = f_\pi$ in the linear sigma model. For simplification we furthermore introduce

$$M_5(x) = g\,[\sigma(x) + \mathrm{i}\gamma_5\boldsymbol{\tau}\cdot\boldsymbol{\pi}(x)]\ . \quad \text{(C.2)}$$

The expectation value of the baryon current solely concerns the fermion part of the generating functional, (2.14) and may be formally written as

H. Weigel: *Baryon Current and Wess–Zumino Term*, Lect. Notes Phys. **743**, 243–252 (2008)
DOI 10.1007/978-3-540-75436-7_14

$$\begin{aligned}\langle B_\mu(y)\rangle &= \frac{1}{N}\int [D\psi]\left[D\bar\psi\right]\bar\psi(y)\gamma_\mu\frac{1}{N_\mathrm{C}}\psi(y)\\ &\quad\times\exp\left[\mathrm{i}\int \mathrm{d}^4x\,\bar\psi(x)\left(\mathrm{i}\partial\!\!\!/ - M_5(x)\right)\psi(x)\right]\\ &= \frac{\mathrm{i}}{N_\mathrm{C}}\frac{\delta}{\delta s_\mu(y)}\ln\mathrm{Det}\left[\mathrm{i}\partial\!\!\!/ - M_5 - s\!\!\!/\right]_{s_\mu=0}\end{aligned}\tag{C.3}$$

since each quark carries baryon number $1/N_\mathrm{C}$. In the first equation the normalization factor N is merely the functional integral without the baryon current. In the second part it is taken care of by the logarithmic derivative. The expectation value on the left hand side is with respect to a prescribed configuration $M(x)$. The interaction via M_5 does not affect color degrees of freedom, hence that part of the determinant can be trivially computed and we write

$$\langle B_\mu(y)\rangle = -\mathrm{i}\mathrm{Tr}'\left[(\mathrm{i}\partial\!\!\!/ - M_5)^{-1}\,\gamma_\mu\delta^{(4)}(\hat x - y)\right]\,,\tag{C.4}$$

where Tr' denotes space–time integration (eventually in momentum space) and the sum over Dirac and flavor indices; the color trace, however, has already been performed. In (C.4) the hat ($\hat{}$) indicates the position operator as defined after (B.11). It should not be confused with the symbol for a unit vector. To set up the gradient expansion we expand

$$M_5(x) = M_5^{(0)} + \delta M_5(x)\,,\tag{C.5}$$

where the first term on the right hand side has the properties

$$M_5^{(0)} = \mathrm{const}\quad\text{and}\quad M_5^{(0)}\left[M_5^{(0)}\right]^\dagger = m^2\,.\tag{C.6}$$

Note that the latter condition does not imply the chiral circle condition which would have to be imposed on the total field $M_5(x)$. The idea is to expand (C.4) in powers of $\delta M_5(x)$. Due to chiral symmetry, the result will be a function of only $M_5^{(0)}$ and derivatives of $\delta M_5(x)$. At the end we replace

$$M_5^{(0)}\longrightarrow M_5(x)\quad\text{and}\quad\partial_\mu\delta M_5(x)\longrightarrow\partial_\mu M_5(x)\,,\tag{C.7}$$

to obtain the gradient expansion approximation. Rather than going through the full calculation it is considerably simplifying to have an educated guess for the result. We know that the baryon current has the quantum numbers of the scalar–isoscalar ω meson which couples to three pions but neither to two pions nor to $\sigma\boldsymbol{\pi}$ due to isospin and G-parity invariance. Defining $\phi_a = (\boldsymbol{\pi},\sigma)_a$ we therefore expect

$$\langle B_\mu(y)\rangle = S(\phi_0^2)\,\epsilon_{abcd}\epsilon_{\mu\nu\rho\sigma}\,\phi_a^{(0)}\partial^\nu\left[\delta\phi_b\right]\partial^\rho\left[\delta\phi_c\right]\partial^\sigma\left[\delta\phi_d\right] + \cdots\,,\tag{C.8}$$

where $\phi_a^{(0)}$and $\delta\phi_a$ are obtained from $M_5^{(0)}$ and $\delta M_5(x)$, respectively and $\phi_0^2 = \sum_{a=1}^4\phi_a^{(0)}\phi_a^{(0)}$. Obviously the above formulation is consistent with the bosonic

character of the (pseudo)scalar mesons. The main task now is to compute the coefficient function $S(\phi_0^2)$. Evidently the educated guess, (C.8) can only emerge from the contribution that is of third order in δM_5 in (C.3). Writing

$$(\mathrm{i}\partial\!\!\!/ - M_5)^{-1} = [1 - (\mathrm{i}\partial\!\!\!/ - M_5^{(0)})^{-1}\delta M_5]^{-1}(\mathrm{i}\partial\!\!\!/ - M_5^{(0)})^{-1} \tag{C.9}$$

the expansion of the factor in square brackets yields the unique third order contribution

$$\begin{aligned}\langle B_\mu(y)\rangle = -\mathrm{i}\mathrm{Tr}'\{&(\mathrm{i}\partial\!\!\!/ - M_5^{(0)})^{-1}\delta M_5(\mathrm{i}\partial\!\!\!/ - M_5^{(0)})^{-1}\delta M_5 \\ &\times(\mathrm{i}\partial\!\!\!/ - M_5^{(0)})^{-1}\delta M_5(\mathrm{i}\partial\!\!\!/ - M_5^{(0)})^{-1}\,\gamma_\mu\delta^{(4)}(\hat{x}-y)\} + \cdots\ .\end{aligned} \tag{C.10}$$

Without loss of generality we may chose the chiral basis such that $M_5^{(0)} = m\mathbb{1} = gf_\pi\mathbb{1}$ and $\delta M_5 = \mathrm{i}g\boldsymbol{\tau}\cdot\boldsymbol{\pi}\gamma_5 = \mathrm{i}g\Pi\gamma_5$. In the last term we have defined a matrix in flavor space. The choice of this basis is helpful to sum over the Dirac indices because then the right hand side of (C.11) contains three factors of γ_5. To get $\epsilon_{\mu\nu\rho\sigma}$ we need to pick up four γ-matrices in (C.11), three of which must emerge from the propagators. As there are four propagators, one of them must deliver $M_5^{(0)}$ and there are four possible combinations to do so. This is most compactly presented in momentum space,

$$\begin{aligned}\langle B_\mu(y)\rangle = 4\mathrm{i}mg^3\epsilon_{\mu\nu\rho\sigma}&\int\frac{\mathrm{d}^4q_1}{(2\pi)^4}\,\frac{1}{q_1^2-m^2}\,\cdots\int\frac{\mathrm{d}^4q_4}{(2\pi)^4}\,\frac{1}{q_4^2-m^2} \\ &\times\{q_2^\nu q_3^\rho q_4^\sigma - q_1^\nu q_3^\rho q_4^\sigma + q_1^\nu q_2^\rho q_4^\sigma - q_1^\nu q_2^\rho q_3^\sigma\}\,\mathrm{e}^{i(q_4-q_1)y} \\ &\times\mathrm{tr}_\mathrm{F}\left[\widetilde{\Pi}(q_1-q_2)\widetilde{\Pi}(q_2-q_3)\widetilde{\Pi}(q_3-q_4)\right] + \cdots\ .\end{aligned} \tag{C.11}$$

The omitted lower index in any of the products of momenta within the curly brackets indicates the propagator that delivered $M_5^{(0)}$ and the alternating signs originate from various anti-commutators of γ_5 and $\not{q}_i$. Furthermore $\widetilde{\Pi}$ denotes the Fourier transformation of Π according to (B.14). Using

$$\begin{aligned}\epsilon_{\mu\nu\rho\sigma}\{&q_2^\nu q_3^\rho q_4^\sigma - q_1^\nu q_3^\rho q_4^\sigma + q_1^\nu q_2^\rho q_4^\sigma - q_1^\nu q_2^\rho q_3^\sigma\} \\ &= \epsilon_{\mu\nu\rho\sigma}\,(q_2-q_1)^\nu\,(q_3-q_2)^\rho\,(q_4-q_3)^\sigma\end{aligned} \tag{C.12}$$

we observe that the momentum factors coincide with the arguments of the Fourier transforms. That is, we may, e.g., write

$$(q_2-q_1)^\nu\,\widetilde{\Pi}(q_1-q_2) = -\mathrm{i}\widetilde{[\partial^\nu\Pi]}(q_1-q_2)\,.$$

After appropriate redefinition of the momenta this yields

$$\langle B_\mu(y)\rangle = 4mg^3\epsilon_{\mu\nu\rho\sigma}\int\frac{\mathrm{d}^4r}{(2\pi)^4}\,\frac{\mathrm{d}^4s}{(2\pi)^4}\,\frac{\mathrm{d}^4t}{(2\pi)^4}\,\mathrm{e}^{-\mathrm{i}(r+s+t)y}\int\frac{\mathrm{d}^4l}{(2\pi)^4}$$

$$\times \frac{\mathrm{tr_F}\,\widetilde{[\partial^\nu \Pi]}(r)\,\widetilde{[\partial^\rho \Pi]}(s)\,\widetilde{[\partial^\sigma \Pi]}(t)}{[l^2-m^2]\,[(l-r)^2-m^2]\,[(l-r-s)^2-m^2]\,[(l-r-s-t)^2-m^2]} + \ldots \quad . \tag{C.13}$$

The gradient expansion is a power series in the external momenta r, s and t; these momenta are assumed small compared to m. In leading order we omit them in the denominator and replace

$$\int \frac{\mathrm{d}^4 l}{(2\pi)^4}\,\frac{1}{\{\ldots\}} \quad \overset{\text{gradient}}{\underset{\text{expansion}}{\blacktriangleright}} \quad \int \frac{\mathrm{d}^4 l}{(2\pi)^4}\,\frac{1}{(l^2-m^2)^4} = \frac{\mathrm{i}}{96\pi^2 m^4} \tag{C.14}$$

where the imaginary unit stems from the Wick rotation. Without the complicated dependences on the external momenta, the Fourier transformations can easily be undone, they just yield the coordinate space analogs. Collecting pieces, we find the leading order (l.o.) gradient expansion to the baryon current,

$$\langle B_\mu(y)\rangle_{\text{l.o.}} = \frac{\mathrm{i}g^3}{24\pi^2 m^3}\epsilon_{\mu\nu\rho\sigma}\,\mathrm{tr_F}\,[\partial^\nu \Pi]\,(y)\,[\partial^\rho \Pi]\,(y)\,[\partial^\sigma \Pi]\,(y)\,. \tag{C.15}$$

This exactly is the Goldstone–Wilczek current [1]. Finally we want to express this result in a chiral invariant fashion in terms of U. We note that a chiral invariant quantity must contain as many Us as $U^\dagger$s and that

$$mU^\dagger \partial_\mu U = m\alpha_\mu = g\mathrm{i}\partial_\mu \Pi + \ldots\,, \tag{C.16}$$

with α_μ defined after (2.40). This then uniquely yields the chirally invariant result

$$\langle B_\mu\rangle_{\text{l.o.}} = \frac{1}{24\pi^2}\,\epsilon_{\mu\nu\rho\sigma}\,\mathrm{tr_F}\left\{\left[U^\dagger\partial^\nu U\right]\left[U^\dagger\partial^\rho U\right]\left[U^\dagger\partial^\sigma U\right]\right\}\,. \tag{C.17}$$

which is nothing but the topological or winding number current.

The Skyrme soliton picture of baryons makes extensive use of and strongly relies on the above identification of the baryon current. For the derivation of that relation spontaneous chiral symmetry breaking is essential as without it, $M^{(0)}$ vanishes and the gradient expansion in (C.14) remains undefined. For spontaneous chiral symmetry to occur it is necessary that $N_\mathrm{f} \geq 2$ since otherwise the symmetry is anyhow broken by the anomaly. Thus, even though the arguments put forward in favor of the soliton picture in Sect. 4.1 appear to be valid for any number of flavors, a cogent consideration requires at least two flavors.

C.2 Gauging the Wess–Zumino Term

In Sect. 2.4 we already encountered the non-local Wess–Zumino term, see (2.50). This time we want to start from that action together with the

transformation properties on the meson fields, (2.30), to show that the winding number current emerges as symmetry current for the baryon charge from $\Gamma_{\rm WZ}$. A straightforward procedure to extract symmetry currents is to introduce gauge fields to elevate global symmetries to local ones. The terms in the gauged action that are linear in the gauge fields then determine the symmetry currents. Unfortunately it is not straightforward to gauge the Wess–Zumino term because the common description of introducing covariant derivatives only works for local action functionals. Rather we have to construct the gauge invariant action by a trial and error method. For our purposes (baryon current and electromagnetic π^0 decay) it is sufficient to only consider $U_{\rm V}(1)$ symmetries and thus abelian gauge fields. This simplifies matters considerably. The result for the general non-abelian case is given in the literature [3, 4].

First of all, we simplify the notation by introducing alternating differential forms, $\alpha = \alpha_\mu {\rm d}x^\mu$, ${\rm d} = \partial_\mu {\rm d}x^\mu$, $\alpha\beta = \alpha_\mu\beta_\nu\, {\rm d}x^\mu \wedge {\rm d}x^\nu$, etc. In that notation the Wess–Zumino term is compactly written as

$$\Gamma_{\rm WZ} = -\frac{{\rm i}N_{\rm C}}{240\pi^2}\int_5 {\rm tr}\,\left(\alpha^5\right)\,. \tag{C.18}$$

Here the integral is over a five-dimensional manifold with Minkowski space as boundary. With respect to vector symmetries, $L = R = 1 + {\rm i}\epsilon Q + \cdots$ in (2.30), the variation of the chiral field is given by the commutator,

$$\delta U = {\rm i}\epsilon[Q, U] \tag{C.19}$$

where ϵ parameterizes the infinitesimal transformation and Q is the generator of the considered $U_{\rm V}(1)$ symmetry. We assume ϵ to be a local quantity,

$$\delta\alpha = {\rm i}\epsilon[Q,\alpha] + {\rm i}{\rm d}\epsilon\left(U^\dagger Q U - Q\right)\,. \tag{C.20}$$

Note that $\delta\alpha$ is a differential one-form. When substituting into $\delta\int{\rm tr}(\alpha^5) = 5\int{\rm tr}(\delta\alpha\alpha^4)$ the first term of (C.20) does not contribute as it merely reflects the global symmetry. The variation due to the derivative term is

$$\delta\Gamma_{\rm WZ} = \frac{N_{\rm C}}{48\pi^2}\int_5 {\rm d}\epsilon\,{\rm tr}\,\left[\left(U^\dagger Q U - Q\right)\alpha^4\right] = -\frac{N_{\rm C}}{48\pi^2}\int_5 {\rm d}\epsilon\,{\rm tr}\,\left[Q\left(\alpha^4 - \beta^4\right)\right]\,. \tag{C.21}$$

where $\beta_\mu = U\partial_\mu U^\dagger = -U\alpha_\mu U^\dagger$. By pure definition we have $\alpha^4 = -{\rm d}(\alpha^3)$ and $\beta^4 = -{\rm d}(\beta^3)$. Thus

$$\delta\Gamma_{\rm WZ} = \frac{N_{\rm C}}{48\pi^2}\int_5 {\rm d}\epsilon\,{\rm d}\,{\rm tr}\,\left[Q\left(\alpha^3 - \beta^3\right)\right] = -\frac{N_{\rm C}}{48\pi^2}\int_4 {\rm d}\epsilon\,{\rm tr}\,\left[Q\left(\alpha^3 - \beta^3\right)\right] \tag{C.22}$$

by Stoke's theorem. Obviously the non-local Wess–Zumino term is not gauge invariant but the gauge variation is local. We introduce a gauge field, $\mathcal{A}_\mu$ to compensate for $\delta\Gamma_{\rm WZ}$,

$$\Gamma^{(1)}_{\rm WZ} = -\frac{{\rm i}N_{\rm C}}{240\pi^2}\int_5 {\rm tr}\,\left(\alpha^5\right) + \frac{N_{\rm C}}{48\pi^2}\int_4 \mathcal{A}\,{\rm tr}\left[Q\left(\alpha^3-\beta^3\right)\right]\,, \tag{C.23}$$

with $\delta\mathcal{A}_\mu = \partial_\mu\epsilon$. Hence $\Gamma^{(1)}_{\rm WZ}$ is invariant to $\mathcal{O}(Q)$, but not completely as the explicit calculation exhibits

$$\begin{aligned}\delta\Gamma^{(1)}_{\rm WZ} &= \frac{{\rm i}N_{\rm C}}{24\pi^2}\int_4 \mathcal{A}\,{\rm d}\epsilon\,{\rm tr}\left[Q^2\left(\alpha^2-\beta^2\right)+Q{\rm d}UQ{\rm d}U^\dagger\right]\\ &= \frac{{\rm i}N_{\rm C}}{24\pi^2}\int_4 \epsilon\,{\rm d}\mathcal{A}\,{\rm tr}\left[Q^2\left(\alpha-\beta\right)+\tfrac{1}{2}\left(Q{\rm d}UQU^\dagger - QUQ{\rm d}U^\dagger\right)\right]\,.\end{aligned} \tag{C.24}$$

Here it has, e.g., been used that $\int {\rm tr}\,[Q\alpha Q\alpha] = 0$, as a reflection of the anti-symmetric nature of differential forms. In addition, the freedom in re-writing the $Q{\rm d}UQ{\rm d}U^\dagger$ term has been fixed by demanding invariance with respect to parity $U \leftrightarrow U^\dagger$ [4]. Again, we add a term, now quadratic in $\mathcal{A}_\mu$, to compensate for the variation $\delta\Gamma^{(1)}_{\rm WZ}$,

$$\begin{aligned}\Gamma^{(2)}_{\rm WZ} = &-\frac{{\rm i}N_{\rm C}}{240\pi^2}\int_5 {\rm tr}\,\left(\alpha^5\right) + \frac{N_{\rm C}}{48\pi^2}\int_4 \mathcal{A}\,{\rm tr}\left[Q\left(\alpha^3-\beta^3\right)\right]\\ &+\frac{{\rm i}N_{\rm C}}{24\pi^2}\int_4 \mathcal{A}\,{\rm d}\mathcal{A}\,{\rm tr}\left[Q^2\left(\alpha-\beta\right)+\tfrac{1}{2}\left(Q{\rm d}UQU^\dagger - QUQ{\rm d}U^\dagger\right)\right]\,.\end{aligned} \tag{C.25}$$

It is now straightforward to verify that the last term in square brackets is indeed gauge invariant and so is $\Gamma^{(2)}_{\rm WZ}$. The term linear in $\mathcal{A}$ contributes to the Noether current; cf. last term in (5.46).

As indicated above, this result can be utilized to obtain the baryon current by setting $Q = \mathbb{1}/N_{\rm C}$, the baryon charge of a quark in a world with $N_{\rm C}$ color degrees of freedom. The term linear in the gauge field (second term in (C.25)) yields,

$$B_\mu = \frac{1}{48\pi^2}\epsilon_{\mu\nu\rho\sigma}{\rm tr}\left[(\alpha^\nu\alpha^\rho\alpha^\sigma - \beta^\nu\beta^\rho\beta^\sigma)\right] = \frac{1}{24\pi^2}\epsilon_{\mu\nu\rho\sigma}{\rm tr}\left[\alpha^\nu\alpha^\rho\alpha^\sigma\right]\,, \tag{C.26}$$

which, as expected, is the same result as obtained from the quark loop in leading order, (C.17). This identity, of course, indirectly proves that the imaginary part of the Euclidean fermion determinant leads to the Wess–Zumino term in the effective meson theory. In (C.25) the terms quadratic in $\mathcal{A}$ vanish for $Q \propto \mathbb{1}$.

Note, however, that a kind of miracle occurred in deriving (C.26). For the $Q \propto \mathbb{1}$ there is no variation of U as in (C.19), hence one would not expect one for the Wess–Zumino term either. Nevertheless a variation occurred in (C.21) in form of a total derivative. In a local theory this would just be fine as such total derivatives would be discarded. Here it is not the case as this total derivative term of the non-local theory contributes locally in four dimensional Minkowski space. This is just one of many examples indicating that it is dangerous to use intuition from local theories to manipulate the Wess–Zumino term. As a rule of thumb, it is unavoidable to perform calculations explicitly. For this end it is occasionally helpful to write $U(x) = V(x)U_0(x)V^\dagger(x)$

with all matrices defined on the five-dimensional manifold. Using that parameterization and applying once again Stoke's theorem the Wess–Zumino term becomes [5]

$$\begin{aligned}\Gamma_{\rm WZ}[U] &= \frac{-{\rm i}N_{\rm C}}{240\pi^2}\int_5 {\rm tr}[v+U_0(\alpha_0-v)U_0^\dagger]^5 \\ &= \Gamma_{\rm WZ}[U_0] - \frac{{\rm i}N_{\rm C}}{48\pi^2}\int_4 {\rm tr}\left[\alpha_0^3 v - v^3\alpha_0 - \frac{1}{2}(\alpha_0 v)^2 + U_0(\alpha_0-v)^3U_0^\dagger v\right. \\ &\qquad \left. -v^3U_0(\alpha_0-v)U_0^\dagger - \frac{1}{2}[vU_0(\alpha_0-v)U_0^\dagger]^2\right] \\ &= \Gamma_{\rm WZ}[U_0] - \frac{{\rm i}N_{\rm C}}{48\pi^2}\int_4 {\rm tr}[\alpha_0^3(v+U_0^\dagger v U_0)] + \mathcal{O}(v^2)\,, \end{aligned} \tag{C.27}$$

where $\alpha_0^\mu = U_0^\dagger\partial^\mu U_0$ and $v^\mu = V^\dagger\partial^\mu V$. A significant simplification occurs when $V(x)$ depends on only a single coordinate, as it happens to be the case in the collective coordinate approach to the $SU(3)$ hedgehog, cf. (6.4). Then only terms linear in v_μ can contribute due to the anti-symmetric structure of the alternating differential forms. This is indicated in the last line of (C.27).

C.3 Wess–Zumino Term in the Bound State Approach

In this section we prove that in the bound state approach the Wess–Zumino term emerges exactly as shown in the last term of (6.39). For this end we will show that the equation of motion (4.44) is the same as applying Euler–Lagrange to (6.39). This is sufficient because the Wess–Zumino term has mainly been introduced to provide that equation of motion. It is obvious that the Skyrme term contributions may be ignored for this discussion. Nevertheless, there is one caveat. Equation (4.44) is only one form of the equation of motion. Equivalently we may write

$$-\frac{f_\pi^2}{2}\,\partial_\mu\beta^\mu + 5{\rm i}\lambda\epsilon_{\mu\nu\rho\sigma}\beta^\mu\beta^\nu\beta^\rho\beta^\sigma = 0 \tag{C.28}$$

since $\beta_\mu = -U\alpha_\mu U^\dagger$ and thus $\partial_\mu\beta^\mu = -U\partial_\mu\alpha^\mu U^\dagger$. We have to find the proper combination to identify the variation of (6.39). Using the parameterization of (6.38) the term linear in Z from (4.44) reads

$$\begin{aligned}\frac{f_\pi^2}{2}\left\{\partial^2 Z - 2{\rm i}\,[v_\mu,\partial^\mu Z] + [\partial_\mu r^\mu, Z] + [l_\mu,[r^\mu,Z]]\right\} \\ -40\lambda\epsilon_{\mu\nu\rho\sigma}\,[p^\mu p^\nu p^\rho, \partial^\sigma Z + [r^\mu, Z]] = 0\,, \end{aligned} \tag{C.29}$$

with $r_\mu = \xi^\dagger\partial_\mu\xi$ and $l_\mu = \xi\partial_\mu\xi^\dagger$. Furthermore p_μ and v_μ are defined as in Sect. 6.6, i.e., (4.62) with $\xi \to \xi_\pi$. This implies $p_\mu = \frac{\rm i}{2}(l_\mu - r_\mu)$ and $v_\mu = \frac{\rm i}{2}(l_\mu + r_\mu)$. From (C.28) we find a similar equation of motion, with l_μ and r_μ exchanged. Combining these two equations yields,

$$\frac{f_\pi^2}{2}\Big\{\partial^2 Z - 2\mathrm{i}\,[v_\mu, \partial^\mu Z] - \mathrm{i}\,[\partial_\mu v^\mu, Z] + \frac{1}{2}\,[l_\mu, [r^\mu, Z]] + \frac{1}{2}\,[r_\mu, [l^\mu, Z]]\Big\}$$
$$-40\lambda\epsilon_{\mu\nu\rho\sigma}\,[p^\mu p^\nu p^\rho, \partial^\sigma Z - \mathrm{i}\,[v^\mu, Z]] = 0\,. \qquad \text{(C.30)}$$

In the isospin reduction we take the same symbols r_μ, etc., to merely denote their (non-zero) $SU(2)$ entries. Since $l \cdot r + r \cdot l = 2(p^2 - v^2)$ the equation of motion for the isospinor K reads,

$$\partial^2 K - 2\mathrm{i}v_\mu\partial^\mu K - \mathrm{i}(\partial_\mu v^\mu)K + \left(p_\mu^2 - v_\mu^2\right) K$$
$$-\frac{80\lambda}{f_\pi^2}\epsilon_{\mu\nu\rho\sigma}p^\mu p^\nu p^\rho\left(\partial^\sigma - \mathrm{i}v^\sigma\right) K = 0\,. \qquad \text{(C.31)}$$

In the isospin reduction p_μ^2 and $\epsilon_{\mu\nu\rho\sigma}p^\mu p^\nu p^\rho$ are both pure isoscalar expressions and we may replace them by the respective traces divided by 2. With $p_\mu = -\frac{\mathrm{i}}{2}\xi\alpha_\mu\xi^\dagger$ we finally obtain

$$\partial^2 K - 2\mathrm{i}v_\mu\partial^\mu K - \mathrm{i}(\partial_\mu v^\mu)K - v_\mu^2 K + \frac{1}{2}\mathrm{tr}\left(p_\mu^2\right) K$$
$$+\frac{\mathrm{i}N_\mathrm{C}}{2f_\pi^2}B_\mu\left(\partial^\mu - \mathrm{i}v^\mu\right) K = 0\,, \qquad \text{(C.32)}$$

where we have inserted $\lambda = \frac{-N_\mathrm{C}}{240\pi^2}$ and used the definition of the baryon current, (C.26). Similarly an equation of motion for $K^\dagger$ can be extracted from (C.30); it is merely the hermitean conjugate of (C.32). It is now a matter of simple algebra to verify that the Euler–Lagrange equations from (6.39) give the same equation of motion (apart from Skyrme and mass terms). This proves the form of the Wess–Zumino term in (6.39) correct. We had to combine the equations of motion in the two equivalent forms, (4.44) and (C.28) simply because the variation for obtaining the kaon equation of motion requires an infinitesimal axial transformation, $\delta U(x) = \{\epsilon(x), U(x)\}$, to maintain its pseudoscalar nature. A right transformation only as in (4.41) in general supplements scalar modes.

C.4 π^0 Decay

On the fundamental level of quark–photon interactions the π^0 decay is described by the Feynman diagrams in Fig. C.1. In these diagrams the pion is represented by an axial current via the PCAC relation, cf. Sect. 2.5. The two fermion axial current vertices contain γ_5 and any symmetry-conversing regularization of the fermion loop momentum shows that the two diagrams do not cancel each other as one would naïvely find if the diagrams were superficially finite. This anomalous non-cancellation gives a non-zero result for the π^0 decay width. We will now work out how such a result emerges in the effective meson theory from the Wess–Zumino term.

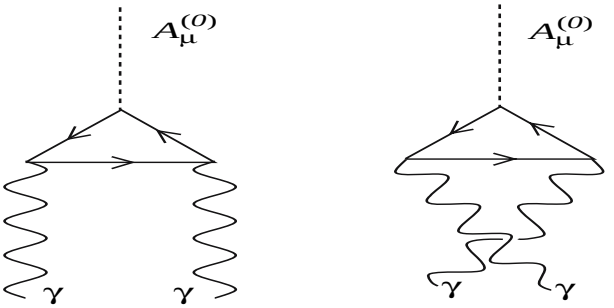

Fig. C.1. Feynman diagrams that describe the π^0 decay. Here $A_\mu^{(0)}$ is the (electrically neutral) axial current that represents (derivative of) the pion field

From the last term in (C.25) we compute the width for the decay $\pi^0 \to \gamma\gamma$ because it contains the coupling of a pseudoscalar meson to two gauge bosons. To gauge with respect to the electromagnetic interaction we first conclude from the baryon number of a single quark $B_\mathrm{q} = \frac{1}{N_\mathrm{C}}$ that the charges of the up and down quarks are $Q_\mathrm{u} = \frac{e}{2}\left(\frac{1}{N_\mathrm{C}} + 1\right)$ and $Q_\mathrm{d} = \frac{e}{2}\left(\frac{1}{N_\mathrm{C}} - 1\right)$ where e is the elementary electric charge. In the case of two light flavors[1] we therefore set

$$Q = \frac{e}{2}\left(\tau_3 + \frac{1}{N_\mathrm{C}}\mathbb{1}\right) . \tag{C.34}$$

We expand the chiral field in powers of the physical pion field $U = 1 + \mathrm{i}\boldsymbol{\tau}\cdot\boldsymbol{\pi}/f_\pi$ and find the relevant interaction Lagrangian after integration by parts

$$\mathcal{L}_{\pi\gamma\gamma} = -\frac{N_\mathrm{C} e^2}{24\pi^2 f_\pi}\epsilon_{\mu\nu\rho\sigma}\partial^\mu \mathcal{A}^\nu \partial^\rho \mathcal{A}^\sigma \mathrm{tr}\left[3Q^2\boldsymbol{\tau}\cdot\boldsymbol{\pi}\right] = -\frac{\pi^0}{8\pi^2 f\pi}\epsilon_{\mu\nu\rho\sigma}\partial^\mu \mathcal{A}^\nu \partial^\rho \mathcal{A}^\sigma . \tag{C.35}$$

Using standard techniques of second quantization we obtain the transition matrix element for the decay of the neutral pion into two photons,

$$\begin{aligned}\mathcal{M}_\mathrm{fi} &= \frac{e^2}{4\pi^2 f_\pi}\epsilon_{\mu\nu\rho\sigma} k_1^\mu \epsilon^{*\nu}(\boldsymbol{k}_1, \lambda_1) k_2^\rho \epsilon^{*\sigma}(\boldsymbol{k}_2, \lambda_2)(2\pi)^4 \delta(p - k_1 - k_2) \\ &=: (2\pi)^4 \delta(p - k_1 - k_2)\mathcal{T}_\mathrm{fi} .\end{aligned} \tag{C.36}$$

[1] For $N_\mathrm{f} = 3$ we furthermore have $Q_\mathrm{s} = \frac{e}{2}\left(\frac{1}{N_\mathrm{C}} - 1\right)$ for the charge of the strange quark and hence

$$Q = \frac{e}{2}\left[\lambda_3 + \frac{1}{\sqrt{3}}\lambda_8 + \left(\frac{1}{N_\mathrm{C}} - \frac{1}{3}\right)\mathbb{1}\right] . \tag{C.33}$$

With $\lambda_8/\sqrt{3} = Y = N_\mathrm{C}\hat{B}/3 + \hat{S}$ and $\mathbb{1} = N_\mathrm{C}\hat{B}$ we have $Q = (2\hat{I}_3 + \hat{B} + \hat{S})/2$ and the charge of any hadron is unambiguously determined by its flavor quantum numbers as for N_C=3.

The pion momentum is p and the photons have momenta k_1 and k_2 with polarizations λ_1 and λ_2, respectively, and $\epsilon^{*\nu}(\boldsymbol{k}_i, \lambda_i)$ are the corresponding polarization vectors. The decay width Γ is computed by squaring $\mathcal{T}_{\rm fi}$, summing over the polarizations of the final photons, taking care of total momentum conservation and integrating over the available phase space of the two photons. Note that a factor $1/2$ arises to comply with Bose statistics of the decay products,

$$\Gamma = \frac{1}{2m_\pi}\frac{1}{2}\sum_{\lambda_1\lambda_2}\int \frac{\mathrm{d}^3k_1}{(2\pi)^3 2k_1^0}\,\frac{\mathrm{d}^3k_2}{(2\pi)^3 2k_2^0}(2\pi)^4\delta^4(p-k_1-k_2)|\mathcal{T}_{\rm fi}|^2\,. \qquad \text{(C.37)}$$

The integrals are most conveniently evaluated in the pion rest frame that is defined by setting the pion momentum to $p^\mu = (m_\pi, \mathbf{0})^\mu$, and implies $k^\mu_{1,2} = (\omega, \pm\boldsymbol{k})^\mu$ for the photon momenta. Hence

$$\Gamma = \frac{\alpha^2 m_\pi^3}{32\pi^2 f_\pi}\int \mathrm{d}\omega\,\delta(m_\pi - 2\omega)\int\frac{\mathrm{d}^2k}{4\pi^2} = \frac{\alpha^2 m_\pi^3}{64\pi^3 f_\pi}\,, \qquad \text{(C.38)}$$

where $\alpha = e^4/4\pi = 1/137$ is the QED fine structure constant. Inserting numerical values yields $\Gamma \approx 7.6\,\mathrm{eV}$. This compares reasonably well with the experimental value, $\Gamma = (8.2 \pm 0.6)\,\mathrm{eV}$ [6]. This is, of course, one of the most striking empirical evidences for the relevance of the Wess–Zumino term.

The final result, (C.38), obtained by gauging the Wess–Zumino term, coincides with that deduced from the triangle anomaly in the microscopic fermion theory in conjunction with PCAC to identify the pion field [7]. The corresponding Feynman diagrams are depicted in Fig. C.1. For this identification, the coefficient of the Wess–Zumino term is crucial, in particular its $N_{\rm C}$ dependence that arises from $N_{\rm C}$ fermions running through the loop. In reversing the line of arguments, Witten [3] concluded that the integer in (4.49) had to equal $N_{\rm C}$.

References

1. J. Goldstone and F. Wilczek, *Phys. Rev. Lett.* **47** (1981) 986. 243, 246
2. I. J. R. Aitchison and C. M. Fraser, *Phys. Rev.* **D31** (1985) 2605. 243
3. E. Witten, *Nucl. Phys.* **B223** (1983) 422, 433. 247, 252
4. O. Kaymakcalan, S. Rajeev, and J. Schechter, *Phys. Rev.* **D30** (1984) 594. 247, 248
5. A. P. Balachandran, F. Lizzi, V. G. J. Rodgers, and A. Stern, *Nucl. Phys.* **B256** (1985) 525. 249
6. S. Eidelman et al. [PDG], *Phys. Lett.* **B592** (2004) 1. 252
7. M. E. Peskin and D. V. Schroeder, *An Introduction to Quantum Field Theory*, Chap. 19.3. Perseus Books, Reading, MA, 1995. 252

Appendix D

$SU(3)$ Euler Angles

In this appendix, we display the explicit forms of the right $SU(3)$ generators R_a $(a = 1, .., 8)$ in terms of differential operators with respect to $SU(3)$ "Euler angles" [1]. The current presentation briefly summarizes the calculations of [2, 3].

An appropriate definition of the $SU(3)$ Euler angles is given by parameterizing the collective flavor rotations (6.4) via

$$\begin{aligned} A = & \, \mathrm{e}^{-\mathrm{i}(\alpha/2)\lambda_3}\mathrm{e}^{-\mathrm{i}(\beta/2)\lambda_2}\mathrm{e}^{-\mathrm{i}(\gamma/2)\lambda_3}\mathrm{e}^{-\mathrm{i}\nu\lambda_4} \\ & \times \mathrm{e}^{-\mathrm{i}(\alpha'/2)\lambda_3}\mathrm{e}^{-\mathrm{i}(\beta'/2)\lambda_2}\mathrm{e}^{-\mathrm{i}(\gamma'/2)\lambda_3}\mathrm{e}^{-\mathrm{i}(\rho/\sqrt{3})\lambda_8} \, . \end{aligned} \tag{D.1}$$

This is merely the $SU(3)$ generalization of (5.12). The group manifold is completely covered by varying the angles $\alpha, \beta, ..., \rho$ according to

$$0 \leq \alpha, \gamma, \alpha', \gamma' < 2\pi, \; 0 \leq \beta, \beta' < \pi, \; 0 \leq \nu < \pi/2, \; 0 \leq \rho < 3\pi. \tag{D.2}$$

Since the $SU(3)$ generators are linear operators, they may in general be written as linear combinations of differential operators [4, 5]

$$R_a = \mathrm{i} d_{ba}(\boldsymbol{\alpha}) \frac{\partial}{\partial \alpha_b}, \tag{D.3}$$

where $\boldsymbol{\alpha} = (\alpha_1, \alpha_2, ..., \alpha_8) = (\alpha, \beta, ..., \rho)$ compactly refers to the eight "Euler angles." The coefficient functions $d_{ab}(\boldsymbol{\alpha})$ will be extracted from the defining equation of the $SU(3)$ algebra

$$A R_a A^\dagger = \frac{1}{2} A \lambda_a A^\dagger = \frac{1}{2} \lambda_b D_{ba}(\boldsymbol{\alpha}). \tag{D.4}$$

As in (5.32), D_{ab} denotes the adjoint representation of the rotation matrix A. The explicit computation of the derivatives defines

$$M_{bc}(\boldsymbol{\alpha}) = \frac{1}{2} \mathrm{tr} \left[\lambda_b A \mathrm{i} \frac{\partial}{\partial \alpha_c} A^\dagger \right] . \tag{D.5}$$

H. Weigel: ***SU(3) Euler Angles***, Lect. Notes Phys. **743**, 253–258 (2008)
DOI 10.1007/978-3-540-75436-7_15

We use this to compute the left hand side of (D.4) and read off the coefficients

$$d_{ab}(\boldsymbol{\alpha}) = \big(M^{-1}(\boldsymbol{\alpha})\big)_{ac} D_{cb}(\boldsymbol{\alpha}) \tag{D.6}$$

and substitute them into (D.3). Then the explicit expressions for the generators are

$$\begin{aligned}
R_1 &= \mathrm{i}\frac{\cos\gamma'}{\sin\beta'}\frac{\partial}{\partial\alpha'} - \mathrm{i}\sin\gamma'\frac{\partial}{\partial\beta'} - \mathrm{i}\cos\gamma'\cot\beta'\frac{\partial}{\partial\gamma'}\,,\\
R_2 &= -\mathrm{i}\frac{\sin\gamma'}{\sin\beta'}\frac{\partial}{\partial\alpha'} - \mathrm{i}\cos\gamma'\frac{\partial}{\partial\beta'} + \mathrm{i}\sin\gamma'\cot\beta'\frac{\partial}{\partial\gamma'}\,,\\
R_3 &= -\mathrm{i}\frac{\partial}{\partial\gamma'}\,,\\
R_4 &= -\,\mathrm{i}\sin\Big(\gamma-\rho+\tfrac{\alpha'-\gamma'}{2}\Big)\frac{\sin\frac{\beta'}{2}}{\sin\beta\sin\nu}\frac{\partial}{\partial\alpha} - \mathrm{i}\cos\Big(\gamma-\rho+\tfrac{\alpha'-\gamma'}{2}\Big)\frac{\sin\frac{\beta'}{2}}{\sin\nu}\frac{\partial}{\partial\beta}\\
&\quad -\,\mathrm{i}\left[2\sin\Big(\rho+\tfrac{\alpha'+\gamma'}{2}\Big)\frac{\cos\frac{\beta'}{2}}{\sin 2\nu} - \sin\Big(\gamma-\rho+\tfrac{\alpha'-\gamma'}{2}\Big)\cot\beta\frac{\sin\frac{\beta'}{2}}{\sin\nu}\right]\frac{\partial}{\partial\gamma}\\
&\quad -\,\frac{\mathrm{i}}{2}\cos\Big(\rho+\tfrac{\alpha'+\gamma'}{2}\Big)\cos\frac{\beta'}{2}\frac{\partial}{\partial\nu} - \frac{3\mathrm{i}}{4}\sin\Big(\rho+\tfrac{\alpha'+\gamma'}{2}\Big)\tan\nu\cos\frac{\beta'}{2}\frac{\partial}{\partial\rho}\\
&\quad +\,\frac{\mathrm{i}}{2}\sin\Big(\rho+\tfrac{\alpha'+\gamma'}{2}\Big)\left[\cos\frac{\beta'}{2}\tan\nu + \frac{\cot\nu}{\cos\frac{\beta'}{2}}\right]\frac{\partial}{\partial\alpha'}\\
&\quad +\,\mathrm{i}\cos\Big(\rho+\tfrac{\alpha'+\gamma'}{2}\Big)\cot\nu\sin\frac{\beta'}{2}\frac{\partial}{\partial\beta'} + \frac{\mathrm{i}}{2}\sin\Big(\rho+\tfrac{\alpha'+\gamma'}{2}\Big)\frac{\cot\nu}{\cos\frac{\beta'}{2}}\frac{\partial}{\partial\gamma'},\\
R_5 &= \mathrm{i}\cos\Big(\gamma-\rho+\tfrac{\alpha'-\gamma'}{2}\Big)\frac{\sin\frac{\beta'}{2}}{\sin\beta\sin\nu}\frac{\partial}{\partial\alpha} - \mathrm{i}\sin\Big(\gamma-\rho+\tfrac{\alpha'-\gamma'}{2}\Big)\frac{\sin\frac{\beta'}{2}}{\sin\nu}\frac{\partial}{\partial\beta}\\
&\quad -\,\mathrm{i}\left[2\cos\Big(\rho+\tfrac{\alpha'+\gamma'}{2}\Big)\frac{\cos\frac{\beta'}{2}}{\sin 2\nu} + \cos\Big(\gamma-\rho+\tfrac{\alpha'-\gamma'}{2}\Big)\cot\beta\frac{\sin\frac{\beta'}{2}}{\sin\nu}\right]\frac{\partial}{\partial\gamma}\\
&\quad +\,\frac{\mathrm{i}}{2}\sin\Big(\rho+\tfrac{\alpha'+\gamma'}{2}\Big)\cos\frac{\beta'}{2}\frac{\partial}{\partial\nu} - \frac{3\mathrm{i}}{4}\cos\Big(\rho+\tfrac{\alpha'+\gamma'}{2}\Big)\tan\nu\cos\frac{\beta'}{2}\frac{\partial}{\partial\rho}\\
&\quad +\,\frac{\mathrm{i}}{2}\cos\Big(\rho+\tfrac{\alpha'+\gamma'}{2}\Big)\left[\cos\frac{\beta'}{2}\tan\nu + \frac{\cot\nu}{\cos\frac{\beta'}{2}}\right]\frac{\partial}{\partial\alpha'}\\
&\quad -\,\mathrm{i}\sin\Big(\rho+\tfrac{\alpha'+\gamma'}{2}\Big)\cot\nu\sin\frac{\beta'}{2}\frac{\partial}{\partial\beta'} + \frac{\mathrm{i}}{2}\cos\Big(\rho+\tfrac{\alpha'+\gamma'}{2}\Big)\frac{\cot\nu}{\cos\frac{\beta'}{2}}\frac{\partial}{\partial\gamma'},\\
R_6 &= -\mathrm{i}\sin\Big(\gamma-\rho+\tfrac{\alpha'+\gamma'}{2}\Big)\frac{\cos\frac{\beta'}{2}}{\sin\beta\sin\nu}\frac{\partial}{\partial\alpha} - \mathrm{i}\cos\Big(\gamma-\rho+\tfrac{\alpha'+\gamma'}{2}\Big)\frac{\cos\frac{\beta'}{2}}{\sin\nu}\frac{\partial}{\partial\beta}\\
&\quad +\,\mathrm{i}\left[2\sin\Big(\rho+\tfrac{\alpha'-\gamma'}{2}\Big)\frac{\sin\frac{\beta'}{2}}{\sin 2\nu} + \sin\Big(\gamma-\rho+\tfrac{\alpha'+\gamma'}{2}\Big)\cot\beta\frac{\cos\frac{\beta'}{2}}{\sin\nu}\right]\frac{\partial}{\partial\gamma}
\end{aligned}$$

$$
\begin{aligned}
&+\frac{\mathrm{i}}{2}\cos\Big(\rho+\tfrac{\alpha'-\gamma'}{2}\Big)\sin\frac{\beta'}{2}\frac{\partial}{\partial\nu}+\frac{3\mathrm{i}}{4}\sin\Big(\rho+\tfrac{\alpha'-\gamma'}{2}\Big)\tan\nu\sin\frac{\beta'}{2}\frac{\partial}{\partial\rho}\\
&-\frac{\mathrm{i}}{2}\sin\Big(\rho+\tfrac{\alpha'-\gamma'}{2}\Big)\left[\sin\frac{\beta'}{2}\tan\nu+\frac{\cot\nu}{\sin\frac{\beta'}{2}}\right]\frac{\partial}{\partial\alpha'}\\
&+\mathrm{i}\cos\Big(\rho+\tfrac{\alpha'-\gamma'}{2}\Big)\cot\nu\cos\frac{\beta'}{2}\frac{\partial}{\partial\beta'}+\frac{\mathrm{i}}{2}\sin\Big(\rho+\tfrac{\alpha'-\gamma'}{2}\Big)\frac{\cot\nu}{\sin\frac{\beta'}{2}}\frac{\partial}{\partial\gamma'}\,,\\
R_7=&\,\mathrm{i}\cos\Big(\gamma-\rho+\tfrac{\alpha'+\gamma'}{2}\Big)\frac{\cos\frac{\beta'}{2}}{\sin\beta\sin\nu}\frac{\partial}{\partial\alpha}-\mathrm{i}\sin\Big(\gamma-\rho+\tfrac{\alpha'+\gamma'}{2}\Big)\frac{\cos\frac{\beta'}{2}}{\sin\nu}\frac{\partial}{\partial\beta}\\
&+\mathrm{i}\left[2\cos\Big(\rho+\tfrac{\alpha'-\gamma'}{2}\Big)\frac{\sin\frac{\beta'}{2}}{\sin 2\nu}-\cos\Big(\gamma-\rho+\tfrac{\alpha'+\gamma'}{2}\Big)\cot\beta\frac{\cos\frac{\beta'}{2}}{\sin\nu}\right]\frac{\partial}{\partial\gamma}\\
&-\frac{\mathrm{i}}{2}\sin\Big(\rho+\tfrac{\alpha'-\gamma'}{2}\Big)\sin\frac{\beta'}{2}\frac{\partial}{\partial\nu}+\frac{3\mathrm{i}}{4}\cos\Big(\rho+\tfrac{\alpha'-\gamma'}{2}\Big)\tan\nu\sin\frac{\beta'}{2}\frac{\partial}{\partial\rho}\\
&-\frac{\mathrm{i}}{2}\cos\Big(\rho+\tfrac{\alpha'-\gamma'}{2}\Big)\left[\sin\frac{\beta'}{2}\tan\nu+\frac{\cot\nu}{\sin\frac{\beta'}{2}}\right]\frac{\partial}{\partial\alpha'}\\
&-\mathrm{i}\sin\Big(\rho+\tfrac{\alpha'-\gamma'}{2}\Big)\cot\nu\cos\frac{\beta'}{2}\frac{\partial}{\partial\beta'}+\frac{\mathrm{i}}{2}\cos\Big(\rho+\tfrac{\alpha'-\gamma'}{2}\Big)\frac{\cot\nu}{\sin\frac{\beta'}{2}}\frac{\partial}{\partial\gamma'}\,,\\
R_8=&-\frac{\mathrm{i}\sqrt{3}}{2}\frac{\partial}{\partial\rho}\,.
\end{aligned}
\tag{D.7}
$$

Here we also want to outline how the eigenvalue problem for the collective Hamiltonian (6.26) reduces to coupled differential equations for functions which only depend on the strangeness changing angle ν. Up to the normalization, a suitable decomposition of the baryon wave functions is given by [1]

$$
\begin{aligned}
\Psi(I,I_3,Y;J,J_3,Y_\mathrm{R})=&\sum_{M_\mathrm{L},M_\mathrm{R}}D^{(I)*}_{I_3,M_\mathrm{L}}(\alpha,\beta,\gamma)f^{(I,Y;J,Y_\mathrm{R})}_{M_\mathrm{L},M_\mathrm{R}}(\nu)\\
&\times\mathrm{e}^{\mathrm{i}Y_\mathrm{R}\rho}D^{(J)*}_{M_\mathrm{R},-J_3}(\alpha',\beta',\gamma').
\end{aligned}
\tag{D.8}
$$

The D-functions refer to $SU(2)$ Wigner functions. It is important to note that the sums over the intrinsic spins ($M_\mathrm{R}=-J,-J+1,...,J$) and isospins ($M_\mathrm{L}=-I,-I+1,...,I$) are subject to the constraint $M_\mathrm{L}-M_\mathrm{R}=(Y-Y_\mathrm{R})/2$. Using the explicit forms for the $SU(3)$ generators (D.7), the action of the quadratic Casimir operator $C_2=\sum_{a=1}^{8}R_a^2$ on the baryon wave function (D.8) is found to be

$$
\begin{aligned}
C_2\Psi(I,I_3,Y;J,J_3,Y_\mathrm{R})=&\sum_{M_\mathrm{L},M_\mathrm{R}}D^{(I)*}_{I_3,M_\mathrm{L}}(\alpha,\beta,\gamma)\mathrm{e}^{\mathrm{i}Y_\mathrm{R}\rho}D^{(J)*}_{J_3,M_\mathrm{R}}(\alpha',\beta',\gamma')\\
\times\Bigg\{&-\frac{1}{4}\left[\frac{\mathrm{d}^2}{\mathrm{d}\nu^2}+(3\cot\nu-\tan\nu)\,\frac{\mathrm{d}}{\mathrm{d}\nu}\right]+\frac{I^2+J^2}{\sin^2\nu}+\frac{M_\mathrm{L}^2}{\cos^2\nu}
\end{aligned}
$$

$$
\begin{aligned}
&+\frac{M_{\rm R}^2}{4}\left(3+\frac{1}{\cos^2\nu}\right)-\frac{1+\cos^2\nu}{\sin^2\nu\cos^2\nu}M_{\rm L}M_{\rm R}+\frac{3Y_{\rm R}M_{\rm L}}{2\cos^2\nu}\\
&\quad -3\frac{1+\cos^2\nu}{4\cos^2\nu}Y_{\rm R}M_{\rm R}+\Big(\frac{3}{4}+\frac{9}{16}\tan^2\nu\Big)Y_{\rm R}^2\Bigg\}f^{(I,Y;J,Y_{\rm R})}_{M_{\rm L},M_{\rm R}}(\nu)\\
&-\frac{\cos\nu}{\sin^2\nu}\sqrt{(I+M_{\rm L}+1)\,(I-M_{\rm L})\,(J+M_{\rm R}+1)\,(J-M_{\rm R})}\;f^{(I,Y;J,Y_{\rm R})}_{M_{\rm L}+1,M_{\rm R}+1}(\nu)\\
&-\frac{\cos\nu}{\sin^2\nu}\sqrt{(I-M_{\rm L}+1)\,(I+M_{\rm L})\,(J-M_{\rm R}+1)\,(J+M_{\rm R})}\;f^{(I,Y;J,Y_{\rm R})}_{M_{\rm L}-1,M_{\rm R}-1}(\nu)\,.
\end{aligned}
\tag{D.9}
$$

Obviously, the dependence on the angles other than ν can be factorized leaving a set of coupled ordinary differential equations in the variable ν. This becomes even more transparent by displaying the ν dependence of the dominating symmetry breaking term in the collective Hamiltonian (6.26):

$$
1-D_{88}=\frac{3}{2}\sin^2\nu. \tag{D.10}
$$

Equation (D.9) also illustrates how the intrinsic functions $f^{(I,Y;J,Y_{\rm R})}_{M_{\rm L},M_{\rm R}}(\nu)$ depend on the spin and isospin quantum numbers.

The eigenvalue equation $C_2\Psi=\mu\Psi$ yields the flavor symmetric $SU(3)$ D-functions, which correspond to states in irreducible representations. As an example, we display the non-vanishing intrinsic isoscalar functions for the baryon octet with $Y_{\rm R}=1$ and $\mu=3$ [5].

$$
\begin{aligned}
N:\;& f^{\frac12,1;\frac12,1}_{\frac12,\frac12}(\nu)=\cos^2\nu\,,\quad f^{\frac12,1;\frac12,1}_{-\frac12,-\frac12}(\nu)=\cos\nu\,;\\
\Sigma:\;& f^{1,0;\frac12,1}_{0,\frac12}(\nu)=\frac{1}{\sqrt{2}}\cos\nu\sin\nu\,,\quad f^{1,0;\frac12,1}_{-1,-\frac12}(\nu)=\sin\nu\,;\\
\Lambda:\;& f^{0,0;\frac12,1}_{0,\frac12}(\nu)=\sqrt{\frac{3}{2}}\sin\nu\cos\nu\;;\qquad \Xi:\;f^{\frac12,-1;\frac12,1}_{-\frac12,\frac12}(\nu)=\sin^2\nu\;.
\end{aligned}
\tag{D.11}
$$

All other octet isoscalar functions vanish because of the constraint $M_{\rm L}-M_{\rm R}=(Y-1)/2$. The normalization is always such that

$$
\int_0^{\frac{\pi}{2}}{\rm d}\nu\sin2\nu\sin^2\nu\sum_{M_{\rm L}M_{\rm R}}\Big[f^{(I,Y;J,Y_{\rm R})}_{M_{\rm L},M_{\rm R}}(\nu)\Big]^2=\frac{(2J+1)(2I+1)}{16}\,. \tag{D.12}
$$

Obviously, none of these wave functions vanish except at the boundaries $\nu=0,\pi/2$. This is, of course, a special feature of the ground states, which reside in the octet representation. The isoscalar wave functions associated with baryons in higher dimensional representations, which carry the same physical quantum numbers (I,J,Y), may well develop nodes.

When the eigenvalue problem is augmented by symmetry breaking terms, the intrinsic function deviate from (D.11) such that they get more pronounced at small ν, i.e., rotations into the direction of strangeness are suppressed. This can also be deduced from Fig. D.1, where the dependencies of the nucleon

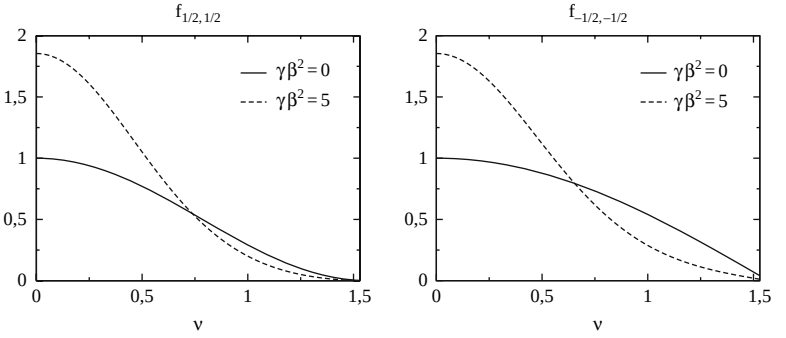

Fig. D.1. The dependencies of the nucleon scalar functions on the strangeness changing angle ν for two values of the symmetry breaking. The case $\gamma\beta^2 = 0$ should be compared with the expressions for (N) in (D.11)

isoscalar functions $f^{\frac{1}{2},1;\frac{1}{2},1}_{\pm\frac{1}{2},\pm\frac{1}{2}}(\nu)$ are displayed for the symmetric case, $\gamma\beta^2 = 0$, as well as for sizable symmetry breaking $\gamma\beta^2 = 5$. We note that this diagonalization approach can indeed be generalized to arbitrary (odd) $N_{\rm C}$ by implementing the constraint $Y_{\rm R} = \frac{N_{\rm C}}{3}$ [6] in (D.9).

Finally, we add a few comments on the treatment of the slow rotator discussed in Sect. 6.5. In a first step, the explicit form (D.9) for the Casimir operator is used in order to express the Hamiltonian, (6.37), as a second-order differential equation for the isoscalar functions $f^{(I,Y;J,Y_{\rm R})}_{M_{\rm L},M_{\rm R}}(\nu)$, which are defined in equation (D.8). These coupled differential equations are then integrated by standard means. In order to evaluate matrix elements, one again employs the decomposition equation (D.8) to reduce them to expressions which only contain functions of the strangeness changing angle ν and $f^{(I,Y;J,Y_{\rm R})}_{M_{\rm L},M_{\rm R}}(\nu)$. The final result is obtained by integrating with respect to the measure, cf. (D.12),

$$\int_0^{\frac{\pi}{2}} {\rm d}\nu\, \sin 2\nu\, \sin^2\nu \left\{ \cdots \right\} . \tag{D.13}$$

As an example, we present the V_1 contribution in (7.7) to the proton magnetic moment,

$$\begin{aligned}
\mu_p = &-\frac{8\pi}{3} M_N \int_0^{\frac{\pi}{2}} {\rm d}\nu\, \sin 2\nu\, \sin^2\nu\, m_1(\nu) \\
&\times \left\{ \frac{2}{3}\sin^2\nu \left(\left(f^{\frac{1}{2},1;\frac{1}{2},1}_{\frac{1}{2},\frac{1}{2}}(\nu) \right)^2 - \left(f^{\frac{1}{2},1;\frac{1}{2},1}_{-\frac{1}{2},-\frac{1}{2}}(\nu) \right)^2 \right) \right. \\
&-\frac{2}{9} \Big[\left(1+\cos^2\nu\right) \left(\left(f^{\frac{1}{2},1;\frac{1}{2},1}_{\frac{1}{2},\frac{1}{2}}(\nu) \right)^2 + \left(f^{\frac{1}{2},1;\frac{1}{2},1}_{-\frac{1}{2},-\frac{1}{2}}(\nu) \right)^2 \right) \\
&\left. +8\cos\nu f^{\frac{1}{2},1;\frac{1}{2},1}_{\frac{1}{2},\frac{1}{2}}(\nu) f^{\frac{1}{2},1;\frac{1}{2},1}_{-\frac{1}{2},-\frac{1}{2}}(\nu) \Big] \right\} .
\end{aligned} \tag{D.14}$$

The ν dependence of m_1 is purely due to the implicit dependence of the chiral angle $F = F(r, \nu)$:

$$m_1(\nu) = \int_0^\infty \mathrm{d}r r^2 \sin^2 F \left[f_\pi^2 + \frac{1}{e^2} \left(F'^2 + \frac{\sin F}{r^2} \right) + \frac{2}{3} (f_K^2 - f_\pi^2) \cos F \right] . \quad \text{(D.15)}$$

Here a prime indicates a derivative with respect to the radial coordinate, i.e., $F' = \partial F(r, \nu)/\partial r$.

References

1. H. Yabu and K. Ando, *Nucl. Phys.* **B301** (1988) 601. 253, 255
2. H. Weigel, *Int. J. Mod. Phys.* **A11** (1996) 2419. 253
3. N. W. Park, J. Schechter, and H. Weigel, *Phys. Rev.* **D43** (1991) 869. 253
4. T. J. Nelson, *J. Math. Phys.* **8** (1967) 857. 253
5. D. F. Holland, *J. Math. Phys.* **10** (1969) 531. 253, 256
6. H. Walliser and H. Weigel, *Eur. Phys. J.* **A26** (2005) 361. 257

Appendix E

Matrix Elements of Momentum Eigenstates

In this appendix we review the evaluation of matrix elements between momentum eigenstates of the soliton that are needed to compute the current matrix elements in Chap. 7. Mostly we will follow the discussion of [1].

E.1 Momentum Eigenstates from Collective Coordinates

In Chapters 5 and 6 we have extensively discussed how to generate states with good flavor quantum numbers from the soliton by means of collective coordinate quantization. However, this is not sufficient to compute form factors. To this end we also need eigenstates with good momentum. The conjugate coordinate is the translation of the soliton and we again introduce respective collective variables, $\boldsymbol{X}(t)$ to parameterize the time-dependent chiral field,

$$U(\boldsymbol{x},t) = U_0\left(\boldsymbol{x} - \boldsymbol{X}(t)\right) , \tag{E.1}$$

where U_0 refers to the hedgehog configuration of (4.23). Due to translational invariance, the Lagrangian that emerges from substituting the configuration, (E.1), will depend on $X(t)$ only through its time derivative $\boldsymbol{V} = \dot{\boldsymbol{X}}(t)$. For the time being and simplicity we omit collective coordinates for the flavor orientation of the soliton for the following reason. As long as we consider effective meson Lagrangians with at most two time derivatives, the coupling between translational and rotational modes can only be proportional to $\boldsymbol{V}\cdot\boldsymbol{\Omega}$, where $\boldsymbol{\Omega}$ is the angular velocity defined in (5.16). Such a coupling is odd under parity and thus disallowed. The Lagrange function obtained for the configuration (E.1) has the general structure

$$L(\boldsymbol{V}) = -E_{\rm cl} + \frac{1}{2} M_{\rm trans} \boldsymbol{V}^2 , \tag{E.2}$$

where $E_{\rm cl}$ is the classical soliton mass and $M_{\rm trans}$ is also a functional of the soliton profiles. In case of the Skyrme model one finds $M_{\rm trans} = \frac{2}{3}\left(M_2 + 2M_4\right)$

H. Weigel: *Matrix Elements of Momentum Eigenstates*, Lect. Notes Phys. **743**, 259–263 (2008)
DOI 10.1007/978-3-540-75436-7_16

where M_2 and M_4 are the contributions to $E_{\rm cl}$ from $\mathcal{L}_{{\rm nl}\sigma}$, (4.22), and $\mathcal{L}_{\rm Sk}$, (4.26), respectively. In the absence of the mass term, simple scaling arguments [2] show that the stationary condition for the soliton implies $M_2 = M_4 = E_{\rm cl}/2$ and thus $M_{\rm trans} = E_{\rm cl}$. In a more general framework we note that (E.1) is merely the non-relativistic form of the Lorentz boost $U_H(\Lambda(\boldsymbol{V}) \cdot x)$ with $\Lambda(\boldsymbol{V})$ being the 4×4 matrix that parameterizes the boost of a four-vector such as $x = (t, \boldsymbol{x})$. Since the Lagrangian density is a Lorentz scalar, the only effect of $\boldsymbol{V} \neq 0$ on L arises from the volume integration yielding a factor $\sqrt{1 - \boldsymbol{V}^2}$ on $E_{\rm cl}$. Expansion with respect to $\boldsymbol{V}$ immediately shows $M_{\rm trans} = E_{\rm cl}$, an identity that we will henceforth adopt.

The conjugate momentum is

$$\boldsymbol{P} = \frac{\partial L(\boldsymbol{V})}{\partial \boldsymbol{V}} = E_{\rm cl} \boldsymbol{V} \,. \tag{E.3}$$

The quantization of $\boldsymbol{P}$ is just that of a free non-relativistic particle with the dispersion relation $E = E_{\rm cl} + \frac{\boldsymbol{P}^2}{2E_{\rm cl}}$. The full wave function for a baryon B becomes

$$\langle B; \boldsymbol{P}; I, J, \ldots | \boldsymbol{X}; A \rangle = \mathcal{N} {\rm e}^{-{\rm i}\boldsymbol{X}\cdot\boldsymbol{P}} D_{I,J,\ldots}(A) \,, \tag{E.4}$$

where we have reintroduced the rotational degrees of freedom and $\mathcal{N}$ is a normalization factor that must be chosen compatible with the normalization of the spinor in (7.4). Its value depends on whether we take $A \in SU(2)$ or $A \in SU(3)$. Here we do not further specify $\mathcal{N}$ nor the Wigner D-functions.

To compute form factors we have to evaluate matrix elements of the form

$$\langle B; \boldsymbol{P}; I, J, \ldots | v(0) | B', \boldsymbol{P}'; I', J', \ldots \rangle \,, \tag{E.5}$$

where $v(0)$ is some current operator to be evaluated at the origin $x = (\boldsymbol{x}, t) = 0$ because the translational piece of matrix element is commonly factored out in the definition of form factors [3]. Within soliton models, the parameterization (5.13) (or its $SU(3)$ generalization, (6.4)) and (E.2) formally yield the current operator

$$v(\boldsymbol{x}, t) = \sum_i f_i \left(\boldsymbol{x} - \boldsymbol{X}(t) \right) \mathcal{O}_i(A) \,, \tag{E.6}$$

that is, a sum of products in which one factor depends on the spatial and the other on the rotational coordinates. We thus find

$$\begin{aligned} &\langle B; \boldsymbol{P}; I, J, \ldots | v(0) | B', \boldsymbol{P}'; I', J', \ldots \rangle = \\ &\int {\rm d}^3X {\rm d}^3X' \int {\rm d}A \int {\rm d}A' \langle B; \boldsymbol{P}; I, J, \ldots \rangle \langle X, A | v(0) | X' A' \rangle \langle B', \boldsymbol{P}'; I', J', \ldots \rangle \\ &= \mathcal{N}\mathcal{N}' \sum_i \int {\rm d}^3X {\rm e}^{{\rm i}\boldsymbol{X}\cdot\boldsymbol{q}} f_i \left(-\boldsymbol{X}(t) \right) \int {\rm d}A D^*_{I,J,\ldots}(A) \mathcal{O}_i(A) D_{I',J',\ldots}(A) \,, \end{aligned} \tag{E.7}$$

where $\boldsymbol{q} = \boldsymbol{P} - \boldsymbol{P}'$ is the momentum transfer. The second integral (over ${\rm d}A$) concerns the spin-flavor degrees of freedom and is processed with techniques described in Chapters 5 and 6, as well as the previous appendix. We read

off quite a simple recipe to handle the linear momentum part of the matrix element: just take the Fourier transformation with respect to (minus) the momentum transfer of the coordinate-dependent factors in the decomposition of the current operators after substituting the soliton configuration. Of course that is precisely reflected by the spherical Bessel function appearing, e.g., in (7.7). In general we may choose any frame to do these calculation. However, it turns out that the Breit frame with,

$$\boldsymbol{P} = -\boldsymbol{P}' = \frac{\boldsymbol{q}}{2} \qquad \text{and} \qquad q^0 = 0 \tag{E.8}$$

is particularly suited not only because it properly reflects the zero energy transfer onto an infinitely heavy (large N_C) soliton but also because it directly connects the electric form factor, G_E and the magnetic form factor, G_M to the time and spatial components of the electromagnetic current, respectively. Specifically, for baryons with spin $\frac{1}{2}$ we find the Sachs form factors from the matrix elements

$$\begin{aligned} \langle B'|J^0(0)|B\rangle &= G_\mathrm{E}(\boldsymbol{q}^2)\langle s_3'|s_3\rangle \\ \langle B'|J^i(0)|B\rangle &= \frac{-\mathrm{i}}{M_\mathrm{B}} G_\mathrm{M}(\boldsymbol{q}^2)\epsilon^{ijk}q^j\langle s_3'|S_k|s_3\rangle\,. \end{aligned} \tag{E.9}$$

Here $\boldsymbol{S}$ is the spin operator and $|s_3\rangle$ indicates the state with spin projection quantum number $s_3 = \pm\frac{1}{2}$.

E.2 Relativistic Recoil Corrections

The formalism discussed above does not take into account recoil corrections. However, they should be significant for momentum transfers of the order of the nucleon mass and larger. Here we will sketch an approach to incorporate these corrections by means of a covariant formulation [4]. The resulting physics is discussed in Sect. 7.2.

The basic idea is to construct a classical moving soliton from the static solution by a Lorentz boost. This is rendered possible because of the covariance of the field equations. As results we will (i) gain a relativistic generalization of (E.3) and (ii) compute the current operators for the relativistically moving soliton. It is convenient to choose a frame such that the boosted coordinates are

$$x' = \gamma(x - Vt)\,, \quad y' = y \quad \text{and} \quad z' = z\,, \tag{E.10}$$

with $\gamma = 1/\sqrt{1-V^2}$. With regard to the discussion in Sect. E.1, Vt should be considered as the collective coordinate. For simplicity of presentation we again refrain from making the rotational coordinates explicit. As already mentioned, the Lagrange function $L = \int \mathrm{d}^3x\mathcal{L}$ for the boosted soliton

$$U(\boldsymbol{x}, t) = U_0(\boldsymbol{x}') \tag{E.11}$$

acquires the factor $1/\gamma$ when compared to the $V = 0$ case. Hence the momentum is

$$\boldsymbol{P} = \gamma \boldsymbol{V} E_{\rm cl} \quad \text{with} \quad \boldsymbol{V} = V \boldsymbol{e}_x \,. \tag{E.12}$$

Upon quantization $\boldsymbol{P}$ is elevated to an operator. The analog of $f(\boldsymbol{X}(t))$ in (E.7) for the isoscalar density is (at $t = 0$ as required for matrix elements)

$$J^0(\boldsymbol{X}) = \gamma J^0_{\rm nr}(\gamma X, Y, Z) \tag{E.13}$$

where the subscript indicates the functional form of the unboosted (non-relativistic) isoscalar density. The computation of matrix elements as in (E.9) becomes complicated because $J^0(\boldsymbol{X})$ is a highly non-linear function of the momentum operator $\boldsymbol{P}$ which induces operator ordering ambiguities. Here again the use of the Breit frame is helpful because γ only depends on $\boldsymbol{P}^2$ and thus its application on $|B\rangle$ and $|B'\rangle$ gives identical results. Therefore it is well justified to replace γ by a c-number [4]. In particular we find

$$1 - V^2 = \frac{1}{1 + \frac{\boldsymbol{q}^2}{4E_{\rm cl}}} \,. \tag{E.14}$$

With these tools at hand we compute

$$\begin{aligned} \langle B'|J^0|B\rangle &\sim G_{\rm E}(q_x^2) \\ &= \int {\rm d}^3X {\rm e}^{{\rm i}q_x X} \gamma J^0_{\rm nr}(\gamma X, Y, Z) = \int {\rm d}^3X {\rm e}^{{\rm i}q_x X/\gamma} J^0_{\rm nr}(X, Y, Z) \\ &= G_{\rm E,nr}\left(\frac{q_x^2}{\gamma^2}\right) , \end{aligned} \tag{E.15}$$

where we have ignored constants arising from the normalization. Next we consider the spatial components of the current, J^i. Since in the chosen frame the velocity is along the X axis and we quantize the baryons to be eigenstates of S_3 it is obvious that only

$$J^2(\boldsymbol{X}) = (\gamma X) J^2_{\rm nr}(\gamma X, Y, Z) S_3 \,, \tag{E.16}$$

has a non-vanishing matrix element. Hence we find

$$\begin{aligned} q_x G_{\rm M}(q_x^2) &\sim \int {\rm d}^3X {\rm e}^{{\rm i}q_x X} (\gamma X) J^2_{\rm nr}(\gamma X, Y, Z) = \frac{1}{\gamma} \int {\rm d}^3X {\rm e}^{{\rm i}q_x X/\gamma} X J^2_{\rm nr}(X, Y, Z) \\ &\sim \frac{1}{\gamma}\left(\frac{q_x}{\gamma}\right) G_{\rm M,nr}\left(\frac{q_x^2}{\gamma^2}\right) . \end{aligned} \tag{E.17}$$

Using (E.14) and returning to a frame-independent formulation suggests the identifications [4]

$$G_{\rm E}(Q^2) = G_{\rm E,nr}\left(\frac{Q^2}{1 + \frac{Q^2}{4M^2}}\right)$$

$$G_{\mathrm{M}}(Q^2) = \frac{1}{1+\frac{Q^2}{4M^2}}\, G_{\mathrm{M,nr}}\left(\frac{Q^2}{1+\frac{Q^2}{4M^2}}\right) . \tag{E.18}$$

We have replaced the classical soliton mass by the baryon mass, which is a self-suggesting approximation to find a model-independent mapping of the non-relativistic (rest frame) form factors to the relativistic ones.

References

1. E. Braaten, S.-M. Tse, and C. Willcox, *Phys. Rev.* **D34** (1986) 1482. 259
2. G. H. Derrick, *J. Math. Phys.* **5** (1964) 1252. 260
3. T. P. Cheng and L. F. Li, *Gauge Theory of Elementary Particles*, Chapters 5 and 16. Clarendon Press, Oxford, 1988. 260
4. X.-D. Ji, *Phys. Lett.* **B254** (1991) 456. 261, 262

Appendix F

Recoupling Coefficients in Adiabatic Scattering

In this appendix, some technicalities concerning the computation of the S-matrix for meson fluctuations about the soliton are discussed.

F.1 Adiabatic Recoupling Coefficients

We first derive the recoupling coefficients that transform the intrinsic S-matrix to the laboratory frame, as used in Sect. 8.1. We present that derivation here because it merely relies on the conservation of the grand spin (see the explanations after (8.4) for detailed definitions)

$$\boldsymbol{G} = \boldsymbol{J} + \boldsymbol{I} = \boldsymbol{L} + \boldsymbol{S} + \boldsymbol{I} \tag{F.1}$$

in the intrinsic frame. This conservation reflects a symmetry of QCD at large $N_{\rm C}$ and is thus more general than the soliton models [1]. Soliton models must satisfy that property because they are consistent with large $N_{\rm C}$ QCD. We will first consider the most simple case of pion–baryon scattering in flavor $SU(2)$ and then describe obvious generalizations.

We start by considering the fluctuations as in (8.1) to relate fluctuations in the intrinsic frame to those in the laboratory frame:

$$\begin{aligned} U(\boldsymbol{x},t) &= A \exp\left[\mathrm{i}\boldsymbol{\tau}\cdot\hat{\boldsymbol{x}}F(r) + \mathrm{i}\boldsymbol{\tau}\cdot\boldsymbol{\eta}(\boldsymbol{x},t)\right] A^\dagger \\ &= \exp\left[\mathrm{i}A\boldsymbol{\tau}\cdot\hat{\boldsymbol{x}}F(r)A^\dagger + \mathrm{i}\boldsymbol{\tau}\cdot\boldsymbol{\xi}(\boldsymbol{x},t)\right] . \end{aligned} \tag{F.2}$$

This implies

$$\eta_\nu(\boldsymbol{x},t) = \sum_{\nu'} D^1_{\nu,\nu'}(A)\xi_{\nu'}(\boldsymbol{x},t)\,, \tag{F.3}$$

where $D^1_{\nu,\nu'}$ is the (iso)spin one representation of the collective rotations A.

Pion fluctuations are labeled by angular momentum (L,m) and isospin projection ν. In $SU(2)$, the soliton models describe baryons with identical spin and isospin. For the time being we call that quantum number s. The respective

H. Weigel: *Recoupling Coefficients in Adiabatic Scattering*, Lect. Notes Phys. **743**, 265–270 (2008)
DOI 10.1007/978-3-540-75436-7_17

projection quantum numbers (σ, τ) may assume different values. We have to couple pion and baryon states to total spin (J, M) and isospin (I, I_3),

$$|(Ls)JM;(1s)II_3\rangle = \sum_{m\sigma\nu\tau} C^{JM}_{Lm,s\sigma} C^{II_3}_{1\nu,s\tau} |Lm,\nu\rangle_{\rm L} \sqrt{\frac{2s+1}{8\pi^2}}\,(-1)^{s+\tau}\, D^s_{\sigma,-\tau}, \tag{F.4}$$

because the pion has unit isospin. The C's are Clebsch–Gordan coefficients and the last factor represents the Wigner D-function for the baryon. This function arises from quantizing the collective coordinates as discussed in Sect. 5.3. The subscript on the pion points out that it is in the laboratory frame. The pion state in the intrinsic (or body-fixed) frame, that is related to the pion state in the laboratory frame by the rotation (F.3)

$$|Lm,\nu\rangle_{\rm B} = \sum_{\nu'} D^1_{\nu,\nu'} |Lm,\nu'\rangle_{\rm L}, \tag{F.5}$$

carries the same quantum numbers. We still have to relate these states to the fluctuations that appear in the differential equations (8.3). The latter possess good grand spin (F.1). It arises from coupling the fluctuations' angular momentum and isospin so that the grand spin states are given by

$$|GG_3, L\rangle = \sum_{m\nu} C^{GG_3}_{Lm,1\nu} |Lm,\nu\rangle_{\rm B}\,. \tag{F.6}$$

The states with good total spin and isospin that we obtain from the grand spin states are therefore

$$|L(GI)JM;II_3\rangle = \sum_{G_3 I_3'} C^{JM}_{GG_3,II_3'} |GG_3,L\rangle D^I_{I_3',-I_3}\,. \tag{F.7}$$

The main task in finding the recoupling coefficients is to relate the states in (F.4) and (F.7). This is mainly a matter of arranging Clebsch–Gordan coefficients and the result is [2]

$$\langle L(GI)JM;II_3|(Ls)JM;(1s)II_3\rangle = (-1)^{L+s+J} \hat{G}\hat{s} \begin{Bmatrix} I & 1 & s \\ L & J & G \end{Bmatrix}, \tag{F.8}$$

where we have defined $\hat{G} = \sqrt{2G+1}$, etc. The object in curly brackets denotes a 6–j symbol that summarizes Clebsch–Gordan coefficients, cf. [3]. We obtain the above recoupling coefficient from (8.8) when we set $s_\phi = 0$ and $I_\phi = 1$. To derive the corresponding generalization from (F.8), we need to (i) replace the orbital angular momentum of the meson by its spin j, where $\boldsymbol{j} = \boldsymbol{L} + \boldsymbol{s}_\phi$, and (ii) introduce a label (I_ϕ) to identify its isospin. Hence, we need to consider the coupling scheme

$$\Big\{ \Big[(Ls_\phi)_j\, s \Big]_J\, (I_\phi s)_I \Big\}_G$$

in the laboratory frame. The subscripts refer to the quantum number to which the quantities in the respective parenthesis are coupled. Equation (F.6) tells

us that the grand spin should now be the vector sum $\boldsymbol{j} + \boldsymbol{I}_\phi$. Hence, we need to generalize (F.7) to the coupling scheme

$$\left\{ \left[(Ls_\phi)_j \, I_\phi \right]_G \, I \right\}_J$$

in the intrinsic frame. As before, the baryon quantum numbers do not explicitly appear in this scheme. This must be so because the corresponding S-matrix is computed from (8.3) which does not contain them either. Thus, the recoupling coefficient from (F.8) turns into

$$\left\langle \left\{ \left[(Ls_\phi)_j \, s \right]_J (I_\phi s)_I \right\}_G \middle| \left\{ \left[(Ls_\phi)_j \, I_\phi \right]_G I \right\}_J \right\rangle = (-1)^{L+s+J} \hat{G} \hat{s} \left\{ \begin{array}{ccc} I & I_\phi & s \\ j & J & G \end{array} \right\} . \tag{F.9}$$

Though this is the final result, it is not of the form encountered in (8.8). This is due to a different intermediate coupling scheme that introduces the total spin $\boldsymbol{S}_\mathrm{t} = \boldsymbol{s} + \boldsymbol{s}_\phi$ rather than $\boldsymbol{j}$ in the laboratory frame as well as the intermediate grand spin $\boldsymbol{K} = \boldsymbol{L} + \boldsymbol{I}_\phi$ in the intrinsic frame. That representation is straightforwardly written in terms of the above basis states, as it merely involves the definition and symmetries of 6–j symbols:

$$\begin{aligned} \left[(ss_\phi)_{S_\mathrm{t}} \, L \right]_J &= \sum_j (-1)^{2s+s_\phi+L+j} \, \hat{S}_\mathrm{t} \hat{j} \left\{ \begin{array}{ccc} s & s_\phi & S_\mathrm{t} \\ L & J & j \end{array} \right\} \left[(s_\phi L)_j \, s \right]_J , \\ \left[(LI_\phi)_K \, s_\phi \right]_G &= \sum_j (-1)^{2I_\phi+s_\phi} \, \hat{K} \hat{j} \left\{ \begin{array}{ccc} I_\phi & L & K \\ s_\phi & G & j \end{array} \right\} \left[(Ls_\phi)_j \, I \right]_G . \end{aligned} \tag{F.10}$$

Putting (F.9) and (F.10) together and utilizing the identity [3]

$$\left\{ \begin{array}{ccc} a & b & c \\ d & e & f \\ g & h & j \end{array} \right\} = \sum_s (-1)^s \hat{s} \left\{ \begin{array}{ccc} a & b & c \\ f & j & s \end{array} \right\} \left\{ \begin{array}{ccc} d & e & f \\ b & s & h \end{array} \right\} \left\{ \begin{array}{ccc} g & h & j \\ s & a & d \end{array} \right\} \tag{F.11}$$

yields the result quoted in the main text (8.8).

Though we have merely considered two-flavor soliton models, the generalization to arbitrary isospin of the scattering meson grasps kaons as well. The only condition is that the target baryon has identical spin and isospin. In particular, we may read off the recoupling coefficient for kaon–nucleon scattering from (F.9) with $j = L$ because the kaons carry spin zero and $I_K = \frac{1}{2}$. These coefficients are important when computing the width of exotic baryons [4], which is discussed at length in Sect. 9.3.

F.2 Jost Function for Intrinsic Fluctuations

We will take the opportunity to sketch one out of several numerical techniques for the computation of the intrinsic S-matrix, $\widetilde{S}_G$, that appears in (8.7). We start from the second-order differential equation for radial functions $\eta_{GJ}(r)$

in the grand spin decomposition (8.5). We define the vector $\widetilde{\eta}_G$ whose entries are the radial functions $\eta_{GJ}(r)$, with all possible J values for a given G. This vector obeys a matrix differential equation of the general form

$$\left\{\mathbb{1}\frac{\mathrm{d}^2}{\mathrm{d}r^2}+\frac{2}{r}D_G^{(1)}(r)\frac{\mathrm{d}}{\mathrm{d}r}-\frac{1}{r^2}K_G+V_G(r)+k^2M(r)\right\}\widetilde{\eta}_G=0\,. \tag{F.12}$$

The coefficient functions are $n\times n$ matrices when n is the number of possible J values. These matrices stem from the Euler–Lagrange equation (8.3). They are block-diagonal with respect to the parity associated with a given channel, η_{GJ}. The radial dependences originate from the soliton profile that acts as background potential about which the fluctuations scatter. The matrices $D^{(1)}$ and M approach unity asymptotically. The matrix $K_G=\mathrm{diag}\,(J_1(J_1+1),\ldots,J_n(J_n+1))$ contains the angular momentum part so that $V_G(r)$ vanishes faster than $1/r^2$ as $r\to\infty$. Furthermore, k is the momentum associated with the dispersion relation for the conserved energy, $\omega=\sqrt{k^2+m^2}$, where m is the meson mass.[1] The appearance of the coordinate-dependent metric function M is unconventional. In (8.13), we have argued it to cause the ever-rising phase shifts at large momenta in the Skyrme model of only pseudoscalar mesons [5]. In the baryon number zero sector, i.e., when all soliton profiles take their vacuum expectation values, we have $D^{(1)}\equiv\mathbb{1}$, $M\equiv\mathbb{1}$ and $V_G\equiv 0$.

In the next step, we elevate the n-component column vector $\widetilde{\eta}_G$ to an $n\times n$ matrix, $\mathcal{N}_G$: its columns contain the linearly independent solutions of the second-order differential equation (F.12). In particular, we may consider those that asymptotically behave like an incoming spherical wave in a given channel,

$$\mathcal{H}_G(kr)=\mathrm{diag}\left(h^{(2)}_{J_1}(kr),\ldots,h^{(2)}_{J_n}(kr)\right), \tag{F.13}$$

where $h^{(2)}_\ell(kr)$ are spherical Hankel functions associated with orbital angular momentum ℓ. Asymptotically, they behave as $h^{(2)}_\ell(z)\to(i^{\ell+1}/z)\mathrm{e}^{-\mathrm{i}z}$ when $z\to\infty$ [6]. Of course, $\mathcal{H}_G(kr)$ is the free solution and we may take it as a starting point for the exact solution by parameterizing,

$$\mathcal{N}_G(r)=\mathcal{F}_G(r)\cdot\mathcal{H}_G(kr)\,. \tag{F.14}$$

Essentially $\mathcal{F}_G(r)$ is the matrix analog of the Jost function in scattering theory. This $n\times n$ matrix is subject to the second-order differential equation

$$\begin{aligned}\frac{\mathrm{d}^2\mathcal{F}_G}{\mathrm{d}r^2}+\frac{2}{r}\frac{\mathrm{d}\mathcal{F}_G}{\mathrm{d}r}\,(\mathbb{1}+rL_G)+\frac{2}{r}\left(D_G^{(1)}-\mathbb{1}\right)\left(\frac{\mathrm{d}\mathcal{F}_G}{\mathrm{d}r}+\mathcal{F}_GL_G\right)\\ -\frac{1}{r^2}\,[K_G,\mathcal{F}_G]+V_G\mathcal{F}_G+k^2\,(M-\mathbb{1})\,\mathcal{F}_G(r)=0\,.\end{aligned} \tag{F.15}$$

[1] If mesons with different masses ($m_1<m_2$) are involved, e.g., pions and vector mesons, k^2 must be considered as a diagonal matrix $\mathrm{diag}\,(\omega^2-m_1^2,\ldots,\omega^2-m_2^2)$. In the regime $m_1<\omega<m_2$, the associated k values are imaginary and the corresponding wave functions are those of bound states, thereby describing closed channels.

Here $L_G = \left(\frac{\mathrm{d}}{\mathrm{d}r}\mathcal{H}_G\right) \cdot \mathcal{H}_G^{-1}$ contains the logarithmic derivatives of the Hankel functions on the diagonal. Equation (F.15) seems complicated but it is easy to see that $\mathcal{F}_G = \mathbb{1}$ is an asymptotic solution and also a solution when the background potentials vanish.

When the boundary condition $\mathcal{F}_G \to \mathbb{1}$ as $r \to \infty$ is imposed, the matrix $\mathcal{N}_G$ contains the solutions that behave as incoming spherical waves. Furthermore, the coefficient functions in the differential equation (F.12) are all real; thus the complex conjugate $\mathcal{N}_G^*$ is a solution as well. So n of the $2n$ linearly independent solutions are contained in $\mathcal{N}_G$ and the remaining n are in $\mathcal{N}_G^*$. Asymptotically, $\mathcal{N}_G^*$ are outgoing spherical waves. This suggests to parameterize the scattering solution as

$$\mathcal{N}_G^{(\mathrm{sc})} = \mathcal{N}_G + \mathcal{N}_G^* \cdot \widetilde{S}_G \,. \tag{F.16}$$

Obviously, $\widetilde{S}_G$ is the scattering matrix for the intrinsic fluctuations. We compute it from the wave functions in $\mathcal{F}_G$ by requiring that $\mathcal{N}_G^{(\mathrm{sc})}$ is regular at the origin, $r \to 0$. Hence,

$$\widetilde{S}_G = -\lim_{r\to 0}\left[(\mathcal{H}_G^*)^{-1} \cdot (\mathcal{F}_G^*)^{-1} \cdot \mathcal{F}_G \cdot \mathcal{H}_G\right] \tag{F.17}$$

provides the entry of (8.7). Technically, we integrate the differential equation (F.15) from sufficiently large $r = R_\infty$ with the boundary conditions $\mathcal{F}_G\big|_{r=R_\infty} = \mathbb{1}$ and $\frac{\mathrm{d}}{\mathrm{d}r}\mathcal{F}_G\big|_{r=R_\infty} = 0$ to the inside and read off $\lim_{r\to 0}\mathcal{F}_G$ from the numerical integration to compute $\widetilde{S}_G$ via (F.17). The method described here is a variant of the variable phase approach, which is exhaustively discussed in [7].

For the application to the vacuum polarization energy in Sect. 8.6, we note that the leading term of $h_\ell^{(2)}(kr)$ as $r \to 0$ is purely imaginary. Therefore, $\lim_{r\to 0}\mathcal{H}_G(kr) \cdot (\mathcal{H}_G^*(kr))^{-1} = -1$, and in each grand spin channel, the sum of eigen phase shifts that appears in (8.57) is obtained from

$$\delta_G^{\mathrm{tot}}(k) = \frac{1}{2\mathrm{i}} \lim_{r\to 0} \mathrm{tr}\left[(\mathcal{F}_G^*)^{-1} \cdot \mathcal{F}_G\right] . \tag{F.18}$$

Finally, let us mention that the approach based on the differential equation (F.15) is well suited to set up the Born series [8, 9]. To do so, let us introduce an artificial order parameter λ whose deviation from unity labels the interaction strength, i.e.,

$$D_G^{(1)} - \mathbb{1} = \mathcal{O}(\lambda) \,, \quad V_G = \mathcal{O}(\lambda) \quad \text{and} \quad M - \mathbb{1} = \mathcal{O}(\lambda) \,. \tag{F.19}$$

Then we expand

$$\mathcal{F}_G = \mathbb{1} + \lambda\mathcal{F}_G^{(1)} + \lambda^2\mathcal{F}_G^{(2)} + \cdots \tag{F.20}$$

and solve (F.15) order by order in λ. The boundary conditions are that all $\mathcal{F}_G^{(n)}$ and their derivatives vanish at spatial infinity. In this manner, the pieces

in (F.19) act as source terms for $\mathcal{F}_G^{(1)}$, which in turn induces $\mathcal{F}_G^{(2)}$ and so on. At the end, we substitute the expansion (F.20) into (F.17) to extract the nth order of the Born series for the scattering matrix as the coefficient of λ^n in (F.17).

References

1. M. P. Mattis and M. Mukherjee, *Phys. Rev. Lett.* **61** (1988) 1344. 265
2. A. Hayashi, G. Eckart, G. Holzwarth, and H. Walliser, *Phys. Lett.* **B147** (1984) 5. 266
3. D. A. Varshalovich, A. N. Moskalev, and V. K. Khersonskii, *Quantum Theory of Angular Momentum*, Chap. 4. World Scientific, Singapore, 1988. 266, 267
4. T. D. Cohen and R. F. Lebed, *Phys. Lett.* **B578** (2004) 150. 267
5. G. Eckart, A. Hayashi, and G. Holzwarth, *Nucl. Phys.* **A448** (1986) 732. 268
6. M. Abramowitz and I. A. Stegun, *Handbook of Mathematical Functions*. Nat. Bureau of Standards, Gaithersburg, MD 1964. 268
7. F. Calegero, *Variable Phase Approach to Potential Scattering*. Acad. Press, New York, 1967. 269
8. N. Graham, R. L. Jaffe, and H. Weigel, *Int. J. Mod. Phys.* **A17** (2002) 846. 269
9. E. Farhi, N. Graham, R. L. Jaffe, and H. Weigel, *Nucl. Phys.* **B630** (2002) 241. 269

Index